Errors in Emergency and Trauma Radiology

Michael N. Patlas
Douglas S. Katz
Mariano Scaglione

Editors

≋ Springer

Errors in Emergency and Trauma Radiology

Michael N. Patlas · Douglas S. Katz
Mariano Scaglione
Editors

Errors in Emergency and Trauma Radiology

Springer

Editors
Michael N. Patlas
Department of Radiology
McMaster University
Hamilton, ON
Canada

Douglas S. Katz
Department of Radiology
NYU Winthrop Hospital
Mineola, NY
USA

Mariano Scaglione
Department of Imaging
Pineta Grande Medical Center
Castel Volturno, Caserta
Italy

To my parents, Ludmila and Dr. Natan Patlas, who showed me the way. To my wife Nataly who made me to believe in myself and continues to inspire me. To my children Michal and Jessica who make me happy and proud.

Michael N. Patlas

To Sebastian Isaiah, who will encounter some pitfalls and will probably make some errors along the way, but whom Darienne and I are confident will find the correct path, and who will have a great journey in life.

Douglas S. Katz, MD

To my parents, Pietro and Ida, for their encouragement, support, and love.

Mariano Scaglione

Foreword

Over the past half century, emergency radiology has come into being as a subspecialty on its own. Corresponding to a dynamic period in CT technology, the evolution of the specialty has been profound. What originally began as an area of interest for some has morphed into a discipline with a potential to make a vital difference in the care of acutely ill patients and victims of trauma.

As a radiologist who trained in the late 1990s, I witnessed firsthand how imaging made major inroads in the care of the emergency department (ED) patient. When I started residency in 1995, we routinely performed angiography for the evaluation of the potentially injured aorta. Some thought that CT would never achieve the accuracy needed for this potentially lethal injury. Over two decades later, it is hard to imagine diagnosing traumatic aortic injury without CT. With the added reliance on imaging, we all became aware of potential pitfalls. Of course, we all wished to be sensitive in our diagnoses but in the ED patient, specificity is equally as important. Chasing an artifact to exclude aortic injury can potentially be lethal in the setting of a pelvic fracture or grade 5 liver laceration.

CT for pulmonary embolism (PE) provides another such example. As a resident, angiography was rarely performed, and ventilation perfusion scintigraphy was the standard for the evaluation of a patient with suspected pulmonary embolism. CT was not felt to be ready to meet this challenge. Boy, how times have changed! A night in the ED rarely passes without at least one PE CT ordered. As with any widely accepted protocol, indication creep occurs and the number of truly positive studies for PE decreases. Understanding of the potential errors helps the reading radiologist make sure they find the unusual PE and prevent overdiagnosis.

In *Errors in Emergency and Trauma Radiology*, Drs. Patlas, Katz, Scaglione, and colleagues address the potential errors and pitfalls in the ED patient. By covering all organ systems, they bring together in one place all of the ways imaging can mislead us in the care of the ED patient. Specific chapters on select patient populations are also incredibly helpful in avoiding the traps of imaging in the ED. For the experienced ED reader, this work will serve as a nice review with creative approaches to reinforce techniques to improve accuracy. For the general reader, it helps put imaging findings in context so that the radiologist may make a meaningful difference and provide effective care in some of our most vulnerable patients.

Anyone taking call will appreciate *Errors in Emergency and Trauma Radiology* as a valuable, concise resource that will help diagnostic accuracy in the ED. Drs. Patlas, Katz, Scaglione, and colleagues deserve much credit for bringing these potential errors together in one place. These chapters represent a compendium of learning in the past half century that will help increase our value in the next half.

<div align="right">

Sanjeev Bhalla, MD
Cardiothoracic Radiology, Emergency Radiology
Mallinckrodt Institute of Radiology
St Louis, MO
USA

</div>

Contents

Errors in Emergency and Trauma Radiology: General Principles

Kate Hames, Michael N. Patlas, Vincent M. Mellnick, and Douglas S. Katz

In 2016, researchers estimated that more than 251,000 patients die in US hospitals annually as a result of preventable errors, ranking medical error as the third most common cause of death in the USA [1]. Many of these preventable deaths are due to diagnostic errors. Multiple large autopsy studies dating from 1957 [2] describe diagnostic error rates across all medical specialties ranging from anywhere between 5% and 47% [2–7]. Diagnostic errors in medicine are a major source of patient harm, and result in death more often than other medical errors including drug-related errors [8]. In addition to affecting patient morbidity and mortality, diagnostic errors also account for the leading type of paid claims (28.6%) and the highest proportion of total payments (35.2%) in malpractice lawsuits, with a 25-year sum of

diagnostic-related payments in the USA totalling $38.8 billion [8].

A diagnostic error is defined as a medical error related to a missed, incorrect, or delayed diagnosis that is discovered by subsequent findings or tests [9, 10]. As medical imaging is central to the overall diagnostic process, it is logical to conclude that the incidence of diagnostic error (missed, incorrect, and delayed) is attributable, at least in part, to radiology-related errors [11]. For example, in a review of closed malpractice claims in the USA, diagnostic radiology was the sixth more frequent specialty involved [12], while approximately three out of four malpractice claims against radiologists mention errors in interpretation resulting in missed diagnoses [5, 13].

Radiology, similar to many other highly complex visual perception-based activities including air traffic control or operating nuclear power plants, relies on a sophisticated interplay of numerous psychophysiological factors and visual perception and is therefore prone to human error [14–17]. Radiological diagnosis also involves decision-making under conditions of often significant uncertainty in which the availability of clinical information, prior examinations, or use of proper technique may be variable [18]. These conditions are amplified in the fast-paced and high-stress environment of emergency and trauma centers in which the acuity of polytrauma patients, involvement of a large multidisciplinary team, and the need to make quick

K. Hames · M. N. Patlas (✉)
Department of Radiology, McMaster University, Hamilton, ON, Canada
e-mail: kathleen.hames@medportal.ca;
patlas@hhsc.ca

V. M. Mellnick
Department of Radiology, Mallinckrodt Institute of Radiology, Washington University School of Medicine, St. Louis, MO, USA
e-mail: mellnickv@wustl.edu

D. S. Katz
Department of Radiology, NYU Winthrop Hospital, Mineola, NY, USA
e-mail: Douglas.Katz@nyulangone.org;
dkatz@nyuwinthrop.org

life-saving decisions all predispose the radiologist to interpretive error. Under such conditions of uncertainty, all diagnostic decisions therefore have inherent error rates [19].

In the first landmark study of its kind, in 1949, California radiologist L.H. Garland published an article entitled, "On the Scientific Evaluation of Diagnostic Procedures," in which he demonstrated a surprising degree of inaccuracy in numerous clinical, laboratory, and radiological tests [20]. Regarding radiological examinations specifically, Garland discovered a 33% retrospective error rate among radiologists interpreting positive chest radiographs and a 2% overall rate for normal examinations [21]. This retrospective experimental error rate translates into an error rate of approximately 3–5% when evaluating the prospective interpretation of all examinations during a routine clinical day [5]. Nearly 70 years later, despite remarkable technological advances in medical imaging, Garland's findings on the incidence of radiological error remain nearly identical. From the 1950s to the present day, studies have repeatedly demonstrated the incidence of diagnostic error in radiology to be approximately 3–5% [17, 19, 22–30].

Unlike physical examination findings, radiological examinations are now easily accessible electronic databases which are available for subsequent scrutiny and analysis. Because of the accessibility and relative permanence of radiological examinations, the extensive collection of examinations also provides a robust data source from which not only to assess inter- and intraobserver variation, but also to retrospectively detect patterns in errors or discrepancies for educational purposes. As dozens of studies have repeatedly shown, radiological errors follow predictable patterns [5, 14, 18, 22, 30–35]. By analyzing these patterns, individual and system-wide measures may be enacted to help prevent similar errors from being made in the future.

1.1 General Errors in Radiology

Radiological errors may be categorized in multiple different ways [5, 11, 30, 32, 33, 36–42]. In the broadest terms, the cause of interpretive error may be either internal (specific to the individual radiologist) or external (due to larger systemic failures). To subdivide these categories further, internal factors include both perceptual and cognitive errors. Among internal sources of error, perceptual errors account for approximately 60–80% of missed or delayed diagnoses in radiological interpretation [5, 11, 36–38]. A perceptual error occurs during the first step of image interpretation. For an error to be categorized as a perceptual error, the imaging finding must be deemed sufficiently conspicuous and detectable in retrospect by the initial radiologist or in the consensus of his or her peers [11]. As such, not all subtle or inconspicuous findings that are subsequently identified and found to represent a pathological process would be classified as perceptual errors [11]. Considering that the radiological error rate has remained stable at 3–5% for nearly 70 years as noted, it is reasonable to assume that every radiologist has committed a perceptual error: a miss that, in retrospect, may appear obvious to both the original radiologist and to her or his peers.

The psychophysiologic and cognitive processes by which an obvious abnormality can simply go unseen when it is so clearly seen in retrospect have yet to be fully explained to anyone's satisfaction. Although an increased incidence of perception error may be due to other specific risk factors including radiologist fatigue, interruptions, distractions, reading too rapidly, satisfaction of search, or various forms of cognitive bias as this chapter will discuss, most perceptual errors lack a clear identifiable cause. However, studies on radiologist perceptual errors from around the world, involving radiologists at all levels of training and experience and across all modalities, conclude that perceptual errors are not a result of carelessness or negligence; rather, perceptual errors are deemed a consequence of the physiological processes of human perception and an inherent feature of the complex system in which radiologists operate [11, 13, 14, 26, 37, 42, 43].

While perceptual errors account for approximately 60–80% of interpretive errors, the remaining 20–40% of internal errors may be classified

as cognitive errors [5, 11, 36–38]. Cognitive errors have been defined as "judgment errors" [5], "faulty reasoning" [22], or "logic fallacies" [44], in which an abnormality is identified, but its clinical significance is misinterpreted, resulting in an inaccurate diagnosis [11]. Cognitive errors may be a result of lack of knowledge, faulty reasoning, or a multitude of cognitive biases. Additionally, these biases may be secondary to undue influence of previous erroneous reports (known as an alliterative error) or misleading clinical information that misdirects the radiological gaze. However, interpretive errors are more likely due to a combination of multiple factors, both intrinsic and extrinsic to the radiologist interpreting the imaging examination.

Of the numerous cognitive biases that may influence a radiologist's interpretive process, four primary types have been repeatedly identified as potential causes of diagnostic error: anchoring, framing, availability, and alliterative [11, 31, 44–46]. Anchoring bias occurs when the radiologist fails to alter his or her initial interpretation despite being provided with contrary information [11, 31, 44]. Framing bias occurs when the radiologist is unduly influenced by the wording or framing of the clinical problem, which leads to restricted diagnostic possibilities [31, 44]. Availability bias is defined as the propensity to consider a diagnosis that comes to mind more readily to be the correct diagnosis [11, 31, 44]. This is more likely to occur after the radiologist has committed an interpretive error, which predisposes him or her to mistakenly attribute the previously "missed" diagnoses to a similar finding in a subsequent patient [44]. An alliterative error occurs when the results from the interpretation of a previous imaging examination biases the radiologist toward the same diagnosis when interpreting the current examination, which results in a diagnostic error [11, 31, 44]. Another cognitive bias described by Bruno et al. [11] is the "zebra retreat," which occurs when the radiologist resists proposing a rare diagnosis (despite supportive findings) due to the rarity of the diagnosis.

Additional cognitive errors include complacency, faulty reasoning, lack of knowledge on the part of the viewer, and underreading [30, 42, 47]. Underreading is the equivalent to a perceptual miss, where the finding is identifiable but was overlooked by the first radiologist [30, 42]. Complacency occurs when a finding is identified but is attributed to the wrong cause and not deemed pathological, while faulty reasoning occurs when a finding is seen and interpreted as abnormal but is subsequently attributed to an incorrect etiology [30, 42]. Satisfaction of search is another common radiological interpretive error and one that produces nearly as much frustration in the radiologist as perceptual errors. Satisfaction of search is the premature discontinuation of a diagnostic search pattern after a primary, usually more obvious abnormality is detected [34, 48–51]. Once a single prominent abnormality is identified, the "search for meaning" is satisfied, and the interpreter ceases to search for additional, usually more subtle abnormalities.

In addition to internal factors, there are numerous external factors that also play a substantial role in radiological error. These external, or system-based, factors include poor or limited radiological technique, lack of access to potentially relevant prior imaging, inadequate or misdirected clinical history, increasing volume and complexity of cases, staff shortages, constant interruptions, and reader fatigue, to list just a few of the more significant external sources potentially contributing to interpretive error [5, 18, 30, 32, 42, 44, 52]. The lack of prior imaging examinations, or the failure to review relevant examinations, also contributes to interpretive error [32, 42]. Both scenarios suggest that interconnected networks of electronic medical records including radiological examinations, and increased ease of access to such prior exams, would help reduce interpretive error.

The ever-increasing volume and complexity of radiological examinations, in addition to staff shortages, have led to mounting pressure on radiologists to read more in a shorter period, which in turn results in longer work hours and mounting reader fatigue, all of which contribute to diagnostic error [44, 53–57]. Not surprisingly, increasing one's speed at image interpretation is also a source of error. Sokolovskaya et al. [58] demonstrated that when radiologists interpreted

examinations at twice the speed of their baseline, the number of significant errors increased from 10% to 26.6%. Constant interruptions and multitasking may also result in increased interpretive error. Balint et al. [59] studied the number of telephone calls on-call radiology residents received at night, and compared the increased interruptions to the rate of interpretive error (defined as a resident-attending discordant report). The study found that in the hour preceding the interpretive error, a single additional phone call above the baseline increased the likelihood of a major discrepancy by 12% [59].

One of the most important sources of radiological error occurs at the start of the imaging cycle with the examination requisition and clinical history. Pinto et al. [40] noted that the study of radiological errors has traditionally been limited to errors in the radiologist's report, which are frequently taken out of the larger diagnostic context, thereby omitting the integral role of the referring physicians. In the majority of studies on radiological errors, researchers have found that a relevant clinical history can improve diagnostic accuracy during both the perception and interpretation phases [46, 60–63]. Loy and Irwig's [60] examination of 16 studies analyzing the accuracy of reports with and without clinical history found that providing relevant clinical history improved the sensitivity of findings without decreasing specificity. Similarly, Leslie et al. [63] found that when referring clinicians provided a clinical history, radiologists changed 19% of their CT reports, more than half of which reflected major changes. Providing accurate clinical information also ensures that the appropriate radiological examination is performed, and ultimately assists the diagnostic workup [44, 46, 64].

While 40–54% of medical malpractice lawsuits against radiologists are due to diagnostic errors [65], the majority of the remaining legal complaints are due to failure to communicate the findings in a timely manner, and the failure to suggest the next appropriate procedure or examination (imaging or otherwise) [47]. Failure to communicate clinically significant findings rapidly is the fourth most frequent medical malpractice claim made against radiologists [66].

Therefore, it is in the patients' and the radiologists' best interests to communicate – and document – urgent findings quickly, and to explicitly recommend appropriate additional imaging or clinical/laboratory follow-up as necessary.

1.2 Errors in Emergency and Trauma Radiology

The potential for diagnostic error, whether due to perceptual errors, cognitive biases, or technical errors, is further magnified in emergency departments and trauma centers. The fast-paced setting and high-stress environment of emergency and trauma departments create a potential "perfect storm" for diagnostic errors: medically unstable and/or uncooperative patients, insufficient histories, multiple concurrent tasks, involvement of a large multidisciplinary trauma team, severity and complexity of trauma injuries, quick life-saving decisions, and often junior physicians with less experience working after hours when the trauma volume is typically highest [67–70]. Radiological errors may also be caused by radiologist fatigue and ocular strain from longer work hours, multiple interruptions, lack of prior imaging for comparison, the pressure to read examinations quickly, and the variable conspicuity of acute abnormalities in difficult-to-image poly-trauma patients. Patients who present to emergency and trauma departments are typically those with more acute injuries, and therefore carry an increased risk of morbidity and mortality at baseline. As such, the diagnostic errors committed in this acute setting carry a greater risk of severe complications and worse patient outcomes, including death.

Multiple studies evaluating missed injuries and delayed diagnoses in the emergency setting have been published, with a reported incidence of 1.3–39% [67, 71–77]. Among patients with missed injuries, 15–22.3% had clinically significant findings [77]. Gruen et al. [67] found that among trauma patients who died from recognizable errors, 16% died from delayed operative or angiographic control of an acute abdominal or pelvic hemorrhage, and 9% died from delayed intervention for on-going intratho-

racic hemorrhage. In autopsy studies involving poly-trauma patients, researchers found that the primary cause of death was due to severe hemorrhage from traumatic bronchopulmonary vessel injury [78]. Of all the missed injuries in emergency and trauma centers, Teixeira et al. [72] report that diagnostic errors are responsible for approximately 10–15% of preventable deaths in trauma center audits. As selective non-operative management has become increasingly feasible after abdominopelvic trauma, diagnosis of injuries requiring surgery or interventional radiology has become more imperative. As such, injuries missed on multi-detector computed tomography (MDCT) have the potential to result in more dire consequences.

Multiple studies have proven MDCT to be superior to both clinical evaluation and diagnostic peritoneal lavage for the diagnosis of clinically significant abdominal injuries in poly-trauma patients [71, 79–82]. Due to multiple factors including decreased consciousness, unreliable histories, and distracting injuries, clinical examination of trauma patients is frequently unreliable [69, 83]. A physical examination of a trauma patient with abdominal injuries is only about 60% reliable [69, 84, 85]. As missed abdominal injuries are a well-documented cause of increased morbidity and mortality in trauma patients [71, 81, 82], early detection of these injuries by CT is crucial to improving patient outcomes. MDCT is also critical to the assessment of head trauma, which is particularly difficult to assess clinically in many poly-trauma patients due to decrease levels of consciousness, distracting injuries, and drug and/or alcohol intoxication. Studies have shown that 25% of unconscious patients with a serious head injury have misleading or equivocal clinical findings on examination [69]. In patients with poly-trauma, blunt cerebral-vascular injuries with associated vertebral and/or carotid injuries in particular are frequently missed if they are only investigated with ultrasound, which has been shown to have a sensitivity of 38.5%, compared to a 100% sensitivity with CT angiography [86].

Over the past two decades, significant developments in CT technology, including faster image acquisition, higher spatial resolution, multi-planar and 3D reformats, and decreased radiation, have resulted in the increased use of MDCT in the emergency setting. The integration of MDCT in emergency departments has improved both the speed and accuracy of diagnostic procedures and has led to early detection of clinically significant injuries [77, 87–89], thereby decreasing mortality in trauma patients [90]. With peritoneal lavage becoming increasingly obsolete [79, 91], the diagnosis of poly-trauma injuries, including acute arterial hemorrhage, now relies almost exclusively on the swift and accurate interpretation of findings from properly performed CT examinations acquired in a timely fashion [83]. In poly-trauma patients in particular, the pan-scan CT (head, chest, abdomen, pelvis, and full spine) is now considered the reference standard for the early assessment of acute potentially life-threatening injuries.

As a key member of the multidisciplinary trauma team, the radiologist not only plays a critical role in diagnosing acute life-threatening injuries but also helps direct the clinical decision-making process for surgical or conservative management. Therefore, errors in image acquisition and image interpretation may lead to suboptimal treatment and potential patient harm. Radiological errors in the emergency setting follow predictable patterns, and recognition of these patterns is crucial to avoiding error and improving patient outcomes.

1.3 Perception and Recognition Errors in Emergency Radiology

Although diagnostic radiology errors are often associated with perception, studies have shown that only 10% of interpretive errors are due to human perception or other nonvisual cues [67, 72, 92], while approximately 60% of radiologic errors are caused by poor technique or image quality [93, 94]. One of the most frequent causes of diagnostic error in trauma patients is the failure to identify fractures on radiographs, which accounts for 41–80% of interpretive errors

in the emergency department [17, 74, 95, 96]. Moreover, missed or delayed diagnosis of skeletal injuries, particularly fractures of the appendicular skeleton, accounts for the majority of malpractice claims against radiologists [74]. The most commonly missed fractures involve the periarticular regions, shoulder girdle, and feet [97]. Approximately 10% of missed fractures involve the spine, with the cranio-cervical junction (40–50%) and the cervicothoracic junction being the most common sites of missed injury [97]. While spinal fractures can have significant orthopedic and neurological implications, they may also direct the radiologist to other associated injuries. For example, although transverse process fractures are only associated with vertebral body fractures in 1% of cases, 50% of patients with transverse process fractures have intra-abdominal injuries [98, 99].

Due to the higher sensitivity and specificity of CT compared to traditional radiography [100], delayed or missed diagnoses of abdominal and pelvic injuries are less frequent than orthopedic injuries; however, interpretive errors in abdominopelvic injuries carry a greater risk of severe complications due to the potentially life-threatening nature of solid and hollow organ injury and active hemorrhage. Among solid organs, injuries of the liver and spleen each account for approximately 10–15% of missed or delayed diagnoses [97]. Although diaphragmatic injuries are relatively uncommon and represent only 5% of delayed diagnoses [101], they remain difficult to detect [102]. Radiological suspicion, attention to secondary signs, and use of multiplanar reconstructed CT images are crucial for the correct identification of diaphragmatic injuries. In addition, vascular injuries account for approximately 5% of delayed diagnoses [97]. In pediatric trauma patients, injuries to the ureteropelvic junction are overlooked in approximately 50% of affected patients on the initial image interpretation [103], which may be due to perceptual error as well as technical error if delayed CT images are not performed. More than 80% of female trauma patients with a previously unknown first-trimester pregnancy are not found to be pregnant during the initial evaluation prior to undergoing CT examination, thereby exposing the embryo to potentially harmful radiation [104].

Other commonly missed injuries in trauma patients involve bowel and mesenteric injuries, which account for approximately 15–20% of diagnostic errors [105]. From a clinical perspective, acute bowel injury often implies surgical exploration, and missed or delayed diagnoses may significantly increase patient morbidity and mortality from sepsis and hemorrhage [106]. However, bowel and mesenteric injuries pose a unique challenge to radiologists, as 9.1–19.4% of patients with surgically proven bowel and mesenteric injuries do not have any identifiable findings on the preoperative MDCT [107, 108]. More recent surgical literature has shown an increased mortality in patients with a diagnostic delay in bowel injury in as little as 5 h [106]; therefore, Patlas et al. [109] suggest that it may be prudent to perform a follow-up CT in 6–8 h for patients with clinically suspected bowel injury or new clinical symptoms concerning for bowel injury.

In addition to recognition errors, interpretive errors may also occur when the radiologist appropriately identifies an abnormality, but mistakenly attributes it to an incorrect etiology. This type of error has been classified as faulty reasoning or a misclassification of a true-positive finding [30, 42]. Provenzale and Kranz [41] use the example of venous infarction and dural venous sinus thrombosis (DST) to illustrate this category of interpretive error. While the radiologist may accurately detect the presence of infarction, she or he may fail to appreciate a thrombosed cortical vein or dural sinus, and mistakenly interpret the finding as an arterial infarct. Similarly, when patients with DST receive IV contrast-enhanced CT and MRI, the abnormal dural enhancement due to collateral vessels may be mistaken for alternative pathologies such as neurosarcoidosis or dural metastases [41, 110].

Errors also occur when the radiologist mistakenly interprets a normal finding as abnormal, which has been described as overcalling or false-positive findings [41, 42, 70]. These findings may be attributed to poor technique, such as artifact, or anatomical variants mistaken for pathology. This type of diagnostic error is more

likely to occur among radiology residents or less experienced radiologists who both lack experience and who tend to be overly cautious [41]. For example, on CT images, respiratory motion artifact may produce an indistinct gray margin around the liver, spleen, kidney, abdominal wall, or ribs [70]. This linear or halo-like appearance may be mistaken for a subcapsular hematoma or even rib fractures [70]. Similarly, cardiac motion artifact in the mediastinum may obscure the aortic root and produce crescentic gray bands within the ascending aorta, which may be mistaken for acute aortic injury. In addition to motion artifact, anatomical variants such as a splenic cleft may also be mistaken for a low-grade splenic laceration [70]. Although this category of error may not result in immediate harm, unlike a missed acute positive finding, it may result in unnecessary hospital admission for observation [70] and unnecessary follow-up examinations, which may indirectly lead to patient harm.

In contrast to overcalling, under-calling is another type of diagnostic error that has the potential to contribute to patient morbidity and mortality. Under-calling occurs when the radiologist identified an abnormality but dismissed it as normal or secondary to artifact. While over-calling may occur more frequently among cautious junior radiologists, under-calling may be more common among experienced radiologists who are accustomed to seeing artifacts and are therefore seemingly more confident in their interpretations. Provenzale and Kranz [41] suggest under-calling may occur subconsciously, without deliberation about the nature of the findings; however, Scaglione et al. [69] suggest these types of errors may occur as a result of external pressure to reduce the number of false-positive interpretations in order to minimize unnecessary follow-up. It may be reasonable to assume these errors may also be a result of lack of knowledge, whereby an abnormality is identified, but because its etiology cannot be confidently deduced, it is erroneously dismissed as insignificant, thus resulting in a missed or delayed diagnosis.

In the faced-paced and high-pressure evaluation of poly-trauma patients, many of whom

present with potentially life-threatening injuries, radiologists are particularly vulnerable to satisfaction of search errors. In satisfaction of search errors, as previously described, once a major abnormality is identified, the radiologist may rapidly shorten her or his search time, thereby overlooking additional abnormalities [30]. As Berbaum et al. [51] noted, satisfaction of search errors are the result of a deliberate truncation of a search rather than a faulty search pattern. Poly-trauma patients, by definition, present with multiple injuries, many of which may be life-threatening. It is therefore the radiologist's responsibility to quickly and accurately identify the most urgent findings that require immediate surgical or other clinical interventions, carefully characterize the findings, and directly communicate critical findings to the appropriate clinical team members. When injuries such as active vascular extravasation, acute aortic injury, pneumoperitoneum, or massive pneumothorax are identified, the radiologist may focus on these findings, and inadvertently abbreviate the remainder of the search, thereby overlooking more subtle, but potentially just as clinically significant abnormalities.

Due to the acuity of patients in the emergency department and the speed with which clinical decisions must be made, strong communication between the radiologist and the treating physician is critical. In many instances, a final written report is not sufficient, as the time delay between the radiologist completing the report and the ER physician or surgeon reading the report is unpredictable. This delay in communication is one of the most frequent causes of medical malpractice claims made against radiologists [66]. In cases of acute, life-threatening findings that require immediate intervention, direct verbal communication between the radiologist and clinician may avoid delays in treatment and prevent any confusion about the severity of injury. Documentation of all verbal reports should include the date, time, name of the clinician(s) with whom the radiologist discussed the findings, and a detailed account of what was discussed [111].

Another important communication error occurs when the radiologist does not expressly

communicate her or his recommendations for additional or follow-up imaging or other examinations. As discussed previously, the ACR practice guidelines state that "follow-up or additional diagnostic studies to confirm the impression should be suggested when appropriate" [112]. Frequently in poly-trauma patients, these recommendations are made at the time of scanning at the CT console. For example, delayed phases may be added if there is suspicion for ureteral injury, or a CT cystogram may be recommended in the case of potential bladder injury. However, in patients with equivocal findings who require follow-up, it is important that the radiologist recommend both the type of follow-up examination and the timeline in which it should be performed. This is particularly crucial for suspected bowel and mesenteric injury, which may not have any imaging findings on the initial MDCT scan, or the findings may be quite subtle [107, 108]. However, if bowel injury is suspected, it is imperative the radiologist recommended follow-up in as little as 6–8 h [109] to avoid potential sepsis and hemorrhage [106].

Emergency physicians and associated health-care practitioners must also communicate clearly with the radiologist and provide an adequate clinical history to avoid potential missed and delayed diagnoses. Without adequate history of the mechanism of trauma and presenting injuries, the radiologist cannot protocol the appropriate cross-sectional examination with the necessary sequences, which predisposes the radiologist to both perceptual and technical diagnostic errors. Scaglione et al. [69] stated that approximately 40% of the patients with delayed diagnoses are due to clinical survey oversight. More specifically, an incomplete history has been shown to result in a 10% likelihood of delayed diagnosis [73]. Additional studies have found that 15% of delayed diagnoses are due to the failure of the clinician to order appropriate imaging of the region of injury identified during clinical examination [73]. Obtaining an adequate history from a trauma patient is notoriously difficult, as noted [97]. However, appropriate imaging and interpretation can only be accomplished if there is clear communication between the treating physi-

cian/health-care practitioner and the radiologist regarding the clinical suspicion of injury.

1.4 Technical Errors in Emergency Radiology

Although there has been a great deal of research conducted on diagnostic errors associated with individual perception and cognitive biases, it is important to remember that a far greater percentage (upward of 60%) of radiological errors are caused by poor technique or image quality [93, 94]. As MDCT has become the reference standard for evaluating poly-trauma patients, adherence to proper technique and protocol is critical to avoid inadequate and potentially non-diagnostic examinations. When imaging a poly-trauma patient with MDCT, it is important that the radiologist and CT technologist work in close collaboration with the trauma team to avoid potential errors and optimize scanning technique. To start, the patient should be undressed to ensure no clothing-related artifacts obscure the image, have at least an 18 g IV to ensure adequate contrast administration, have their arms raised above their head (if possible in the context of injury) to avoid bony artifact in the chest and abdomen, have their arms down if the area of interest is in the head or neck, and either be cooperative or sedated to minimize motion artifact [113].

Once the patient is properly prepared for the CT scan, the appropriate protocol must be selected based on the clinical history and mechanism of injury. While in some patients this may include a full-body scan (head, chest, abdomen, pelvis, and spine) with arterial and portal venous phases, other patients may require more tailored approaches with additional phases of imaging. This includes patients with acute hemorrhage who may require multiphasic imaging to accurately characterize the source of hemorrhage. At the minimum, a CT angiogram of the chest, abdomen, and pelvis is recommended to detect the source of acute arterial hemorrhage [114–117], although non-contrast and/or delayed CT acquisitions may be useful to better characterize the source of bleeding. However, not all sources

of hemorrhage are arterial; therefore, it is imperative to attempt to identify whether the source of extravasation is due to either an arterial or venous injury, which will help direct interventional and surgical management as necessary [69, 118].

After the biphasic (arterial and portal venous) examination has been performed, the radiologist may detect potential renal, ureteral, or bladder injuries requiring additional phase images. If the emergency radiologist is not at the scanner at the time of CT image acquisition to direct further imaging, multiple injuries only detectable on delayed phases may potentially be missed. For example, if there is suspicion for renal or ureteral injury, a delayed excretory phase is recommended at an 8–12-min delay. If there is suspicion for bladder injury, an MDCT cystogram should be performed to assess the extent of injury and to characterize if it is intra- or extraperitoneal or both, which will dictate surgical management [119]. Delayed CT images also help to further characterize solid visceral organ injuries that involve the vasculature and which may also require surgical or urgent interventional management [120–123].

Appropriate MDCT technique is also crucial in the evaluation of cerebral trauma. As blunt cerebral-vascular injuries are frequently underdiagnosed in poly-trauma patients [86], full evaluation with a CT angiogram of the carotid and vertebral arteries as well as of the circle of Willis may help avoid missed or delayed diagnoses of vascular injury and potentially prevent neurological complications. With advances in MDCT techniques, a full-body CT angiogram from the circle of Willis to the pelvis is possible and has been advocated in patients with severe poly-trauma [124–126]. In order to maximize image quality and prevent missed or delayed diagnoses, appropriate MDCT protocols must be used. This includes important follow-up examinations for patients with equivocal findings on the initial MDCT, such as those with potential bowel or mesenteric injury, as well as in patients with new or worsening symptoms.

Once all of necessary phases of an MDCT examination have been obtained, multi-planar reformatted images must also be evaluated. Coronal and sagittal reconstructions are particularly helpful for localizing the source of any acute hemorrhage [17], characterizing spinal fractures, assessing bowel and mesenteric injury [127], and identifying diaphragmatic injuries which are notoriously difficult to detect only on axial images [102] and are therefore easily missed.

1.5 Solutions and Prevention of Radiological Errors

When considering potential solutions to preventing diagnostic error in radiology, it is important to consider both person-centered and system-based solutions. However, care must be taken when defining a person-centered approach, as the aim is not to focus on an individual who has committed an error and thereby subject him or her to blame, shame, or disciplinary action [18]. Such targeted shame-based approaches have been proven counterproductive and ill-suited to the health-care domain [128]. Instead, the focus should be on the larger forces that have created the conditions for the error to occur. This is not to say that solutions such as improved education cannot be directed at particular individuals, specifically radiologists-in-training and junior attendings; rather, continuing education and adherence to standards of care should be directed toward all members of the radiology department.

Education on radiological errors, including cognitive biases and the propensity to commit satisfaction of search errors, may help raise awareness of the common "error traps" [18] and thereby decrease the incidence of these errors. For example, if awareness is raised about alliterative bias, whereby reading the previous report may unduly influence the interpretation of the current examination, radiologists may choose to avoid consulting the prior report until they have completed their own evaluation of the current examination. To decrease satisfaction of search errors, education on complete search strategies and common mechanism-based multiple injury patters may prove beneficial [127]. For example, knowledge of trauma injury "packages" (such as right-sided injuries or left-sided injuries) may

help focus the radiologist's attention on organ systems and adjacent structures most likely to be involved in particular mechanisms of injury, thereby decreasing the potential for missed or delayed diagnoses. Additionally, the use of checklists or dictation templates (especially for residents and junior attendings) may reduce diagnostic error by promoting a more systematic and complete search process [127].

Intradepartmental and multidisciplinary meetings focusing on clinical and radiological diagnostic errors may also prove beneficial from an educational standpoint. However, for such meetings to be productive and to have a positive learning outcome, the culture of the meeting must not be one of blame. Fitzgerald [18] noted in 2001 that the culture at that time was to embarrass and shame the radiologist who committed the error. This approach has the potential to undermine the educational value and instead foster a culture of fear and animosity. Radiological error/quality assurance meetings (or morbidity and mortality rounds) may be more beneficial if they are conducted according to the principles outlined by Chandy et al. [129]: a confidential reporting system, anonymous presentation, written reports by peers at the meeting, and consensus adjudication on the presence or absence of error. Encouraging radiologists to share their diagnostic misses and mistakes with others in a supportive learning environment may not only help others avoid similar errors but may also lead to greater self-awareness of one's own search errors and cognitive biases, thereby decreasing diagnostic errors overall.

At the system level, it is important that all equipment is functioning optimally in order to maximize the quality of image production. Standardized MDCT protocols are also important, particularly in the evaluation of poly-trauma patients. Depending on the mechanism of injury and the clinical suspicion, whole-body MDCT protocols including angiographic examinations from the circle of Willis to the pelvis may prove beneficial in detecting otherwise occult injuries [124–126]. The radiologist should also be encouraged to be present, when possible, at the

CT scanner at the time of image acquisition in order to assess the need for delayed imaging or a CT cystogram.

As fatigue and ocular strain have also been proven to contribute to diagnostic errors [56], optimizing ergonomics, encouraging breaks, and promoting physical activity whenever possible may prove beneficial in reducing error rates [130]. Optimal lighting and individualized ergonomic settings of PACS stations may reduce physical stressors and improve the reading experience, which may potentially decrease diagnostic error [44]. Decreasing the number of interruptions may also prove beneficial, as disrupting radiologists' focus during image interpretation has been shown to result in interpretive errors [59]. For example, Rosenkrantz et al. [131] found that the introduction of reading room coordinators to assist radiologists with phone calls and other administrative tasks significantly decreased interruptions and improved radiologists' workflow efficiency. Implementing similar programs throughout radiology departments may also help to reduce diagnostic errors.

Recent advancements in artificial intelligence (AI) and machine learning (ML) algorithm also promise to streamline the data mining and organizational tasks that often detract from radiological interpretation of examinations [132–135]. For example, Thrall et al. [133] argued that, more than improve diagnostic accuracy, AI can be applied to numerous practical issues that radiologists encounter on a daily basis: optimizing work lists to prioritize cases, pre-analyzing cases in high-volume settings to help eliminate observer fatigue, extracting information from images not readily apparent to the human eye, and improving the quality of reconstructed images [133]. The application of AI may also assist with the timeliness of image interpretation and communication of urgent findings. If algorithms can be used to prescreen examinations rapidly and detect urgent findings such as pulmonary emboli, pneumothorax, pneumoperitoneum, or other potentially life-threatening conditions, the program could

alert the radiologist to prioritize the case for immediate interpretation [133]. For example, Prevedello et al. [136] developed a machine learning algorithm to identify critical findings on non-contrast-enhanced CT examinations of the brain. The program was found to be highly accurate in detecting intracranial hemorrhage, mass effect, and hydrocephalus, with an area under the receiver operating characteristic curve of 0.91 [136].

By prioritizing examinations for urgent review, AI may potentially reduce interpretive error by decreasing delays in diagnosis and improving communication. Prescreening algorithms may also help to identify critical findings and prevent errors of omission and satisfaction of search errors [135], which would also help to avert delayed and missed diagnoses. In their study on identifying strokes, Griffis et al. [137] developed an algorithm using naïve Bayes classification to automatically identify strokes on T1-weighted MRI images, which correctly predicted lesion locations for 30/30 untrained cases. Additionally, Thornhill et al. [138] have used advanced morphometric analysis to help distinguish free-floating intraluminal thrombus from atherosclerotic plaque in patients presenting with TIA or stroke. By more accurately characterizing a symptom-related intravascular lesion as thrombus or plaque, the application of this algorithm may help to optimize patient management and improve patient outcomes [138].

While some may argue that AI will eventually replace human radiologists [139] (and other specialists including dermatologists, neurologists, radiation oncologists, and many more), others see AI as a valuable tool that will ultimately increase radiologists value, efficiency, accuracy, and personal satisfaction [132–135]. As Recht et al. [132] argued, using AI algorithms to perform the quantification tasks and data mining of electronic medical records will help radiologists refocus their energies on more value-added functions that computers cannot provide. With the help of AI, radiologists can increase their professional interactions, become more visible to patients, and ultimately play a more active, visible role in integrated clinical teams to improve patient care [132].

1.6   Conclusion

Radiological diagnosis in an emergency and trauma setting demands quick decision-making under conditions of significant uncertainty in which the availability of clinical information, prior examinations, or the use of proper techniques is often highly variable [18]. Therefore, all such decisions have inherent error rates [19]. While diagnostic errors are responsible for only approximately 10–15% of preventable deaths in trauma center audits [72], as selective non-operative management has become increasingly feasible after abdominopelvic trauma, the accurate diagnosis of injuries requiring surgical or interventional management has become more imperative. As such, injuries missed on MDCT have the potential to result in more dire consequences. Radiologists are key members of the multidisciplinary trauma team, and play a critical role in not only diagnosing acute, potentially life-threatening injuries, but also in directing the clinical decision-making process toward appropriate surgical, interventional, or conservative management.

Radiological errors in the emergency setting follow predictable patterns. By analyzing these patterns, individual and system-wide measures may be enacted to help prevent similar errors from being made in the future. For example, diagnostic errors may be reduced by on-going education on the individual sources of error, including satisfaction of search error and cognitive biases, as well as through the use of standardized reporting or checklists. Additionally, implementing supportive intra- and interdisciplinary morbidity and mortality rounds may allow radiologists to learn from each other's mistakes, while becoming more cognizant of their own search patterns and biases. Finally, at the system level, ensuring appropriate MDCT and other imaging protocols are followed, attempting to limit interruptions, and promoting radiologists' physical and mental well-being through optimization of ergonomics and minimization of fatigue, may all help to reduce interpretive error.

References

1. Makary MA, Daniel M. Medical error: the third leading cause of death in the US. BMJ. 2016;353:2139.
2. Gruver RH, Freis ED. A study of diagnostic errors. Ann Intern Med. 1957;47:108–20.
3. Anderson RE, Hill RB, Key CR. The sensitivity and specificity of clinical diagnostics during five decades: toward an understanding of necessary fallibility. JAMA. 1989;261:1610–7.
4. Roosen J, Frans E, Wilmer A, Knockaert DC, Bobbaers H. Comparison of premortem clinical diagnoses in critically ill patients and subsequent autopsy findings. Mayo Clin Proc. 2000;75:562–7.
5. Berlin L. Radiologic errors, past, present and future. Diagnosis. 2014;1(1):79–84.
6. Leape LL, Brennan TA, Laird N, Lawthers AG, Localio AR, Barnes BA, et al. The nature of adverse events in hospitalized patients: results of the Harvard medical practice Study II. N Engl J Med. 1991;324(6):377–84.
7. Berner ES, Graber ML. Overconfidence as a cause of diagnostic error in medicine. Am J Med. 2008;121(5 suppl):S2–23.
8. Saber Tehrani AS, Lee H, Mathews SC, Shore A, Makary MA, Pronovost PJ, et al. 25-year summary of US malpractice claims for diagnostic errors 1986-2010: an analysis from the National Practitioner Data Bank. BMJ Qual Saf. 2013;22(8):672–80.
9. Kohn LT, Corrigan JM, Donaldson MS. Executive summary. In: To err is human: building a safer heath system. Washington, DC: National Academy Press; 2000. p. 1–16.
10. Graber ML, Franklin N, Gordon R. Diagnostic error in internal medicine. Arch Intern Med. 2005;165(13):1493–9.
11. Bruno MA, Walker EA, Abujudeh HH. Understanding and confronting our mistakes: the epidemiology of error in radiology and strategies for error reduction. Radiographics. 2015;35:1668–76.
12. Whang JS, Baker SR, Patel R, Luk L, Castro A. The causes of medical malpractice suits against radiologists in the United States. Radiology. 2013;266(2):548–54.
13. Berlin L. Radiologic errors and malpractice: a blurry distinction. Am J Roentgenol. 2007;189(3):517–22.
14. Tuddenham WJ. Roentgen image perception – a personal survey of the problem. Radiol Clin North Am. 1969;7:499–501.
15. Yerushalmy J. The statistical assessment of the variability in observer perception and description of roentgenographic pulmonary shadows. Radiol Clin North Am. 1969;7:381–92.
16. Leape LL. Error in medicine. JAMA. 1994;272:181–7.
17. Berlin L. Defending the "missed" radiographic diagnosis. Am J Roentgenol. 2001;176:317–22.
18. Fitzgerald R. Error in radiology. Clin Radiol. 2001;56(12):938–46.
19. Potchen EJ, Cooper TG, Sierra AE. Measuring performance in chest radiography. Radiology. 2000;217:456–9.
20. Garland LH. On the scientific evaluation of diagnostic procedures. Radiology. 1949;52(3):309–28.
21. Garland LH. Studies on the accuracy of diagnostic procedures. Am J Roentgenol. 1959;82:25–38.
22. Smith MJ. Error and variation in diagnostic radiology. Springfield, IL: Thomas; 1967. 4, 73–74, 144–69.
23. Stevenson CA. Accuracy of the X-ray report. JAMA. 1969;207:1140–1.
24. Berlin L. Does the "missed" radiographic diagnosis constitute malpractice? Radiology. 1977;123:523–7.
25. Markus JB, Somers S, Franic SE, Moola C, Stevenson GW. Interobserver variation in the interpretation of abdominal radiographs. Radiology. 1989;171:69–71.
26. Siegle RL, Baram EM, Reuter SR, Clarke EA, Lancaster JL, McMahan CA. Rates of disagreement in imaging interpretation in a group of community hospitals. Acad Radiol. 1998;5:148–54.
27. Soffa DJ, Lewis RS, Sunshine JH, Bhargavan M. Disagreement in interpretation: a method for the development of benchmarks for quality assurance in imaging. J Am Coll Radiol. 2004;1:212–7.
28. Abujudeh HH, Boland GW, Kaewlai R, Rabiner P, Halpern EF, Gazelle GS, et al. Abdominal and pelvic computed tomography (CT) interpretation: discrepancy rates among experienced radiologists. Eur Radiol. 2010;20(8):1952–7.
29. Borgstede JP, Lewis RS, Bhargavan M, Sunshin JH. RADPEER quality assurance program: a multifactorial study of interpretive disagreement rates. J Am Coll Radiol. 2004;1:59–65.
30. Renfrew DL, Franken EA, Berbaum KS, Weigelt FH, Abu-Yousef MM. Error in radiology: classification and lessons in 182 cases presented at a case conference. Radiology. 1992;183:145–50.
31. FitzGerald R. Radiological error: analysis, standard setting, targeted instruction and teamworking. Eur Radiol. 2005;15(8):1760–7.
32. Brady A, Laoide RÓ, McCarthy P, McDermott R. Discrepancy and error in radiology: concepts, causes and consequences. Ulster Med J. 2012;81(1):3–9.
33. Lev MH, Rhea JT, Bramson RT. Avoidance of variability and error in radiology. Lancet. 1999;354(9175):272.
34. Ashman CJ, Yu JS, Wolfman D. Satisfaction of search in osteo-radiology. Am J Roentgenol. 2000;175:541–4.
35. Rogers LF. Keep looking: satisfaction of search. Am J Roentgenol. 2000;175:287.
36. Samei E, Krupinski E, editors. The handbook of medical image perception and techniques. 1st ed. Cambridge: Cambridge University Press; 2014. 438 p
37. Donald JJ, Barnard SA. Common patterns in 558 diagnostic radiology errors. J Med Imaging Radiat Oncol. 2012;56:173–8.
38. Kundel HL, Nodine CF, Carmody D. Visual scanning, pattern recognition and decision-making in pulmonary nodule detection. Invest Radiol. 1978;13(3):175–81.
39. Brook OR, O'Connell AM, Thornton E, Eisenberg RL, Mendiratta-Lala M, Kruskal JB. Quality initia-

tives: anatomy and pathophysiology of errors occurring in clinical radiology practice. Radiographics. 2010;30(5):1401–10.

40. Pinto A, Scuderi MG, Daniele S. Errors in radiology: definition and classification. In: Errors in radiology. Milano: Springer; 2012. p. 1–7. Available from: https://link.springer.com/chapter/10.1007/978-88-470-2339-0_1.

41. Provenzale JM, Kranz PG. Understanding errors in diagnostic radiology: proposal of a classification scheme and application to emergency radiology. Emerg Radiol. 2011;18(5):403–8.

42. Kim YW, Mansfield LT. Fool me twice: delayed diagnoses in radiology with emphasis on perpetuated errors. Am J Roentgenol. 2014;202(3):465–70.

43. Revesz G, Kundel HL. Psychophysical studies of detection errors in chest radiology. Radiology. 1977;123(3):559–62.

44. Waite S, Scott J, Gale B, Fuchs T, Kolla S, Reede D. Interpretive error in radiology. Am J Roentgenol. 2017;208(4):739–49.

45. Lee CS, Nagy PG, Weaver SJ, Newman-Toker DE. Cognitive and system factors contributing to diagnostic errors in radiology. Am J Roentgenol. 2013;201(3):611–7.

46. Berlin L, Berlin JW. Malpractice and radiologists in Cook County, IL: trends in 20 years of litigation. Am J Roentgenol. 1995;165(4):781–8.

47. Pinto A, Brunese L. Spectrum of diagnostic errors in radiology. World J Radiol. 2010;2(10):377–83.

48. Fleck MS, Samei E, Mitroff SR. Generalized "satisfaction of search": adverse influences on dual-target search accuracy. J Exp Psychol Appl. 2010;16:60–71.

49. Berbaum KS, Franken EA, Caldwell RT. Satisfaction of search in radiographic modalities. Radiology. 2011;261:1000–1.

50. Berbaum KS, Schartz KM, Caldwell RT. Satisfaction of search from detection of pulmonary nodules in computed tomography of the chest. Acad Radiol. 2013;20:194–201.

51. Berbaum KS, Brandser EA, Franken EA, Dorfman DD, Caldwell RT, Krupinski EA. Gaze dwell times on acute trauma injuries missed because of satisfaction of search. Acad Radiol. 2001;8(4):304–14.

52. Waite S, Scott JM, Legasto A, Kolla S, Gale B, Krupinski EA. Systemic error in radiology. Am J Roentgenol. 2017;209(3):629–39.

53. McDonald RJ, Schwartz KM, Eckel LJ, Diehn FE, Hunt CH, Bartholmai BJ, et al. The effects of changes in utilization and technological advancements of cross-sectional imaging on radiologist workload. Acad Radiol. 2015;22(9):1191–8.

54. Krupinski EA, Berbaum KS, Caldwell RT, Schartz KM, Kim J. Long radiology workdays reduce detection and accommodation accuracy. J Am Coll Radiol. 2010;7(9):698–704.

55. Vertinsky T, Forster B. Prevalence of eye strain among radiologists: influence of viewing variables on symptoms. Am J Roentgenol. 2005;184(2):681–6.

56. Rohatgi S, Hanna TN, Sliker CW, Abbott RM, Nicola R. After-hours radiology: challenges and strategies for the radiologist. Am J Roentgenol. 2015;205(5):956–61.

57. Hanna TN, Lamoureux C, Krupinski EA, Weber S, Johnson J-O. Effect of shift, schedule, and volume on interpretive accuracy: a retrospective analysis of 2.9 million radiologic examinations. Radiology. 2017;287(1):205–12.

58. Sokolovskaya E, Shinde T, Ruchman RB, Kwak AJ, Lu S, Shariff YK, et al. The effect of faster reporting speed for imaging studies on the number of misses and interpretation errors: a pilot study. J Am Coll Radiol. 2015;12(7):683–8.

59. Balint BJ, Steenburg SD, Lin H, Shen C, Steele JL, Gunderman RB. Do telephone call interruptions have an impact on radiology resident diagnostic accuracy? Acad Radiol. 2014;21(12):1623–8.

60. Loy CT, Irwig L. Accuracy of diagnostic tests read with and without clinical information: a systematic review. JAMA. 2004;292(13):1602–9.

61. Berbaum KS, el-Khoury GY, Franken EA, Kathol M, Montgomery WJ, Hesson W. Impact of clinical history on fracture detection with radiography. Radiology. 1988;168(2):507–11.

62. Doubilet P, Herman PG. Interpretation of radiographs: effect of clinical history. Am J Roentgenol. 1981;137(5):1055–8.

63. Leslie A, Jones AJ, Goddard PR. The influence of clinical information on the reporting of CT by radiologists. Br J Radiol. 2000;73(874):1052–5.

64. Robinson PJA. Radiology's Achilles' heel: error and variation in the interpretation of the Roentgen image. Br J Radiol. 1997;70:1085–98.

65. Berlin L. Malpractice and radiologists, update 1986: an 11.5-year perspective. Am J Roentgenol. 1986;147(6):1291–8.

66. Harrigal CL, Erly WK. On-call radiology: community standards and current trends. Semin Ultrasound CT MRI. 2007;28(2):85–93.

67. Gruen RL, Jurkovich GJ, McIntyre LK, Maier RV. Patterns of errors contributing to trauma mortality: lessons learned from 2594 deaths. Ann Surg. 2006;244(3):371–80.

68. Pinto A, Reginelli A, Pinto F, Lo Re G, Midiri F, Muzj C, et al. Errors in imaging patients in the emergency setting. Br J Radiol. 2016;89(1061):20150914.

69. Scaglione M, Iaselli F, Sica G, Feragalli B, Nicola R. Errors in imaging of traumatic injuries. Abdom Imaging. 2015;40(7):2091–8.

70. West CO, Anderson J, Lee JS, Finnell CW, Raval BK. Patterns of diagnostic error in trauma abdominal CT. Emerg Radiol. 2002;9(4):195.

71. Janjua KJ, Sugrue M, Deane SA. Prospective evaluation of early missed injuries and the role of tertiary trauma survey. J Trauma. 1998;44(6):1000–6.

72. Teixeira PG, Inaba K, Hadjizacharia P, et al. Preventable or potentially preventable mortality at a mature trauma center. J Trauma Acute Care Surg. 2007;63(6):1338–47.

73. Sung CK, Kim KH. Missed injuries in abdominal trauma. J Trauma. 1996;41(2):276–82.
74. Brooks A, Holroyd B, Riley B. Missed injury in major trauma patients. Injury. 2004;35(4):407–10.
75. Houshian S, Larsen MS, Holm C. Missed injuries in a level I trauma center. J Trauma. 2002;52(4):715–9.
76. Vles WJ, Veen EJ, Roukema JA, Meeuwis JD, Leenen LPH. Consequences of delayed diagnoses in trauma patients: a prospective study. J Am Coll Surg. 2003;197(4):596–602.
77. Pfeifer R, Pape H. Missed injuries in trauma patients: a literature review. Patient Saf Surg. 2008;2:20.
78. Barendregt WB, de Boer HH, Kubat K. Quality control in fatally injured patients: the value of necropsy. Eur J Surg. 1993;159:9–13.
79. Catre MG. Diagnostic peritoneal lavage versus abdominal computed tomography in blunt abdominal trauma: a review of prospective studies. Can J Surg. 1995;38(2):117–22.
80. Gonzales RP, Ickler J, Gachassin P. Complementary roles of diagnostic peritoneal lavage and computed tomography in the evaluation of blunt abdominal trauma. J Trauma. 2001;51(6):1128–34.
81. Ekeh AP, Saxe J, Walusimbi M, et al. Diagnosis of blunt intestinal and mesenteric injury in the era of multidetector CT technology - are results better? J Trauma. 2008;65(2):354–9.
82. Velmahos GC, Tabbara M, Gross R, et al. Blunt pancreatoduodenal injury: a multi-center study on the Research Consortium of New England Centers for Trauma (Re-CONECT). Arch Surg. 2009;144(5):413–9.
83. Soto JA, Anderson SW. Multidetector CT of blunt abdominal trauma. Radiology. 2012;265(3):678–93.
84. Poletti P-A, Wintermark M, Schnyder P, Becker CD. Traumatic injuries: role of imaging in the management of the polytrauma victim (conservative expectation). Eur Radiol. 2002;12(5):969–78.
85. Schurink GW, Bode PJ, van Luijt PA, van Vugt AB. The value of physical examination in the diagnosis of patients with blunt abdominal trauma: a retrospective study. Injury. 1997;28(4):261–5.
86. Mutze S, Rademacher G, Matthes G. Blunt cerebrovascular injury in patients with blunt multiple trauma: diagnostic accuracy of duplex Doppler US and early CT angiography. Radiology. 2005;237:884–92.
87. Hessmann MH, Hofmann A, Kreitner KF, Lott C, Rommens PM. The benefit of multislice CT in the emergency room management of polytraumatized patients. Acta Chir Belg. 2006;106(5):500–7.
88. Hilbert P, zur Nieden K, Hofmann GO, Hoeller I, Koch R, Stuttmann R. New aspects in the emergency room management of critically injured patients: a multi-slice CT-oriented care algorithm. Injury. 2007;38(5):552–8.
89. Kanz K-G, Paul AO, Lefering R, Kay MV, Kreimeier U, Linsenmaier U, et al. Trauma management incorporating focused assessment with computed tomography in trauma (FACTT) - potential effect on survival. J Trauma Manag Outcomes. 2010;4:4.
90. Huber-Wagner S, Lefering R, Qvick L-M, Körner M, Kay MV, Pfeifer K-J, et al. Effect of whole-body CT during trauma resuscitation on survival: a retrospective, multicentre study. Lancet. 2009;373(9673):1455–61.
91. Drost TF, Rosemurgy AS, Kearney RE, Roberts P. Diagnostic peritoneal lavage. Limited indications due to evolving concepts in trauma care. Am Surg. 1991;57(2):126–8.
92. Ivatury RR, Guilford K, Malhotra AK, Duane T, Aboutanos M, Martin N. Patient safety in trauma: maximal impact management errors at a level I trauma center. J Trauma. 2008;64(2):265–70.
93. Hirshberg A, Wall MJ, Allen MK, Mattox KL. Causes and patterns of missed injuries in trauma. Am J Surg. 1994;168(4):299–303.
94. Nicolaou S, Eftekhari A, Sedlic T, Hou DJ, Mudri MJ, Aldrich J, et al. The utilization of dual source CT in imaging of polytrauma. Eur J Radiol. 2008;68(3):398–408.
95. Guly H. Diagnostic errors in an accident and emergency department. Emerg Med J. 2001;18(4):263–9.
96. Williams SM, Connelly DJ, Wadsworth S, Wilson DJ. Radiological review of accident and emergency radiographs: a 1-year audit. Clin Radiol. 2000;55(11):861–5.
97. Stanescu L, Talner LB, Mann FA. Diagnostic errors in polytrauma: a structured review of the recent literature. Emerg Radiol. 2006;12(3):199–23.
98. Krueger MA, Green DA, Hoyt D, Garfin SR. Overlooked spine injuries associated with lumbar transverse process fractures. Clin Orthop. 1996;327:191–5.
99. Patten RM, Gunberg SR, Brandenburger DK. Frequency and importance of transverse process fractures in the lumbar vertebrae at helical abdominal CT in patients with trauma. Radiology. 2000;215(3):831–4.
100. Cain G, Shepherdson J, Elliott V. Imaging suspected cervical spine injury: plain radiography or computed tomography? Systematic review. Radiography. 2010;16:68–77.
101. Voeller GR, Reisser JR, Fabian TC, Kudsk K, Mangiante EC. Blunt diaphragm injuries. A five-year experience. Am Surg. 1990;56:28–31.
102. Reber PU, Schmied B, Seiler CA, Baer HU, Patel AG, Buchler MW. Missed diaphragmatic injuries and their long-term sequelae. J Trauma Inj Infect Crit Care. 1998;44(1):183–8.
103. Onuora VC, Patil MG, al-Jasser AN. Missed urological injuries in children with polytrauma. Injury. 1993;24(9):619–21.
104. Bochicchio GV, Napolitano LM, Haan J, Champion H, Scalea T. Incidental pregnancy in trauma patients. J Am Coll Surg. 2001;192(5):566–9.
105. Lawson CM, Daley BJ, Ormsby CB, Enderson B. Missed injuries in the era of the trauma scan. J Trauma. 2011;70(2):452–6.

106. Malinoski DJ, Patel MS, Yakar DO, Green D, Qureshi F, Inaba K, et al. A diagnostic delay of 5 hours increases the risk of death after blunt hollow viscus injury. J Trauma. 2010;69(1):84–7.

107. LeBedis CA, Anderson SW, Bates DDB, Khalil R, Matherly D, Wing H, et al. CT imaging signs of surgically proven bowel trauma. Emerg Radiol. 2016;23(3):213–9.

108. Matsushima K, Mangel PS, Schaefer EW, Frankel HL. Blunt hollow viscus and mesenteric injury: still underrecognized. World J Surg. 2013;37(4):759–65.

109. Patlas MN. Invited commentary on "MDCT imaging of surgically proven blunt bowel and mesenteric injury". Radiographics. 2017;37:625–7.

110. Provenzale JM, Joseph GJ, Barboriak DP. Dural sinus thrombosis: findings on CT and MR imaging and diagnostic pitfalls. Am J Roentgenol. 1998;170(3):777–83.

111. Raskin MM. Survival strategies for radiology: some practical tips on how to reduce the risk of being sued and losing. J Am Coll Radiol. 2006;3(9):689–93.

112. American College of Radiology. ACR practice guideline for communication of diagnostic imaging findings. In: 2005 practice guideline and technical standards. Reston, VA: American College of Radiology; 2005. p. 5–9.

113. Guida F, Bocchini G, Sica G, Frezza A, Scaglione M. Errors in polytrauma. In: Errors in radiology. Milano: Springer; 2012. p. 27–37. Available from: https://link.springer.com/chapter/10.1007/978-88-470-2339-0_4.

114. Weninger P, Mauritz W, Fridrich P, Spitaler R, Figl M, Kern B, et al. Emergency room management of patients with blunt major trauma: evaluation of the multislice computed tomography protocol exemplified by an urban trauma center. J Trauma. 2007;62(3):584–91.

115. Yao DC, Jeffrey RB, Mirvis SE, Weekes A, Federle MP, Kim C, et al. Using contrast-enhanced helical CT to visualize arterial extravasation after blunt abdominal trauma: incidence and organ distribution. Am J Roentgenol. 2002;178(1):17–20.

116. Willmann JK, Roos JE, Platz A, Pfammatter T, Hilfiker PR, Marincek B, et al. Multidetector CT: detection of active hemorrhage in patients with blunt abdominal trauma. Am J Roentgenol. 2002;179(2):437–44.

117. Hamilton JD, Kumaravel M, Censullo ML, Cohen AM, Kievlan DS, West OC. Multidetector CT evaluation of active extravasation in blunt abdominal and pelvic trauma patients. Radiographics. 2008;28(6):1603–16.

118. Albrecht T, Foert E, Holtkamp R, Kirchin MA, Ribbe C, Wacker FK, et al. 16-MDCT angiography of aortoiliac and lower extremity arteries: comparison with digital subtraction angiography. Am J Roentgenol. 2007;189(3):702–11.

119. Deck AJ, Shaves S, Talner L, Porter JR. Computerized tomography cystography for the diagnosis of traumatic bladder rupture. J Urol. 2000;164(1):43–6.

120. Anderson SW, Varghese JC, Lucey BC, Burke PA, Hirsch EF, Soto JA. Blunt splenic trauma: delayed-phase CT for differentiation of active hemorrhage from contained vascular injury in patients. Radiology. 2007;243(1):88–95.

121. Mulligan JM, Cagiannos I, Collins JP, Millward SF. Ureteropelvic junction disruption secondary to blunt trauma: excretory phase imaging (delayed films) should help prevent a missed diagnosis. J Urol. 1998;159(1):67–70.

122. Ortega SJ, Netto FS, Hamilton P, Chu P, Tien HC. CT scanning for diagnostic blunt ureteral and ureteropelvic junction injuries. BMC Urol. 2008;8(3):3.

123. Stuhlfaut JW, Lucey BC, Varghese JC, Soto JA. Blunt abdominal trauma: utility of 5-minute delayed CT with a reduced radiation dose. Radiology. 2006;238(2):473–9.

124. Pinto A, Niola R, Tortora G, et al. Role of multidetector-row CT in assessing the source of arterial haemorrhage in patients with pelvic vascular trauma. Comparison with angiography. Radiol Med. 2010;115(4):648–67.

125. Nguyen D, Platon A, Shanmuganathan K, Mirvis SE, Becker CD, Poletti PA. Evaluation of a single-pass continuous whole-body 16-MDCT protocol for patients with polytrauma. Am J Roentgenol. 2009;192(1):3–10.

126. Foster BR, Anderson SW, Uyeda J, Brooks JG, Soto JA. Integration of 64-detector lower extremity CT angiography into whole-body trauma imaging: feasibility and early experience. Radiology. 2011;261(3):787–95.

127. Patlas MN, Dreizin D, Menias CO, Tirada N, Bhalla S, Nicolaou S, et al. Abdominal and pelvic trauma: misses and misinterpretations at multidetector CT: *trauma/emergency radiology*. Radiographics. 2017;37(2):703–4.

128. An organisation with a memory: report of an expert group on learning from adverse events in the NHS chaired by the Chief Medical Officer. | AHRQ Patient Safety Network. Accessed 2 Apr 2018. Available from: https://psnet.ahrq.gov/resources/resource/1568/an-organisation-with-a-memory-report-of-an-expert-group-on-learning-from-adverse-events-in-the-nhs-chaired-by-the-chief-medical-officer.

129. Chandy J, Goodfellow T, Vohrah A. Clinical governance in action: radiology. Hosp Med. 2000;61(5):326–9.

130. Hoffmann JC, Mittal S, Hoffmann CH, Fadl A, Baadh A, Katz DS, et al. Combating the health risks of sedentary behavior in the contemporary radiology reading room. Am J Roentgenol. 2016;206(6):1135–40.

131. Rosenkrantz AB, Kang SK, Rybak L, Alexa D, Recht MP. The reading room coordinator: reducing radiologist burnout in the digital age. J Am Coll Radiol. 2018;15(1):65–8.

132. Recht M, Bryan RN. Artificial Intelligence: threat or boon to radiologists? J Am Coll Radiol. 2017;14(11):1476–80.

133. Thrall JH, Li X, Li Q, Cruz C, Do S, Dreyer K, et al. Artificial intelligence and machine learning in radiology: opportunities, challenges, pitfalls, and criteria for success. J Am Coll Radiol. 2018;15(3): 504–8.

134. McGinty GB, Allen B. The ACR Data Science Institute and AI Advisory Group: Harnessing the power of artificial intelligence to improve patient care. J Am Coll Radiol. 2018;15(3):577–9.

135. Kahn CE. From images to actions: opportunities for artificial intelligence in radiology. Radiology. 2017;285(3):719–20.

136. Prevedello LM, Erdal BS, Ryu JL, Little KJ, Demirer M, Qian S, et al. Automated critical test findings identification and online notification system using artificial intelligence in imaging. Radiology. 2017;285(3):923–31.

137. Griffis JC, Allendorfer JB, Szaflarski JP. Voxel-based Gaussian naïve Bayes classification of ischemic stroke lesions in individual T1-weighted MRI scans. J Neurosci Methods. 2016;257:97–108.

138. Thornhill RE, Lum C, Jaberi A, Stefanski P, Torres CH, Momoli F, et al. Can shape analysis differentiate free-floating internal carotid artery thrombus from atherosclerotic plaque in patients evaluated with CTA for stroke or transient ischemic attack? Acad Radiol. 2014;21(3):345–54.

139. Obermeyer Z, Emanuel EJ. Predicting the future - big data, machine learning, and clinical Medicine. N Engl J Med. 2016;375(13):1216–9.

Mistakes in Imaging Interpretation of Traumatic and Non-traumatic Brain Emergencies

Carlos Torres, Nader Zakhari, Francisco Rivas-Rodriguez, Angela Guarnizo-Capera, Ashok Srinivasan, and Diego Nunez

The Merriam-Webster Dictionary defines an error as an act that through ignorance, deficiency, or accident departs from or fails to achieve what should be done. Errors in medicine can arise from different causes including technical failure, perceptual problem, cognitive biases, system errors, etc., and mitigation of these errors requires a thorough understanding of the root causes in each scenario since it may be multifactorial. Errors in radiology are unique within the practice of medicine, since the missed imaging finding or misinterpretation of an imaging examination stays for posterity and can be accessed easily much later in time, unlike errors in clinical examinations that often are not accessible for investigation at a later time. They are also unique due to the inherent differences in the acquisition and interpretation of imaging examinations, and are more prone toward perceptual and cognitive biases.

For the sake of simplicity, errors in radiology can be broadly divided into perceptual and interpretive errors, but it is important to understand that these categories are not mutually exclusive. There are different system and cognitive factors which can lead to diagnostic error. In the field of emergency radiology, errors often occur due to repeating themes, which are particularly specific to this subspecialty. These include the need for a quick turnaround time (implying less time to spend on each image in cross-sectional examinations, which typically have hundreds of images, if not thousands for some MR examinations), inadequate clinical history (which can lead to misdirection of the focused search for abnormalities), relative inexperience of the radiologist in

C. Torres (✉)
Department of Radiology, University of Ottawa, Ottawa, ON, Canada

Department of Diagnostic Imaging, The Ottawa Hospital, Ottawa, ON, Canada

Ottawa Hospital Research Institute OHRI, Ottawa, ON, Canada
e-mail: catorres@toh.ca

N. Zakhari
Department of Radiology, University of Ottawa, Ottawa, ON, Canada

Department of Diagnostic Imaging, The Ottawa Hospital, Ottawa, ON, Canada
e-mail: nzakhari@toh.ca

F. Rivas-Rodriguez · A. Srinivasan
Department of Radiology, University of Michigan, Ann Arbor, MI, USA
e-mail: frivasro@med.umich.edu;
ashoks@med.umich.edu

A. Guarnizo-Capera
Department of Radiology, University of Ottawa, Ottawa, ON, Canada
e-mail: aguarnizocapera@toh.ca

D. Nunez
Department of Radiology, Brigham and Women's Hospital, Harvard Medical School, Boston, MA, USA
e-mail: dnunez@bwh.harvard.edu

a specific subspecialty, and suboptimal imaging examinations which may be technically inadequate (motion artifacts, thicker slices, lack of multi-planar reformations, etc.).

2.1 Clinical Information and Imaging Techniques: Valuable Tools to Reduce Errors in the Imaging Evaluation of Brain Emergencies

The diagnosis of neurological emergencies is imperfect with underdiagnosis (threatening patient safety) and overtesting (leading to the suboptimal use of resources). Stroke, dizziness, headache, and seizures are the clinical scenarios with a greater potential for diagnostic error [1]. Approximately 4% of diagnostic radiology examinations have associated interpretation errors. Specific features of medical care in the emergency setting, including uncooperative patients, inadequate clinical histories, time-critical decisions, concurrent tasks, and varying experience of the radiologist working afterhours in busy emergency departments, all contribute to the potential for error in the interpretation of imaging examinations of brain emergencies [2].

Awareness of variable clinical and imaging presentations of brain emergencies, appropriateness criteria in the imaging evaluation of such entities, technical requirements, proper imaging protocols, attempting to obtain relevant and accurate clinical information, peer review following imaging interpretation, timely communication of abnormal findings to the treating clinicians, and the recommendation of follow-up imaging examinations when appropriate, all substantially minimize the potential for error [3].

Headache accounts for approximately 2% of emergency department (ED) visits, of which only a small number have serious causes [4]. Deciding which patients need further investigation can be difficult. The need for imaging should be triggered by the presence of "red flags" in the clinical history and physical examination [5].

Subarachnoid hemorrhage (SAH) misdiagnosis stems from three recurring, correctable patterns of diagnostic error: failure to consider the spectrum of clinical presentation, not following an algorithm workup, and failure to understand the limitations of diagnostic tests, including computed tomography (CT) and lumbar puncture (LP) [6].

Most patients with subarachnoid hemorrhage have abrupt onset of a severe and unique headache or neck pain. Many patients may additionally have abnormal findings on neurologic examination, while others only complain of subtle meningismus or ocular findings. Understanding this wide spectrum of clinical presentation, paired with careful history taking and physical examination, is the best strategy for identifying patients who should be evaluated for subarachnoid hemorrhage [6].

Among patients presenting to emergency departments with headaches, approximately 1% have subarachnoid hemorrhage [7]. This proportion increases to 12% when a headache is referred to as "the worst headache" of their life. If patients additionally have a neurological deficit, up to 25% have SAH [8].

Initial subarachnoid hemorrhage may be fatal, may result in devastating neurologic sequela, or alternatively may produce minor symptoms. Accurate early diagnosis is critical, as early aneurysm repair reduces short-term complications, primarily recurrent bleeding and vasospasm, and improves outcomes. Despite the widespread availability of neuroimaging, misdiagnosis of subarachnoid hemorrhage is still common [9, 10] (Fig. 2.1), and it is an important cause of litigation related to emergency medicine.

The first imaging examination in the diagnostic workup of SAH should be a non-contrast head CT. Attention to CT technique and systematic interpretation algorithms increase the sensitivity for the diagnosis of SAH. It is well known that thin cuts (3 mm or smaller), especially at the skull base, increase conspicuity for identification using CT of small hemorrhagic collections. The use of different planes, in particular the coronal plane, is critical in order to identify or exclude SAH within the olfactory sulci. Adjustments in window width and window level increase soft-tissue contrast between adjacent
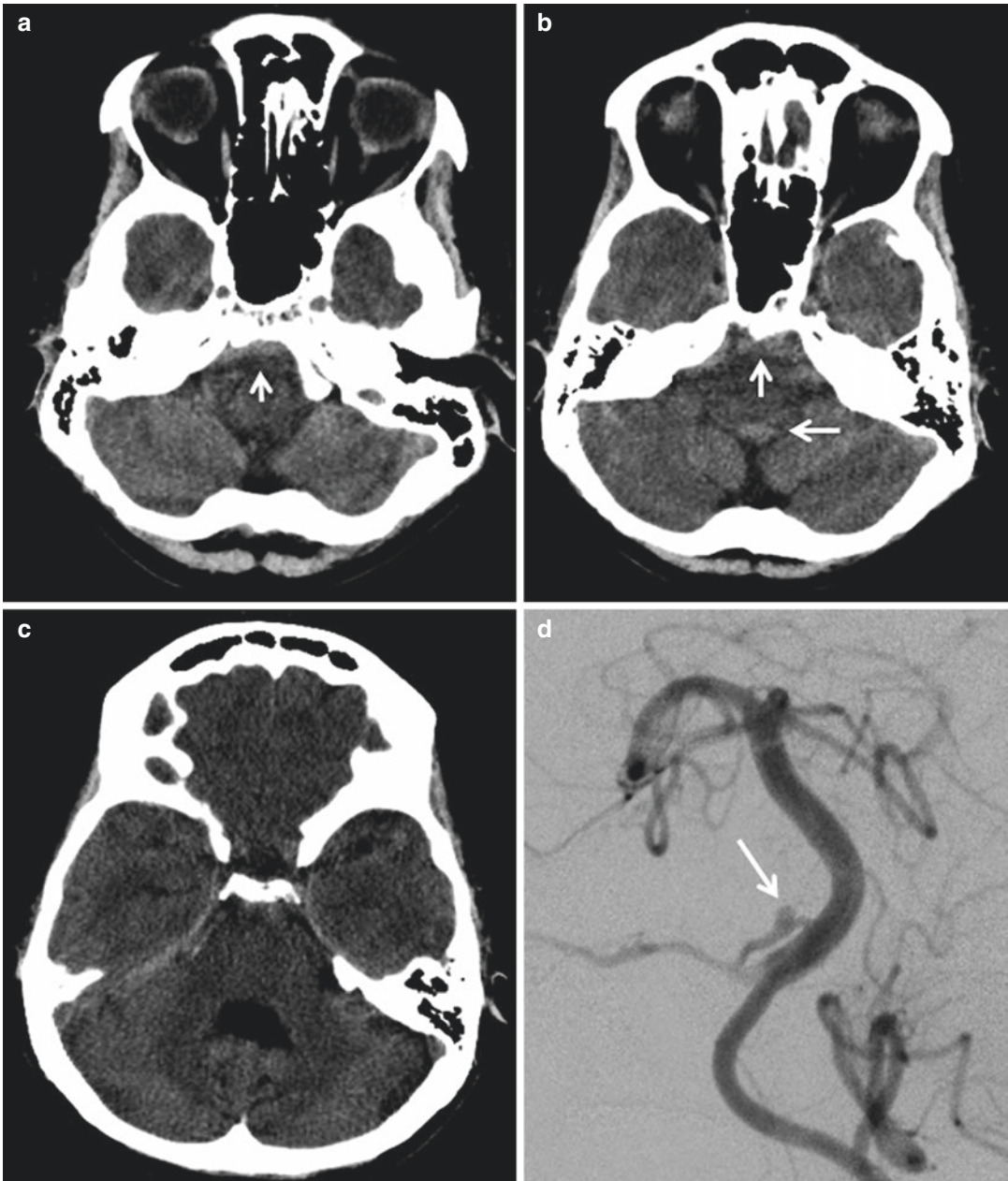
Fig. 2.1 Axial images of a non-contrast head CT (**a**, **b**) in a 40-year-old man with headache and nausea show hyperdensity in the prepontine and pre-medullary cisterns, as well as in the foramen of Magendie (arrows). Given the location, low in the posterior fossa, the findings were thought to be artifactual in nature. Of note, the supra- and infratentorial ventricular systems were prominent (**c**) for the patient's age, suggesting hydrocephalus. Given the persistence of symptoms, a CT angiogram was performed (not shown), which demonstrated an aneurysm at the origin of the right anterior inferior cerebellar artery (AICA), a finding which was then confirmed with a catheter angiogram (arrow **d**)

hyperattenuating structures, including bone and hemorrhagic collections, which is of paramount importance in preventing CT misdiagnosis/overlooking of isoattenuating extra-axial hemorrhagic collections (Fig. 2.2).

CT attenuation of blood is a direct function of hemoglobin concentration. Hemoglobin concentration lower than 10 mg/dL may be isoattenuating to brain parenchyma. Likewise, CT sensitivity for the detection of SAH decreases over time from the onset of symptoms, most notably on those CT scans performed 5–7 days after onset of symptoms/aneurysm rupture [11, 12] (Fig. 2.3). Sensitivities of 98% and 93% have been reported for the identification of SAH on CT scans obtained before 12 and 24 h from the beginning of symptoms, respectively. These percentages have been proven to decline to 76% and 58% when patients were imaged after 3 or 5 days from aneurysm rupture [13]. Therefore, patients with aneurysm-related subarachnoid hemorrhage presenting with milder headaches and absence of neurological deficits may seek medical evaluation later from initial aneurysm rupture/leak. These patients may have subarachnoid collections which are already isoattenuating to the brain parenchyma, or are closely attenuating to cerebrospinal fluid (CSF), making them very difficult to identify on CT [14] (Fig. 2.3).

Skills in accurately identifying intracranial hemorrhage on imaging vary widely among emergency physicians and other clinicians, neurologists, neurosurgeons, general radiologists, and neuroradiologists. More experienced subspecialized physicians are less likely to miss subtle imaging abnormalities.

Attention to detail in technical parameters is a must for an accurate high-resolution multi-detector CT (HR MDCT) evaluation of intracranial vascular abnormalities. CTA of the head is critical in the evaluation of intracranial vessel occlusion, aneurysms, and post-traumatic injuries. Potential technique-related sources of error include suboptimal contrast injections and inadequate bolus delay. After confirming intravascular catheter access, the intravenous injection of contrast should be done at a rate of at least 3.5 mL/s, to guarantee diagnostic-level contrast opacification of the vascular lumen. A proper bolus timing triggered for optimal and selective opacification of the arterial vessels is critical in the evaluation of saccular aneurysms in the setting of SAH, as well as in the evaluation of post-traumatic or spontaneous intracranial arterial wall dissections. Suboptimal prolonged contrast delay on a CTA of the head will render undesired contrast opacification of venous structures which are in the immediate vicinity of major artery bifurcations and may render the false-positive appearance of a saccular aneurysm. Likewise, on CT venography, a longer delay triggered to opacify the dural venous sinuses is needed for
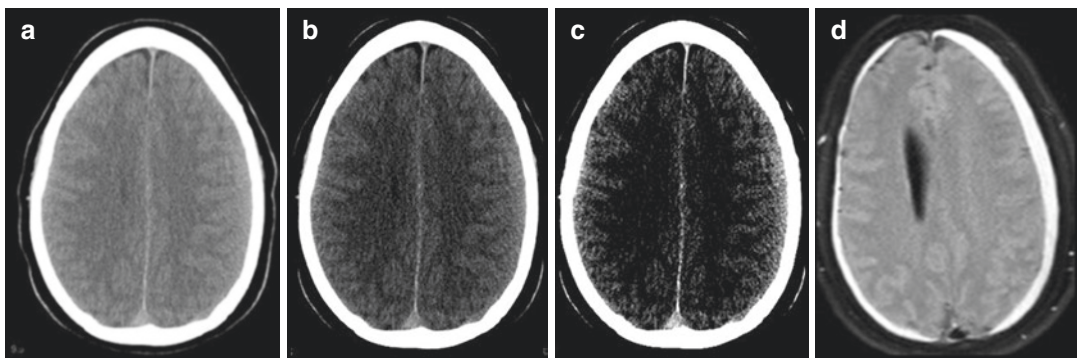
Fig. 2.2 Axial image of a non-contrast head CT (**a**) in a 39-year-old woman with worsening postural headache was considered normal; however, in retrospect, after adjusting the window width and window level (**b**, **c**), it becomes apparent that there is a left holohemispheric sub-dural hematoma, isodense to the cortex. Follow-up MRI with axial fluid-attenuated inversion recovery (FLAIR) sequence (**d**), obtained few days later, shows bilateral subdural hematomas in this patient with spontaneous intracranial hypotension (SIH)
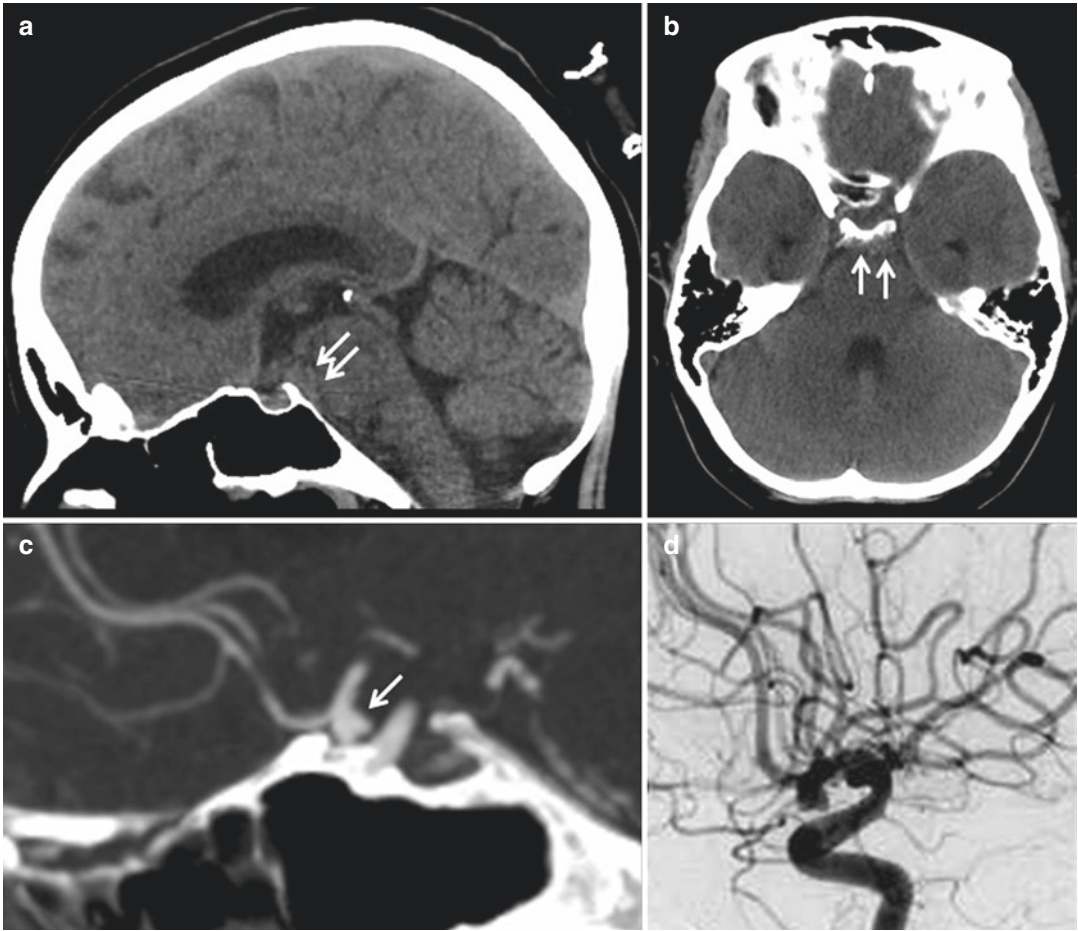
Fig. 2.3 Sagittal (**a**) and axial (**b**) images of a non-contrast head CT in a 45-year-old woman with abrupt "worst" headache of her life 5 days prior show subtle subarachnoid hemorrhage in the prepontine and suprasellar cisterns (arrows). Given the delay in presenting to the ED, the blood in the subarachnoid space is isodense to the brain parenchyma. Sagittal image of a subsequent CTA (**c**) shows a bilobed aneurysm in the region of the anterior communicating artery complex (arrow), a finding which was confirmed with a catheter angiogram (**d**), prior to endovascular treatment. The aneurysm was successfully coiled, and the patient did not have any neurological deficits

the identification of venous filling defects in the setting of venous sinus thrombosis [2].

Brain imaging should be performed promptly in comatose patients whose clinical assessment suggests a structural injury or those with head trauma. Imaging evaluation could be done with either CT or MRI, but CT is the preferred initial modality. While non-contrast CT reveals the shift of midline structures, hydrocephalus, intracranial hemorrhage, parenchymal herniation, thalamic abnormalities, and hyperdense arteries, it may not reveal treatable vascular causes of coma, including basilar artery occlusion, posterior reversible encephalopathy syndrome, reversible vasoconstriction syndrome, early thalamic and brainstem ischemic strokes, and cerebral venous sinus thrombosis [15]. If a non-contrast head CT does not reveal any abnormality, advanced and vascular imaging including diffusion-weighted MR imaging (DWI), MR angiography (MRA), or CTA should expeditiously be done [16]. Patients with posterior reversible encephalopathy syndrome (PRES) present with rapid-onset headache, visual deficits, and seizures before mental
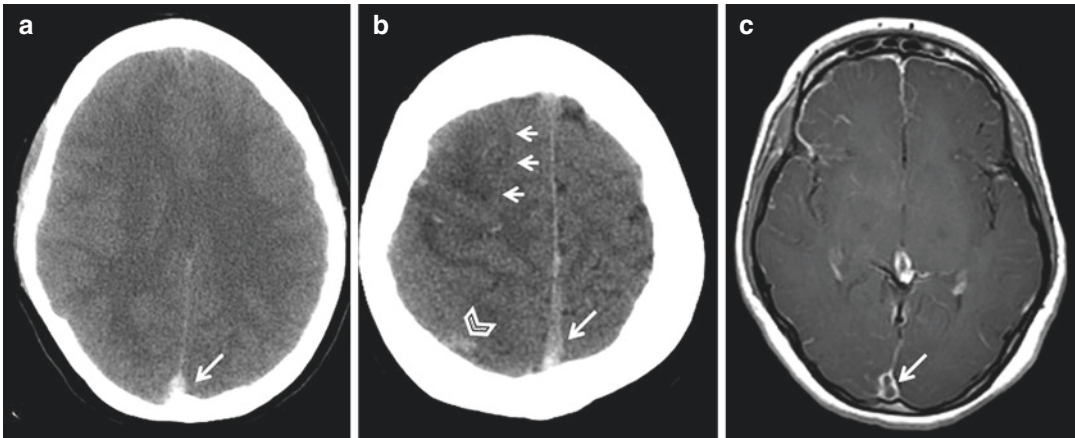
Fig. 2.4 20-year-old man with new seizures in the context of progressive headache without focal deficit. Axial non-contrast head CT images (**a**, **b**) show increased density along the posterior aspect of the superior sagittal sinus (arrows) suggestive of thrombus, loss of gray-white matter differentiation in the right frontal lobe (small arrows in **b**) consistent with acute infarction, and foci of subarachnoid hemorrhage (chevron in **b**). Axial T1-weighted image with IV contrast on follow-up MRI (**c**) shows the "empty delta" sign within the superior sagittal sinus (arrow), confirming the diagnosis of venous sinus thrombosis

status changes; MRI in these patients will likely demonstrate increased T2 signal in the posterior cerebral parenchyma. Patients with new seizures in the context of a progressive headache and focal deficits not localizing to a vascular territory need to be evaluated with a head CT, including CT venography, or with MRI, including MR venography, to exclude venous thrombosis [17] (Fig. 2.4).

2.2 Cognitive Errors Secondary to Framing Bias

Framing bias is a cause of cognitive error in which the radiologist is influenced in his or her interpretation by the wording of the clinical question [18]. A retropharyngeal non-enhancing fluid collection on a CT scan of the neck of a patient presenting to the ED with odynophagia and mild fever, for example, with a request to evaluate for retropharyngeal abscess, was inadequately diagnosed as a retropharyngeal abscess requiring surgical drainage. The effect of the framing bias here is clear, since the fluid collection is non-enhancing, and is associated with a focal calcification along the longus colli at the level of C1–C2 (Fig. 2.5), representing

acute longus colli calcific tendinitis, a known self-limited inflammatory reaction to calcium hydroxyapatite deposition in the longus colli tendons [19, 20]. This example can also be attributed to satisfaction of search error, where the second abnormality (the calcification) was missed due to failure to continue the search for other abnormalities after an obvious finding (fluid collection) was identified [21].

Another example of framing bias is the interpretation of a focal temporal lobe parenchymal hyperdensity in a patient with history of head injury, as a post-traumatic hemorrhagic contusion (Fig. 2.6a–c), which is known to occur more commonly in the temporal and frontal lobes [22]. However, if the clinical indication had also included the history of seizures as a cause of head injury, other possibilities might have been considered, including hemorrhagic and hypercellular neoplasms, i.e., glioblastoma and lymphoma (Fig. 2.6d–f).

There are different approaches to avoid this type of bias. One approach is to assess the images, blinded to the clinical information, to reduce its initial influence on the interpretation. The second approach is to seek more clinical information, to ensure the interpretation appropriately explains the abnormality [23].
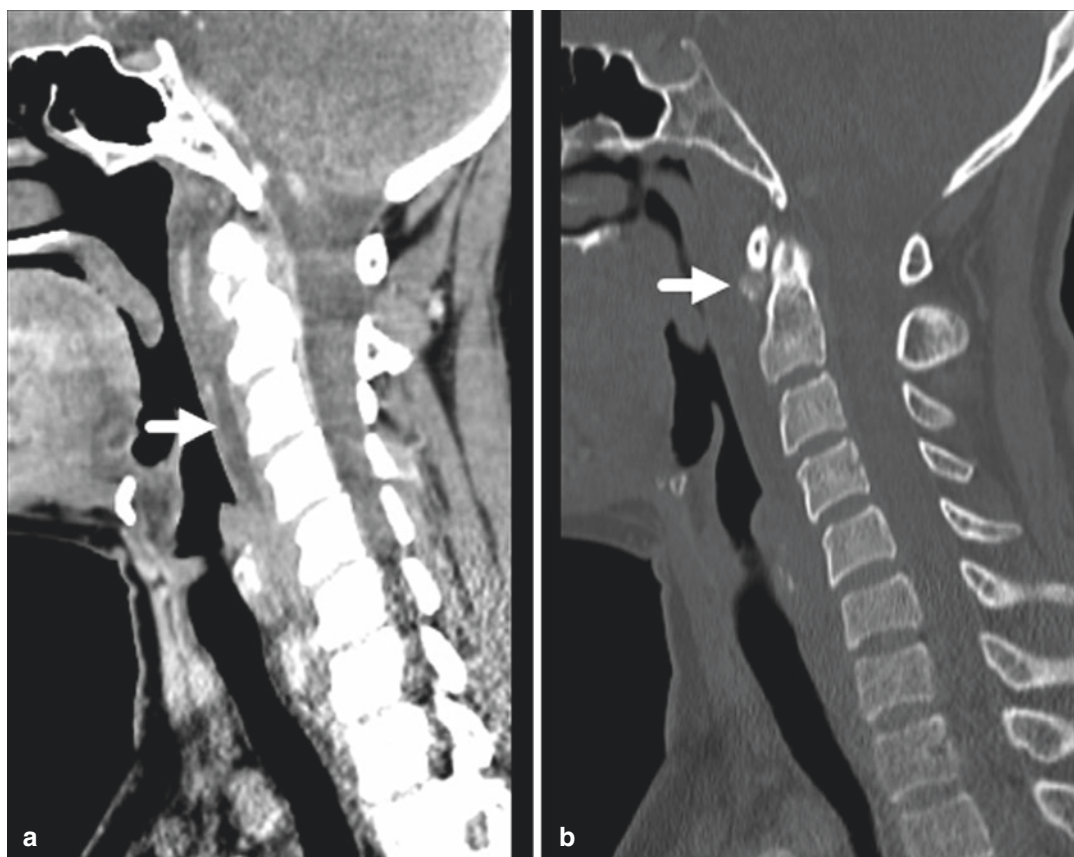
Fig. 2.5 Acute longus colli calcific tendinitis in a patient presenting with odynophagia and mild fever. Sagittal IV contrast-enhanced CT images of the neck with soft-tissue and bone algorithms show a retropharyngeal non-enhancing fluid collection (arrow in **a**), and an associated focal calcification along the tendon of the longus colli muscles at C1–C2 (arrow in **b**)

2.3   Cognitive Errors Secondary to Anchoring Bias

Anchoring bias reflects the influence of the radiologist's first impression. In this type of error, the radiologist fails to change her or his initial impression in light of new or conflicting information [18, 24]. For example, an isodense biconcave extra-axial process in an elderly patient presenting to the ED with confusion was interpreted as a subacute subdural hematoma despite the additional clinical information provided of known prostate cancer metastatic to the bones. Careful assessment would also have revealed adjacent sclerotic bony metastatic disease pointing toward dural-based metastases, which would easily be confirmed with an IV contrast-enhanced MRI (Fig. 2.7). This is a well-known form of metastatic disease, especially in the context of breast, lung, and prostate cancer [25]. To avoid this error, one should carefully and objectively consider alternate differential diagnoses, even when confident of the initial diagnostic impression [18].

2.4   Cognitive Errors Secondary to Alliterative Bias

Alliterative bias is another source of cognitive error, which reflects the influence of one radiologist's interpretation on the judgment of another radiologist [18]. For example, a patient
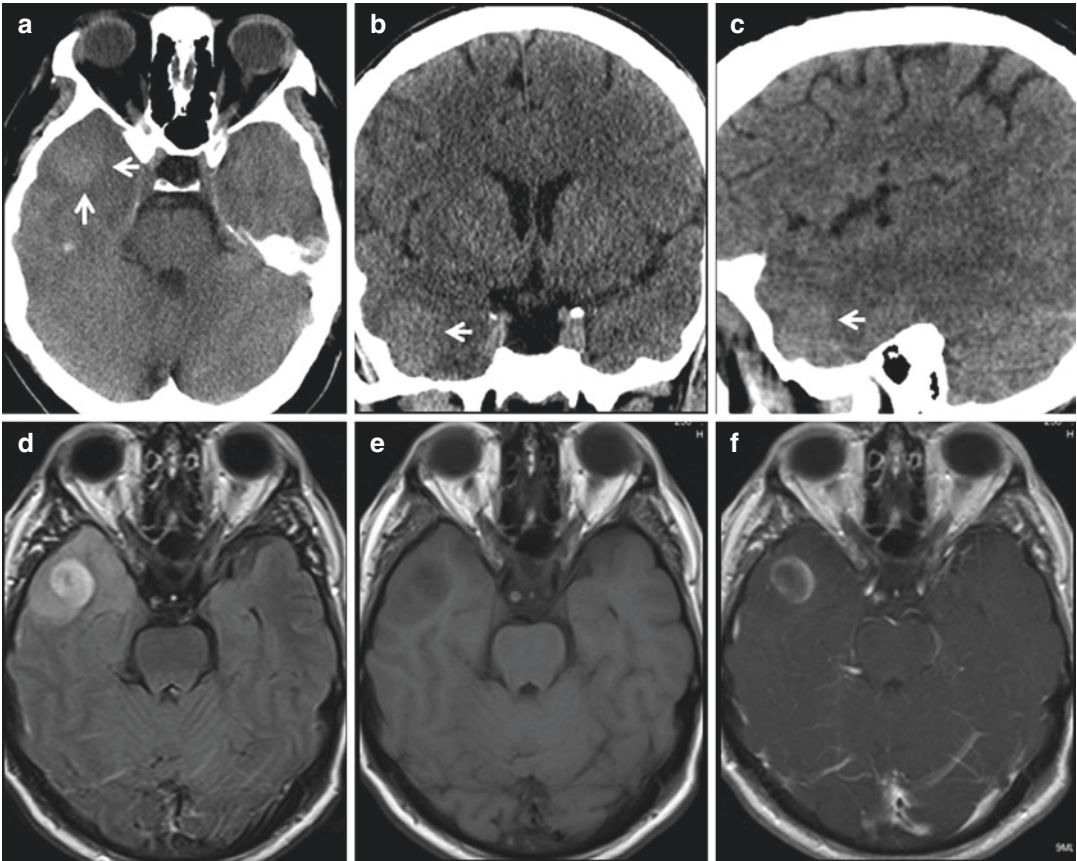
Fig. 2.6 Right temporal lobe glioblastoma in a patient with head trauma. Axial, coronal, and sagittal images of a non-contrast head CT (**a**–**c**) show a focal right temporal lobe parenchymal hyperdensity (arrows), interpreted as a hemorrhagic parenchymal contusion, given the history of head trauma from a motor vehicle collision (MVC). Axial FLAIR, T1-weighted pre- and T1-weighted post-contrast MR images (**d**–**f**) obtained the next day, after additional history of seizures was provided, show an intra-axial enhancing mass in the right temporal lobe, pathologically proven to represent a glioblastoma (GBM)
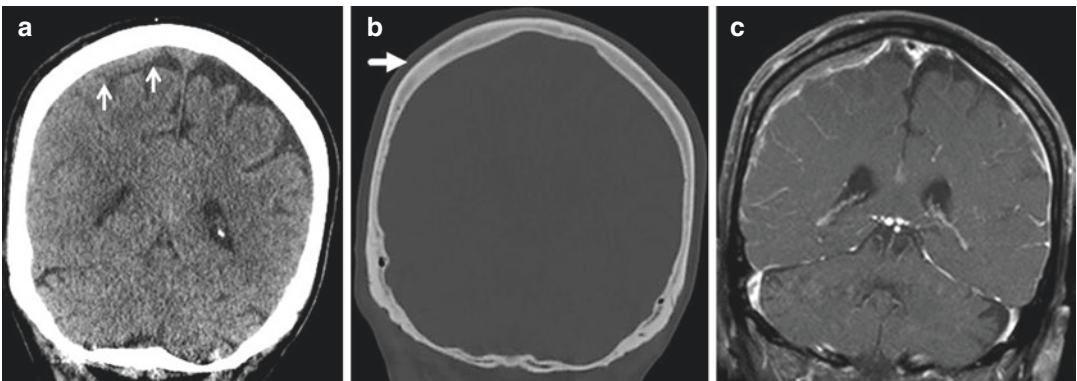
Fig. 2.7 Dural-based metastatic disease in a patient with prostate cancer. Coronal non-contrast head CT (**a**) shows an isodense extra-axial abnormality interpreted prospectively shows a subtle subacute subdural hematoma. Coronal image in bone window (**b**) shows a subtle adja- cent sclerotic bony metastatic deposit (arrow). Coronal T1-weighted MR image with IV contrast (**c**) performed the same week shows enhancement of the dural-based abnormality representing metastatic disease

transferred from another hospital arrives with a non-contrast head CT showing a parenchymal hyperdensity involving the right caudate nucleus and putamen interpreted as an intra-axial hematoma, a diagnosis which was then confirmed by a second radiologist. However, the involvement of the caudate nucleus and putamen without vasogenic edema or mass effect, as well as the additional clinical information of abnormal movements affecting one side of the body and associated hyperglycemia, points toward the correct diagnosis of nonketotic hyperglycemia hemichorea-hemiballismus [26, 27] (Fig. 2.8). Reviewing the imaging findings and formulating one's own interpretation before reviewing the prior reports can help avoid this type of bias [18].

However, the cognitive error in this patient illustrates another type of bias: "zebra retreat bias," where the radiologist avoids a correct but rare diagnosis "zebra," despite supporting findings, in favor of a more common alternate diagnosis [21]. In this patient, the parenchymal hyperdensity was interpreted as the more common intraparenchymal hematoma, rather than the correct but unusual diagnosis of nonketotic hyperglycemia [26, 27].

2.5   Cognitive Errors Secondary to Satisfaction of Search

Satisfaction of search is one of the most common types of error, where the radiologist is cognitively satisfied after identifying an abnormality, and fails to complete her or his search pattern, making additional important findings more likely to be missed [18, 21, 28]. This becomes of even greater impact in complicated clinical scenarios, e.g., trauma and ICU patients. A CT of the head and facial bones for a polytrauma patient, for example, showed multiple calvarial, skull base, and facial fractures, which were predominantly left-sided, but the radiologist did not prospectively identify a contrecoup right cerebellar non-hemorrhagic contusion (Fig. 2.9).

Another common example of satisfaction of search is a missed non-displaced calvarial fracture associated with a correctly identified adjacent hemorrhagic contusion and extra-axial hemorrhage. The fracture could be visualized on the scout view in this patient, and on the reformatted coronal and sagittal images, after window setting adjustment for bone evaluation (Fig. 2.10). This patient also illustrates another
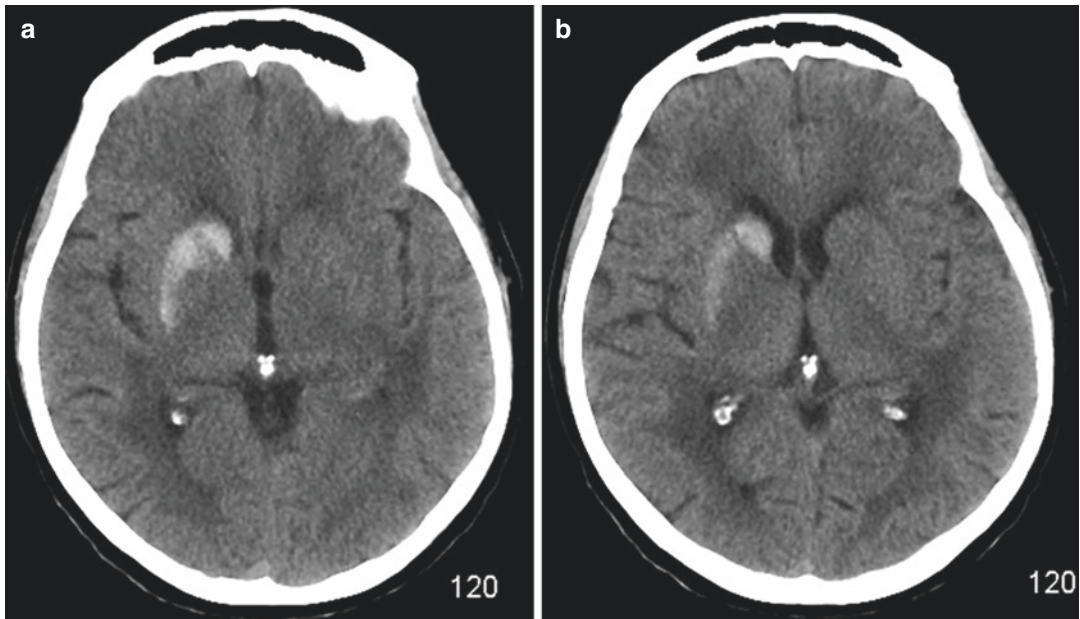

Fig. 2.8 Nonketotic hyperglycemia hemichorea-hemiballismus. Axial non-contrast head CT (**a**, **b**) shows parenchymal hyperdensity involving the head of the right caudate nucleus and the putamen, without vasogenic edema or mass effect, in a patient with hyperglycemia and abnormal movements
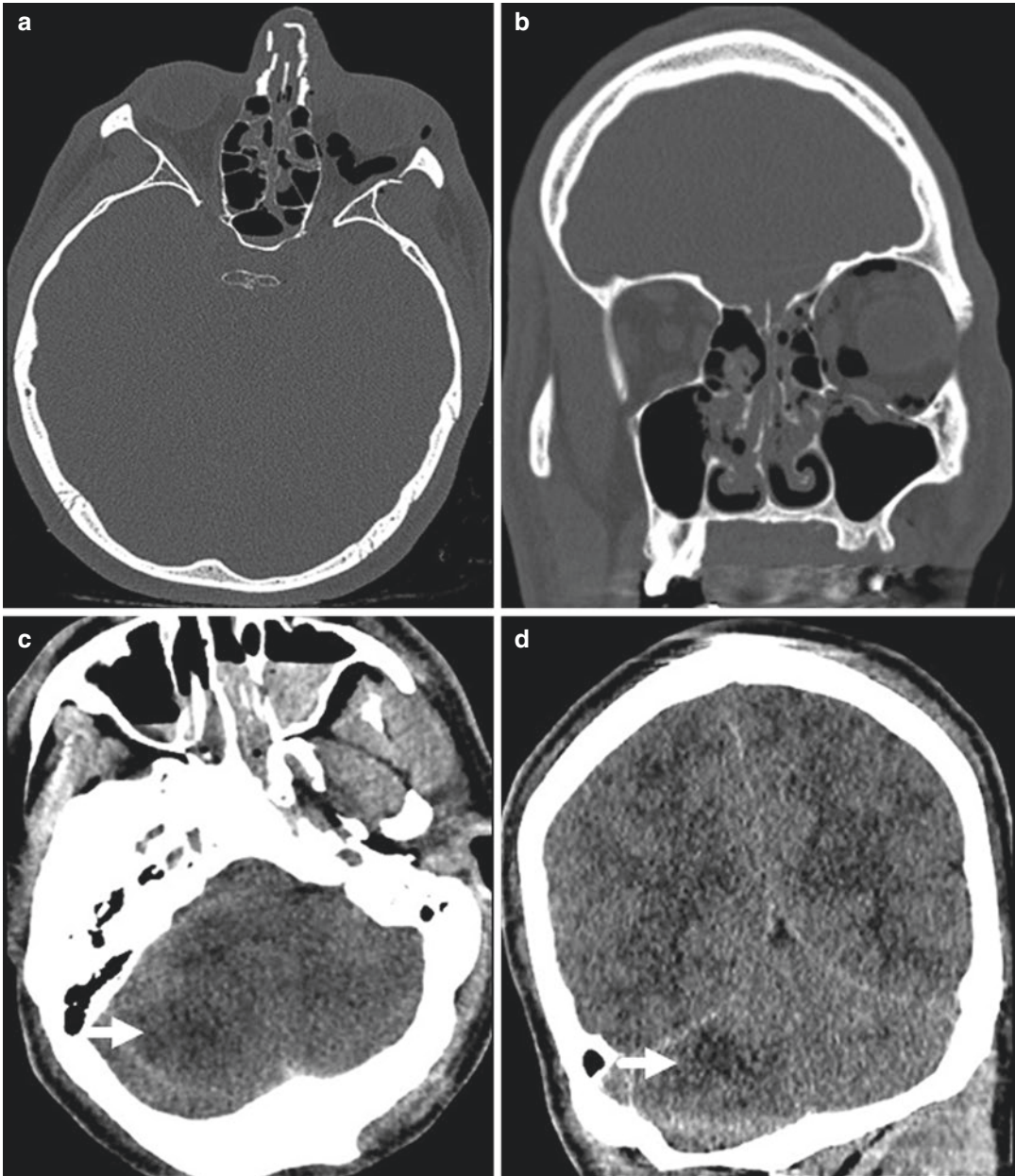
Fig. 2.9 Right cerebellar non-hemorrhagic contusion and facial fractures in a patient with head trauma. Axial and coronal images of a CT of the facial bones (**a**, **b**) demonstrate multiple nasal and left orbital fractures with orbital emphysema. Axial and coronal non-contrast head CT in the same patient (**c**, **d**) show a contrecoup parenchymal hypodensity (arrows) in the right cerebellar hemisphere, representing a nonhemorrhagic contusion, which was missed at the time of interpretation

type of bias, which is called "scout neglect bias," [18] where an abnormality can be seen on the initial scout images but is not diagnosed if the radiologist reporting the CT does not examine the scout images. As in this patient, the fracture line can be better appreciated on the scout view compared to the axial CT images, where it was not well visualized because it was in the same plane as the images. In other patients, an abnormality clearly seen on the large field-of-view of the
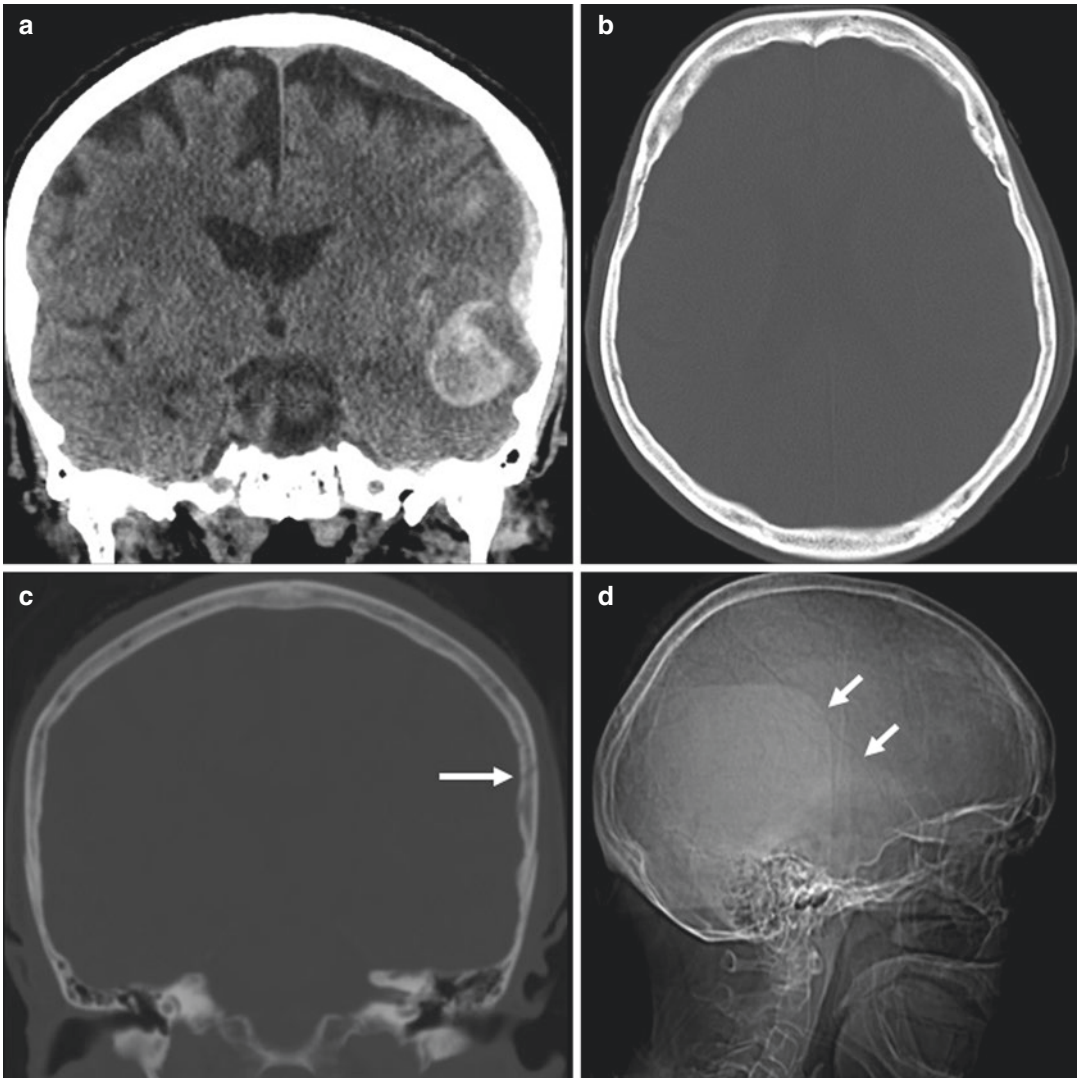
Fig. 2.10 Linear fracture of the squamous portion of the left temporal bone with adjacent post-traumatic intracranial hemorrhage. Coronal CT of the head (**a**) shows a left temporal hemorrhagic contusion, an acute subdural hematoma, and a small amount of acute subarachnoid hemorrhage. No convincing fracture was seen on the axial CT image with bone algorithm (**b**). Coronal CT image after window settings adjustment for bone evaluation (**c**), however, shows a non-displaced fracture of the left temporal bone (arrow). Scout view (**d**) shows a lucent fracture line in the temporal region (arrows)

scout images may not be included on the smaller field-of-view cross-sectional images. A similar error occurs when the reformatted additional planes are not evaluated, or when the window settings are not adjusted for proper evaluation of the bone and different soft-tissue structures.

Promoting awareness of these errors; using reporting templates; identifying injury patterns, e.g., coup and contrecoup patterns of head injury;

and reviewing all available images on a provided examination, can help reduce these errors [18].

2.6   Undercalling

In undercalling, an abnormality is detected but is not interpreted as an abnormal finding, as the radiologist dismisses the finding either as a nor-

mal structure or an artifact. This type of error can be due to lack of knowledge, but can also be made by experienced radiologists who are accustomed to seeing many artifacts [29]. For example, a small venous epidural hematoma adjacent to the transverse venous sinus in a patient with head injury was dismissed as part of the transverse sinus. Identification of the non-displaced adjacent occipital fracture which would have supported the true nature of the abnormality, rather than a normal structure—i.e., a venous sinus—was not prospectively identified (Fig. 2.11).
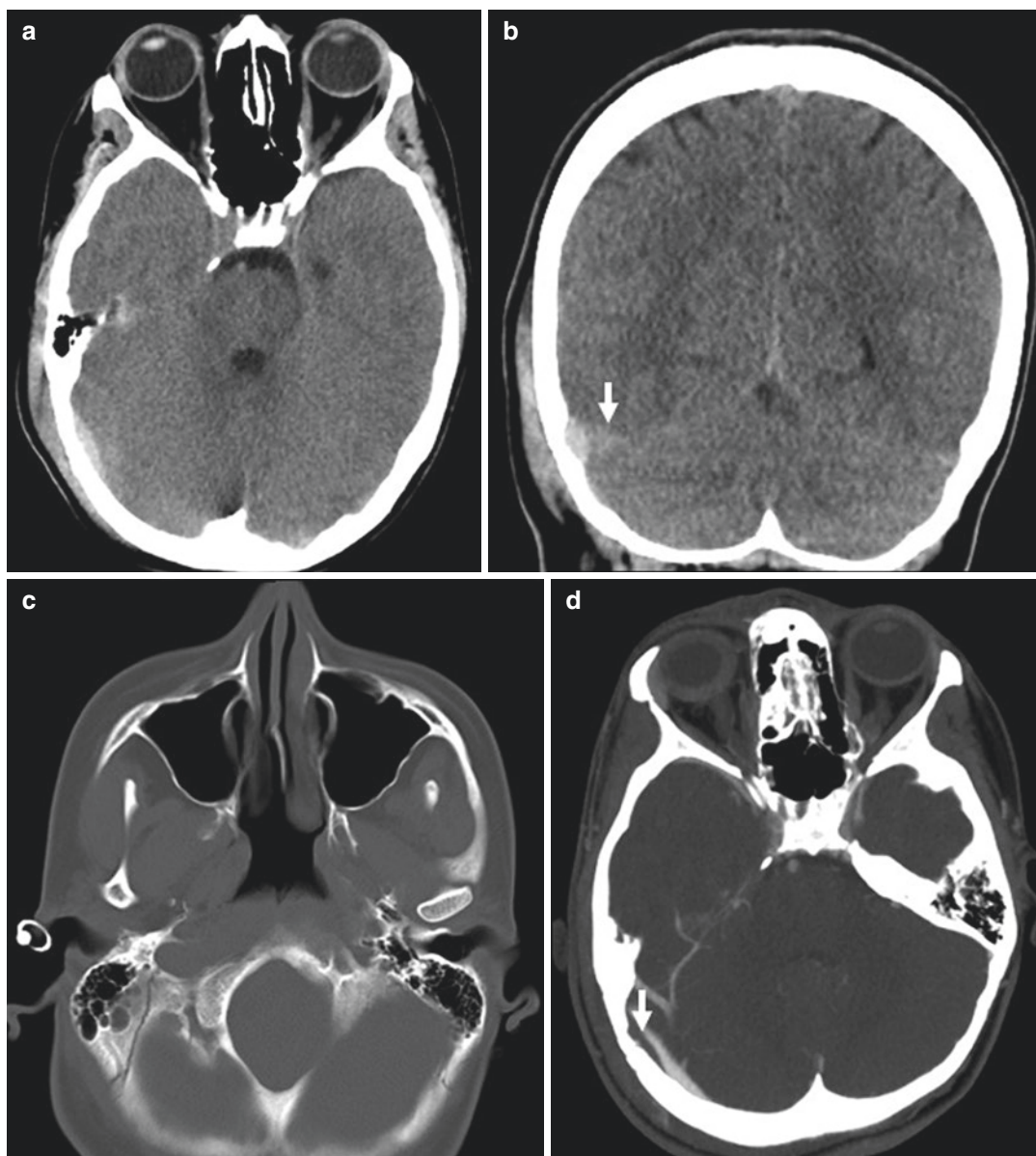
Fig. 2.11 Small right venous epidural hematoma in a patient with head injury. Axial image of a non-contrast head CT (**a**) shows a small acute right temporo-occipital epidural hematoma. Coronal image of the same examination (**b**) shows the hematoma with different density, in comparison to the adjacent right transverse venous sinus, which is displaced medially (arrow). Axial CT image with bone algorithm (**c**) demonstrates a right occipital fracture/diastasis. Axial CT venogram image (**d**) confirms the displacement and mild compression of the right transverse venous sinus by the small adjacent epidural hematoma (arrow)

2.7   Cognitive Errors Secondary to Availability Bias

Availability bias causing cognitive errors occurs when certain patients are easily recalled given their association with an unusual diagnosis or personal error or when a similar patient has been recently interpreted or presented in a conference. Unfortunately, such patients may exert unduly influence on near future prospective imaging diagnosis [18]. To illustrate such a bias, we present a patient seen in the ED with left hemiparesis who had a head CT (Fig. 2.12a–c) which was interpreted as having a large acute/early subacute infarct in the right middle cerebral artery territory. That diagnosis was offered without any differential diagnosis, given a very similar patient had been presented earlier the same day during multi-disciplinary rounds. The follow-up MRI obtained to further assess the findings showed an extra-axial enhancing mass consistent with a meningioma in the right middle cranial fossa, with associated mass effect and extensive surrounding vasogenic edema (Fig. 2.12d–f). In order to avoid this type of bias, radiologists should seek second opinions from colleagues or refer to sources of information beyond the radiologist's own personal experience [18, 23, 30, 31].
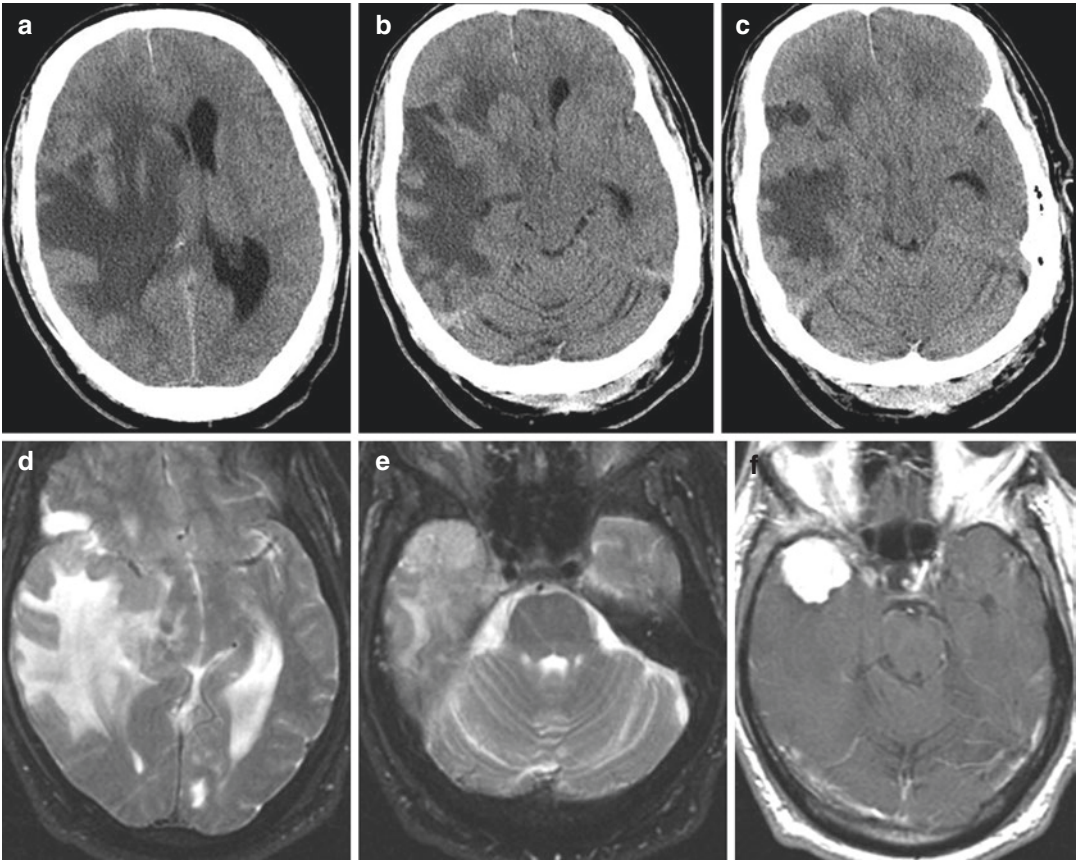

Fig. 2.12 Non-contrast head CT (**a**–**c**) of a patient seen in the ED with left hemiparesis shows substantial hypodensity of the white matter in the right frontal and temporal lobes, with focal cortical hypodensity and mass effect interpreted as a large acute/early subacute infarct in the right middle cerebral artery territory. Axial T2-weighted MR images (**d**, **e**) and axial T1-weighted image with IV contrast (**f**) on a short-term follow-up MRI demonstrate an extra-axial enhancing mass along the right sphenoid wings, representing a meningioma. There is associated mass effect and surrounding vasogenic edema
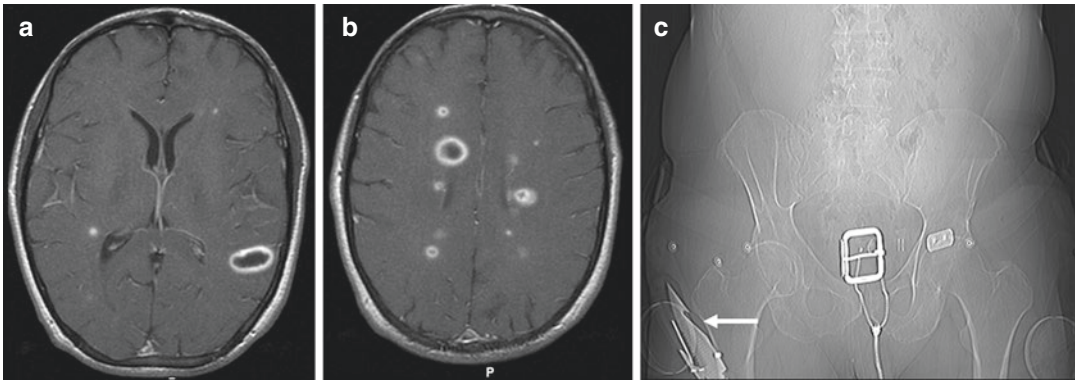
Fig. 2.13 Axial T1-weighted MR images with IV contrast (**a**, **b**) from an MRI of the brain from the ED show multiple ring-enhancing nodules. A knife is seen in the patient's pocket (arrow), on the scout view of a CT scan of the abdomen and pelvis (**c**) performed earlier the same day. The ring-enhancing nodules were interpreted as abscesses, probably related to intravenous drug abuse, given the finding on the scout view

2.8 Cognitive Errors Secondary to Attribution Bias

Attribution bias causing cognitive errors occurs when a specific characteristic is attributed to a person or a thing only because it belongs to a certain class [18, 32]. For instance, an MRI of the brain from the ED shows multiple ring-enhancing nodules (Fig. 2.13). While reviewing the prior imaging examinations, a knife was seen in the patient's pocket, on the scout view of a CT of the abdomen and pelvis performed earlier the same day (Fig. 2.13c). The ring-enhancing nodules were then interpreted as abscesses, and the report stated that they were probably related to intravenous drug abuse. Although the diagnosis of cerebral abscesses was ultimately correct, stating that the patient is a drug abuser because there is a knife in his or her pocket is a clear bias. Structured reporting using report templates and/ or interpreting the imaging examinations without initially reviewing the clinical history may help avoid this bias [18].

2.9 Perceptual Errors

Perceptual errors occur in the initial detection phase of image interpretation [21], when an abnormality which is present on imaging is not prospectively identified by the interpreting radi-

ologist. They account for approximately 60–80% of radiologist's errors, and represent a significant cause of radiology-related litigation [21, 33–35]. This type of error is deemed to have occurred when, in retrospect, the abnormality was not only present but was sufficiently discrete in order to be detectable by the interpreting radiologist or by a consensus of peers. A classic example of this type of error can be seen in the context of head injury and acute post-traumatic subarachnoid or subdural hemorrhage. A small acute post-traumatic subdural hematoma (SDH) in the right temporal region was not identified on an initial head CT (e.g., Fig. 2.14a). The patient was discharged and returned to the emergency department with increased headache and signs of increased intracranial pressure. The follow-up CT demonstrated substantial interval increase in size of the subdural hematoma, with extension to the tentorium and associated mass effect on the underlying temporal lobe (Fig. 2.14b). In another patient with head trauma involved in a motor vehicle collision, the initial head CT was reported as normal; however, several subtle but important findings were missed by the radiologist, including a linear fracture of the lesser wing of the left sphenoid bone, a fracture of the lateral wall of the left sphenoid sinus, a small SDH in the anterior aspect of the left middle cranial fossa, minimal pneumocephalus within the left sylvian fissure, and an air-fluid level within the sphenoid sinus (hemo-sinus), overall
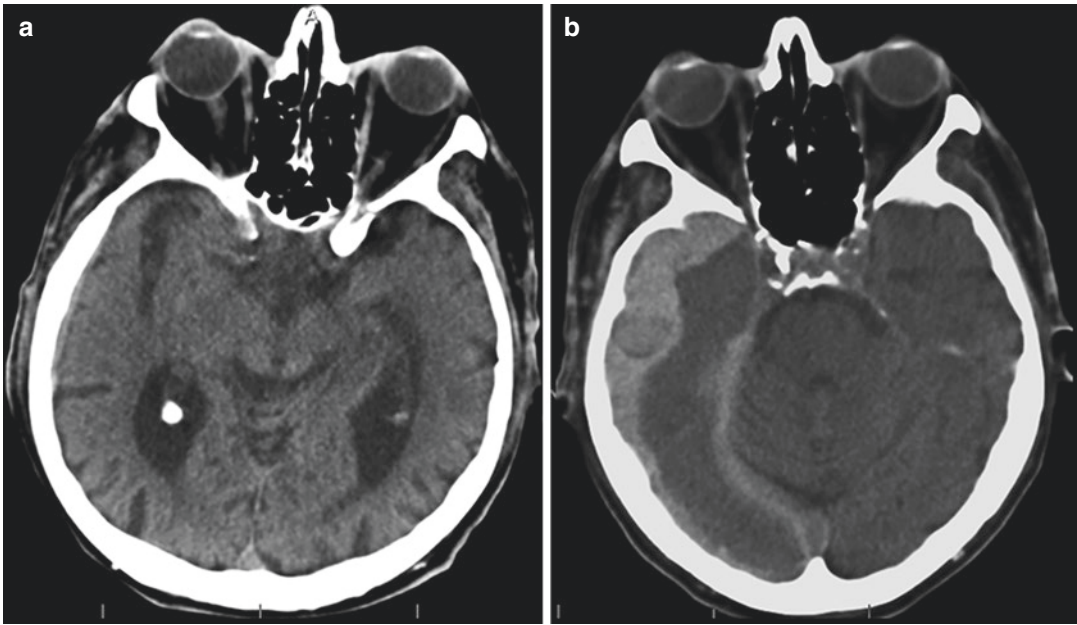
Fig. 2.14 A small acute subdural hematoma in the right temporal region was not identified on the initial head CT (**a**) of a 75-year-old man with head trauma. The patient was discharged and returned to the emergency department with increased headache and signs of increased intracra-nial pressure. The follow-up CT (**b**) demonstrates sub-stantial interval increase in size of the subdural hematoma, with extension to the tentorium, and associated mass effect on the underlying temporal lobe

findings representing a substantial blow to the head (Fig. 2.15a–c). Given that the head CT was reported as normal, the patient was discharged home but returned to the hospital 2 weeks later with intractable headache, fever, and neck rigid-ity, symptoms highly suggestive of meningitis. A follow-up head CT performed at this time showed marked communicating hydrocephalus second-ary to meningitis in the context of a missed skull base fracture communicating the sphenoid sinus, a known source of infection, with the left middle cranial fossa. In addition, there was an infectious basilar artery pseudoaneurysm, a complication of the meningitis (Fig. 2.15d–f).

One of the most challenging and often missed diagnoses is the subacute subdural hematoma as it blends with the adjacent cortex, given the similar density on non-contrast CT (Fig. 2.16). Particular attention to asymmetric cerebral sulci may prove helpful in order to recognize the presence of this entity. In addition and, in the appropriate clinical context (e.g. fall, anticoagu-lation, etc.), the CT images should be reviewed

using norrow windows in order to avoid missing this diagnosis. Loss of gray-white matter differ-entiation can be another difficult scenario where the radiologist fails to see the abnormality on CT, given the symmetry of the findings (Fig. 2.17).

The cause for this type of error is poorly under-stood to our knowledge. Factors which have been associated with perceptual errors include rapid pace of interpretation, mental fatigue, and poor conspi-cuity, as well as numerous and various distractions including interruptions by phone calls, pagers, and emails. Satisfaction of search bias has also been linked to perceptual error, when there is a second or more abnormalities on a given imaging exami-nation, which then tend to be overlooked [21].

2.10   Summary

Diagnostic errors in radiology often arise from faulty mental shortcuts, cognitive biases, and perceptual errors. Being aware of the spectrum of cognitive bias may help create a comprehen-
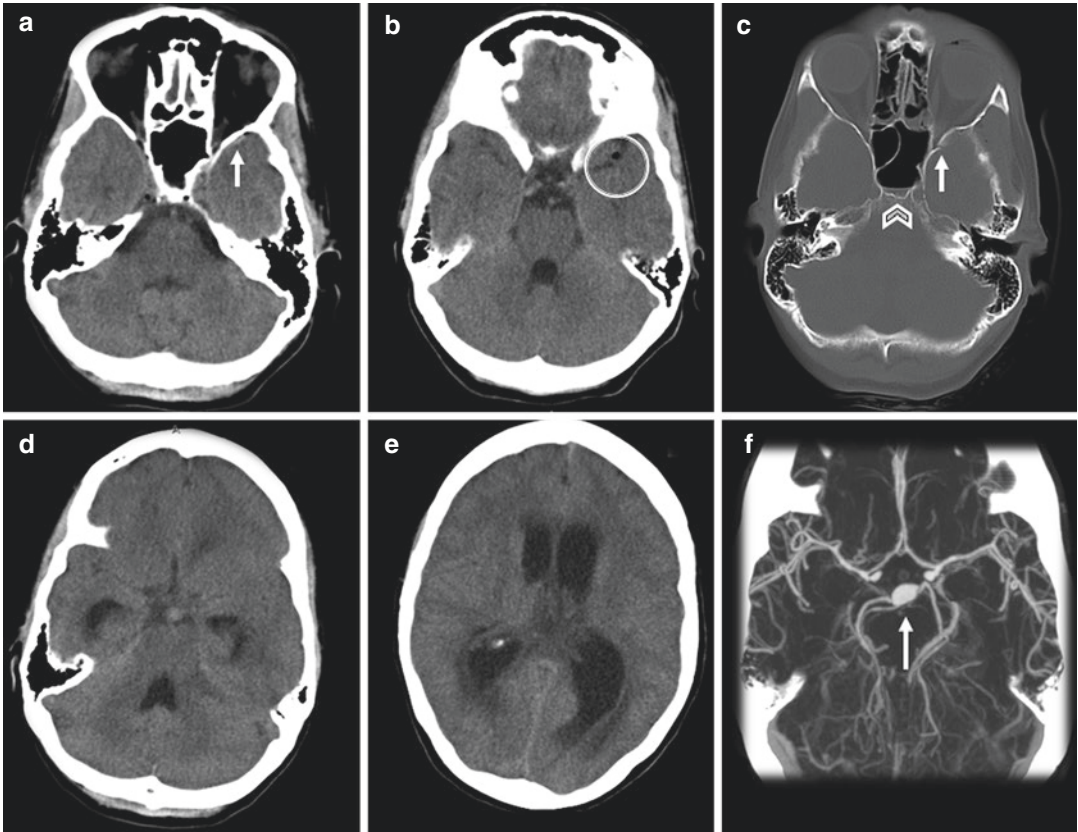
Fig. 2.15 Patient with head trauma, involved in a motor vehicle collision. Initial head CT was reported as normal; however, several subtle but important findings including a small subdural hematoma (SDH) in the anterior aspect of the left middle cranial fossa (arrow in **a**), minimal pneumocephalus within the left sylvian fissure (circle in **b**), a linear fracture of the lesser wing of the left sphenoid bone (arrow in **c**), and an air-fluid level within the sphenoid sinus (chev-ron in **c**) were all initially missed prospectively. The patient returned to the hospital 2 weeks later with intractable headache, fever, and neck rigidity, suggestive of meningitis. The head CT at that point showed marked communicating hydrocephalus secondary to meningitis (**d**, **e**) in the context of a missed skull base fracture. Additionally, there was an infectious basilar artery pseudoaneurysm (arrow in **f**), as seen on the axial CT angiogram image of the head (**f**)
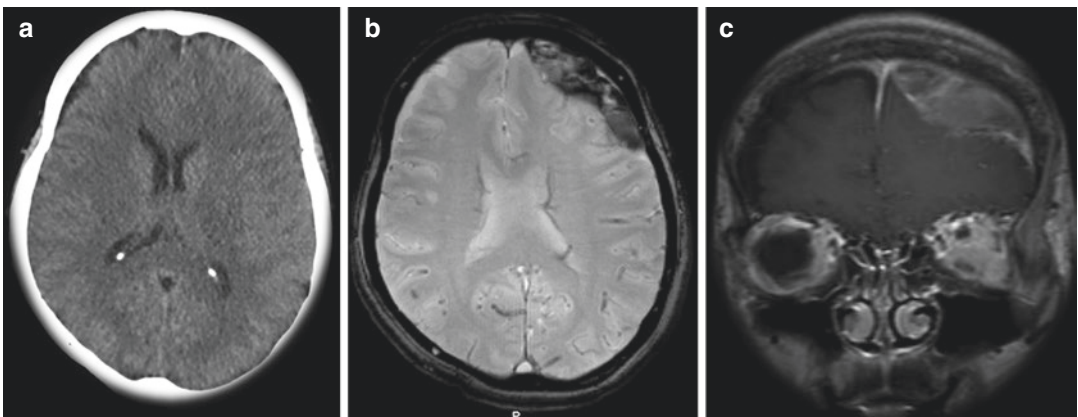

Fig. 2.16 Representative axial head CT image without contrast (**a**), of a 50 year-old patient who presented with persistent headache 2 weeks after a head trauma. The scan was reported as normal. Axial GRE (**b**) and coronal T1-weighted MR images with IV contrast (**c**) performed the following day show a large subdural hematoma in the left frontal region, which in retrospect could be seen but is more subtle on the head CT
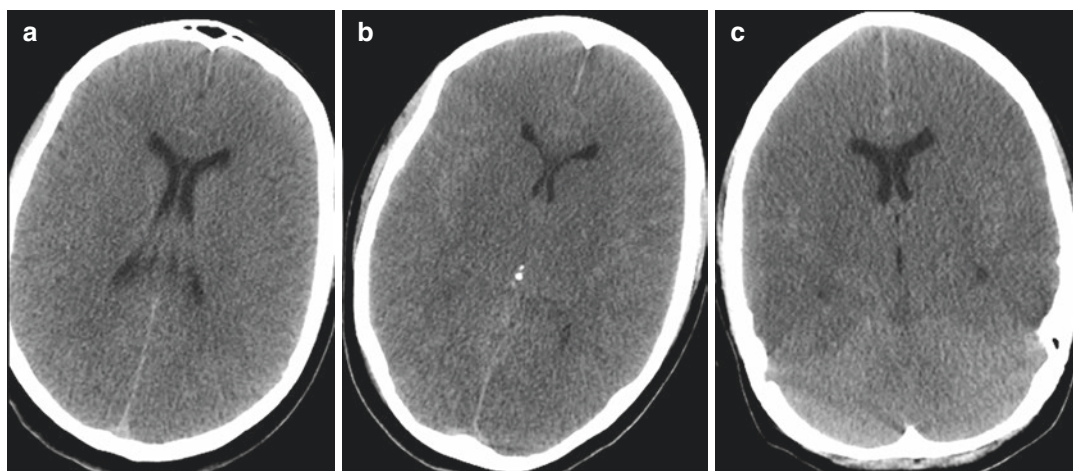
Fig. 2.17 Axial non-contrast head CT (**a**) of a 22-year-old woman who presented with cardiac arrest was initially reported as normal; however, there is loss of gray-white matter differentiation and there is poor visualization of the cerebral sulci. Follow-up head CT obtained 24 h later (**b**) now shows hypodensity of the basal ganglia and thalami, representing diffuse anoxic brain injury. The head CT performed 72 h later (**c**) shows diffuse hypodensity of the brain parenchyma, with total loss of gray-white matter differentiation, confirming the diagnosis. Note the "white cerebellum" sign in (**c**), which has been described in diffuse anoxic brain injury

sive strategy to learn from diagnostic errors and hence to help prevent them [18]. Some solutions may include structured reporting, peer review, continuing medical education, decreased interruptions, and improved communication with emergency physicians and other clinicians. Quality improvement strategies and solutions based on information technology may also prove beneficial [21].

References

1. Pope JV, Edlow JA. Avoiding misdiagnosis in patients with neurological emergencies. Emerg Med Internat. 2012;2012:1–10.
2. Pinto A, Reginelli A, Pinto F, et al. Errors in imaging patients in the emergency setting. Br J Radiol. 2016;89:20150914.
3. Caranci F, Tedeschi E, Leone G, et al. Errors in neuroradiology. Radiol Med. 2015;120(9):795–801.
4. Goldstein JN, Camargo CA Jr, Pelletier AJ, et al. Headache in United States emergency departments: demographics, work-up and frequency of pathological diagnoses. Cephalalgia. 2006;26(6):684–90.
5. Edlow JA, Panagos PD, Godwin SA, et al. Clinical policy: critical issues in the evaluation and management of adult patients presenting to the emergency department with acute headache. Ann Emerg Med. 2008;52(4):407–36.
6. Edlow JA, Caplan LR. Avoiding pitfalls in the diagnosis of subarachnoid hemorrhage. N Engl J Med. 2000;342(1):29–36.
7. Ramirez-Lassepas M, Espinosa CE, Cicero JJ, et al. Predictors of intracranial pathologic findings in patients who seek emergency care because of headache. Arch Neurol. 1997;54:1506–9.
8. Linn FH, Wijdicks EF, van der Graff Y, et al. Prospective study of sentinel headache in aneurysmal subarachnoid haemorrhage. Lancet. 1994;344:590–3.
9. Neil-Dwyer G, Lang D. Brain attack' — aneurysmal subarachnoid haemorrhage: death due to delayed diagnosis. J R Coll Physicians. 1997;31:49–52.
10. Mayer PL, Awad IA, Todor R, et al. Misdiagnosis of symptomatic cerebral aneurysm: prevalence and correlation with outcome at four institutions. Stroke. 1996;27:1558–63.
11. Kassell NF, Torner JC, Haley EC Jr, et al. The international cooperative study on the timing of aneurysm surgery. 1. Overall management results. J Neurosurg. 1990;73:18–36.
12. van Gijn J, van Dongen KJ. The time course of aneurysmal haemorrhage on computed tomograms. Neuroradiology. 1982;23:153–6.
13. Morgenstern LB, Luna-Gonzales H, Huber JC Jr, et al. Worst headache and subarachnoid hemorrhage: prospective, modern computed tomography and spinal fluid analysis. Ann Emerg Med. 1998;32:297–304.
14. Van der Wee N, Rinkel GJ, Hasan D, et al. Detection of subarachnoid haemorrhage on early CT: is lumbar puncture still needed after a negative scan? J Neurol Neurosurg Psychiatry. 1995;58:357–9.

15. Edlow JA, Rabinstein A, Traub SJ, et al. Diagnosis of reversible causes of coma. Lancet. 2014;384:2064–76.
16. Liman TG, Bohner G, Heuschmann PU, et al. The clinical and radiological spectrum of posterior reversible encephalopathy syndrome: the retrospective Berlin PRES study. J Neurol. 2012;259:155–64.
17. Roth C, Ferbert A. The posterior reversible encephalopathy syndrome: what's certain, what's new? Pract Neurol. 2011;11:136–44.
18. Itri JN, Patel SH. Heuristics and cognitive error in medical imaging. Am J Roentgenol. 2018;210(5):1097–105.
19. Alamoudi U, Al-Sayed AA, AlSallumi Y, et al. Acute calcific tendinitis of the longus colli muscle masquerading as a retropharyngeal abscess: a case report and review of the literature. Int J Surg Case Rep. 2017;41:343–6.
20. Zibis AH, Giannis D, Malizos KN, et al. Acute calcific tendinitis of the longus colli muscle: case report and review of the literature. Eur Spine J. 2013;22(Suppl 3):S434–8.
21. Bruno MA, Walker EA, Abujudeh HH. Understanding and confronting our mistakes: the epidemiology of error in radiology and strategies for error reduction. Radiographics. 2015;35(6):1668–76.
22. Ratnaike TE, Hastie H, Gregson B, et al. The geometry of brain contusion: relationship between site of contusion and direction of injury. Br J Neurosurg. 2011;25(3):410–3.
23. Lee CS, Nagy PG, Weaver SJ, et al. Cognitive and system factors contributing to diagnostic errors in radiology. Am J Roentgenol. 2013;201(3):611–7.
24. Waite S, Scott J, Gale B, et al. Interpretive error in radiology. Am J Roentgenol. 2017;208(4):739–49.
25. Savage NM, Alleyne CH, Vender JR, et al. Dural-based metastatic carcinomas mimicking primary CNS neoplasia: report of 7 cases emphasizing the role of timely surgery and accurate pathologic evaluation. Int J Clin Exp Pathol. 2011;4(5):530–40.
26. Carrion DM, Carrion AF. Non-ketotic hyperglycemia hemichorea-hemiballismus and acute ischemic stroke. BMJ Case Rep. 2013;2013:bcr2012008359.
27. Wilson TJ, Than KD, Stetler WR, et al. Non-ketotic hyperglycemic chorea-hemiballismus mimicking basal ganglia hemorrhage. J Clin Neurosci. 2011;18(11):1560–1.
28. Ashman CJ, Yu JS, Wolfman D. Satisfaction of search in osteoradiology. Am J Roentgenol. 2000;175(2):541–4.
29. Provenzale JM, Kranz PG. Understanding errors in diagnostic radiology: proposal of a classification scheme and application to emergency radiology. Emerg Radiol. 2011;18(5):403–8.
30. Tversky A, Kahneman D. Judgment under uncertainty: heuristics and biases. Science. 1974;185:1124–31.
31. Gunderman RB. Biases in radiologic reasoning. Am J Roentgenol. 2009;192:561–4.
32. Block J, Funder DC. Social roles and social perception: individual differences in attribution and error. J Pers Soc Psychol. 1986;51:1200–7.
33. Donald JJ, Barnard SA. Common patterns in 558 diagnostic radiology errors. J Med Imaging Radiat Oncol. 2012;56:173–8.
34. Quekel LG, Kessels AG, Goei R, van Engelshoven JM. Miss rate of lung cancer on the chest radiograph in clinical practice. Chest. 1999;115:720–4.
35. Rosenkrantz AB, Bansal NK. Diagnostic errors in abdominopelvic CT interpretation: characterization based on report addenda. Abdom Radiol. 2016;41:1793–9.

Errors in Emergency and Trauma Radiology: C-Spine Imaging

Sadia R. Qamar, Yuhao Wu, Luck Louis,
and Savvas Nicolaou

3.1 Introduction

In the past two decades, the use of imaging in emergency and trauma settings has rapidly expanded. According to the 2015 National Hospital Ambulatory Medical Care Survey, the number of emergency visits totaled 136.9 million in the United States, and 47.0% of these visits resulted in the performance of at least one imaging examination [1]. The demand for the rapid availability of high-quality imaging, immediate reporting, and 24 h, 7 days a week service makes emergency radiology an environment which is particularly susceptible to increasing medical errors and misdiagnosis.

Acute or suspected cervical trauma accounts for more than one million visits to emergency departments and $3.4 billion dollars in diagnostic imaging costs in the United States alone each year [2, 3]. Because the possibility of missing cervical spine (c-spine) trauma can have catastrophic consequences, it is essential to have accurate diagnostic imaging to guide prompt management. This chapter will discuss some of the common types of radiological errors, will describe the use of imaging in acute cervical spine trauma, and will review the pearls and pitfalls for imaging the acute cervical spine using a case-based approach.

3.2 Errors in Diagnostic Radiology

Radiologists make approximately 4% of errors in interpretation of imaging examinations [4]. Errors in diagnostic radiology can be attributed to technical factors, work environment factors, or radiologist-specific factors. Technical errors can include choice of inappropriate image modality, poor image resolution, and inadequate clinical information [5]. In order to make an accurate diagnosis, the appropriate imaging modality should be chosen, and image quality should be optimized so that the relevant anatomy can be visualized while minimizing patient exposure to ionizing radiation. In addition, adequate clinical information should be provided to maximize the utility of available diagnostic imaging. However, radiologists often lack access to clinical information, especially in emergency settings. In a retrospective study, Trianopoulo et al. [6] found that 14% of the radiology requisitions ($n = 1708$) had no clinical information, and an additional 9.3% had inadequate clinical information. In the same

S. R. Qamar (✉) · Y. Wu · L. Louis
Vancouver General Hospital, University of British Columbia, Vancouver, BC, Canada
e-mail: Sadia.Qamar@vch.ca;
Yuhao.wu@alumni.ubc.ca; Luck.Louis@vch.ca

S. Nicolaou
Department of Radiology, Jim Pattison Pavilion South, Vancouver General Hospital,
Vancouver, BC, Canada
e-mail: savvas.nicolaou@vch.ca

study, the provisional clinical diagnosis was only included on 54% of the requisitions [6]. Technical factors and lack of adequate clinical history is estimated to account for approximately 4% of radiologic errors [7].

The role of diagnostic radiology has also expanded enormously with increasing volumes and the advent of more complex diagnostic imaging modalities including computed tomography (CT) and magnetic resonance imaging (MRI). This, when accompanied with the demand for more rapid interpretation and longer working hours, leads to a work environment where radiologists are more prone to making diagnostic errors [8].

Radiologist-specific errors can be broadly categorized into perceptual errors and cognitive errors [9]. Perceptual errors, which account for 60–80% of the errors, occur when an apparent abnormality on imaging is missed by the interpreting radiologist [10]. Under-reading, which occurs when conspicuous findings are missed prospectively, is the most common type of perceptual error and accounts for 42% of such errors. Twenty-two percent of the errors are attributable to "satisfaction of search," when the radiologist fails to continue to look for additional abnormalities after the initial abnormality has been identified. Another 7% of errors are due to abnormalities seen outside of the area of interest but which are still visible on imaging (i.e., on the first and last images of the sequence or on the corner of an image) [7]. Cognitive errors occur when the abnormality is spotted on imaging, but its significance is misinterpreted or miscommunicated to clinicians. These errors can be secondary to complacency and faulty reasoning, lack of knowledge, failure to review previous relevant imaging, or failure to communicate findings to clinicians in a clear and organized manner [7].

3.3 Indications for Imaging the C-Spine

Diagnostic imaging of the cervical spine in acute trauma is crucial for guiding early treatment for injuries which would otherwise have serious neurological sequelae. To ensure the accurate diagnosis of cervical spine trauma, both the National Emergency X-Radiography Utilization Study (NEXUS) and the Canadian Cervical Spine Rule (CCR) have developed clinical decision tools to ensure the appropriate use of diagnostic imaging. NEXUS, which has a sensitivity of 99.6% and negative predictive value of 99.9%, utilizes five clinical criteria to select for patients who do not require diagnostic imaging: (1) no tenderness at the posterior midline of the cervical spine, (2) no focal neurological deficits, (3) normal level of consciousness/alertness, (4) no evidence of intoxication, and (5) no other painful injuries which might distract patients from the pain of cervical spine trauma [11]. Diagnostic imaging is indicated for patients who fail to meet any one of these criteria.

The Canadian Cervical Spine Rule (CCR), as shown in Fig. 3.1, categorizes patients based on three high-risk criteria and five low-risk criteria and the ability to rotate their necks to 45° [12]. It has similar sensitivity (99.4% vs. 99.6%) but higher specificity (42.5% vs. 12.9%) compared to the NEXUS study [11–13], and has been validated in several multicenter prospective randomized trials [14, 15]. However, CCR is only applicable to patients between 16 and 65 years of age, whereas the NEXUS study applies to patients of all age groups. Compared to CCR, NEXUS provides more validity in pediatric patients under the age of 16. However, its reliability in elderly patients over the age of 65 may still be limited [16].

According to the American College of Radiology (ACR) Appropriateness Criteria for suspected cervical trauma imaging, computed tomography (CT) should be the initial imaging modality for patients over the age of 14 who screen positive for either the NEXUS or CCR algorithm. Compared to cervical spine radiographs, multi-detector CT has a higher sensitivity and is more time-efficient [17]. Cervical spine radiography is only recommended for patients under the age of 14 or as follow-up imaging for patients who initially had negative findings on CT but remain in a cervical spine collar due to persistent neck pain or those who need surgical planning for a mechanically unstable cervical spine,
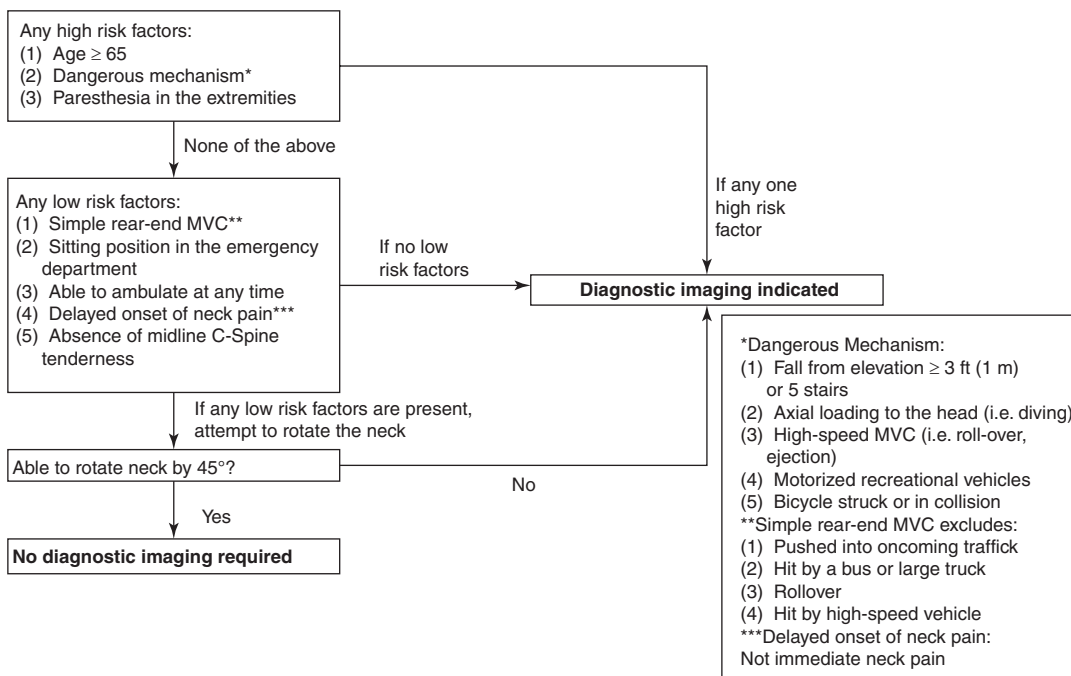
```
┌─────────────────────────────────┐
│ Any high risk factors:          │
│ (1) Age ≥ 65                    │
│ (2) Dangerous mechanism*        │
│ (3) Paresthesia in the extremities │
└─────────────────────────────────┘
         │
    None of the above
         │
┌─────────────────────────────────┐
│ Any low risk factors:           │
│ (1) Simple rear-end MVC**        │
│ (2) Sitting position in the emergency │
│     department                  │
│ (3) Able to ambulate at any time │
│ (4) Delayed onset of neck pain*** │
│ (5) Absence of midline C-Spine  │
│     tenderness                  │
└─────────────────────────────────┘
         │
  If any low risk factors are present,
  attempt to rotate the neck
         │
┌─────────────────────────────────┐
│ Able to rotate neck by 45°?     │
└─────────────────────────────────┘
         │
        Yes
         │
┌─────────────────────────────────┐
│ No diagnostic imaging required  │
└─────────────────────────────────┘
```

If no low risk factors → **Diagnostic imaging indicated**

If any one high risk factor → **Diagnostic imaging indicated**

No

*Dangerous Mechanism:
(1) Fall from elevation ≥ 3 ft (1 m) or 5 stairs
(2) Axial loading to the head (i.e. diving)
(3) High-speed MVC (i.e. roll-over, ejection)
(4) Motorized recreational vehicles
(5) Bicycle struck or in collision
**Simple rear-end MVC excludes:
(1) Pushed into oncoming traffick
(2) Hit by a bus or large truck
(3) Rollover
(4) Hit by high-speed vehicle
***Delayed onset of neck pain:
Not immediate neck pain

Fig. 3.1 Canadian C-spine rule [12]

when used as an adjunct to CT and/or MRI [18]. Despite this recommendation, it is estimated that 32.7% of the initial cervical spine imaging examinations ordered on adult patients (age ≥ 18) in the emergency department are cervical spine radiographs, which would be considered to be "inappropriate imaging" by the ACR criteria [2].

3.4 Imaging Techniques

At the authors' institution—Emergency and Trauma Radiology Center, Vancouver General Hospital (Vancouver, BC, Canada)—a standard non-enhanced cervical spine CT utilizing trauma protocol is carried out for suspected isolated cervical spine injuries. Patients are scanned in the craniocaudal direction with a tube voltage of 120 or 140 kV, a rotation time of 1 s, and a pitch of 0.8, using a detector configuration of 64×0.6 mm. All images are reconstructed using standard bone deconvolution kernel, B75H, very sharp, ASA (Siemens Healthcare, Forchheim, Germany) in the axial, sagittal, and coronal planes, as well as a soft-tissue deconvolution kernel using hybrid

iterative reconstruction, 130 strengths 2 SAFFIRE (Siemens Healthcare, Forchheim, Germany) in the axial, sagittal, and coronal planes. Thin axial sections (i.e., 0.75 or 1 mm) with coronal and sagittal reconstructions at 1–2 mm thickness are used. Three-dimensional rendering including volume and cinematic rendering is used on an as-needed basis for problem-solving and preoperative planning, and to enhance communication with the trauma surgery team.

Dose reduction strategies including tube current modulation, adaptive collimation, automated exposure control, and iterative reconstructions are used whenever possible [19]. At the authors' institution, a 40% dose reduction is achieved by reducing kilovolt (peak) from 140 to 120 in younger patients. Further reduction in dose can be achieved by reducing both kilovolt and quality milliamp seconds (mA s) and by utilizing iterative reconstructions techniques to account for the increased image noise.

In poly-trauma patients with high-velocity collisions, an intravenous contrast-enhanced standard neck CT angiography protocol is used with dedicated osseous and soft-tissue recon-

structions for the cervical spine. CT angiography provides supplemental information on vascular injuries resulting from traction of vessels due to associated fractures or dislocations, especially in hyperflexion and hyperextension injuries [20], and in blunt cerebrovascular injuries which are difficult to assess in obtunded patients [21].

3.5 Approaches to Interpreting Cervical Imaging

3.5.1 Cervical Spine Anatomy and Biomechanics

The cervical spine has two separate anatomical and functional units [22, 23]. The craniocervical junction includes the skull base (the occipital condyles), the first cervical vertebra (C1), and the second cervical vertebra (C2). The subaxial spine consists of the third through seventh vertebrae (C3–C7). However, rigid spine diseases including ankylosing spondylitis (AS) and diffuse idiopathic skeletal hypertrophy (DISH) do not follow this division, as these spines respond differently to external traumatic forces [22]. The vertebral bodies increase in strength from C1 through C7. The compressive forces are transmitted through the vertebral bodies in the cervical spine. The facets carry 30% of the cervical spine load and further contribute to 45% of the torsional strength [23].

An unstable cervical spine is defined as a spine which cannot maintain normal alignment and is not able to protect the spinal cord and exiting nerve roots under physiological conditions [23, 24]. Cervical spine stability is determined by the integrity of osseous and ligamentous structures along with the intervertebral discs and facet joints. It is deemed unstable if more than one of these structures is disrupted, thus allowing abnormal movements at, above, or below the level of injury [23, 24]. However, the complex anatomy of the cervical spine with a potentially wide range of injury mechanisms and baseline patient factors pose challenges to determine the stability of the cervical spine based on the use of one imaging modality alone.

In the craniocervical junction, the unique anatomy of the atlas (C1) and axis (C2) vertebrae and the distinct articulation with the skull base allow for a wide range of movements [23]. The anatomically intricate craniocervical junction is comprised of vital associations between joints and ligaments, namely, the atlanto-occipital, the occipitoaxial, and the atlantoaxial joints [23, 25]. These anatomical relationships are shown in Fig. 3.2.

The atlanto-occipital joint between the occipital condyles and C1 is composed of the atlanto-occipital ligaments (anterior, posterior, and lateral), the paired atlanto-occipital joints, and the atlanto-dental joints (anterior or posterior). The anterior atlanto-occipital membrane connects the anterior margin of the foramen magnum to the superior border of the anterior arch of the atlas. The posterior atlanto-occipital ligament connects the posterior arch of C1 to the posterior aspect of the foramen magnum [19]. The lateral atlanto-occipital ligament connects the transverse process of C1 to the jugular process of the occipital bone [20].

The occipito-axial relationship between the occipital condyles and C2 consists of the apical, tectorial, and paired alar ligaments. The apical ligament connects the basion to the tip of the dens. The tectorial ligament connects the basilar groove of the occipital bone to the posterior body of C2. The alar ligament arises from the lateral margins of the dens and inserts onto the occipital condyles. It limits occipital and atlantal rotation in relation to C2 and is stretched with rotation of the head to the contralateral side. It also functions to stabilize the atlantoaxial joint by preventing anterior subluxation of C1 against the dens.

The atlantoaxial relationship consists of two paired atlantoaxial joints and the cruciate ligament complex (which is composed of the transverse ligament and the superior and inferior longitudinal bands). The transverse ligament courses posterior to the dens and attaches to the lateral tubercles of C1. Together with the superior and inferior longitudinal bands, the transverse ligament forms the cruciate ligament complex, which holds the dens securely against C1 and prevents anterior displacement of C1 [23].
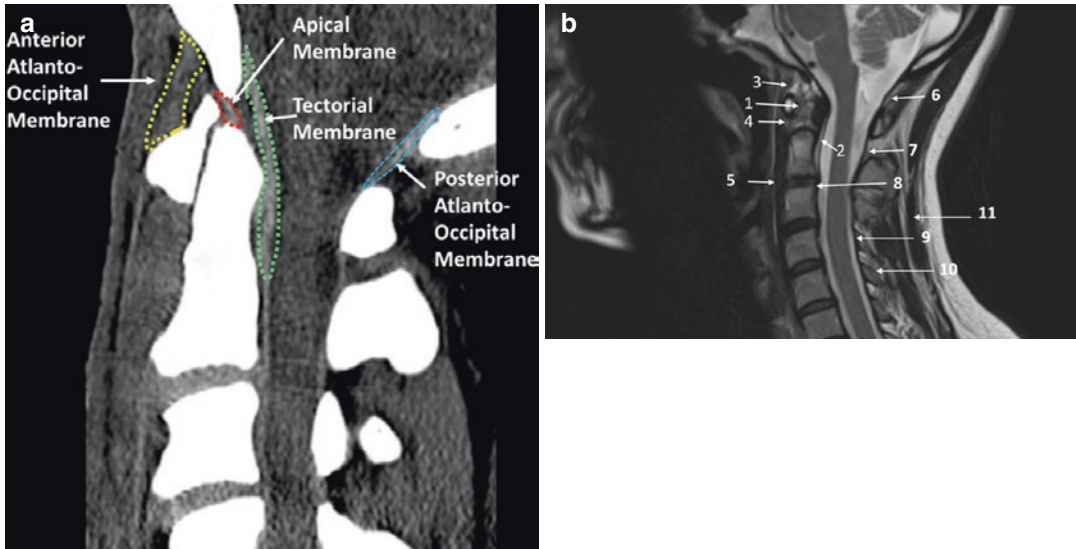
Fig. 3.2 (**a**) Sagittal soft-tissue window cervical spine CT: anterior and posterior atlanto-occipital membranes, apical membrane, and tectorial membrane. (**b**) Normal sagittal view of cervical spine on a T2-weighted MRI image, showing (1) apical membrane, (2) tectorial membrane, (3) anterior atlanto-occipital membrane, (4) ante-rior atlantoaxial membrane, (5) anterior longitudinal ligament, (6) posterior atlanto-occipital membrane, (7) posterior atlantoaxial membrane, (8) posterior longitudinal ligament, (9) ligamentum flavum, (10) interspinous ligament, and (11) nuchal ligament

The subaxial spine is primarily supported by the ligaments which extend from the axis (C2) through the sacrum, anterior and posterior to the vertebral bodies, namely, the anterior and posterior longitudinal ligaments [23]. Additional support to the posterior elements is provided by the ligamentum flavum, the interspinous ligaments, and the supraspinous ligaments. Intervertebral discs and facet joints add further integrity to the lower cervical spine [25].

The three-column model of Denis is typically used to assess the stability of the subaxial spine [26]. The anterior longitudinal ligament (ALL), the anterior half of the vertebral body, and the anterior half of the intervertebral disc and annulus fibrosis comprise the anterior column. This bears axial loads and resists extension. The posterior longitudinal ligament, the posterior half of the vertebral body, and the posterior half of intervertebral disc and annulus fibrosis create the middle column. This bears axial loads and resists flexion. The posterior osseous elements, facet joints, and the posterior ligamentous complex (PLC, which is composed of the ligamentum fla-

vum, interspinous ligament, nuchal ligament, and facet joint capsule) form the posterior column, which is responsible for stabilization of the spine during rotation and lateral flexion and resists flexion. Disruption of two or more columns strongly suggests instability. Because ligament disruption often begins in either the anterior or posterior columns, involvement of the middle column is synonymous with instability.

One classification scheme to predict the stability and prognosis of the subaxial cervical injuries is the Subaxial Cervical Injury Spine Classification (SLIC) system, which accounts for the degree of osseous and ligamentous injury and the neurological status of the patient to assess the stability or lack of stability of injuries [26]. The classification system awards points to each of the following components: (1) osseous morphology, (2) disco-ligamentous complex, and (3) neurological status. A higher score on the SLIC system suggests a potentially unstable injury. However, this classification system is limited in emergency settings where isolated initial CT is unable to provide information about the disco-ligamentous

complex, which needs to be determined utilizing MR imaging. Furthermore, this scale cannot be used in intubated and obtunded patients.

3.6 Cervical Radiographs

Before the advent of multi-detector CT, cervical radiographs were the initial imaging modality for suspected cervical trauma. The most commonly utilized cervical spine series consists of three views: (1) anterior-posterior (AP) view, (2) lateral view, and (3) odontoid view [27]. Compared to CT, cervical spine radiographs have low sensitivity (52%) and should not be utilized as the initial imaging for cervical spine trauma. Normal cervical radiographs are shown and described in Fig. 3.3.

3.6.1 Imaging Approach

1. For adequate assessment, all seven cervical vertebrae and the first thoracic vertebra should all be visualized.
2. The lateral view is most important, and most injuries seen on cervical spine radiographs can be identified on this view. A detailed approach to interpreting the lateral view of a cervical radiograph is described and is shown in Fig. 3.3a, b.
3. The AP view is important for visualizing soft-tissue abnormalities and for evaluating the cervical-thoracic junction. In the normal AP view, the spinous processes, which may appear as bifid, should be aligned and spaced out evenly (see Fig. 3.3c). Misalignment of the cervical spine suggests flexion and rotational injuries, and increased interspinous distances may indicate a ligamentous disruption [28].
4. The odontoid view (also known as the open-mouth view) is valuable in assessing for the odontoid and the relationship between C1 and C2, as seen in Fig. 3.3d. The dens should be located symmetrically midline to the lateral masses (i.e., the discrepancy in the lateral atlanto-dental space should be less than 2 mm), and the lateral masses of C1 should align with the vertebral body of C2 (with less than 7 mm of lateral mass overhang) [29].

3.7 Cervical Spine CT

Computed tomography (CT), with a sensitivity of 98% [26], should be the initial imaging modality in patients presenting with suspected cervical spine trauma. A standard cervical CT should include the spine from the craniocervical junction to the T3 vertebral body. Coronal and sagittal reformations are critical for assessing alignment and the soft tissues, and the axial reformations are useful for diagnosing osseous fractures. Misalignment and soft-tissue swelling without osseous fractures are suspicious for ligamentous injury, and MRI should be obtained for confirmatory diagnosis [27]. A normal cervical spine CT with reformations is shown and described in Fig. 3.4.

3.7.1 Imaging Approach

3.7.1.1 General Considerations

In busy emergency radiology departments, a systematic approach to interpreting imaging examinations is extremely vital to avoid missing potential injuries. The following is an outline of a stepwise, systematic approach used at the authors' institution to interpret cervical spine CT:

1. Label the cervical spine using the annotation tool on the workstation; it helps anatomical correlation across multi-planar reformations.
2. On axial reformations, look for:
    (a) Integrity and rotational alignment of each vertebra
    (b) The cervical soft tissues
    (c) The spinal canal diameter
    (d) Neuroforaminal patency
3. Sagittal reconstruction plane:
    (a) Assess for alignment: The anterior vertebral, posterior vertebral, spinolaminar, and posterior spinous lines are used to interpret the alignment, similar to the interpretation of the lateral cervical spine radiograph; a subluxation beyond 3 mm for anterior and posterior vertebral lines is considered abnormal.
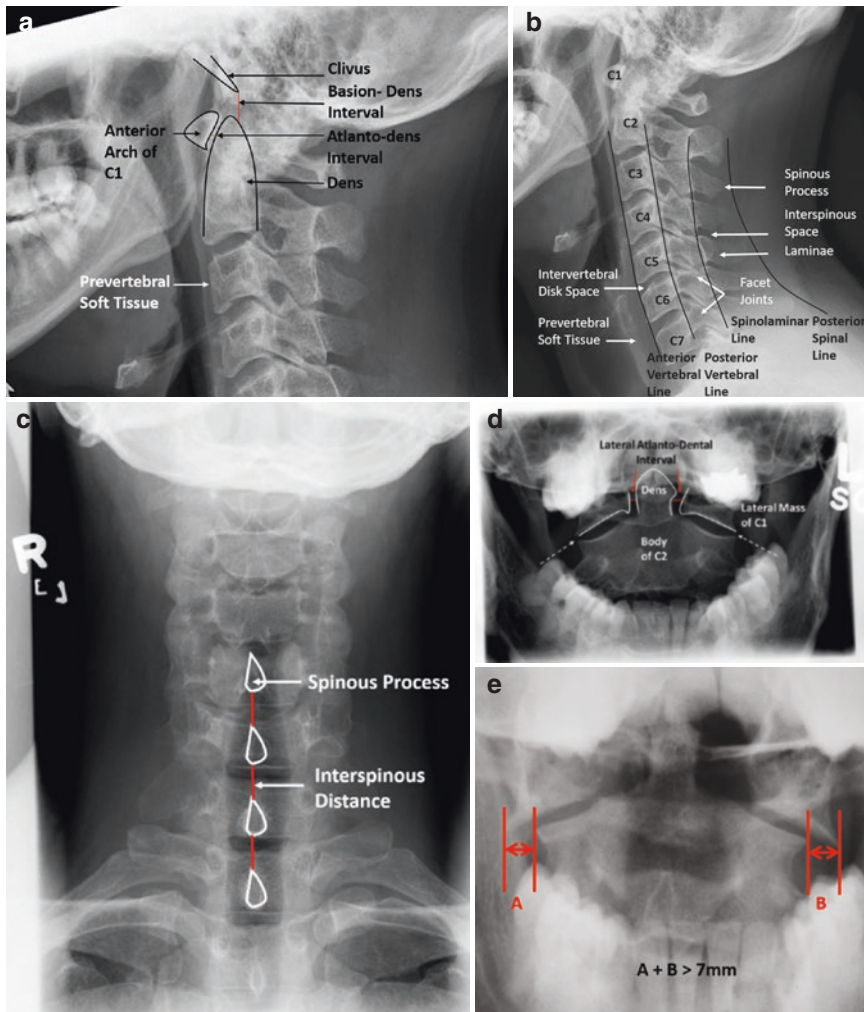   (b) Assess the vertebral bodies and intervertebral discs for their heights.

Fig. 3.3 (**a**) Lateral view on cervical radiograph, showing the upper cervical anatomy: (1) The tip of the clivus (basion) should point to the dens, and the distance between the basion and the tip of the dens (basion-dens interval) should be less than 12 mm; (2) the distance from the anterior arch of C1 to the anterior aspect of the dens (atlanto-dens interval) should be less than 3 mm; and (3) the prevertebral soft tissue should be less than 7 mm anterior to C1–C3 (i.e., less than 50% width of the C2 vertebral body). The contour of the prevertebral soft tissue should generally follow the contour of the vertebrae: it should be slightly convex anteriorly to the anterior arch of C1 and take on a concave shape posteriorly. However, endotracheal tube reduces aeration to the nasopharynx and can make visualization of the prevertebral soft tissues difficult. (**b**) Lateral view on cervical radiograph, showing lower cervical spine anatomy: (1) the anterior vertebral, posterior vertebral, spinolaminar, and spinous process lines should be smooth and free of abrupt discontinuity; (2) the intervertebral disc spaces should be approximately equal in size; (3) the facet joints should be smooth and regular; (4) the interspinous spaces should be equal in size at all levels; and (5) the width of the prevertebral soft tissue should be less than 24 mm anterior to C4–C7. However, if present, an endotracheal tube reduces aeration to the nasopharynx and can make visualization of the prevertebral soft tissues difficult. (**c**) Anterior-posterior view on cervical radiography: the spinous process should be bifid and vertically aligned, and the interspinous distances should be equal. Discrepancy in the interspinous distances suggests possible hyperflexion or rotational injuries. (**d**) Open-mouth (odontoid) view on cervical radiograph: the dens should be situated in between the two lateral masses of C1, with an equidistant lateral atlanto-dental interval (LADI) bilaterally. There may be up to 2 mm of asymmetry between LADI, especially if there is lateral tilt or rotation of a patient's head (with the widening to the side on which the patient's head is tilted or rotated). However, asymmetry >2 mm may be suggestive of atlantoaxial dissociation, and CT or MRI should be obtained. In addition, the lateral masses of C1 should not extend over the lateral mass of C2 by a combined sum of 7 mm. (**e**) Spence's rule can be used to determine the integrity of the transverse ligament on the odontoid view: If the combined sum of the overhang of C1 over C2 exceeds 7 mm, then MRI should be obtained to assess for possible transverse ligament injury
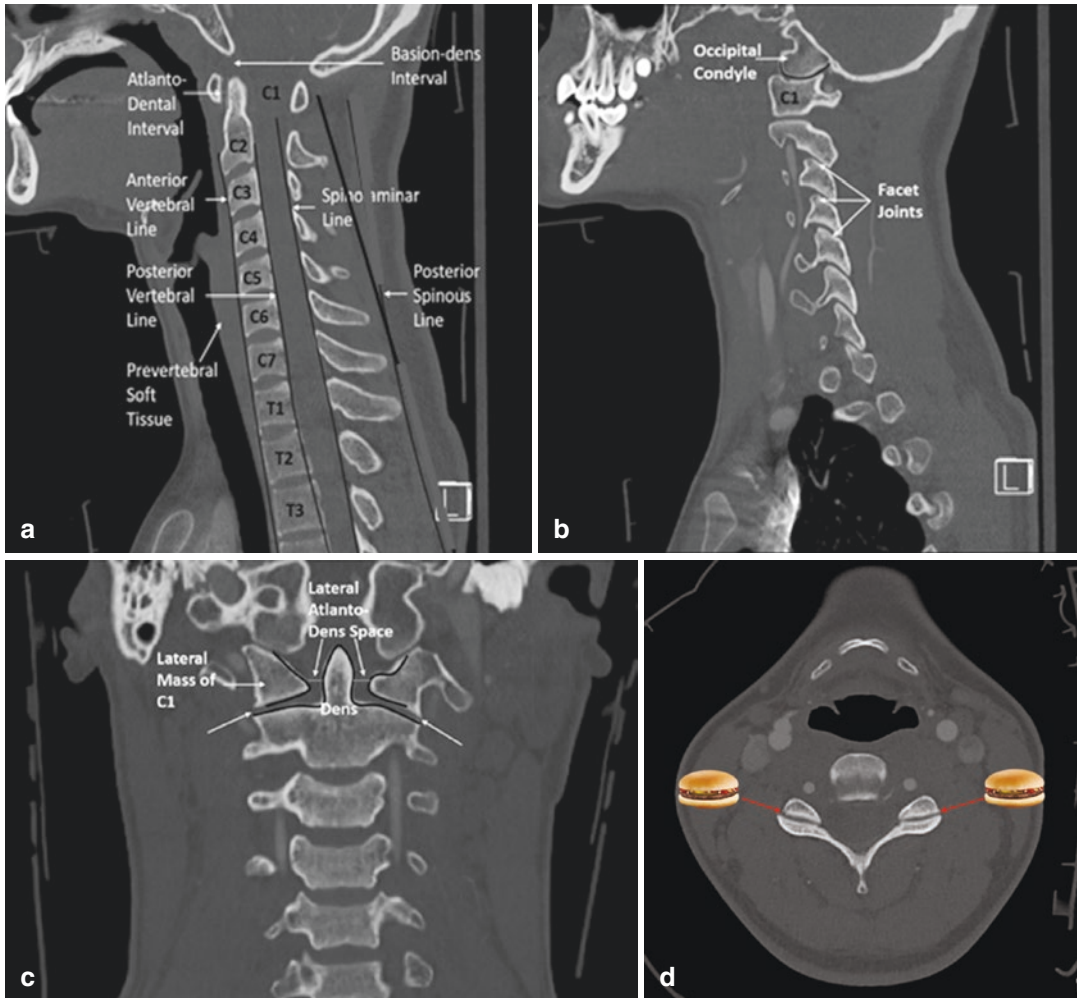
Fig. 3.4 (**a**) Sagittal reformat cervical spine CT: The anterior vertebral, posterior vertebral, spinolaminar, and posterior spinous lines should be smooth and free of abrupt discontinuity. The basion-dens interval should be less than 9 mm, and the atlanto-dental interval should be less than 3 mm. (**b**) Parasagittal view on cervical spine CT: the occipital condyle should be aligned with C1, and the sum of the atlanto-occipital distance bilaterally (condylar sum) should not exceed 4 mm. Increased condylar sum may be a sign of atlanto-occipital dislocation. The joint facets should be well aligned with one another without widening, subluxation, or dislocation. (**c**) On a coronal view on cervical CT, it is important to examine for the lateral atlanto-dens space, as well as for the alignment of the lateral masses of C1 in relationship to C2. (**d**) On the axial images of the cervical CT, it is important to look for the "hamburger sign," which represents normal facet joints. Loss or reversal of the "hamburger sign" suggests facet joint dislocation

   (c) Analyze the interspinous distance; a widened interspinous distance suggests ligamentous injury.

   (d) Assess for spinal canal hematomas on window settings for hemorrhage (window, 135; level, 72 Hounsfield units).

4. Sagittal soft-tissue window:

   (a) Assess the prevertebral tissues on soft-tissue windows; soft-tissue thickness should be less than 5 mm at C2 or 15 mm at C5.

   (b) Analyze the spinal canal, especially for epidural hematomas.

   (c) Look for traumatic disc herniations.

3.7.1.2 Craniocervical Junction

The craniocervical junction is a potential blind spot on CT. The assessment can be further compromised in severely injured patients. The following considerations are an aid in the systematic assessment of the craniocervical junction.

1. Consider occipital condyles as cervical vertebra zero (C0) to ensure individual assessment [23].
2. C0, C1, and C2 are assessed on all three planes.
3. On the axial plane, the anterior atlanto-dental interval is measured; it should be less than 2 mm.
4. Sagittal planes with bone algorithm:
   (a) Atlanto-occipital relationship: the basion-dens interval (BDI), the distance from the basion to the dens, should be less than 9 mm on CT [30]; measurements more than 9 mm suggest craniocervical dissociation [31, 32].
   (b) The congruity between the occipital condyles and the C1 lateral masses.
   (c) The condyle-to-C1 interval should be less than or equal to 2 mm [33].
   (d) Condylar sum: the sum of the distance between each condyle and the condylar fossa of C1 should be less than 4 mm [33].
5. Coronal reconstruction plane: assess for offset at the atlantoaxial junction; any offset of the lateral masses of C1 on C2 should be less than 2 mm [33].
6. Parasagittal images:
   (a) Occipital condyles
   (b) The atlanto-occipital and atlantoaxial congruity
   (c) Facet joint alignment

3.7.1.3 Subaxial Spine
1. All three planes should be utilized to assess fractures.
2. Vertically-oriented fractures are assessed on coronal and axial planes.
3. Horizontally-oriented fractures are assessed on coronal and sagittal planes.
4. The alignment of the facet joints is best assessed on the axial plane.
5. The facet joints should be assessed for overlap or widening; widening of more than 2 mm is abnormal.

3.7.2 Interpretation Pitfalls

The recoil and the muscle spasm after the initial impact of trauma can reduce the osseous displacement, and the neck immobilization in a hard cervical collar can further mask instability by maintaining vertebral alignment. If CT findings are normal and the patient has persistent pain or neurological symptoms, ligamentous injuries must be excluded. MR imaging can be used to identify ligamentous injuries by displaying edema; however, these findings can also be seen in clinically stable injuries. In the setting of acute neurological deficits, MRI provides information on epidural hematoma, traumatic disc herniation, and spinal cord contusion.

3.8 Injuries at the Craniocervical Junction

3.8.1 Occipital Condylar Fracture

Occipital condyle fractures have a 3% incidence in severe blunt cervical trauma patients and indicate a high-energy injury mechanism [34, 35]. Associated C1, C2, and basal skull fractures are frequently seen [19, 34]. The Anderson and Montesano classification is the most widely used radiologic classification system for occipital condylar fractures [36]. The classification encompasses three different mechanisms of injury: (a) Type I, axial loading resulting in comminution-impaction injury with minimal or no fracture displacement (Fig. 3.5); (b) Type II, direct blow to the skull resulting in skull base fracture extending through the occipital condyles (Fig. 3.6); and (c) Type III, forced rotation and lateral bending, resulting in tension on the alar ligament with subsequent avulsion fracture (Fig. 3.7). Type III fractures with alar ligament disruption are unstable [36–38]. These fractures are unstable due to the location of the fractured fragment in the foramen magnum and the avulsed alar ligament. Coronal reconstructions with bone algorithm clearly depict the displacement of the fragment in the foramen magnum, in addition to accurately providing size measurements. Furthermore, bilateral occipital condyle fractures are also considered unstable [20].

3.8.2 Atlanto-occipital Dissociation or Distractions

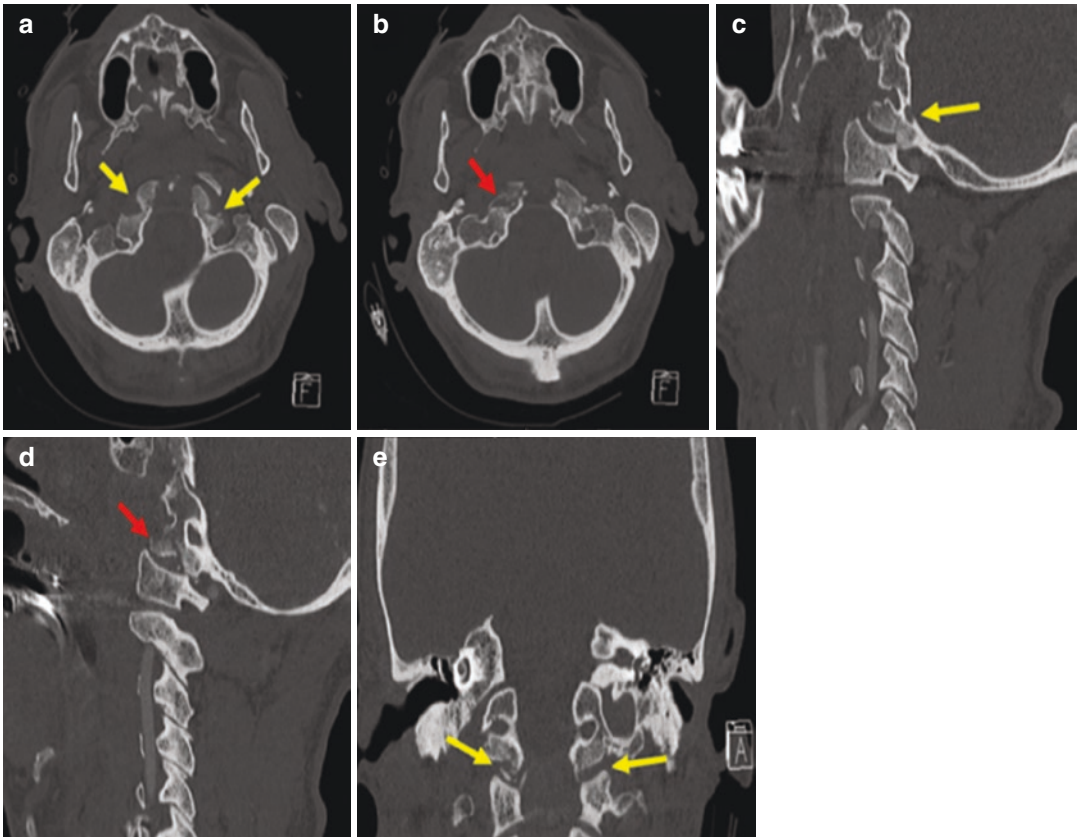Atlanto-occipital dissociation consists of two entities: (a) complete dislocation seen in fatal

Fig. 3.5 Cervical spine CT (**a**, **b**) axial, (**c**, **d**) sagittal, and (**e**) coronal reformatted images show Type I bilateral occipital condyle fractures (yellow arrows) in a 56-year-old woman involved in a motor vehicle collision. The anterior aspect of the right occipital condyle (red arrows) is depressed and comminuted, suggesting crush-type injury
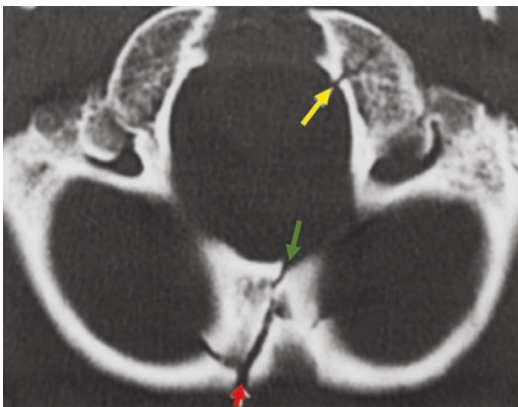

Fig. 3.6 Type 2 occipital condyle fracture in a 45-year-old man involved in a motor vehicle collision. The right occipital base fracture (red arrow) extends through the posterior margin of the foramen magnum (green arrow) to the left occipital condyle (yellow arrow)

motor vehicle and other severe trauma and (b) subluxation or distraction injuries, which are more subtle but potentially survivable injuries [30, 39]. Multiple intervals are measured to assess the craniocervical junction on CT. These include (a) the atlanto-dental interval, which in the axial plane should be less than 2 mm [33]; (b) basion-dens interval which should be less than 9.5 mm [33]; (c) the basion-to-posterior axial line interval which should be less than 5.5 mm [33]; (d) the C1–C2 spinolaminar distance which should be less than 7.8 mm [33]; and (e) the occipital-to-posterior arch of C1 distance which should be less than 8 mm [33]. Examples of normal and abnormal relationship and interval measurements are shown in Figs. 3.8, 3.9, and 3.10. Values greater than normal tend to be sensitive,
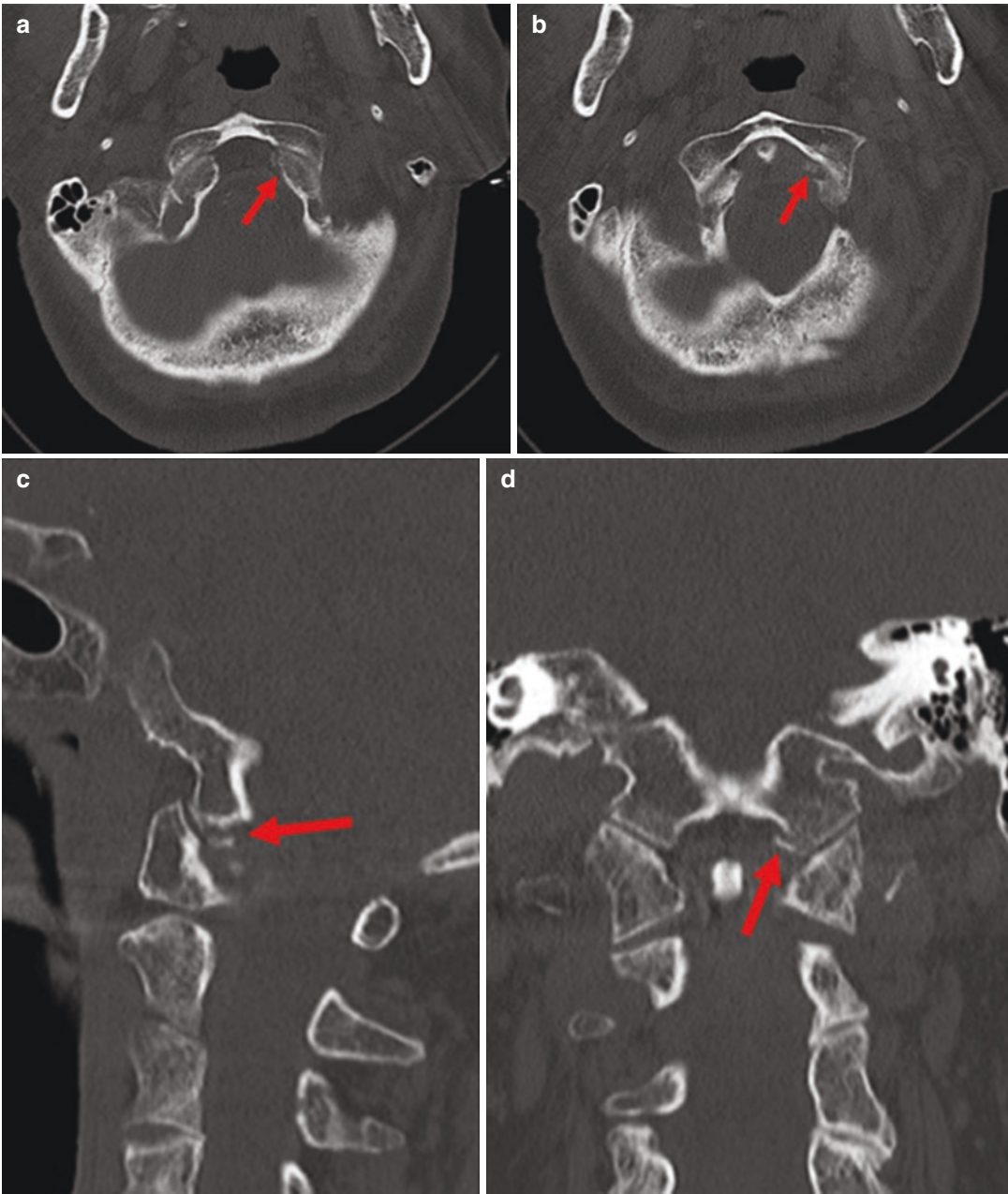
Fig. 3.7 Cervical spine CT with (**a**, **b**) axial images and (**c**) sagittal and (**d**) coronal reformations showing a Type 3 occipital condyle fracture (red arrows) in a 76-year-old woman with a fall from a standing height

but not specific. Normal values virtually exclude craniocervical dissociation or distraction; however, greater than normal values can be normal in some patients but abnormal in others.

The presence of a cranially divergent predental angle ("V sign") is suggestive of trans-verse ligament injury, and increases the likelihood of atlanto-occipital distraction (relative risk ratio = 2.95) [33]. Isolated distraction of the C1–C2 lateral masses is uncommon and is classically seen without cruciate ligament injury.

Normal	Abnormal		Normal	Abnormal	
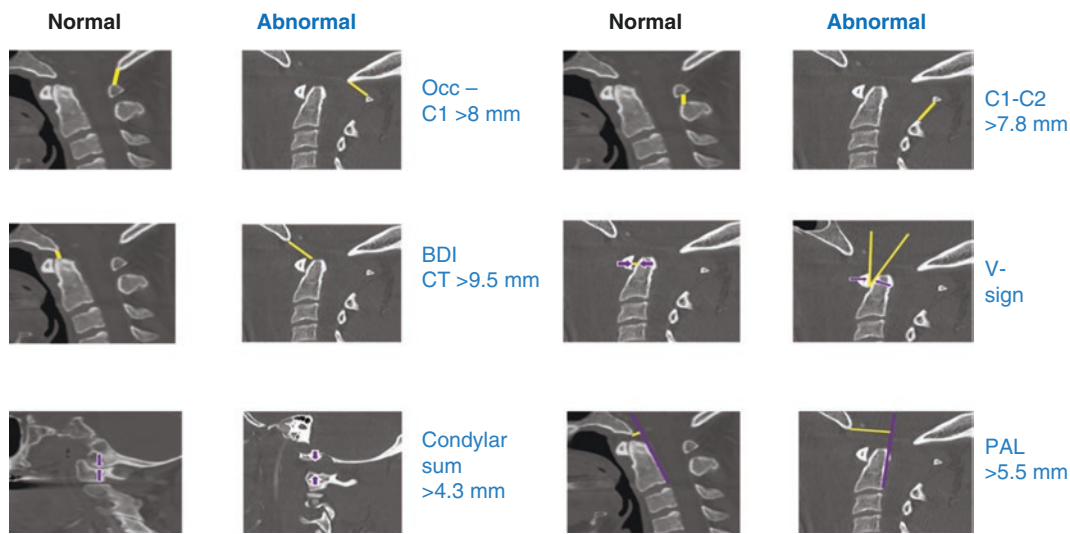
Fig. 3.8 MDCT cervical spine sagittal reconstruction plane with standard measurements indicating atlanto-occipital dissociation (AOD)

V-sign (positive)
ADI = 4.5 mm
PAL = 26.8 mm
BDI = 41.3 mm

C1-C2 = 28.1 mm
Occ-C1 = 27.9 mm
Condylar sum = 28.4 mm
Posterior cortical surface
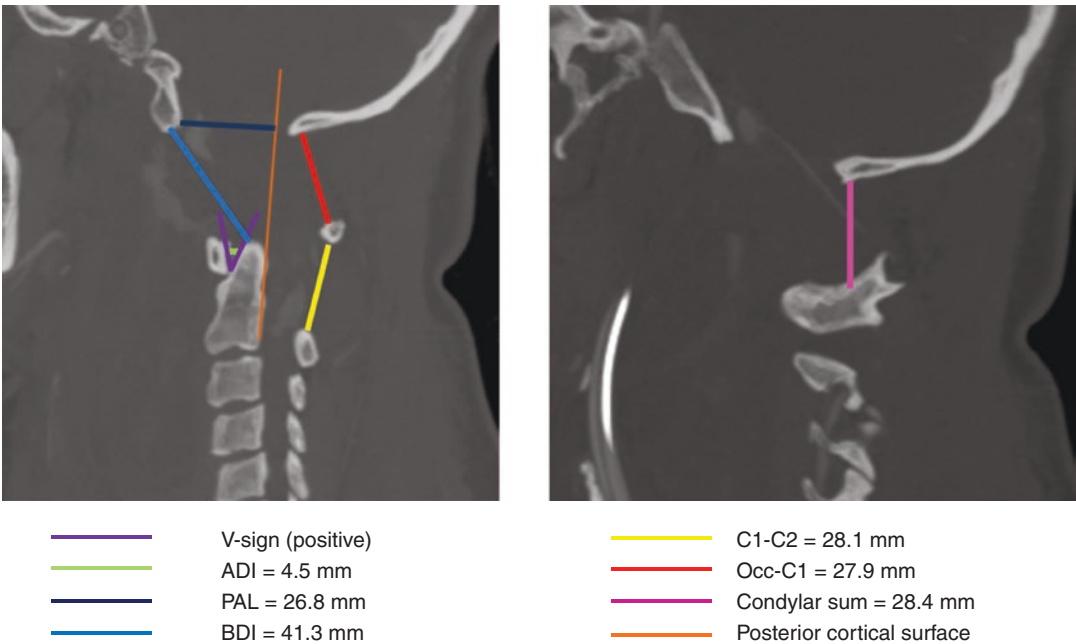
Fig. 3.9 A 56-year-old man involved in a non-lethal high-speed motorcycle collision with craniocervical dissociation. CT cervical spine with sagittal reconstruction plane displaying multiple abnormal measurements. The "V sign" indicates cranially divergent predental angle which is suggestive of transverse ligament injury, and increases the likelihood of atlanto-occipital distraction. (*ADI* atlanto-dental interval, *PAL* posterior axial line, *BDI* basion-dental interval, *occ-C1* atlanto-occipital interval)
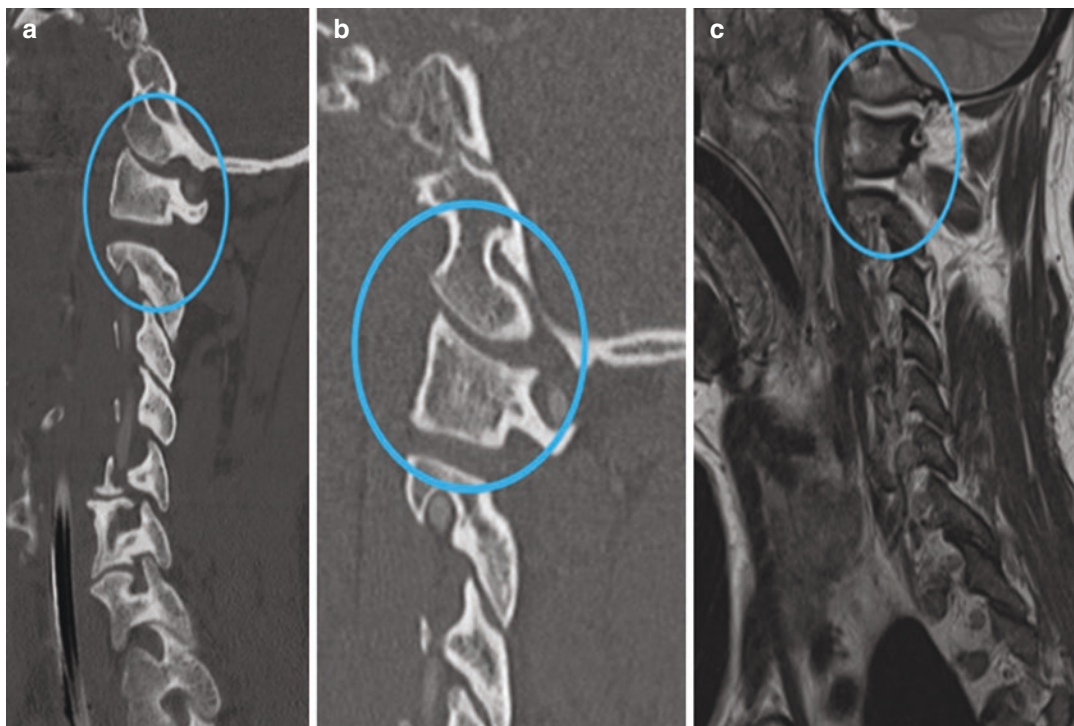
Fig. 3.10 A 58-year-old man with craniocervical dissociation. (**a**) Sagittal, (**b**) magnified sagittal reconstruction planes of a cervical spine CT and (**c**) sagittal T2W MR cervical spine images show that there is a widening of C0–C1 (atlanto-occipital joint) and C1–C2 (atlantoaxial joint), with anterior displacement of the occipital condyles in relation to the lateral mass of C1

Pitfalls A partially ossified atlanto-occipital membrane, a well-corticated osseous fragment posterior to the lateral mass of atlas (C1), or an osseous excrescence termed "ponticulus posticus," Latin for little posterior ridge, can be a source of diagnostic confusion [40].

3.8.3 Jefferson Fractures

Burst fracture of the atlas (C1) is considered to be the result of axial loading with radial displacement of the fragments away from the spinal canal [41]. Fractures may occur at the weakest points of the ring, typically at the anterior or posterior junctions of the arches and lateral masses. As an isolated injury, the classic Jefferson burst fracture is a four-part fracture involving the anterior and posterior arches. It is mechanically and neurologically stable due to the tendency for the fractured bony fragments to spread apart from the spinal canal, and can be managed with external immobilization for 8–12 weeks [21]. Atypical Jefferson fractures are produced by asymmetric axial loading and involve two- or three-part fractures (Fig. 3.11). Because they are commonly associated with transverse ligament injuries, atypical Jefferson fractures often cause atlantoaxial instability [42].

Pitfalls Congenital fusion anomalies, clefts, or aplasia involving anterior and posterior arches
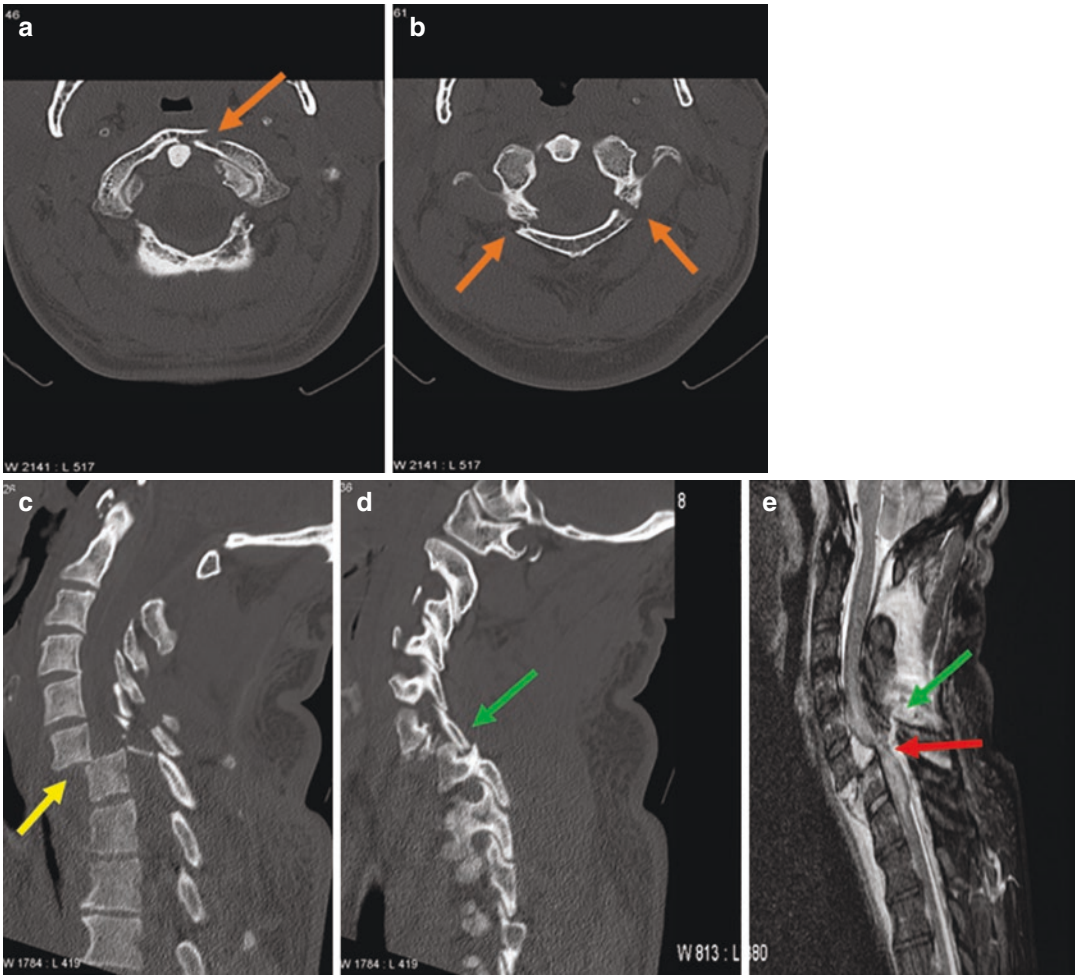
Fig. 3.11 A 41-year-old jogger with history of poly-trauma after a tree fell on him, with an axial loading mechanism. CT cervical spine (**a**, **b**) axial images with a three-part atypical Jefferson fracture, with single fracture through the anterior arch, and bilateral fractures through the posterior arch of C1 (orange arrows). (**c**) Sagittal plane shows greater than 50% C6–C7 subluxation (yellow arrow), and (**d**) parasagittal plane through the facets displays a dislocated facet at C6–C7 (green arrow). (**e**) Sagittal T2 STIR image shows marked cord compression at C6–C7, with intramedullary edema (red arrow)

may simulate fractures or dislocations. Typically, smooth well-corticated margins can help reveal these entities, in contrast to sharp and non-sclerotic fracture margins [40].

3.8.4 Odontoid Fracture

Odontoid fractures represent the most common fractures of the axis and are typically seen in elderly patients or in patients with stiff spondy-lotic spines [41]. A widely accepted three-part classification was proposed by Anderson and D'Alonxo [38]. *Type 1 fractures* are obliquely oriented fractures at the superolateral aspect of the dens, which are caused by alar ligament avulsion. These are unstable owing to ligamentous disruption. *Type 2 fractures* are horizontally oriented fractures at the odontoid base. *Type 3 fractures* are fractures which extend into the vertebral body (Fig. 3.12). A sagittal reconstruction plane should be used to assess the degree and direction
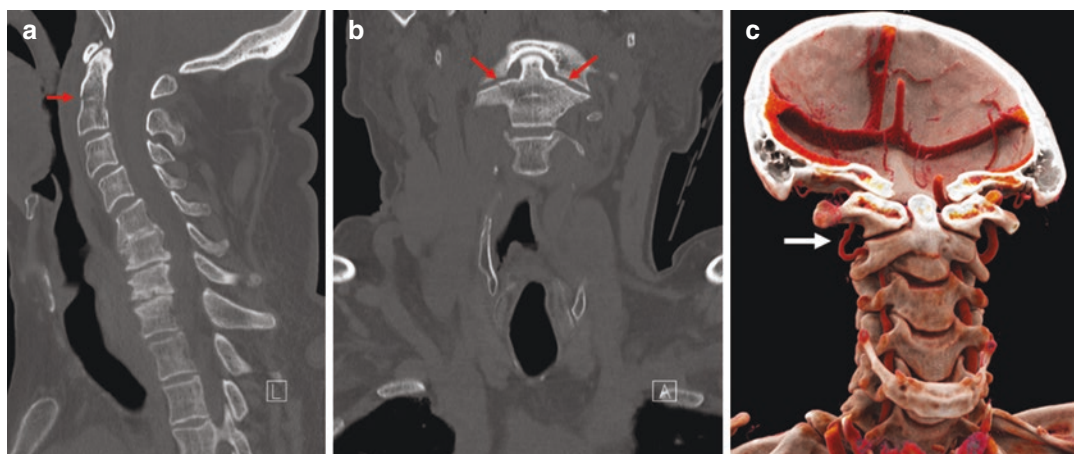
Fig. 3.12 A 60-year-old man fell down the stairs while drunk. (**a**) Sagittal (**b**) coronal CT cervical spine images show a non-displaced Type 3 non-displaced odontoid process fracture. (**c**) Cinematic-rendered image (different patient) showing irregular contour of the right vertebral artery (white arrow), representing blunt cerebrovascular injury

of the odontoid angulation, to ascertain the integrity of the transverse ligament.

Pitfalls Os odontoideum, an unstable entity, can potentially be mistaken for a fracture. According to a general consensus, this is now increasingly considered as sequelae of childhood trauma rather than a congenital anomaly. Os odontoideum should be distinguished from a chronic type II fracture by the presence of a large gap between the os and the axis (C2) body. Os terminale, a secondary ossification center at the odontoid tip, is characterized by its smaller size relative to the os odontoideum.

3.8.5 Hangman's Fractures

The "Hangman's fracture" refers to the traumatic spondylolisthesis of the axis (C2), which is seen in patients involved in motor vehicle collisions, particularly following sudden deceleration injuries [40]. Axial and parasagittal CT images best depict the pars interarticularis fractures. Often these fractures are asymmetric and atypical with fracture lines extending into the posterior vertebral body. If the transverse foramen is involved, these fractures pose a potential risk for vertebral artery injury [20, 33]. A modified classification system by Levine and Edwards subdivides the fracture to the following types [40]:

1. *Type 1 fracture*—bilateral pars fractures without angulation or significant translation, due to hyperextension and axial loading.
2. *Type 2 fracture*—disruption of the C2–C3 disc with anterior C2 body translation owing to hyperextension with axial loading followed by hyperflexion; a small posterior fracture fragment is separated in this type, and causes spinal canal narrowing with subsequent spinal cord injury.
3. *Type 2A fracture*—C2 angulation without translation seen in flexion-distraction injuries.
4. *Type 3 fractures*—combination of anterior translation and angulation with facet subluxation or frank dislocation secondary to hyperflexion and compression (Fig. 3.13).

Pitfalls Type I fractures are radiologically subtle and can be overlooked. Multi-planar reconstructions should be utilized on CT to help identify these fractures [40]. Vertebral artery injury can be missed in fractures involving the transverse foramen. Therefore, such fractures should be fol-
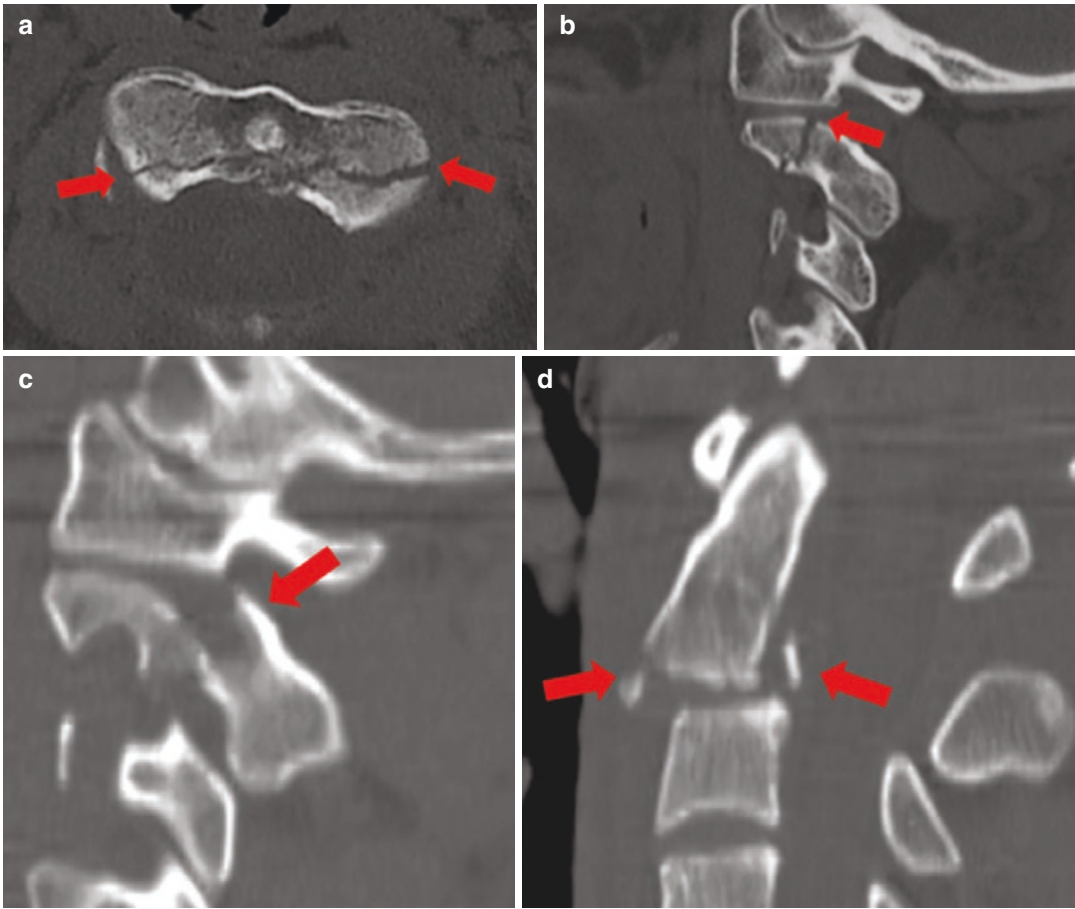
Fig. 3.13 Three types of Hangman's fractures in three different patients. Type 1, CT cervical spine (**a**, **b**) axial and sagittal images show a coronal fracture involving body of C2 extending through the bilateral pars interar- ticularis, without anterior C2 translation; Type 2, sagittal plane (**c**) shows disruption of the C2–C3 disc with anterior C2 translation; and Type 3, (**d**) there is a combination of anterior C2 translation and angulation

lowed with CT angiography [40]. Inability to differentiate Type 1 from Type 2 fractures can result in worse outcomes, as the latter require sur- gical reduction and internal fixation [40].

3.9   Injuries at Subaxial Cervical Spine

3.9.1   Flexion Injuries

Hyperflexion injuries are the most common type of cervical spine injuries and can be divided into hyperflexion sprain (anterior subluxation), flexion-compression, flexion-teardrop, and flexion-distraction injuries [43].

3.9.1.1   Hyperflexion Sprain and Anterior Subluxation

In normal physiological flexion, the cervical verte- bral bodies translate anteriorly, and each succes- sively higher vertebral body becomes more anteriorly translated. The inferior articular facet of the higher vertebral body moves forward and upward relative to the superior articular facet of the lower vertebral body, and the interspinous spaces becomes widened. Hyperflexion sprain occurs when the posterior longitudinal ligament, which normally limits cervical spine flexion, becomes disrupted by a mild-to-moderate flexion force (usu- ally less than 49 kg/cm^2) [31]. If the posterior annu- lus fibrosis is also involved, this results in anterior subluxation of the involved vertebral body.

CT findings include [31] (1) increased interspinous distances (also known as "fanning" of the spinous process); (2) increased posterior vertebral disc space; (3) localized kyphosis limited to the level of the disruption; (4) anterior and superior dislocation of the superior facet in relation to the inferior facet, thus increasing the posterior interfacetal space (also known as "uncovering" of the facets); and (5) anterior subluxation.

Pitfalls Cervical kyphosis may also result from muscle spasm and can be mistaken for anterior subluxation. This, however, should be differentiated from kyphosis due to traumatic anterior subluxation by examining for the alignment of the facet joints and the posterior vertebral disc spacing [40]. Degenerative changes can be confused with traumatic subluxation. In contrast to traumatic anterior subluxation, cervical spondylosis usually results in retrolisthesis due to normal cervical lor-dosis and posteriorly inclined articular facets. Additionally, the narrowed facet joint and thinned osseous facets further point to degenerative changes. On the contrary, the facet joints are abnormally widened in traumatic subluxation [19, 40].

3.9.1.2 Flexion-Compression Injury and Teardrop Fractures

Flexion-compression injuries occur when there is a compressive force vector exerted on the flexed cervical spine. These injuries result in the blunting of the anterior-superior margin of the vertebral body and with more severity, creating a triangular-shaped fracture fragment at the anterior-inferior margin of the vertebral body known as a "teardrop" fragment (Fig. 3.14). Teardrop fracture occurs when there is accompanying retrolisthesis of the posterior-inferior edge of the vertebral body into the spinal canal, causing disruption to the posterior longitudinal liga-
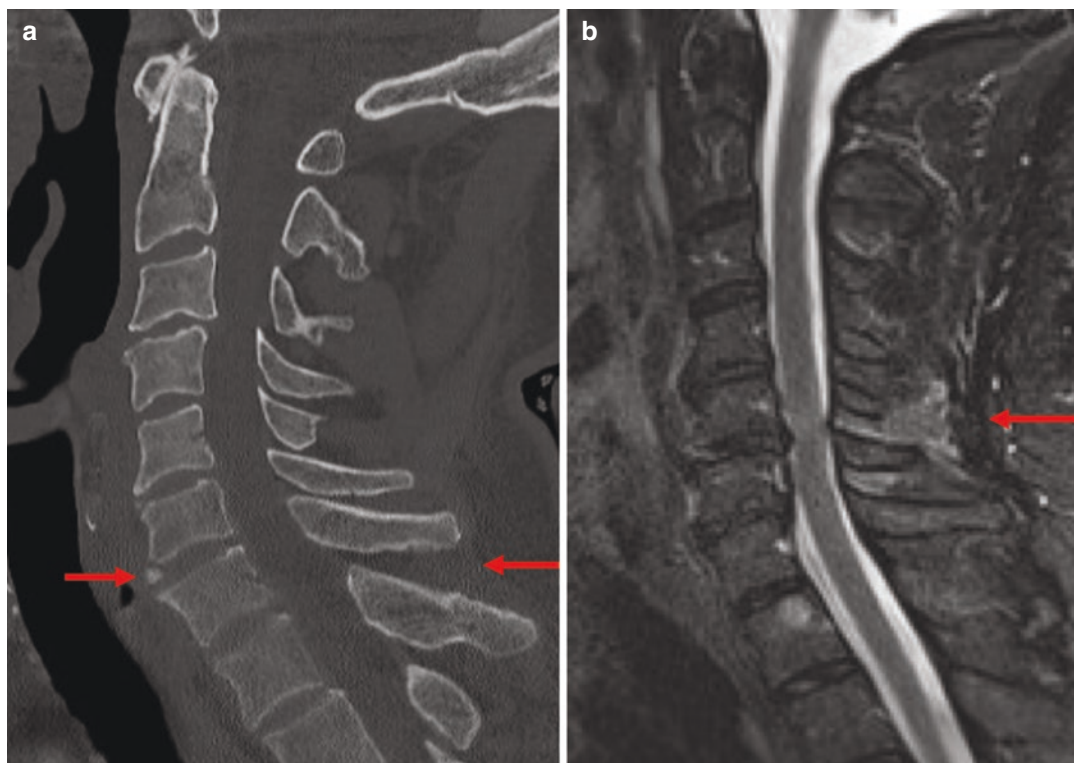
Fig. 3.14 Flexion-teardrop fracture in a 37-year-old woman involved in a motor vehicle collision. (**a**) Sagittal cervical spine CT reformation shows a teardrop fracture at the anterior-inferior aspect of the C6 vertebral body (red arrow), with fanning of the C6–C7 interspinous space (red arrow). (**b**) Sagittal T2W fat-suppressed MR cervical spine image of another patient with hyperflexion injury displays edema at the C5–C6 interspinous ligament

ment and posterior ligamentous complex (PLC). Other signs of PLC disruption include increased interspinous distance, facet dislocation, vertebral body subluxations, and localized kyphosis [44]. Flexion-teardrop fractures have a poor prognosis, with approximately 56% of patients progressing to quadriplegia [44]. Because it is a highly unstable injury and has severe neurological consequences, teardrop fractures require immediate surgical fixation.

3.9.1.3 Flexion-Distraction Injuries

Flexion-distraction injuries (Fig. 3.15) occur when there is tension or shear forces applied to the cervical spine while it is in flexion, resulting in vertical disassociation of the spinous components [21]. The ligaments are disrupted in a posterior-to-anterior sequence. Flexion-distraction injuries proceed in four stages: (1) first, there is disruption to the PLC, resulting in facet subluxation and increased interspinous dis-

tances; (2) second is unilateral facet dislocation; (3) third is bilateral facet dislocation, and up to 50% anterior displacement of the superior vertebral body; and (4) fourth, in the most severe stage, it produces a "floating vertebrae" phenomenon, with more than 50% displacement of the anterior vertebral body. Facet joint dislocation is best visualized on axial CT and manifests in the "reverse hamburger" sign, resulting from the dislocated facet. Both unilateral and bilateral facet dislocations are associated with traumatic disc herniation, and MRI should be obtained prior to spinal stabilization or reduction. A posterior approach is preferred in patients without disc herniation, but anterior decompression and stabilization with discectomy should be utilized in patients with disc damage [45].

3.9.1.4 Clay-Shoveler Fracture

The clay-shoveler fracture is a rare type of stress-avulsion fracture resulting from shear stress
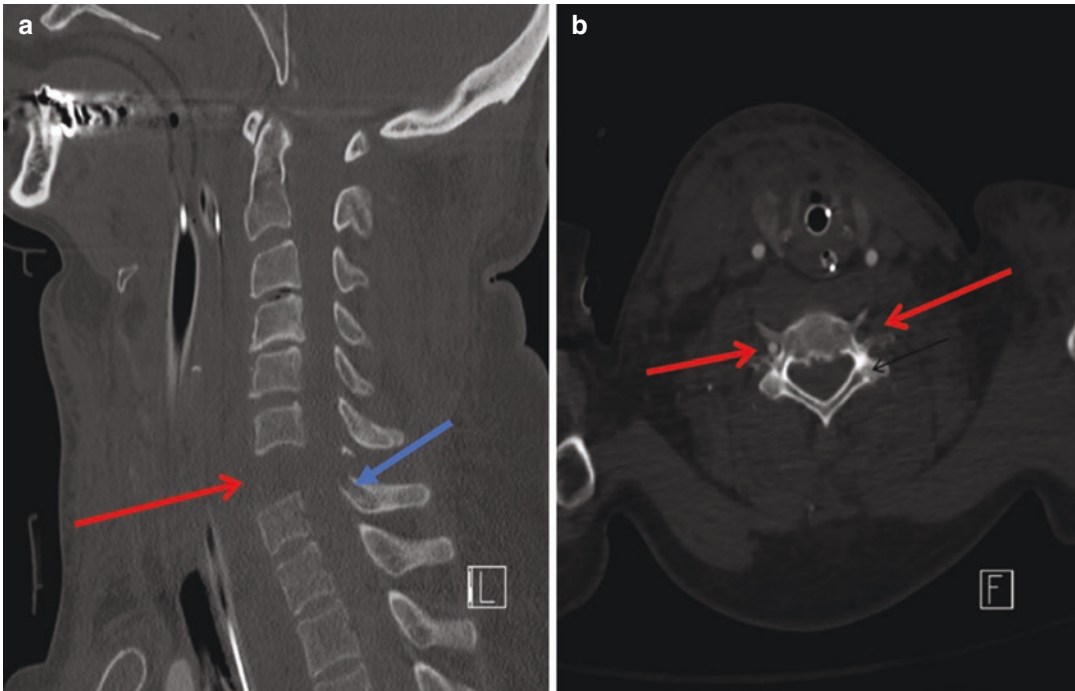
Fig. 3.15 CT cervical spine (**a**) sagittal reformation shows flexion distraction with complete avulsion of the C6/C7 interspace, with disc space widening of approximately 1.5 cm (red arrow). There is also an associated fracture through the superior endplate of C7 extending

through the posterior elements (blue arrow), with grade 1 retrolisthesis at C6/C7. Axial image (**b**) displays complete occlusion of the left vertebral artery at the level of injury (red arrows)

exerted by the trapezius and rhomboid muscles on the spinous processes of the lower cervical and upper thoracic vertebrae [46]. It is associated with direct trauma to the posterior aspect of the neck or cervical hyperflexion and hyperextension injuries following acute trauma. The avulsed spinous process fragment becomes dislocated inferiorly and posteriorly. It is one of the more readily missed fractures on cervical radiography due to obscuration by the patient's shoulders, and CT should be obtained in the setting of acute trauma [47]. On an AP view, it manifests as misalignment of the spinous processes. On a lateral view, the fracture can usually be seen, which results in the downward and posterior dislocation of the fractured fragment. It is considered to be a stable injury, and treatment usually consists of 4–6 weeks of immobilization [48].

3.9.2 Extension Injuries

Extension injuries account for fewer than 25% of the cervical spine injuries [23]. Predisposing factors include senile and intoxicated patients who may have impaired ability to break a fall and baseline rigid spine diseases [49, 50]. The mechanism of injury includes hyperextension with axial compression or rotation. The traumatic force is directed through the posterior column, which results in a spectrum of injuries including sprain, ligamentous rupture, and fractures [49, 50].

3.9.2.1 Hyperextension Sprain Dislocation

Hyperextension sprain dislocation is seen in patients with head trauma and assaults [51]. The injury begins with disruption of anterior longitudinal ligament, resulting in widening of the anterior disc space [23]. With increasing force, the intervertebral disc and posterior ligaments can rupture. The vertebral body may translate posteriorly, causing neurological compromise [24]. A high-velocity trauma may cause ligamentous damage in the middle column as well, resulting in dislocation of the vertebral body a level above the injury [40].

Pitfalls Middle column ligamentous injuries, even without evidence of dislocation on initial CT, should be reduced immediately. A high index of suspicion should be maintained based on the mechanism of injury, to warrant further evaluation by MR imaging [40].

3.9.2.2 Hyperextension Fracture Dislocation

When there is a severe hyperextension force applied to the cervical spine, there is posterior dislocation of the vertebral body causing spinal cord compression. This is known as hyperextension fracture dislocation. In this fracture pattern, the ALL, annulus fibrosis, intervertebral disc, PLL, and ligamentum flavum are all disrupted. In approximately two-thirds of the patients, there is also an associated bony fragment due to the avulsion of the intact annulus fibrosis on the anterior-inferior endplate of the vertebral body. In contrast with the "teardrop" fragments, the bony fragments produced in hyperextension fracture dislocations are longer in the horizontal dimension than in the vertical dimension. The injury is often accompanied with central cord syndrome and neurological deficits, ranging from upper extremity weakness to complete quadriplegia [22].

Senile and rigid spines (AS, DISH) are prone to undergo hyperextension fracture-dislocation [23]. The rigid spine behaves like a solid continuous pipe, with fractures extending through the anterior bridging osteophytes and/or the fused anterior spine, with asymmetric widening of the anterior disc space, and fracture lines traversing into the adjacent vertebrae and posterior elements [52] (Fig. 3.16).

Pitfalls Because the alignment of the involved spinal segments often returns to neutral position after the impact force is removed, the extent of hyperextension fracture dislocation can be underestimated on CT. The injury should be suspected when there is normal alignment of the vertebral body with extensive prevertebral soft-tissue swelling, and MRI should be obtained to detect the extent of spinal cord involvement [22]. Nondisplaced subtle bone fragments in rigid spines
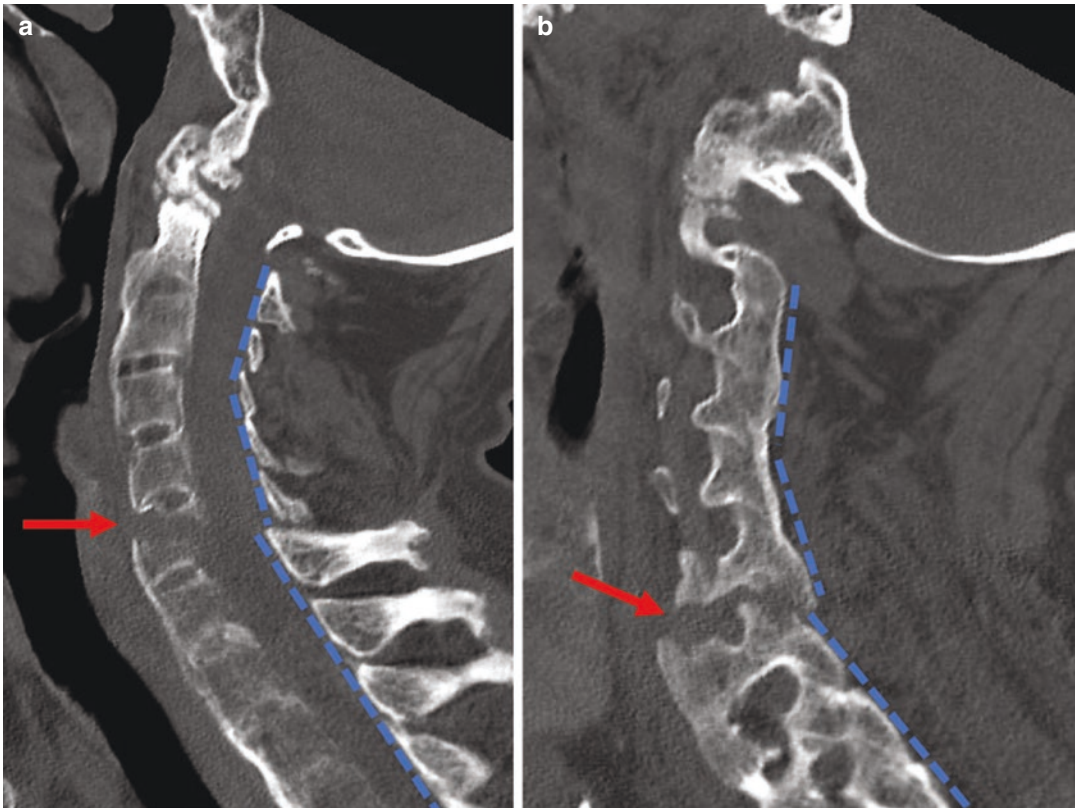
Fig. 3.16 Extension fracture dislocation in a 62-year-old man with ankylosing spondylitis. (**a**) Sagittal and (**b**) parasagittal CT cervical spine images show a fracture through an anterior bridging osteophyte and a fused facet joint (red arrows), with disruption of the anterior and posterior spinal lines (not outlined) and of the spinolamellar line (dotted blue line)

are difficult to assess on in the axial plane because of the horizontal configuration. Sagittal CT reconstructed images should be used [40].

3.9.2.3 Extension-Teardrop Fracture

Similar to flexion-teardrop fractures, extension-teardrop fractures result in the production of anterior-inferior corner "teardrop" fragments. However, in extension teardrop, this is due to avulsion injury, whereby the anterior longitudinal ligament (ALL) pulls away a bone fragment from the lower aspect of the vertebral body in the context of forced extension and rotation [52]. There may also be associated intervertebral disc space widening. Although unstable in extension, extension-teardrop fractures are relative stable in flexion, and can be treated with immobilization in cervical collars [23].

Pitfalls Extension teardrop fractures commonly involve the C2 vertebrae, whereas the location for the flexion-teardrop fractures is usually at C5 and C6 [40]. In contrast to flexion-teardrop fractures, the PLL and the PLC are usually intact in extension-teardrop fractures.

3.10 Limitations of Multi-detector CT

Multi-detector CT (MDCT) is considered the initial modality of choice for the assessment of cervical spine injuries. However, MDCT is limited in determining important factors affecting management including ligamentous details, spinal cord injury (edema, contusion, or hemorrhage), and epidural hematomas. MRI is complementary

to initial CT scan to assess abovementioned spectrum of injury.

3.11 Magnetic Resonance Imaging

MRI of the cervical spine is usually performed with head and neck coils to allow for the best spatial and contrast resolution. It should include axial T2-weighted and T2-weighted gradient-recalled echo (GRE) sequences, sagittal T1-weighted, T2-weighted and T2-weighted GRE fat-saturated sequences, and short-tau inversion recovery (STIR) sequences, which provides fat suppression [53]. T1-weighted images are useful for identifying osseous abnormalities. T2-weighted images are used to identify spinal cord edema, and T2-weighted GRE sequences are used to detect hemorrhage surrounding the spinal cord. STIR can be very sensi-

tive for revealing soft-tissue and ligamentous injuries (Fig. 3.17). A normal cervical spine MRI sequence is shown and is described in Fig. 3.2.

MRI is often the confirmatory imaging modality for visualizing injuries to the soft tissues, which includes ligaments, spinal cord, vasculature, and intervertebral discs. MRI is indicated when there are neurological deficits or there is clinical suspicion for vascular abnormalities following cervical trauma. It should be obtained within 72 h after an acute injury, as post-traumatic edema increases the conspicuity of ligaments which are normally seen as low-signal structures [53].

3.12 Spinal Cord Injuries

The evaluation for the integrity of the spinal cord is the most important indication for the use of MRI following acute cervical spine trauma.
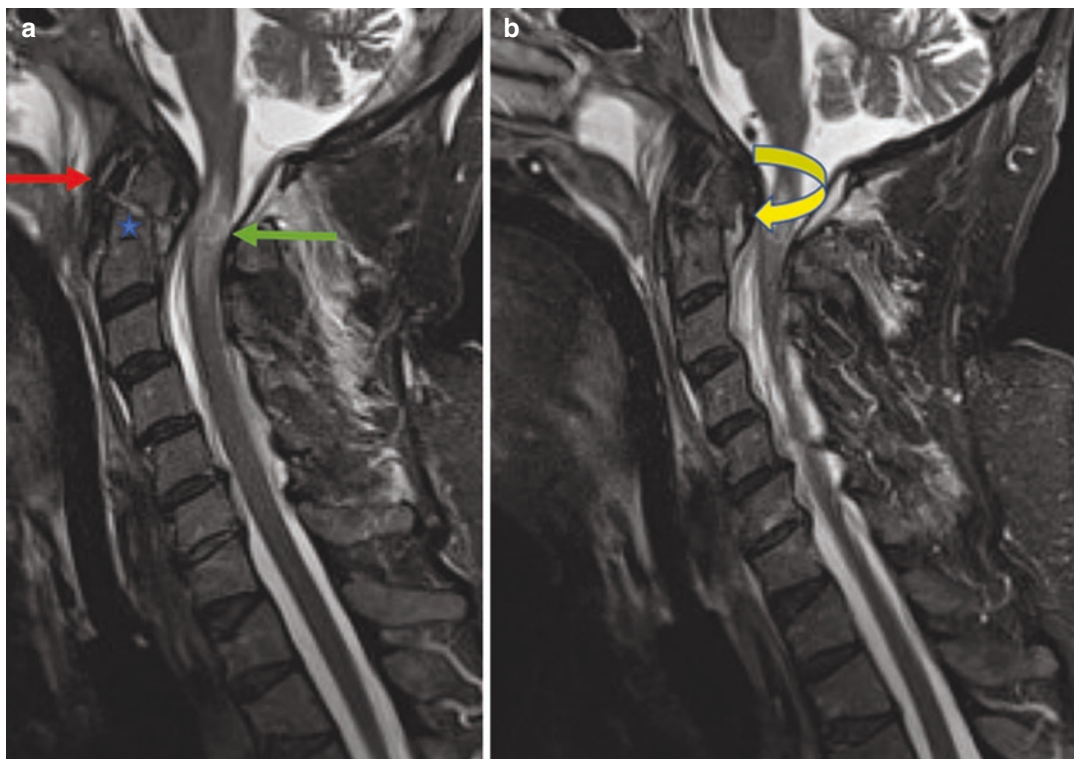
Fig. 3.17 (**a**, **b**) Sagittal T2-weighted fat-suppressed MR cervical spine images show disruption of the anterior longitudinal (red arrow) and posterior longitudinal ligaments (curved yellow arrow), with edema. Hyperintense intra-medullary signal suggests cord edema at the level of C2 (green arrow) due to an associated odontoid process fracture (blue star)

Selden et al. identified four findings which are associated with a worse prognosis [54]: (1) the presence of intra-axial hematoma, (2) the extent of spinal cord hematoma, (3) the extent of spinal cord edema, and (4) spinal cord compression by extra-axial hematoma and/or intervertebral discs.

Cord edema appears as abnormal hyperintense signals on T2-weighted sequences (Fig. 3.17). Cord hemorrhage appears as hypointense signal surrounded by a thin rim of hyperintense signal. The degree of cord compression can be estimated by comparison with the diameter of the nearest normal spinal cord, and greater compression is associated with a worse prognosis [55, 56].

Spinal cord injury can be classified into complete and incomplete cord injuries. Complete spinal cord injury results in loss of all motor and sensory functions below the level of injury. It is a rare type of injury, which occurs following extreme distraction and penetrating injuries. MRI demonstrates complete cord transection of the spinal cord, with hyperintense cerebrospinal fluid occupying the intramedullary space, as is seen on T2-weighted images [56].

Traumatic central cord syndrome is the most common incomplete spinal cord injury. It presents with disproportionate motor and sensory deficits in the upper extremities compared to the lower extremities. Elderly patients who have baseline degenerative changes are more likely to be affected, as osteophytes and buckled ligamentum flavum can compress the central gray matter in the setting of hyperflexion injuries [54]. On MRI, this manifests as intramedullary hyperintense signal on T2-weighted images.

Prevertebral hyperintensity and disruption of the posterior ligaments, which are associated with spinal instability, suggest a worse prognosis [57]. Other signs of spinal instability include angular displacement >12° and vertebral body translation >3.5 mm on cervical radiographs [25]. Although most patients with central cord syndrome can be treated with supportive measures, patients who demonstrate spinal instability require surgical decompression and spinal fixation to prevent delayed cord compromise [58].

Anterior cord syndrome is caused by occlusion in the anterior spinal artery, which results in ischemia of the anterior two-thirds of the spinal cord. Patients present with motor paralysis, as well as loss of pain and temperature below the level of the injury due to infarcted corticospinal and spinothalamic tracts. Touch and proprioception usually remains intact due to preserved dorsal column, which is supplied by the posterior spinal artery. On MRI, this syndrome has a characteristic "owl-eye" pattern, which consists of bilateral foci of hyperintense T2-weighted signal in the anterior horn of the spinal cord [59]. Brown-Sequard syndrome results from rotational injuries or penetrating trauma, which causes hemisection of the spinal cord, and manifests with ipsilateral motor and contralateral sensory deficits. Posterior cord syndrome is a rare spinal cord injury which results from insult to the posterior column of the spinal cord or an occlusion of the posterior spinal artery. MRI shows hyperintense T2-weighted signals in the posterior columns, which is consistent with cord edema and infarction in the area [60].

3.13 Spinous Ligamentous Injuries

On MRI, ligaments appear as linear, low-signal intensity structures. Hyperextension injuries may result in disruption to the anterior column or to both the anterior and middle columns. Hyperflexion injuries may result in disruption to the posterior and middle columns. If two adjacent columns are disrupted, the cervical spine will be unstable [61]. Injuries to the spinal ligaments are visualized as focal disruptions to the low-signal ligaments, with edema best seen on a STIR sequence [53] (Fig. 3.17).

3.14 Traumatic Disc Injuries

Traumatic disc herniations are often associated with unstable cervical spine injuries and occur in association with fracture subluxation or hyperflexion injuries (particularly in flexion-dislocation or flexion-compression injuries) [61]. They result from injuries to the annulus fibrosis, which causes nucleus pulposus extrusion, and may lead to compression of the spinal cord.
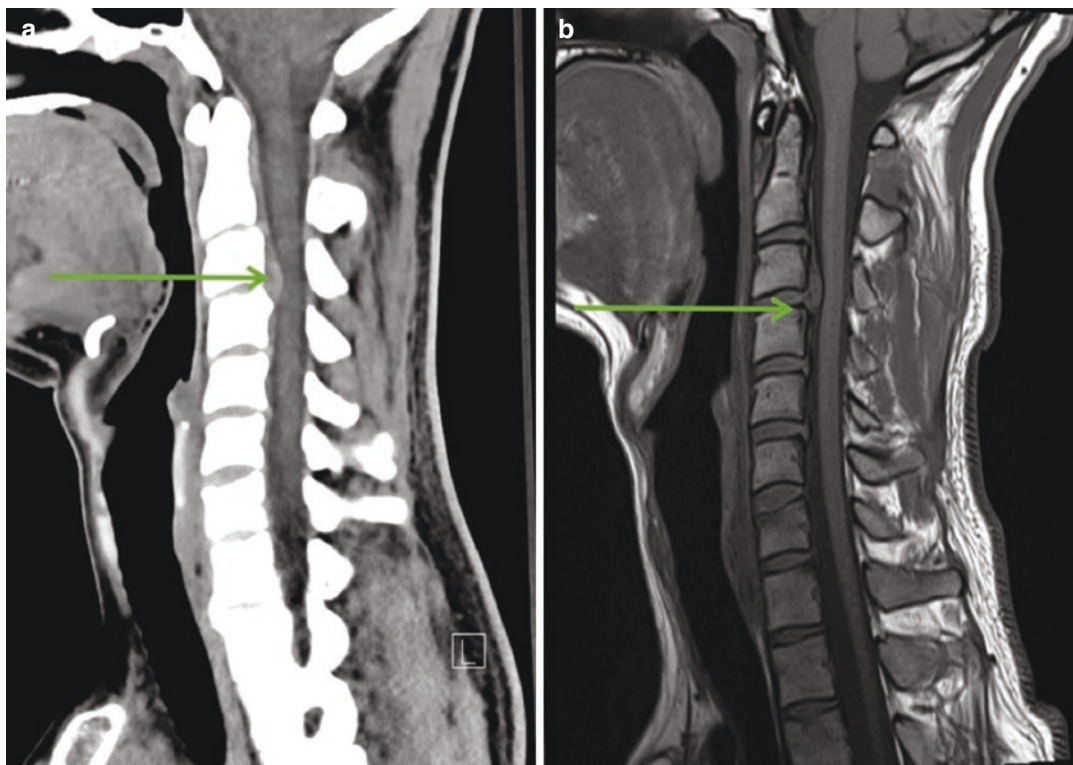
Fig. 3.18 27 year-old male with history of fall to the ground during a soccer game. (**a**) Sagittal CT cervical spine image in soft-tissue window and (**b**) sagittal T1W

MR image display post-traumatic disc protrusion at C2/C3 (green arrows)

Narrowing of the intervertebral disc space seen on radiographs or CT may increase the suspicion for disc herniation, and may warrant further investigation by MRI (Fig. 3.18). It is important to confirm the diagnosis as occult disc herniations may further lead to neurological compromise [62]. Pre-reduction MRI to exclude traumatic disc herniation should be obtained before attempting closed traction or open posterior reduction of cervical fractures to avoid further neurological deterioration [63].

3.15   Newer Techniques

Cervicothoracic junction injuries are the second most common cervical spine injuries after atlantoaxial joint injuries and can result in significant morbidity and mortality if the diagnosis is missed or delayed [64]. Therefore, optimization

of spinal canal soft-tissue detail at the cervicothoracic junction is crucial in assessment of trauma patients. Evaluation of the cervicothoracic junction is frequently limited by beam hardening and scatter radiation artifacts, due to photon depletion and hardening of the normally utilized polychromatic X-ray beam. The following newer CT techniques can be helpful for improved visualization of cervicothoracic junction abnormalities.

3.16   C-Spine Imaging with Tin Filter

Cervical spine imaging at 140 kV with a tin filter can provide superior details at the cervicothoracic junction, by reducing the lower energy X-rays, thus minimizing the beam hardening and scatter radiation artifacts (Fig. 3.19).
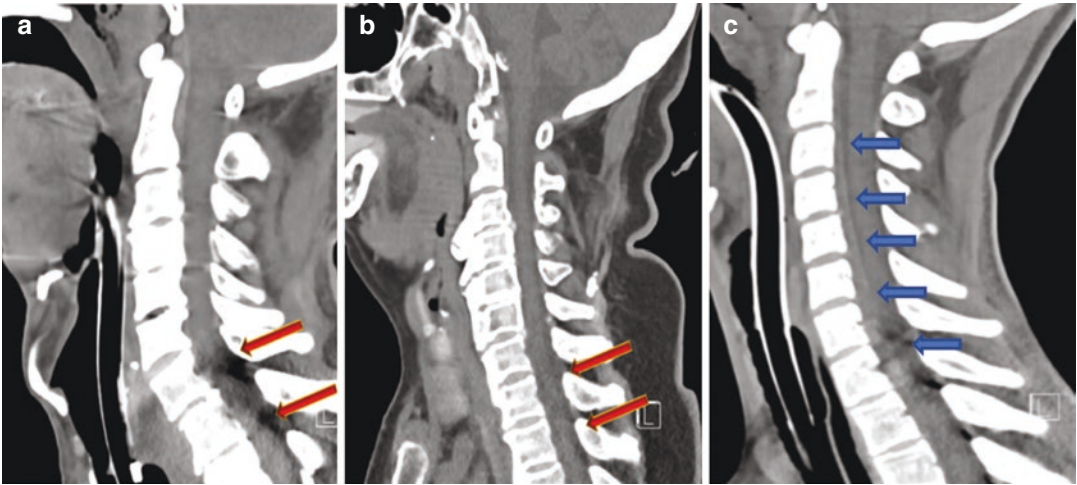
Fig. 3.19 Sagittal cervical spine CT reformations at (**a**) 120 kV and (**b**) 140 kV with tin filter imaging, depicting superior spinal canal soft-tissue details, especially at cervicothoracic junction. (**c**) Sagittal cervical spine CT refor- mation of a different patient with tin filter imaging displays an acute hematoma extending posterior to C2 through to the cervicothoracic junction
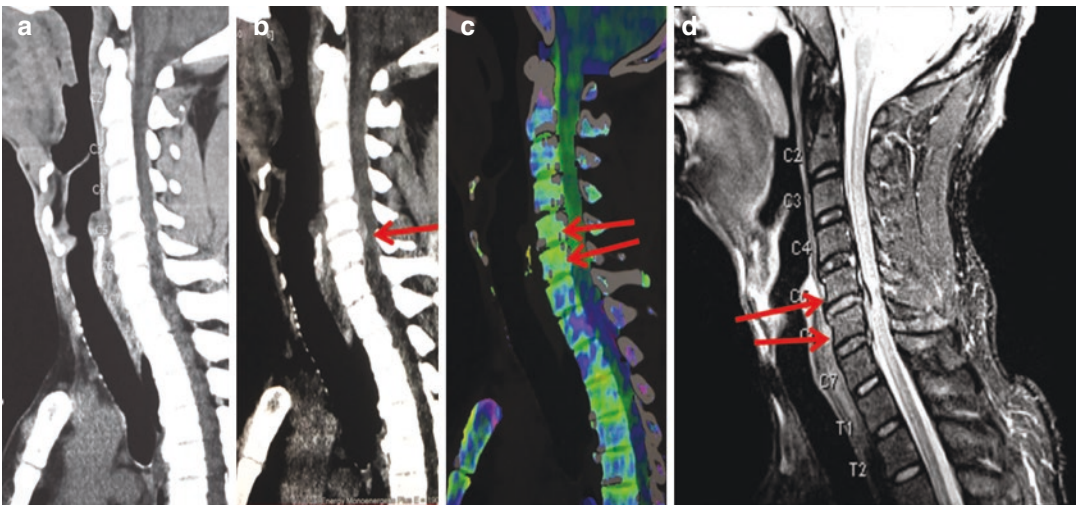
Fig. 3.20 Monoenergetic sagittal cervical spine CT reformations acquired at (**a**) 120 kV and (**b**) 190 kV, the latter of which provides superior imaging details for identifying the epidural hematoma. Virtual non-calcium (VNCa) image (**c**) of the same patient shows associated bone marrow edema displayed in green (red arrows) in the fifth and sixth cervical vertebrae, with no fracture identified on source images. (**d**) Sagittal T2 STIR MR image shows similar altered signals indicative of acute fractures

3.17 Dual-Energy Imaging

Dual-energy CT (DECT) provides image recon- struction at different energy levels with a monoen- ergetic post-processing algorithm (Monoplus) enabling increased attenuation at simultaneously low image noise, by reducing the beam hardening and scatter radiation artifacts [64] (Fig. 3.20).

3.18 Dual-Energy Virtual Non-calcium Imaging with Bone Marrow Edema

Dual-energy CT (DECT) imaging with a virtual non-calcium (VNCa) technique based on information of mass attenuation coefficients at different energy levels can be used to depict bone marrow edema in cervical spine in patients with acute trauma and can improve detection of acute vertebral fractures [65] (Fig. 3.20).

3.19 Conclusion

Prompt and correct identification and classification of cervical spine injury is imperative to patient management in acute trauma. Multi-detector CT has become the standard of care for evaluating blunt cervical spine trauma. A systematic approach for evaluating the cervical spine is key to accurate radiologic and clinical diagnosis. Understanding the mechanism-based classic patterns of the cervical spine injury can be helpful to an extent. However, it is important to realize that in severe poly-trauma, these patterns may be difficult to appreciate, as patients may be subjected to two or more vector forces (i.e., a whiplash injury involving both hyperflexion and hyperextension forces). Having a high radiologic and clinical key index of suspicion based on mechanism of injury, associated stigmata, and baseline predisposing risk factors, including senile or rigid spine, is crucial to correctly suspect and then identify the potential spectrum of injuries. Supplementing MDCT with CT angiography in suspected vascular injuries and MR imaging in obtunded patients, and in potential ligamentous and spinal cord injuries, should be deemed necessary.

References

1. Centers for Disease Control and Prevention. National Hospital ambulatory medical care survey. Atlanta, GA: Centers for Disease Control and Prevention; 2015.

2. Sheikh K, Belfi LM, Sharma R, et al. Evaluation of acute cervical spine imaging based on ACR Appropriateness Criteria®. Emerg Radiol. 2012;19(1):11–7.

3. Munera F, Rivas LA, Nunez DB, et al. Imaging evaluation of adult spinal injuries: emphasis on multidetector CT in cervical spine trauma. Radiology. 2012;263(3):645–60.

4. Berlin L. Radiologic errors and malpractice: a blurry distinction. Am J Roentgenol. 2007;189(3):517–22.

5. Pinto A, Reginelli A, Pinto F, et al. Errors in imaging patients in the emergency setting. Br J Radiol. 2016;89(1061):20150914.

6. Triantopoulou C, Tsalafoutas I, Maniatis P, et al. Analysis of radiological examination request forms in conjunction with justification of X-ray exposures. Eur J Radiol. 2005;53(2):306–11.

7. Kim YW, Mansfield LT. Fool me twice: delayed diagnoses in radiology with emphasis on perpetuated errors. Am J Roentgenol. 2014;202(3):465–70.

8. Krupinski EA, Berbaum KS, Caldwell RT, et al. Long radiology workdays reduce detection and accommodation accuracy. J Am Coll Radiol. 2010;7(9):698–704.

9. Renfrew DL, Franken EA, Berbaum KS, et al. Error in radiology: classification and lessons in 182 cases presented at a problem case conference. Radiology. 1992;183(1):145–50.

10. Bruno MA, Walker EA, Abujudeh HH. Understanding and confronting our mistakes: the epidemiology of error in radiology and strategies for error reduction. Radiographics. 2015;35(6):1668–76.

11. Hoffman JR, Mower WR, Wolfson AB, et al. Validity of a set of clinical criteria to rule out injury to the cervical spine in patients with blunt trauma. National Emergency X-Radiography Utilization Study Group. N Engl J Med. 2000;343(2):94–9.

12. Stiell IG, Wells GA, Vandemheen KL, et al. The Canadian C-spine rule for radiography in alert and stable trauma patients. JAMA. 2001;286(15):1841–8.

13. Stiell IG, Clement CM, McKnight RD, et al. The Canadian C-spine rule versus the NEXUS low-risk criteria in patients with trauma. N Engl J Med. 2003;349(26):2510–8.

14. Stiell IG, Clement CM, O'Connor A, et al. Multicentre prospective validation of use of the Canadian C-Spine Rule by triage nurses in the emergency department. CMAJ. 2010;182(11):1173–9.

15. Stiell IG, Clement CM, Grimshaw J, et al. Implementation of the Canadian C-Spine Rule: prospective 12 centre cluster randomised trial. BMJ. 2009;339:b4146.

16. Paykin G, O'Reilly G, Ackland HM, et al. The NEXUS criteria are insufficient to exclude cervical spine fractures in older blunt trauma patients. Injury. 2017;48(5):1020–4.

17. Daffner RH. Helical CT of the cervical spine for trauma patients: a time study. Am J Roentgenol. 2001;177(3):677–9.

18. Daffner RH, Weissman BN, Wippold FJ II, Angtuaco EJ, et al. Expert panels on musculoskeletal and neurologic imaging. ACR Appropriateness Criteria® suspected spine trauma. Reston, VA: American College of Radiology; 2012.

19. Becce F, Ben Salah Y, Verdun FR, et al. Computed tomography of the cervical spine: comparison of image quality between a standard-dose and a low dose protocol using filtered back-projection and iterative reconstruction. Skeletal Radiol. 2013;2(7):937–45.

20. Sliker CW. Blunt cerebrovascular injuries: imaging with multidetector CT angiography. Radiographics. 2008;28(6):1689–708. discussion 1709–1710.

21. Burlew CC, Biffl WL, Moore EE, Barnett CC, Johnson JL, Bensard DD. Blunt cerebrovascular injuries: redefining screening criteria in the era of noninvasive diagnosis. J Trauma Acute Care Surg. 2012;72(2):330–5. discussion 336–337.

22. White AA, Panjabi MM. Clinical biomechanics of the spine. 2nd ed. Philadelphia, PA: Lippincott; 1990.

23. Schwartz ED, Flanders AE. Spinal trauma: imaging, diagnosis, and management. Philadelphia, PA: Lippincott Williams & Wilkins; 2007.

24. Denis F. Spinal stability as defined by the three-column spine concept in acute spinal trauma. Clin Orthop Relat Res. 1984;Oct(189):65–76.

25. Daffner RH, Deeb ZL, Rothfus WE. "Fingerprints" of vertebral trauma-a unifying concept based on mechanism. Skeletal Radiol. 1986;15(7):518–25.

26. Dvorak MF, Fisher CG, Fehlings MG, et al. The surgical approach to subaxial cervical spine injuries: an evidence-based algorithm based on the SLIC classification system. Spine. 2007;32(23):2620–9.

27. Holmes JF, Akkinepalli R. Computed tomography versus plain radiography to screen for cervical spine injury: a meta-analysis. J Trauma. 2005;58(5):902–5.

28. Berquist TH. Imaging of adult cervical spine trauma. Radiographics. 1988;8(4):667–94.

29. Banerjee A, Clayton-Jolly A, Mbamalu D. The radiological assessment of injuries to the atlanto-axial-occipital complex (C1 and C2 vertebrae). Trauma. 2008;10(4):231–8.

30. Rojas CA, Bertozzi JC, Martinex CR, et al. Reassessment of the craniocervical junction: normal values on CT. Am J Neuroradiol. 2007;28(9):1819–23.

31. Green JD, Harle TS, Harris JH Jr. Anterior subluxation of the cervical spine: hyperflexion sprain. Am J Neuroradiol. 1981;2(3):243–50.

32. Smoker WR. Craniovertebral junction: normal anatomy, craniotomy, and congenital anomalies. Radiographics. 1994;14(2):255–77.

33. Chang W, Alexander MT, Mirvis SE. Diagnostic determinants of craniocervical distraction injury in adults. Am J Roentgenol. 2009;192(1):52–8.

34. Hanson JA, Deliganis AV, Baxter AB, et al. Radiologic and clinical spectrum of occipital condyle fractures: retrospective review of 107 consecutive fractures in 95 patients. AJR Am J Roentgenol. 2002;178(5):1261–8.

35. Leone A, Cerase A, Colosimo C, Lauro L, Puca A, Marano P. Occipital condylar fractures: a review. Radiology. 2002;2016(3):635–44.

36. Anderson PA, Montesano PX. Morphology and treatment of occipital condyle fractures. Spine (Phila Pa 1976). 1988;13(7):731–6.

37. Gehweiler JA Jr, Duff DE, Martinex S, Miller MD, Clark WM. Fractures of the atlas vertebra. Skeletal Radiol. 1976;1(2):97–102.

38. Anderson LD, D'Alonxo RT. Fractures of the odontoid process of the axis. J Bone Joint Surg Am. 1974;56(8):1663–74.

39. Junewick JJ. Pediatric craniocervical junction injuries. Am J Roentgenol. 2011;196(5):1003–10.

40. Dreizin D, Michael L, Sliker CW, Chokshi FH, Bodanapally U, Mirvis S, et al. Multidetector CT of blunt cervical spine trauma in adults. Radiographics. 2014;34(7):1842–65.

41. Levine AM, Edwards CC. Fractures of the atlas. J Bone Joint Surg Am. 1991;73(5):680–91.

42. Hagedorn JC II, Emery SE, France JC, et al. Does CT angiography matter for patients with cervical spine injuries? J Bone Joint Surg Am. 2014;96(11):951–5.

43. Rankine JJ. Spinal trauma. In: Adam A, editor. Grainger & Allison's diagnostic radiology. 6th ed. London: Churchill Livingstone Elsevier; 2015. p. 1374–89.

44. Raniga SB, Menon V, Al Muzahmi KS, et al. MDCT of acute subaxial cervical spine trauma: a mechanism-based approach. Insights Imaging. 2014;5(3):321–38.

45. Kim KS, Chen HH, Russell EJ, et al. Flexion teardrop fracture of the cervical spine: radiographic characteristics. Am J Roentgenol. 1989;152(2):319–26.

46. Posthuma de Boer J, van Wulfften Palthe AF, Stadhouder A, et al. The clay shoveler's fracture: a case report and review of the literature. J Emerg Med. 2016;51(3):292–7.

47. Lin JT, Lee JL, Lee ST. Evaluation of occult cervical spine fractures on radiographs and CT. Emerg Radiol. 2003;10(3):128–34.

48. Han SR, Sohn MJ. Twelve contiguous spinous process fracture of cervicothoracic spine. Korean J Spine. 2014;11(3):212–3.

49. Regenbogen VS, Rogers LF, Atlas SW, et al. Cervical spine cord injuries in patients with cervical lordosis. Am J Roentgenol. 1986;146(2):277–84.

50. Scher AT. Hyperextension trauma in the elderly: an easily overlooked spinal injury. J Trauma. 1983;23(12):1066–8.

51. Edeiken-Monroe B, Wagner LK, Harris JHJ. Hyperextension dislocation of the cervical spine. Am J Roentgenol. 1986;146(4):803–8.

52. Daffner RH, Daffner SD. Vertebral injuries: detection and implications. Eur J Radiol. 2002;42(2):100–16.

53. Kumar Y, Hayashi D. Role of magnetic resonance imaging in acute spinal trauma: a pictorial review. BMC Musculoskelet Disord. 2016;17:310–41.

54. Selden NR, Quint DJ, Patel N, et al. Emergency magnetic resonance imaging of cervical spinal cord inju-

ries: clinical correlation and prognosis. Neurosurgery. 1999;44(4):785–92. discussion 792–783.

55. Chandra J, Sheerin F, Lopez de Heredia L, et al. MRI in acute and subacute post-traumatic spinal cord injury: pictorial review. Spinal Cord. 2012;50(1):2–7.

56. Song J, Mizuno J, Inoue T, et al. Clinical evaluation of traumatic central cord syndrome: emphasis on clinical significance of prevertebral hyperintensity, cord compression, and intramedullary high-signal intensity on magnetic resonance imaging. Surg Neurol. 2006;65(2):117–23.

57. Wu SK, Kuo LC, Lan HC, et al. The quantitative measurements of the intervertebral angulation and translation during cervical flexion and extension. Eur Spine J. 2007;16(9):1435–44.

58. Molliqaj G, Payer M, Schaller K, et al. Acute traumatic central cord syndrome: a comprehensive review. Neurochirurgie. 2014;60(1-2):5–11.

59. Harada K, Chiko Y, Toyokawa T. Anterior spinal cord syndrome-"owl's eye sign". J Gen Fam Med. 2018;19(2):63–4.

60. Matsubayashi J, Tsuchiya K, Shimizu S, et al. Posterior spinal artery syndrome showing marked swelling of the spinal cord: a clinico-pathological study. J Spinal Cord Med. 2013;36(1):31–5.

61. Pratt ES, Green DA, Spengler DM. Herniated intervertebral discs associated with unstable spinal injuries. Spine (Phila Pa 1976). 1990;15(7):662–6.

62. Harrington JF, Likavec MJ, Smith AS. Disc herniation in cervical fracture subluxation. Neurosurgery. 1991;29(3):374–9.

63. Hadley MN, Walters BC, Grabb BC, et al. Initial closed reduction of cervical spine fracture-dislocation injuries. Neurosurgery. 2002;50(3 Suppl):S44–50.

64. Andreas C, Johannes H, Christoph O, Christian W, Stefan U, Lukas E. CT dose and image quality in the last three scanner generations. World J Radiol. 2013;5(11):421–9.

65. Piazzolla A, Solarino G, Lamartina C, et al. Vertebral bone marrow edema (VBME) in conservatively treated acute vertebral compression fractures (VCFs): evolution and clinical correlations. Spine. 2015;40(14):E842–8.

Errors in Imaging of Thoracic Trauma

4

Ashwin Jain, John Lee, David Dreizin, Gene Kim, and Christina A. LeBedis

4.1 Introduction

Approximately 25% of trauma-related deaths are secondary to thoracic injuries [1]. Thoracic trauma is categorized into two major categories, blunt and penetrating trauma. Blunt trauma makes up an estimated 90% of chest trauma-related cases, with penetrating trauma being less common [1]. The estimated overall fatality rate of thoracic trauma is approximately 10%, which is highest in those with tracheobronchial-esophageal or cardiac-related injuries [2]. In patients with multi-systemic trauma (i.e., abdominal, vascular, extremity), the presence of thoracic injuries increases the overall mortality rate. In developed countries, over 66% of blunt thoracic trauma is secondary to motor vehicle collisions, with falls and blows from non-penetrating objects making up the remaining cases [2]. Understanding and knowing the mechanism of blunt or penetrating trauma are vital for diagnosis and utilizing the correct type of imaging. Although all structures should be closely examined, being able to tailor the radiologist's search pattern for primary injuries and associated related injuries is very important to ensure accurate and efficient diagnosis.

Conventional radiography remains the first initial examination in thoracic trauma, regardless of whether or not computed tomography (CT) is to be performed [2]. Portable chest radiographs allow for the detection of tension pneumothorax, large hemothorax, tube or line mispositioning, and other conditions which require emergent treatment [2]. Other thoracic trauma-related injuries, including small pleural injuries, parenchymal lung contusion/laceration, minimal aortic injury, cardiac injuries, small diaphragmatic injuries, and other skeletal-related fractures require further evaluation with CT. Management in approximately 20% of thoracic trauma patients with abnormal initial radiographs is changed due to CT findings [2]. Multi-detector CT (MDCT) has become increasingly used for imaging in thoracic trauma and has helped to markedly reduce the number of catheter aortographic examinations necessary to detect and characterize thoracic aortic injury [2]. This technology has allowed trauma physicians to decide whether patients should be managed conservatively, sent for exploration, or referred to interventional radiology [3].

Disclosure: The authors have no relevant financial disclosures related to this topic.

A. Jain (✉) · J. Lee · G. Kim · C. A. LeBedis
Department of Radiology, Boston University Medical Center, Boston University School of Medicine, Boston, MA, USA
e-mail: ashwin.jain@bmc.org;
Christina.LeBedis@bmc.org

D. Dreizin
Diagnostic Radiology and Nuclear Medicine, Department of Radiology, University of Maryland Medical Center, University of Maryland School of Medicine, Baltimore, MD, USA
e-mail: ddreizin@umm.edu

4.2 MDCT

MDCT is crucial in the assessment of the acutely injured patient, as it provides rapid image acquisition with essentially isotropic voxels. Although there is no standard protocol for trauma computed tomography (CT) in North America to our knowledge, there are two commonly used techniques: whole-body CT angiogram (CTA) and the segmental CT scanning approach. The whole-body CTA technique employs a CTA of the chest, abdomen, and pelvis, followed by a portal venous-phase acquisition through the abdomen and pelvis. The drawback of this approach is the increased radiation dose due to scan overlap. In the segmental CT scanning technique, a CTA of the chest through the entire spleen is acquired, followed by portal venous-phase imaging through the abdomen and pelvis. The drawback of this approach is the lack of an arterial phase in the lower abdomen and pelvis. Optional delayed phase (at approximately 5 min) images can be obtained with either imaging protocol at the discretion of the radiologist, through an area of suspected positive findings.

Torso trauma imaging includes a single 100 mL bolus of iodinated contrast injected through at least a 20-gauge intravenous catheter at 3–5 mL/s. A 30 mL saline chaser bolus is then administered. The CTA acquisition is performed with a 30-s delay, while the portal venous phase is obtained at 70 s. At the author's institutions, axial reconstructions are obtained with 1.25 and 3.75 mm slice thickness. Coronal and sagittal 2.5 mm reformations are imperative for injury detection and troubleshooting [3].

4.3 Aortic Injury

4.3.1 Acute Traumatic Aortic Injury

The prompt diagnosis of acute traumatic aortic injury (ATAI) by the radiologist is crucial in order to facilitate the proper next steps by the primary clinical team, given the 70–90% survival rate for those patients who reach the hospital alive and undergo repair [4]. Acute traumatic aortic injury can be classified by specific location: intrapericardial/ascending aorta, aortic arch, and descending aorta [4]. Since the clinical signs of ATAI are non-specific, diagnosis relies heavily on imaging. Angiography was previously considered the imaging reference standard for evaluating the aorta and great vessels; however, CTA with or without three-dimensional reconstructions has nearly completely replaced catheter angiography [5–7, 31].

Chest radiograph findings which should raise suspicion for ATAI include mediastinal widening, indistinct aortic contour (with loss of the normal interface with the lung and aorticopulmonary window), depression of the left mainstem bronchus, tracheal deviation, nasogastric tube deviation rightward of the T3 or T4 spinous processes, and increased density of the left subclavian artery reflection [4]. Although these relatively non-specific radiographic findings may represent sequelae of other complications of blunt or penetrating trauma, any suspicion for ATAI warrants further investigation with CT.

On CT there are several indirect and direct signs the radiologist should be aware of. One of the main indirect signs of ATAI is a mediastinal hematoma abutting the aorta (hyperattenuating material measuring 40–70 HU) which displaces the normal mediastinal fat and results in the absence of the normal fat plane-vessel distinction (Fig. 4.1) [4]. If the mediastinal hematoma does not abut the aorta, then it does not represent an indirect sign of ATAI but instead may represent venous bleeding or complication from an adjacent fracture. One misconception regarding mediastinal hematoma is that it is thought to be the result from blood extravasation from the vessel lumen. In actuality, the mediastinal hematoma is instead more likely from avulsed perivascular veins or from the arterial vaso vasorum [4]. Additionally, the absence of contrast extravasating into the mediastinal hematoma does not exclude aortic injury.

Direct signs of ATAI on CT include disruption of the aortic wall (focal wall outpouching, contour irregularity, or contrast extravasation from aorta into adjacent mediastinal hematoma), intraluminal thrombus (resulting from luminal wall injury forming a nidus for thrombus), and abrupt caliber change (from blood within the vessel wall or mass effect from adjacent hematoma) (Fig. 4.2). Regarding penetrating trauma,
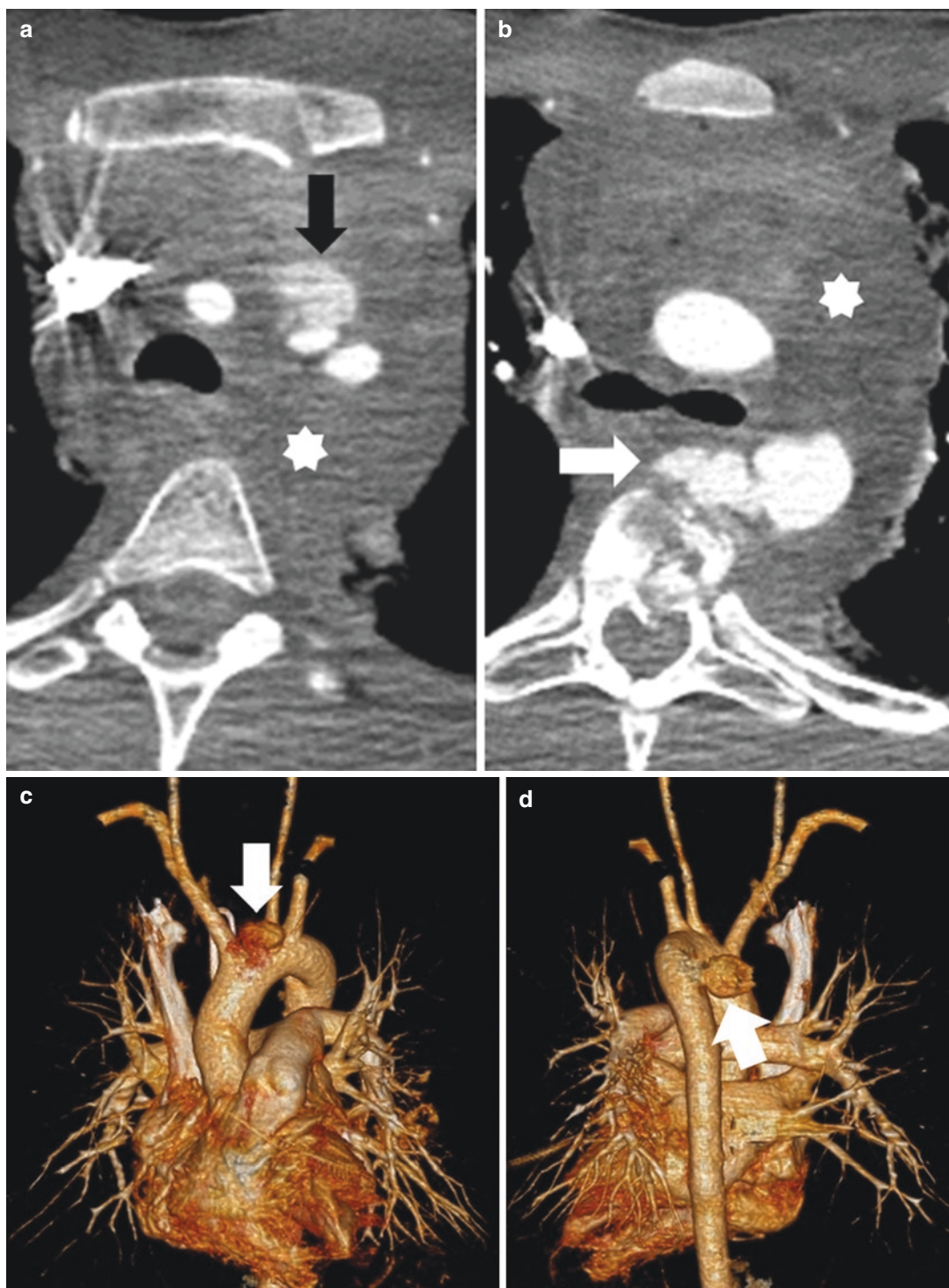
Fig. 4.1 Nineteen-year-old man presenting after a gunshot wound to the thoracic aorta and spine. Axial IV contrast-enhanced CT image (**a**, **b**) show active extravasation of contrast from the aortic arch/left common carotid artery junction (black arrow), contained rupture of the descending aorta with pseudoaneurysm (white arrow), and mediastinum hematoma (asterisks). 3D reformatted images demonstrate the aortic arch injury (**c**, arrow) and descending thoracic aortic injury (**d**, arrow) to better advantage. Sagittal IV contrast-enhanced CT images (**e**, **f**) again demonstrate these injuries, as well as fracture of the manubrium and T5/T6 vertebral bodies with bone/bullet fragments within the thoracic spinal canal (arrows). The patient survived, underwent an emergent thoracic endovascular aortic repair, and was planned for spinal fusion
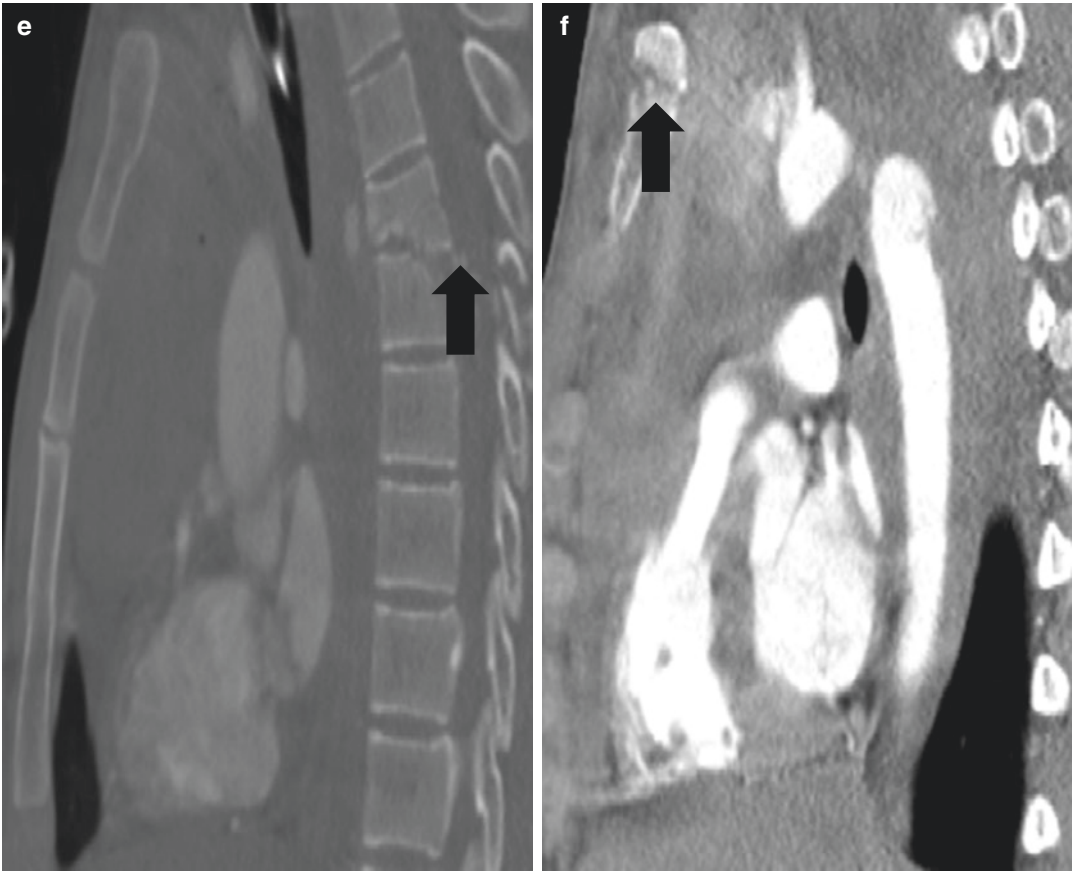
Fig. 4.1 (continued)
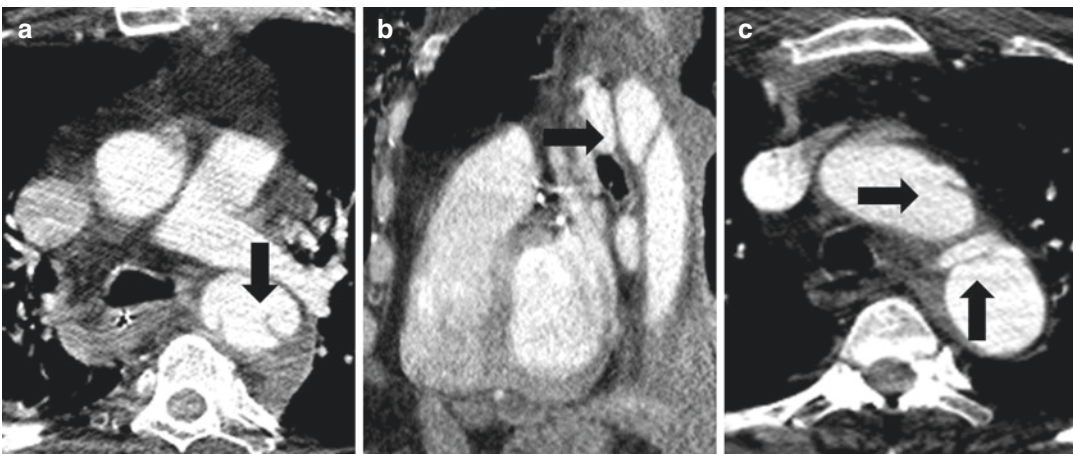
Fig. 4.2 Sixty nine-year-old woman following a motor vehicle collision. Axial (**a**) and sagittal (**b**) IV contrast-enhanced CT images show a traumatic aortic transection (arrows) with associated periaortic fat stranding/ hemorrhage. (**c**) 62-year-old man following motor vehicle collision. Axial IV contrast-enhanced CT image (arrows) demonstrates another example of a traumatic aortic transection
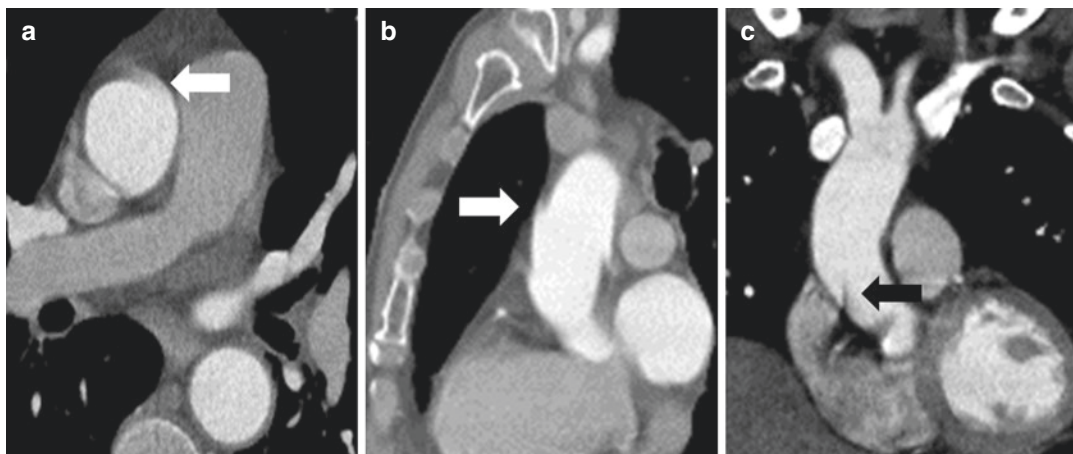
Fig. 4.3 Fifty four-year-old man presenting after a motor vehicle collision. Axial (**a**), sagittal (**b**), and coronal (**c**) IV contrast-enhanced CT images show the potential pitfall of cardiac pulsations creating pseudo-aortic intimal flaps (arrows)

the wound trajectory and tract is of high importance. If the wound tract passes adjacent to the aorta or through it, then the likelihood for an ATAI is high [4].

In the presence of direct signs of ATAI, further investigation with conventional angiography is not necessary. However, in stable patients without direct signs of ATAI with only indirect signs of injury, the clinical team may proceed with a repeat CT in 48–72 h, transcatheter intravascular ultrasound, or transesophageal echocardiography to assess for occult injuries. For the subset of patients with penetrating trauma and a wound trajectory intersecting or adjacent to the aorta, follow-up CT may be obtained in 24–48 h [4, 23–26, 33].

Awareness of the CT pitfalls of the thoracic aorta is important to avoid inaccurate diagnosis of ATAI. Anatomic variants such as the ductus diverticulum may incorrectly lead the radiologist to interpreting this normal anatomic variant as a direct sign of ATAI. Aortic ductus diverticulum is a developmental outpouching of the thoracic aorta that is typically seen along the anteromedial aspect of the aorta at the level of the aortic isthmus. In ATAI, the outpouching may have an irregular margin with acute angles at the base, whereas a ductus diverticulum will have smooth margins and form obtuse angles with the aorta. Aortic spindles are another anatomic variant, which appear as fusiform dilatation of the aorta.

Other anatomic variants which may be mistaken for an ATAI include small infundibula at the origins of branching vessels (bronchial and intercostal arteries) and mediastinal process (i.e., normal thymic tissue) which may be mistaken for a mediastinal hematoma [4]. The infundibula are conical in shape, and the artery can be seen at the apex of the outpouching. In mediastinal findings not otherwise related to aortic injury, secondary findings of injury, particularly fat stranding will be absent. Technical nonanatomic CT pitfalls include breath-hold artifacts, patient arm placement (resulting in linear streak artifact), and cardiac pulsation artifacts (Fig. 4.3) [4].

4.3.2   Traumatic Aortic Pseudoaneurysm

Disruption of the aortic intima and media causing adventitial outpouching, i.e., a pseudoaneurysm, is another important traumatic injury to look for in the setting of blunt and penetrating thoracic trauma. The use of the term "pseudoaneurysm" has been controversial in some practices given the concern that it may underestimate the extent of vascular injury [4, 15, 30]. However, for the purposes of this chapter, we will use the terms outpouching and pseudoaneurysm interchangeably. This is considered a partially contained rup-

ture of the aorta, with luminal blood only being held by the adventitia or by mediastinal structures. Traumatic aortic pseudoaneurysms typically occur adjacent to the aortic isthmus from the origin of the left subclavian artery to the ligamentum arteriosum [6]. Given the higher propensity to rupture compared to true aneurysms due to the weak support of the pseudoaneurysm adventitial wall, traumatic pseudoaneurysms typically require urgent treatment. In hemodynamically unstable patients, endovascular treatment with stent grafts has shown to provide a good alternative to open surgical intervention [30].

On CT chest angiogram, axial and sagittal planes will demonstrate a saccular outpouching, demarcated from the aortic lumen by the torn intima (Fig. 4.4). Clues to the accurate diagnosis of a traumatic aortic pseudoaneurysm on CT include continuity with the aortic wall, with obtuse margins, and occasionally atheromatous plaque and surrounding mediastinal hematoma [5–7, 15, 30].

4.3.3 Minimal Aortic Injury

With the advent of MDCT, there has been increasing ability to detect small injuries only affecting the intima of the aortic vessel wall, also known as minimal aortic injury (MAI). In a 2014 study at the University of Washington investigating MAI, the inclusion criteria for MAI on CTA were post-traumatic abnormality of the internal contour of the aorta wall projecting into
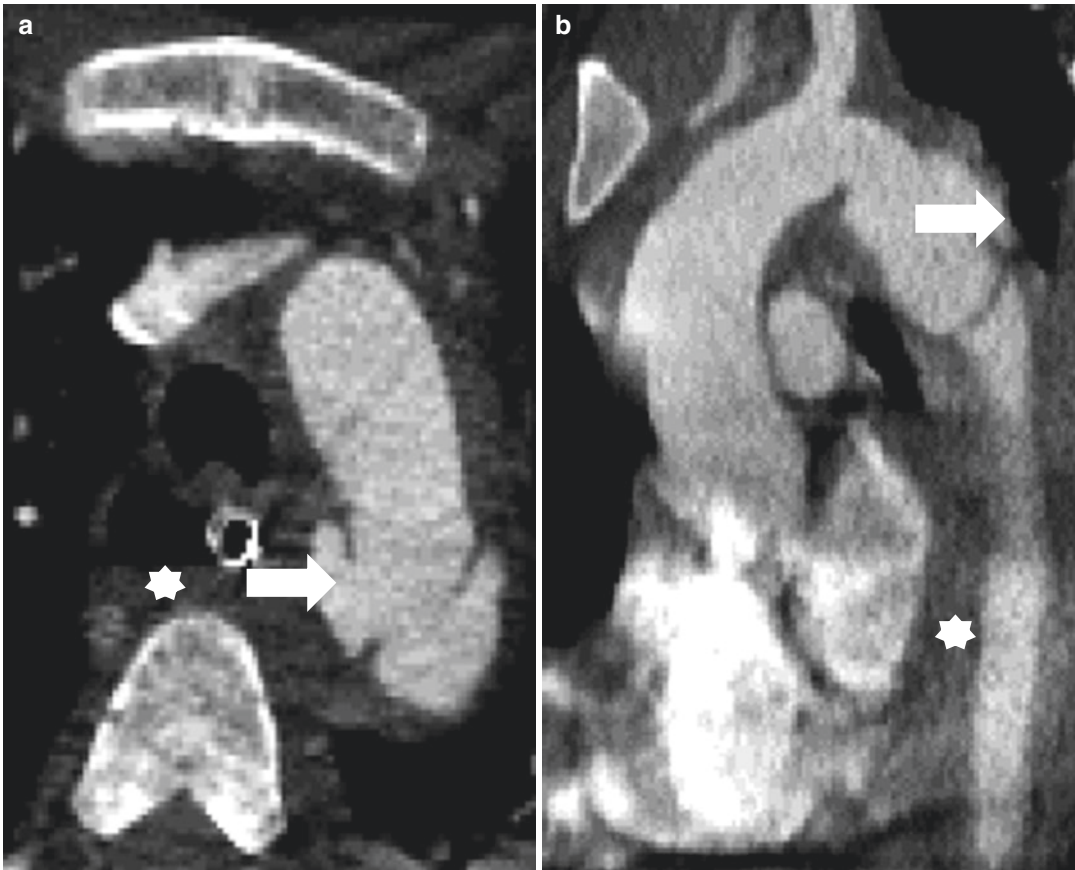
Fig. 4.4 Twenty two-year-old woman presenting after a motor vehicle collision. Axial (**a**) and sagittal (**b**) IV contrast-enhanced CT images of the thoracic aorta show traumatic descending thoracic aortic injury with associated pseudoaneurysm (arrows). Periaortic hematoma is noted (asterisks)

the lumen, an intimal flap, an intraluminal filling defect, an intramural hematoma, and no evidence of an abnormality to the external contour of the aorta [8–10, 32]. The study reviewed 81 patients with blunt traumatic aortic injury and identified a subset of 23 patients with MAI. A majority (69%) of MAI occurred in the descending thoracic aorta, and the most common CT appearance of MAI was a rounded or triangular intraluminal filling defect [9, 10]. Overall, MAI represents a milder form of blunt traumatic aortic injury, and a more conservative approach to management is generally feasible, rather than the more invasive approach taken with significant traumatic aortic injuries [9, 10, 32].

4.4 Blunt Cardiac Injury

4.4.1 Myocardial Contusion/ Myocardial Concussion

On the basis of mechanism, cardiac injury is classified into two categories, blunt and penetrating injury. Given its ability to provide accurate means for diagnosis and ability to expedite overall treatment, MDCT is the test of choice in the evaluation of acute cardiac injury. Approximately 25% of traumatic deaths are caused by cardiac-related injuries, with the majority predominantly involving cardiac or great vessel damage [2, 7, 10, 11]. Crush injuries characteristically cause injury to the pericardium, myocardium, and coronary vessels. The mechanism is often due to direct compression between the sternum and spine, or rapid deceleration and shearing forces, including flexion, stretching, and twisting [6, 8, 10, 11, 29, 34].

Blunt cardiac injury can be further subclassified into myocardial concussion and myocardial contusion. Myocardial "concussion" refers to a subset of blunt cardiac injuries which present with wall motion abnormalities with preservation of the anatomic and cellular components. In contrast, myocardial "contusion" refers to bruising of the myocardium, which manifests as increased cardiac enzymes or tissue damage seen at surgery or autopsy [8, 10]. Diagnosis has largely been difficult due to the non-specific associated clinical symptoms and lack of an ideal diagnostic examination. Diagnosis of myocardial contusion is typically established by a combination of several methods including electrocardiography (ECG), echocardiography, nuclear cardiac imaging, and cardiac biomarkers (troponin I and troponin T) [23–26, 29].

Echocardiography will demonstrate segmental wall motion abnormality in myocardial concussion. However, in contusion, echocardiography will show increased myocardial echogenicity, along with a focal systolic wall hypokinesis. Other echocardiographic findings associated with myocardial contusion include traumatic ventricular septal defect and valvular injury [10, 11].

4.4.2 Pericardial Injury

Injuries to the pericardium can be life-threatening if resultant cardiac tamponade occurs [10–13]. In the setting of trauma, hemopericardium (Fig. 4.5) is the most common etiology potentially resulting in tamponade. As blood accumulates between the visceral and parietal serosal layers, compression of the cardiac chambers ensues, which can result in complete cardiovascular collapse. Pneumopericardium,
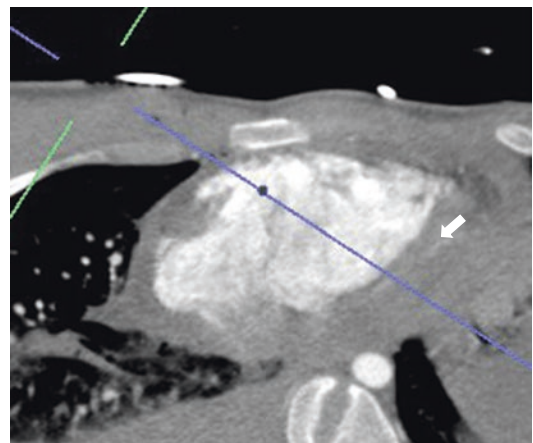

Fig. 4.5 Twenty one-year-old man presenting with precordial stab wound. Oblique trajectography CT image shows wound extension to the right ventricle (line) with small hemopericardium (arrow). Figure adapted with the author's permission from Dreizin D, Munera F. Multidetector CT for penetrating torso trauma: state of the art. Radiology. 2015. 338–55

air within the pericardial space, is less likely to cause cardiac tamponade [24].

Diagnosis of cardiac tamponade is usually confirmed by characteristic clinical signs including tachycardia, diminished cardiac output, increased central venous pressure, distended neck veins, and muffled cardiac sounds. On CT, in the setting of blunt trauma, one should suspect tamponade in the presence of high-attenuation pericardial effusion (>35 Hounsfield units (HU) suggestive of hemorrhagic effusion); dilated inferior vena cava (IVC), superior vena cava (SVC), and renal veins; deformed ventricular contour; interventricular septal straightening; compression of right-sided cardiac chambers; reflux of contrast into the IVC and azygous vein; and congestive hepatomegaly with periportal edema [10–13]. Other etiologies of tamponade in the setting of trauma include extrapericardial mediastinal hematoma, ventricular rupture, aortic root injury, myocardial contusion, and coronary artery laceration. Treatment of cardiac tamponade is emergent pericardiocentesis.

4.5 Pleural Injuries

4.5.1 Hemothorax

Following blunt or penetrating trauma, accumulation of blood between the parietal and visceral pleura is referred to as a hemothorax, and is defined as a pleural effusion having a hematocrit equal to 50% of the blood hematocrit level. Hemothorax occurs in approximately 30–50% of blunt thoracic trauma patients, with motor vehicle collision being the most common etiology [10–12]. Clinical signs and symptoms are nonspecific and include pain on the affected side and dyspnea. In hemodynamically unstable patients, laceration of the intercostal or internal mammary vessels should be suspected when hemothorax is present. Treatment may involve chest tube thoracostomy, video-assisted thoracoscopic surgery (VATS), or thoracotomy.

Chest radiography will demonstrate blunting of the costophrenic angles on upright positioning and increased ipsilateral lung density on supine
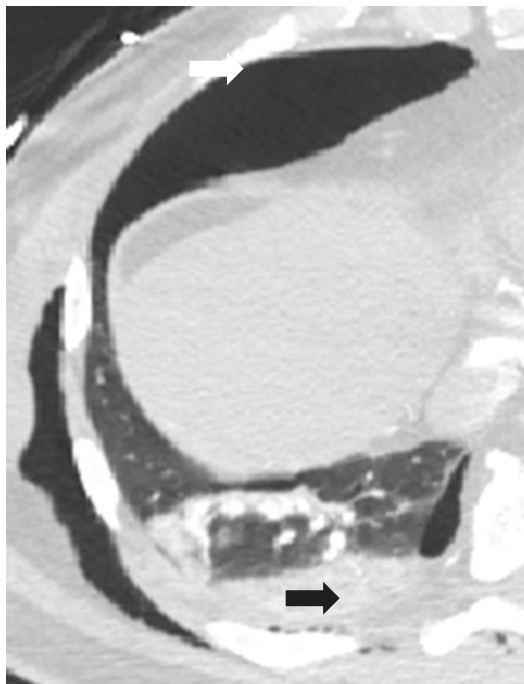
Fig. 4.6 Sixty two-year-old man presenting after MVC. Axial IV contrast-enhanced CT image of the right lung shows pneumothorax (white arrow) and hemothorax (black arrow)

positioning due to layering pleural fluid. CT may show a dense (>50 HU) or an inhomogeneous fluid collection, with some areas demonstrating higher attenuation than the surrounding fluid (Fig. 4.6). A "hematocrit effect" refers to heterogeneous pleural fluid with a layered appearance (fluid-fluid level) of high-attenuation fluid, which represents dependent clot [2, 11–13].

4.5.2 Pneumothorax

Air within the pleural space from blunt or penetrating trauma occurs in approximately 15–40% of patients with acute chest trauma [2, 12, 13]. The most common cause is from lung injury associated with rib injury. Other etiologies include tracheobronchial injury, esophageal rupture, pleural laceration, blunt trauma with elevation of alveolar pressure, and rupture of air into the pleural space and other forms of penetrating lung injury. Detection of pneumothorax in the

ventilated patient is important due to the propensity to enlarge from positive-pressure ventilation. Tension pneumothorax results from a lung or airway injury associated with a one-way accumulation of air within the pleural space, causing a rapid increase in intrapleural pressure. As the intrapleural pressure increases, mediastinal and intrathoracic structures become compressed, venous return to the heart decreases, and hemodynamic instability ensues [2, 12, 13, 17, 18]. For this reason, prompt diagnosis and rapid treatment with emergent chest decompression with needle thoracostomy and chest tube placement are required.

Most pneumothoraces will be evident on upright chest radiographs by visualization of the visceral pleural line without peripheral lung markings. Subtle findings on supine chest radiographs include deepening of the costophrenic sulcus due to air collecting within the nondependent locations (the "deep sulcus" sign), sharply outlined cardiac and diaphragmatic borders, and depression of the ipsilateral hemidiaphragm [2, 12, 13]. Smaller pneumothoraces are better detected on CT, and are referred to as "occult" if not visualized on standard chest radiographs. In the setting of tension pneumothorax, both radiographs and CT will show contralateral mediastinal shift, ipsilateral increased intercostal spaces, and ipsilateral depression of the hemidiaphragm.

4.6 Lung Injuries

4.6.1 Pulmonary Contusion

Pulmonary contusion remains the most common lung parenchymal injury from blunt chest trauma, with an estimated prevalence of approximately 30–70% in blunt chest trauma [2, 12, 13]. Interstitial or alveolar injury occurs secondary to disruption of the capillaries of the alveolar walls and septa and leakage of blood into the alveolar septa and interstitium. The primary mechanism is due to compression and tearing of lung parenchyma adjacent to the site of impact. Contralateral lung parenchymal injuries may also be seen and represent a "contrecoup" contusion. Clinical symptoms may be non-specific and present as dyspnea, chest pain, hemoptysis, or respiratory distress, with hemodynamic instability in severe cases. Unless there is a superimposed air-space infection or the presence of respiratory distress syndrome, pulmonary contusions will typically resolve beginning after 24–48 h, with complete resolution at 3–10 days [13].

CT is the imaging modality of choice and is more sensitive than chest radiography. Pulmonary contusions may be occult on chest radiographs for the first 6 h after trauma; however, they become more radiographically evident after 24 h [12, 13] (Fig. 4.7a). The typical imaging appearance of pulmonary contusion on CT consists of non-segmental peripheral geographic regions of ground-glass/nodular opacities and consolidations which do not respect lobar boundaries. Subpleural sparing consisting of 1–2 mm of clear parenchyma beneath the pleural surface may be observed. Focal parenchymal opacities detected on CT after 24 h from injury should raise suspicion for alternative diagnoses other than contusion, including aspiration, pneumonia, and/or fat embolism. Aspiration will typically follow a bronchovascular distribution, whereas contusion will not. Additionally, contusions typically do not worsen after 48 h, whereas superimposed pneumonia can [2, 12, 13].

4.6.2 Pulmonary Laceration

Pulmonary laceration refers to disruption of the alveoli and lung parenchyma. Due to the intrinsic pulmonary elastic recoil, the lung parenchyma surrounding a laceration will retract centrifugally. This centrifugal retraction causes the appearance of a round or oval cavity, instead of a linear "tear" which is seen in other solid organ lacerations. This cavity may fill with air (traumatic pneumatocele), blood (traumatic hematocele), or both (traumatic hematopneumocele) (Fig. 4.7c). Pulmonary lacerations typically take longer to resolve compared to contusions and often leave a residual scar [2, 13].

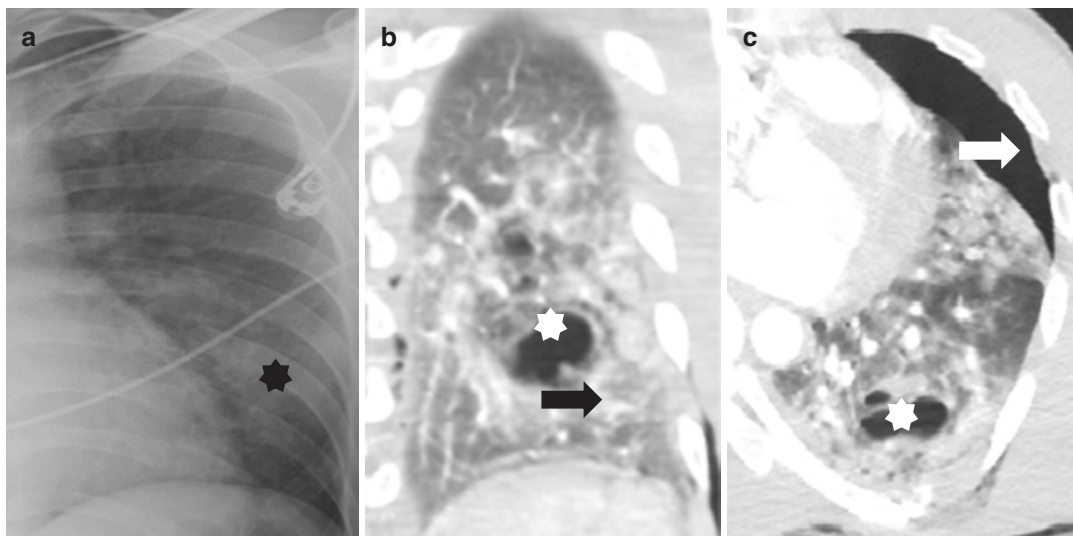**Fig. 4.7** Twenty nine-year-old man presenting after motorcycle collision. Chest radiograph (**a**) shows left basilar opacity (asterisk), suggestive of pulmonary contusion in the setting of trauma. Coronal (**b**) and Axial IV (**c**) contrast-enhanced CT images demonstrate left-sided pneumothorax (white arrow) and pulmonary contusion (black arrows) with associated regions of cavitation, indicating pulmonary laceration and/or traumatic pneumatoceles (asterisk)

There are four types of pulmonary lacerations, according to mechanism of injury, CT pattern, and location of associated rib fractures [2, 13]. Type 1 lacerations (most common) are centrally located and are due to direct compressive forces of the lung against the central tracheobronchial tract. Type 2 lacerations result from a compression shear injury and occur in a paravertebral lower lobe of the lung. The mechanism involves compression of the lower chest wall, ultimately causing the lower lobe to shift rapidly across the vertebral body in a shearing-type injury [2, 13]. Type 3 lacerations are located peripherally, occur due to penetration from a rib fracture, and are often associated with a pneumothorax. Type 4 lacerations represent tearing of prior pleural-parenchymal adhesions and are usually diagnosed at the time of surgery or on autopsy.

It is important to also investigate for pulmonary vascular injuries when pulmonary laceration is present. One direct sign of pulmonary vascular injury in the setting of blunt or penetrating trauma is the presence of a pulmonary artery pseudoaneurysm (Fig. 4.8). The rarity of this finding is likely due to the innate low pressure system of
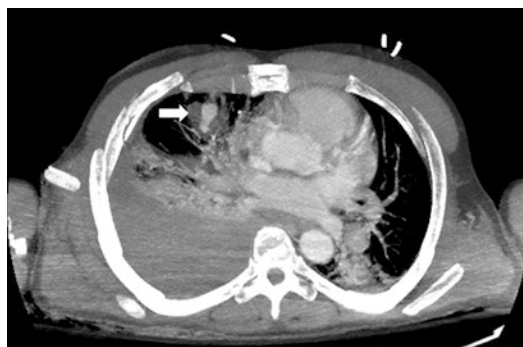
Fig. 4.8 Forty eight-year-old man presenting with a stab wound. Maximum intensity projection (MIP) reconstruction image from CT angiography demonstrates a right mid-lung anterior pulmonary artery pseudoaneurysm (arrow)

the pulmonary artery. Endovascular treatment by direct coil embolization, stent placement, or embolization of the feeding vessel has shown to be effective in occluding pseudoaneurysms [14, 35]. Other direct CT signs of vascular injury include lacerations with active contrast extravasation, intimal tears, dissection, intraluminal thrombosis, vessel narrowing, and arteriovenous fistulas [14, 35].

4.7 Tracheobronchial Injury

4.7.1 Tracheobronchial Laceration

Disruption of the tracheobronchial tract during blunt or penetrating trauma is rare and occurs in approximately 1.5% of blunt trauma patients. Delayed diagnosis can occur due to the difficulty in recognition on initial imaging. Over 70% of patients are diagnosed after 24 h and approximately 40% after 1 month. Approximately 80% of tracheobronchial tract injuries occur within 2 cm of the carina, and tears most commonly occur at the junction of membranous airway with cartilage rings [2, 12, 13]. Tracheal lacerations typically are longitudinal to the cartilage rings, whereas bronchial lacerations are more commonly parallel to the cartilage rings. Tracheal lacerations can lead to pneumomediastinum and cervical emphysema; however, pneumothorax is not usually seen. Bronchial injuries are more commonly associated with pneumothorax and pneumomediastinum. In the setting of blunt trauma, causes include direct compression of the tracheobronchial tract between the sternum and spine and/or sudden deceleration of the lung. Iatrogenic causes can occur from endotracheal tube placement or mispositioned enteric tubes. The classic clinical sign is a non-resolving pneumothorax despite chest tube suction. This occurs due to continuous air leakage through the airway rupture. Additionally, subcutaneous emphysema may persist or may progressively increase, despite chest tube placement [2, 12, 13].

On chest radiographs, the presence of pneumothorax, pneumomediastinum, and subcutaneous emphysema may be apparent (Fig. 4.9). One of the pathognomonic signs of tracheobronchial tract injury is the "fallen lung" sign [2, 13]. This occurs when complete bronchial transection occurs resulting in the ipsilateral lung collapsing away from the hilum toward the lateral chest wall or diaphragm. CT demonstrates these findings more clearly and will also allow visualization of the exact site of injury. Direct signs of injury on CT include focal wall defects, complete loss of
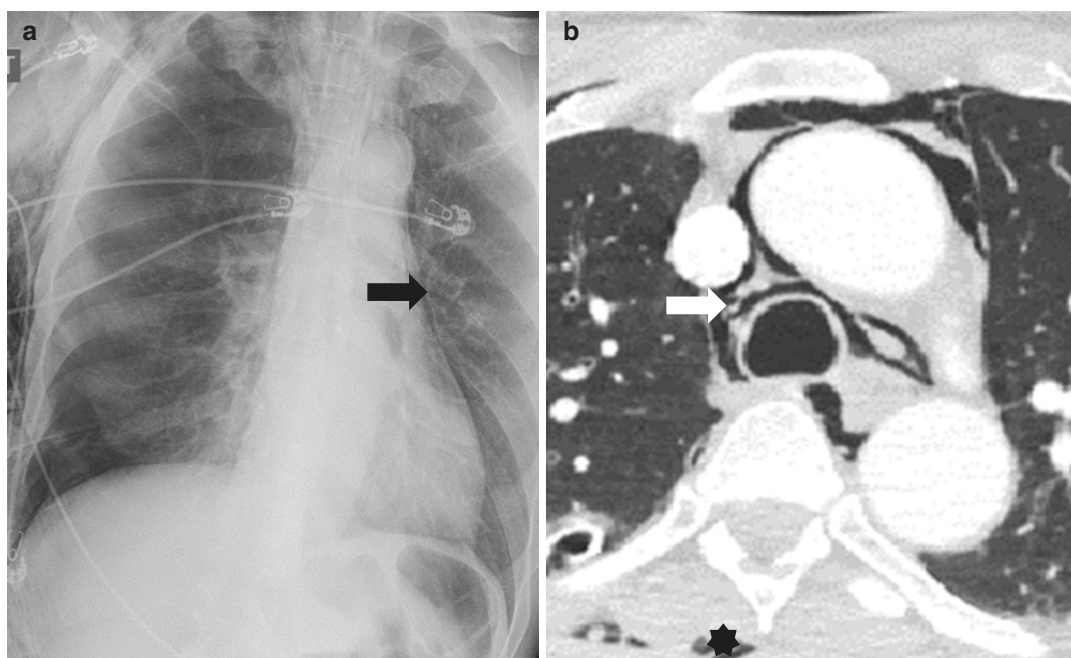
Fig. 4.9 Fifty eight-year-old man presenting with chest pain after fall and blunt trauma to the chest. Chest radiograph (**a**) and Axial IV contrast-enhanced CT chest image (**b**) show pneumomediastinum (black arrow, **a**; white arrow, **b**) and subcutaneous emphysema (asterisk). There was no evidence of tracheobronchial injury
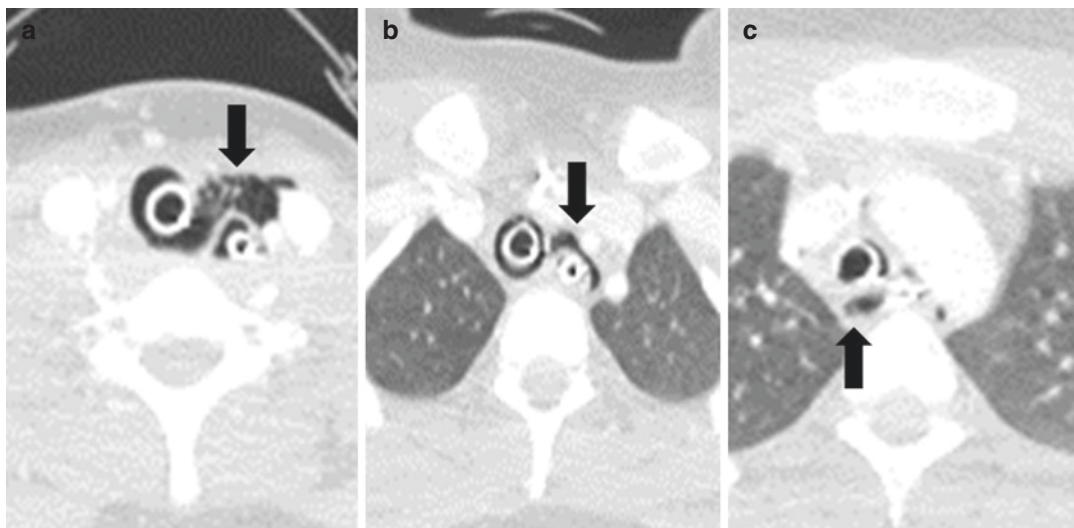
Fig. 4.10 (**a**–**c**) Twenty-year-old woman presenting after MVC. Axial IV contrast-enhanced CT images of the upper thorax at different levels show tracheal injury (arrow). Tracheal injury was confirmed intraoperatively.

There is a definitive left upper thoracic tracheal disruption with a tracheoesophageal fistula. Endotracheal and nasogastric tubes are seen within the upper trachea and esophagus, respectively

the circumferential wall, contour deformities, or abnormal communications with other mediastinal structures (Fig. 4.10). Other CT signs which should raise suspicion include sharply angulated bronchus, cutoff of the tracheobronchial wall with extraluminal air surrounding the airway, extratracheal location of an endotracheal tube, or overinflation of the endotracheal balloon [12, 13]. Although imaging plays an important role in diagnosing tracheobronchial injuries, examination should be performed for confirmation.

4.8   Diaphragmatic Injury

Traumatic diaphragmatic injuries occur in an estimated 0.2–5% of blunt trauma patients and are prevalent more in abdominal trauma compared to thoracic trauma. The most common causes of diaphragmatic injuries include penetrating trauma from knife or gunshot wounds and blunt trauma from motor vehicle collisions. The posterolateral surface of the left hemidiaphragm is affected three times more commonly than the right hemidiaphragm [16, 17]. This is postulated to be secondary to an area of embryologic weakness in the posterolateral left diaphragm. Right-

sided injuries occur less frequently due to the intrinsic increased strength of the right hemidiaphragm and the protective effect of the liver. The mechanism causing rupture involves distortion and elongation of the chest wall, which results in shearing of the diaphragm or avulsion of its attachments. Diaphragmatic tears from blunt diaphragmatic rupture are typically longer than 10 cm; however, penetrating injuries are shorter and measure approximately 1–2 cm [16]. Blunt diaphragmatic rupture almost never occurs as an isolated injury. In addition to the more commonly associated abdominal injuries, thoracic injuries including rib fracture, pneumothorax, and pleural effusion are also present in approximately 90% of patients [16, 23].

Although chest radiographs can demonstrate elevation of one side of the diaphragm, intrathoracic air-filled bowel, air-fluid levels above the expected level of the diaphragm, intrathoracic ending enteric tubes, and other secondary signs, MDCT remains the modality of choice. There are numerous direct and indirect signs suggestive of blunt diaphragmatic rupture [16, 17]. Direct signs include direct visualization of diaphragmatic discontinuity and segmental or partial absence of the hemidiaphragm. Several well-known indi-

rect CT signs of diaphragmatic injury are related to intrathoracic herniation of abdominal organs or peritoneal fat through a diaphragmatic defect (Fig. 4.11). The "collar sign," also known as the "hourglass sign," refers to a waist-like constriction of the herniated contents at the diaphragmatic rupture site. This is most easily detected on sagittal and coronal CT reformations. The "dependent viscera sign" refers to direct contact between the herniated abdominal organs and the posterior chest wall, without interposed lung between. When there is loss of diaphragmatic support after a rupture and the patient is supine, the abdominal organs will naturally move to the dependent position against the posterior thoracic wall. This sign is reportedly seen in 90% of moderate to large diaphragmatic ruptures [16]. Like any other herniations, the intrathoracic herni-

ated contents are at risk of strangulation, incarceration, and perforation, which makes close examination of such findings on CT crucial to recognize to avoid complications. Other indirect signs on CT of diaphragmatic injury are related to loss of the border between the thorax and abdomen, and include abdominal fluid abutting a thoracic structure, pneumothorax and pneumoperitoneum, hemothorax, and hemoperitoneum and abdominal viscera abutting thoracic fluid or a thoracic organ (Fig. 4.12). Potential diagnostic pitfalls at CT include pre-existent congenital hernias (Bochdalek or Morgagni hernias), acquired chronic defects (diaphragmatic fenestrations or discontinuities most commonly at the posterior crura), and diaphragmatic eventration (abnormal area of diaphragmatic relaxation and elevation) [16].
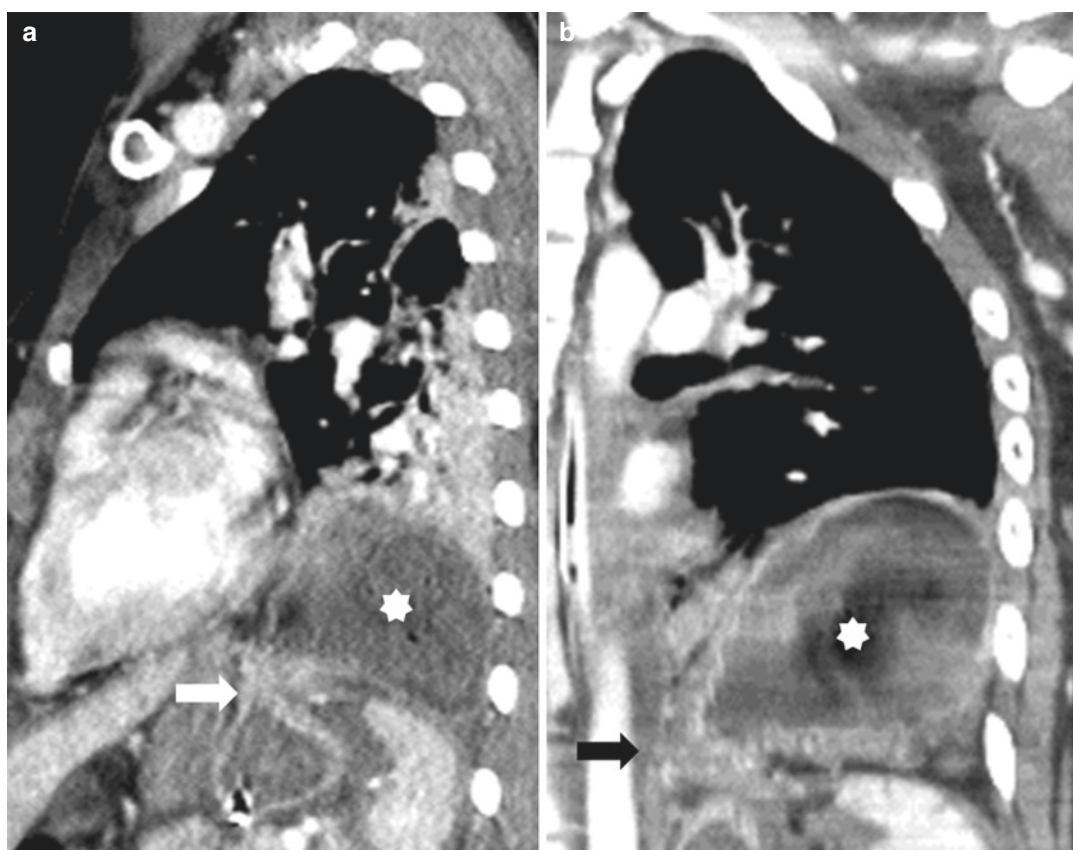
Fig. 4.11 Nineteen-year-old woman presenting after MVC. Sagittal (**a**) and coronal (**b**) contrast-enhanced CT images show left diaphragm injury (white and black arrows), with superior herniation of the stomach (asterisks)
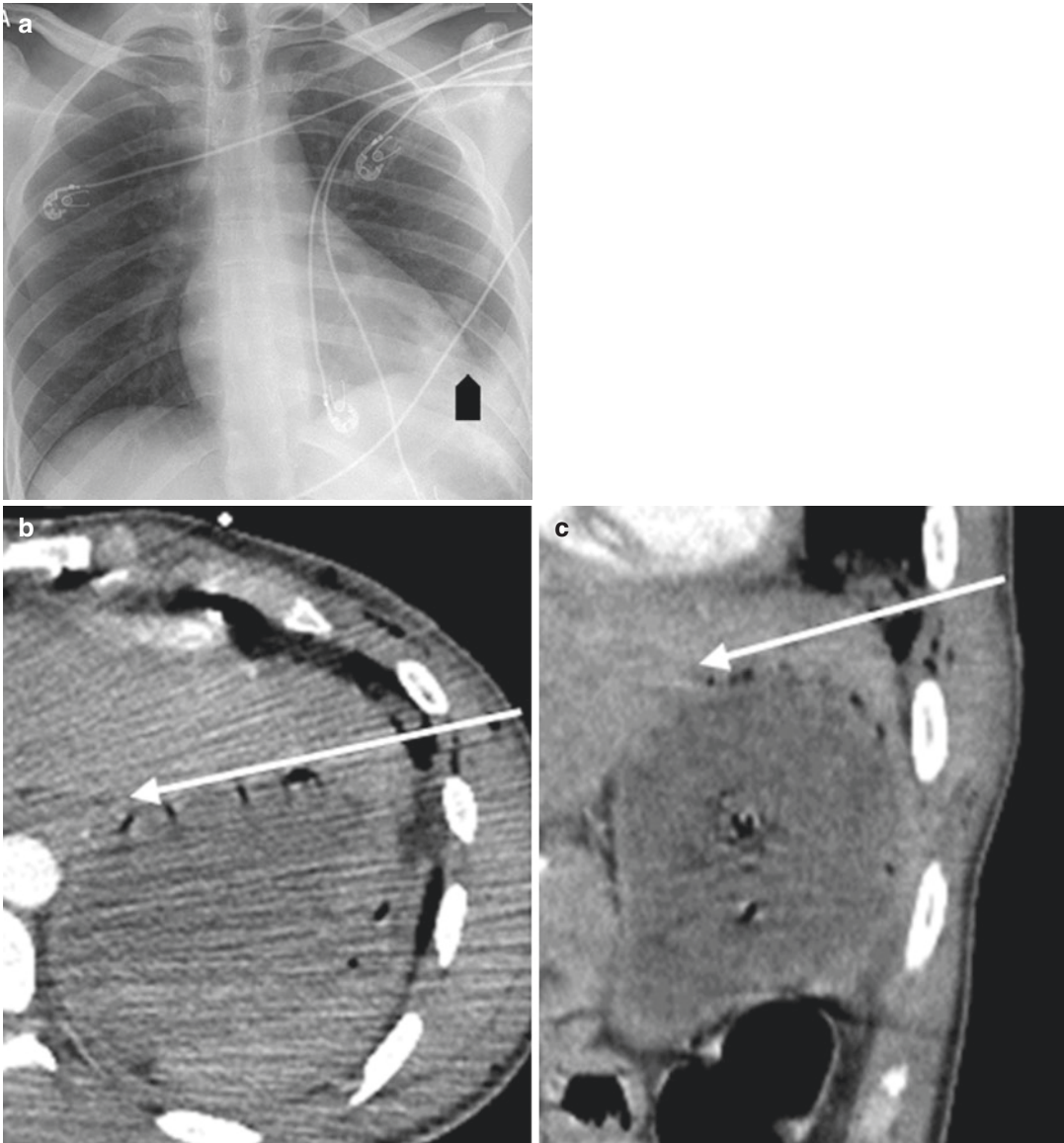
Fig. 4.12 Twenty four-year-old man presenting after multiple gunshot injuries. Chest radiograph (**a**) shows obscuration of the left hemidiaphragm (arrow). Axial (**b**) and coronal (**c**) IV contrast-enhanced CT images show left diaphragm injury along the trajectory of the bullet, as outlined by the arrows

4.9   Thoracic Skeleton Injuries

4.9.1   Rib Fractures

Portable chest radiographs in the trauma setting often have a limited ability to depict non-displaced and even displaced rib fractures due to several factors, including patient positioning, poor inspiratory effort, or other superimposed pulmonary and non-pulmonary processes. Since rib fractures may only be detectable on approximately 40–50% of chest radiographs [2, 17], CT has become the definitive modality for confirmation of cortical breaks/step-offs, as well as for the evaluation of underlying visceral injuries due to fractures [17]. Multiple or bilateral rib fractures is an indication of more severe thoracic injury [17].

The thoracic ribs are divided into three zonal segments according to the degree of trauma required for injury and the associated injuries [17]. Fractures involving the upper zone (ribs 1–4) are seen in high-velocity trauma, because enough energy force must overcome the protection from the scapulae, clavicles, and musculature. Associated injuries seen in upper zone fractures include brachial plexus and/or subclavian vessel injury. Fractures involving the middle zone (ribs 5–9) commonly occur posterior or lateral. Associated injuries more commonly seen in middle zone injuries include pulmonary laceration, pulmonary contusion, extrapleural hematoma, hemothorax, and pneumothorax [17]. Fractures involving the lower zone (ribs 10–12) should raise suspicion for solid organ injury affecting the liver, spleen, or kidneys.

Flail chest (clinical diagnosis) is seen in up to 20% of patients with major trauma, and is defined as three or more contiguous segmental fractures (two or more fracture in the same rib), or greater than five contiguous simple rib fractures [2, 17]. This type of rib injury can create a flail segment which can move paradoxically relative to the remainder of the chest, inward with inspiration and outward with expiration. Although flail chest may not be clinically evident in up to one-third of patients, physical examination should be utilized in conjunction with imaging. Although rib fracture treatment is mostly supportive (analgesia), nearly 50% of patients with flail chest may require intubation and mechanical ventilation [17]. Along with improving oxygenation and ventilation, the positive-pressure ventilation also provides an internal stabilization to the thoracic cage, and temporarily helps resolve the paradoxical movement [17].

4.9.2   Scapular Fractures

Significant blunt or penetrating force is required to fracture the scapula and accounts for 3–5% of all shoulder girdle fractures [2]. Scapular body fractures account for 50–85% of scapular fractures, while fractures of the scapular neck account for approximately 10–60% of scapular fractures [1, 2, 22]. In up to 80–90% of scapular fractures, other injuries are frequently associated, including thoracic (rib fractures, lung contusions/lacerations), glenohumeral joint, brachial plexus, and axillary artery injuries [22]. CT is more reliable and accurate for the detection and staging of scapular injuries compared to radiographs (Fig. 4.13). Due to reformatted 2-D
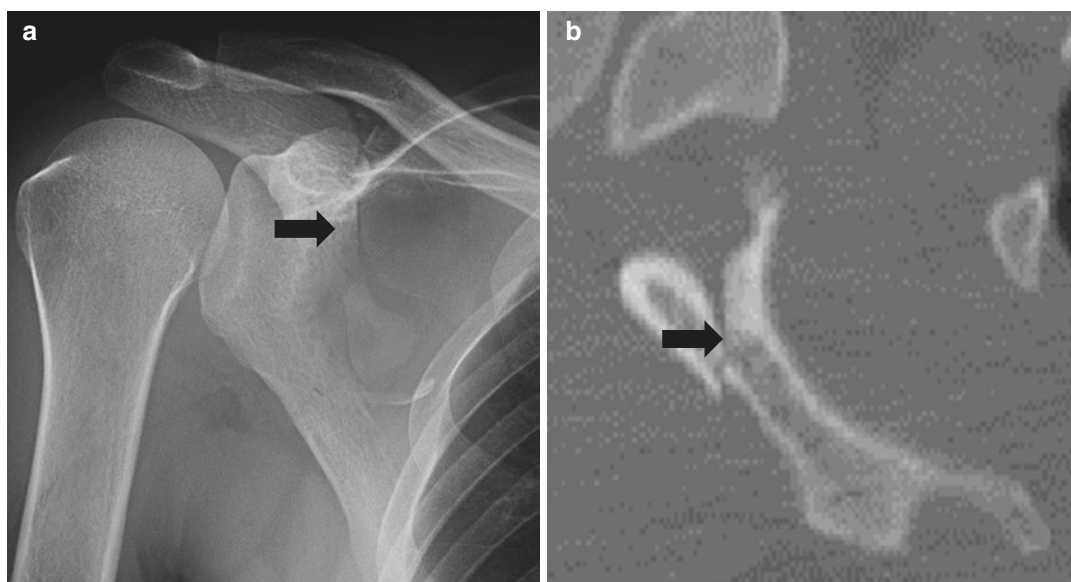
Fig. 4.13 Forty six-year-old man presenting after MVC. Right shoulder radiograph (**a**) and Axial IV contrast-enhanced CT image of the right scapula in bone window (**b**) show acute right fracture through the scapular spine (arrow)

and 3-D CT images which are routinely acquired from admission chest CT, dedicated shoulder CT is not necessary in the setting of trauma and suspected scapular injury [22]. Once a scapular fracture is identified, it is important to inspect the glenoid fossa and glenoid rim for involvement. Fractures involving the glenoid have the potential to disrupt the shoulder girdle function, and ultimately lead to glenohumeral joint instability, arthrosis, and disruption of the rotator cuff and shoulder girdle musculature [22]. Since most scapular fractures are minimally displaced or non-displaced, treatment is usually conservative; however, glenoid involvement may require open reduction and internal fixation. Imaging pitfalls to consider in order to avoid misdiagnosis include noting anatomic variants including an os acromiale, glenoid hypoplasia, and unfused apophyses [22].

4.9.3 Sternal Fracture

Direct blunt trauma to the anterior chest wall or injuries involving rapid deceleration can result in fractures of the sternum. Although MDCT with multi-planar reformatted images improves the diagnostic sensitivity of fracture detection and is the imaging modality of choice, a lateral chest radiograph is often sufficient enough for visualization of sternal cortical discontinuity (Fig. 4.14). Injuries associated with sternal fractures include retrosternal hematoma, mediastinal hematoma, cardiac contusion/concussion, and aortic injury. For unstable or severely displaced fractures, sternal fixation can be performed using sternal wires or with formal osteosynthesis with plate and screws [19]. It is important to note that non-united ossification centers may simulate a fracture.
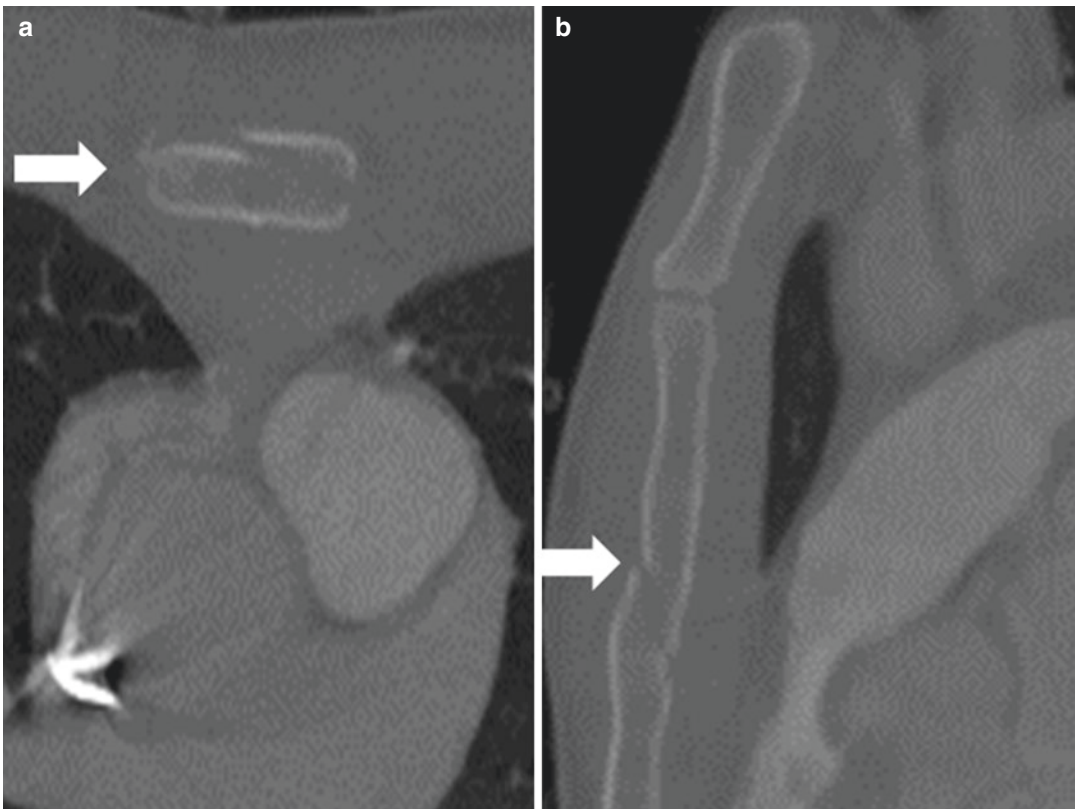
Fig. 4.14 Fifty-year-old man presenting after MVC. Axial (**a**) and sagittal (**b**) IV contrast-enhanced CT images of the sternum in bone windows show a mildly displaced sternal body fracture (arrows)

4.9.4   Sternoclavicular Injury

Injuries to the sternoclavicular joint can range from sprain, subluxation, dislocation, or dissociation. In the setting of blunt trauma, anterior dislocations commonly occur due to indirect forces to the shoulder and lateral clavicle. Although less common than anterior dislocations, posterior sternoclavicular dislocations typically represent a more serious injury and result from a posterior blunt force to the shoulder, or blunt force against the medial aspect of the clavicle [1, 2, 27]. When there is high clinical suspicion for a posterior sternoclavicular injury, it is important to evaluate for life-threatening vascular injuries and/or damage superior mediastinal structures with intravenous contrast-enhanced CT [1, 27].

4.9.5   Thoracic Spine Injuries

Accurate and early diagnosis of thoracic spine fractures is imperative in reducing the potential for irreversible neurologic deficits and to help improve overall mortality. Approximately 75–90% of spinal fractures occur in the thoracic and lumbar regions [20, 21, 28]. The thoracolumbar junction, T10–L2, is the most common site of injury [20, 21, 28]. In the setting of trauma, fractures found at any level of the spine warrant screening of the entire spine, as 15–20% of spinal fractures occur in a discontinuous fashion [20, 21, 28]. Compression fracture is the most common type of thoracic spine fracture due to blunt trauma [20, 21, 28]. Burst fractures occur due to severe axial loading (most commonly from falls from height), typically on the anterior and middle spinal columns, and most commonly at the thoracolumbar junction. Retropulsion of fracture fragments can lead to canal narrowing and neurologic injury (Fig. 4.15). Chance fractures (seatbelt fractures) occur from compressive/hyperflexion injury of the anterior column, with distraction of the posterior elements and ligaments. This will usually occur at the levels of T12, L1, and L2. CT will show wedging of the anterior vertebral body and bony/ligamentous injury to the posterior column, with increased interspinous distance. The
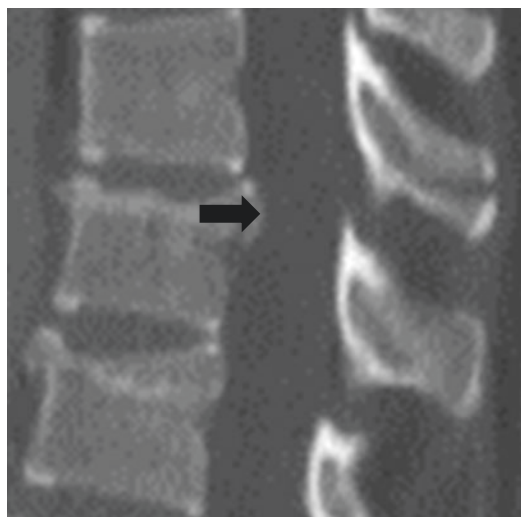
Fig. 4.15 Twenty four-year-old woman presenting after fall from 15 ft, with back pain. Detail of sagittal CT image in bone window shows compression fracture deformities of T12 and L1, with posterior retropulsion of the T12 fracture fragment (arrow). MRI spine was recommended for evaluation of possible spinal cord injury

orientation of posterior element fractures can help distinguish between burst fractures and chance fractures. In contrast to the vertically-oriented posterior element fractures seen in burst fractures, the posterior elements will fracture horizontally, which reflects the distraction force [28].

4.9.6   Clavicular Fractures

Clavicular fractures represent 5% of all fractures [27]. The middle third of the clavicle is the most common site of fracture (involved in 65–80% of all clavicular fractures), which results from blunt trauma to the superolateral shoulder [27] (Fig. 4.16). Most fractures heal without difficulty with conservative treatment. It is important to look for associated injuries in clavicular fractures, including compression of subclavian vessels, injury to the brachial plexus, and sternoclavicular ligament injury. While CT is limited for assessment of neurovascular injury and ligamentous injury, there must be a high suspicion for these types of associated injuries in conjunction with the clinical examination, prior to ordering further imaging.

Fig. 4.16 Twenty eight-year-old woman presenting after MVC. AP clavicle radiograph shows a comminuted and distracted left clavicle fracture

4.9.7 Glenohumeral Dislocation

Anterior shoulder dislocations are at least ten times more common than posterior dislocations [2]. The humeral head will lie anterior and medial to the glenoid. Hill-Sachs lesions, indentation of the posterosuperior aspect of the humeral head, are associated with anterior dislocations and may indicate higher likelihood of recurrent dislocation. Bankart deformities represent irregularities of the inferior glenoid and are also associated with anterior dislocations. Posterior glenohumeral dislocations represent 2–5% of all traumatic glenohumeral dislocations [36]. Associated abnormalities with posterior dislocations include the reverse Hill-Sachs lesion (anteromedial humeral head), the reverse Bankart lesion, a posterior labrocapsular periosteal sleeve avulsion (POLPSA), a tear of the posterior band of inferior glenohumeral ligament (IGHL), lesser tuberosity fractures, humeral neck fractures, and less commonly neurovascular injuries.

4.10 Conclusion

Thoracic trauma remains one of the most important and relevant medical and imaging topics across the world. With the combination of both conventional radiography and the major advancements with multi-detector CT, the accurate diagnosis of thoracic trauma-related injuries is achievable. Understanding the mechanism of injury is vital. The recognition of major thoracic injuries including aortic, cardiac, pleural, pulmonary, tracheobronchial, diaphragmatic, and skeletal injuries on different imaging modalities, especially on CT, is crucial in the overall management of trauma patients.

References

1. Whitesell RT, Avery LL. Chest trauma. Emergency radiology: the requisites, vol. 2. Philadelphia, PA: Elsevier; 2017. p. 61–80.
2. Kaewlai R, Avery LL, Asrani AV, Novelline RA. Multidetector CT of blunt thoracic trauma. Radiographics. 2008;28:1555–70.
3. Hsu MJ, Gupta A, Soto JA, Lebedis CA. Imaging of torso and extremity vascular trauma. Semin Roentgenol. 2016;51:165–79.
4. Raptis CA, Hammer MM, Raman KG, Mellnick VM, Bhalla S. Acute traumatic aortic injury: practical considerations for the diagnostic radiologist. J Thorac Imaging. 2015;30:202–13.
5. Creasy JD, Chiles C, Routh WD, Dyer RB. Overview of traumatic injury of the thoracic aorta. Radiographics. 1997;17:27–45.
6. Steenburg SD, Ravenel JG, Ikonomidis JS, Schönholz C, Reeves S. Acute traumatic aortic injury: imaging evaluation and management. Radiology. 2008;248:748–62.
7. Batra P, Bigoni B, Manning J, Aberle DR, Brown K, Hart E, Goldin J. Pitfalls in the diagnosis of thoracic aortic dissection at CT angiography. Radiographics. 2000;20:309–20.
8. Mcmahon MA, Squirrell CA. Multidetector CT of aortic dissection: a pictorial review. Radiographics. 2010;30:445–60.
9. Gunn ML, Lehnert BE, Lungren RS, Narparla CB, Mitsumori L, Gross JA, Starnes B. Minimal aortic injury of the thoracic aorta: imaging appearances and outcome. Emerg Radiol. 2014;21:227–33.
10. Restrepo CS, Gutierrez FR, Marmol-Velez JA, Ocazionez D, Martinez-Jimenez S. Imaging patients with cardiac trauma. Radiographics. 2012;32:633–49.
11. Alborzi Z, Zangouri V, Paydar S, Ghahramani Z, Shafa M, Ziaeian B, Khodaei S. Diagnosing myocardial contusion after blunt chest trauma. J Tehran Univ Heart Cent. 2016;11:49–54.
12. Groskin SA. Selected topics in chest trauma. Radiology. 1992;183:605–17.
13. Oikonomou A, Prassopoulos P. CT imaging of blunt chest trauma. Insights Imaging. 2011;2:281–95.
14. Donaldson B, Ngo-Nonga B. Traumatic pseudoaneurysm of the pulmonary artery: case report and review of the literature. Am Surg. 2002;68:414–6.
15. Beslic S, Beslic N, Beslic S, Sofic A, Ibralic M, Karovic J. Diagnostic imaging of traumatic pseudoaneurysm of the thoracic aorta. Radiol Oncol. 2010;44:158–63.
16. Desir A, Ghaye B. CT of blunt diaphragmatic rupture. Radiographics. 2012;32:477–98.
17. Talbot BS, Gange CP, Chaturvedi A, Klionsky N, Hobbs SK, Chaturvedi A. Traumatic rib injury: patterns, imaging pitfalls, complications, and treatment. Radiographics. 2017;37:628–51.

18. Eckstein M, Suyehara D. Needle thoracostomy in the prehospital setting. Prehosp Emerg Care. 1998;2:132–5.

19. Khoriati AA, Rajakulasingam R, Shah R. Sternal fractures and their management. J Emerg Trauma Shock. 2013;6:113–6.

20. Gamanagatti S, Rathinam D, Rangarajan K, Kumar A, Farooque K, Sharma V. Imaging evaluation of traumatic thoracolumbar spine injuries: radiological review. World J Radiol. 2015;7: 253–65.

21. Raniga SB, Skalski MR, Kirwadi A, Menon VK, Al-Azri FH, Butt S. Thoracolumbar spine injury at CT: trauma/emergency radiology. Radiographics. 2016;36:2234–5.

22. Ropp AM, Davis DL. Scapular fractures: what radiologists need to know. Am J Roentgenol. 2015;205:491–501.

23. Aronchick JM, Epstein DM, Gefter WB, Miller WT. Chronic traumatic diaphragmatic hernia: the significance of pleural effusion. Radiology. 1988;168:675–8.

24. Co SJ, Yong-Hing CJ, Galea-Soler S, Ruzsics B, Schoepf UJ, Ajlan A, Nicolaou S. Role of imaging in penetrating and blunt traumatic injury to the heart. Radiographics. 2011;31:E101–15.

25. Huguet M, Tobon-Gomez C, Bijnens BH, Frangi AF, Petit M. Cardiac injuries in blunt trauma. J Cardiovasc Magn Reson. 2009;11:35.

26. Kaewlai R, De Moya MA, Santos A, Asrani AV, Avery LL, Novelline RA. Blunt cardiac injury in trauma patients with thoracic aortic injury. Emerg Med Int. 2011;2011:848013.

27. Khan LK, Bradnock TJ, Scott C, Robinson M. Fractures of the clavicle. J Bone Joint Surg Am. 2009;91:447–60.

28. Khurana B, Sheehan SE, Sodickson A, Bono CM, Harris MB. Traumatic thoracolumbar spine injuries: what the spine surgeon wants to know. Radiographics. 2013;33:2031–46.

29. Kuhlman JE, Pozniak MA, Collins J, Knisely BL. Radiographic and CT findings of blunt chest trauma: aortic injuries and looking beyond them. Radiographics. 1998;18:1085–106.

30. Li P, Tsai C, Lin T, Hung S, Hu S. Endovascular treatment for traumatic thoracic aortic pseudoaneurysm: a case report. J Card Surg. 2013;8:36.

31. Morgan TA, Steenburg SD, Siegel EL, Mirvis SE. Acute traumatic aortic injuries: posttherapy multidetector CT findings. Radiographics. 2010;30:851–67.

32. Mosquera VX, Marini M, Gulías D, Cao I, Muñiz J, Herrera-Noreña JM, Lopez-Perez JM, Cuenca JJ. Minimal traumatic aortic injuries: meaning and natural history. Interact Cardiovasc Thorac Surg. 2012;14:773–8.

33. Patel NH, Stephens KE, Mirvis SE, Shanmuganathan K, Mann FA. Imaging of acute thoracic aortic injury due to blunt trauma: a review. Radiology. 1998;209:335–48.

34. Van Hise ML, Primack SL, Israel RS, Muller NL. CT in blunt chest trauma: indications and limitations. Radiographics. 1998;18:1071–84.

35. Shin S, Shin T, Choi H, Choi JS, Kim YH, Kim CW, Jung G, Kim Y. Peripheral pulmonary arterial pseudoaneurysms: therapeutic implications of endovascular treatment and angiographic classifications. Radiology. 2010;256:656–64.

36. Sharma P, Meena S, Rastogi D, Chowdhury B. A case of posterior shoulder dislocation with ipsilateral humeral shaft fracture. Ann Med Health Sci Res. 2014;4:314–6.

Errors in Non-traumatic Thoracic Imaging

5

Daria Manos

5.1 Introduction

Grouped together, chest pain, fever, and respiratory complaints are the most common emergency department presentation in the United States [1]. Not surprisingly, the chest radiograph (CXR) is the most common imaging examination obtained in the emergency department [2]. Unfortunately, even severe disease can result in subtle abnormalities, many findings have multiple possible causes, and there is substantial overlap between normal and abnormal imaging. Errors can be minimized through awareness of blind spots, comparison with prior imaging, tailoring interpretation to the clinical context, and understanding common artifacts.

A systematic approach is essential for interpretation of both radiographs and cross-sectional imaging. However, very few published systematic approaches to chest imaging include arguably the most important element—clinical correlation. With the advent of electronic medical records, it is easier than ever to obtain clinical information. Even patient age alone should alter the radiologists' search pattern and greatly influences the differential diagnosis (Fig. 5.1).

D. Manos (✉)
Department of Diagnostic Radiology, Dalhousie University, Halifax, NS, Canada
e-mail: daria.manos@nshealth.ca

5.2 Lung

5.2.1 Acute Diffuse Ground-Glass Opacity

Diffuse ground-glass opacity visible either on CXR as widespread hazy increase in density or more clearly on computed tomography (CT) has a wide differential. Because cardiogenic pulmonary edema is such a common cause, other potentially fatal diagnoses may be overlooked. Unfortunately, several different disease entities can have a near identical imaging appearance, even with CT, and clinical clues are often more informative than imaging features (Fig. 5.2) (Table 5.1).

When diffuse bilateral air-space disease can be identified on chest radiographs, the utility of CT both for diagnosis and to guide therapy is relatively low. Nonetheless, CT is often requested in patients with moderate to severe respiratory distress in the hopes that some useful clues can be identified. Pulmonary edema (both hydrostatic and increased permeability), infection (atypical and opportunistic), and diffuse pulmonary hemorrhage are the most likely considerations when diffuse ground-glass opacity presents acutely in the ED.

5.2.1.1 Diffuse Pulmonary Hemorrhage

Diffuse pulmonary hemorrhage (DPH) may be missed as a cause of diffuse ground-glass opacity
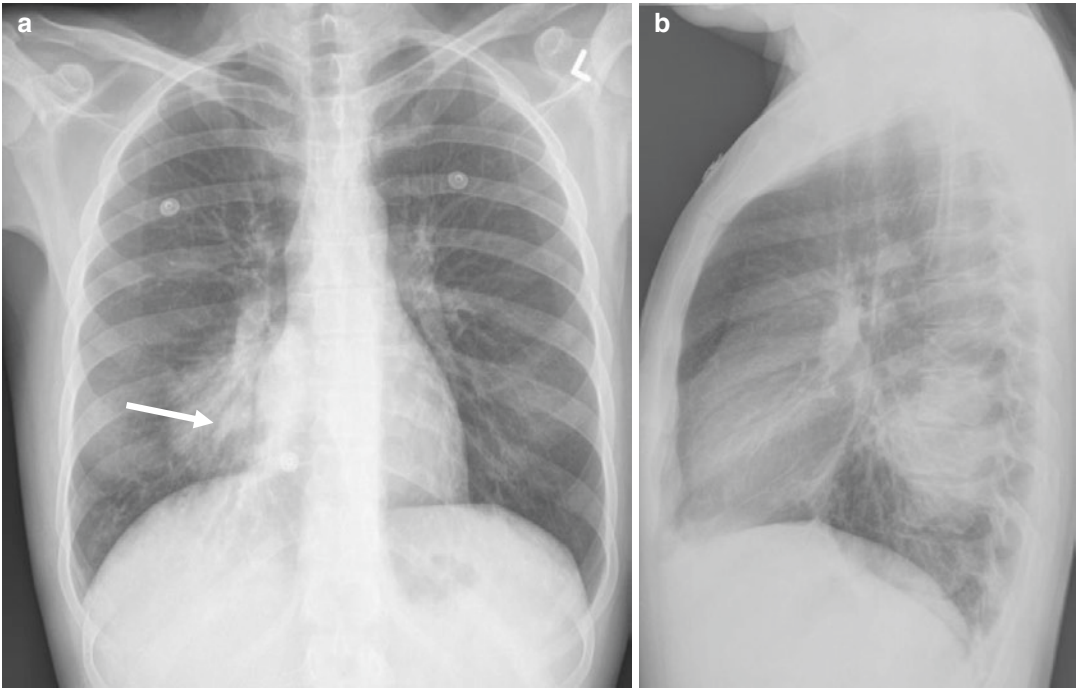
Fig. 5.1 (**a**, **b**) Rounded opacity in a 29-year-old man presenting with cough. PA and lateral chest radiographs demonstrate a rounded opacity in the right lower lobe. Air bronchograms (arrow) suggest pneumonia, but the rounded shape and relatively well-defined margins are concerning for malignancy. The patient age, however, strongly favors pneumonia rather than malignancy. The finding resolved on follow-up imaging
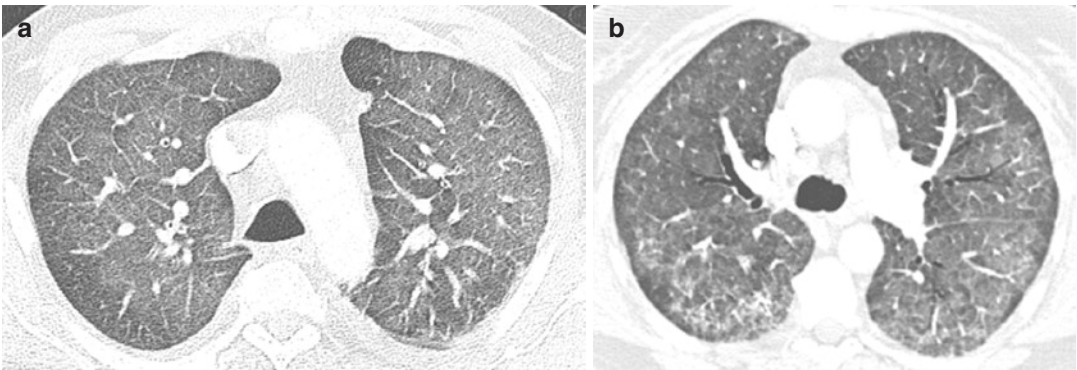
Fig. 5.2 Acute diffuse ground-glass opacity. Axial chest CT images with lung algorithm in two different patients, one with cardiogenic edema (**a**) and one with *Pneumocystis jirovecii* pneumonia (**b**). While the appearance of the lungs is quite similar, note the presence of bypass grafting and small bilateral pleural effusions in (**a**). These features strongly suggest cardiogenic edema. Nonetheless, clinical history is more helpful for diagnosis

by both radiologists and emergency physicians. The diagnosis can be particularly difficult in the up to 30% of patients with DPH who do not present with hemoptysis [3]. Pulmonary hemorrhage should be strongly considered in any patient with diffuse ground-glass opacity and an acute other-wise unexplained drop in hemoglobin, even in the absence of hemoptysis. CT findings are of ground-glass opacity, often with some areas demonstrating a centrilobular pattern (Fig. 5.3). Areas of more dense consolidation, septal thickening (as blood becomes absorbed into the intersti-

Table 5.1 Acute diffuse ground-glass opacity in the emergency department

Diagnosis	Clinical clues (more helpful)	Imaging clues (less helpful)
Diffuse pulmonary hemorrhage	Decline in hemoglobin with or without hemoptysis; previously healthy patient or known vasculitis	CT may demonstrate centrilobular nodular pattern; CT may demonstrate "crazy paving" pattern
Opportunistic infection (including PJP and viral pneumonia)	Known immunocompromise or risk factors for immunocompromise; often subacute gradual decline	May spare lung periphery; PJP often demonstrates "crazy paving" pattern on CT
Hydrostatic edema	Known heart or renal disease	Pleural effusions, septal thickening; enlarged heart
Permeability edema without diffuse alveolar damage	Risk factors (drug use, transfusion, or causes of ARDS)	Rapid clearing; consolidation uncommon
Diffuse alveolar damage (acute respiratory distress syndrome, including acute interstitial pneumonia)	Meet clinical criteria for ARDS, including acute deterioration; risk factors (massive aspiration, toxic inhalation, severe illness including trauma, sepsis, shock, and pneumonia) or idiopathic (AIP) in a previously healthy patient with rapid decline	Often superimposed areas of consolidation which may be basal predominant; septal thickening and pleural effusion less common or mild
Mixed edema	Risk factors (high-altitude edema, neurologic compromise, and postpartum)	Often "crazy paving" on CT; may have consolidation
Acute exacerbation of chronic interstitial pneumonia	Known chronic lung disease, such as idiopathic pulmonary fibrosis	CT evidence of superimposed chronic fibrotic lung disease, such as honeycombing

PJP Pneumocystis jirovecii pneumonia, *AIP* acute interstitial pneumonia, *ARDS* acute respiratory distress syndrome, *CT* computed tomography
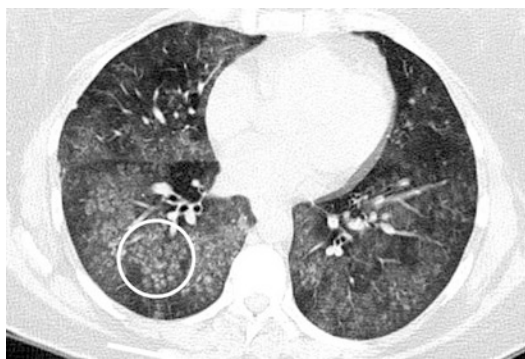
Fig. 5.3 Diffuse pulmonary hemorrhage. Axial CT image of the chest in a 38-year-old woman shows bilateral ground-glass opacity in many areas demonstrating a centrilobular pattern (circle), with sparing around the larger vessels. This patient presented with dyspnea and was subsequently diagnosed with ANCA-positive vasculitis

tium), and atelectasis (related to intrapulmonary aspirated hemorrhage) may also be seen. However, the CT findings are not specific. If CT is performed, it can reveal which areas of the lung are most severely affected, and this can guide bronchoscopy and intervention. Evaluating

for abnormal vessels (pulmonary and systemic), focal masses, endobronchial disease, and evidence of underlying lung disease including bronchiectasis and lung cancer is also important, but these findings are much more commonly seen in focal rather than in diffuse hemorrhage. For diffuse pulmonary hemorrhage, the radiologists should report the size, location, and laterality of the bronchial arteries, if interventional radiology needs to help control the hemorrhage.

5.2.1.2 Infection

Infection, particularly opportunistic and atypical infection, is an important cause of acute diffuse ground-glass opacity. The findings may be subtle, and early disease can be occult by CXR (Fig. 5.4). With widespread use of antibiotic prophylaxis, patients immunocompromised due to transplantation or patients with known HIV and good health care are often protected against *Pneumocystis jirovecii* pneumonia (PJP). Nonetheless, it remains the most common opportunistic infection in patients with HIV. It may present in a subacute fashion (weeks) with gradual respiratory
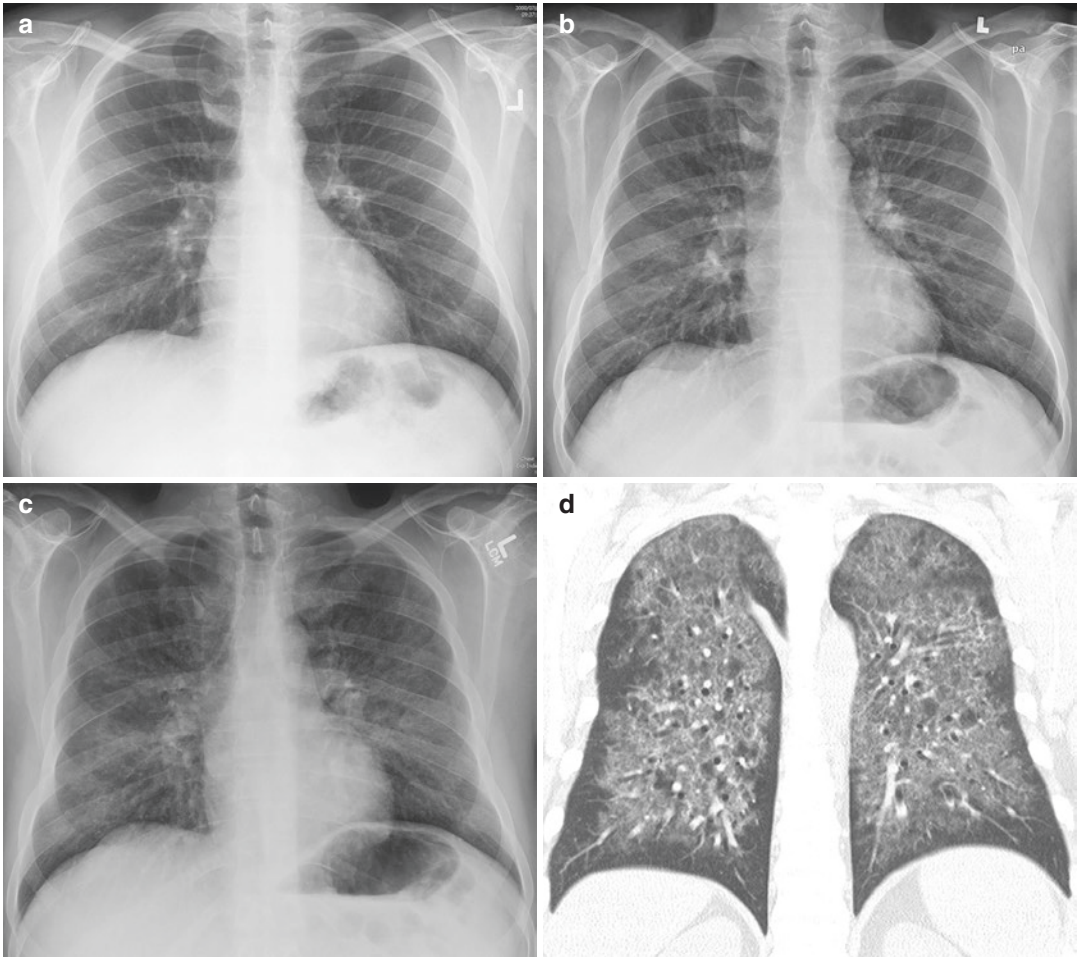
Fig. 5.4 *Pneumocystis jirovecii* pneumonia in a 45-year-old man not known to be immunocompromised but who was later diagnosed with HIV. Baseline PA radiograph from the prior year is normal (**a**). Outpatient PA radiograph for shortness of breath was reported as subtle increase in lung density diffusely (**b**). This is very difficult to appreciate without the prior radiograph. Emergency department PA radiograph (**c**), obtained for increase in shortness of breath not improving with antibiotics, more clearly demonstrates a hazy increase in lung density, with progressive obscuration of lung vasculature. Coronal CT reformation (**d**) performed 3 days later shows diffuse ground-glass opacity. *Pneumocystis jirovecii* pneumonia was confirmed by bronchoscopic lavage

compromise [4]. Unfortunately, opportunistic infection is easily overlooked in patients without the immunocompromised label. PJP remains a common initial presenting diagnosis of HIV with up to 45% of PJP diagnosed immediately prior to HIV diagnosis [5]. The emergency radiologist should look for risk factors for HIV but should also consider the diagnosis if there is any history to suggest immunocompromising medication (including steroid use or chemotherapy), malignancy, or transplantation. In practice, we have seen several instances where patients developed fatal PJP due to failure to consider the diagnosis in a patient with unrecognized immunocompromise such as a chronic hematological malignancy with concomitant chronic steroid use for an unrelated condition. Regardless, the radiologist should consider atypical and opportunistic infection in the setting of acute ground-glass opacity associated with respiratory compromise and fever. Cytomegalovirus (CMV) will present with similar clinical and imaging features but is less

common. The distinction is better made by analysis of bronchoalveolar lavage than by imaging features. Remember, however, that community-acquired pneumonia (CAP) is the most common respiratory infection in immunocompromised patients and that lobar consolidation or a bronchopneumonia pattern is usually a result CAP, rather than PJP or other opportunistic infections.

5.2.1.3 Pulmonary Edema

Not all pulmonary edema is cardiogenic or hydrostatic. Non-hydrostatic edema should be considered for the ED patient with diffuse ground-glass opacity but no suggestion of heart disease, renal failure, or fluid overload. The heart usually is normal in size, and if pleural effusions are present, they are small. The causes are reviewed in Table 5.1 and include acute lung injury resulting from inhaled toxins, drug reaction (often chemotherapy agents such as bleomycin) and overdose, sepsis, aspiration, trauma, neurologic compromise, transfusion reaction, and reaction to severe illness, including sepsis and shock. However, acute interstitial edema (AIP) can also be considered in the absence of a clear insult. AIP is the idiopathic form of ARDS and is seen in previously healthy patients, often with a preceding history of viral upper respiratory tract illness. Symptoms progress rapidly (less than 1 week), and there is extensive diffuse lung abnormality on imaging. On CT, the overall extent of ground-glass opacity and consolidation and associated findings of architectural distortion, bronchiolectasis, and honeycombing correlate with an increased risk of death [6]. Overall mortality rates in AIP have been reported to be as high as 70% [7].

Cardiogenic or hydrostatic edema as a cause of acute diffuse ground-glass opacity is usually not a difficult diagnosis clinically or radiographically, and patients seldom require CT. However, the diagnosis may be missed when demonstrated in unexpected patient populations, such as in a young patient with new cardiomyopathy.

5.2.1.4 Mimics of Acute Diffuse Ground-Glass Opacity

Mimics of acute diffuse ground-glass opacity and/or pulmonary edema on CXR include imaging in expiration, enlarged chest wall, and layering pleural effusions (especially on a supine radiograph) (Fig. 5.5). In addition, due to physiologic breast changes, a pregnant or lactating patient may demonstrate marked apparent increase lung density on a frontal chest radiograph when compared to priors.

5.2.2 Focal Opacity

Focal pulmonary opacities seen in the emergency department often represent community-
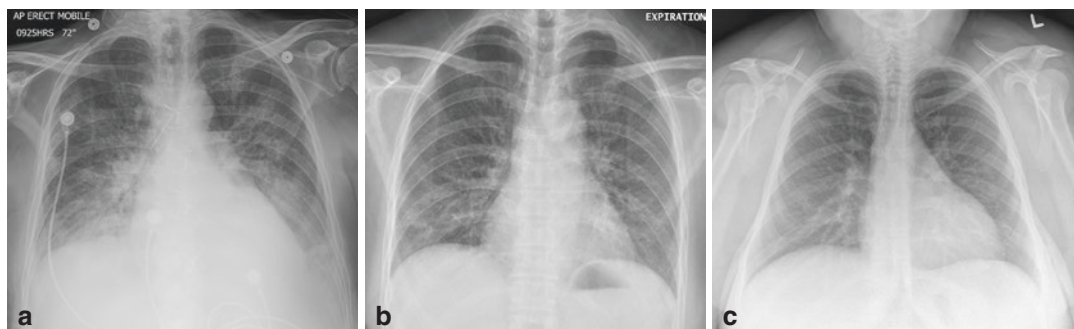
Fig. 5.5 True ground-glass opacity and common mimics. AP radiograph (**a**) demonstrates true ground-glass opacity related to hydrostatic edema in a patient with acute on chronic renal failure. Note the pulmonary vessels are ill-defined. There is also bibasal atelectasis and bilateral pleural effusions. Expiratory PA radiograph (**b**) in a patient without pulmonary pathology demonstrates artifactual increased lung density due to poor lung expansion. The vessels appear crowded but remain well defined. PA radiograph in a third patient (**c**) demonstrates hazy increase in lung density related to the large body habitus and thick anterior chest wall

acquired pneumonia. Difficulties can arise with subtle or unusual patterns of pneumonia and when other possible causes are not considered.

5.2.2.1 Community-Acquired Pneumonia

Community-acquired pneumonia may be missed when early or retrocardiac, particularly when only a frontal radiograph has been obtained. Even with PA and lateral radiographs and an excellent inspiratory effort, it can be difficult to distinguish early subtle pneumonia from artifacts. Evaluating symmetry and comparing with prior imaging if available can be helpful. Occasionally it is difficult for the radiologist to be definitive either way. In these patients, it is helpful to discuss the findings with the referring clinician. If the clinical assessment is also equivocal, patients can be brought back for repeat radiograph in 2 days if the symptoms persist.

Antimicrobial coverage is usually more influenced by clinical rather than imaging features, although there are some important exceptions including aspiration (discussed below), atypical infections (including viral and mycoplasma), tuberculosis, and opportunistic infection. Regardless, it is always essential to assess for any evidence of cavitation as this is associated with greater disease severity. Severe streptococcal infections can cause cavitation, but klebsiella and tuberculosis more frequently result in cavitation. Careful attenuation should also be paid to identifying and emphasizing the presence of an effusion, even if small, in association with pneumonia. This is discussed in more detail in the pleural effusion section.

Exercise caution when diagnosing community-acquired pneumonia in a patient with chest pain, with involvement confined to the upper lobes or without fever. While community-acquired pneumonia remains a likely consideration even with atypical presentation, it is important to consider alternate explanations (see below). Remember also that the term "consolidation" may be considered a synonym for pneumonia by the busy ED clinician.

Box 5.1 Does Pneumonia Need a Follow-Up Radiograph in 6 Weeks?

There is very little high-quality evidence to our knowledge regarding the benefit of routine follow-up of community-acquired pneumonia. American College of Radiology Appropriateness Criteria do not specifically address this. Follow-up is not usually appropriate for those at low risk of thoracic malignancy (non-smokers under the age of 50) and with typical radiographic and clinical features of pneumonia. However, regardless of patient risk of malignancy, there may be radiographic features (rounded configuration, upper lung location, questionable endobronchial or hilar lesion, repeat or persistent opacity) or clinical features (absence of fever, prolonged symptoms) prompting the radiologist to recommend 6-week follow-up to exclude the possibility of underlying malignancy. Note that 6 weeks is optimal because radiographic clearing of pneumonia often lags clinical improvement. Earlier repeat imaging should be considered only if the patient's condition does not improve (consider antibiotic failure, empyema, alternate cause of consolidation including organizing pneumonia, eosinophilic pneumonia, and pulmonary infarct).

5.2.3 Mimics of Community-Acquired Pneumonia in the Emergency Department Setting

5.2.3.1 Pulmonary Embolism

Hemorrhage associated with pulmonary embolism ("infarct") is a cause of consolidation difficult to accurately diagnose if a history of pleuritic chest pain is overlooked or not provided. The telltale peripheral wedge-shaped pattern is not always present and when present may be difficult to recognize on radiography, particularly if only one view has been obtained (Fig. 5.6). In addition, the location of the pain may be misleading. For exam-
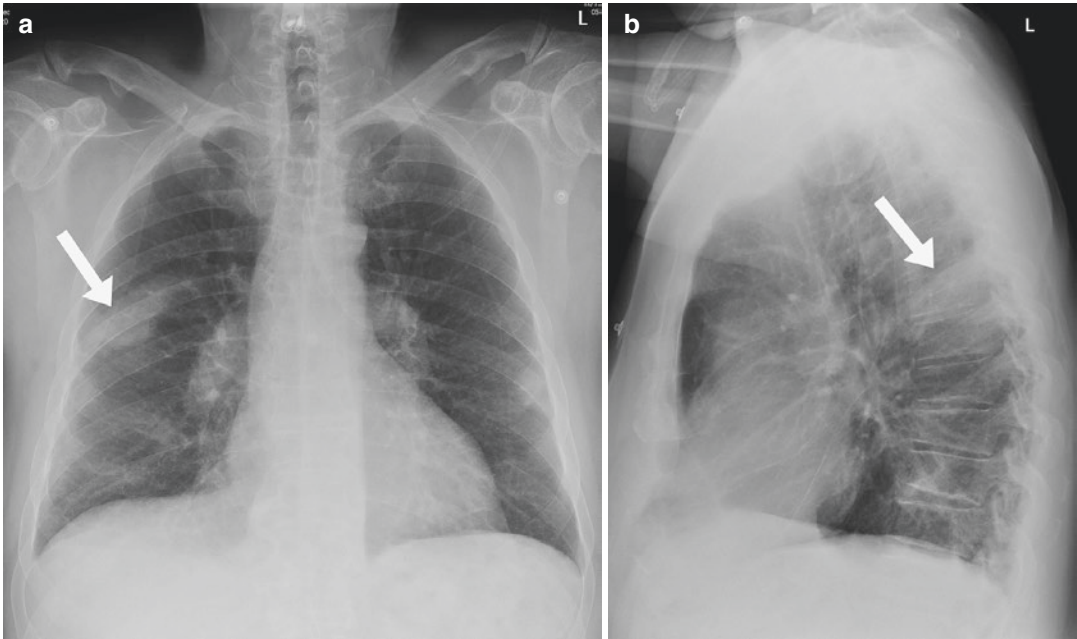
Fig. 5.6 (**a**, **b**) Pulmonary embolus. PA and lateral radiograph in a 62-year-old man demonstrate a well-defined wedge-shaped opacity (arrows) in the superior segment of the right lower lobe. The patient presented to the ED with acute-onset chest pain waking him from sleep and

3 weeks of dyspnea. The patient was diagnosed with pneumonia and was sent home with arrangements for follow-up CT to exclude malignancy. The follow-up CT (not shown) demonstrated pulmonary embolus and pulmonary infarction

ple, basal infarct may present with flank pain, and the patient may receive evaluation for a suspected renal calculus rather than for pulmonary embolus. When peripheral wedge-shaped air-space disease is seen on a non-contrast CT, discuss with the ED clinician the possibility of pulmonary embolus as the cause rather than pneumonia.

5.2.3.2 Aspiration
Distinguishing between aspiration-related consolidation and other causes of lower lobe community-acquired pneumonia is typically better performed clinically; however, in practice, the radiologist may be the first to consider aspiration by recognizing imaging clues (cavitation or necrosis, endobronchial debris, or esophageal dilation/fluid), prior radiographs demonstrating repeat episodes of basilar consolidation, and risk factors (hiatal hernia, advanced age, and bowel obstruction or ileus). While not completely definitive, CT clues suggesting aspiration include dependent distribution (including in the posterior portion of the upper lobes), a tree-in-bud pattern,

and associated endobronchial, tracheal, and/or esophageal fluid/mucus/other materials [8, 9]. A well-demarked horizontal line between normal lung and consolidated lung is used by some radiologists as a sign of acute aspiration but has not been well evaluated in the literature to our knowledge.

5.2.3.3 Atelectasis
Associated findings of volume loss can be helpful to distinguish atelectasis from pneumonia. On CT, atelectasis may be misinterpreted as pneumonia. Air bronchograms have been suggested as a way to distinguish atelectasis from consolidation. However, passive atelectasis (as seen with poor lung inflation or associated with an effusion) will demonstrate air bronchograms. On an IV contrast-enhanced CT, atelectasis will enhance avidly, while consolidation will not.

5.2.3.4 Lung Cancer
Lung cancer may appear similar to pneumonia. Endobronchial obstruction can result in lobar

consolidation with cough and fever, and lung cancer may sometimes demonstrate an irregular and ill-defined margin more suggestive of pneumonia than a mass. Recurrent consolidation or persistent consolidation without interval clearing should especially raise the suspicion for underlying malignancy. If the radiologist is concerned regarding a focal or rounded opacity suggesting coexistent malignancy in a patient with clinical history suggestive of acute pneumonia and chest radiographic signs of air-space disease, consider recommending a follow-up PA and lateral radiograph in 6 weeks. If CT is performed immediately, it may be difficult for the radiologist to distinguish pneumonia from malignancy. See Box 5.1 regarding when to recommend a follow-up radiograph in a patient with probable pneumonia.

5.2.4 Multifocal Opacity

On chest radiography, multiple masses or large nodules can be misinterpreted as multifocal air-space disease, and therefore these two patterns will be grouped together here. Multifocal air-space opacity or mixed nodular and air-space opacity on emergency department chest radiographs most commonly indicates bronchopneumonia. Errors can result from failure to consider clinical history that suggests alternate causes and from overcalling malignancy.

5.2.4.1 Organizing Pneumonia and Eosinophilic Pneumonia

Organizing pneumonia (OP) and eosinophilic pneumonia (EP) are causes of multifocal air-space disease, more commonly demonstrating a subacute rather than emergent presentation. Nonetheless, these entities may be seen in the emergency department and may be misinterpreted as community-acquired pneumonia. Patients typically present with respiratory and generalized symptoms, including fever and malaise. Peripheral predominant multifocal opacity (more often lower lung for OP and upper lung for EP) is seen on chest radiographs and may demonstrate a fleeting or migratory pattern (Fig. 5.7). Highly suggestive CT signs for both entities include the atoll sign or reverse halo (ground-glass opacity surrounded by a ring or partial ring of consolidation) and perilobular consolidation (consolidation surrounding one or more pulmonary lobules). Secondary causes, particularly drug reactions, should be considered although both entities may be idiopathic. Among the most common etiologic drugs are bleomycin, methotrexate, cyclophosphomate, nitrofurantoin, and penicillamine [10].

5.2.4.2 Septic Emboli and Vasculitis

Septic emboli and vasculitis (particularly granulomatosis with polyangiitis) may present in the emergency department with basal and peripheral
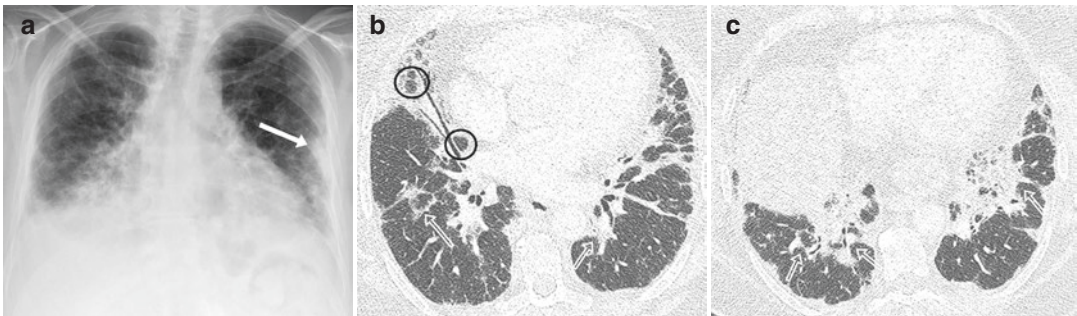
Fig. 5.7 A 59-year-old woman with organizing pneumonia secondary to nitrofurantoin. This patient presented to the emergency department with 3 weeks of dyspnea, not improving on antibiotics. The PA chest radiograph (**a**) demonstrates bilateral basal and peripheral predominant consolidation. Note the peripheral consolidation in the left lung (arrow). Two axial CT images (**b**, **c**) show both a peripheral and peribronchovascular predominance, perilobular consolidation (open arrows), and lobular sparing (circle), findings typical for organizing pneumonia. The patient had been on nitrofurantoin for 1 year
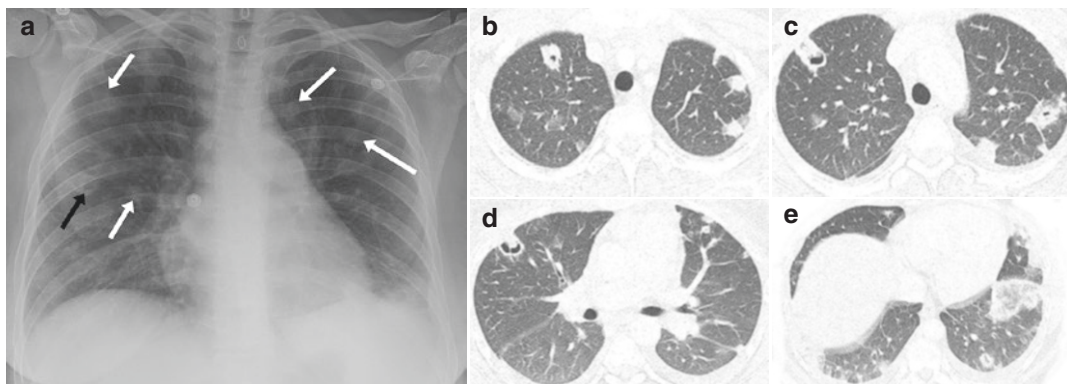
Fig. 5.8 Septic emboli in a 28-year-old woman with a history of intravenous drug use. AP chest radiograph (**a**) demonstrates multiple nodules (white arrows) and area of ill-defined air-space consolidation in the left lower lobe. A single focus of cavitation is demonstrated (black arrow). Axial CT images (**b**–**e**) obtained later the same day better demonstrate multiple nodules (some cavitating) with air-space disease in the left lower lobe

predominant multifocal or patchy opacities on radiography (Fig. 5.8). While mass-like configuration and cavitation should markedly increase the suspicion for either, these imaging characteristics may be hard to appreciate without CT. Septic emboli should be considered in a patient with risk factors (known or suspected IV drug use, valvular heart disease). Vasculitis may present with low-grade fever and cough, making the clinical distinction from pneumonia surprisingly difficult. Hemoptysis should increase the suspicion of vasculitis but is neither a sensitive nor specific sign. On CT, the differential for multiple masses and nodules, some cavitating, includes septic emboli, vasculitis, and metastases. Clinical history, more than imaging characteristics, is most helpful for ordering the differential. However, metastases are usually better defined, whereas septic emboli and granulomatosis with polyangiitis typically demonstrate ill-defined or ground-glass margins.

5.3 Pleura

5.3.1 Pneumothorax

Pneumothorax may be missed particularly when present in an unusual location. Even in an upright patient, all or part of the pneumothorax may be loculated inferiorly or medially, often due to adhesions. Clues include loculated peripheral areas of hyperlucency. As pneumothorax is often accompanied by at least a small amount of pleural fluid, another clue for a basal pneumothorax in an upright patient is an unusually perfect horizontal margin of the effusion (Fig. 5.9), rather than the typical curved meniscus.

In a supine patient, pneumothorax collects anteriorly and/or inferiorly. The classic sign of supine pneumothorax, the deep sulcus sign, is an asymmetric deepening and increased lucency in the lateral costophrenic angle. More subtle signs of supine pneumothorax include asymmetric hyperlucency resulting in increased contrast between the lung and soft tissue, including the hemidiaphragm or mediastinum. In a supine patient, the pleural reflection line may not be visible.

Artifact may result in overcalling pneumothorax. Skinfolds may cause a curvilinear vertical density, but unlike with pneumothorax, there will be no clear avascular lucency peripheral to the line. In addition, skinfolds will often demonstrate a thin peripheral dark line just external to the interface and an absence of the sharp white line at the pleural reflection, which is seen in a true pneumothorax (Fig. 5.10). Skinfolds are typically seen in older patients and demonstrate a predominantly vertical orientation. Also check
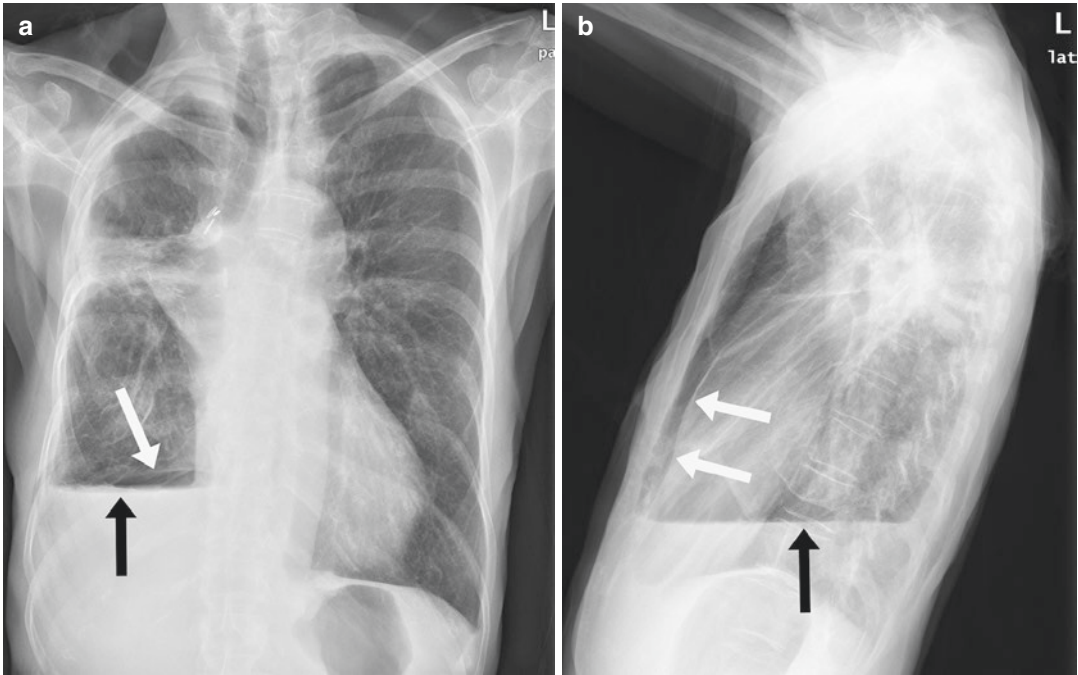
Fig. 5.9 (**a**, **b**) Basal pneumothorax in an upright patient (who had prior treatment for lung cancer). PA and lateral views demonstrate areas of abnormal lucency anteriorly and inferiorly (white arrows). The unusual horizontal margin of the pleural effusion (black arrows) reflects the interface between gas and fluid in the pleural space

that the apparent pneumothorax does not represent gas trapped between the chest wall and the arms (Fig. 5.11).

5.3.2   Pleural Effusions and Empyema

Small bilateral pleural effusions are a common finding and are often seen in patients with renal or heart disease or in those receiving IV fluids. Pleural effusions of unknown etiology and unilateral pleural effusions deserve special attention; failure to recognize these effusions may lead to severe consequences.

On a frontal upright radiograph, effusions are typically occult unless measuring more than 200 mL (Fig. 5.12) [11]. Supine radiographs are more problematic, with even large effusions often manifesting as nothing more than a hazy increase in opacity without obscuration of vascular markings. Subpulmonic effusions can be difficult to identify because the normal shape of the lateral

costophrenic sulcus appears preserved. Look for what appears to be an elevated hemidiaphragm with a lateral peak.

Unilateral effusions are a concerning finding and may be caused by pulmonary embolus, trauma, parapneumonic effusion, or malignancy. The presence and size of a unilateral pleural effusion associated with pneumonia should be highlighted in the radiology report. Thoracentesis for effusions associated with pneumonia is often recommended, even for patients without clinical evidence of sepsis, although guidelines vary as to the size threshold [11]. Regardless, any size effusion associated with pneumonia requires close radiographic and clinical follow-up (within a week) due to the risk of empyema (Figs. 5.13 and 5.14). Empyema should be suspected in patients with evidence of bacteremia or septicemia, or when the effusion demonstrates complex imaging findings, particularly loculation or, more rarely, gas without iatrogenic explanation. Complex effusions are discussed in more detail below.
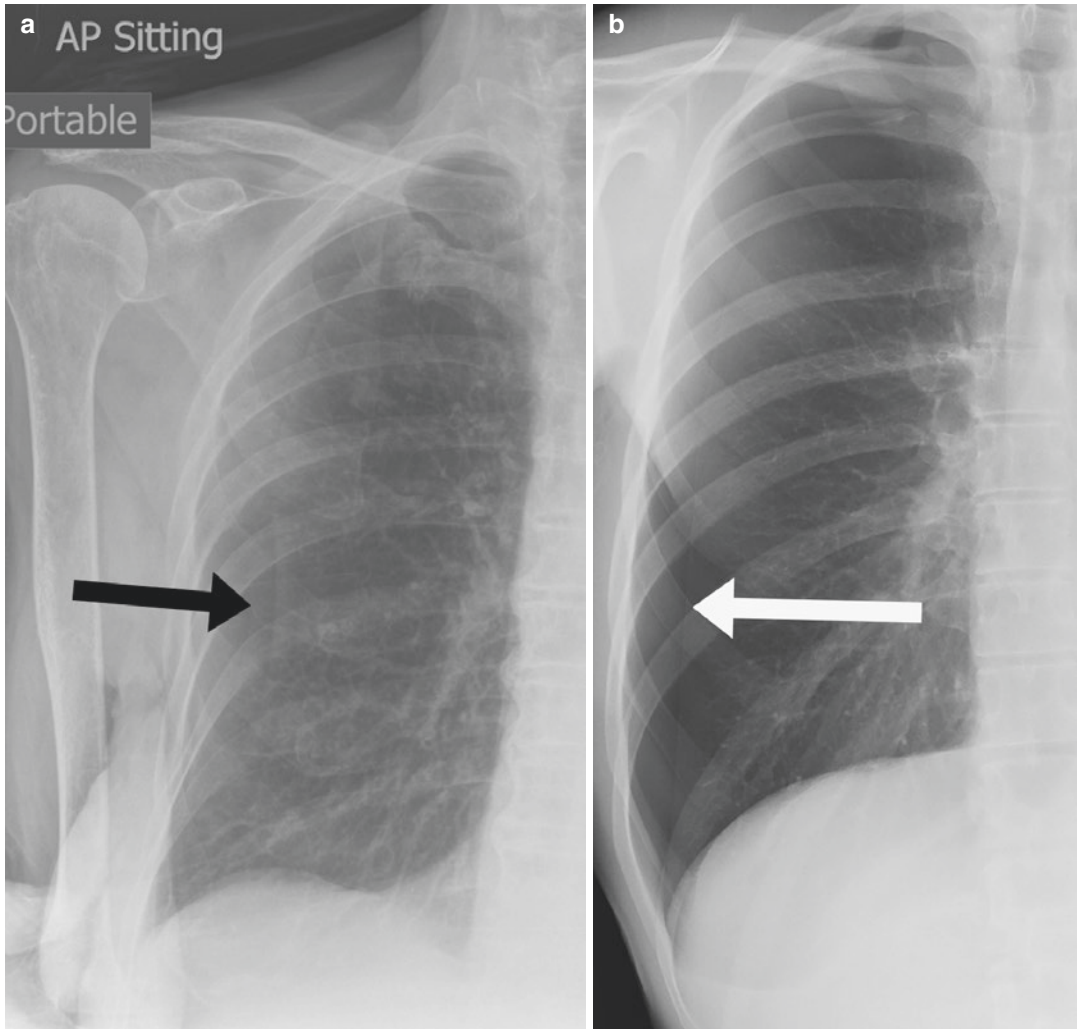
Fig. 5.10 Skinfold versus pneumothorax. AP radiograph (**a**) demonstrates a curvilinear line in the right thorax secondary to a skinfold. Note the presence of subtle pulmonary vasculature markings peripheral to the line and the black outline immediate external to the line (black arrow). These are findings of a skinfold. In contrast, there are no peripheral vascular markings on the PA radiograph of a true pneumothorax (**b**). Note also in (**b**) the presence of a thin white pleural reflection line (white arrow), another finding of a true pneumothorax

An effusion associated with chest pain in a patient without trauma or evidence of pneumonia often requires evaluation for pulmonary embolus. When pulmonary embolus is associated with pleural effusion, the effusion is typically small or small-to-moderate (less than one third of the hemithorax) and is often associated with both chest pain and dyspnea out of proportion to the effusion [12]. Pulmonary embolus is discussed in more detail later in the chapter.

Surprisingly, hemothorax may be difficult to identify as the cause of a unilateral pleural effusion, as some patients (including those with cognitive difficulties or substance abuse) may sustain significant trauma without recollection. These patients may present to the emergency department several days following the trauma. Patients may also deny trauma when the trauma is non-accidental. For all pleural effusions without clear cause, carefully review the ribs on both radiograph and CT for subtle signs of acute rib fractures (Fig. 5.15).
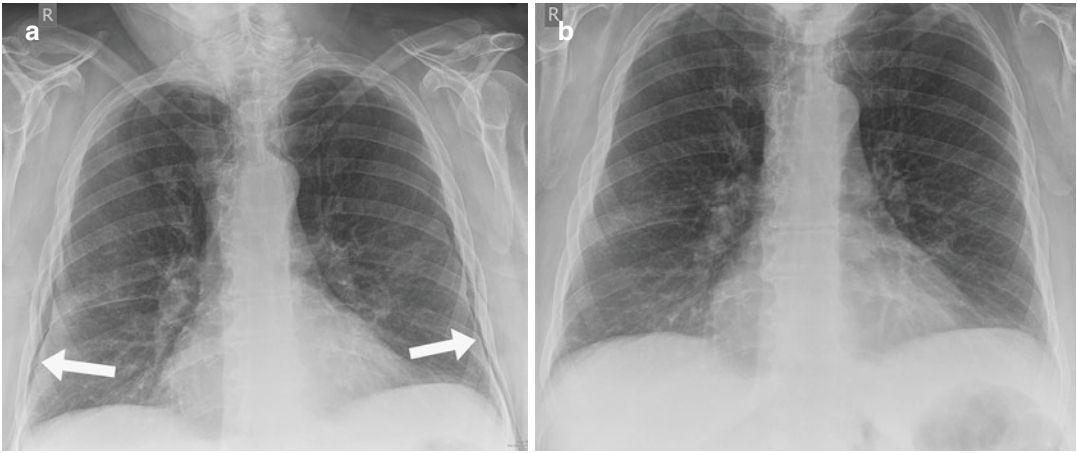
Fig. 5.11 Skinfolds resulting in pneumothorax mimic. This 67-year-old woman presented to the ED with dsypnea. PA radiograph with arms down (**a**) demonstrates gas trapped between the arms and chest wall, giving the illusion of bilateral pneumothoraces (arrows). A repeat PA radiograph in the same patient with arms slightly abducted (**b**) confirms the artifact
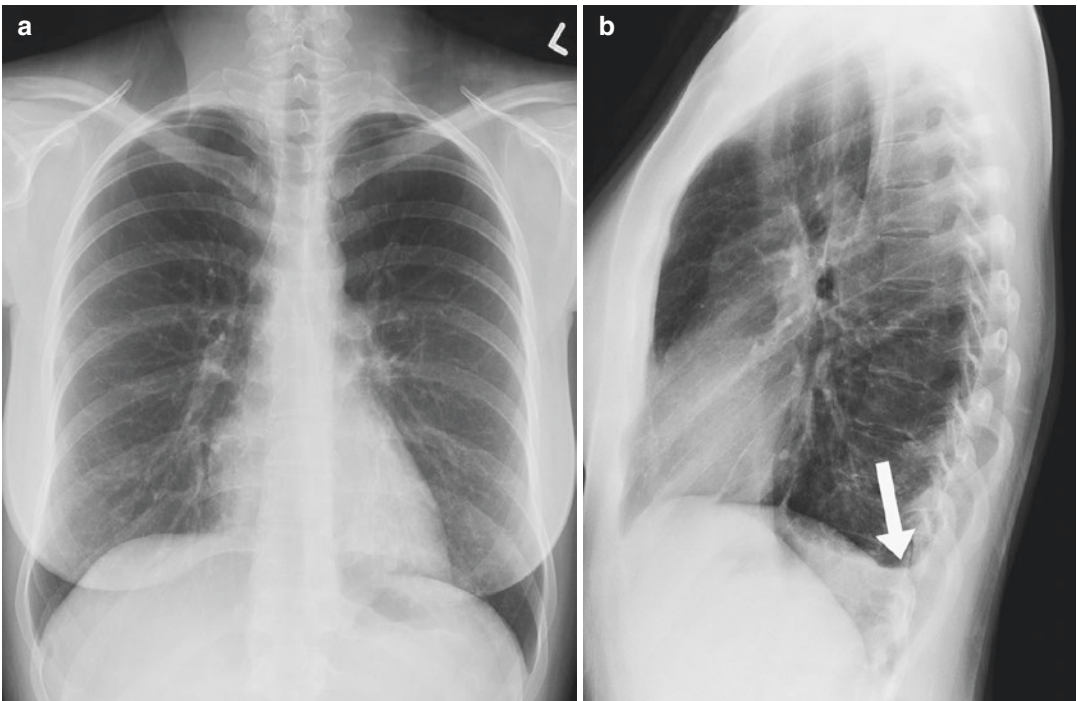
Fig. 5.12 (**a**, **b**) PA and lateral radiograph in a 33-year-old woman demonstrates a small left pleural effusion (arrow) visible on the lateral radiograph only

A unilateral pleural effusion without obvious cause should be considered highly concerning for malignancy, especially metastatic disease. If the suspicion of malignancy is high, IV contrast-enhanced CT is often indicated. Even if the suspicion of malignancy is low, unilateral pleural effusions of unknown etiology should be followed to resolution with PA and lateral radiographs.

Complex effusions may be caused by prior trauma (particularly remote or subacute trauma
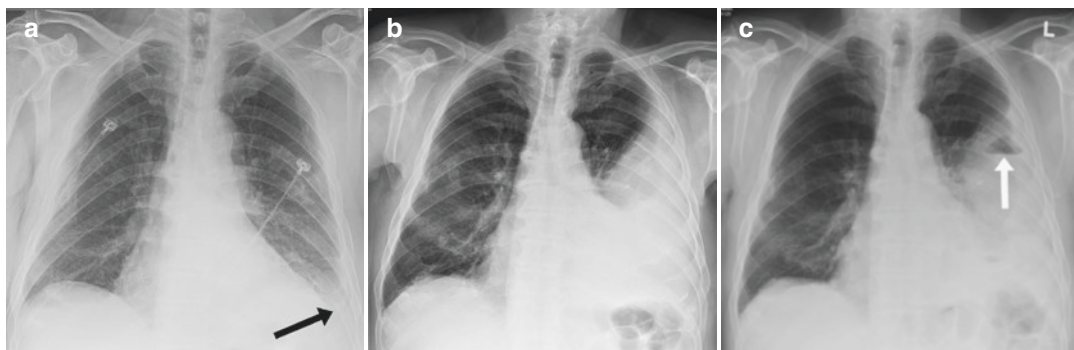
Fig. 5.13 Serial radiographs in a 77-year-old man demonstrating evolution of empyema. AP radiograph at initial presentation (**a**) was reported as concerning for left lower lobe pneumonia. The presence of a pleural effusion was not discussed in the report but is suspected in retrospect due to increased density laterally (black arrow). The patient represented with pain at which time a pleural effusion was reported (**b**). However, the size of the effusion and the possibility of empyema were not discussed. A 6-week follow-up was recommended. PA radiograph 3 weeks later (**c**) for increasing fever and pain demonstrates gas (white arrow) within the effusion consistent with empyema. Any size effusion associated with pneumonia is at risk for becoming an empyema and if not drained should be followed closely
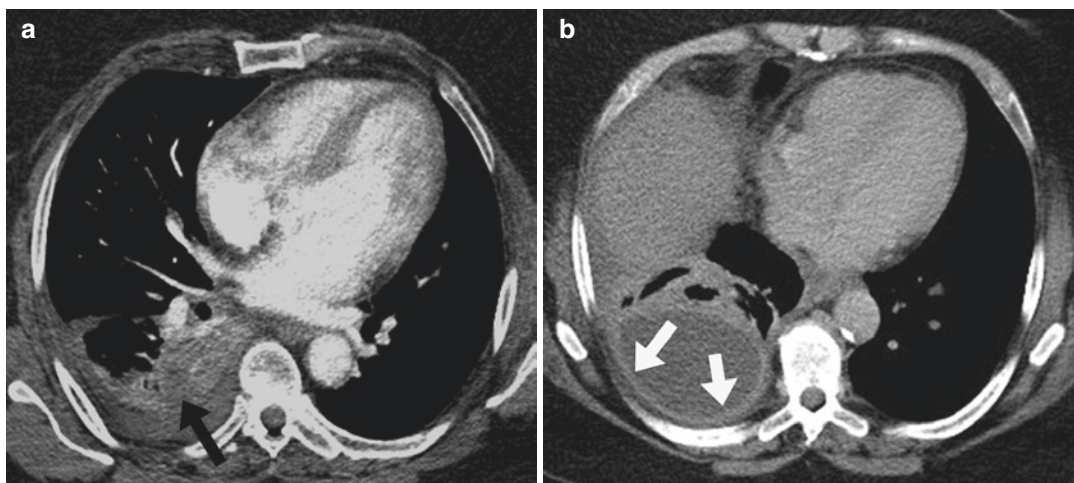
Fig. 5.14 Development of empyema in a 58-year-old woman. Axial image from CTPA (**a**) demonstrates low-density consolidation (black arrow) in the right lower lobe. The exam was negative for pulmonary embolus, and a diagnosis of pneumonia was made. The presence of the small simple-appearing pleural effusion was reported but was not emphasized. The patient returned 3 weeks later with increasing pain, at which time convex margins and new thickened enhancing pleura (white arrows) were seen, which are highly concerning for empyema (**b**). Diagnosis was confirmed by thoracentesis

or iatrogenic trauma (such as cardiac surgery)), empyema, and solid pleural malignant deposits. Loculation is the most common sign of a complex effusion and can be identified on CXR and CT by convex margins and nondependent collections. Fluid loculated within the fissures or adjacent to the upper mediastinum may be misinterpreted as a lung mass. Note that prior episodes of pleural inflammation, pleural hemorrhage, or intervention may lead to scarring and adhesions and will cause a simple effusion to appear loculated. Gas within the effusion, especially small pockets of loculated gas, is very rare in the absence of intervention but is a strong predictor of empyema. Pleural thickening and enhancement are also often described as signs of empyema and are important observations.
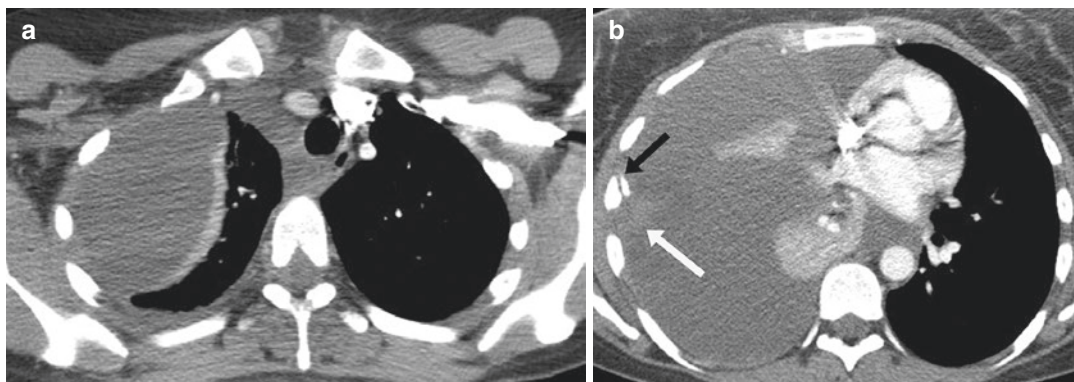
Fig. 5.15 (**a**, **b**) Large hemothorax in a 34-year-old presenting with pleuritic chest pain. Two axial images from a CTPA demonstrate a large partially loculated right pleural effusion, with collapse of the right middle and lower lobes and shift of the mediastinum to left. The pleura does not demonstrate the thickening and enhancement typical of an empyema. The emergency physicians did not elicit a history of trauma, and the patient initially did not recall trauma. Acute fracture of the sixth rib (black arrow) was missed by the initial radiologist, along with the small area of adjacent high attenuation (white arrow) consistent with acute hemmorhage

However, pleural thickening and enhancement are also common with any cause of chronic pleural inflammation. Remote undrained hemothorax will result in pleural thickening, which may appear slightly hyperdense to simple pleural fluid. Patients who have had cardiac surgery will often demonstrate chronic mildly complex-appearing pleural effusions. Errors can be avoided by reviewing prior films and noting that the pleural effusion first appeared after cardiac surgery.

5.4 Mediastinum

5.4.1 Aorta

Failure to identify aortic pathology can have devastating effects. Common sources of error result from failure to identify change in the aortic contour on chest radiographs or failure to identify aortic pathology on non-dedicated imaging (e.g., on CTPA or routine CT rather than on CT angiography).

5.4.1.1 Acute Aortic Syndrome

Acute aortic syndrome is an umbrella term which includes acute dissection, intramural hematoma, and symptomatic penetrating atheromatous ulcers. Typically, patients present with severe sharp chest or back pain and are usually evaluated with both chest radiography and dedicated aortic CT [13]. To minimize errors, some radiologists recommend that IV-contrast-enhanced CT should be performed with ECG gating. The enhanced scan should also include the abdominal aorta. The necessity of non-enhanced CT images is controversial. Non-enhanced CT images may help distinguish intramural hematoma (hyperdense) from chronic non-calcified plaque, but supporting evidence based on current CT technology and techniques is poor, to our knowledge. Rarely a pericardial recess can be confused with aortic pathology if unenhanced CT is not performed (Fig. 5.16). Intramural hematoma and acute mediastinal hemorrhage will appear high density on non-enhanced CT.

Diagnosis can be difficult when presentation is atypical. Patients under 40 are much less likely to have a history of the classic risk factors, hypertension or atherosclerotic disease, and are more likely to have connective tissue disease or a bicuspid aortic valve [13]. Women are less likely to present with pulse deficits but are more likely to present with altered mental status [14].

The chest radiograph is abnormal in up to 88% of patients, but findings, including widening of the superior mediastinum, displacement of atherosclerotic calcification, and abnormal
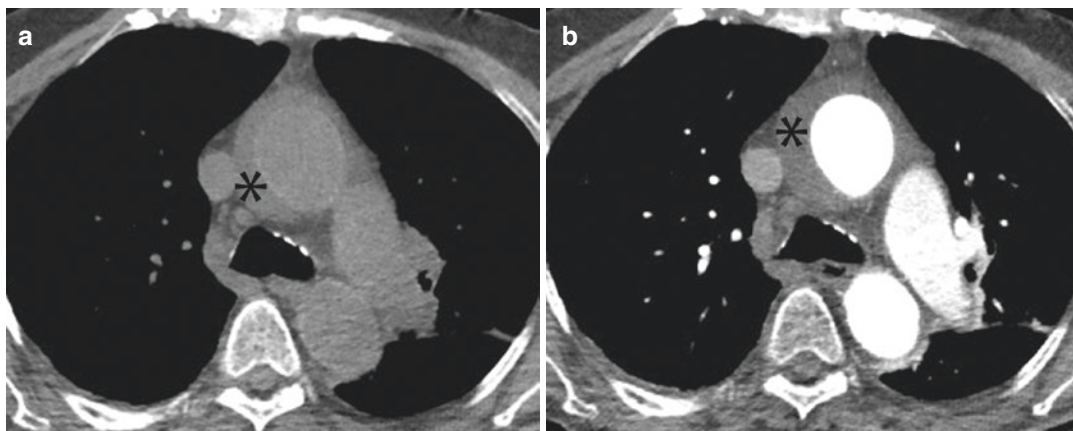
Fig. 5.16 Pericardial recess mimicking intramural hematoma in an 87-year-old woman. Axial CT images without IV contrast (**a**) and with IV contrast (**b**) demonstrate fluid (*) around the ascending aorta. On the non-enhanced CT, the fluid measures below 20 HU (simple fluid) and is hypodense to the aorta. On the enhanced CT, the density of the fluid collection is more difficult to evaluate as beam hardening from dense IV contrast in the aorta causes pseudoenhancement of the fluid surrounding the aorta. Echocardiogram (not shown) did not demonstrate evidence of acute aortic syndrome, and follow-up CT scans (not shown) demonstrated no change
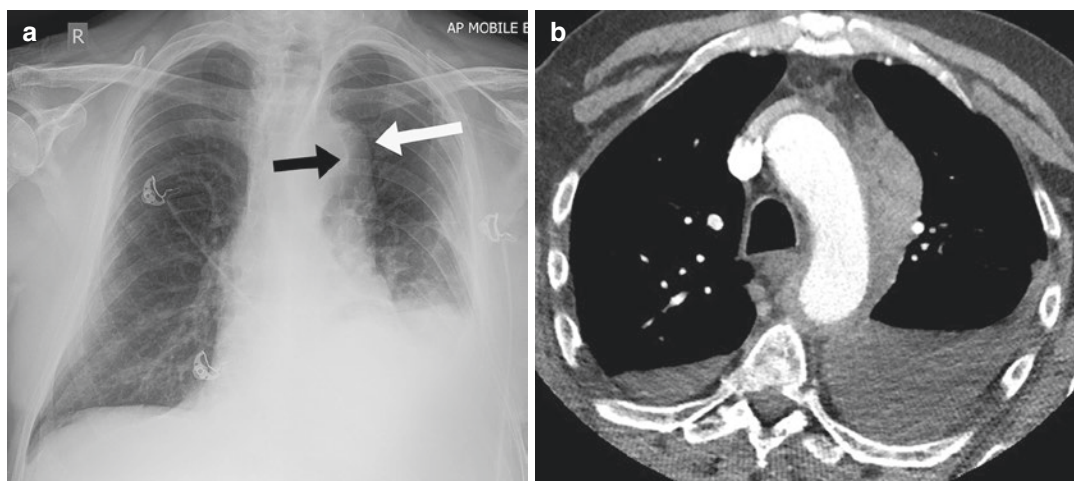
Fig. 5.17 AP radiograph (**a**) demonstrates widening of the superior mediastinum in an 83-year-old man, with the apparent contour of the aorta (white arrow) extending beyond the crescent of atherosclerotic calcification (black arrow). CT (**b**) confirms intramural hematoma and associated periaortic hemorrhage. Bilateral pleural effusions are also present

or altered aortic contour, may not be appreciated prospectively (Figs. 5.17 and 5.18) [15]. Identification can be optimized when the mediastinum is carefully compared to prior radiographs.

Evaluation is more straightforward on multidetector CT. Mistakes in CT interpretation can be caused by cardiac motion affecting the ascending aorta (false positive), failure to identify complications (including poor enhancement of branch vessels), and inability to distinguish the true from the false lumen. The false lumen is often larger (compresses the true lumen), is usually less dense on contrast-enhanced images (delayed enhancement), and is typically hyperdense on non-enhanced images (due to hemorrhage). Typically, mural calcification will be
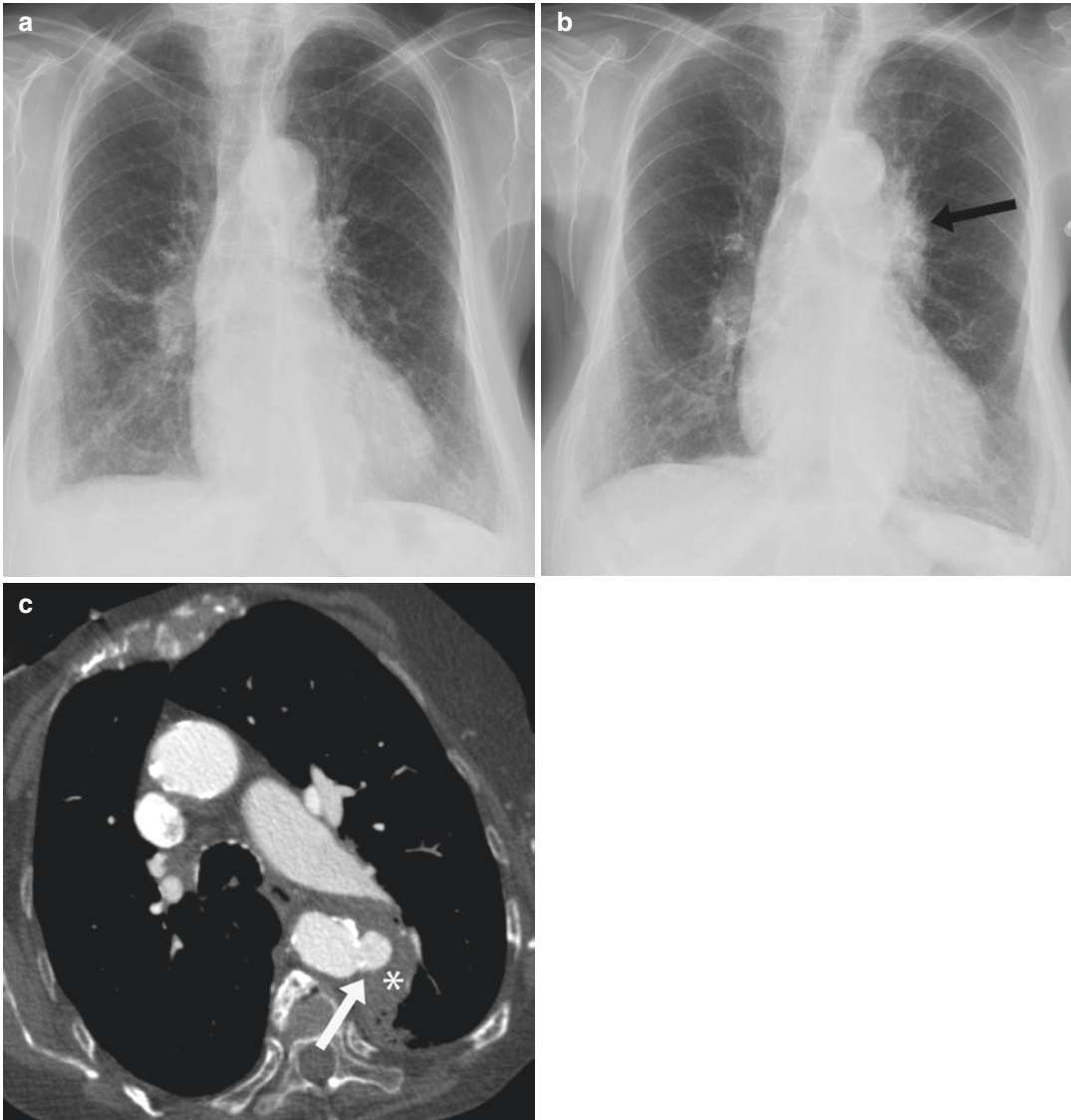
Fig. 5.18 Symptomatic penetrating ulcer in a 94-year-old woman. Remote baseline PA radiograph (**a**) demonstrates normal contour of the aorta. PA radiograph obtained in the emergency department (**b**) during the work-up of chest pain demonstrates new opacity in the aortic-pulmonary window (black arrow). Axial CT image (**c**) demonstrates ulcer-like projection in the proximal descending aorta (white arrow) and associated intramural hematoma (*)

peripheral in the setting of chronic mural thrombus. In dissection, however, calcification is displaced by the false lumen.

For acute aortic syndome, it is important to note prognostic CT signs including the diameter of the ascending aorta, periaortic hematoma, pericardial effusion/hemorrhage, and pleural effusion/hemorrhage. In the setting of dissection, also specify the entry tear size, location of entry tear relative to the subclavian artery origin, the presence of any extension into branch arteries, and evidence of organ ischemia.

For intramural hematoma and penetrating atherosclerotic ulcer, be careful to identify
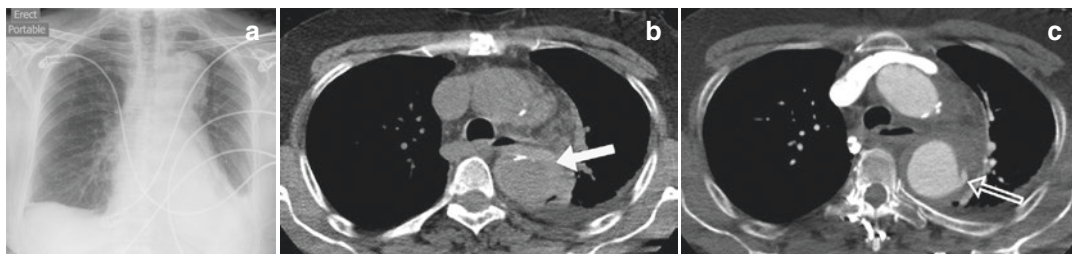
Fig. 5.19 Intramural hematoma in a 74-year-old woman. Portable AP radiograph (**a**) demonstrates a widened mediastinum, with enlargement of the aortic arch. Non-enhanced CT axial image (**b**) demonstrates hyperdense crescent (white arrow) surrounding the proximal descending aorta and external to mural calcification. CT angiography (**c**) reveals an enhancing ulcer-like projection extending into an intramural hematoma (open arrow)

signs of severity, including mural thickness and ulcer-like projections not associated with plaque (Figs. 5.18 and 5.19) [16, 17]. Note that penetrating ulcers typically become symptomatic when associated with intramural hematoma.

5.4.1.2 Arteritis

Aortitis is an uncommon cause of acute chest pain and can be very difficult to diagnose clinically. The CT manifestations, including aortic wall thickening, focal dilation, and/or stenosis of the aorta and its branches, may be overlooked by the radiologist, particularly when attention is focused elsewhere, such as excluding pulmonary embolus. Takayasu and giant cell arteritis are the most common causes. While patients may present with systemic symptoms including fever and malaise, more serious symptoms of ischemia, including limb pulselessness, angina, syncope, visual changes, and claudication may result if there is severe vascular compromise. Takayasu arteritis is most common in patients under 40 and preferentially affects women. In contrast, giant cell arteritis is rare under the age of 50 and is often associated with temporal artery involvement. Behçet's disease may also involve the aorta but more commonly affects the pulmonary arteries. Hughes-Stovin syndrome is considered a rare variant of Behçet's disease. It predominantly affects males between 20 and 40 years, with involvement limited to pulmonary arteries (typically central pulmonary artery aneurysms).

5.4.2 Pneumomediastinum

Pneumomediastinum, even when extensive, can be overlooked on chest radiographs. A lateral examination may increase detection and is helpful to distinguish artifact from true pathology (Fig. 5.20). On both the frontal and lateral radiographs, look for linear streaky lucencies outlining the mediastinal structures. The Mach effect (artifactual hyperlucency adjacent to areas of high contrast, such as the interface between the lung and the mediastinum) can be mistaken for pneumomediastinum [18]. Because pneumomediastinum frequently extends into the neck, identifying lucencies around the vascular and musculature structures of the neck can increase the interpreting radiologist's confidence (Fig. 5.21).

Pneumomediastinum without a history of significant external trauma can be seen in Boerhäave's syndrome (esophageal rupture associated with vomiting), foreign-body-related esophageal perforation, asthma and other underlying chronic lung diseases, inhaled drugs, and mediastinal infection [19]. Gas may also track into the mediastinum secondary to pneumothorax or pneumatosis intestinalis.

5.5   Pulmonary Embolus

Evaluation for pulmonary embolus is the most common indication for thoracic CT in emergency department patients [20]. Although the vast majority of CTPA examinations are negative, its
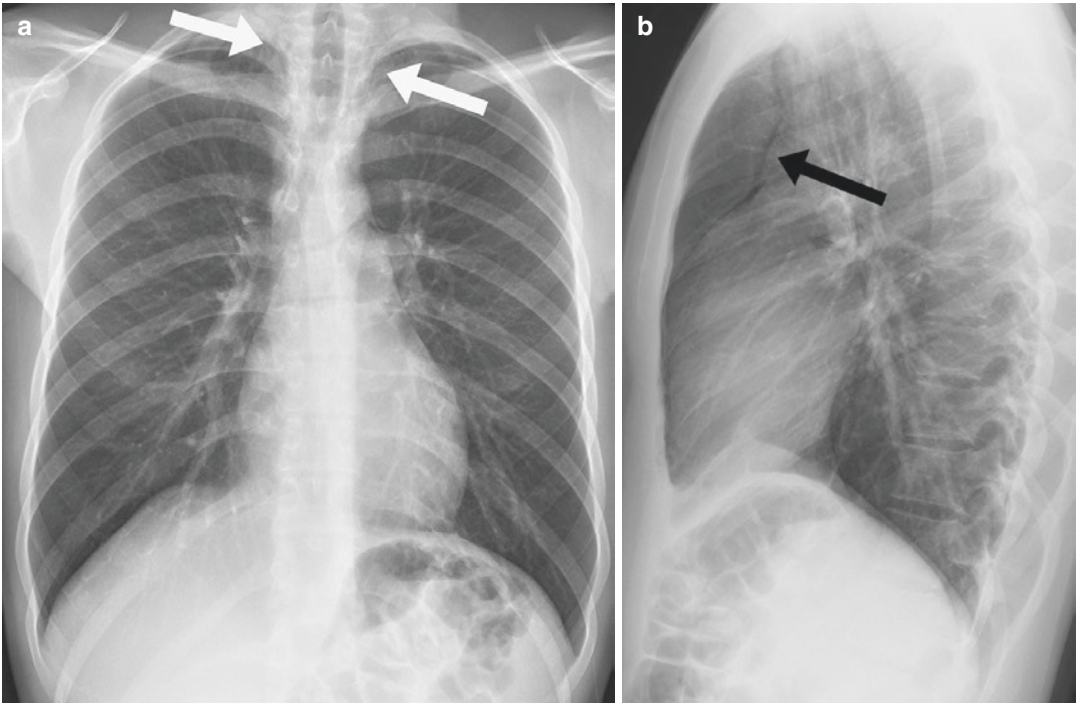
Fig. 5.20 Pneumomediastinum. Very subtle linear lucencies (white arrows) are demonstrated in the lower neck on the PA radiograph (**a**). Pneumomediastinum is more obvious on the lateral radiograph (**b**), where a lucent line (black arrow) is visible anterior to the mediastinal structures
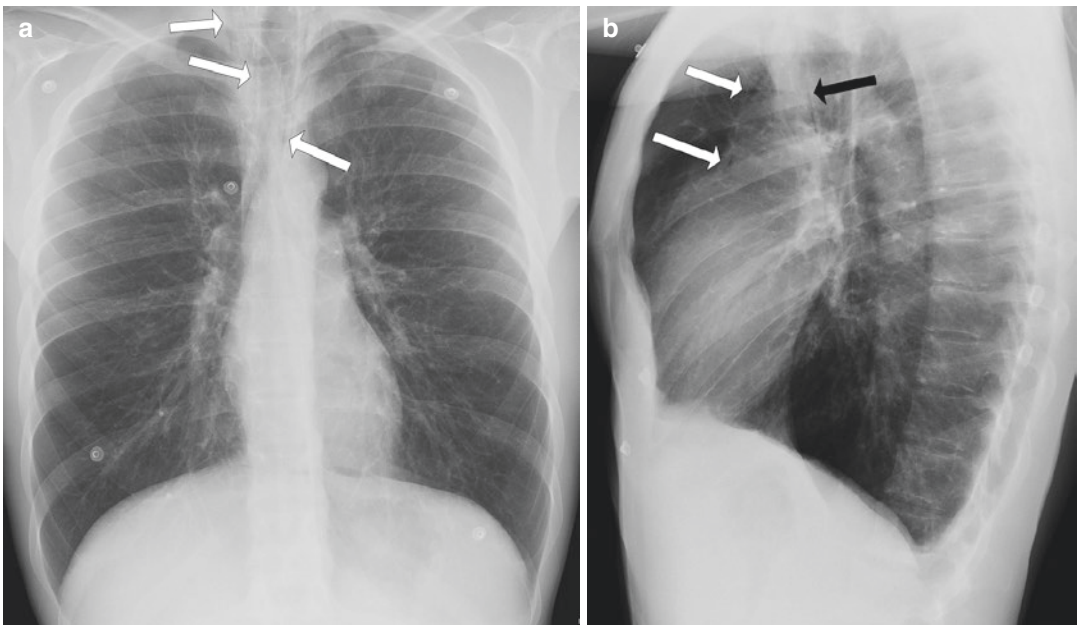

Fig. 5.21 Pneumomediastinum in a 21-year-old man with asthma. Linear lucencies (white arrows) are seen in the lower neck and the superior mediastinum on the PA radiograph (**a**) and anterior to the aorta and the trachea (black arrow) on the lateral radiograph (**b**)

Table 5.2 Technical errors and problem-solving tips for CTPA

Problem	Possible cause	Solution
Poor concentration of contrast in the main pulmonary artery but bright contrast in the SVC, and contrast is in the peripheral pulmonary arteries/pulmonary veins	Transient interruption of contrast from unopacified blood in the IVC. This may occur due to increased abdominal pressure (in particular, Valsalva, abdominal mass, pregnancy, and obesity)	Image without breath holding (Fig. 5.22). Consider a *V/Q* scan especially in pregnant patients
Good concentration of contrast in the main pulmonary artery and bright SVC, but poor concentration in the peripheral pulmonary arteries	Imaging too early. Even with appropriate bolus trigger or test bolus, this can occur due to poor cardiac output. When right ventricular function is severely compromised, contrast concentration in the central pulmonic arteries may also be low or may appear streaky	Increase scan delay by 2–3 s (Figs. 5.23 and 5.24)
Poor concentration of contrast in the main pulmonary artery and SVC, but good opacification of the peripheral pulmonary arteries, veins, and/or aorta	Imaging too late. This can occur in young patients (especially when cardiac output is further increased by tachycardia)	Decrease scan delay by 1–2 s
Examination doesn't trigger	Region of interest may be placed poorly. ROI may be difficult to place with congenital heart disease or anatomic alteration, including due to surgery or severe thoracic deformity	Check technologist's ROI and reposition as necessary
Examination too noisy. Pixelated appearance of the pulmonary arteries	Obesity, large diameter of the chest wall	Even with variable mA, it may be necessary to design separate protocols for large and very large patients. Before repeating the scan, determine if the examination is diagnostic for evaluation to the segmental vessels

IVC Inferior vena cava, *SVC* superior vena cava, *V/Q* ventilation perfusion, *ROI* region of interest

utility remains paramount [21]. Diagnostic imaging remains critical to determining who is treated and how. Undertreatment increases the risk of PE-related mortality, but overtreatment also places the patient at increased risk for treatment complications, including intracranial and other hemorrhages.

5.5.1 CTPA Technical Errors

Although ensuring a minimum threshold opacification (usually at least 250 HU) in the main pulmonary artery is an accepted method to judge the technical adequacy of a CTPA examination, evaluating motion artifacts, signal-to-noise ratio, and contrast opacification in the more peripheral pulmonary arteries is equally important but may be overlooked. All four factors can result in interpretative errors or can render a CT nondiagnostic. Additional common technical difficulties are summarized in Table 5.2.

5.5.2 Interpretative Errors

In the early days of CT, much attention was paid to the possibility of confusing incompletely opacified pulmonary veins and arteries and avoiding streak artifacts from dense contrast in the superior vena cava, metal implants, or structures outside the thorax (Fig. 5.25). With technical advancements and increased experience, these specific issues are rarely a concern, and the challenge now is to avoid more subtle errors. Unfortunately, the conse-
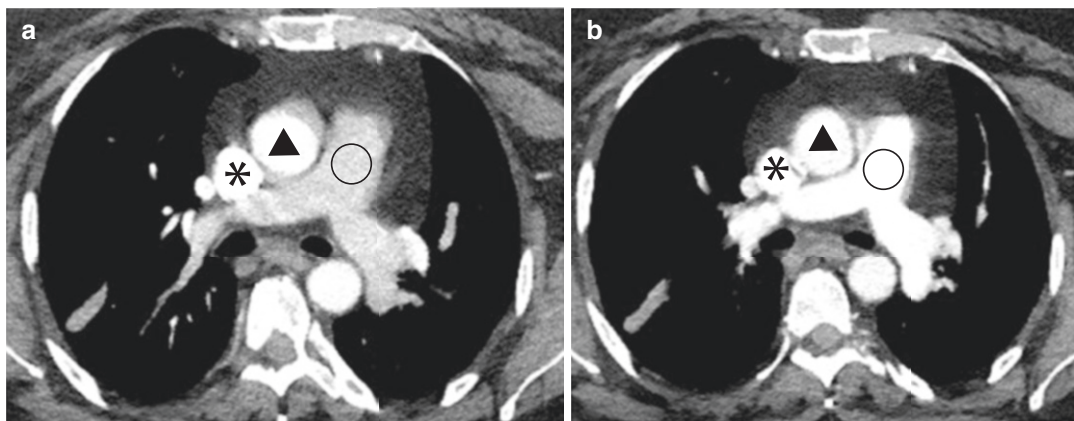
Fig. 5.22 CTPA with axial images in a 43-year-old with obesity. Initial scan (**a**) performed with standard breath hold instruction demonstrates high-density IV contrast in both the superior vena cava (*) and the ascending aorta (triangles) but unacceptably low contrast concentration in the main pulmonary artery (circles). Repeating the scan with no breath hold (**b**) reduces Valsalva-related return of unopacified blood from the IVC. In (**b**), Hounsfield units in the main pulmonary artery are now at a diagnostic level
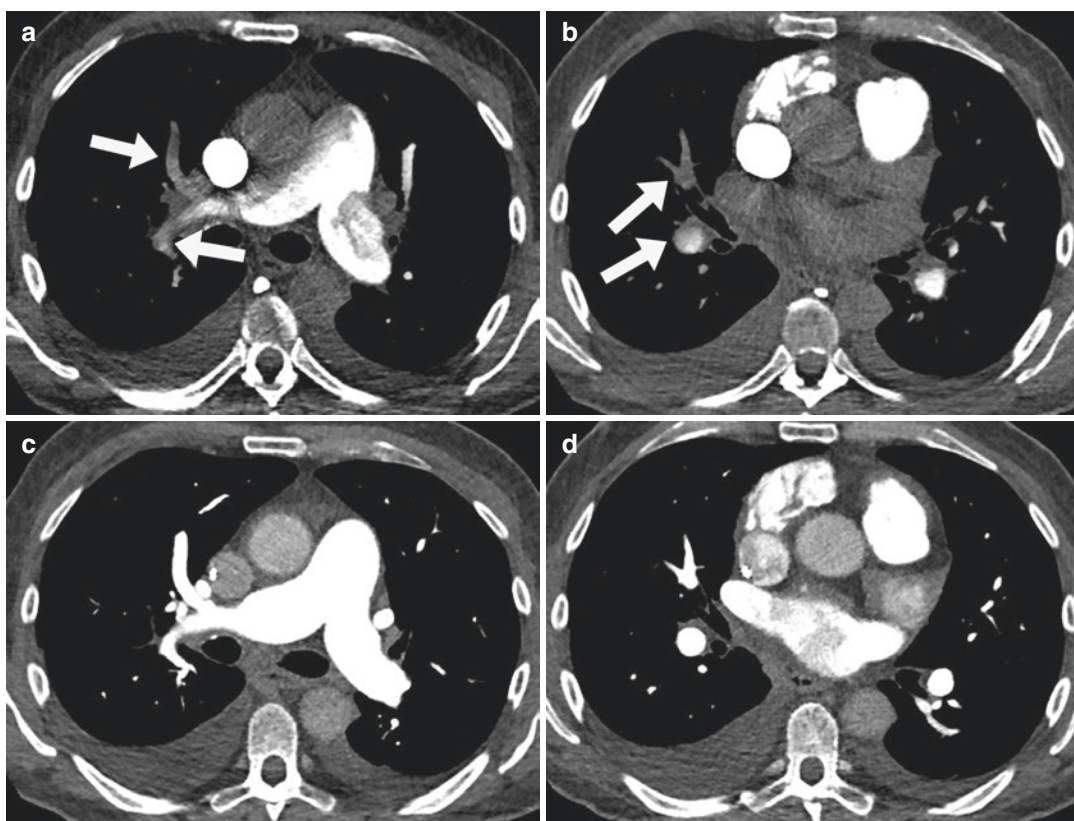
Fig. 5.23 Poor right heart function resulting in flow artifact. Axial images from CTPA protocol (**a**, **b**) performed on a 64-year-old man demonstrate multiple apparent filling defects in the main right and left pulmonary arteries despite excellent contrast opacification of the main pulmonary artery. There is poor contrast opacification of the right lobar and segmental arteries (arrows). Density in the abnormal vessels measure over 150 HU, greater than expected for true pulmonary emboli. Because of the known history of right heart disease, the examination was repeated (**c**, **d**) with a 3 second increase in scan delay, resulting in a normal appearance of the pulmonary vessels. Bilateral pleural effusions are present

Fig. 5.24 Flow artifact in a 62-year-old man. Selected axial images from a CTPA (**a–d**) demonstrating excellent contrast opacification of the main pulmonary artery (circle) but low attenuation within the basal trunk of the right lower lobar artery (arrows). Repeating the examination immediately with a second IV bolus and a slightly longer delay (**e–h**) demonstrates normal enhancement of the artery. The patient was known to have chronic severe right heart dysfunction. Enlargement of the right ventricle and atrium reflects right heart dysfunction. Bilateral effusions are present

Fig. 5.25 Artifact mimicking pulmonary emboli in a 61-year-old man. Linear areas of low attenuation (arrows) are seen in the superior segmental artery of the right lower lobe (**a**) and in the basal trunk of the left lower lobar artery (**b**) on two axial CTPA images. Similar lines are seen coursing outside the vessels (open arrows), and confirm the finding represents streak artifacts, in this patient due to imaging with the arms down as demonstrated on the scout radiograph (**c**)

quence of overcalling pulmonary embolus may be significant, particularly with respect to potential bleeding complications.

CTPA-specific windowing should be used so that small clots will not be obscured by very high-density contrast. However, even with advanced scanners, respiratory and cardiac motion can cause a normal vessel to demonstrate low density. Before raising the possibility of embolus, alter the window settings as motion artifacts are better appreciated on lung windows. A double arterial shadow alerts the radiologist that the abnormal
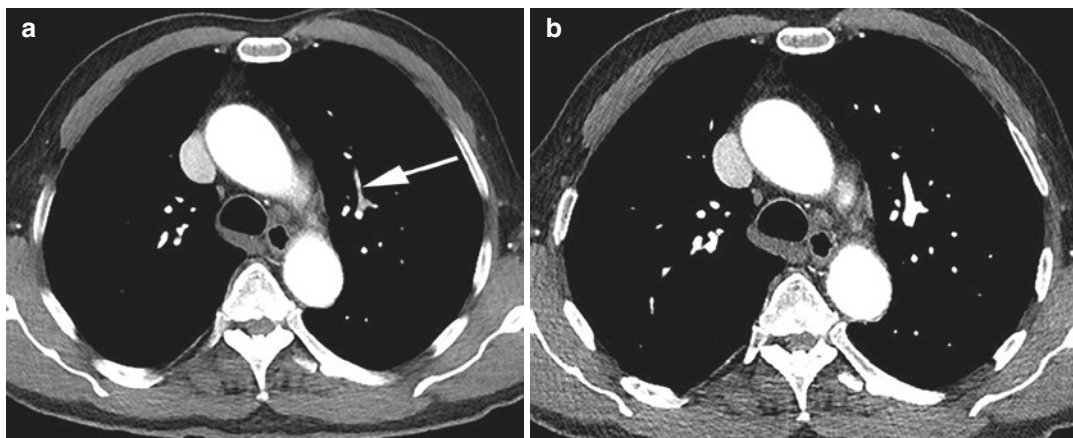
Fig. 5.26 Volume averaging artifact in an 83-year-old man. Axial contrast-enhanced CT (**a**) with 5 mm collimation appears to show low attenuation in a central artery within the left upper lobe (arrow). (**b**) The source images were reformatted to 1.5 mm collimation for clarification and demonstrate a normal vessel. The appearance suggestive of embolus on the thicker slice collimation is due to volume averaging with adjacent lung

appearance is likely secondary to motion rather than an embolus. A similar appearance of low density can occur with thicker slice collimation. In practice, this is an issue when an examination is not performed with a specific CTPA protocol. Reformatting the source images with thinner collimation can prevent both errors and repeat scanning (Fig. 5.26).

Distinguishing poorly opacified but normal arteries from pulmonary embolus can also be difficult. A clot-free vessel can appear low density due to one of three phenomena: (1) imaging before contrast has completely reached the artery (often seen in patients with very poor cardiac output); (2) reduced local arterial flow secondary to abnormal lung (hypoxic vasoconstriction); and (3) poor enhancement secondary to non-enhanced blood return from the abdomen. This phenomenon known as "flow artifact" can be evaluated by measuring the density within the apparent thrombus. Small studies have shown that on an CTPA examination, true acute pulmonary embolus should measure less than 70 HU [22, 23]. Flow artifacts also often tend to be less well defined than emboli.

Pulmonary embolus can also be missed if the entire vessel is involved. When the interface between clot and normally enhancing vessel is not obvious, pulmonary embolus can be confused with a normal vein (Fig. 5.27). It may be helpful to identify all 18 segmental arteries to ensure large emboli are not missed. Reviewing reformations in other planes and evaluating the global appearance of the pulmonary vasculature can also be helpful.

Even for experienced expert radiologists, there will always be some difficult CTPA examinations to interpret. In these patients, it may be helpful to take a more holistic approach. An isolated equivocal abnormality is more easily dismissed than several equivocal abnormalities in separate areas of the lung. If the study is truly equivocal, it is important that the report discuss whether or not the scan demonstrates an alternate possibility (such as aspiration) for the clinical presentation.

5.5.3 Signs of Severity

In the setting of a positive or equivocal CTPA examination, it is standard of practice for the radiologist to report on the CT findings of right ventricular dysfunction (Fig. 5.28). While the ratio of the right ventricle (RV) short-axis diameter versus the left ventricle (LV) short-axis diam-
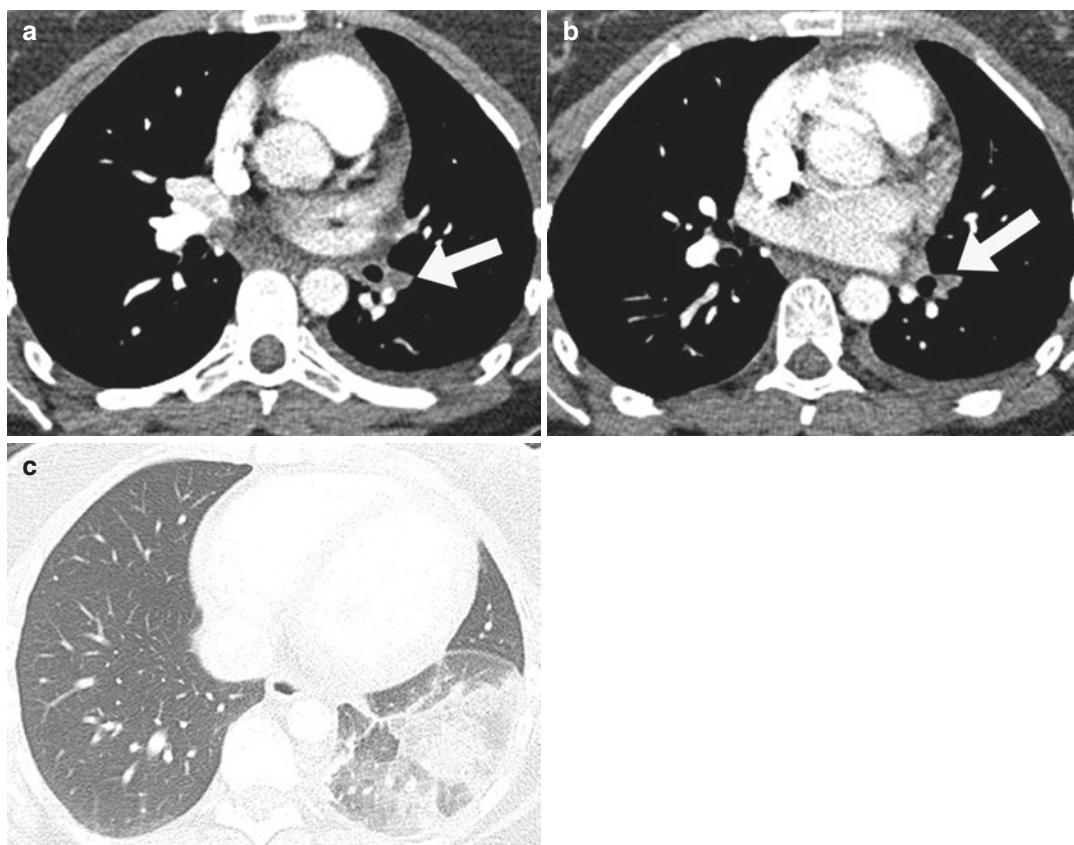
Fig. 5.27 Missed acute pulmonary embolus reported as pneumonia. Axial images with mediastinal windowing (**a**, **b**) on a CTPA examination demonstrate complete absence of contrast enhancement in the anteromedial basal segment of the left lower lobar pulmonary artery (arrow), which was missed by the radiologist. The ground-glass opacity and consolidation in the left lower lobe demonstrated on axial lung windows (**c**) represents associated hemorrhage/pulmonary infarction
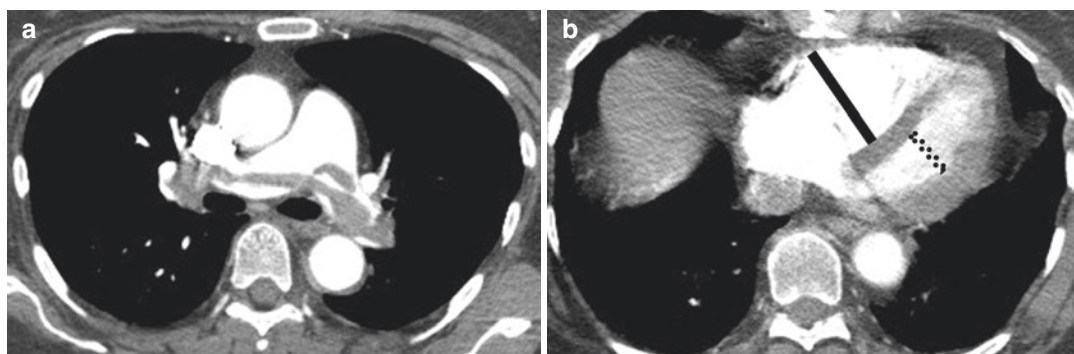

Fig. 5.28 (**a**, **b**) Saddle embolus resulting in acute right heart strain in a 52-year-old man. Axial images from a CTPA examination with large central embolus demonstrate short axis diameter of the right ventricle (solid line) to be substantially larger than that of the left ventricle (dashed line). Note also bowing of the intraventricular septum
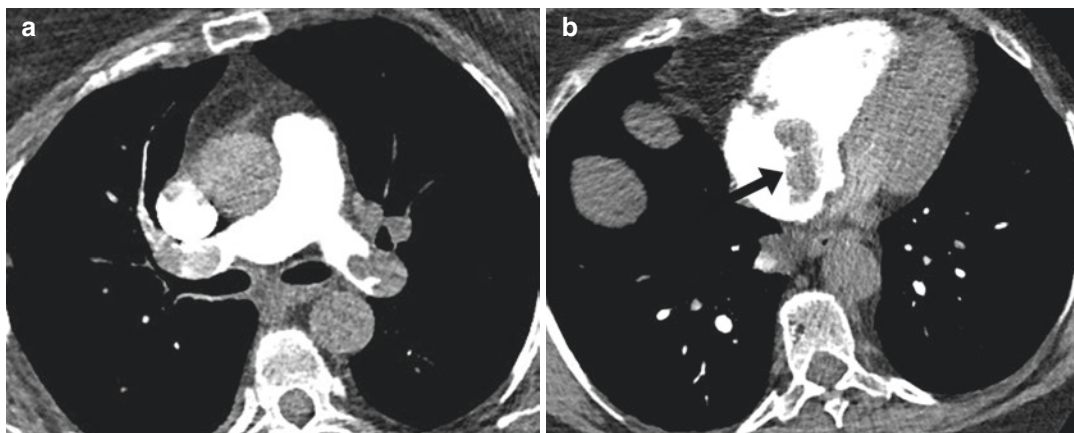
Fig. 5.29 (**a**, **b**) Right atrial thrombus in a 66-year-old woman. Axial images from a CTPA demonstrating right and left central pulmonary emboli but also thrombus in the right atrium (arrow). This requires urgent consultation and possibly surgical or interventional radiology treatment. Note also that the right ventricle is substantially larger than the left ventricle, a sign of right heart strain

eter as seen on a single axial image is easy to measure on CT, studies on the predictive value of this measurement are mixed to our knowledge [24, 25]. Similarly, deviation of the intraventricular septum does not appear to be a useful sign on non-gated CTPA [26]. RV-to-LV ratio >1.5, RV-to-LV ratio on a four-chamber view >1, and RV volume to LV volume >1 are all better predictors of adverse outcome and are associated with a greater risk of sudden death [25]. Severity of contrast reflux into the IVC and hepatic veins is also associated with right ventricular strain but may be affected by the rate and volume of contrast administration [27].

Approximately 4% of patients with pulmonary embolus will have right atrial thrombus [28]. This can be missed unless the right atrium is systematically reviewed on every CTPA examination (Fig. 5.29). The finding of right atrial embolus should be brought specially to the attention of the ED clinician, as these patients will require echocardiogram for further confirmation and may require surgical or percutaneous embolectomy [29].

and PE can be overlooked in those without apparent risk factors. Regardless of the information provided on the requisition, the radiologists should consider pulmonary embolus in the following emergency imaging scenarios:

1. Consolidation or ground-glass opacity with a focal peripheral distribution on CXR. While infection would be the most likely consideration, review the clinical history to ensure it is concordant. If there are risk factors or unusual clinical features such as chest pain or absence of fever, it may be prudent to perform dedicated PE imaging.
2. Peripheral basal pulmonary consolidation/ground-glass opacity on a CT of the abdomen (Fig. 5.30), particularly when the CT is performed for pain.
3. Unilateral pleural effusion on CXR or CT without explanation (i.e., no history of trauma, pneumonia, or malignancy). At minimum, the clinical history and physical examination should be reviewed.

5.5.4 Missed Pulmonary Embolus on Non-dedicated Imaging

Pulmonary embolus may be difficult to detect clinically; basal embolus may present with flank pain, some patients may not present with pain,

5.5.5 Negative PE Examination: Are You Missing Something?

Before signing off a negative CTPA examination report, the radiologist should consider the following checklist:

Fig. 5.30 Pulmonary hemorrhage (i.e., infarct) on a renal colic CT. Axial CT with lung windows from a non-contrast renal colic CT in an afebrile 43-year-old man presenting with right flank and shoulder pain demonstrates ground-glass opacity at the right lower lobe. Dedicated CTPA (not shown) confirmed acute pulmonary embolus
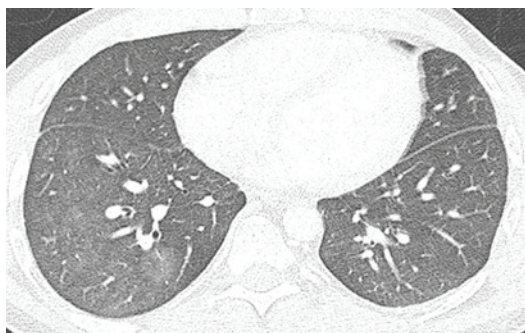

Fig. 5.31 Pneumonia on CTPA in a 43-year-old man with fever and dyspnea. Axial image from a CTPA with lung window demonstrates subtle ground-glass opacity in the right lower lobe. This is an early pneumonia that was not visible on the chest radiograph obtained earlier the same day (not shown)

– Osseous: Is there an acute rib fracture, a verte-bral body compression fracture, or evidence of discitis?
– Cardiac: Even in a young patient, is there any CT evidence of cardiomyopathy such as increased chamber size or increased ventricu-lar wall thickness? Is there a pericardial effusion?
– Aorta: Any evidence of intramural hematoma? Any circumferential non-calcified wall thick-ening to suggest vasculitis?
– Lung: Is there evidence of subtle pneu-monia that may have been occult on chest radiography (Fig. 5.31)? Is there any evi-

dence of aspiration, including bronchial fluid/mucus/debris?
– Abdomen: If the field of view allows, is there any evidence of a renal calculus or obstruction, pancreatitis, or cholecystitis, for example?

5.6 Special Considerations for Vulnerable Patient Groups

5.6.1 Pregnant and Postpartum Patients

Pregnant and postpartum patients are at higher risk for pulmonary embolism, aortic dissection, cardiomyopathy, pulmonary edema, ARDS, and infection (the latter due to immunosuppression). PE is the most common cause of maternal death [30]. Due to the normal physiologic changes in pregnancy, heart rate and respiratory rate may be elevated. D-dimer is frequently elevated and may not return to normal values until 6 weeks postpar-tum. Unfortunately, pregnant patients have a high rate of nondiagnostic CTPA [31, 32], usually due to transient interruption of contrast. Modified *V/Q* and *V/Q* SPECT examination may be appro-priate alternatives and result in reduced maternal breast radiation [33]. If CTPA is performed, non-diagnostic imaging due to unopacified abdominal blood return to the heart can be reduced by careful instruction to avoid both deep inspiration and forceful breath holding.

5.6.2 Oncology Patients

Oncology patients are frequent users of the emergency department including for diagnosis, disease complications, treatment complications, and end-of-life care. In the patient with known malignancy, treatment-related pulmonary tox-icity can be seen with chemotherapy agents, medications targeting specific oncologic muta-tions, immunotherapy, and radiation therapy. Diffuse findings of pulmonary edema (acute lung injury) is a medical emergency and may reflect life-threatening acute radiation pneumonitis or drug-related pulmonary toxicity. These patients

may deteriorate rapidly if misdiagnosed with pneumonia. Non-specific interstitial pneumonia, organizing pneumonia, eosinophilic pneumonia, and hypersensitivity pneumonitis are other manifestations of treatment-related injury.

Oncologic patients are at higher risk for opportunistic infections, including invasive fungal infections (aspergillosis and candidiasis) and *Pneumocystis jirovecii* pneumonia. Do not hesitate to perform a CT in a patient with immunocompromise (particularly febrile neutropenia) with respiratory symptoms or without apparent non-pulmonary cause, even if the CXR is normal. CT allows for earlier diagnosis and improved outcomes.

Pulmonary embolus is an incidental finding in up to 4% of oncologic patients who have a thoracic CT [34, 35]. If thicker reformations have been obtained and result in a questionable incidental pulmonary embolus, the source images should be able to be reformatted with thin sectioning. If reformats remain unclear, a dedicated CTPA may be required.

Finally, sometimes radiologists are so intent on reporting a new diagnosis of malignancy or changes of an existing malignancy that we forget to emphasize the possible emergent manifestations of the chronic process. In the setting of lung cancer or metastatic disease to the thorax, pay careful attention for tracheal and main stem or lobar bronchial narrowing, complete or impending SVC compromise, spinal canal compromise, and impending vertebral body collapse.

5.6.3 Chronic Disease in the Emergency Department

As discussed above, chest radiographs are the most frequently ordered imaging examination in the ED. Patients with poor health care and without family physician care are more likely to present to the ED. Subsequently, the ED chest radiograph is an important pathway to chronic disease diagnosis, including lung cancer and chronic interstitial lung disease. However, it is essential to note that patients with acute respiratory complaints may demonstrate acute findings mimicking significant chronic diseases. In a patient with the possibility of an acute explanation for a concerning CXR finding, consider follow-up PA and lateral radiographs, instead of immediate CT. In particular, pulmonary edema can mimic interstitial lung disease, and acute inflammatory and infectious consolidation can mimic malignancy. Consider that even for asymptomatic patients, 50% of sub-solid or part-solid nodules and masses seen on CT are transient [36]. When a patient has clinical evidence of an acute inflammatory/infectious process or when there is evidence of pneumonia elsewhere in the lung, short-term interval surveillance imaging (6–12 weeks) for a focal ill-defined or sub-solid nodule should be performed before more intensive work-up for underlying malignancy. There is no easy formula to protect the radiologist from over or under calling chronic disease. However, reviewing prior films, risk factors, and clinical presentation can help ensure more appropriate care.

5.7 Conclusion

Given the ubiquity of chest radiography in the emergency department and the non-specific nature of radiographic findings, there is potential for significant error in ED thoracic imaging. Radiologist initiated correlation with clinical information, careful wording of reports, and understanding of common pitfalls may all contribute to decreasing avoidable errors.

References

1. Rui P, Kang K. Emergency department summary tables. In: National hospital ambulatory medical care survey; 2015. http://www.cdc.gov/nchs/data/ahcd/nhamcs_emergency/2015_ed_web_tables.pdf. Accessed 15 Jun 2018.
2. Fatihoglu E, Aydin S, Gokharman FD, Ece B, Kosar PN. X-ray use in chest imaging in emergency department on the basis of cost and effectiveness. Acad Radiol. 2016;23:1239–45.
3. Lara AR, Schwarz MI. Diffuse alveolar hemorrhage. Chest. 2010;137:1164–71.

4. Tasaka S. Pneumocystis pneumonia in human immunodeficiency virus–infected adults and adolescents: current concepts and future directions. Clin Med Insights Circ Resp Pulm Med. 2015;9(Suppl 1):19–28.

5. Walzer PD, Evans HER, Copas AJ, Edwards SG, Grant AD, Miller RF. Early predictors of mortality from pneumocystis jirovecii pneumonia in HIV-infected patients: 1985–2006. Clin Infect Dis. 2008;46:625–33.

6. Ichikado K, Suga M, Muller NL. Acute interstitial pneumonia: comparison of high-resolution computed tomography findings between survivors and nonsurvivors. Am J Respir Crit Care Med. 2002;165:1551–6.

7. Bouros D, Nicholson AC, Polychronopoulos V, du Bois RM. Acute interstitial pneumonia. Eur Respir J. 2000;15:412–8.

8. Komiya K, Ishii H, Umeki K, Kawamura T, Okada F, et al. Computed tomography findings of aspiration pneumonia in 53 patients. Geriatr Gerontol Int. 2013;13:580–5.

9. Nambu A, Ozawa K, Kobayashi N, Tago M. Imaging of community-acquired pneumonia: roles of imaging examinations, imaging diagnosis of specific pathogens and discrimination from noninfectious diseases. World J Radiol. 2014;6:779–93.

10. Rossi SE, Erasmus JJ, McAdams HP, Sporm TA, Goodman PC. Pulmonary drug toxicity: radiologic and pathologic manifestations. Radiographics. 2000;20:1245–59.

11. Blackmore CC, Black WC, Dallas RV, Crow HC. Pleural fluid volume estimation: a chest radiograph prediction rule. Acad Radiol. 1996;3:103e9.

12. Yap E, Anderson G, Donald J, Wong CA, Lee YCG, et al. Pleural effusion in patients with pulmonary embolism. Respirology. 2008;13:832e6.

13. Tsai TT, Nienaber CA, Eagle KA. Acute aortic syndromes. Circulation. 2005;112:3802–13.

14. Nienaber CA, Fattori R, Mehta RH, Richartz BM, Evangelista A, et al. Gender-related differences in acute aortic dissection. Circulation. 2004;109:3014–21.

15. Hagan PG, Nienaber CA, Isselbacher EM, Bruckman D, Karavite DJ, et al. The international registry of acute aortic dissection (IRAD): new insights into an old disease. JAMA. 2000;283:897–903.

16. Kruse MJ, Johnson PT, Fishman EK, Zimmerman SL. Aortic intramural hematoma: review of high-risk imaging features. J Cardiovasc Comput Tomogr. 2013;7:267–72.

17. Gahana F, Miller DC, Sugimoto K, Do YS, Minamiguchi H, et al. Prognosis of aortic intramural hematoma with and without penetrating atherosclerotic ulcer: a clinical and radiological analysis. Circulation. 2002;106:342–8.

18. Buckle CE, Udawatta V, Straus CM. Now you see it, now you don't: visual illusions in radiology. Radiographics. 2013;33:2087–102.

19. Caceres M, Ali SZ, Braud R, Weiman D, Garrett HE. Spontaneous pneumomediastinum: a comparative study and review of the literature. Ann Thorac Surg. 2008;86:962–6.

20. Weiner RS, Oulette DR, Diamond E, Fan VS, Mauer JR, et al. An official American Thoracic Society/American College of Chest Physicians policy statement: the choosing wisely top five list in adult pulmonary medicine. Chest. 2014;145:1383–91.

21. Stein P, Matta F. Epidemiology and incidence: the scope of the problem and risk factors for development of venous thromboembolism. Clin Chest Med. 2010;31:611–28.

22. Wittram C, Maher MM, Halpern E, Shepard JO. Attenuation of acute and chronic pulmonary emboli. Radiology. 2005;235:1050–4.

23. De Luca F, Modolon C, Buia F, Attinà D, Fughelli P, et al. Densitometric CT evaluation of acute and chronic thromboembolic filling defects of the pulmonary arteries before and after contrast injection. Radiol Med. 2012;117:979–91.

24. Meinel FG, Nance JW Jr, Schoepf UJ, Hoffmann VS, Thierfelder KM, et al. Predictive value of computed tomography in acute pulmonary embolism: systematic review and meta-analysis. Am J Med. 2015;128:747–59.e2.

25. Kang DK, Thilo C, Schoepf UJ, Barraza JM Jr, Nance JW Jr, et al. CT signs of right ventricular dysfunction: prognostic role in acute pulmonary embolism. JACC Cardiovasc Imag. 2011;4:841–9.

26. Ghaye B, Ghuysen A, Willems V, Lambermont B, Gerard P, et al. Severe pulmonary embolism: pulmonary artery clot load scores and cardiovascular parameters as predictors of mortality. Radiology. 2006;239:884–91.

27. Aviram G, Rogowski O, Gotler Y, Bendler A, Steinvil A, et al. Real-time risk stratification of patients with acute pulmonary embolism by grading the reflux of contrast into the inferior vena cava on computerized tomographic pulmonary angiography. J Thromb Haemost. 2006;6:1488–93.

28. Torbicki A, Galie N, Covezzoli A, Rossi E, De Rosa M, et al. Right heart thrombi in pulmonary embolism: results from the international cooperative pulmonary embolism registry. J Am Coll Cardiol. 2003;41:2245–51.

29. Jaff MR, McMurtry MS, Archer SL, Cushman M, Goldenberg N, et al. Management of massive and submassive pulmonary embolism, iliofemoral deep vein thrombosis, and chronic thromboembolic pulmonary hypertension. Circulation. 2011;123:1788–830.

30. Bhatia P, Bhatia K. Pregnancy and the lungs. Postgrad Med J. 2000;76:683–9.

31. Devaraj A, Sayer C, Sheard S, Grubnik S, Nair A, et al. Diagnosing acute pulmonary embolism with computed tomography: imaging update. J Thorac Imaging. 2015;30:176–92.

32. Parker MS, Hui FK, Camacho MA, et al. Female breast radiation exposure during CT pulmonary angiography. Am J Roentgenol. 2005;85:1228–33.

33. Leung AN, Bull TM, Jaeschke R, Lockwood CJ, Boiselle PM, et al. American Thoracic Society documents: an official American Thoracic Society/Society of Thoracic Radiology clinical practice guideline-evaluation of suspected pulmonary embolism in pregnancy. Radiology. 2012;262:635–46.

34. Engelke C, Manstein P, Rummeny EJ, Marten K. Suspected and incidental pulmonary embolism on multidetector-row CT: analysis of technical and morphological factors influencing the diagnosis in a cross-sectional cancer centre patient cohort. Clin Radiol. 2006;61:71–80.

35. Sebastian AJ, Paddon AJ. Clinically unsuspected pulmonary embolism – an important secondary finding in oncology CT. Clin Radiol. 2006;61:81–5.

36. Feliz L, Serra-Tosio G, Lantuejoul S, Timsit JF, Moro-Sibilot D, et al. CT characteristics of resolving ground glass opacities in a lung cancer screening program. Eur J Radiol. 2011;77:410–6.

Errors in Imaging of Abdominal and Pelvic Trauma

6

Mariano Scaglione, Ettore Laccetti, Roberto Picascia, Michele Altiero, Francesca Iacobellis, Mathew Elameer, and Roberto Grassi

6.1 Introduction

Abdominal and pelvic trauma represents a common clinical problem in the emergency department. The mechanism of trauma is the most important issue influencing the choice of imaging work-up, regardless of the age of the patient. We face at least two major clinical scenarios: minor trauma and major (poly-)trauma.

In minor trauma, most European trauma centers recommend ultrasonography (US) as the first-line imaging technique in the evaluation of most abdominal and pelvic trauma. In Europe, US is usually performed by a consultant radiologist working 24/7 in the emergency department, for rapid assessment of free fluid in the peritoneal, pericardial, and pleural spaces. Moreover, US also has a high sensitivity and specificity for the identification of intra-abdominal solid organ injuries, including to the liver and spleen [1]. Nevertheless, this technique has low sensitivity and specificity for injuries to the retroperitoneum and hollow viscus. Furthermore, US may be limited by abdominal gas or bowel distention (ileus), patient habitus, and lack of patient cooperation. Errors can be related to inappropriate technical equipment or probes, suboptimal image settings, and inadequate training in emergency ultrasound [2–6]. Intravenous (IV) contrast-enhanced US (CEUS) is a technique frequently used in Europe to improve the intrinsic limitations of a standard US examination. IV administration of microbubbles acts as contrast and proves to be particularly useful in young patients with minor, localized trauma to diagnose or exclude liver and splenic injuries, as well as in the follow-up of stable adult patients with known isolated liver, splenic, or renal lacerations, thus substantially reducing the number of CT scans and the associated dose exposure.

M. Scaglione (✉)
Department of Diagnostic Imaging, "Pineta Grande" Hospital, Castel Volturno, CE, Italy

Department of Radiology, Sunderland Royal Hospital, NHS, Sunderland, UK
e-mail: mariano.scaglione@pinetagrande.it

E. Laccetti · M. Altiero
Department of Diagnostic Imaging, "Pineta Grande" Hospital, Castel Volturno, CE, Italy

R. Picascia · R. Grassi
Department of Radiology, University of Campania "L. Vanvitelli", Naples, Italy

F. Iacobellis
Department of General and Emergency Radiology, "A. Cardarelli" Hospital, Naples, Italy

M. Elameer
Department of Radiology, Sunderland Royal Hospital, NHS, Sunderland, UK

The second scenario is major trauma (i.e., poly-trauma).

Poly-trauma is an acute multi-organ potentially life-threatening disease requiring prompt assessment and treatment. It is characterized by injury involving two or more body parts, with an injury severity score (ISS) greater than or equal to 16, and a series of systemic reactions, which increases the incidence of injuries in distant organs from the site of the primary injury [7]. In terms of average life expectancy, the years lost by poly-trauma patients exceed those caused by cancer and cardiovascular disease combined.

In Western countries, poly-trauma represents the third most common cause of death and is the first leading cause of death in people under 45 years [8], even though its mortality has significantly dropped from 40% to 10%, between 1907 and 2008 [9]. Regardless of the patient's age, in the context of poly-trauma, multi-detector CT (MDCT) is the reference imaging standard, with a sensitivity of 95% and a negative predictive value approaching 100%, to depict injuries [10–13]. MDCT has markedly contributed to the change of the "classic paradigm" established decades ago, which has moved from an invasive laparotomy routinely to non-operative management whenever possible, thus reducing mortality and morbidity from trauma and related complications [14].

In the emergency setting, radiologists play a crucial role in the diagnosis and management of trauma patients. They are members of the Trauma Team [2]. Together with other trauma specialists including emergency physicians, surgeons, anaesthesiologists, and ancillary staff, radiologists have the responsibility to care for trauma patients and specifically to advise, protocol, and expedite accurate diagnosis, providing important information for timely management. However, despite the advances in imaging technology and the powerful MDCT scanners available today, numerous diagnostic and management errors still continue to exist, with serious potential consequences for patients [15, 16].

Two main categories of errors, resulting in the failure or delay in diagnosis of abdominal and pelvic injuries in poly-trauma patients, are associated with MDCT:

- *Technical and methodological errors*: representing approximately 60%, are related to incomplete imaging, poor quality imaging, or inadequate technique
- *Diagnostic errors*: related to perceptual errors or non-visual errors [17–19]

6.2 Technical and Methodological Errors

In the past, older-generation CT technology was not used for the evaluation of poly-trauma patients due to the long time for a whole-body CT acquisition. Most patients were imaged with a protocol including a head CT, lateral cervical spine radiograph, AP chest radiograph, AP pelvis radiograph, an extended focused assessment with sonography for trauma (FAST), and clinical observation. It has been proven that this "old

Fig. 6.1 A 37-year-old man was admitted to the emergency department after a motor bicycle accident. This patient was initially imaged with a CT head, chest X-ray, and an extended FAST examination (eFAST), which showed no abnormalities. After 3 h, the patient became rapidly hypotensive and dropped his hemoglobin level to 10 g/dL. Therefore, he was immediately taken to CT for evaluation. Contrast-enhanced CT shows a deep laceration in the segment VIII of the liver (grade 3, according to AAST) and massive free hemoperitoneum around the liver and spleen. Comment: this patient demonstrates the value of CT in the initial assessment of trauma patients compared to the "old clinical paradigm," which included CT head, chest radiography, FAST examination, and observation

fashioned approach" potentially leads to severe errors, delayed diagnosis, and a prolonged period of clinical observation [20, 21] (Fig. 6.1).

Currently, faster MDCT scanners with a tailored protocol for high-energy trauma allow optimal identification of subtle but potentially life-threatening injuries, directing the patient toward the most appropriate and timely management. Furthermore, given its high negative predictive value, MDCT can be used to exclude nearly 100% of all injuries, thus permitting discharge of the patient and saving the costs of unnecessary hospitalization, when it is appropriate to do so [22].

From the authors' perspective, although in the literature there is no general agreement regarding the "best" CT protocol approach in the context of high-energy trauma, the "whole-body MDCT protocol for trauma" is strongly advised [23]. The "whole-body CT scan protocol" includes a non-contrast scan of the head, followed by an arterial-phase scan from the circle of Willis to the symphysis pubis, and a venous-phase scan from the diaphragm to the iliac crests. Intravenous contrast material (80–130 mL iodinated contrast medium, according to the patient's weight) at a high concentration (370–400 mg I/mL), injected at 4–5 mL/s, is followed by a 40 mL saline chaser at the same flow rate, to obtain optimal vessel depiction. Automated bolus tracking identifies the arterial phase; a region of interest (ROI) is placed on the aortic arch, and scanning begins when an attenuation threshold of 100 HU is reached. The venous phase is performed at a 60- to 70-s delay from the beginning of the injection. Post-processing with three-dimensional (3D) multi-planar reconstructions (MPR) and volume rendering reconstructions is helpful for identifying injuries of the vessels and sites of active bleeding, as well as for searching for osseous injuries which can be missed on the axial images. Faster MDCT technology, high flow rates of injection, and high concentrations of iodinated contrast result in optimal vascular and parenchymal image quality.

For accurate vascular evaluation, a slice thickness ranging from 0.5 to 3 mm, and preferably 0.5–1.5 mm, in the arterial phase is recommended, while to detect solid organ injuries, a slice thickness ranging from 3 to 5 mm, and preferably 3 mm, in the venous phase, is sufficient [17].

In Europe, a consultant radiologist is always present in the CT suite 24/7. She/he supervises, modifies the standard CT protocol if needed, and provides a first reading for immediate and appropriate patient management (i.e., tension pneumothorax, shattered spleen or kidney, etc.).

Moreover, in selected patients, an additional late phase at 3–5 min may be required to differentiate arterial bleeding from lower-pressure venous bleeding [16]. Bleeding may be classified into three main categories according to its size and morphology: a spot of bleeding (punctiform self-limiting bleeding), a jet (linear bleeding with no significant morphological change), or pooling (active extravasation of contrast media, with significant change in its shape and volume over multiple phases of acquisition) [24]. This classification may provide additional information to help decide the urgency and need for treatment, independently from the origin (arterial or venous) of bleeding. In some patients, this late phase also helps to distinguish active bleeding from non-traumatic organ benign findings (i.e., hemangiomas). If renal or ureteral injury is suspected, a low-dose delayed phase acquired 5–20 min after injection of contrast media is advised. This "excretory phase" provides crucial information about urinary extravasation, which can be effectively managed non-operatively in up to 95% of patients [17, 25].

When bladder injuries are suspected, irrespective of the presence or absence of pelvic fractures, it is necessary to obtain a high-quality MDCT cystogram. CT cystography, performed by active distension of the bladder with diluted iodinate contrast material through a urethral catheter (about 300–350 mL of 5% diluted contrast media), helps to identify bladder injuries [26–29]. Passive distension of the bladder during the "excretory phase" usually does not permit an overall assessment of bladder injuries. Injuries of the dome in particular may be easily overlooked, even if the bladder is passively distended [30, 31]. From the authors' perspective, MDCT cystography should be performed after the IV

contrast-enhanced CT acquisition of the abdomen and pelvis [32, 33]. This technique allows to get pre- and post-cystography CT images, to ensure that extra-luminal contrast material actually comes from the bladder. If the bladder is filled before CT, a urinary leak can be confused with, interfere with, or even hide active bleeding, thus potentially resulting in a delay of localization of bleeding and plans for embolization [32–35]. In patients with penetrating or gunshot injuries passing through the pelvis, a CT cystogram is advised, as well as the use of "triple contrast CT" to exclude bladder and/or bowel perforation [36, 37] (Fig. 6.2).

A controversial topic is the use of a noncontrast CT phase. This initial acquisition may be useful to detect hyperdense clot, i.e., the "sentinel clot sign": areas of higher attenuation near an

injury site, likely to indicate the source of bleeding. Non-contrast images may also be useful to improve the detection of intramural vascular hematomas [1, 17]. These two features may be difficult to identify after IV contrast injection. With modern MDCT scanners, dual-phase scanning (arterial and portal venous phases) appears adequate in most instances [38]. If any intraabdominal fluid is seen, the use of ROI analysis is necessary to classify and characterize the nature of the fluid.

Poor image quality and inadequate technique can also be the cause of errors of interpretation. New generation of MDCT scanners with faster acquisitions and thinner slice thickness have substantially improved routine imaging quality. Therefore, a correct protocol requires a minimum slice thickness which is necessary together
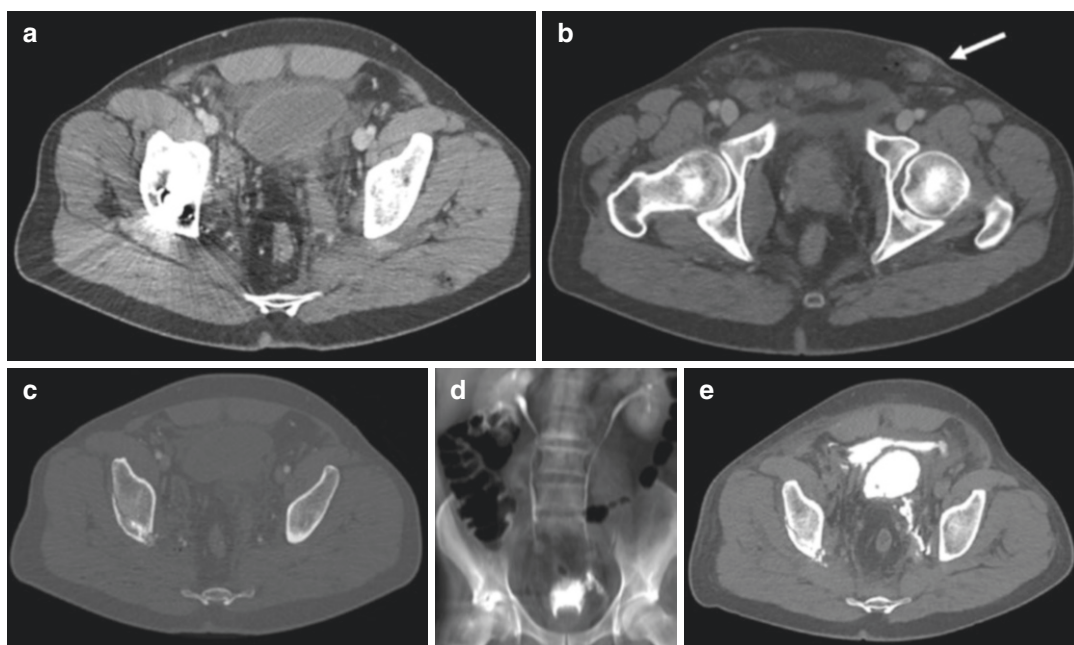
Fig. 6.2 A 50-year-old man admitted to the emergency department after a gunshot injury to the pelvis who underwent a dual-phase MDCT protocol. IV contrast-enhanced axial MDCT image shows a bullet in the right hip (**a**) causing a fracture of the acetabular roof (**c**) from the left anterior wall of the pelvis, with gas in the left inguinal soft tissues (entry point, **b**, arrow). Note also a small amount of fluid in the pelvis, with no active extravasation (**a**). Follow-up MDCT after 1 day included a delayed phase (**d**) and retrograde filling of the bladder after catheteriza- tion, depicting opacified urine distribution in the extraperitoneal spaces of the pelvis (**e**). Comment: this patient shows the importance of the excretory phase and retrograde filling of the bladder on CT for an optimal assessment of possible urine extravasation after a gunshot passing through the pelvis. This phase is mandatory in the initial CT examination of patients involving gunshot injuries in the pelvis and/or with evidence or suspicion of pelvic involvement in blunt trauma

with isotropic datasets to obtain high-quality post-processed images, including multi-planar reformations (MPRs) and maximum-intensity projections (MIPs) [17, 34, 39]. Reconstructions are particularly helpful to detect spinal and pelvic fractures, diaphragmatic injuries, hematomas, and regions of active bleeding. MPRs are useful in the evaluation of urinary (ureteral and bladder) injuries, and in particular for the detection of the most frequent site for a bladder injury: the dome of the bladder [17, 32].

Nevertheless, the main goal in abdominal and pelvic trauma is the early identification and accurate characterization of vascular injuries. This is more relevant and of greater clinical significance than purely detecting an abdominal solid organ injury [40], which may be treated non-operatively, regardless of the anatomical/surgical grade, if the patient is hemodynamically stable. Today, the use of newer MDCT scanners allows radiologists to identify sites of bleeding and in differentiating arterial from venous hemorrhage, which may require different management approaches. As a result of the use of MDCT in abdominal trauma, the vast majority of patients are now treated non-operatively: patients with vascular injuries can be safely sent to the interventional radiology department for embolization if appropriate, and surgery is indicated in only a small percentage of patients (e.g., with a shattered spleen or kidney, and when hemorrhage cannot otherwise be controlled). In most patients, this has saved time and lives, significantly reducing morbidity, death from sepsis and other complications, and financial costs.

Faster MDCT scanners, a rapid rate of IV contrast material injection, and high iodine concentration are the most important factors determining the quality of arterial enhancement. The sensitivity and specificity of MDCT for the depiction of vascular injuries is very high [41–43]. For this reason, it is essential to adopt a "biphasic" MDCT protocol with MPR and MIP reconstructions, producing an "angiogram" which increases diagnostic sensitivity, with important therapeutic and prognostic implications as mentioned above [18]. The use of this biphasic protocol permits the differentiation of contained bleeding injuries from actively bleed-

ing injuries and the identification and characterization of parenchymal injuries. Contained vascular injuries (i.e., pseudoaneurysms and arteriovenous fistulas) can generally be safely treated non-operatively with embolization and conversely, if untreated, may increase in volume and occasionally in number and can rupture causing active bleeding [27, 44] (Fig. 6.3). Active bleeding can also safely be treated non-operatively with embolization, or alternatively patients may be sent for surgical laparotomy,
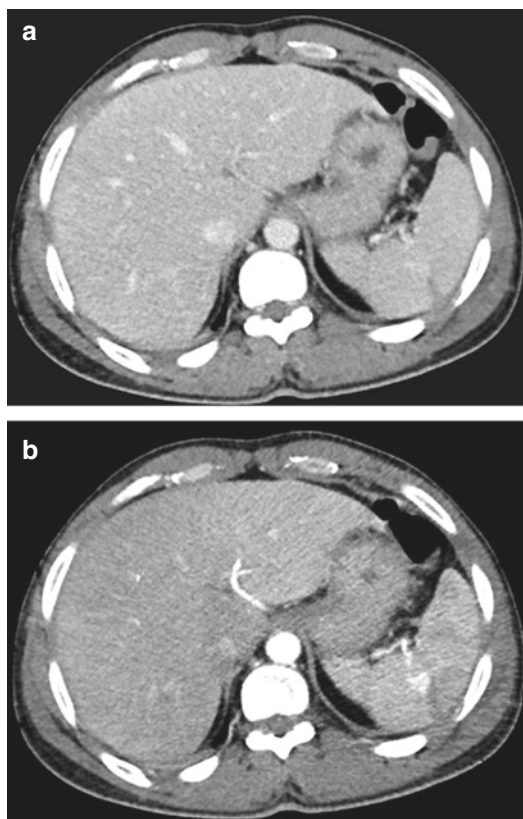
Fig. 6.3 A 40-year-old man who underwent an initial single portal-phase MDCT protocol after a motor vehicle collision. IV contrast-enhanced CT image shows a small laceration in the spleen without significant free hemoperitoneum (**a**). Follow-up CT shows a well-defined, rounded splenic pseudoaneurysm in the arterial phase (**b**). In comparison, note that the pseudoaneurysm was faintly seen on the initial scan. Comment: this patient emphasizes the value of a dual-phase MDCT protocol in high-energy trauma and the importance of the arterial phase in the detection of traumatic pseudoaneurysms. Using a single-phase MDCT protocol, contained vascular injuries may be easily overlooked

depending on the hemodynamic stability. In patients with active bleeding, axial, sagittal, and coronal MPRs can help reveal the bleeding vessel of origin and the severity of hemorrhage, by revealing the areas of active bleeding in three dimensions [34, 45]. Alternatively in patients with contained vessel injury, MPRs can be useful to distinguish a pseudoaneurysm from an arteriovenous fistula, providing crucial information to the interventional radiologist and/or surgeon, which is necessary for planning therapeutic intervention. Finally, the use of a biphasic MDCT protocol for trauma can help differenti-

ate traumatic vascular injuries from preexistent solid organ findings, by providing optimal parenchymal assessment (Fig. 6.4).

The main drawback of the whole-body MDCT protocol for trauma technique is related to the doubled radiation dose as a consequence of the two acquisition phases. Another CT protocol for poly-trauma patients has therefore been recommended: the "split-bolus technique." This CT protocol consists of two boluses (arterial and portal venous) and a single pass through the CT gantry [46]. The main drawbacks of this technique are the limited capacity to differentiate traumatic
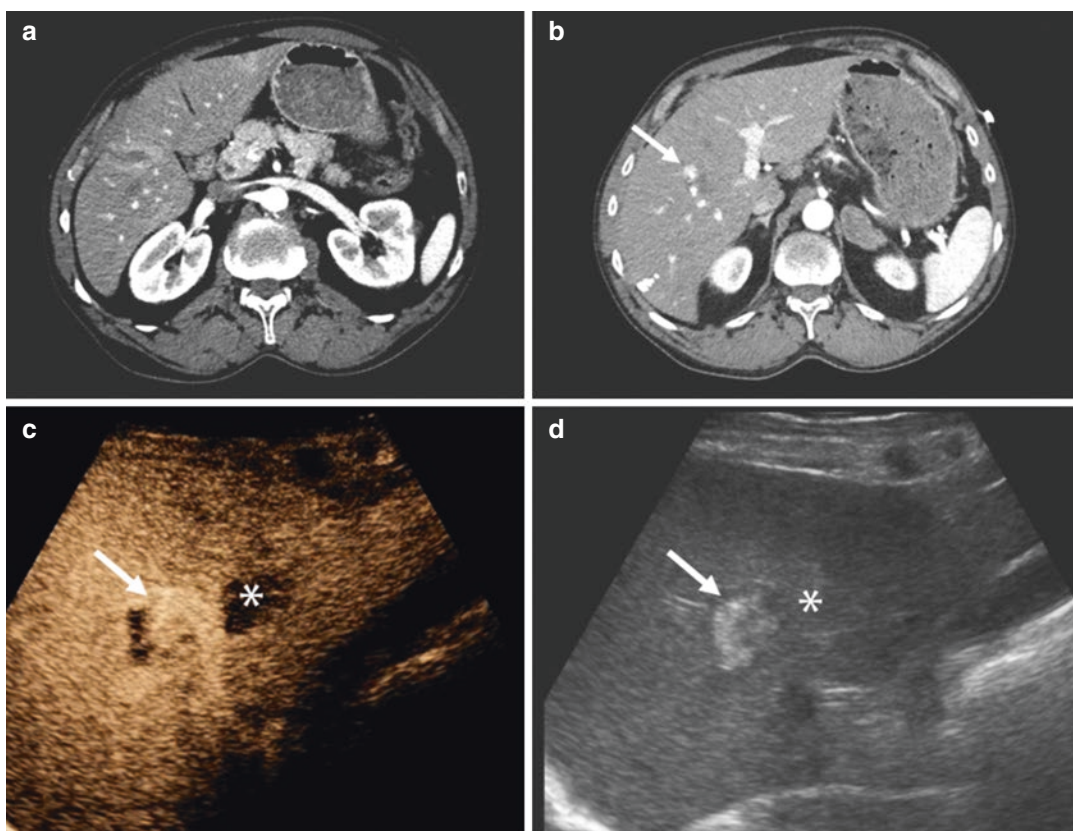
Fig. 6.4 A 13-year-old male patient with major trauma underwent "split-bolus CT technique" to lower the radiation dose. IV contrast-enhanced CT image shows a laceration in segment V of the liver (**a**) and a contiguous focal hyperdensity which was interpreted as a possible traumatic pseudoaneurysm (**b**, arrow). A follow-up contrast-enhanced ultrasound (CEUS) was performed, showing a classical hemangioma (**c**, **d**, arrow) and the laceration (**c**, **d**, asterisks). Comment: in the context of major trauma,

a dual-phase CT protocol should be adopted, regardless of the patient's age. While the use of "split-bolus technique" results in radiation dose reduction, this patient demonstrates that one acquisition phase may be insufficient in the differential diagnosis of vascular abnormalities. Furthermore, also note that in the follow-up of isolated solid organ injuries, CEUS is strongly advised by most European trauma centers
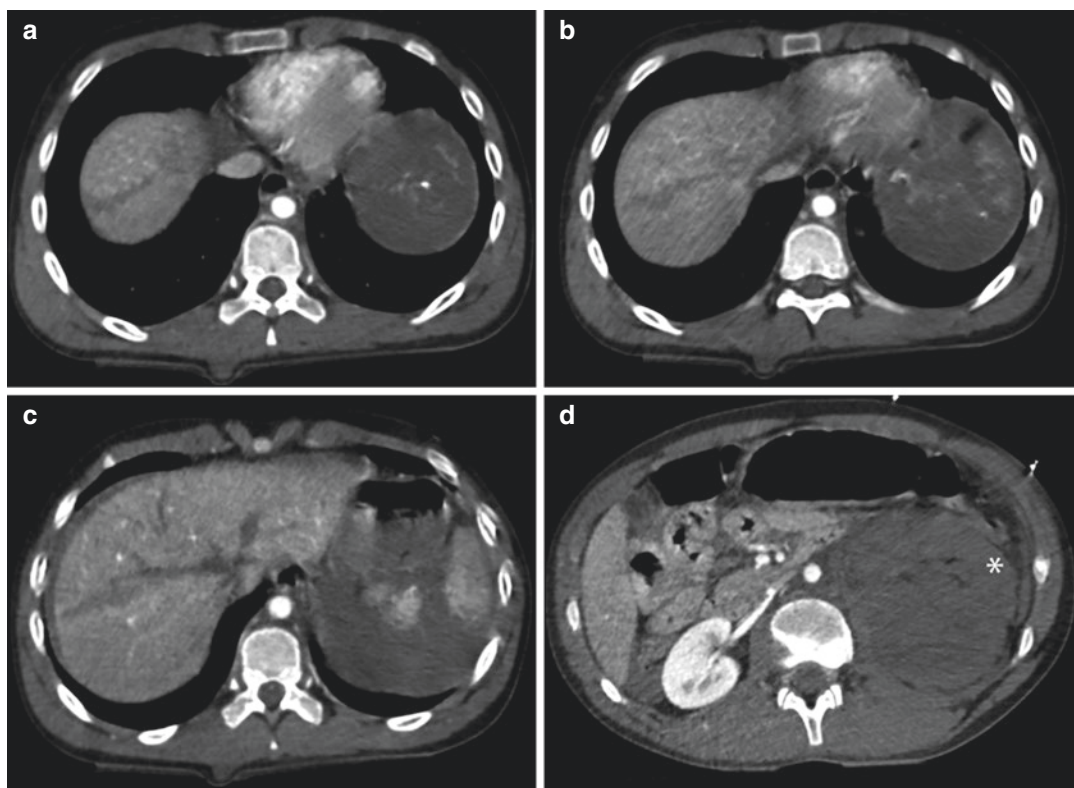
Fig. 6.5 A 16-year-old male patient admitted to the emergency department after high-energy trauma, who was imaged with a "split-bolus" CT protocol to lower the radiation dose. IV contrast-enhanced CT image shows a linear hypodensity at segment VIII of the liver (**a**–**c**), which was misinterpreted as a deep laceration, a shattered spleen (**c**), and a left renal avulsion (**d**, asterisk). At surgery, no liver injuries were identified. A follow-up CT in the portal venous phase demonstrated homogenous enhancement of the liver (not shown). Comment: in the context of a major trauma, a dual-phase CT protocol should be adopted, regardless of the patient's age. While the use of the "split-bolus technique" results in a radiation dose reduction, this patient demonstrates that the use of only one acquisition phase may potentially lead to important errors of interpretation of solid organ injuries

arterial from venous vascular findings and to distinguish vascular injuries from pre-existing parenchymal findings (Fig. 6.5).

6.3   Diagnostic Errors

In the context of abdominal trauma, small and large bowel injuries are involved in 15–20% of diagnostic errors, followed by the liver and spleen, which represent approximately 10–15%. Vascular injuries constitute only approximately 5% of delayed diagnoses. Because of intrinsic difficulty in accurate diagnosis, injuries of the diaphragm (representing 5% of underestimated or non-diagnosed injuries) are not identified in the first 24 h in up to half of affected patients, with the sensitivity of initial CT approaching only 50–73% [47]. Ureteropelvic junction injuries are missed in approximatively 50% of patients, especially on initial analysis, due to an inadequate or incomplete CT protocol [32]. A schematic classification of diagnostic errors includes observer errors, errors in interpretation, errors in suggesting the next step for patient management, and errors in communication (time and manner) [48]. The most important are the errors in interpretation, which can be divided into cognitive errors (caused by lack of knowledge including poor clinical informa-
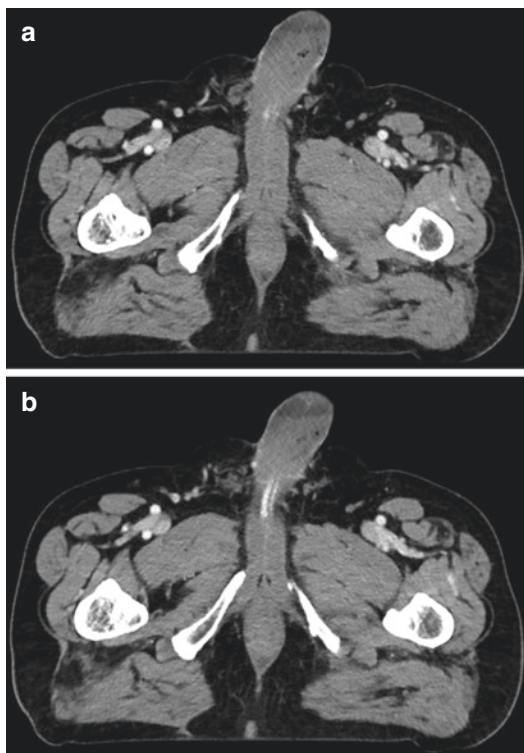
Fig. 6.6 A 71-year-old man was admitted to the emergency department following a motor vehicle collision. Two contiguous IV contrast-enhanced CT images show the penis swelling midway down the shaft of the corpus spongiosum and gas bubbles (**a**, **b**), which was initially interpreted as a penis injury. Review of the history revealed that the patient had a prostaglandin injection into the cavernous bodies just before getting into the car. Comment: in trauma patients, a careful medical history, when possible, is strongly advised to avoid image misinterpretation

tion) and perceptual errors (when the abnormality is simply not seen) [2]. The absence of clinical history and the absence of comparison imaging examinations are factors which may lead to errors [49].

Knowledge of the type of trauma (deceleration, penetrating, or direct trauma), its dynamics and its direction, allows the prediction of the type and site of injuries, which helps the radiologist to avoid a missed diagnosis and to correctly interpret otherwise potentially equivocal images [50, 51] (Fig. 6.6).

Furthermore, any type of injury should be considered in the context of patient age. It should

be kept in mind that seemingly minor, direct abdominal and pelvic trauma in the elderly can lead to more severe consequence than in an adult or a child because of the intrinsic fragility of their body structures. For this reason, "minor" abdominal trauma in elderly people with abdominal complaints should be investigated with CT (Fig. 6.7) [52].

One of the most common errors is the failure to detect an abnormality which may have serious clinical consequences. In this situation the abnormality is visible in retrospect on the scan but has not been reported [18, 53]. In some patients, the "miss" occurs when it is not noted that an abnormal finding is present or when there is low contrast between the abnormality and adjacent normal tissue.

Another common error is "overcall." This is a false-positive finding related to incorrect interpretation of a normal finding, or an anatomical variant. This is more common among inexperienced radiologists and radiology residents who tend to be overcautious and may cause unnecessary worry, hospitalization, and overtreatment [54, 55]. Peripheral lobulations or clefts (most commonly seen in the spleen) can be misinterpreted as lacerations and may falsely cause critical concern in the context of abdominal trauma, especially if there is an adjacent hemoperitoneum. Careful evaluation of the edges of solid organs is required. A cleft usually has a rounded edge and is not associated with perisplenic fluid [56, 57] (Fig. 6.8). In such patients, a timely consultant opinion and urgent reviews are necessary.

Breathing artifacts are a potential cause of this kind of error. They usually appear as indistinct or double edges surrounding moving structures including the liver, spleen, kidney, abdominal wall, ribs, or vessels, associated with bands of hyperdensity in the periphery of structures. Today, fast MDCT acquisitions have markedly reduced this source of artifacts [39, 58]. Ideally, in such patients, rescanning the patient when she/he is still on the CT table is the best practice. This is only possible when a radiologist is present in the CT suite and is supervising the scan in real time.

Streak artifacts from foreign bodies or from overlying arms along the body can simulate a
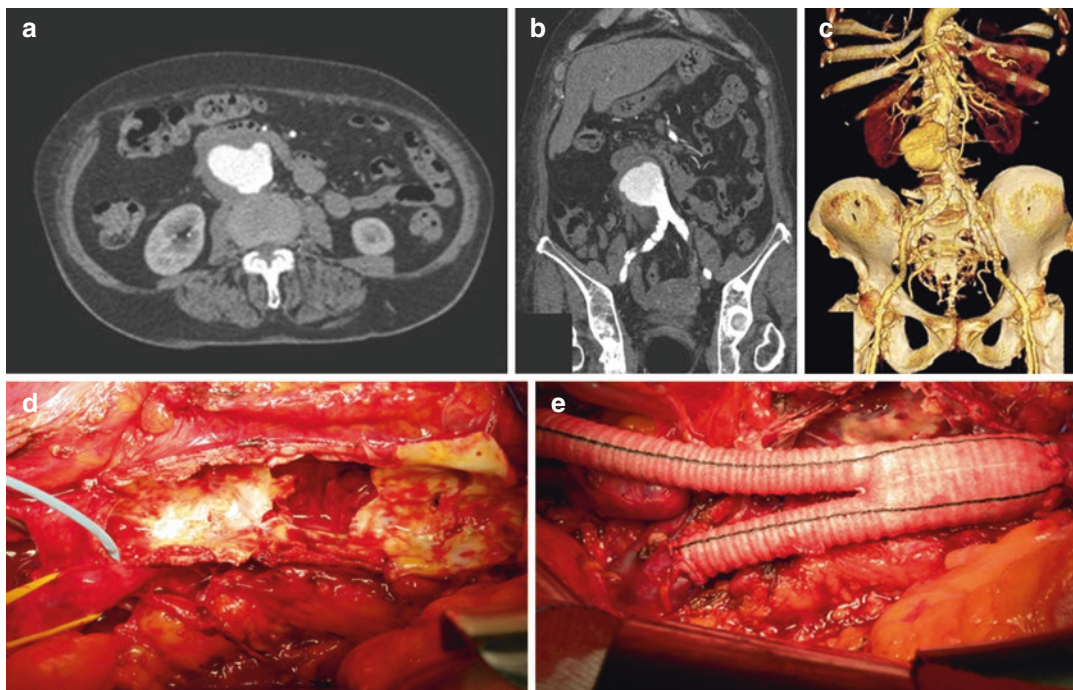
Fig. 6.7 An 89-year-old man complained of abdominal pain after a seemingly minor abdominal trauma (fall off a bed). Axial (**a**) and coronal (**b**) IV contrast-enhanced CT images show a large abdominal aortic pseudoaneurysm. 3D reconstruction image (**c**) gives optimal spatial depiction of the aortic injury. The surgical specimen (**d**) demonstrates a hole in the abdominal aorta, as result of the direct trauma. This injury was surgically treated with graft placement (**e**). Comment: this patient demonstrates how a seemingly minor trauma may lead to severe abdominal injuries in the elderly patients. In such cases patients complaining of abdominal pain should be investigated with MDCT

parenchymal laceration in solid organs or may mask substantial parenchymal injuries [56, 57] (Fig. 6.9). Again, if doubts exist, rescan the patient to allow definitive assessment of the abdomen and pelvis.

A sign which often is underestimated or incorrectly interpreted is "periportal tracking." This is defined as a hypodense lines extending along the main portal tract and/or its intrahepatic branches. It is considered a non-specific sign of liver laceration due to hemorrhage tracking along the portal veins but can also be found in patients with high central venous pressure (e.g., tension pneumothorax or pericardial tamponade). In a poly-trauma patient with periportal tracking, some features may be useful to differentiate fluid shifts from a liver laceration. In particular, if the patient has been infused with a high volume of IV fluids, the vena cava may be

dilated, and there should be no other signs of injury. However, the only sign which unequivocally identifies a laceration is the presence of hemoperitoneum and/or an adjacent retroperitoneal hematoma [59].

Another frequent error occurs when CT signs of hypovolemic or hypotensive shock are misinterpreted as active bleeding, as in the "depending pooling sign." The "dependent pooling sign" is a typical CT feature of cardiac arrest due to the retrograde flow of blood from the inferior vena cava into the liver (Fig. 6.10). This may have tremendous consequences in terms of patient treatment and management.

Another common type of error is "satisfaction of search." This situation may happen when there are multiple injuries in the same patient. The radiologist identifies one abnormality, so her or his attention decreases, and she or he fails to see
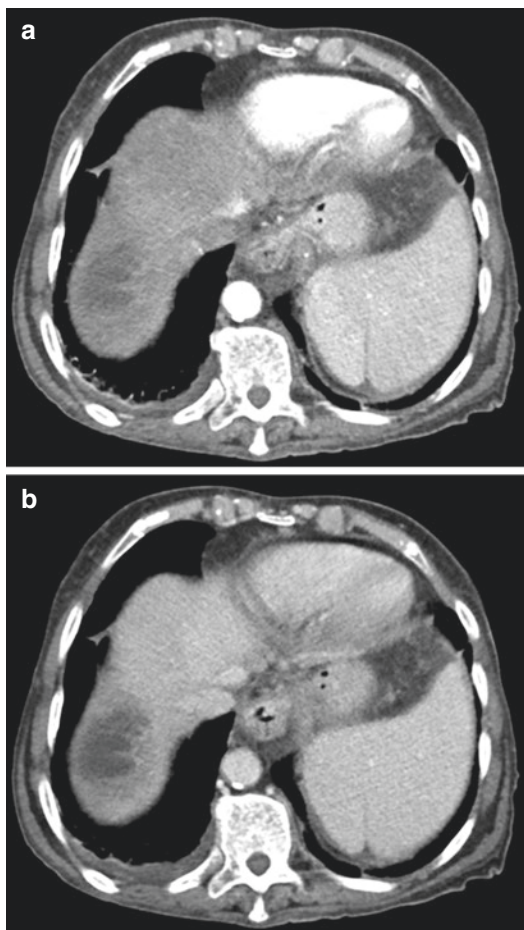
Fig. 6.8 An 80-year-old woman with a history of hepatocellular carcinoma (HCC) was admitted to the emergency department with abdominal pain after a fall down the stairs. IV contrast-enhanced axial MDCT images (**a**, **b**) show a deep hypodense area in the spleen, with rounded edges and small amount of fluid in between, representing a splenic cleft (**a**, **b**). This finding might be misinterpreted as a splenic laceration, especially when there is perisplenic fluid. Careful evaluation of the edges, rounded in case of a splenic cleft, is helpful in the differential diagnosis

Fig. 6.9 A 36-year-old man was admitted to the emergency department following a gunshot injury. IV contrast-enhanced CT axial image shows a bullet within the left iliopsoas muscle and a large retroperitoneal hematoma. Note also multiple streak artifacts (**a**) extending up to the abdominal wall, passing through the pancreatic tail. Follow-up CT after bullet removal clearly demonstrates a deep laceration in the pancreatic tail (**b**). Comment: streak artifacts may mask significant injuries. Repeat CT after removal of radiopaque foreign bodies after trauma, if possible, may be advisable for definitive assessment

a second or more abnormality [53]. The initial pattern of the search is adequate, but it ends prematurely when the first abnormality is found [60]. To avoid this mistake, radiologists can take advantage of a systematic approach, with the use of a checklist of anatomic regions for interpreting trauma abdominal CT. This approach places special emphasis on efficiently identifying life-threatening injuries [61, 62].

Another responsibility for radiologists is to timely communicate a potentially life-threatening injury to the trauma team. Radiologists must be aware that their role in the emergency setting is greater than just writing a report or identifying an injury. Failing to timely communicate a potentially life-threatening injury or to suggest the most appropriate next step can lead to unacceptable delays in the correct management of a patient and can even result in unnecessary invasive surgery (Figs. 6.11 and 6.12) [63–66].
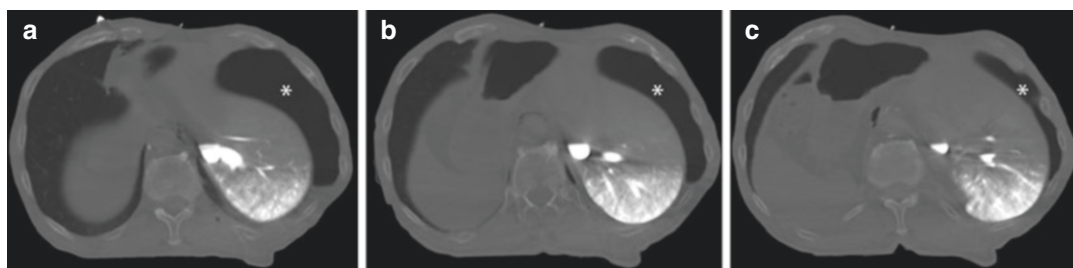
Fig. 6.10 An 89-year-old man was admitted to the emergency department after a suicide attempt (an intentional fall from a balcony). Three contiguous IV contrast-enhanced CT images show incidental "situs inversus" and pooling of intravenous contrast within the inferior vena cava and dependent liver. It is a typical CT feature of cardiac arrest, but in this patient was prospectively misinterpreted as contrast extravasation (**a–c**). Note also a large left pneumothorax (asterisks). Comment: the "dependent pooling sign" is a typical CT feature of cardiac arrest due to the retrograde flow of blood from the inferior vena cava into the liver. This sign should not be confused with contrast extravasation
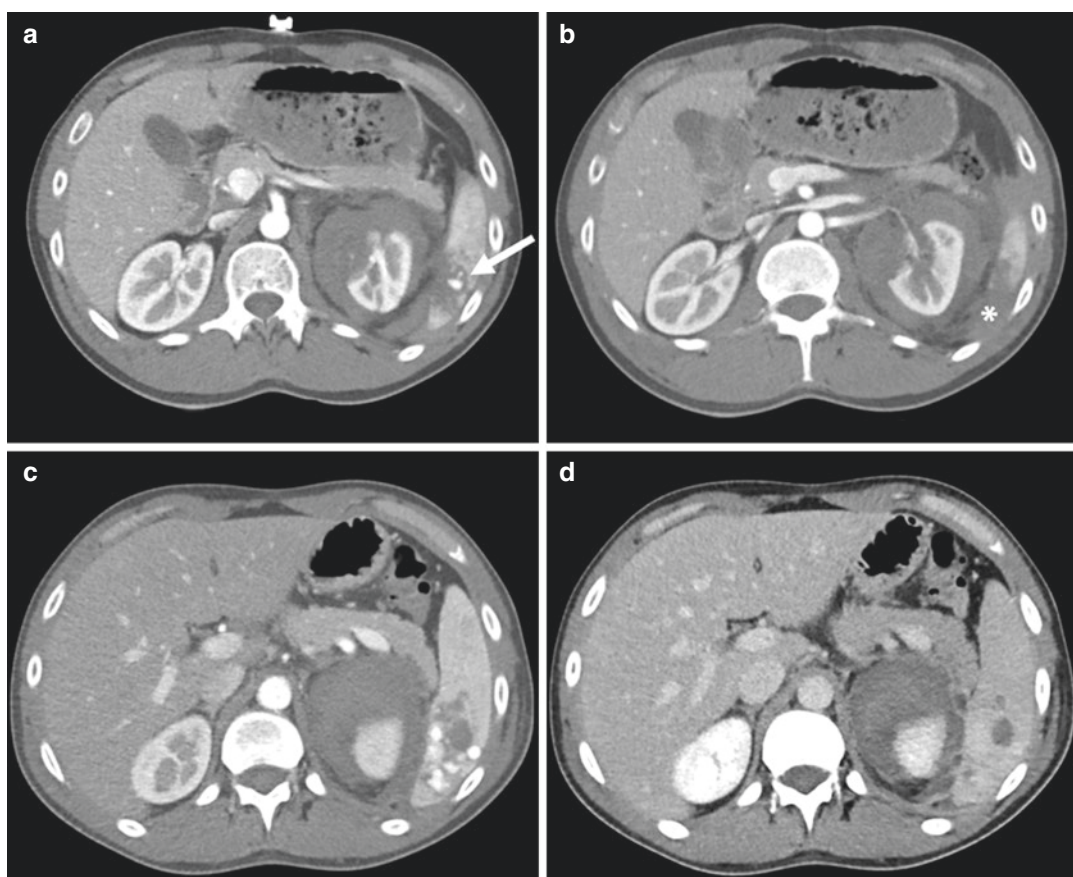
Fig. 6.11 A 28-year-old man was admitted to the emergency department following motor vehicle collision. Two contiguous axial contrast-enhanced CT images (**a**, **b**) demonstrate deep lacerations in the left kidney with perirenal hematoma (grade 3 according to AAST) and a pseudoaneurysm in the spleen (A, arrow), with an adjacent small amount of hemoperitoneum (**b**, asterisk). Both findings were initially treated non-operatively. Follow-up CT images (**c**, **d**) after 3 days show multiple pseudoaneuryms in the spleen and a stable left perirenal hematoma. Comment: while grade 3 renal injuries were correctly managed non-operatively, the presence of a splenic pseudoaneurysm required embolization. If untreated, pseudoaneurysms may increase in volume and number as in this patient, with the potential to rupture and bleed, causing immediate hemodynamic instability
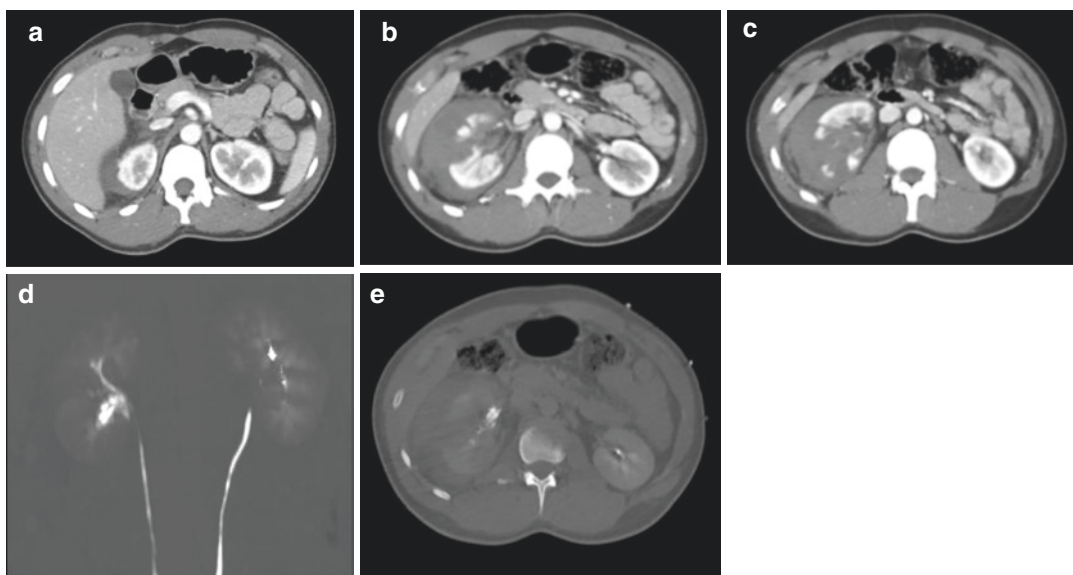
Fig. 6.12 A 16-year-old male admitted to the emergency department after a motor vehicle collision. IV contrast-enhanced CT images (**a**–**c**) demonstrate deep lacerations in the right kidney and a perirenal hematoma (grade 3 according to AAST). Delayed-phase images demonstrate a right inferior calyceal leak with normal ureteral opacification consistent with a minor leak (**d**, **e**). This patient was clinically stable, with a hemoglobin of 12 g/dL, and incorrectly underwent nephrectomy. Comment: in such patient with deep lacerations in the kidney (grade 3 according to AAST) with associated minor urinary leak, there is no indication for surgery. Indications for surgery include a shattered kidney, renal avulsion, and uncontrollable hemorrhage. Furthermore, in this patient, vascular injuries and active bleeding were excluded

6.4 Conclusion

Poly-trauma is an acute systemic disease requiring immediate assessment and an individualized approach to therapy. With the advent of MDCT, patient outcomes have substantially improved, but diagnostic errors still persist and can result in mismanagement with potentially serious consequences. Unfortunately, radiologists are responsible for such errors, as they play a pivotal role in the assessment of trauma. Radiologists are key members of the Trauma Team and should be available within the emergency department 24/7. Their role is greater than simply to write a remote report or to just describe an injury. Diagnostic error rate can be markedly reduced by adopting optimal CT protocols according to the mechanism of trauma, following shared guidelines, organizing institutional clinical governance and quality assurance meetings, discussing difficult clinical cases and unexpected deaths with the Trauma Team, and improving research and development in the fields of emergency radiology and trauma care. Finally, in our opinion, young radiologists participating in trauma care should have at least 1 year of experience working at a major trauma hospital and are strongly encouraged to complete a post-residency fellowship program in emergency radiology.

References

1. Guida F, Bocchini G, Sica G, Freeze A, Scaglione M. Errors in polytrauma. In: Romano L, Pinto A, editors. Errors in radiology. Milan: Springer; 2012. p. 27–37.

2. Pinto A, Reginelli A, Pinto F, et al. Errors in imaging patients in the emergency setting. Br J Radiol. 2016;89(1061):20150914.

3. Farina R, Sparano A. Errors in sonography. In: Romano L, Pinto A, editors. Errors in radiology. Milan: Springer; 2012. p. 79–85.

4. Pinto A, Pinto F, Faggian A, et al. Sources of error in emergency ultrasonography. Crit Ultrasound J. 2013;5(Suppl. 1):S1.

5. Casciani E, De Vincentiis C, Mazzei MA, et al. Errors in imaging the pregnant patient with acute abdomen. Abdom Imaging. 2015;40:2112–26.

6. Chang PT, Schooler GR, Lee EY. Diagnostic errors of right lower quadrant pain in children: beyond appendicitis. Abdom Imaging. 2015;40:2071–90.

7. Gebhard F, Huber-Lang M. Polytrauma—pathophysiology and management principles. Langenbecks Arch Surg. 2008;393(6):825–31.

8. World Healt Organization. Injuries and violence: the facts. Geneva: WHO; 2010. http://www.who.int/violence_injury_prevention/key_facts/en/. Accessed 16 Jun 2018.

9. Nicolaou S, Eftekhari A, Sedlic T, et al. The utilization of dual source CT in imaging of polytrauma. Eur J Radiol. 2008;68:398–408.

10. Linsenmaier U, Kanz KG, Rieger J, et al. Structured radiologic diagnosis in polytrauma [in German]. Radiologe. 2002;42(7):533–40.

11. Philipp MO, Kubin K, Hörmann M, et al. Radiological emergency room management with emphasis on multidetector-row CT. Eur J Radiol. 2003;48(1):2–4.

12. Huber-Wagner S, Lefering R, Qvick LM, et al. Working Group on Polytrauma of the German Trauma Society. Effect of whole-body CT during trauma resuscitation on survival: a retrospective, multicentre study. Lancet. 2009;373(9673):1455–61.

13. Gunn ML, Lehnert BE, Lungren RS, et al. Minimal aortic injury of the thoracic aorta: imaging appearances and outcome. Emerg Radiol. 2014;21:227–33.

14. Fanucci E, Fiaschetti V, Rotili A, et al. Whole body 16-row multislice CT in emergency room: effects of different protocols on scanning time, image quality and radiation exposure. Emerg Radiol. 2007;13:251–7.

15. Gruen RL, Jurkovich GJ, McIntyre LK, et al. Patterns of errors contributing to trauma mortality: lessons learned from 2,594 deaths. Ann Surg. 2006;244:371–80.

16. West OC, Anderson J, Lee JS, et al. Patterns of diagnostic error in trauma abdominal CT. Emerg Radiol. 2002;9:195–200.

17. Scaglione M, Iaselli F, Sica G, et al. Errors in imaging of traumatic injuries. Abdom Imaging. 2015;40:2091–8.

18. Sica G, Guida F, Bocchini G, et al. Errors in imaging assessment of polytrauma patients. Semin Ultrasound CT MR. 2012;33:337–46.

19. Hirshberg A, Wall MJ Jr, Allen MK, et al. Causes and patterns of missed injuries in trauma. Am J Surg. 1994;168:299–303.

20. Sampson MA, Colguhoun KB, Hennessy NL. Computed tomography whole body imaging in multi-trauma: 7 years experience. Clin Radiol. 2006;61(4):365–9.

21. American College of Surgeons. ATLS textbook. Chicago, IL: American College of Surgeons; 2001.

22. Mirvis SE, Shanmuganathan K. The 2008 RadioGraphics monograph issue: emergency imaging in adults. Radiographics. 2008;28(6):1539–40.

23. Ptak T, Rhea J, Novelline R. Experience with a continuous, single-pass whole-body multi-detector CT protocol for trauma: the three-minute multiple trauma CT scan. Emerg Radiol. 2001;8:250–6.

24. Anderson SW, Lucey BC, Rhea JT, et al. 64 MDCT in multiple trauma patients: imaging manifestations and clinical implications of active extravasation. Emerg Radiol. 2007;14:151–9.

25. Stuhlfaut JW, Anderson SW, Soto JA. Blunt abdominal trauma. Current imaging techniques CT findings in patients with solid organ, bowel and mesenteric injury. Semin Ultrasound CT MRI. 2007;28:115–29.

26. Vaccaro JP, Brody JM. CT cystography in the evaluation of major bladder trauma. Radiographics. 2000;20:1373–81.

27. Quagliano PV, Delair SM, Malhotra AK. Diagnosis of blunt bladder injury: a prospective comparative study of computed tomography cystography and conventional retrograde cystography. J Trauma. 2006;61:410–21.

28. Deck AJ, Shaves S, Talner L, et al. Computerized tomography cystography for the diagnosis of traumatic bladder rupture. J Urol. 2000;164:43–6.

29. Peng MY, Parisky YR, Cornwell EE, et al. CT cystography versus conventional cystography in evaluation of bladder injury. Am J Roentgenol. 1999;173:1269–72.

30. American College of Radiology. ACR Appropriateness Criteria® suspected lower urinary tract trauma. 2013.; https://www.guidelinecentral.com/summaries/acr-appropriateness-criteria-suspected-lower-urinary-tract-trauma/ Accessed 05 Aug 2018.

31. Mee SL, McAninch JW, Federle MP. Computerized tomography in bladder rupture: diagnostic limitations. J Urol. 1987;137:207–9.

32. Chan DP, Abujudeh HH, Cushing GL Jr, et al. CT cystography with multiplanar reformation for suspected bladder rupture: experience in 234 cases. Am J Roentgenol. 2006;187:1296–302.

33. Joshi G, Kim EY, Hanna TN, Siegel CL, Menias CO. CT cystography for suspicion of traumatic urinary bladder injury: indications, technique, findings, and pitfalls in diagnosis: radioGraphics fundamentals | online presentation. Radiographics. 2018;38(1):92–3.

34. Vu M, Anderson SW, Shah N, et al. CT of blunt abdominal and pelvic vascular injury. Emerg Radiol. 2010;17:21–9.

35. Spencer Netto FA, Hamilton P, et al. Retrograde urethrocystography impairs computed tomography diagnosis of pelvic arterial hemorrhage in the presence of a lower urologic tract injury. J Am Coll Surg. 2008;206:322–7.

36. Dreizin D, Munera F. Multidetector CT for penetrating torso trauma: state of the art. Radiology. 2015;277(2):338–55.

37. Gross JA, Lehnert BE, Linnau KF, et al. Imaging of urinary system trauma. Radiol Clin North Am. 2015;53(4):773–88.

38. Iacobellis F, Ierardi AM, Mazzei MA, et al. Dual-phase CT for the assessment of acute vascular injuries in high-energy blunt trauma: the imaging findings and management implications. Br J Radiol. 2016;89(1061):20150952.

39. Rieger M, Czermak B, El Attal R, et al. Initial clinical experience with a 7064-MDCT whole-body scanner in an emergency department: better time management and diagnostic quality? J Trauma. 2009;66:648–57.

40. Pinto A, Niola R, Tortora G, et al. Role of multidetectorrow CT in assessing the source of arterial haemorrhage in patients with pelvic vascular trauma. Comparison with angiography. Radiol Med. 2010;115:648–67.

41. Yao DC, Jeffrey RB Jr, Mirvis SE, et al. Using contrast-enhanced helical CT to visualize arterial extravasation after blunt abdominal trauma: incidence and organ distribution. Am J Roentgenol. 2002;178:17–20.

42. Willmann JK, Roos JE, Platz A, et al. Multidetector CT: detection of active hemorrhage in patients with blunt abdominal trauma. Am J Roentgenol. 2002;179:437–44.

43. Hamilton JD, Kumaravel M, Censullo ML, et al. Multidetector CT evaluation of active extravasation in blunt abdominal and pelvic trauma patients. Radiographics. 2008;28:1603–16.

44. Guida F, Bocchini G, Chef GM, et al. Traumi intestinali e dei meso. Radiol Med. 2010;115:S161–5.

45. Rieger M, Mallouhi A, Tauscher T, et al. Traumatic arterial injuries of the extremities: initial evaluation with MDCT angiography. AJR Am J Roentgenol. 2006;186:656–64.

46. Leung V, Sastry A, Woo TD, et al. Implementation of a split-bolus single-pass CT protocol at a UK major trauma centre to reduce excess radiation dose in trauma pan-CT. Clin Radiol. 2015;70(10):1110–5.

47. Stanescu L, Talner LB, Mann FA. Diagnostic errors in polytrauma: a structured review of the recent literature. Emerg Radiol. 2006;12:119–23.

48. Onuora VC, Patil MG, al-Jasser AN. Missed urological injuries in children with polytrauma. Injury. 1993;24:619–21.

49. Sung CK, Kim KH. Missed injuries in abdominal trauma. J Trauma. 1996;41:276–82.

50. Tomczak PD, Buikstra JE. Analysis of blunt trauma injuries: vertical deceleration versus horizontal deceleration injuries. J Forensic Sci. 1999;44:253–62.

51. Fitzharris M, Franklyn M, Frampton R, et al. Thoracic aortic injury in motor vehicle crashes: the effect of impact direction, side of body struck, and seat belt use. J Trauma. 2004;57:582–90.

52. Newgard CD. Defining the "older" crash victim: the relationship between age and serious injury in motor vehicle crashes. Accid Anal Prev. 2008;40:1498–505.

53. Samuel S, Kundel HL, Nodine CF, et al. Mechanism of satisfaction of search: eye position recordings in the reading of chest radiographs. Radiology. 1995;194:895–902.

54. Pinto A, Brunese L. Spectrum of diagnostic errors in radiology. World J Radiol. 2010;2:377–83.

55. Provenzale JM, Kranz PG. Understanding errors in diagnostic radiology: proposal of a classification scheme and application to emergency radiology. Emerg Radiol. 2011;18:403–8.

56. West RW. Radiology malpractice in the emergency room setting. Emerg Radiol. 2000;7:14–8.

57. Scaglione M, Romano L, Forner AL, et al. Computerized tomography in the differential diagnosis of congenital lobulations and traumatic lacerations of the spleen. Radiol Med. 1996;92:324–6.

58. Anderson SW, Lucey BC, Varghese JC, et al. Sixty-four multi-detector row computed tomography in multitrauma patient imaging: early experience. Curr Probl Diagn Radiol. 2006;35:188–98.

59. Macrander SJ, Lawson TL, Foley WD, et al. Periportal tracking in hepatic trauma: CT features. J Comput Assist Tomogr. 1989;13(6):952–7.

60. Berbaum KS, Brandser EA, Franken EA, et al. Gaze dwell times on acute trauma injuries missed because of satisfaction of search. Acad Radiol. 2001;8:304–14.

61. Ely JW, Graber ML, Croskerry P. Checklists to reduce diagnostic errors. Acad Med. 2011;86:307–13.

62. Graber ML, Wachter RM, Cassel CK. Bringing diagnosis into the quality and safety equations. JAMA. 2012;308:1211–2.

63. Harrigal CL, Erly WK. On-call radiology: community standards and current trends. Semin Ultrasound CT MR. 2007;28:85–93.

64. Thomson CB, Greaves I. Missed injury and the tertiary trauma survey. Injury. 2008;39:107–14.

65. Pinto A, Acampora C, Pinto F, et al. Learning from diagnostic errors: a good way to improve education in radiology. Eur J Radiol. 2011;78:372–6.

66. Raskin MM. Survival strategies for radiology: some practical tips on how to reduce the risk of being sued and losing. J Am Coll Radiol. 2006;3:689–93.

Errors in Imaging of Non-traumatic Abdominal Emergencies

7

Maria Zulfiqar, Vincent M. Mellnick, and Michael N. Patlas

Abdominal/pelvic pain is one of the most common chief complaints in patients presenting to emergency departments [1]. Making a specific diagnosis is often not possible using only history and physical examination, particularly in the fast-paced environment typically seen in emergency departments. Therefore, imaging plays a crucial and increasingly utilized role in the evaluation of the patient with acute abdominal pain [2]. Studies have largely shown high diagnostic accuracy for radiologic identification of causes for acute abdominal pain, particularly using CT. For instance, Perry et al. demonstrated 88% accuracy for CT in this patient population [3]. Despite very good performance of CT for this indication, radiologists can certainly make errors in interpreting these examinations, often for similar reasons as encountered in other clinical scenarios—broadly, perceptual and cognitive errors [4].

7.1 Perceptual Errors

Radiologic perceptual errors in patients with abdominal pain result from a failure to observe an abnormality which retrospectively can be seen by peers and/or by the original interpreters. These observations can be broadly grouped into a few categories: inflammation; extraluminal gas, fluid, or blood; abnormal size or thickness of an anatomic structure; abnormal positioning of anatomic structures; or abnormal organ perfusion. Most perceptual radiologic errors in a patient with abdominal/pelvic pain will occur when a radiologist does not recognize one or more of these abnormalities on cross-sectional imaging.

7.2 Inflammation

Inflammation in the abdomen and pelvis is often recognized by the presence of thickening of a previously normal structure and by the presence of surrounding increased blood flow and capillary permeability resulting in edema. Radiologists rely on infiltration of the adipose tissue—"fat stranding"—to detect inflammatory abnormalities, typically on CT and MRI [5]. On CT, fat stranding results in increased attenuation of the tissues surrounding an inflamed structure (Fig. 7.1a). On MRI, this can result in increased T2 signal reflecting fluid (Fig. 7.1b); however, it is important to remember that this is more conspicuous on

M. Zulfiqar (✉) · V. M. Mellnick
Abdominal Imaging, Mallinckrodt Institute of Radiology, Washington University School of Medicine, St. Louis, MO, USA
e-mail: mariazulfiqar@wustl.edu; mellnickv@wustl.edu

M. N. Patlas
Department of Radiology, McMaster University, Hamilton, ON, Canada
e-mail: patlas@hhsc.ca
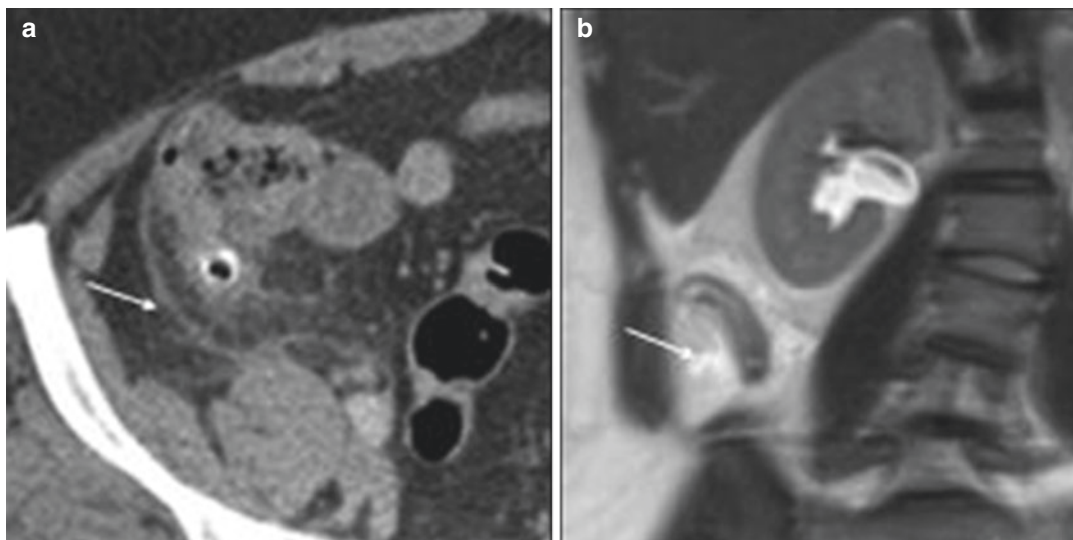
Fig. 7.1 Fat stranding (arrows), a common sign of inflammation, as seen on an axial abdominal CT image (**a**) in a 40-year-old woman with cecal diverticulitis. On MRI of another patient, fat stranding manifests with increased T2 signal in the fat surrounding the dilated appendix on a coronal image (**b**)

fat-saturated images [6]. On ultrasound, inflammation is more readily detected as an increase in blood flow on color Doppler, focal tenderness, and increased echogenicity in the adjacent fat during the examination [7]. Regardless of modality, detection of inflammation requires comparison of tissues within the abdomen and pelvis for asymmetry [5]. This may be particularly difficult in pediatric and thin patients who have little peritoneal fat, and particular in patients who have generalized third spacing of fluid.

7.3 Extraluminal Gas, Fluid, and Blood

Although not mutually exclusive from these inflammatory changes, extraluminal gas, fluid, and blood are critical findings which must be observed on imaging by the interpreting radiologist. Extraluminal gas in particular carries a strong connotation of hollow viscous perforation in the absence of a recent procedure and may be easily missed when present in small quantities. It is important to remember patient positioning when searching for extraluminal gas. Most often, patients undergoing diagnostic imaging are supine, resulting in gas collecting anti-dependently in the anterior abdomen, often around the diaphragm if the patient has been upright or semi-upright. On CT, the use of lung or bone window settings can help improve conspicuity of small quantities of gas (Fig. 7.2a). On MRI, gas results in blooming artifact due to susceptibility. Therefore, extraluminal gas may be easiest to observe on gradient-echo imaging such as T1 in-phase sequences (Fig. 7.2b). On ultrasound, "dirty" acoustic shadowing is the classic appearance of extraluminal gas, and may be easiest to observe along the liver surface.

In contrast to the anti-dependent distribution of gas, extraluminal fluid and blood layer dependently in the abdomen and pelvis. In the supine patient, this occurs in the pelvis and in the paracolic gutters, as well as around the liver and spleen. Although small volumes of free fluid can be physiologic in reproductive age women, it is much more commonly abnormal in men, and should be regarded as a potential sign of an acute process, especially in the absence of volume overload or recent intravenous resuscitation. Differentiating between simple fluid and blood is also a crucial observation since hemoperitoneum is always pathologic. On CT, this distinction is typically
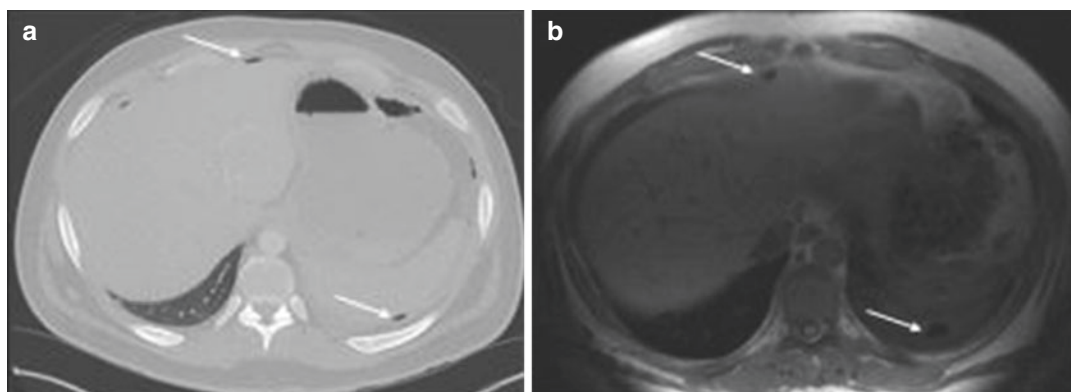
Fig. 7.2 Free intraperitoneal air appears in the non-dependent abdomen of a supine patient. Axial abdominal CT image (**a**) utilizing lung windows shows multiple foci of gas along the diaphragm (arrows). On T1 axial in-phase MRI (**b**, arrows), these foci of gas demonstrate blooming artifact due to susceptibility
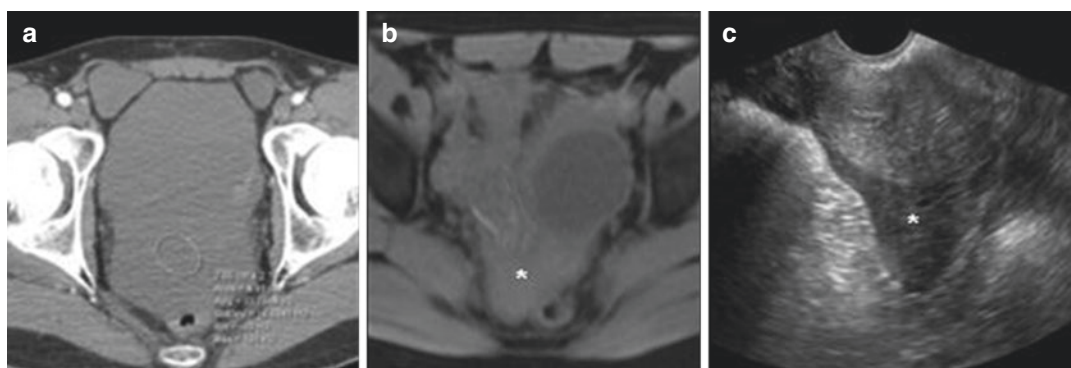
Fig. 7.3 Hemoperitoneum on CT, MRI, and US. On CT, hemoperitoneum has higher attenuation than simple fluid (**a**). On MRI, blood has T1 iso- to hyperintense signal relative to skeletal muscle, seen here in the cul-de-sac (**b**, asterisk) from a ruptured ectopic pregnancy in the left adnexa. Hemorrhagic fluid has low-level internal echoes on ultrasound (**c**, asterisk)

achieved by comparing free fluid to internal reference points e.g., urine in the bladder or skeletal muscle—and by noting the relatively higher attenuation of hemoperitoneum to urine or iso-attenuation to the muscle (Fig. 7.3a). Measuring Hounsfield units (HU) is a more quantitative method of performing this comparison, with hemoperitoneum typically measuring 30–60 HU [8]. Important pitfalls in observing hemoperitoneum on CT include anemic patients whose blood is less attenuating than typically seen. In addition, blood may not distribute uniformly through the abdomen, resulting in areas which appear to be simple fluid. On MRI, observing increased T1 and decreased T2 signal in free fluid is key to diagnosing extraluminal blood (Fig. 7.3b), whereas ultrasound may demonstrate complex fluid with areas of increased echogenicity (Fig. 7.3c) [8].

7.4 Abnormal Size or Thickness of an Anatomic Structure

In addition to surrounding ancillary findings, observing abnormal size or thickness of an anatomic structure can be the key to diagnosing a cause for acute abdominal pain (Fig. 7.4). Obstruction of the ureters, bile ducts, and bowel leads to distention and conspicuity of these structures. However, it is important to note that this dilation may be transient and, if very early, may
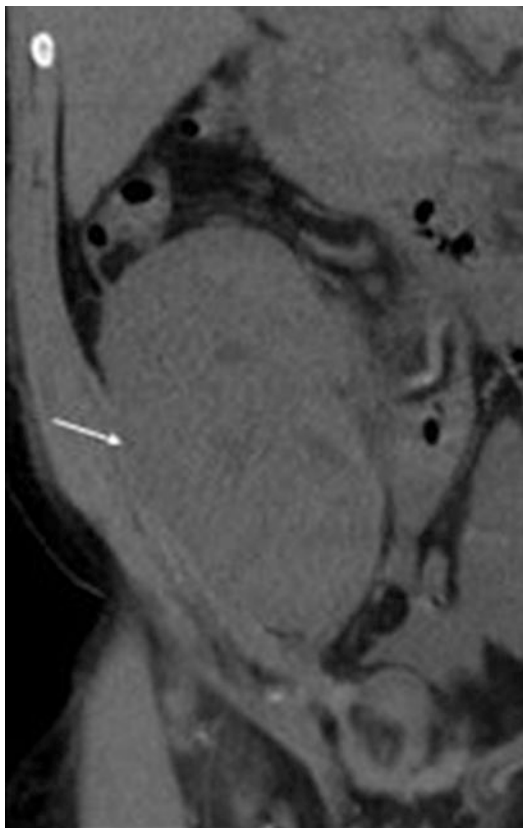
Fig. 7.4 Enlarged organ size as an indicator of acute inflammation. Non-enhanced coronal CT image shows an enlarged right lower quadrant transplant kidney (arrow). Abnormal renal enlargement in this 36-year-old man was due to acute transplant rejection

be subtle, leading to a possible missed diagnosis if applied too dogmatically. Examples include decompression of the proximal gastrointestinal tract with vomiting in the setting of bowel obstruction, gallbladder perforation with an occluded cystic duct, and calyceal rupture resulting from an obstructing ureteral calculus. Although these examples often have other findings of an acute process including surrounding inflammation, relying on the sizes of these organs alone will lead to a missed diagnosis. Knowledge of the normal range of sizes for abdominopelvic anatomic structures is important, as is comparison to the contralateral side in paired structures, although sometimes both may be abnormal. One such example is the ovaries: increased ovarian size is a common observation in ovarian torsion

and should be assessed relative to the size of the ovary on the patient's asymptomatic side [9].

Along with the size of an organ or structure, the thickness should be evaluated as well. This is typically an observation related to the wall of gas or fluid-filled structures, including the bowel, urinary tract, and biliary tract. When evaluating for wall thickening, it is important to place an observation in the context of distention, particularly in the gastrointestinal tract. The gastric antrum and jejunum are classic sites of apparent wall thickening that commonly result from peristalsis rather than a pathologic process when non-distended, especially now with the generalized decline in the use of oral contrast [10]. Similarly, the bladder and gallbladder may have a range of thickness depending on the degree of distention. In contrast, the bile ducts and ureters should have a nearly imperceptible wall, and increased conspicuity of these structures may indicate an inflammatory, infectious, or neoplastic process, or some combination [11, 12].

7.5 Abnormal Anatomic Positioning

An abnormal anatomic position of an organ may be an easily overlooked observation that leads to a missed diagnosis. One such example is that of internal hernias, which may not always have bowel dilation or inflammation as ancillary signs. The presence of bowel behind the root of the small bowel mesentery, abnormal clustering of bowel loops, or a shifting enteric anastomosis can all be anatomic positional clues to this important diagnosis (Fig. 7.5) [13]. Ovarian torsion may also result in shifting of the uterus to the torsed side, and positioning of the ovary across the midline and may be the only clue to this diagnosis on CT or MRI [9]. Abnormal positioning may not always carry an emergent connotation, however. One such example is that of gastric volvulus, in which the greater curvature of the stomach is abnormally positioned. However, the presence of an abnormally positioned stomach is not diagnostic of volvulus. Large hiatal hernias may result in organoaxial positioning of the stomach in asymptomatic patients without obstruction [14].

Fig. 7.5 Non-obstructed transmesocolic internal hernia identified by abnormal organ position. Axial abdominal CT image with intravenous contrast from a 32-year-old woman who had previous Roux-en-Y gastric bypass shows the transverse colon (asterisk) posterior to the small bowel mesentery. Despite the lack of obstruction, an internal hernia was diagnosed and was confirmed operatively

Fig. 7.6 Bowel ischemia on a portal venous phase coronal abdominal CT image in a 56-year-old man. Absent small bowel perfusion is demonstrated by hypoenhancing and mildly dilated small bowel loops in the left abdomen (asterisk), which are ischemic due to an occluded superior mesentery artery (arrow)

7.6   Abnormal Perfusion

Ischemia of abdominal organs encompasses a wide range of diagnoses and underlying causes. Regardless of the organ or the etiology, ischemia is diagnosed most commonly by observing decreased or absent blood flow to a vascular territory. On CT and MRI, this is often evaluated by assessing contrast enhancement in an organ. Decreased enhancement of an organ certainly suggests a diagnosis of ischemia, but must be viewed in the context of the specific patient and the other abdominal organs. Issues with contrast injection, decreased cardiac output, and inflammatory processes may all cause decreased enhancement of a non-ischemic organ. Conversely, multi-focal organ hypoperfusion may occur from a global hypotensive episode or an embolic source, and may lead to an error in diagnosis due to the multiplicity of findings. An examination protocol may also not be optimized to evaluate the vasculature and/or perfusion. One example of this can be seen in the imaging diagnosis of bowel ischemia. Commonly pre-contrast, arterial phase, and portal venous phase scans (with CT and occasionally with MR) with thin collimation will be performed in this setting to assess the bowel enhancement, arteries, and veins [15]. However, this may not be suspected a priori, leading to many patients in

this scenario being evaluated with routine portal venous phase-imaging which may make the findings less conspicuous (Fig. 7.6).

7.7   Cognitive Errors

Although a majority of radiologic errors are perceptual, cognitive errors remain an important cause of misdiagnosis in the evaluation of patients with abdominal pain. Due to anchoring, framing, availability, and alliteration errors (see Chap. 1), radiologists may often be prone to suggesting the most common or most recently seen diagnoses that occur in a given clinical scenario. Just as clinicians tend to take a quadrant-based approach to their diagnostic algorithm for abdominal pain, radiologists similarly tend to gravitate toward the common culprits in the four quadrants—cholecystitis, appendicitis, diverticulitis, and pancreatitis in the right upper, right lower, left lower, and left upper quadrants, respectively [16]. Focusing on a limited list of diagnoses can lead to a failure to suggest other inflammatory or infectious etiologies of abdominal pain. Furthermore, neoplastic

processes of the gallbladder, appendix, colon, pancreas, and surrounding structures may mimic the more common diseases that first come to mind and lead to a delayed cancer diagnosis, particularly if there is resultant inflammation.

7.8 Right Upper Quadrant Pain

In a patient with right upper quadrant pain, gallbladder pathology and specifically gallstones and/or cholecystitis are often the first diagnosis considered by both clinicians and radiologists. Errors in the diagnosis of acute cholecystitis may occur in patients with chronic cholecystitis who may not have gallbladder distention. In addition, patients who have received pain medication or those with gangrenous cholecystitis may have a falsely negative sonographic/clinical Murphy's sign [17].

7.9 Gallbladder Carcinoma

In addition, gallbladder carcinoma can be deceivably similar, not only in clinical presentation but also on imaging, especially when there is diffuse gallbladder wall thickening, gallbladder perforation, or fistula formation to adjacent bowel. Gallbladder cancer should be suspected when there are findings of focal, asymmetric wall thickening, lymphadenopathy, hepatic metastases, and biliary obstruction [18].

7.10 Xanthogranulomatous Cholecystitis

Xanthogranulomatous cholecystitis (XGC) is an uncommon variant of chronic cholecystitis and can be difficult to differentiate from gallbladder carcinoma. It is characterized by gallbladder inflammation with intramural accumulation of lipid-laden macrophages. On CT and MRI, it can appear aggressive with marked and irregular gallbladder wall thickening, with extension into adjacent liver parenchyma or even fistula formation into bowel loops. Hypoattenuating intramural nodules with loss of signal on opposed-phase

MRI sequence indicates intravoxel fat. In addition, an intact mucosal line, luminal surface enhancement, and gallstones are suggestive of XGC rather than carcinoma [19].

7.11 Peptic Ulcer Disease

Complicated or uncomplicated duodenal ulcer (DU) is a common cause of epigastric and sometimes right upper quadrant pain. DU is two- to three-times times more common than gastric ulcer. The most frequent site involved is the duodenal bulb, which may project into the hepatic hilum near the gallbladder. Giant duodenal ulcers greater than 3 cm can be mistaken for the duodenal bulb itself. On CT, duodenal wall thickening and adjacent fat stranding with a mucosal defect and outpouching are diagnostic. However, the proximity to the gallbladder may lead to a misattribution of this inflammation to cholecystitis (Fig. 7.7). Free retroperitoneal or intraperitoneal air and paraduodenal fluid are seen with perforation. Sometimes chronic DUs can cause stricture and gastric outlet obstruction [20].

Post-bulbar DUs should raise the possibility of excessive gastrin secretion, especially when multiple. Caused by a gastrin-secreting tumor, Zollinger-Ellison syndrome (ZES) is characterized by marked thickening of gastric rugal folds and hypervascular tumor in the duodenum or pancreas with or without metastases. ZES is seen in 20–60% of patients with multiple endocrine neoplasia type 1 (MEN1) [21] [22].

7.12 Groove Pancreatitis

Another cause of right upper quadrant inflammation, groove pancreatitis is an uncommon form of pancreatitis, which focally involves the pancreatic head, leading to inflammation in the potential space between the pancreatic head and the second portion of the duodenum. Usually, there is serum lipase elevation, but this may be falsely negative. There may be associated mass effect on the distal common bile duct, resulting in elevated serum bilirubin and alkaline phosphatase levels. On CT and MRI, fat
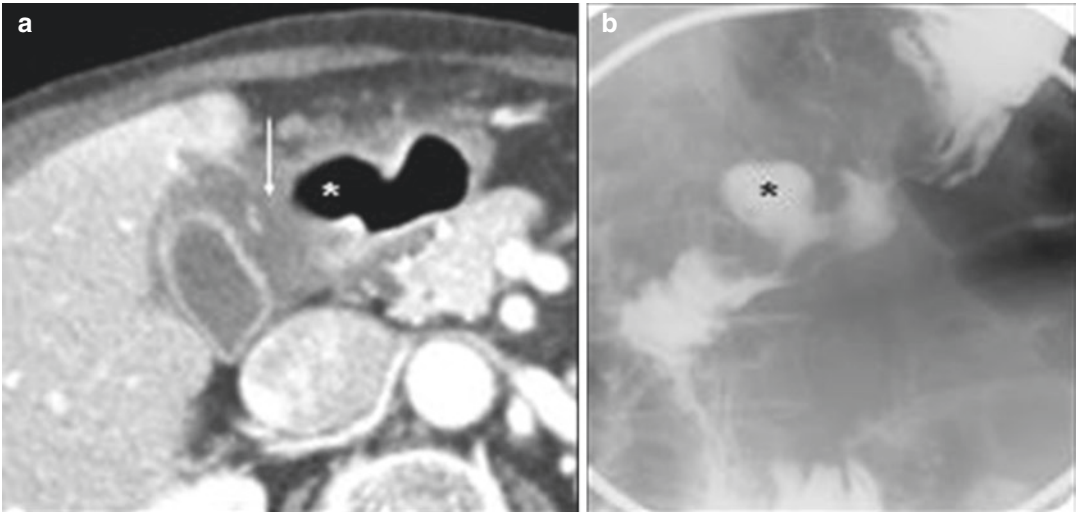
Fig. 7.7 Penetrating duodenal bulb ulcer causing secondary cholecystitis in an 80-year-old woman presenting with right upper quadrant pain. Axial abdominal CT image with intravenous contrast (**a**) shows a large duodenal bulb ulcer (asterisk), with surrounding fat stranding and thickening of the gallbladder wall (arrow). The ulcer fills with contrast on a subsequent upper GI examination (**b**, asterisk)
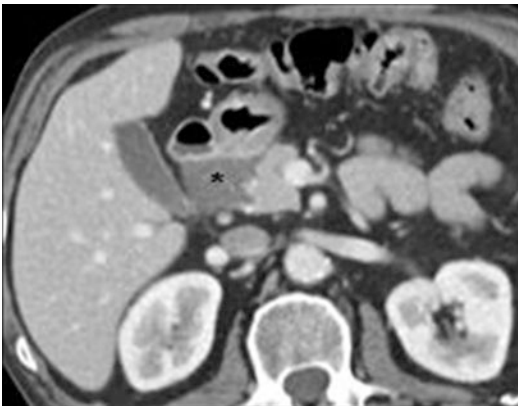

Fig. 7.8 Groove pancreatitis in a 47-year-old man with right upper quadrant pain and normal serum amylase. Axial abdominal CT image with intravenous contrast shows low attenuation mass-like soft tissue in the pancreaticoduodenal groove (asterisk), which is consistent with groove pancreatitis, and which was confirmed with endoscopic ultrasound and biopsy

stranding and inflammatory changes are seen in the pancreaticoduodenal groove, classically with associated "cystic degeneration." This may be mischaracterized as a routine duodenitis, pancreatic or duodenal tumor, or cholangitis. Chronically, soft tissue can be seen in the groove, which demonstrates delayed enhancement from fibrotic change (Fig. 7.8) [23].

7.13 Ascending Cholangitis

Acute cholangitis or ascending cholangitis is typically clinically diagnosed and is characterized by the Charcot triad of right upper quadrant pain, fever, and jaundice. Choledocholithiasis, recent ERCP, and biliary malignancy are some of the risk factors. Although imaging findings are nonspecific, ultrasound may show biliary dilatation and wall thickening and sometimes intraluminal debris/pus. CT and MRI show heterogeneous peripheral enhancement of the liver parenchyma on the arterial phase and biliary enhancement with or without dilatation [24]. Secondary inflammation of the gallbladder may occur, and in the case of biliary obstruction, there may also be gallbladder distention.

7.14 Left Upper Quadrant Pain

Acute pancreatitis is one of the most common diagnoses considered in the patient presenting with acute left upper quadrant pain [25]. On ultrasound, interstitial edema in acute pancreatitis is manifested as enlargement and decrease in echogenicity of the gland. However, sonography is most of the time limited due to bowel gas from

ileus and is mostly utilized to detect cholelithiasis and choledocholithiasis [26]. CT is often the initial imaging modality used to assess for complications of pancreatitis, including necrosis and fluid collections. Magnetic resonance imaging with cholangiopancreatography (MRCP) is employed to characterize ductal anatomy and to detect subtle underlying masses. Potential pitfalls in the diagnosis of acute pancreatitis include atypical cases such as from autoimmune inflamma-

tion (Fig. 7.9). Underlying malignancy may also mimic pancreatitis but is suggested when there is a focal mass, abrupt dilatation of the pancreatic duct, and upstream gland atrophy (Fig. 7.10). Other findings including lymphadenopathy and distant metastases help with suggesting an underlying malignancy [27]. In patients where the radiologist is unsure, follow-up imaging can be obtained to look for a mass once the inflammation has subsided.
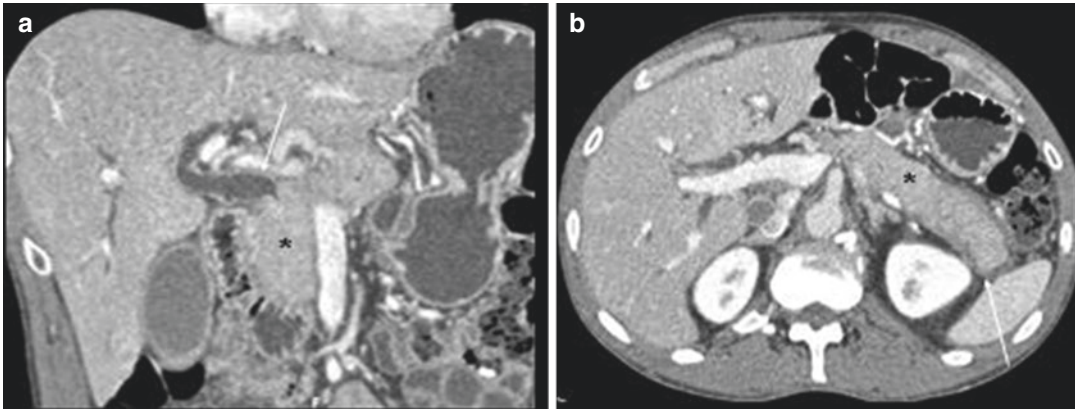
Fig. 7.9 Autoimmune pancreatitis in this 37-year-old man with left upper quadrant pain. Coronal (**a**) and axial (**b**) abdominal CT images with intravenous contrast show mass-like enlargement of the pancreatic head (**a**, asterisk), with upstream biliary ductal dilatation (**a**, arrow). Note the sausage shape of the pancreas (**b**, asterisk), with loss of normal lobulations. There is peripancreatic fat stranding (**b**, arrow), representing acute inflammation
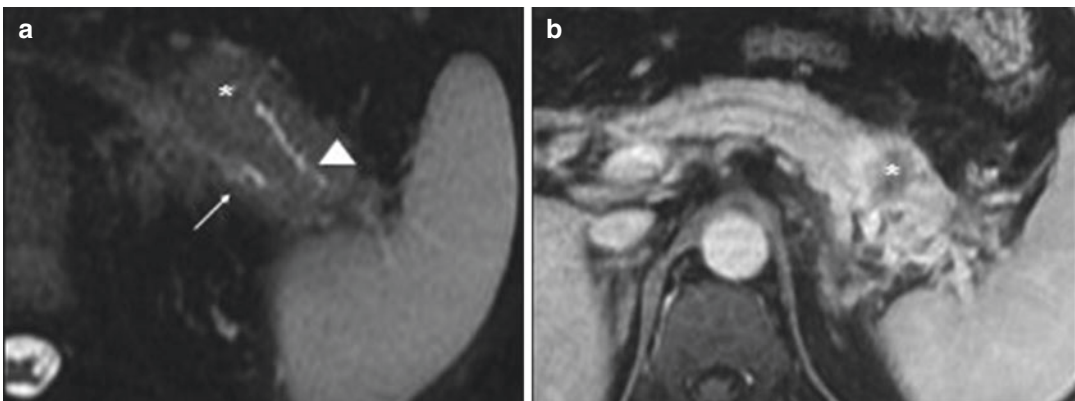
Fig. 7.10 Acute interstitial edematous pancreatitis of the tail caused by an obstructing mass in a 55-year-old man presenting with left upper quadrant pain. Endoscopic biopsy confirmed pancreatic adenocarcinoma. Axial T2-weighted (**a**) and post-contrast T1-weighted (**b**) MR images show abrupt cutoff of a dilated main pancreatic duct (**a**, arrowhead), which is due to a T2 intermediate intensity (**a**, asterisk) and hypoenhancing mass (**b**, asterisk) in this region. Note the T2 hyperintense changes in the fat surrounding the pancreatic tail (**a**, arrow), representing associated pancreatitis

7.15   Splenic Rupture

A ruptured spleen is typically caused by blunt or penetrating trauma to the left upper abdomen or the left lower chest. Less commonly rupture may be spontaneous or occur from iatrogenic injury such as after colonoscopy or colonic surgery, which is generally due to tension on the spleno-colic ligament (Fig. 7.11) [28]. Patients commonly present with left upper quadrant or left shoulder tip pain due to irritation of the left diaphragm from the blood. Computed tomography (CT) is commonly the first imaging performed, and shows perisplenic hemorrhage with or without a laceration or a pseudoaneurysm. The high attenuation of perisplenic blood is one of the key differentiating imaging features from acute pancreatitis.

7.16   Gastritis

Gastritis is commonly seen in patients with alcohol or nonsteroidal anti-inflammatory drug (NSAID) abuse. Although the most common site is the gastric antrum, which leads to epigastric pain, involvement of the gastric body and fundus can lead to left upper quadrant pain and inflammation. When present, associated peptic ulcers can perforate, bleed, or penetrate into adjacent structures. On CT, inflammation of the stomach presents with mural stratification of the gastric wall, with mucosal hyperenhancement and submucosal edema. When complicated by ulcers, these may be seen as an outpouching in the gastric mucosa with associated inflammation manifested with fluid and/or fat stranding (Fig. 7.12). Free gas and/or fluid may also be observed with perforation [29].

7.17   Right Lower Quadrant Pain

Uncomplicated or complicated acute appendicitis is the most common cause of right lower quadrant pain. An inflamed appendix can be seen on imaging as thick-walled, edematous, and dilated, with mucosal hyperenhancement, along with periappendiceal fat stranding and fluid. A dilated appendix is usually defined as having a transverse diameter of greater than 6 mm. An obstructing appendicolith may or may not be identified. In the general adult population, CT has a high sensitivity and specificity, reportedly between 88–100% and 91–99%, respectively [30]. However, in the pediatric population and
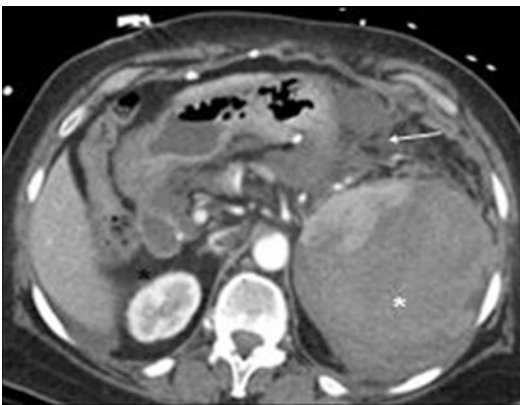
Fig. 7.11 Traumatic splenic rupture following colonoscopy in a 60-year-old-man. Axial abdominal CT image with intravenous contrast shows a large subcapsular splenic hematoma, compressing the spleen, which is small and anteromedially displaced (asterisk), with blood extending along the stomach and pancreas (arrow)
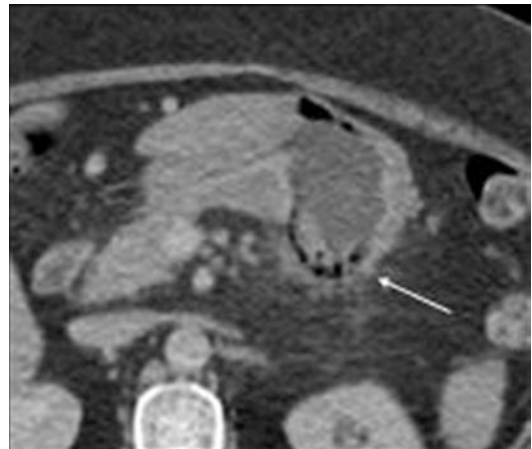
Fig. 7.12 Gastric ulcer. Axial abdominal CT image of a 48-year-old man with NSAID use presenting with left upper quadrant pain shows a focal outpouching representing an ulcer along the lesser curvature of the stomach (arrow), with wall thickening and perigastric fat stranding representing associated gastritis
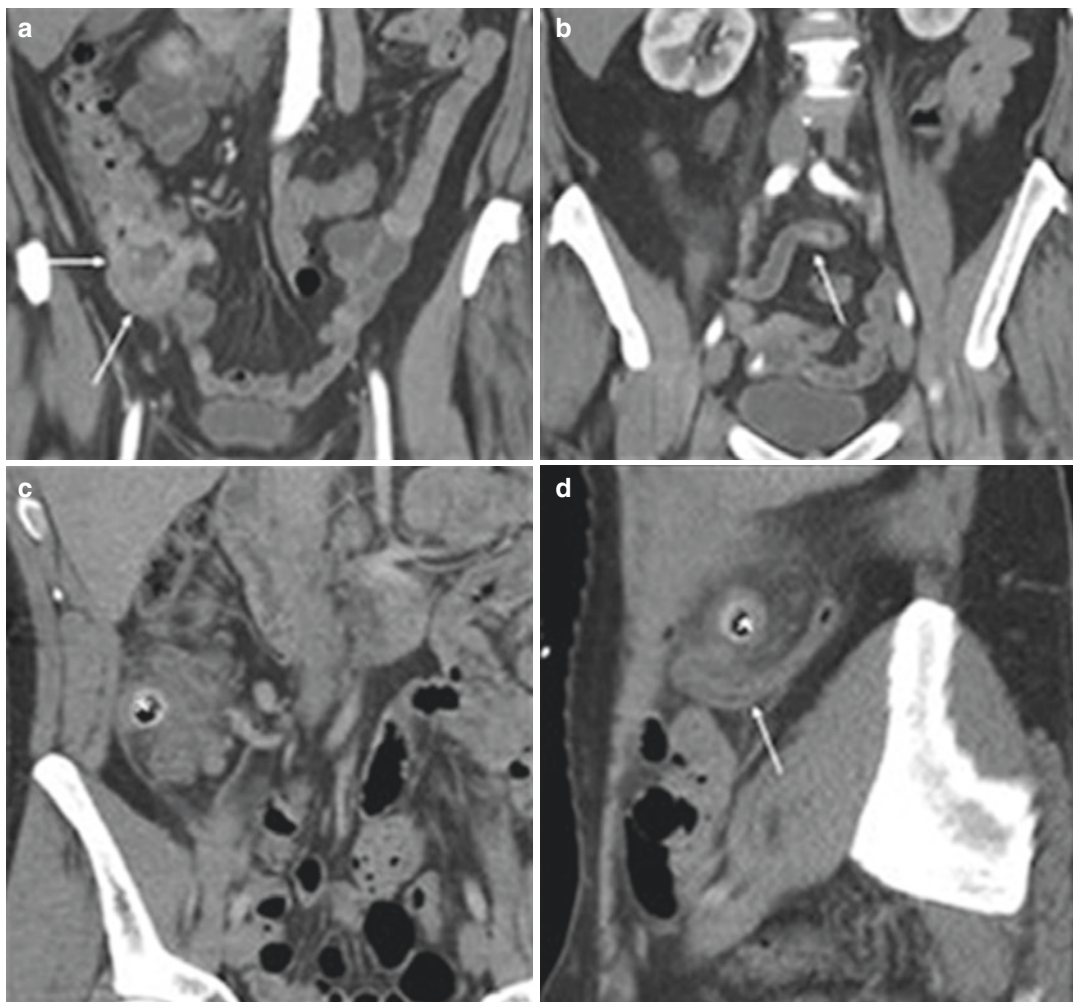
Fig. 7.13 Cecal causes of right lower quadrant pain. Coronal abdominal/pelvic CT images show a soft-tissue mass in the cecum (**a**, arrows) representing adenocarcinoma with obstruction and dilatation of the appendix in a 58-year-old patient (**b**, arrow). Cecal diverticulitis in a 29-year-old woman is depicted on coronal (**c**) and sagittal (**d**) CT images, with secondary inflammation of the appendix (**d**, arrow)

pregnant women, ultrasound and alternatively MRI now are often employed to avoid radiation which is associated with CT. Appendiceal tumors are rare but may mimic acute appendicitis, particularly when mucinous, which may present with luminal dilation and fluid density collections around the appendix. Cecal carcinoma can obstruct the appendiceal orifice and mimic acute appendicitis (Fig. 7.13a, b). Also, small appendiceal cancers in the adult or elderly population can obstruct the appendiceal lumen and lead to secondary appendicitis. CT findings include nodular

or mass-like asymmetric or irregular thickening of the cecum and/or base of the appendix.

7.18 Cecal Diverticulitis

Right-sided colonic diverticula are seen more commonly in younger adult patients and in the Asian population [31]. When diverticula become occluded, inflammation can occur, manifested on imaging as a thick-walled, rounded outpouching from the colon, potentially with extraluminal gas

or an abscess when perforated. Cecal diverticulitis may be confused for appendicitis since it presents as an inflamed projection near the ileocecal valve, and because inflammation from diverticulitis may secondarily inflame the appendix (Fig. 7.13c, d). The radiologist needs to differentiate between cecal diverticulitis and appendicitis, because most patients with diverticulitis are stratified to non-operative management.

7.19   Terminal Ileitis

Terminal ileitis presents on imaging with wall thickening of the ileum with surrounding fat stranding and engorgement of the vasa recta. Similar to cecal diverticulitis, terminal ileitis may also cause secondary inflammation of the appendix, potentially leading to a misdiagnosis of appendicitis. Crohn's disease is a common cause of terminal ileitis, and can lead to segmental inflammation manifested with asymmetric nodular wall thickening and potentially penetrating disease, resulting in abscesses and/or enteroenteric or enterocolic fistulae. In addition to Crohn's disease, bacterial, fungal, parasitic, and viral pathogens can cause terminal ileitis with or without mesenteric adenitis, including *Mycobacterium tuberculosis*, *Salmonella*, and *Yersinia enterocolitica* [32]. Non-occlusive ischemic enteritis may also appear similar [33].

7.20   Meckel's Diverticulitis

Meckel's diverticula are present in approximately 2% of the population. Meckel's diverticulitis is the most common congenital anomaly of the gastrointestinal tract, which is caused by failure of the omphalomesenteric duct to regress. These diverticula arise from the antimesenteric border of the ileum, between 40 and 100 cm from the ileocecal valve. They can harbor ectopic gastric and pancreatic tissue, and can become inflamed and ulcerated. Enteroliths can form within Meckel's diverticula, with subsequent obstruction leading to diverticulitis. Patients with Meckel's diverticulitis will present with right lower quadrant pain.
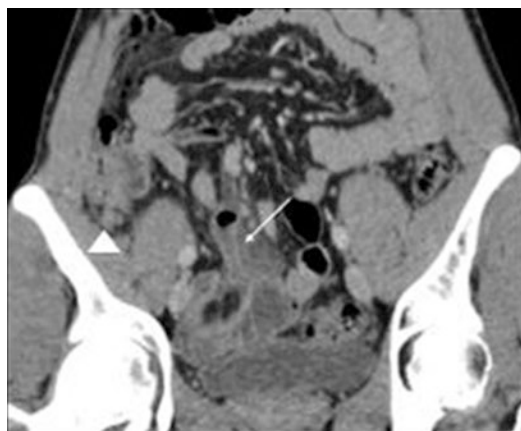
Fig. 7.14 Meckel's diverticulitis in a 25-year-old man with right lower quadrant pain. Coronal abdominal/pelvic CT image shows a blind-ending dilated tubular structure arising from the antimesenteric border of the ileum in the right lower quadrant, with trace surrounding fluid and fat stranding, representing an inflamed Meckel's diverticulum (arrow). Note the presence of a normal appendix adjacent to the cecum (arrowhead)

Meckel's diverticula can also serve as a lead point for intussusception or volvulus [34]. Inflamed Meckel's diverticula may be potentially confused for appendicitis, but can be differentiated on CT by increased distance from the ileocecal valve relative to the expected location of the appendix at the cecal base, and by finding a separate, normal appendix (Fig. 7.14).

7.21   Pelvic Inflammatory Disease

Pelvic inflammatory disease may present with right lower quadrant abdominal pain and clinically mimic appendicitis. Findings on ultrasound, CT, and MR may include hydro- or pyosalpinx, usually associated with an adnexal inflammatory mass and/or rim-enhancing fluid collections. More subtle cases may simply have generalized pelvic fat stranding, some of which may involve the appendix and can be confused for appendicitis [35]. In contrast to appendicitis, however, pelvic inflammatory disease should present with a normal-caliber appendix and inflammatory stranding extending beyond the periappendiceal fat (Fig. 7.15). Sometimes, infection can ascend
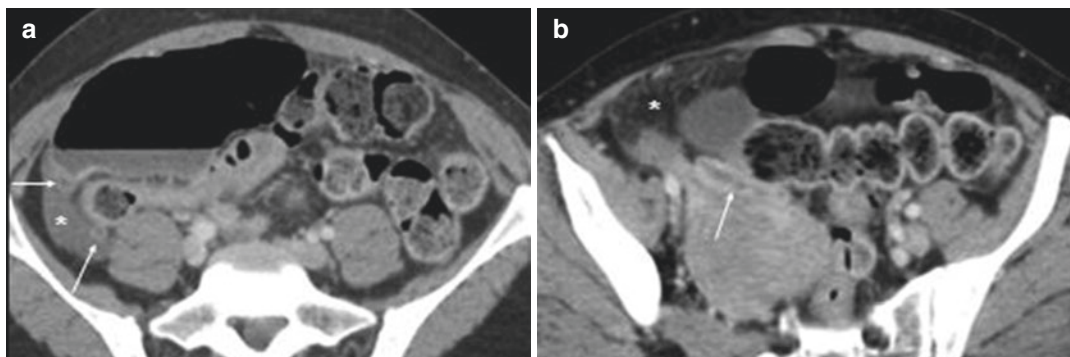
Fig. 7.15 Pelvic inflammatory disease presenting with right lower quadrant pain, clinically mimicking appendicitis. Axial abdominal/pelvic CT images of this 27-year-old woman presenting with right lower quadrant pain show free fluid in the right lower quadrant (**a**, asterisk) surrounding a non-dilated appendix (**a**, arrows). There is fat stranding in the right lower quadrant (**b**, asterisk), with a thickened, dilated right fallopian tube (**b**, arrow)

along the peritoneum and cause perihepatitis, a condition termed Fitz-Hugh-Curtis syndrome, which is characterized by hepatic capsular hyperemia, as well as periportal and gallbladder wall edema [35].

7.22 Ovarian Torsion

Ovarian torsion is considered a gynecological emergency and has a slight right-sided predilection due to the presence of the sigmoid colon on the left. On ultrasound, the affected ovary is enlarged with or without an underlying lead mass, is midline in position, and is often hypoechoic due to edema or hyperechoic due to hemorrhage or infarction. There is often peripheral migration of the ovarian follicles. Doppler evaluation may show diminished or no intraovarian venous flow, and less commonly absent or reversed arterial diastolic flow. Despite the potential for these findings, radiologists should be mindful that due to the dual arterial supply of the ovary from the ovarian and uterine arteries, normal arterial flow does not exclude torsion [9]. CT and MRI show a unilateral enlarged ovary with uterine deviation to the twisted side, fallopian tube thickening, peripheral cystic structures representing displaced follicles due to central stromal edema and/or hemorrhage, and ascites (Fig. 7.16) [9, 36]. These features can help differentiate surrounding pelvic inflammation from appendicitis.

7.23 Left Lower Quadrant

Sigmoid diverticulitis is one of most common causes of left lower quadrant abdominal pain. It is readily diagnosed when an inflamed, rounded outpouching(s) is(are) observed extending from the colon, and may be complicated by bowel perforation and subsequent abscess formation [37]. Sometimes acute diverticulitis can appear mass-like and may be difficult to differentiate from malignancy. In such patients, the presence of lymphadenopathy is a feature more commonly seen in adenocarcinoma [38]. Chronically, sigmoid diverticulitis results in muscular hypertrophy and potentially stenosis of the lumen. Although radiologists have traditionally advised follow-up optical colonoscopy to exclude an underlying mass in all or most patients with apparent diverticulitis on CT, more recent evidence has not supported this practice [39].

7.24 Epiploic Appendagitis

Epiploic appendages are small pouches of peritoneal fat arising from subserosa of the colon, the largest of which are in the sigmoid region. They can be seen on CT primarily when they are surrounded by fluid or when they become inflamed and/or infarcted after getting torsed, a condition termed as epiploic appendagitis. The most
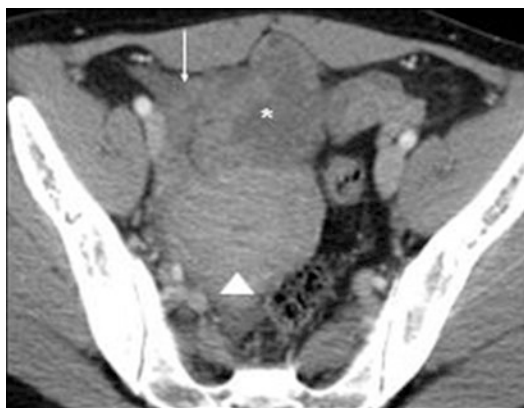
Fig. 7.16 Ovarian torsion causing right lower quadrant pain. Axial upper pelvic CT image of a 26-year-old woman presenting with right lower quadrant abdominal pain shows an enlarged and edematous right ovary (asterisk) displaced to the midline, with peripheral distribution of the follicles, compatible with torsion. There is also ipsilateral uterine deviation (arrowhead) and hemorrhagic fluid (arrow) in the right lower quadrant anteriorly
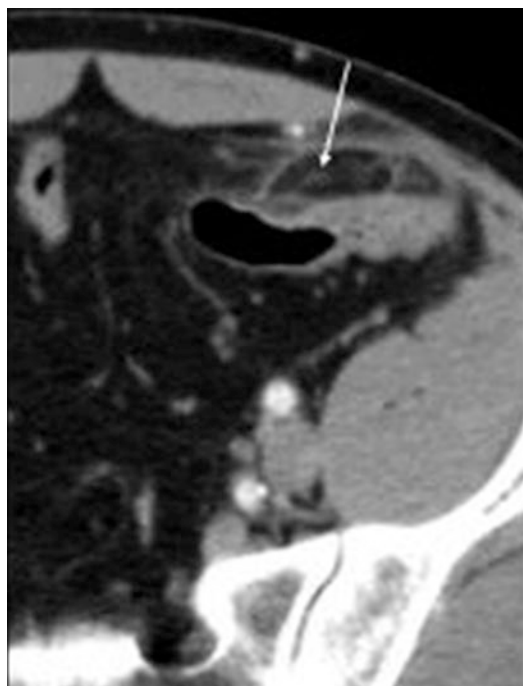
common CT finding is a less than 5 cm round or oval nodule abutting the colonic wall and with fat attenuation (Fig. 7.17). A central area of high attenuation is often seen, representing a centrally thrombosed vessel [40]. These features help distinguish this predominately self-limiting condition from that of diverticulitis, as both most commonly occur in the left lower quadrant.

7.25   Colitis

Although patients with colitis tend to present more often with bloody diarrhea than those with diverticulitis, there is substantial overlap in the clinical presentation of these two diseases. Inflammation involving the sigmoid colon can be due to ischemia, infection, or autoimmune causes, and can be difficult to distinguish from diverticulitis in patients with underlying diverticulosis. Typically, the degree of wall thickening and length of colonic involvement are more severe in colitis compared to diverticulitis (Fig. 7.18) [31]. Diverticulitis is also more likely to present with a focally swollen diverticulum on CT or MRI, more pronounced fat stranding, as well as microperforation and/or abscesses compared to in most patients with colitis [41].

Fig. 7.17 Epiploic appendagitis. Axial lower abdominal CT image with intravenous contrast shows an inflamed, oval-shaped focus of fat in the left lower quadrant anteriorly, with stranding stranding and a central area of vessel thrombosis (arrow), representing epiploic appendagitis in a 42-year-old patient. Note the lack of associated diverticulosis

7.26   Endometriosis

Endometriosis is an important cause of infertility and chronic pelvic pain. Although the most common site of involvement is the ovary, endometrial implants can involve the sigmoid colon, rectum, and cul-de-sac, and therefore cause left lower quadrant and pelvic pain. These implants can bleed, get inflamed, and lead to fibrosis and adhesions, and may even present as bowel obstruction. The classic sonographic appearance of an endometrioma is a homogenous, hypoechoic round or oval mass, with thin walls and posterior acoustic enhancement demonstrating low-level internal echoes and no internal blood flow. MRI is very useful for detecting small implants. Endometriomas appear T1 hyperintense, with corresponding low signal on T2-weighted imaging, which is referred to as T2 shading [42]. However, CT may simply demonstrate inflammation surrounding a mass or
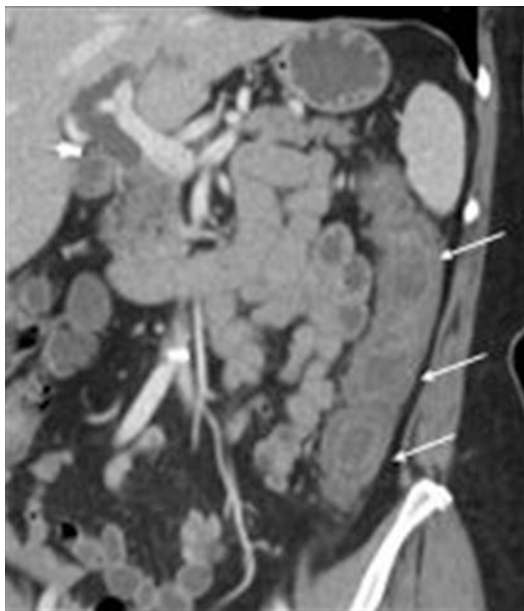
Fig. 7.18 Ischemic colitis causing left lower abdominal pain. Coronal abdominal CT image with intravenous contrast image shows wall thickening in the descending colon (arrows) in a recently hypotensive 80-year-old patient. Although the submucosal edema is non-specific, ischemic colitis was diagnosed endoscopically
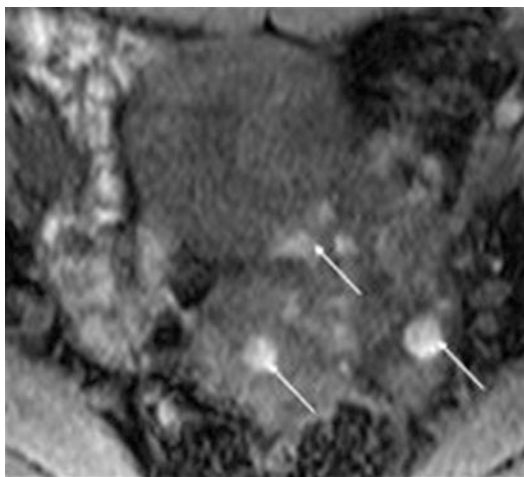

Fig. 7.19 Endometriosis in the left lower quadrant. Axial T1-weighted MR image of a 25-year-old woman presenting with left lower abdominal pain shows multiple hyperintense serosal endometriosis deposits involving the sigmoid colon (arrows), the cause for her acute pain, which potentially could be confused with diverticulitis

ill-defined area of colonic wall thickening, and may potentially lead to a misdiagnosis of a primary colonic process (Fig. 7.19).

7.27 Conclusion

Radiologists may make perceptual or cognitive errors in evaluating patients with abdominal pain. These stem from either failure to observe an important finding or from attributing findings, to a more common but not necessarily accurate diagnosis. Either scenario can lead to delayed diagnosis and/or inappropriate treatment. Therefore, it is incumbent upon radiologists to be aware of the common sources of these errors on a variety of imaging modalities.

References

1. Niska R, Bhuiya F, Xu J. National hospital ambulatory medical care survey: 2007 emergency department summary. Natl Health Stat Rep. 2010;26:1–31.
2. Raja AS, Mortele KJ, Hanson R, Sodickson AD, Zane R, Khorasani R. Abdominal imaging utilization in the emergency department: trends over two decades. Internal J Emerg Med. 2011;4:19.
3. Perry H, Foley KG, Witherspoon J, et al. Relative accuracy of emergency CT in adults with non-traumatic abdominal pain. Br J Radiol. 2016;89(1059):20150416.
4. Bruno MA, Walker EA, Abujudeh HH. Understanding and confronting our mistakes: the epidemiology of error in radiology and strategies for error reduction. Radiographics. 2015;35(6):1668–76.
5. Pereira JM, Sirlin CB, Pinto PS, Jeffrey RB, Stella DL, Casola G. Disproportionate fat stranding: a helpful CT sign in patients with acute abdominal pain. Radiographics. 2004;24(3):703–15.
6. Singh A, Danrad R, Hahn PF, Blake MA, Mueller PR, Novelline RA. MR imaging of the acute abdomen and pelvis: acute appendicitis and beyond. Radiographics. 2007;27(5):1419–31.
7. Sasaki T, Kunisaki R, Kinoshita H, et al. Doppler ultrasound findings correlate with tissue vascularity and inflammation in surgical pathology specimens from patients with small intestinal Crohn's disease. BMC Res Notes. 2014;7(1):363.
8. Lubner M, Menias C, Rucker C, et al. Blood in the belly: CT findings of hemoperitoneum. Radiographics. 2007;27(1):109–25.

9. Chang HC, Bhatt S, Dogra VS. Pearls and pitfalls in diagnosis of ovarian torsion. Radiographics. 2008;28(5):1355–68.

10. Pickhardt PJ, Asher DB. Wall thickening of the gastric antrum as a normal finding: multidetector CT with cadaveric comparison. Am J Roentgenol. 2003;181(4):973–9.

11. Potenta SE, D'Agostino R, Sternberg KM, Tatsumi K, Perusse K. CT urography for evaluation of the ureter. Radiographics. 2015;35(3):709–26.

12. Yeh BM, Liu PS, Soto JA, Corvera CA, Hussain HK. MR imaging and CT of the biliary tract. Radiographics. 2009;29(6):1669–88.

13. Lockhart ME, Tessler FN, Canon CL, et al. Internal hernia after gastric bypass: sensitivity and specificity of seven CT signs with surgical correlation and controls. Am J Roentgenol. 2007;188(3):745–50.

14. Peterson CM, Anderson JS, Hara AK, Carenza JW, Menias CO. Volvulus of the gastrointestinal tract: appearances at multimodality imaging. Radiographics. 2009;29(5):1281–93.

15. Wiesner W, Khurana B, Ji H, Ros PR. CT of acute bowel ischemia. Radiology. 2003;226(3):635–50.

16. Stoker J, van Randen A, Lameris W, Boermeester MA. Imaging patients with acute abdominal pain. Radiology. 2009;253(1):31–46.

17. Rosenthal SJ, Cox GG, Wetzel LH, Batnitzky S. Pitfalls and differential diagnosis in biliary sonography. Radiographics. 1990;10(2):285–311.

18. Levy AD, Murakata LA, Rohrmann CA. Gallbladder carcinoma: radiologic-pathologic correlation. Radiographics. 2001;21(2):295–314.

19. Zhao F, Lu P-X, Yan S-X, et al. CT and MR features of xanthogranulomatous cholecystitis: an analysis of consecutive 49 cases. Eur J Radiol. 2013;82(9):1391–7.

20. Jayaraman MV, Mayo-Smith WW, Movson JS, Dupuy DE, Wallach MT. CT of the duodenum: an overlooked segment gets its due. Radiographics. 2001;21(1):147–60.

21. Roy PK, Venzon DJ, Shojamanesh H, et al. Zollinger-Ellison syndrome. Clinical presentation in 261 patients. Medicine. 2000;79(6):379–411.

22. Rodallec M, Vilgrain V, Zins M, Couvelard A, Ruszniewski P, Menu Y. Helical CT of pancreatic endocrine tumors. J Comput Assist Tomogr. 2002;26(5):728–33.

23. Raman SP, Salaria SN, Hruban RH, Fishman EK. Groove pancreatitis: spectrum of imaging findings and radiology-pathology correlation. Am J Roentgenol. 2013;201(1):W29–39.

24. Catalano OA, Sahani DV, Forcione DG, et al. Biliary infections: spectrum of imaging findings and management. Radiographics. 2009;29(7):2059–80.

25. Ecanow JS, Gore RM. Evaluating patients with left upper quadrant pain. Radiol Clin N Am. 2015;53(6):1131–57.

26. O'Connor OJ, McWilliams S, Maher MM. Imaging of acute pancreatitis. Am J Roentgenol. 2011;197(2):W221–5.

27. Shanbhogue AKP, Fasih N, Surabhi VR, Doherty GP, Shanbhogue DKP, Sethi SK. A clinical and radiologic review of uncommon types and causes of pancreatitis. Radiographics. 2009;29(4):1003–26.

28. Levenson RB, Troy KM, Lee KS. Acute abdominal pain following optical colonoscopy: CT findings and clinical considerations. Am J Roentgenol. 2016;207(3):W33–40.

29. Zulfiqar M, Shetty A, Shetty V, Menias C. Computed tomography imaging of non-neoplastic and neoplastic benign gastric disease. Curr Probl Diagn Radiol. 2018;48(1):75–96.

30. Lane MJ, Liu DM, Huynh MD, Jeffrey RB Jr, Mindelzun RE, Katz DS. Suspected acute appendicitis: nonenhanced helical CT in 300 consecutive patients. Radiology. 1999;213(2):341–6.

31. Ben Yaacoub I, Boulay-Coletta I, Jullès MC, Zins M. CT findings of misleading features of colonic diverticulitis. Insights Image. 2011;2(1):69–84.

32. Pinto Leite N, Pereira JM, Cunha R, Pinto P, Sirlin C. CT Evaluation of appendicitis and its complications: Imaging techniques and key diagnostic findings. Am J Roentgenol. 2005;185(2):406–17.

33. Berritto D, Iacobellis F, Mazzei MA, et al. MDCT in ischaemic colitis: how to define the aetiology and acute, subacute and chronic phase of damage in the emergency setting. Br J Radiol. 2016;89(1061):20150821.

34. Elsayes KM, Menias CO, Harvin HJ, Francis IR. Imaging manifestations of Meckel's diverticulum. Am J Roentgenol. 2007;189(1):81–8.

35. Revzin MV, Mathur M, Dave HB, Macer ML, Spektor M. Pelvic inflammatory disease: multimodality imaging approach with clinical-pathologic correlation. Radiographics. 2016;36(5):1579–96.

36. Duigenan S, Oliva E, Lee SI. Ovarian torsion: diagnostic features on CT and MRI with pathologic correlation. Am J Roentgenol. 2012;198(2):W122–W31.

37. Horton KM, Corl FM, Fishman EK. CT evaluation of the colon: inflammatory disease. Radiographics. 2000;20(2):399–418.

38. Chintapalli KN, Esola CC, Chopra S, Ghiatas AA, Dodd GD. Pericolic mesenteric lymph nodes: an aid in distinguishing diverticulitis from cancer of the colon. Am J Roentgenol. 1997;169(5):1253–5.

39. Sai VF, Velayos F, Neuhaus J, Westphalen AC. Colonoscopy after CT diagnosis of diverticulitis to exclude colon cancer: a systematic literature review. Radiology. 2012;263(2):383–90.

40. Singh AK, Gervais DA, Hahn PF, Sagar P, Mueller PR, Novelline RA. Acute epiploic appendagitis and its mimics. Radiographics. 2005;25(6):1521–34.

41. Childers BC, Cater SW, Horton KM, Fishman EK, Johnson PT. CT evaluation of acute enteritis and colitis: is it infectious, inflammatory, or ischemic? Radiographics. 2015;35(7):1940–1.

42. Bennett GL, Slywotzky CM, Cantera M, Hecht EM. Unusual manifestations and complications of endometriosis—spectrum of imaging findings. Am J Roentgenol. 2010;194(6):WS34–46.

Errors in Imaging of the Acute Female Pelvis: Where Do They Occur and How Can We Reduce Them?

8

Ania Z. Kielar, Shauna Duigenan, and Darcy J. Wolfman

Key Teaching Points

- An HCG level should be checked in all women of childbearing age before imaging to prevent unnecessary radiation of an unexpected pregnancy and to look for complications of pregnancy, including ectopic pregnancy, in women presenting with acute pelvic pain.
- Endometriosis is an underdiagnosed condition which can be identified on ultrasound and on MRI in particular, and should be a consideration in women with chronic pain or with unusual, cyclical symptoms.
- Differentiation of large fibroids versus a sarcoma of the uterus can be very challenging; growth or an invasive appearance of a "fibroid"

in postmenopausal women should be carefully evaluated for a possible sarcoma.

- Use of meticulous sonographic technique including providing two planes of imaging of any abnormality and cine imaging is important for accurate diagnosis of pelvic findings in women.
- Pelvic inflammatory disease and other inflammatory conditions in the pelvis can have overlapping features. Careful assessment of cross-sectional imaging by radiologists can help arrive at the correct diagnosis.

8.1 Introduction

"To err is human"; however, as physicians it is incumbent upon us to reduce potential sources of error in our daily work in order to reduce the risk of patient harm [1].

In addition to acute conditions involving the bowel, urinary tract, and musculoskeletal system, women also have a number of conditions specific to their gender which substantially increases the number of differential diagnoses to choose from when a female patient presents with pelvic pain. For example, in general, a history of right lower quadrant pain could represent appendicitis or inflammatory bowel disease, but in women, right-sided adnexal abnormalities including ovarian torsion, pelvic inflammatory disease, hemorrhagic cyst, endometriosis, malignancy of the

A. Z. Kielar (✉)
C1-Imaging, The Ottawa Hospital,
University of Ottawa, Ottawa, ON, Canada

University of Toronto, Toronto, ON, Canada

Ottawa Hospital Research Institute,
Ottawa, ON, USA

S. Duigenan
C1-Imaging, The Ottawa Hospital,
University of Ottawa, Ottawa, ON, Canada
e-mail: sduigenan@toh.ca

D. J. Wolfman
Community Radiology Division,
Department of Radiology, Johns Hopkins School
of Medicine, Baltimore, MD, USA

American Institute for Radiologic Pathology,
American College of Radiology,
Silver Spring, MD, USA

reproductive organs, and ectopic pregnancy are additional considerations.

8.2 Type of Errors

There are many postulated reasons why errors occur in radiology, with active and latent errors being the two main categories. Quantification and categorization of errors specifically involving acute pelvic conditions in women have not been reported in the literature to our knowledge [2]. Latent errors include system-wide organizational processes; these are felt to be responsible for the majority of errors in medicine. In the case of women's imaging, this can include the use of outdated technology such as ultrasound equipment without adequate transabdominal penetration in a patient population with a larger body mass index or lack of stirrups for a hysterosonogram. It can also include lack of access to non-irradiating modalities including magnetic resonance imaging (MRI) and after-hours ultrasound (US). Additionally, latent errors include hospital-wide processes which allow the incorrect imaging test to be requested without input from a radiologist, and protocols that result in incomplete field-of-view imaging to ensure all pertinent parts are included [3]. However, active errors, which are attributable to human causes, also account for identifiable errors, and these should be closely evaluated to reduce their incidence. In certain patients, an incomplete history can lead the radiologist to choose an imaging examination which is suboptimal for diagnosing the abnormality (e.g., CT performed for evaluation of chronic endometriosis). Even if the correct examination is performed, technical errors including incorrect timing of contrast injection, motion artifact, or incomplete imaging of the area of interest can all prevent the radiologist from correctly identifying the abnormality. There are also limitations of various imaging modalities with regard to certain diagnoses, as well as patient-related factors. For example, too much intrapelvic fat can limit transabdominal sonographic interrogation of pelvic structures, whereas too little intrapelvic fat and crowding of the bowel and gynecologic structures

can make CT evaluation more challenging [4]. In women, the digestive, retroperitoneal, musculoskeletal, and urinary system structures are all located within the pelvic girdle in close proximity to the reproductive organs. Thus, non-specific symptoms can make it difficult to choose the best imaging for patient evaluation.

The most common active error in interpretation of cross-sectional pelvic radiologic images is a false-negative (FN) error, which means that a finding is missed [5]. Satisfaction of search error falls into the category of FN error. In this scenario, one finding is identified on a patient's imaging examination, but there may be another finding of significance which is not described (e.g., a patient with appendicitis is correctly diagnosed; however, the incidental adnexal mass is not reported) (Figs. 8.1 and 8.2).

Cognitive errors are also common in women's imaging, in that an abnormality is identified, but the incorrect diagnosis is chosen (Fig. 8.3a, b).

Women presenting with acute pelvic pain should always be screened for possible pregnancy with either urine or blood tests, particularly if they are of childbearing age and regardless of the reported use of contraception (Fig. 8.4).

Even with a negative HCG level, evaluation of reproductive organs for acute abnormalities may be required if initial findings related to other structures in the pelvis are noted to be normal (Fig. 8.5a–c).

When a woman presents with acute pelvic pain, the most clinically appropriate imaging for the differential diagnosis should be chosen. A team effort is thus required to have the highest likelihood for correct diagnosis; this includes input from the referring physician (often in the emergency department), the radiologist protocoling the examination, and the technologists performing the examination. A review of the American College of Radiology's (ACR) Appropriateness Criteria is often of value when trying to determine the safest and most effective imaging to perform. For evaluation of female reproductive organs, ultrasound is often the first imaging examination of choice [6]; however, if gastrointestinal or other structures are being evaluated, CT may be favored.
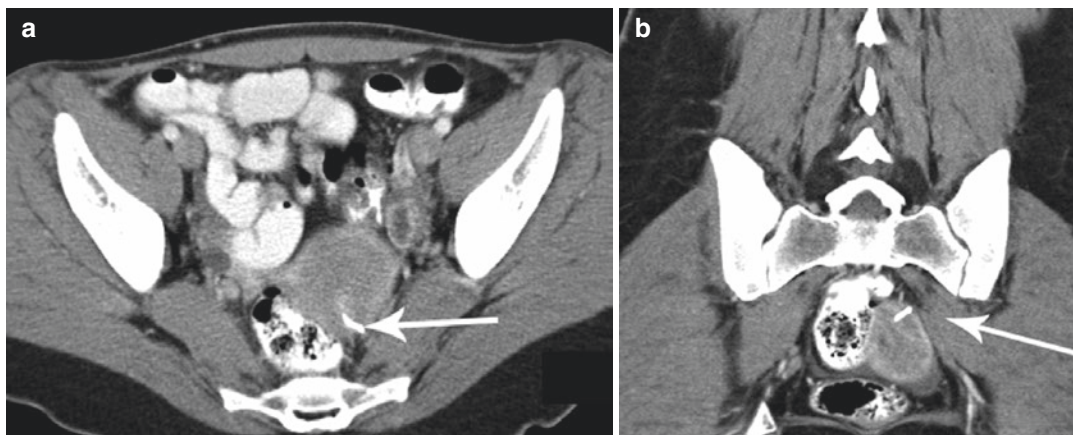
Fig. 8.1 (**a**) Axial CT image with oral and IV contrast image in a patient with a history of lymphoma perforation of an IUD through the uterine wall (arrow). (**b**) Coronal CT image of the same patient shows a missed perforated IUD through the uterine wall (arrow). The patient later developed a pelvic abscess adjacent to the time of the IUD which required drainage
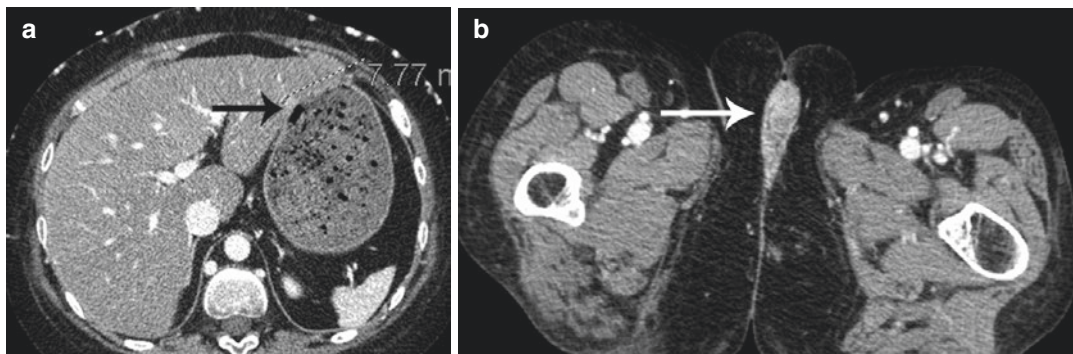

Fig. 8.2 (**a**) Axial CT image of the abdomen with IV contrast in a 68 year old woman being investigated for an echogenic liver mass incidentally found on US shows an 8 mm hyperdense/hyperenhancing area in the left lobe (arrow) which on follow-up MRI was found to represent focal fat infiltration. (**b**) CT in the same patient with field of view which extended into the pelvis shows an incidental mass in the vulva that was missed (arrow). The patient presented 6 months later with a mass which had almost doubled in size. This was proven to be a vaginal squamous cell carcinoma. Follow up imaging not shown

In the case of ultrasound, technologists as well as radiologists performing hands-on scans have an opportunity to interact with the patient and to obtain a more detailed history, as well as to determine the area of maximal discomfort. This is especially vital in assessing possible ovarian torsion and endometriosis [7]. This can help direct the current imaging and potential follow-up imaging. Ultrasound technologists should also strive to provide easily interpretable and reproducible imaging quality. This can include use of split-screen images (two planes of imaging for a structure of interest), as well as the routine use of cine loops [8].

CT technologists have an important role in limiting radiation exposure, particularly in younger women (of childbearing age). They should double check that patients have undergone HCG testing prior to scanning, when possible, although in severe trauma, scanning may proceed regardless of pregnancy status. CT technologists can also ensure that two or three planes of image reconstruction are provided to radiologists, to help radiologists in their interpretations.

In countries where available, MRI technologists can administer hyoscine-*N*-butylbromide (Buscopan) or glucagon, if that is the standard of care at their institution, to reduce bowel motion
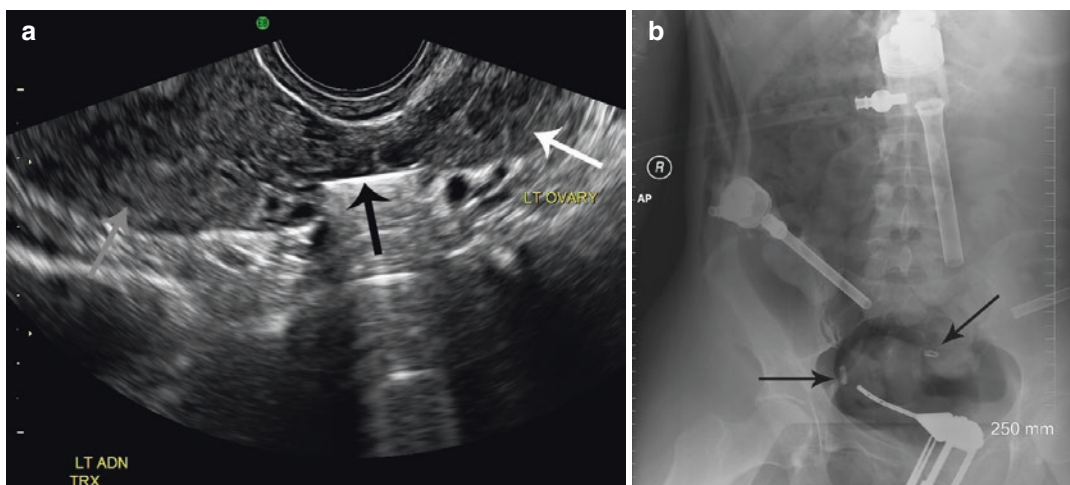
Fig. 8.3 (**a**) Transvaginal US image in a 36-year-old woman with pelvic pain. The echogenic structure with posterior shadowing between the uterus and left adnexa (arrow) was interpreted as an intra-abdominal IUD which had perforated through the uterine wall. (**b**) Intra-operative radiograph demonstrates that the echogenic structure seen on ultrasound was actually one of two tubal ligation clips (arrows)

Fig. 8.4 Abdominal radiograph performed in a 26-year-old woman with a known history of Crohn disease. A radiograph was performed to determine if there was a bowel obstruction related to Crohn disease to explain her symptoms. An HCG level was not checked. The radiograph reveals a 35-week gestation in a patient who did not realize that she was pregnant

artifacts and thus improve image quality [9]. These technologists can confer with radiologists to ensure that efficient and appropriate sequences are used and that instructions provided to the patients are clear, including breath holding, as needed.

Use of evidence-based medicine and following published guidelines are important for efficient use of limited health-care resources.

Standardized template reports, rather than free prose reporting, for findings in the pelvis may be helpful to trainees (including radiology residents, fellows, and junior faculty), to ensure all structures of interest have been evaluated. Use of template reports has been shown to improve consistency and quality of reporting, ultimately leading to clearer communication between radiologists and requesting physicians [10–12]. These template reports should be designed to answer the clinical questions, using appropriate, published, evidence-based management guidelines. For example, if an ovarian cyst is incidentally identified in a woman who is postmenopausal, the most up-to-date published guidelines should be used to prevent either the patient getting lost to follow-up, or unnecessary additional imaging and patient anxiety [13].
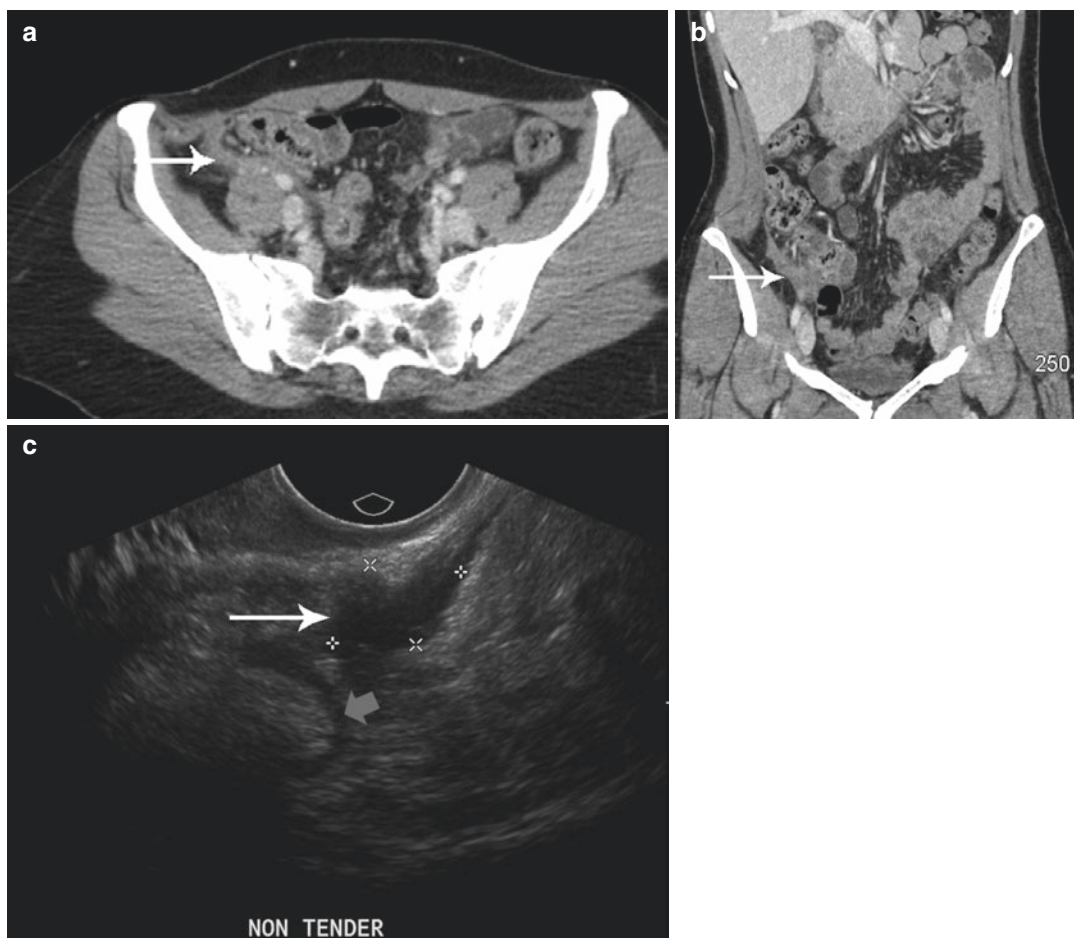
Fig. 8.5 (**a**) CT of a 32-year-old woman presenting with right lower quadrant pain who was brought to the OR subsequent to a CT diagnosis of acute-on-chronic appendicitis. Irregular-shaped soft tissue was seen in the right lower quadrant next to the external iliac vessels (short gray arrow). These were found to be endometriotic plaques at the OR. (**b**) Right lower quadrant irregular-shaped soft tissue is also shown on the coronal CT reformation, representing an endometriotic plaque (short gray arrow). (**c**) Transvaginal ultrasound image in the same patient demonstrates a hypoechoic, non-mobile, irregular-shaped endometrial plaque (white arrow) located next to the ascending colon (short gray arrows)

In acute imaging of the female pelvis, there are imaging findings which may overlap for more than one diagnosis. Examples of various pearls and pitfalls are provided in an organ-based fashion below.

8.2.1 Uterus

Uterine myomas, also known as fibroids, are common in North American women and have the highest prevalence in African-Americans [14]. Fibroids can grow quite large and undergo degeneration if they outgrow their blood supply. This can be a source of acute pelvic pain. Exophytic fibroids are also at risk for torsion, which can also be a cause of acute pelvic pain in women. In both of these conditions, intravenous contrast-enhanced MRI can show a reduction in enhancement of these fibroids and often, if there is internal hemorrhage, high signal on T1-weighted
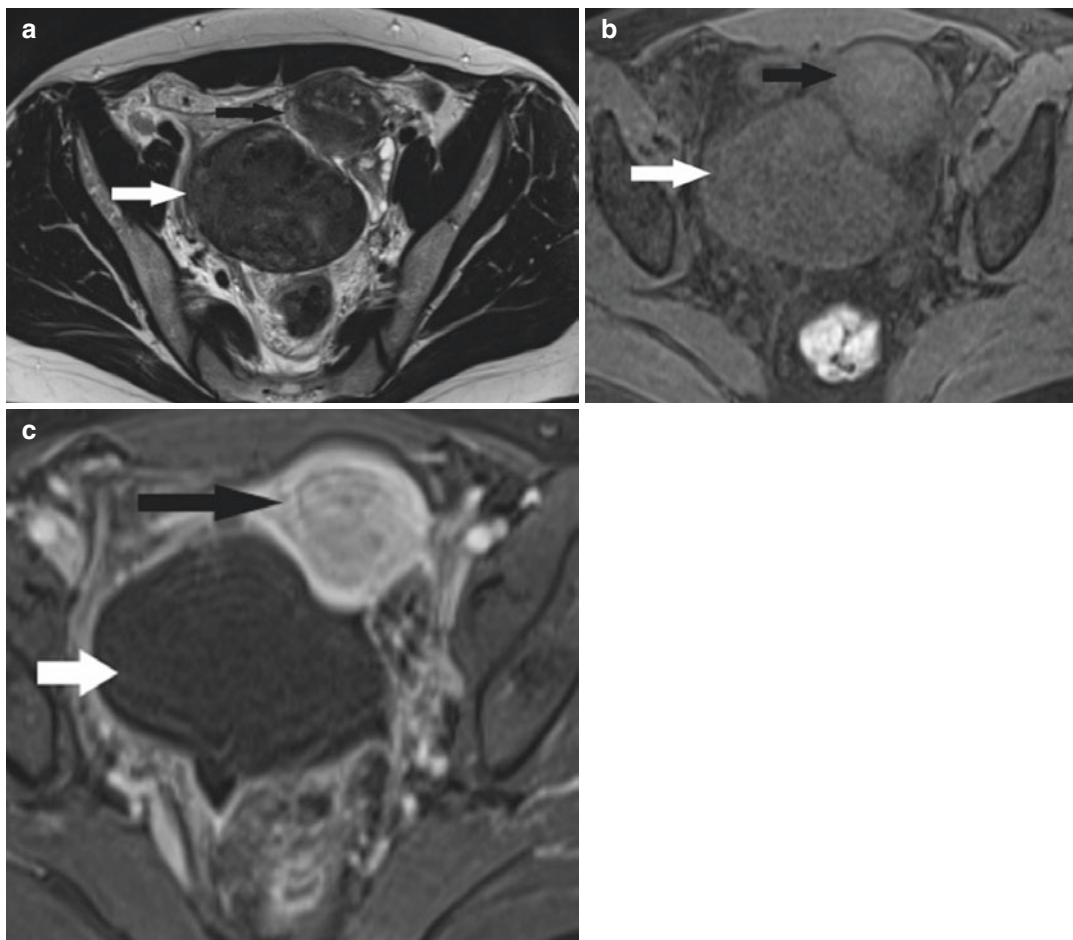
Fig. 8.6 (**a**) T2-weighted axial image of a 47-year-old woman with acute pelvic pain. Exophytic fibroid was present on prior ultrasound (not shown). The posteriorly located fibroid (white arrow) is larger than the uterus (black arrow). (**b**) Pre-contrast fat-saturated T1-weighted axial MR image shows similar signal intensity of the fibroid (white arrow) when compared to the uterus (black arrow). (**c**) Post-gadolinium axial MR image shows no enhancement of the fibroid (white arrow) when compared to the normal uterus (black arrow), due to torsion of the pedicle of the fibroid

images (Fig. 8.6a–c). During sonographic interrogation, evaluation is more limited; however, patients may sometimes have pain when the probe is placed over the fibroid of concern [15].

Rarely, patients may develop uterine sarcomas. These can be very difficult to differentiate from a large fibroid, which are far more common. This can be a source of error, particularly when a patient presents to the ED with non-specific abdominal or pelvic pain and a large pelvic mass is identified. There are some ways to help differentiate a sarcoma from a large fibroid. This includes growth of a "fibroid" in postmenopausal women, as well as direct extension into

adjacent structures or organs [16]. It is important to note that uterine leiomyosarcoma do not arise from uterine fibroids, so the presence of a new "fibroid" in a postmenopausal patient is worrisome.

Size of the uterine mass, presence or lack of areas of enhancement, and heterogeneous signal intensity on MRI are not specific findings for differentiating the two diagnoses. However, invasion of adjacent structures by a soft-tissue mass arising from the myometrium is a highly specific finding associated with malignancy. A comparison with previous is recommended, when possible. Substantial increase in size, and especially
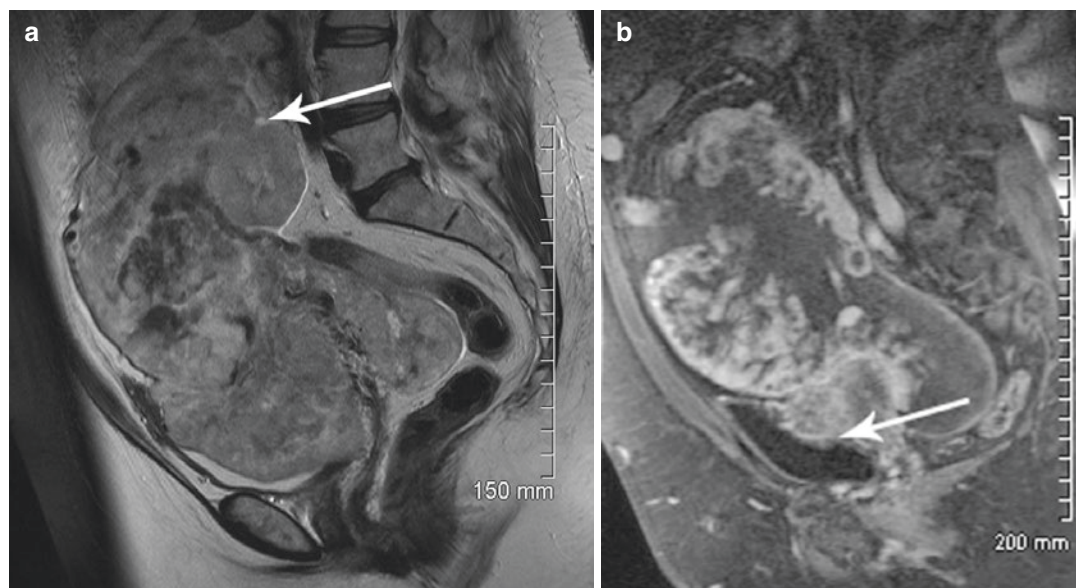
Fig. 8.7 (**a**) Sagittal T2-weighted MR image of a 57-year-old woman with uterine sarcoma mimicking a large fibroid (arrow). Imaging done 10 years before demonstrated a normal uterus without any mass or fibroid (not shown). (**b**) Post-gadolinium sagittal T1-weighted LAVA, image shows abnormal enhancement along the anterior/inferior margin of the mass, and direct extension of mass into the bladder (arrow)

increase in size in postmenopausal women, is a concerning feature (Fig. 8.7a, b).

Congenital abnormalities of the uterus occur in 5.5% of women in the general population and in up to 24.5% of those with prior miscarriage and infertility. These congenital abnormalities are often incidental findings which can easily be missed, but have potentially clinically significant effects on attempts at future pregnancy [17].

There are six main classes of uterine anomalies; however, unicornuate and septate uteri have the highest risks of complications. Unicornuate uteri are clinically significant due to increased risk of uterine rupture in the third trimester due to a reduced capacity for a growing intrauterine pregnancy. This is particularly of high risk in women who have a rudimentary horn associated with their unicornuate uterus, and when the gestation forms within the communicating rudimentary horn. Unicornuate uteri can be challenging to diagnose, but can be identified as having a banana shape. Hysterosalpingogram has been traditionally used for characterizing uterine anomalies; however, many of these findings can now be identified on MRI or ultrasound [18, 19] (Fig. 8.8).
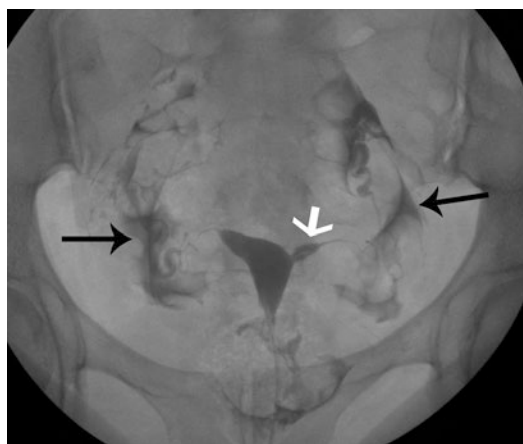
Fig. 8.8 Hysterosalpingogram in a 27-year-old undergoing an infertility workup demonstrates a unicornuate uterus with a rudimentary left horn (white arrow). This small left horn communicates with the cervix, and there is free spillage of the contrast agent through both fallopian tubes (black arrows on both sides)

It is important to diagnose unicornuate uteri, as these patients are at risk for complications of pregnancy, especially uterine rupture of the rudimentary horn if a subsequent pregnancy develops there [20] (Fig. 8.9a, b).
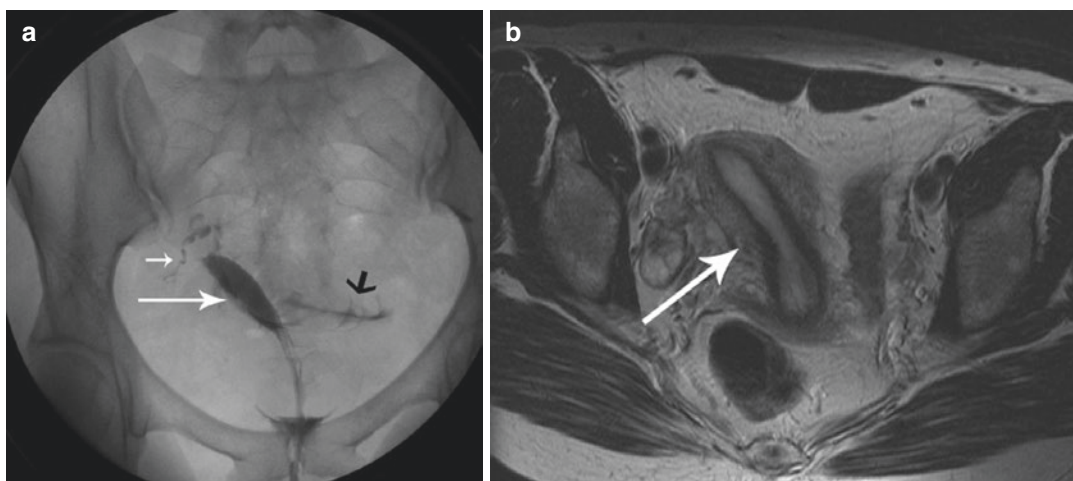
Fig. 8.9 (**a**) Hysterosonogram in a 28-year-old woman undergoing an infertility workup shows a right unicornuate uterus without a rudimentary horn. The spillage (black arrows) of injected contrast is from the single patent right fallopian tube. (**b**) Corresponding T2-weighted axial MR image demonstrates the typical banana-shaped uterus, confirming the uterine anomaly

A septate uterus is the most common uterine anomaly and is the result of partial or complete failure of resorption of the uterovaginal septum. The outer contour of the uterus is usually preserved or only mildly indented. Septate uteri are associated with recurrent pregnancy losses, since the septum does not have enough blood supply to support the growing fetus and placenta [21].

8.2.2 Endometrium

Endometrial thickness varies during the menstrual cycle of women of childbearing age, which can make evaluation challenging. The upper limit of thickness is not well established in women with regular menstrual cycles, although an endometrial thickness of >15 mm in a patient with dysfunctional uterine bleeding should prompt investigation, such as endometrial sampling/biopsy. If there is no dysfunctional bleeding, then the upper limit for endometrial thickness has not been clearly established to our knowledge [22–24].

In postmenopausal women, an endometrial stripe thickness of >5 mm (bilayer midline sagittal transvaginal image) is considered abnormal in women who are symptomatic (with dysfunctional uterine bleeding). It is also considered abnormal in asymptomatic women who have risk factors for endometrial cancer (including obesity, hypertension, or late menopause) or who have other imaging features on transvaginal US which are suspicious for malignancy, including increased vascularity, inhomogeneity, or particulate fluid. Endometrial hyperplasia and endometrial carcinoma are the main concerns in postmenopausal women, particularly in those who have higher endogenous estrogen levels (e.g., are overweight due to accumulation of estrogen in fat stores), as well as in women who are on hormone replacement therapy [25].

Endometriosis is a commonly underdiagnosed condition, and often women have signs and symptoms for an average of 10 years before diagnosis [26]. Both ultrasound and MRI have been shown to be helpful for making this diagnosis, though use of ultrasound requires operator experience and is often relatively time-consuming [27]. It can also be uncomfortable for women as symptoms are typically reproduced during the examination. MRI has been
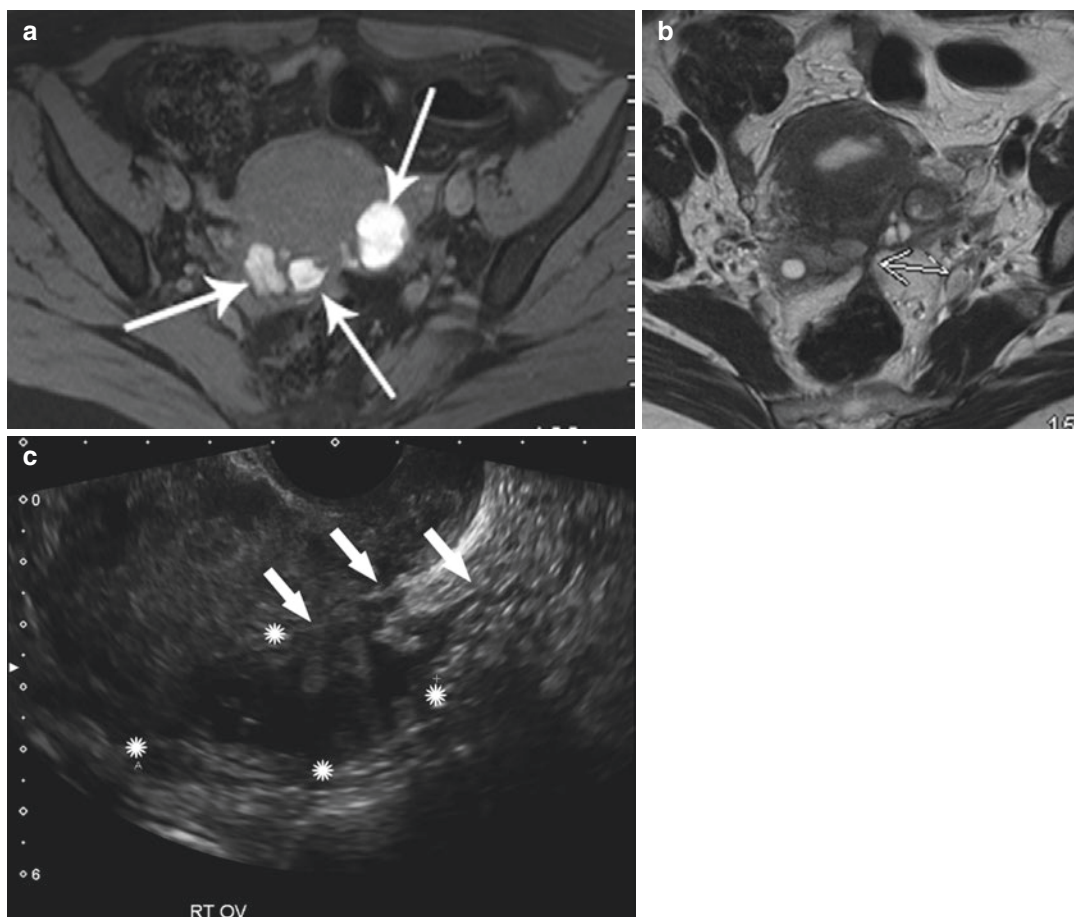
Fig. 8.10 (**a**) Follow-up MR done on a 43-year-old woman with acute-on-chronic pelvic pain. The initial diagnosis was missed on ultrasound. Endometriosis deposits are seen as high signal intensity on the fat-saturated T1-weighted axial MR image (white arrows). (**b**) Axial T2 MR showing a low signal intensity linear structure tethering both adnexa and the posterior aspect of the uterus to the anterior aspect of the rectum (white arrow). This represent chronic endometriosis plaque. (**c**) Corresponding ultrasound image, in retrospect, demonstrates tethered areas (arrows and asteriks)

shown to be accurate for revealing endometrial plaques, which are often of low signal intensity on T2WI and high T1WFS signal, causing tethering of nearby structures, most commonly in the posterior cul-de-sac (Fig. 8.10a–c).

Real-time imaging or cine clips in these areas of tethering from chronic endometriosis plaques demonstrate lack of smooth movement of the various structures with respect to one another with inspiration. Also, there is often pain described by the patient when the probe is place next to these tethering plaques. Symptoms can be vague, and imaging characteristics are variable, depending if there is an active endometrial implant versus chronic endometriosis causing adhesions. Also, endometriosis implants can be found in many locations, and may not always be associated with the typical ovarian findings. Many radiologists are not familiar with appearance of chronic endometriosis and deep endometriosis, and can potentially miss it (Fig. 8.11a–d).

Endometriosis can affect any part of the body including the brain as well as the lungs, leading to catamenial hemoptysis (Fig. 8.12).
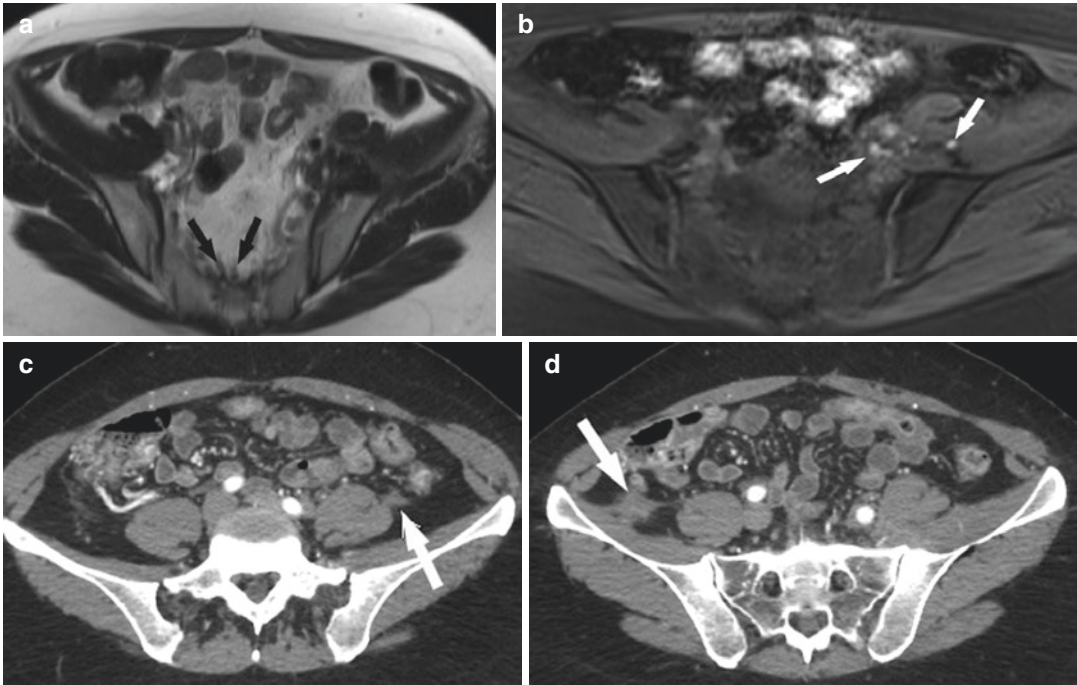
Fig. 8.11 (**a**) T2-weighted axial MR image of the pelvis of a 28-year-old woman patient with a history of unexplained left-sided deep venous thrombosis, shows areas of low T2 signal intensity along the left sacroiliac joint not seen prospectively (dark linear areas just anterior to the sacrum outlined by two black arrows). (**b**) Fat-saturated T1-weighted axial MR image shows several foci of high signal intensity, separate from the colon, located next to the muscles of the pelvic girdle (arrows) which represent missed deep endometriotic implants. (**c**) Axial follow-up CT image with IV contrast of the pelvis shows peritoneal deposits along the left paracolic gutter and psoas (arrow). (**d**) Axial follow-up CT showing right-sided peritoneal deposits (arrow). Follow-up biopsy of one of the peritoneal deposits yielded a diagnosis of endometriosis, which explained the patient's long-standing pain
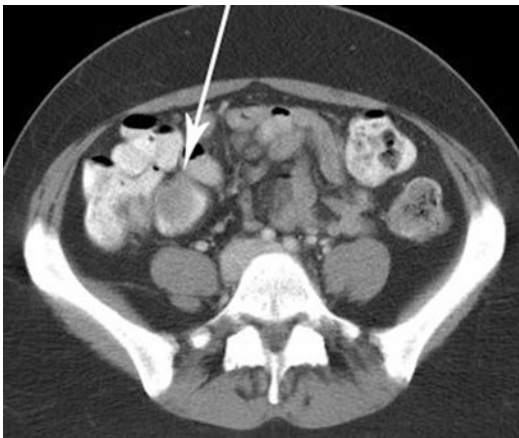
Fig. 8.12 Axial CT image of the pelvis with oral and IV contrast of a 46-year-old woman presenting with GI bleeding and abdominal pain. A filling defect was identified in the terminal ileum (white arrow). At surgery, a polypoid-shaped endometriosis deposit was diagnosed in this location

Endometriosis should be considered in women with cyclical symptoms, including pain, partial bowel obstruction, and various locations of bleeding (Fig. 8.13a, b).

8.2.3 Cervix

There are a few emergent conditions involving the cervix; however, cervical malignancy should be considered when a pelvic mass is being evaluated. Of note, however, patients with sexually transmitted infection may have cervicitis and resultant pain during transvaginal ultrasound. Thus, despite lack of imaging findings in the cervix itself, cervical motion tenderness should alert technologists and radiologists to the possibility of an infectious cervicitis and pelvic inflammatory disease [28].
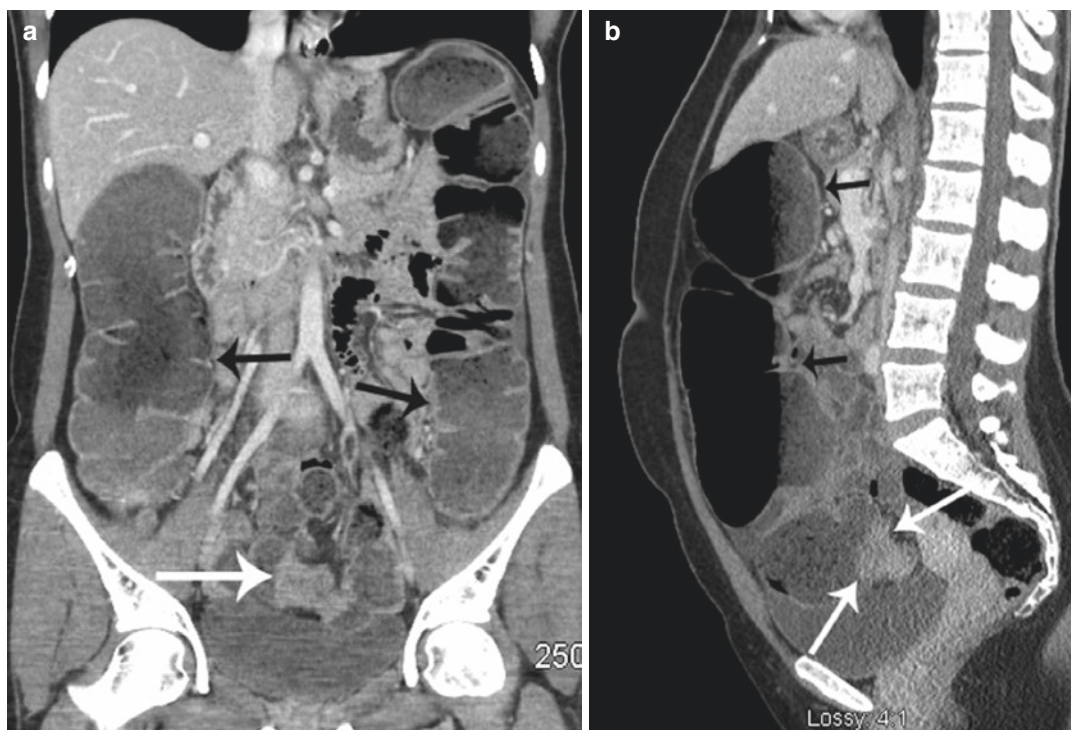
Fig. 8.13 (**a**) Coronal CT image with IV contrast of a 29-year-old woman presenting to the emergency department demonstrated a large bowel obstruction with dilated loops of the colon (black arrow) and a transition point caused by a mass (white arrow). (**b**) Sagittal CT image shows dilated colon (black arrows, (**a**, **b**) and a mass at the point of transition in the sigmoid colon (white arrow). At surgery, the obstructing sigmoid mass was discovered to be endometriosis, and the patient later revealed that she had cyclical abdominal pain corresponding with her periods for several years, including worsening monthly bloating

8.2.4   Ovaries and Fallopian Tubes

The diagnosis of ovarian torsion is a common situation where a cognitive error can occur, and it is imperative that radiologists be attuned to the findings in order to reduce the risk of missing this diagnosis. Ovarian torsion is defined as partial or complete rotation of the ovarian vascular pedicle, which causes obstruction to venous outflow and arterial inflow. In ovarian torsion, patients often present with acute pelvic pain. Some of the imaging findings which may be present on any type of cross-sectional imaging and which are helpful toward the diagnosis include:

(a) A central location of the ovary, rather than off midline as normally seen (Fig. 8.14a, b).
(b) Enlargement of the abnormal ovary, with presence of peripherally located, small folli-cles within it. A normal pre-menopausal ovarian volume is in the range of 5 cc, with an upper limit of normal of 20 cc [29].
(c) Uterine deviation of displacement to the opposite/normal side.
(d) Thickening or twisting of the fallopian tube (Fig. 8.15a–e).
(e) Free fluid in the pelvis [30, 31].
(f) Ovarian stromal edema/heterogeneity [7].
(g) Coexistent mass within the twisted ovary [7].

Ultrasound is typically the first imaging modality used to evaluate for possible torsion. Doppler interrogation is a very important aspect of sonographic assessment in the setting of potential ovarian torsion. Specifically, it is important to note that the presence of arterial flow does not exclude torsion, whereas assessment for decreased or absent venous flow is more helpful. Loss of arterial flow
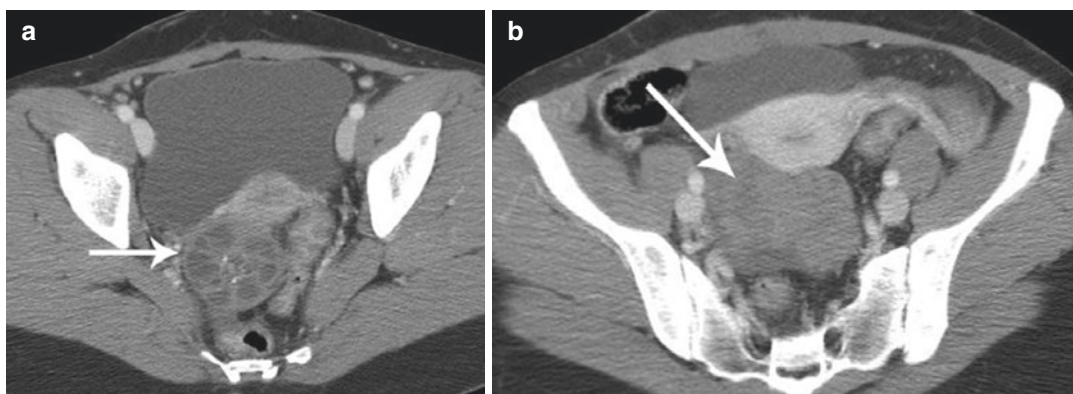
Fig. 8.14 (**a**) Axial CT image with IV contrast of the pelvis of a 31-year-old woman with fever and sudden severe abdominal pain demonstrating a prominent right adnexa (arrow). (**b**) Axial CT image at a slightly higher level in the pelvis shows an enlarged ovary which was midline in location, and which contained numerous, peripherally located follicles (arrow)
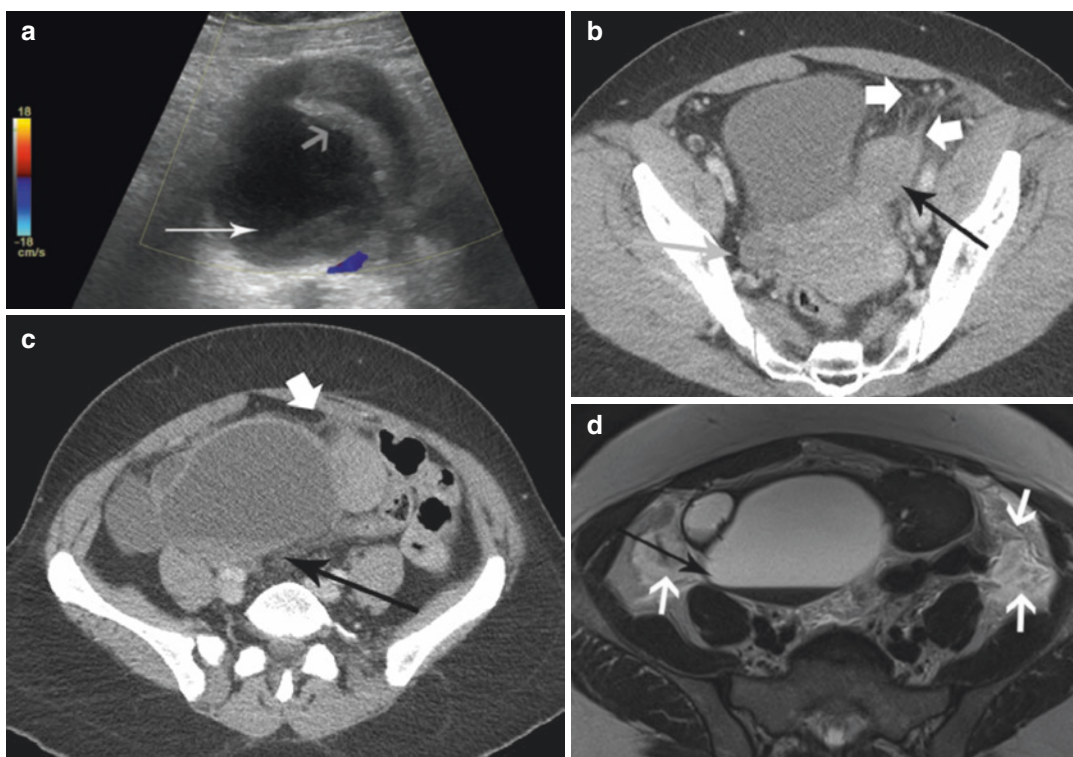

Fig. 8.15 30-year-old woman who presented with left pelvic pain. (**a**) Color Doppler ultrasound image demonstrates a fluid-fluid level (white arrow) in a dilated, tubular cystic structure. A "cogwheel" appearance of the fallopian tube (gray arrow) is difficult to confidently identify on only one plane of imaging. (**b**) CT performed with intravenous contrast to clarify the diagnosis shows a prominent left adnexa (black arrow) and some adjacent inflammation (white arrows). The right-sided structure is consistent with the right ovary (gray arrow). (**c**) CT image at a slightly higher level shows a cystic structure in the midline containing a fluid level (black arrow). Some adjacent inflammatory change is seen (white arrow). A tubu-ovarian abscess was suspected based on the CT. (**d**) MRI was performed for further assessment. On this T2-weighted MR image, there is a layering fluid level in the cystic structure (black arrows) and edema (white arrows). (**e**) Sagittal post-contrast, fat-saturated MR shows a tubular non-enhancing structure suggestive of a pyosalpinx (white arrow) and a subtle fluid level (gray arrow). At surgery, a pyosalpinx in the left fallopian tube was found as well as an ischemic left ovary
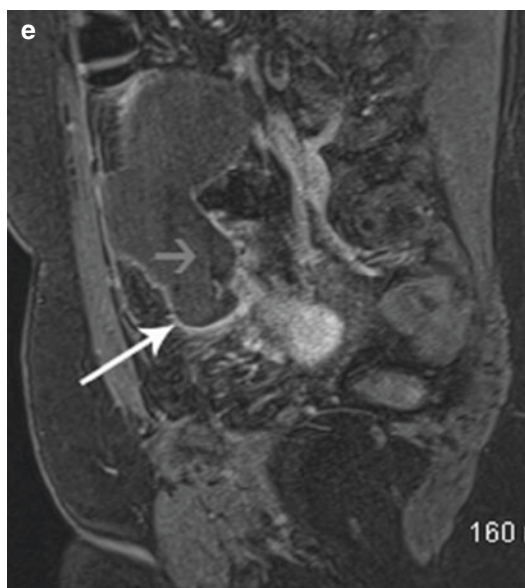
Fig. 8.15 (continued)

to the ovary is a late finding and is often associated with ovarian loss at surgery (Fig. 8.16a–c).

Ovarian enlargement is also seen in patients of polycystic ovarian syndrome (PCOS), as well as hyperstimulation syndrome, which is usually related to medication used for fertility treatment. In patients with PCOS, elevated testosterone levels, increased number of peripherally located follicles, and ovarian volume enlargement are often seen in conjunction to making the diagnosis, although radiologists should be familiar with the imaging findings of peripherally located follicles to suggest this diagnosis [32] (Fig. 8.17a, b).

Patients with hyperstimulation syndrome can present with acute, severe abdominal pain as well as nausea. On imaging, severe enlargement of the ovaries, replaced with numerous large cysts, is often seen. Free fluid can also develop [33]. Knowing the history of fertility treatment is important for the final diagnosis (Figs. 8.18 and 8.19).

Hemorrhagic cysts can present with acute pelvic pain and are usually physiologic. They usually resolve in a few menstrual cycles. On ultrasound, hemorrhagic cysts can show classic imaging features including internal cystic complexity with a reticular pattern of internal echoes or a solid-appearing area with concave margins, but acute hemorrhagic cysts can show overlap in imaging features with endometriomas, thus can lead to diagnostic dilemmas [13]. Follow-up US or MR can be helpful in distinguishing between the two [34]. On MRI, endometriomas typically have a shaded appearance on T2-weighted MRI sequences and high signal on T1-weighted images [35] (Fig. 8.20a, b).

Pelvic inflammatory disease can prove to be a diagnostic dilemma for the referring clinicians and for radiologists, and it can often be difficult to diagnose as the early imaging features can be subtle. While pelvic ultrasound is the imaging examination of initial choice, CT may be the first examination due to the vague and non-specific clinical presentation [36]. Imaging features include thickening of the fascial planes, uterosacral ligaments, and peritoneal reflections. Hepatic capsular enhancement and para-aortic lymphadenopathy along the gonadal vein drainage pathway are also associated with PID. Pelvic fat infiltration, pelvic edema, and free fluid in the cul-de-sac are commonly seen. Pelvic fat haziness, best seen on CT or MR, is one of the most sensitive findings of acute PID, as is peritonitis, which manifests as peritoneal enhancement [37]. The fallopian tubes can appear thickened from salpingitis (>5 mm), and changes of cervicitis with an abnormally enhancing or hyperemic endocervical canal and parametrial fat stranding can be seen [37] (Fig. 8.21a–c).

Pelvic inflammatory disease can have an insidious presentation in women and can be far advanced at the time of presentation [38]. Without treatment, risk of infertility increases. A study by Wiesenfeld et al. demonstrated subclinical PID diagnosed at enrollment had a 40% reduced incidence of pregnancy [39]. This diagnosis may be challenging, as the history provided may not suggest this diagnosis, and the imaging appearances of advanced PID
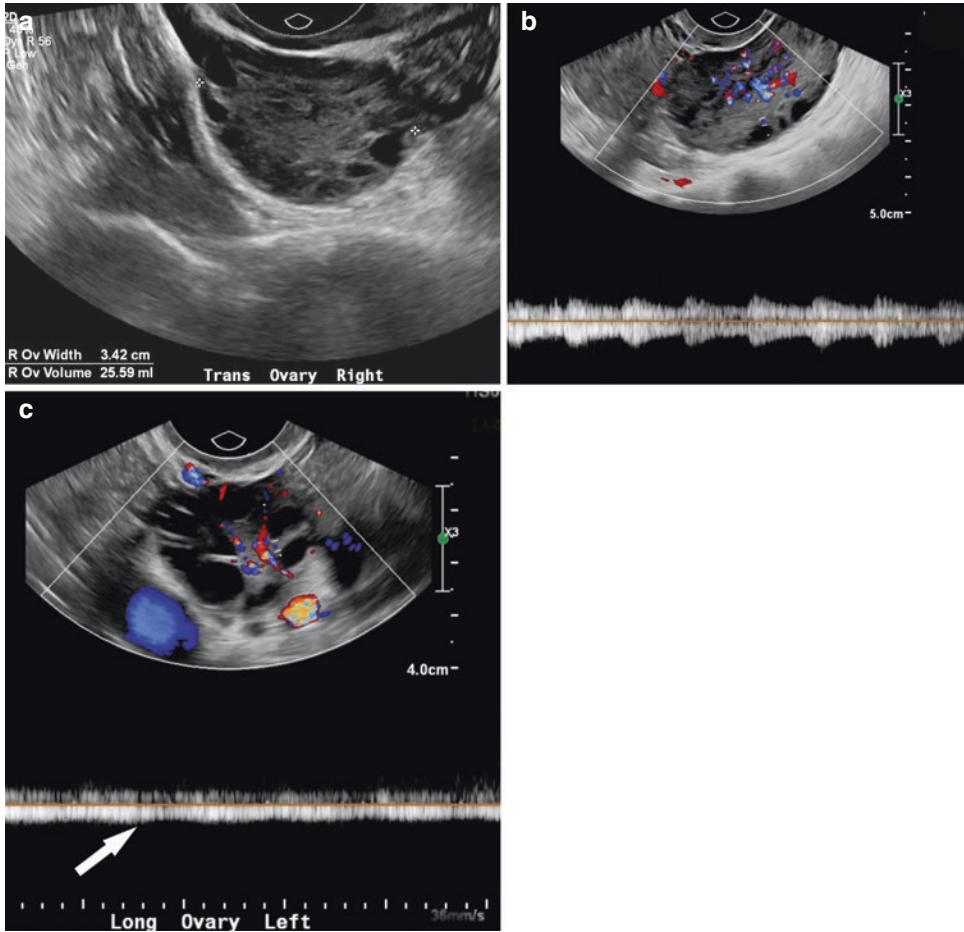
Fig. 8.16 (**a**) Transvaginal US image of a 26-year-old woman with a 3-day history of right pelvic pain. Ovarian torsion was found in the OR. The right ovary is enlarged with a volume of 25 cc with peripherally located follicles. (**b**) Pulsed Doppler sagittal image through the same ovary shows only arterial flow. No venous flow was visible. (**c**) The normal left ovary, for comparison, demonstrates venous flow (arrow) in addition to arterial flow (not shown). The right ovary was detorsed and salvaged in the OR
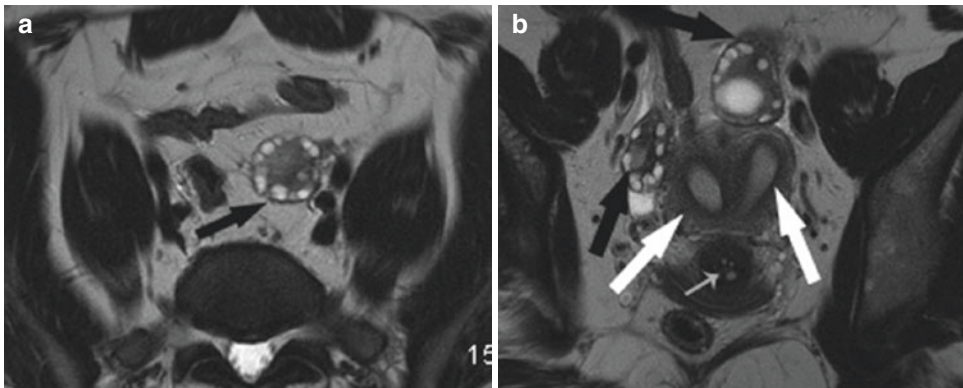
Fig. 8.17 (**a**) Axial T2-weighted MR image in a 32-year-old woman being assessed for abnormal uterine shape on ultrasound. The left ovary has numerous peripheral follicles (black arrow). (**b**) Coronal T2-weighted MR image shows both ovaries with peripheral follicles (black arrows). Nabothian cysts are seen in the cervix (small gray arrow). A bicornuate uterus is present (white arrows)
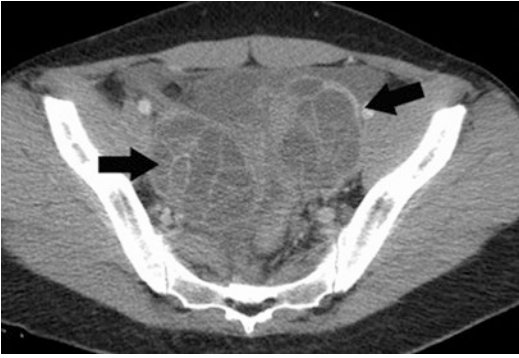
Fig. 8.18 Axial CT image of a 33-year-old woman with hyperstimulation syndrome who presented to the emergency department with acute abdominal pain. Both ovaries are substantially enlarged (black arrows). The patient was on fertility induction medications. The free fluid noted in the pelvis was felt to be the consequence of the fertility treatment as well

Fig. 8.19 Axial CT image of a 19-year-old woman with acute sepsis presenting to the ED. Bilateral adnexal cystic structures are present due to acute pelvic inflammatory disease and bilateral tubo-ovarian abscesses (and are not due to ovarian hyperstimulation syndrome; compare with Fig. 8.18)

may overlap with the appearance of other acute pelvic infectious and inflammatory conditions, including ruptured appendicitis, ruptured mucocele of the appendix, or metastatic gastrointestinal tumor of the small bowel (Fig. 8.22a–d).

8.2.5 Ectopic Pregnancy

Incidence of ectopic pregnancy varies around the world but is more common in older women,

those with prior pelvic inflammatory disease, and those undergoing assisted reproduction. In a study by Tay et al., the incidence was 11.5/1000 pregnancies in the United Kingdom [40]. Women presenting to the ED with pelvic pain may not know they are pregnant. Thus, any woman of reproductive age should have a HCG level determined in the case of pelvic pain. If this is positive, it is imperative on ultrasound to confirm an intrauterine location of the gestation. Various types of ectopic pregnancy locations can occur, which radiologists need to be aware of in order to prevent errors in diagnosing this potentially life-threatening condition.

An intrauterine gestation should first be identified in patients being investigated for ectopic pregnancy. This includes finding a gestational sac which is an eccentrically-placed intrauterine structure showing a "double decidual sign," and not just a cystic space in the uterus, which is also known as a pseudogestational sac. Ideally a fetal heart rate will be identified on transvaginal ultrasound, around or just beyond 6 weeks gestation [41]. If an empty uterus is identified and there is a positive HCG level, then further evaluation of the adnexa for ectopic pregnancy is warranted (Fig. 8.23a, b). Even if an intrauterine gestation is confirmed, the adnexa should still be evaluated, and the presence of a corpus luteum follicle should be identified. Also, a heterotopic pregnancy (one intrauterine and one ectopic) should be excluded at the same time. This is a rare occurrence in the general population, with an incidence of approximately 1 in 30,000 pregnancies, but the risk of this type of ectopic pregnancy increases in women on fertility treatments, with rates as high as 1 in 900 in ovulation induction [42].

Identifying C-section scar ectopic pregnancies, cervical ectopic pregnancies, and interstitial ectopic pregnancies can be challenging, as these are all rare but clinically important types of ectopic pregnancies. These interstitial ectopic pregnancies are sometimes called cornual ectopic pregnancies, but this is a misnomer and should be reserved for women with a unicornuate uterus. Interstitial ectopic pregnancies can be diagnosed using ultrasound or MRI, when the gestational sac or decidual reaction is located
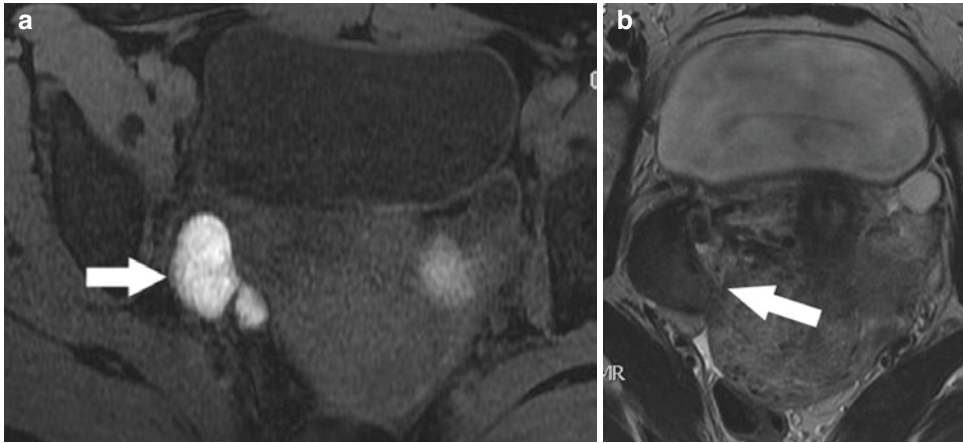
Fig. 8.20 27 year old woman with chronic pelvic pain. (**a**) Axial fat-saturated T1-weighted MR image shows a high signal intensity structure in the right adnexa (white arrow) with signal intensity suggestive of endometriosis. (**b**) T2-weighted MR image in the same patient shows typical "shading" appearance of an endometrioma (arrow)
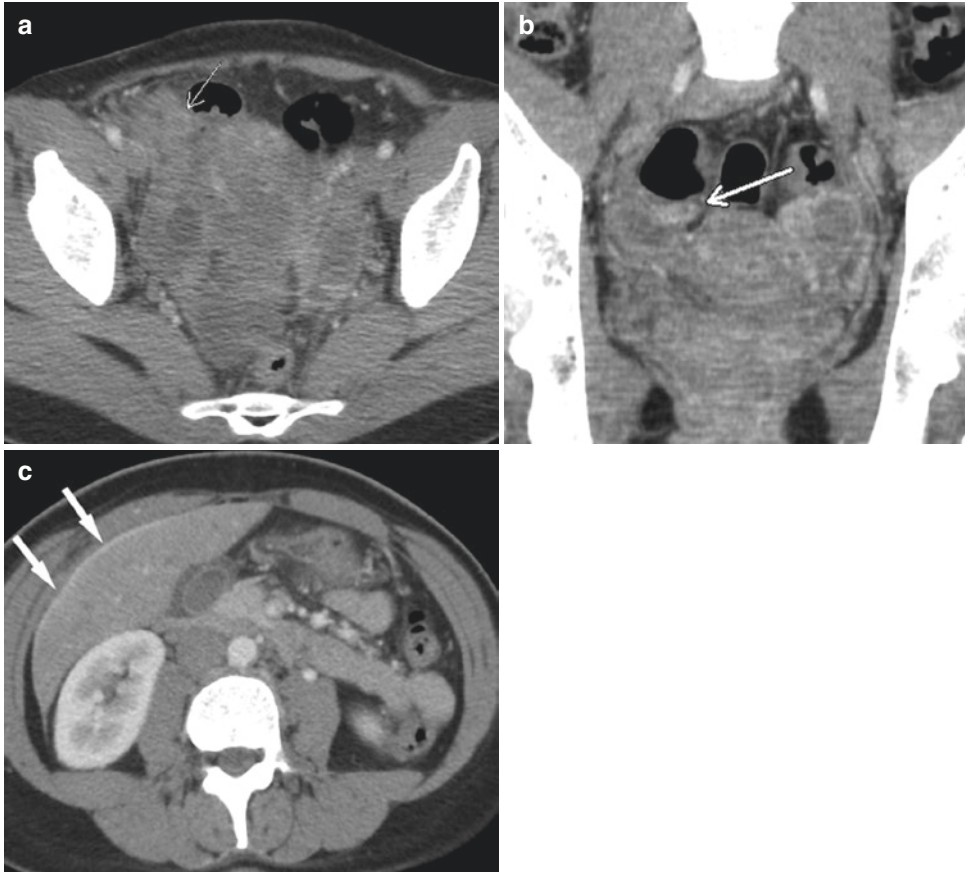

Fig. 8.21 (**a**) CT of a 31-year-old woman who presented with peritoneal signs and fever with a rounded enhancing structure in the RLQ initially diagnosed as an inflamed appendix (arrow). (**b**) Coronal CT image show a tubular enhancing structure (arrow) called the inflamed appendix. (**c**) CT in the same patient showing enhancement of the liver capsule (arrow) in keeping with Fitz-Hugh-Curtis syndrome. At surgery, the appendix was noted to be normal, but there was pus arising from both fallopian tubes with the final diagnosis being pelvic inflammatory disease
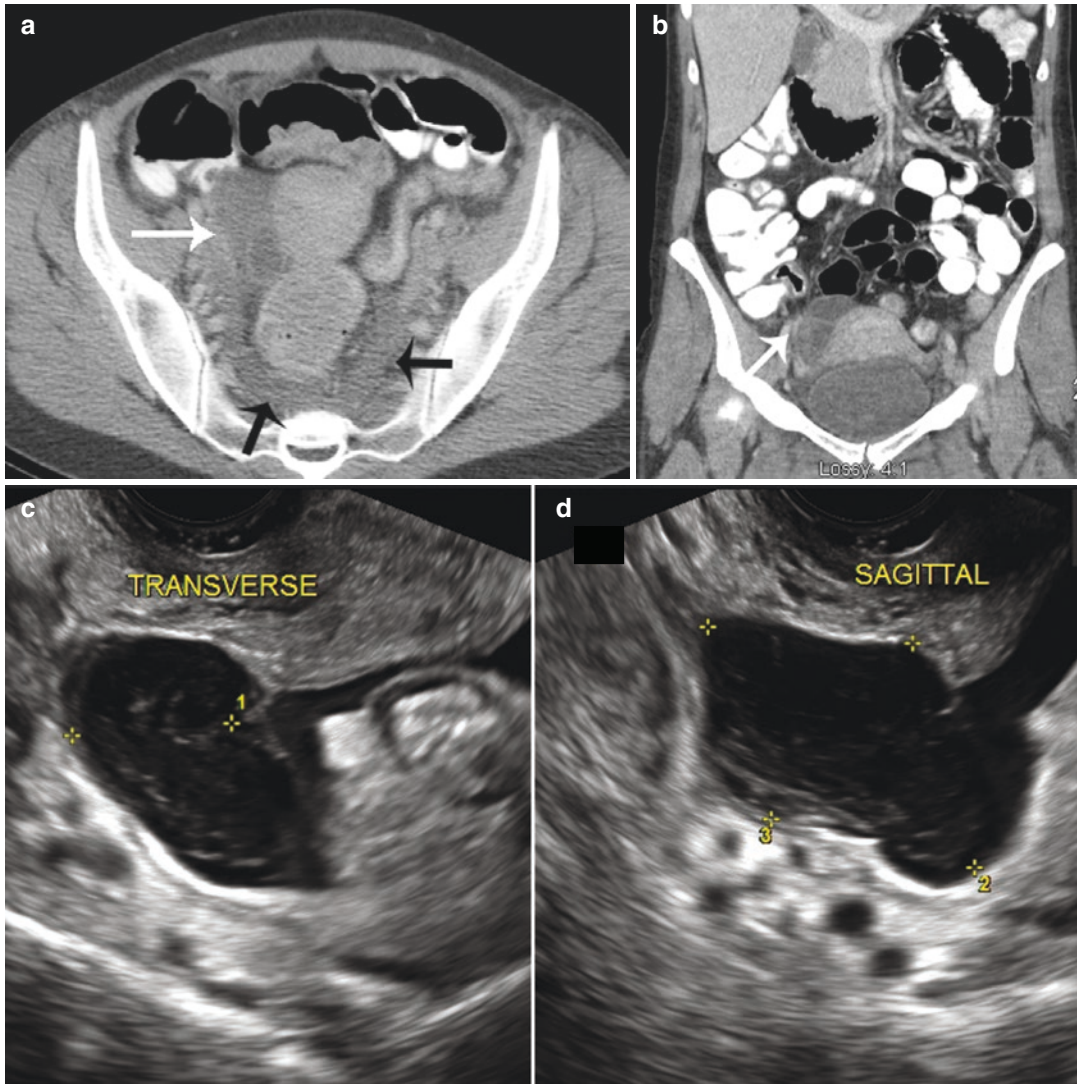
Fig. 8.22 (**a**) Axial CT image with oral and IV contrast of an 18-year-old woman who presented with a 1-week history of worsening pelvic pain. Diffuse fluid and inflammatory changes were seen in the pelvis (arrows). (**b**) A dilated tubular structure on the right (white arrow, (**a**, **b**); (**b**) – coronal CT image) was thought to represent an abnormally dilated fallopian tube. At surgery, this tubular structure was attached to the cecum and represented a perforated appendiceal mucocele. (**c**) Transvaginal 2D ultrasound image show a cystic structure in the right adnexa. (**d**) Transvaginal ultrasound with transverse and sagittal images show that the cystic structure is actually tubular, and represents an appendiceal mucocele (arrows). (**e**) Transvaginal 3D ultrasound shows the mucocele (arrow)
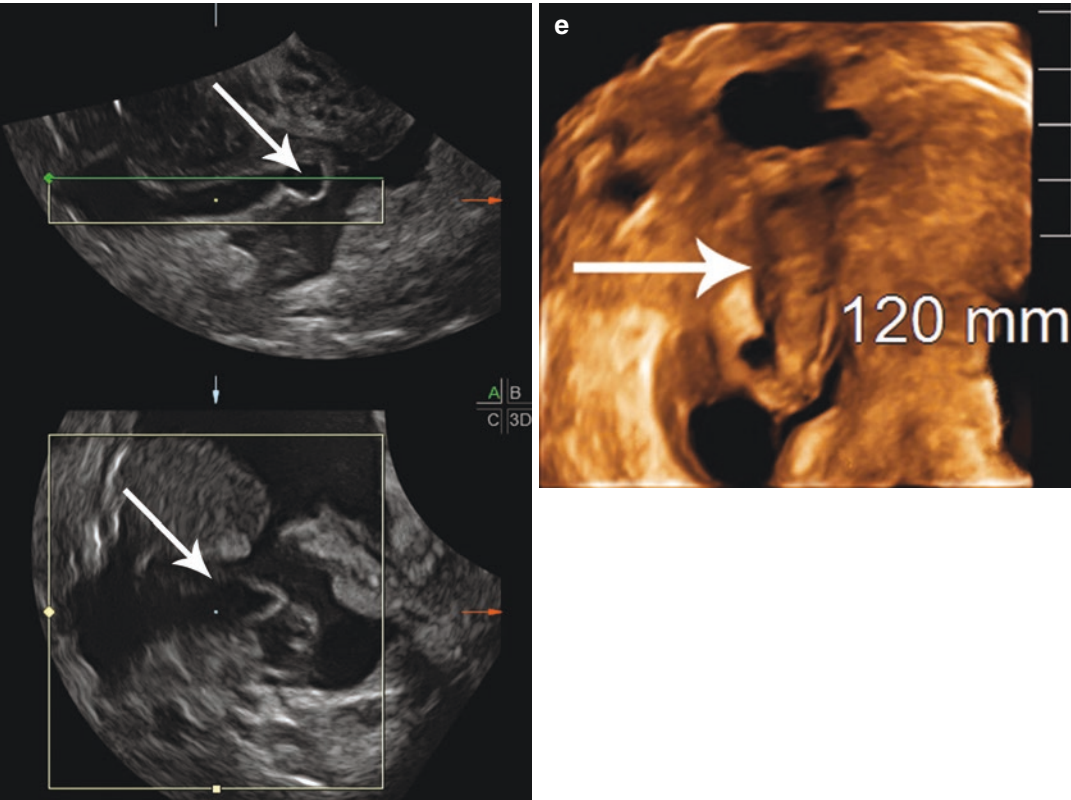
Fig. 8. 22 (continued)
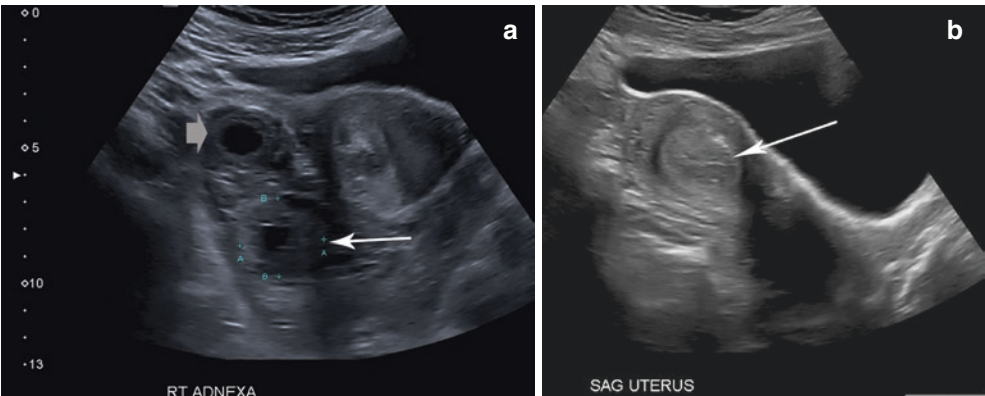
Fig. 8.23 (**a**) Ultrasound of the right adnexa in a 37-year-old woman with pelvic pain and a positive HCG level showing a corpus luteum cyst (gray arrow) and a thick-walled cystic right adnexal structure (white arrow) in keeping with a tubal ectopic pregnancy. (**b**) Ultrasound showing an empty uterus without gestational sac. The ectopic pregnancy was treated with methotrexate and resolved

high in the fundus, usually off toward either the right or left side, with <5 mm of surrounding myometrium in all planes [43] (Fig. 8.24a, b).

Cervical ectopic pregnancies can be confused with a spontaneous abortion in progress, although usually in spontaneous abortion, the gestation sac has a more oval appearance and there is rarely a heartbeat identified. Early diagnosis of cervical ectopic pregnancy is important due to the risk of severe bleeding [44].

8.2.6   Post-operative Changes

It is important to use a standardized approach when evaluating post-operative pelvis. Having a checklist to look for each organ is helpful both for identifying abnormalities of expected structures and also for determining if each organ is present or absent. Postoperatively, organs or structures

may be missing, and others may move into the potential space, changing their usual location and shape (Fig. 8.25a, b). Understanding the type of surgery which took place is also important to prevent misinterpretation of the normal postoperative findings as potential complications (Fig. 8.3).

8.2.7   Iatrogenic

Intrauterine devices (IUD) are used as a method of contraception whereby a structure is placed in the endometrial cavity. The shape and makeup of this structure can vary. IUDs can migrate from their original position. This includes falling out (and therefore become ineffective), or being malrotated (as a cause of pelvic pain), and rarely perforating through the wall of the myometrium, ending up as a foreign body in the peritoneal
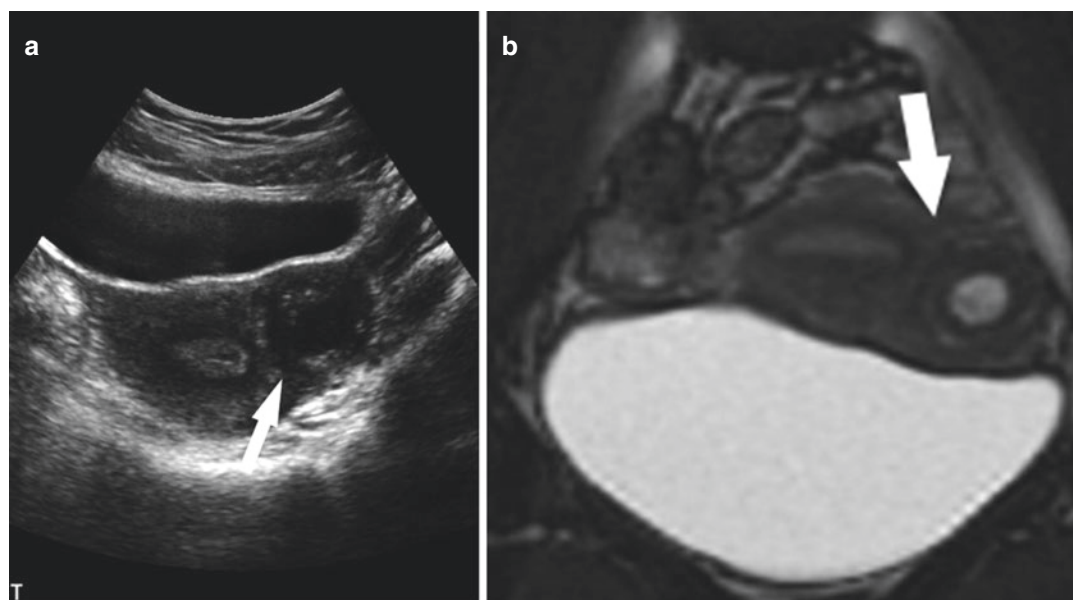

Fig. 8.24 (**a**) Transabdominal ultrasound in a 36-year-old woman with an estimated gestational age by dates of 7 weeks. Ultrasound shows a gestational sac which is eccentrically located near the origin of the left fallopian tube (arrow). (**b**) Coronal follow-up T2-weighted MR image (MR was performed for additional evaluation and treatment planning) confirmed an interstitial location (arrow), showing <5 mm of myometrium around the gestational sac
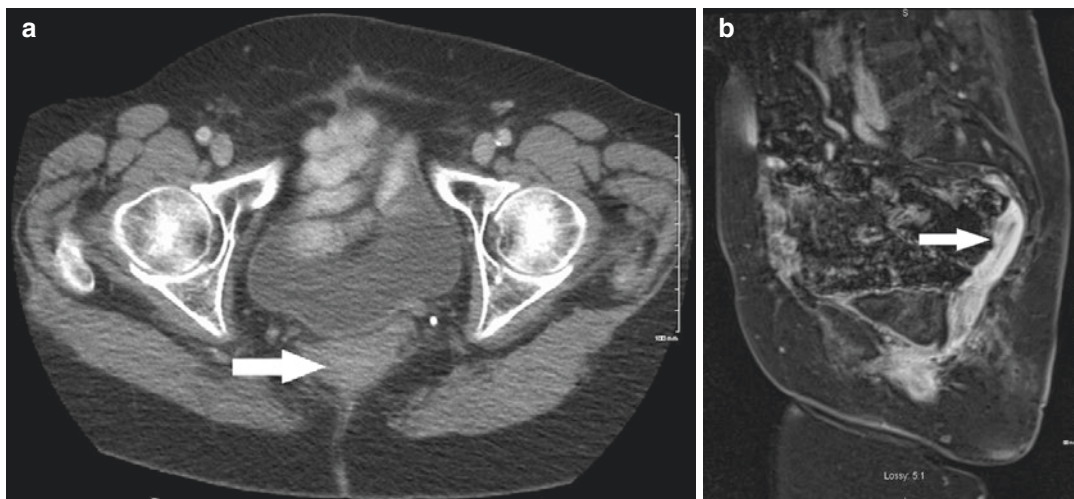
Fig. 8.25 (**a**) Axial CT image of a 57-year-old woman who had surgery for rectal cancer 2 years earlier presenting with upper abdominal pain. CT shows some soft tissue anterior to the sacrum that was called tumor recurrence (arrow). (**b**) Sagittal fat-saturated post-contrast MR image shows that the area of soft tissue is the uterus, which had fallen posteriorly in the surgically created potential space (arrow)
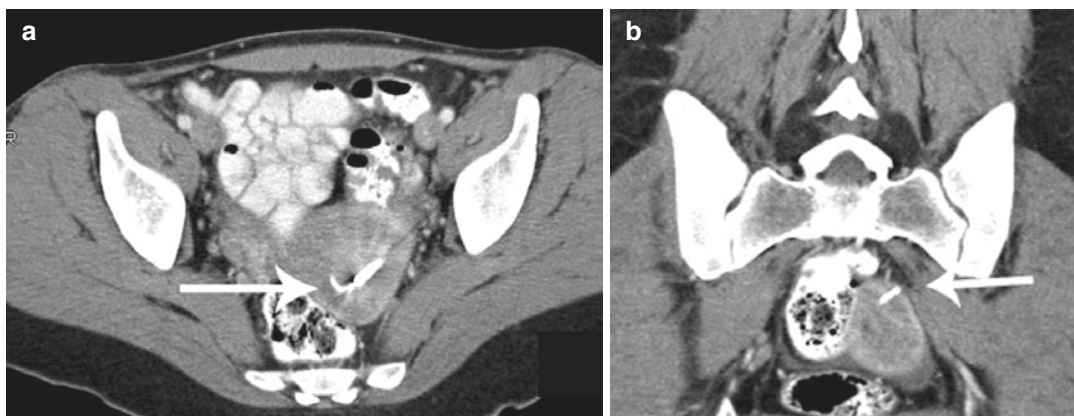

Fig. 8.26 (**a**) Axial CT image of the pelvis with oral and IV contrast in a 42-year-old woman who presented for evaluation of mid-abdominal pain with an IUD present (arrow). (**b**) Coronal CT image shows that the IUD is embedded in the myometrium of the uterus extending to the serosal surface (arrow). This was not commented upon prospectively. The patient presented 6 months later with a pelvic abscess on the left as a complication of the migrated and misplaced IUD

cavity [45]. 3D ultrasound can be helpful for confirming the location and position of the IUD. CT can also help identify the position of IUDs which are thought to have ended up in the peritoneal cavity. In order to prevent a satisfaction of search error, all such placed structures should be carefully evaluated to ensure their proper position (Fig. 8.26a, b).

Patient with malignancies in the pelvis often undergo radiation therapy as part of their treatment. Radiation can cause damage to adjacent structures and render their tissue friable. Fistulas may form and can lead to various symptoms. Cross-sectional imaging may be required to identify and characterize these fistulas. Fluoroscopy has previously been the

reference standard for identifying patent fistula tracts, and CT has a role too, although MRI has best contrast resolution in the pelvis for identifying various communications and for determining which organs or structures are involved (Fig. 8.27).

Fig. 8.27 Sagittal T2-weighted MR image in a 77-year-old woman patient with previous urethral malignancy treated with radiation therapy, who presented to the emergency department with urinary leakage from the vagina. A communication (black arrow) is seen between the posterior urethra and the vagina with fluid (urine) within the vaginal canal

8.2.8 GI Tract Abnormalities

It is possible for acute conditions from the gastrointestinal tract or urinary tract to secondarily affect reproductive organs in women. For example, diverticulitis can focally perforate, form an abscess, and eventually form a fistula either to the ovary or the endometrium (Fig. 8.28a, b).

Crohn disease is a granulomatous condition which can lead to bowel obstruction, abscess formation, and fistula tracks, including fistulous communications to reproductive structures including the endometrium (Fig. 8.29a, b).

Non-gynecologic conditions involving the GI tract or urinary system can also lead to interpretation errors when imaging features appear similar to abnormalities of the reproductive organs. This includes confusion between chronic appendicitis and endometriosis, or an appendiceal mucocele versus a dilated fallopian tube from PID. A helpful distinguishing feature of mucocele of the appendix is the presence of thin peripheral calcification, which is almost never seen in abnormalities of the fallopian tube (Fig. 8.30a, b).

The demonstration of a tubular appearance makes the diagnosis unlikely to represent an ovarian cyst,
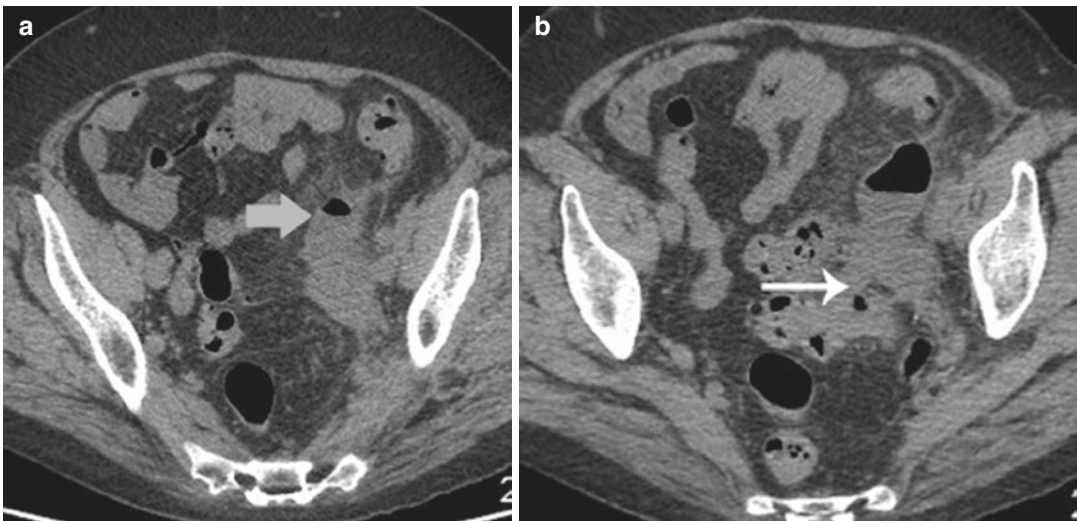

Fig. 8.28 (**a**) Non-enhanced axial CT image of the pelvis without contrast in a 66-year-old woman with left lower quadrant pain showing an area of inflammation in the area of the sigmoid colon related to focal diverticulitis (white arrow). (**b**) A second axial image at a slightly lower level demonstrates an air-fluid level (gray arrow) denoting an abscess in the left ovary. This was a sequela of direct communication with the perforated sigmoid diverticulitis
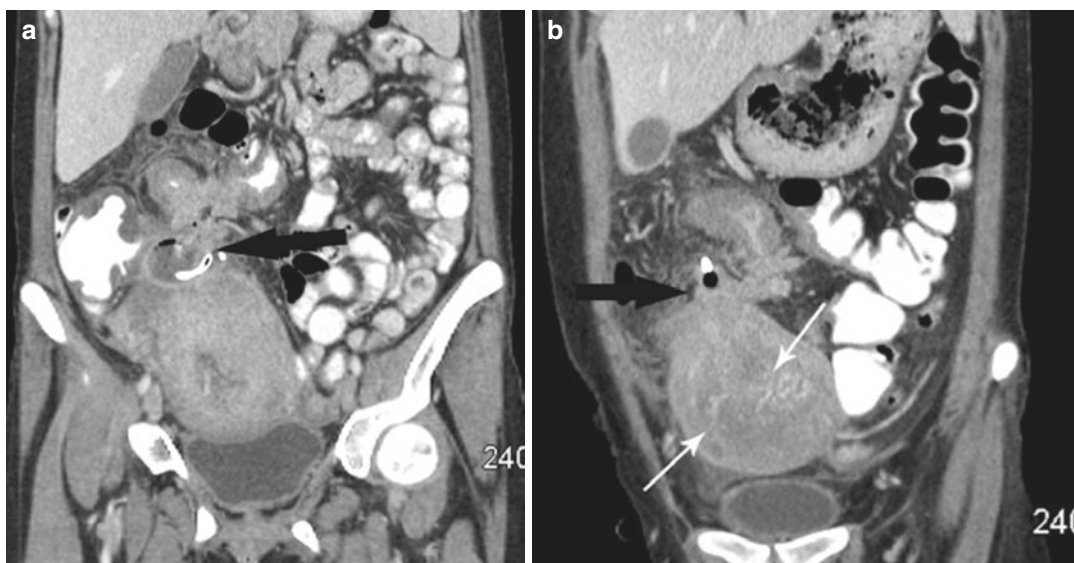
Fig. 8.29 (**a**) Coronal abdominal and pelvic CT image with oral and IV contrast of a 23-year-old woman with known Crohn disease for follow-up of catheter drainage of an abscess from a Crohn flare-up and focal perforation of the transverse colon (black arrow). (**b**) A more poste-rior coronal CT image shows tethering of the uterine fun-dus toward the abscess containing a percutaneous drain (black arrow). The endometrium is also heterogeneous due to pus (white arrows)
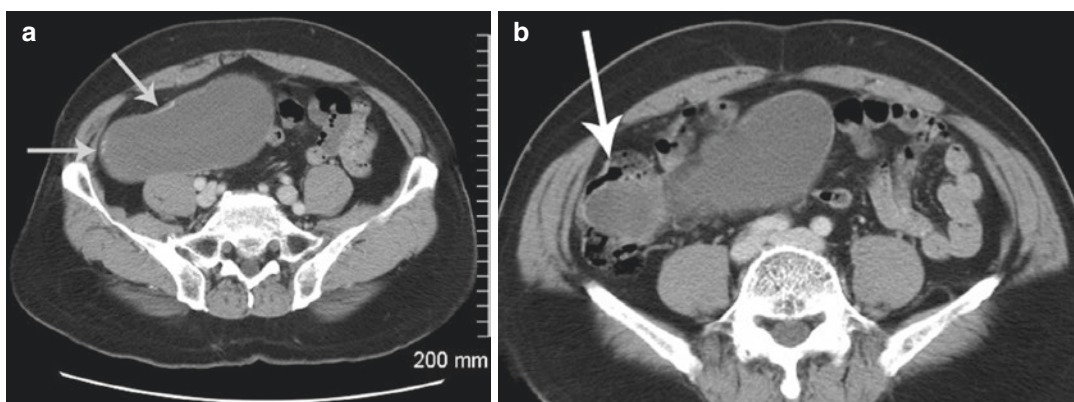

Fig. 8.30 (**a**) Axial CT of a 47-year-old woman with right lower quadrant pain showing a long tubular structure measuring 6.6 × 2.3 cm in the right lower quadrant with-out any surrounding inflammatory changes (arrows). (**b**) The cystic structure appears to communicate with the cecum (arrow). This was proven at surgery to represent a ruptured appendiceal mucocele

even though ovarian malignancies can also present with various types of calcification. This highlights the importance of obtaining two planes of imaging with ultrasound, CT, and MRI (although calcifica-tions are not reliably seen on MRI).

Making the distinction between gyneco-logic origin and gastrointestinal tract origin of an abnormality on cross-sectional imaging can sometimes be challenging, but this has improved with better-quality imaging and meticulous evaluation by the radiologist. Although clinical symptoms and history can sometimes be help-ful (e.g., patients with endometriosis may have a history of cyclical pain corresponding with the
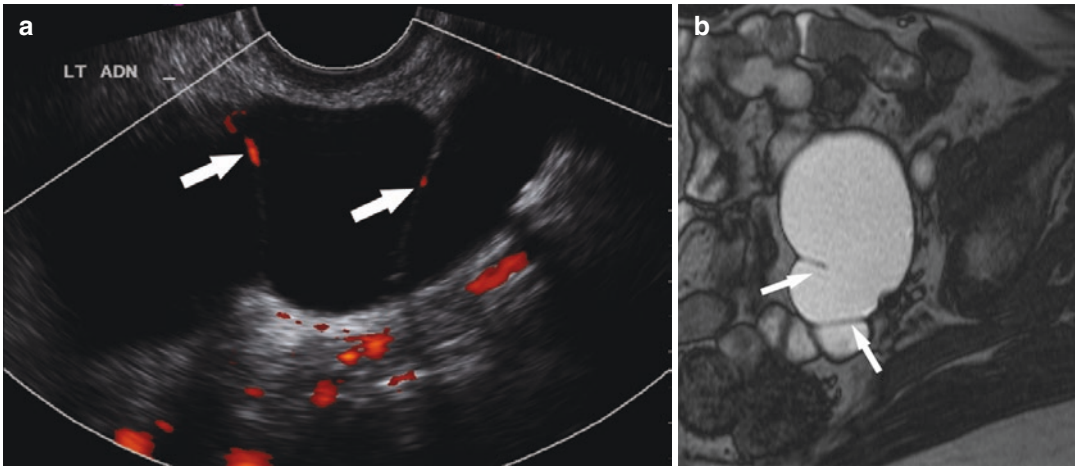
Fig. 8.31 (**a**) Power Doppler transvaginal US image of a 48-year-old woman with a chronic left hydrosalpinx showing some flow in a fold of the fallopian tube (white arrows). (**b**) Corresponding T2-weighted MR image shows the hydrosalpinx with indented, partial septa of the fallopian tube walls (arrows). There are no inflammatory changes in the surrounding fat to suggest an acute process

menstrual cycle), there are many instances in the acute setting where clinical symptoms are non-specific. For example, fever and leukocytosis commonly occur with appendicitis and diverticulitis, but are also associated with pelvic inflammatory disease. Nausea, vomiting, and anorexia are also non-specific findings [46]. Thus, careful assessment of the anatomy by the radiologist is very important. For example, a dilated appendix (related to acute appendicitis, chronic appendicitis, and/or mucocele of the appendix) should demonstrate an origin or attachment to the base of the cecum and be blind-ending. If the attachment to the cecum cannot be determined, a dilated fallopian tube can be considered in the differential diagnosis, as well as a vascular structure or a lymphangioma [47]. Distinctive features of a dilated fallopian tube include longitudinal folds which produce a characteristic "cogwheel" appearance. These normal folds within the fallopian tube often become more pronounced in chronic cases of hydrosalpinx, and are well seen on ultrasound. On Doppler interrogation, these soft tissue folds can demonstrate some flow in them (Fig. 8.31a, b). However, hydrosalpinx can be missed on ultrasound if images are captured in only one plane (Fig. 8.15a).

In some patients, a hydrosalpinx can be misinterpreted as a cyst rather than a tubular structure. This highlights once again the importance of either interrogating in two planes, or providing radiologists with cine images. Use of Doppler in any anechoic or "cystic" structure is also important to exclude an aneurysm or other vascular structure in the pelvic area.

There are many benign pelvic cystic structures which occur in women. They are often identified incidentally and often are of no clinical significance. Being aware of these generally benign cystic conditions can prevent misdiagnosis, unnecessary follow-up, and patient anxiety. Some of the common cysts in the pelvic area, particularly in the perineal area, include:

Nabothian cysts are cystic areas commonly found in the cervix. They are usually round and avascular. They can be solitary or multiple. Rarely, due to their size, there can be obstruction of the cervical canal causing hydrometria [48]. When multiple, the diagnosis of adenoma malignum may be considered in the differential diagnosis, although this is a rare malignancy which usually presents with copious clear vaginal discharge [49], a feature which is not associated with Nabothian cysts (Fig. 8.17b).
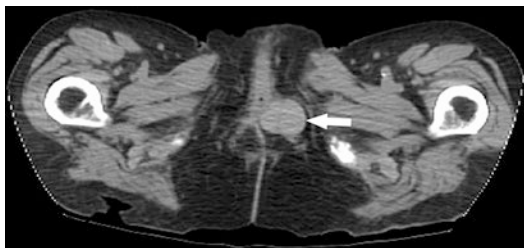
Fig. 8.32 CT image of the pelvis of a 62-year-old with an incidentally discovered hyperdense Bartholin gland cyst on the left (arrow). It is important to ensure there is no solid component, and not to confuse this with a vulvar malignancy

Bartholin's gland cysts are located on either side of the vaginal opening. They produce fluid that lubricates the outer lips of the vagina and may become enlarged. They do not have internal flow (Fig. 8.32).

Other cysts which may occur in the pelvis include:

(a) Epidermoid inclusion cysts: These cysts form on the lower back of the vaginal wall. They may be caused by injury during childbirth or surgery [50].

(b) Müllerian duct cysts: These are another common type of cyst that form as a result of material left behind during embryological development. They grow anywhere on the vaginal walls and often contain mucus [50].

(c) Gartner's duct cysts: These vaginal cysts develop over time from a duct that normally regressed in embryo [51].

(d) Skene's gland cysts: Skene gland cysts are retention cysts located lateral to the external urethral meatus and inferior to the pubic symphysis. They can be mistaken with Bartholin's gland cysts due to their caudal location [52].

8.3 Conclusion

Imaging of acute pelvic conditions in women is challenging, as findings may be related to gynecologic causes in addition to gastrointestinal, urinary tract, or musculoskeletal etiologies. Being aware that gynecologic conditions can often

manifest as subtle or non-specific findings and may require additional clinical information is important in order for radiologists to make the most efficient and accurate diagnosis.

Key points to remember include:

- Ensure that an HCG level is determined for all women of childbearing age at the time of imaging decision making, since ectopic pregnancy is a potentially life-threatening event which should not be missed.
- Ovarian torsion can also present with acute pelvic pain and imaging findings including central location of an ovary and lack of venous flow (arterial flow can be preserved early on).
- Pelvic inflammatory disease can have a subtle presentation and be confused with other causes of peritonitis, including perforated appendicitis with the diagnosis being rendered more challenging when there is difficulty definitely visualizing the appendix on imaging, or in a patient with a paucity of intrapelvic fat.
- Finally, there are many incidental gynecologic findings which can be identified on imaging of acute pelvic pain of other cause. It is thus important to prevent satisfaction of search errors. Standardized reporting tools may help with this, so that the radiology report is clear and complete, thereby helping to prevent future errors or misses of early pathology.

References

1. Pope A. Phrases, saying, proverbs and idioms at The Phrase Finder. 2018. https://www.phrases.org.uk/meanings/to-err-is-human.html. Accessed 5 Jun 2018.
2. Brook OR, O'Connell AM, Thornton E, et al. Quality initiatives: anatomy and pathophysiology of errors occurring in clinical radiology practice. Radiographics. 2010;30(5):1401–10.
3. Kohn LT, Corrigan JM, Donaldson MS, editors. To err is human: building a safer health system. Washington, DC: Institute of Medicine Committee on Quality of Health Care in America. National Academies Press; 2000.
4. Glanc P, O'Hayon BE, Singh DK, Bokhari SA, Maxwell CV. Challenges of pelvic imaging in obese women. Radiographics. 2012;32(6):1839–62.
5. Bruno MA, Walker EA, Abujudeh HH. Understanding and confronting our mistakes: the epidemiology of

error in radiology and strategies for error reduction. Radiographics. 2015;35(6):1668–76.

6. Bhosale PR, Javitt MC, Atri M, Harris RD, Kang SK, Meyer BJ, et al. ACR appropriateness criteria$^{(R)}$ acute pelvic pain in the reproductive age group. Ultrasound Q. 2016;32(2):108–15.

7. Chang HC, Bhatt S, Dogra VS. Pearls and pitfalls in diagnosis of ovarian torsion. Radiographics. 2008;28(5):1355–68.

8. Dormagen JB, Gaarder M, Drolsum A. Standardized cine-loop documentation in abdominal ultrasound facilitates offline image interpretation. Acta Radiol. 2015;56(1):3–9.

9. Johnson W, Taylor MB, Carrington BM, et al. The value of hyoscine butylbromide in pelvic. MRI Clin Radiol. 2007;62(11):1087–93.

10. Marcal LP, Fox PS, Evans DB, et al. Analysis of free-form radiology dictations for completeness and clarity for pancreatic cancer staging. Abdom Imaging. 2015;40(7):2391–7.

11. Nielsen JW, Boomer L, Kurtovic K, et al. Reducing computed tomography scans for appendicitis by introduction of a standardized and validated ultrasonography report template. J Pediatr Surg. 2015;50(1):144–8.

12. Larson DB, Towbin AJ, Pryor RM, et al. Improving consistency in radiology reporting through the use of department-wide standardized structured reporting. Radiology. 2013;267(1):240–50.

13. Levine D, Brown DL, Andreotti RF, et al. Management of asymptomatic ovarian and other adnexal cysts imaged at US: Society of Radiologists in Ultrasound Consensus Conference Statement. Radiology. 2010;256(3):943–54.

14. Sparic R, Mirkovic L, Malvasi A, et al. Epidemiology of uterine myomas: a review. Int J Fertil Steril. 2016;9(4):424–35.

15. Kim H-G, Song YJ, Na YJ, et al. A case of torsion of a subserosal leiomyoma. J Menopausal Med. 2013;19(3):147–50.

16. Tanos V, Berry KE. Benign and malignant pathology of the uterus. Best Pract Res Clin Obstet Gynaecol. 2018;46:12–30.

17. Chan YY, Jayaprakasan K, Zamora J, et al. The prevalence of congenital uterine anomalies in unselected and high-risk populations: a systematic review. Hum Reprod Update. 2011;17(6):761–71.

18. Sawada M, Kakigano A, Matsuzaki S, et al. Obstetric outcome in patients with a unicornuate uterus after laparoscopic resection of a rudimentary horn. J Obstetr Gyaenecol Res. 2018;44(6):1080–6.

19. Fukunaga T, Fujii S, Inoue C, et al. The spectrum of imaging appearances of mullerian duct anomalies: focus on MR imaging. Jpn J Radiol. 2017;35(12):697–706.

20. Caserta D, Mallozzi M, Meldolesi C, et al. Pregnancy in a unicornuate uterus: a case report. J Med Case Rep. 2014;8:130.

21. Ghi T, De Musso F, Maroni E, et al. The pregnancy outcome in women with incidental diagnosis of septate uterus at first trimester scan. Hum Reprod. 2012;27(9):2671–5.

22. Baker ME, Rendon NC, Rosen MO et al (2013) .ACR. https://acsearch.acr.org/docs/69468/Narrative. Accessed June 5 2018.

23. Williams PL, Laifer-Narin SL, Ragavendra N. US of abnormal uterine bleeding. Radiographics. 2003;23(3):703–18.

24. Dubinsky TJ. Value of sonography in the diagnosis of abnormal vaginal bleeding. J Clin Ultrasound. 2004;32(7):348–53.

25. Wolfman W, Leyland N, Heywood M, et al. Asymptomatic endometrial thickening. J Obstet Gynaecol Can. 2010;32(10):990–9.

26. Kuligowska E, Deeds L, Lu K. Pelvic pain: overlooked and underdiagnosed gynecologic conditions. Radiographics. 2005;25(1):3–20.

27. Guerriero S, Ajossa S, Minguez JA, et al. Accuracy of transvaginal ultrasound for diagnosis of deep endometriosis in uterosacral ligaments, rectovaginal septum, vagina and bladder: systematic review and meta-analysis. Ultrasound Obstet Gynecol. 2015;46(5): 534–45.

28. Romosan G, Bjartling C, Skoog L, et al. Ultrasound for diagnosing acute salpingitis: a prospective observational diagnostic examination. Hum Reprod. 2013;28(6):1569–79.

29. Pavlik EJ, DePriest PD, Gallion HH, et al. Ovarian volume related to age. Gynecol Oncol. 2000;77(3): 410–2.

30. Dhanda S, Quek ST, Ting MY, et al. CT features in surgically proven cases of ovarian torsion-a pictorial review. Br J Radiol. 2017; https://doi.org/10.1259/bjr. 20170052.

31. Rha SE, Byun JY, al JSE. CT and MR imaging features of adnexal torsion. Radiographics. 2002;22(2):283–94.

32. Indran IR, Huang Z, Khin LW, et al. Simplified 4-item criteria for polycystic ovary syndrome: a bridge too far? Clin Endocrinol. 2018; https://doi.org/10.1111/ cen.13755.

33. Nastri CO, Teixeira DM, Moroni RM. Ovarian hyperstimulation syndrome: pathophysiology, staging, prediction and prevention. Ultrasound Obstet Gynecol. 2015;45(4):377–93.

34. Corwin MT, Gerscovich EO, Lamba R, et al. Differentiation of ovarian endometriomas from hemorrhagic cysts at MR imaging: utility of the T2 dark spot sign. Radiology. 2014;271(1):126–32.

35. Glastonbury CM. The shading sign. Radiology. 2002;224(1):199–201.

36. Spain J, Rheinboldt M. MDCT of pelvic inflammatory disease: a review of the pathophysiology, gamut of imaging findings, and treatment. Emerg Radiol. 2017;24(1):87–93.

37. Revzin MV, Mathur M, Dave HB. Pelvic inflammatory disease: multimodality imaging approach with clinical-pathologic correlation. Radiographics. 2016;36(5):1579–96.

38. Iraha Y, Okada M, Iraha R, et al. CT and MR imaging of gynecologic emergencies. Radiographics. 2017;37(5):1569–86.

39. Wiesenfeld HC, Hillier SL, Meyn LA, et al. Subclinical pelvic inflammatory disease and infertility. Obstet Gynecol. 2012;120(1):37–43.

40. Tay JI, Moore J, Walker JJ. Ectopic pregnancy. West J Med. 2000;173(2):131–4.

41. Bickhaus J, Perry E, Schust DJ. Re-examining sonographic cut-off values for diagnosing early pregnancy loss. Gynecol Obstet. 2013;3(1):141.

42. Mj G, Rajan R. Heterotopic pregnancy in natural conception. J Hum Reprod Sci. 2008;1(1):37–8.

43. Ramanathan S, Raghu V, Ladumor SB, et al. Magnetic resonance imaging of common, uncommon, and rare implantation sites in ectopic pregnancy. Abdom Radiol (NY). 2018;43(12):3425–35.

44. Hirakawa M, Tajima T, Yoshimitsu K, et al. Uterine artery embolization along with the administration of methotrexate for cervical ectopic pregnancy: technical and clinical outcomes. Am J Roentgenol. 2009;192(6):1601–7.

45. Gunbey HP, Sayit AT, Idilman IS, et al. Migration of intrauterine devices with radiological findings: report on two cases. BMJ Case Reports. 2014; https://doi.org/10.1136/bcr-2013-202522.

46. Vandermeer FQ, Wong-You-Cheong JJ. Imaging of acute pelvic pain. Clin Obstet Gynecol. 2009;52(1): 2–20.

47. Boyd CA, Riall TS. Unexpected gynecological findings during abdominal surgery. Curr Probl Surg. 2012;49(4):195–251.

48. Torky HA. Huge nabothian cyst causing hematometra (case report). Eur J Obstet Gynecol Reprod Biol. 2016;207:238–40.

49. Umesaki N, Nakai Y, Honda K, et al. Power Doppler findings of adenoma malignum of uterine cervix. Gynecol Obstet Investig. 1998;45(3):213–2116.

50. Jayaprakash S, Lakshimidevi M, Kumar GS. A rare case of posterior vaginal wall cyst. BMJ Case Reports. 2011; https://doi.org/10.1136/bcr.02.2011.3804.

51. Tiwari U, Relia N, Shailesh F, et al. Gartner duct cyst: CT and MRI findings. J Obstet Gynaecol India. 2014;64(Suppl 1):150–1.

52. Chaudhari VV, Patel MK, Douek M, et al. MR imaging and US of female urethral and periurethral disease. Radiographics. 2010;30(7):1857–74.

Errors in Acute Musculoskeletal Imaging

9

Travis J. Hillen, Michael V. Friedman,
and Jonathan C. Baker

9.1 Introduction

Many traumatic and nontraumatic emergencies affect the musculoskeletal system. Radiologists play an important role in both the diagnosis of disease and as a consultant who recommends the best imaging modality for further evaluation of initially demonstrated or suspected pathology.

Clinical history and physical examination typically lead to the appropriate radiographic evaluation of the affected joint or body part. In many circumstances, the radiographs provide the necessary information needed to make the diagnosis, e.g., the obvious fracture or flagrant osteomyelitis next to a large wound. Sometimes the information needed may be visible on the radiographs but is missed by the referring clinician, radiologist, or both. Other times, the information needed to make the diagnosis is occult by radiographs, and further imaging should be recommended to make the diagnosis.

In this chapter, we will discuss multiple commonly missed upper and lower extremity fractures, which are often very subtle even to the well-trained radiologist, and ways to avoid misdiagnosis. We will also highlight fractures which

are commonly identified but are associated with more serious injuries. Additionally, we will discuss multiple musculoskeletal pathologies for which radiographs lack the appropriate sensitivity to establish the diagnosis early in the disease course and the need for the radiologist to recommend the appropriate imaging examination to confirm the diagnosis.

9.2 Lower Extremities

9.2.1 The Hip

A number of important, easily missed traumatic injuries affect the hip and thigh in adults. The initial radiographic evaluation of hip trauma should include at minimum an anteroposterior (AP) view including the entire pelvis and at least one lateral projection of the symptomatic hip, usually a cross-table lateral radiograph. The frog-leg lateral view is useful but is often difficult or impossible to obtain if the patient has a fracture.

9.2.1.1 Femoral Neck Fracture
Femoral neck fractures are frequently encountered in the emergency department. These intracapsular fractures are classified with the Garden or Pauwels systems and are typically managed surgically by percutaneous screw fixation or joint replacement [1]. Complications include non-union, osteonecrosis of the femoral head, and the risk of

T. J. Hillen (✉) · M. V. Friedman · J. C. Baker
Musculoskeletal Section, Mallinckrodt Institute of
Radiology, St. Louis School of Medicine, Washington
University in St. Louis, St. Louis, MO, USA
e-mail: tjhillen@wustl.edu; mvfriedman@wustl.edu;
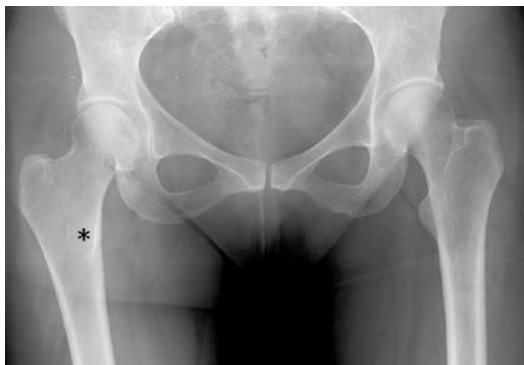jonathancbaker@wustl.edu

Fig. 9.1 Sixty-two-year-old woman with normal AP pelvic radiograph demonstrating the importance of hip positioning for adequate assessment of the femoral neck. The right hip is internally rotated, thereby elongating the femoral neck and optimizing detection of a femoral neck fracture. Adequate internal rotation is present when the lesser trochanter (asterisk) is superimposed on the femur. On the left, the hip is externally rotated, which both foreshortens the femoral neck and causes the greater trochanter to obscure the inferolateral femoral neck

Fig. 9.2 Eighty-six-year-old woman with acute left femoral neck fracture. The fracture was difficult to appreciate on an AP pelvic radiograph (not shown), but is well demonstrated (arrows) on a right posterior oblique view

Fig. 9.3 Sixty-eight-year-old woman with right femoral neck fracture, initially overlooked. Subtle clues include a double density crossing the femoral head-neck junction (arrow) and interruption of the compressive and tensile trabecular lines in the femoral neck (normal lines indicated by arrowheads in the left femur)

deconditioning or even mortality, particularly in elderly patients. Some femoral neck fractures result from high-energy trauma, such as a motor vehicle collision or fall from a height, and have a readily identifiable fracture line which courses vertically through the femoral neck. In contrast, more subtle injuries of the femoral neck occur in older adults with a low-energy mechanism, such as a same-level fall. Many of these injuries represent fragility fractures in the setting of osteoporosis, which reduces bone mineral density and strength, particularly in the region of Ward's triangle in the femoral neck [2]. Demineralization of the bone in patients with osteoporosis or other metabolic bone diseases may obscure the fracture line. An important technical factor that hinders the detection of a femoral neck fracture is incorrect patient positioning. Proper profiling of the femoral neck requires internal rotation of the hip. When the hip is externally rotated, the femoral neck is foreshortened and partially overlaps the greater trochanter (Fig. 9.1) [3]. When pain prevents internal rotation of the hip, a posterior oblique Judet view of the pelvis may help to profile the symptomatic hip (Fig. 9.2) [4]. Familiarity with subtle radiographic clues indicating a non-displaced femoral neck fracture may aid the radiologist in fracture detection. These findings include interruption of the primary trabecular lines and a double density over the femoral neck (Fig. 9.3) [3].

Radiographs remain insensitive for femoral neck fracture even when there is a high index of clinical suspicion [5]. In such cases of suspected proximal femur fracture with normal or indeterminate radiographs, MRI is useful to demonstrate radiographically occult injuries [6]. MRI is the preferred imaging modality of the authors to detect occult femoral fractures, a practice supported by the American College of

Radiology Appropriateness Criteria [7]. Many emergency departments have access to MRI, and a rapid screening MRI examination may be done to detect occult hip fracture using 2–4 pulse sequences [8, 9]. The authors prefer to obtain a four-sequence examination, using a field-of-view covering the entire pelvis, with T1-weighted and fat-suppressed, fluid-sensitive sequences in the coronal and axial planes. For patients who have no fracture, MR reveals an alternate source of pain in up to 73% of patients [5]. We recognize that CT is obtained rather than MR in many situations, whether because of pressure to speed patient throughput in the ED or because of patient contraindication to MR. However, CT is less sensitive than MR for hip fractures [10, 11]. Dual-energy CT has promise because of its ability to depict bone marrow edema, but comparison with the MR standard is lacking at this time to our knowledge. Bone scintigraphy is very sensitive for fracture detection but is not commonly employed, as there may be a 2- to 3-day delay before uptake is seen at the fracture site, and the lack of specificity often requiring another examination.

9.2.1.2 Isolated Greater Trochanter Fracture

An apparently "isolated" fracture of the greater trochanter represents another potential pitfall. Most patients with a non-displaced fracture of the greater trochanter on hip radiography actually have intertrochanteric extension of the fracture on MR (Fig. 9.4) [12]. The distinction is clinically significant, because a true isolated greater trochanter fracture is managed non-operatively, whereas a fracture with intertrochanteric extension undergoes surgical fixation [13]. Identification of a greater trochanter fracture on hip radiographs should prompt an MR to detect occult intertrochanteric extension.
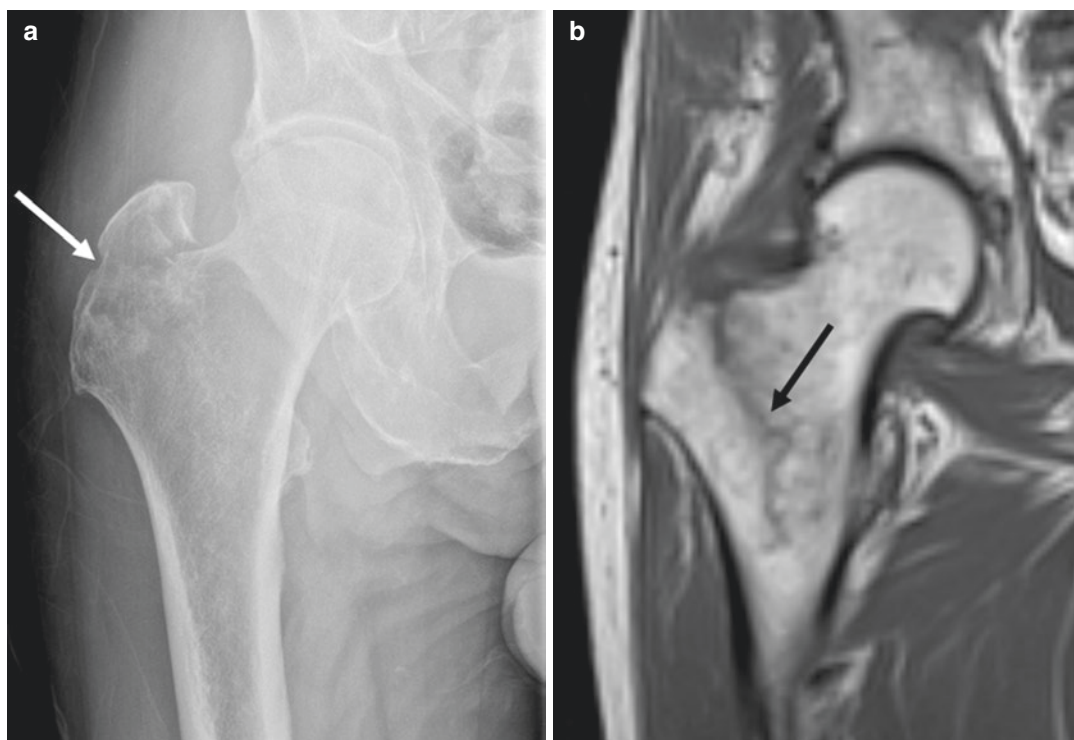

Fig. 9.4 Seventy-year-old man with intertrochanteric right femur fracture. AP hip radiograph (**a**) shows a non-displaced fracture of the greater trochanter. Coronal T1-weighted MR image (**b**) demonstrates intertrochanteric extension of the fracture line (arrow), which was not appreciated on the radiograph. The patient underwent open reduction and internal fixation of the fracture

9.2.1.3 Femoral Stress Fracture

Stress fractures of the proximal femur may occur after excessive loading of a normal bone (fatigue fracture), typically seen in runners, or after normal loading of an abnormal bone (insufficiency fracture) weakened by osteoporosis or another metabolic bone disease [14]. Radiographs obtained in the early stage of injury are either normal or show easily overlooked findings, including periosteal bone formation and linear endosteal sclerosis. Most fractures are incomplete and involve the compressive side of the bone along the medial femoral neck. These generally heal with appropriate rest. Tensile side fractures are less common, begin at the lateral cortex, and are at higher risk of completion.

9.2.2 The Knee

Imaging of a patient with blunt trauma or twisting injury of the knee accompanied by joint effusion, focal tenderness, or difficulty bearing weight begins with a dedicated four-view knee trauma series. This includes supine AP, bilateral oblique, and cross-table lateral radiographs. A tangential patellar or sunrise view may be obtained in select circumstances.

9.2.2.1 Tibial Plateau Fracture

Intra-articular fractures of the proximal tibia are frequently encountered. Displaced fractures are readily identified with routine radiographs. However, fractures with minimal displacement or depression may be overlooked, especially if only AP and lateral views are obtained (Fig. 9.5). The presence of a lipohemarthrosis in a patient with knee trauma indicates the presence of an intracapsular fracture and should prompt close scrutiny of the tibial plateau. Subtle radiographic clues to this injury include the presence of trabecular double density (Fig. 9.6), and depression or increased downsloping of the tibial plateau on the lateral view.
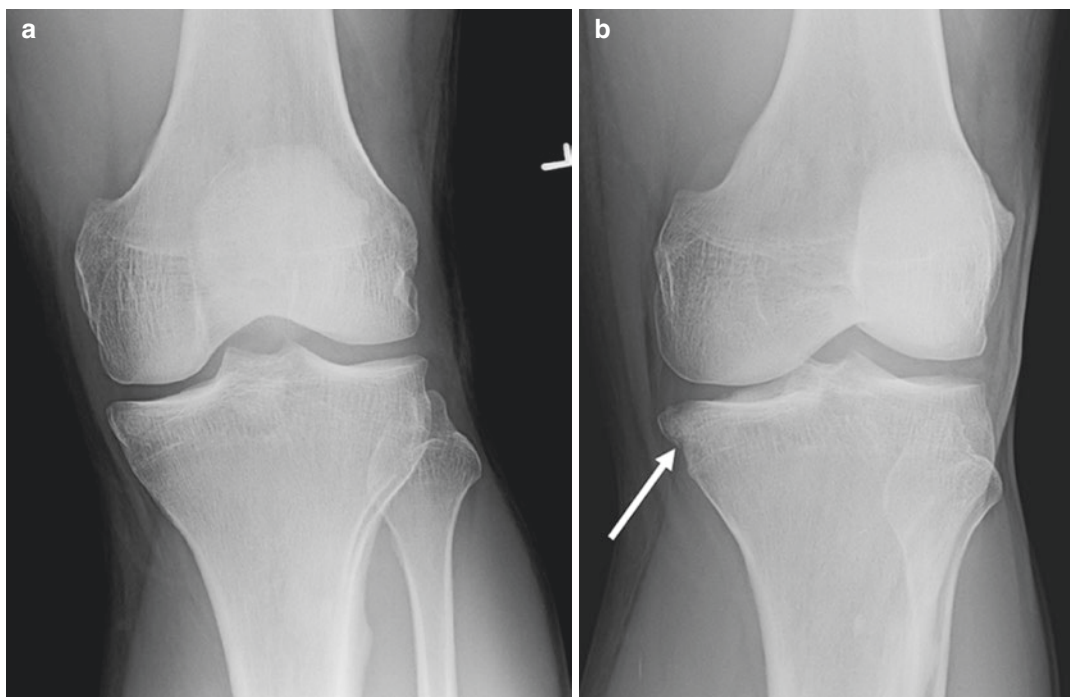

Fig. 9.5 Thirty-six-year-old man with initially missed medial tibial plateau fracture. The initial examination (**a**) included only an AP view and a lateral view (not shown), with a knee effusion but no apparent fracture. Subsequent oblique view (**b**) demonstrates a non-displaced fracture of the posteromedial tibial plateau (arrow)

9.2.2.2 Subtle Fractures Associated with Ligament Injury

The knee serves as the attachment point for multiple stabilizing ligaments and tendons. Subtle avulsion fractures at any of these ligament footprints may generate a small, linear crescent of cortical bone referred to as the "fleck sign." Recognition of this finding on radiography points to a potential ligament injury and should prompt further evaluation with MR. The ligament injury can be inferred from the location of the cortical fragment and knowledge of the ligamentous anatomy in the knee. Avulsion fractures to consider include the Segond (lateral capsular ligament) (Fig. 9.7), reverse Segond (deep medial collateral ligament fibers), and arcuate (conjoint tendon) avulsion fractures [15].

9.2.2.3 Patellar Fracture

Patellar fractures in adults are easily detected in most patients, provided that a quality trauma series of radiographs is obtained. However, two subtle fractures deserve specific mention. The first is a sagittal fracture of the patella (Fig. 9.8). When non-displaced, this fracture may be occult

on the routine trauma series. If the patient has anterior pain and direct trauma, a tangential patellar radiograph is useful to detect this fracture [16]. The second fracture is a non-displaced avulsion fracture of the medial patella following transient lateral dislocation of the patella. This finding is generally seen only with a tangential patellar radiograph.

9.2.2.4 Extensor Mechanism Disruption

Ruptures of the quadriceps and patellar tendon may be inferred by the presence of certain subtle radiographic findings. Both tendons are normally well seen on the lateral knee radiograph, as they are depicted in long axis, and their margins outlined by fat attenuation tissue. Clues include abnormal patellar position (low-lying patella

Fig. 9.6 Fifty-six-year-old woman with tibial plateau fracture initially missed in the emergency department. A double density on the AP radiograph (arrow) is an important clue to a depressed fracture involving the articular surface

Fig. 9.7 Sixty-three-year-old man with missed Segond fracture. AP radiograph shows a small fleck of cortical bone (arrow) adjacent to the lateral tibial plateau, which was not prospectively identified. Identification of this fracture is important due to its strong association with internal derangements, particularly an anterior cruciate ligament tear, which was found on subsequent MRI (not shown)
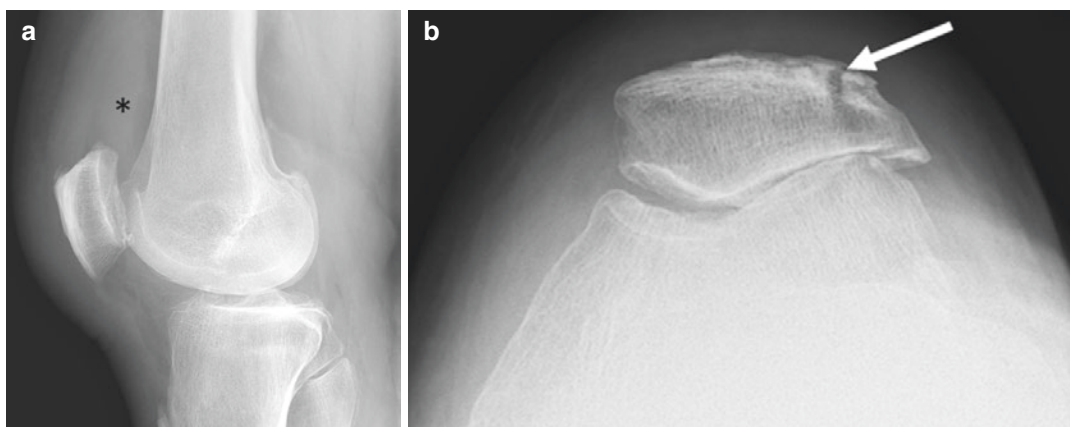
Fig. 9.8 Sixty-two-year-old man with patellar fracture. Lateral (**a**) and AP (not shown) knee radiographs showed anterior soft-tissue swelling and a joint effusion (asterisk). Subsequent tangential patellar view (**b**) demonstrates a sagitally-oriented fracture of the lateral patella (arrow)

with quadriceps rupture or high-riding patella with patellar tendon rupture) and obscuration of the injured tendon margin [17].

9.2.3 The Ankle and Foot

9.2.3.1 Calcaneus Fracture

Fractures of the calcaneus typically result from an axial load after a fall from a height. The common intra-articular fracture pattern with central depression and extension into the subtalar joint is seldom overlooked on routine foot and ankle radiographs. However, fractures with less severe comminution and displacement may be difficult to appreciate on radiography. An important clue in these cases is flattening of Bohler's angle, normally 25–40°, due to subtle depression of the calcaneal fracture fragments [18]. Extra-articular calcaneal fractures at several locations are often subtle and are easily missed. The anterior calcaneal process should be scrutinized, particularly on lateral and oblique foot radiographs. Avulsion fractures of the lateral calcaneal cortex at the origin of the extensor digitorum brevis muscle are best seen on the AP ankle radiograph, frequently accompanied by lateral soft-tissue swelling centered distal to the lateral malleolus. Finally, non-displaced fractures of the posteroinferior calcaneal tuberosity may be seen only with a Harris-Beath, or axial, view of the heel (Fig. 9.9) [19].

9.2.3.2 Capsular Avulsion Fractures

Capsular avulsion fractures at the talonavicular and calcaneocuboid joints are subtle injuries manifest by dorsal soft-tissue swelling and a tiny, linear fleck of cortical bone. Recognition of these subtle findings is important, as they may indicate a more extensive injury to the Chopart joint (Fig. 9.10) [20].

9.2.3.3 Lisfranc Ligament Injury

Injuries of the tarsometatarsal (Lisfranc) joint complex are important to recognize because prompt treatment is needed to treat midfoot instability and forestall the development of post-traumatic midfoot osteoarthritis. Close inspection of the alignment at the tarsometatarsal joints is essential. Important clues that suggest Lisfranc joint injury include dorsal soft-tissue swelling in the midfoot, malalignment at the tarsometatarsal joints, and tiny avulsion fracture fragments, particularly in the space between the first and second metatarsal bases [21]. If possible, a weight-bearing dorsoplantar radiograph including both feet is useful to detect subtle malalignment at the tarsometatarsal joints.

9.2.3.4 Achilles Tendon Tear

Because the Achilles tendon abuts the subcutaneous fat posteriorly and Kager's fat pad anteriorly, the tendon silhouette is depicted on lateral radiographs of the foot and ankle.
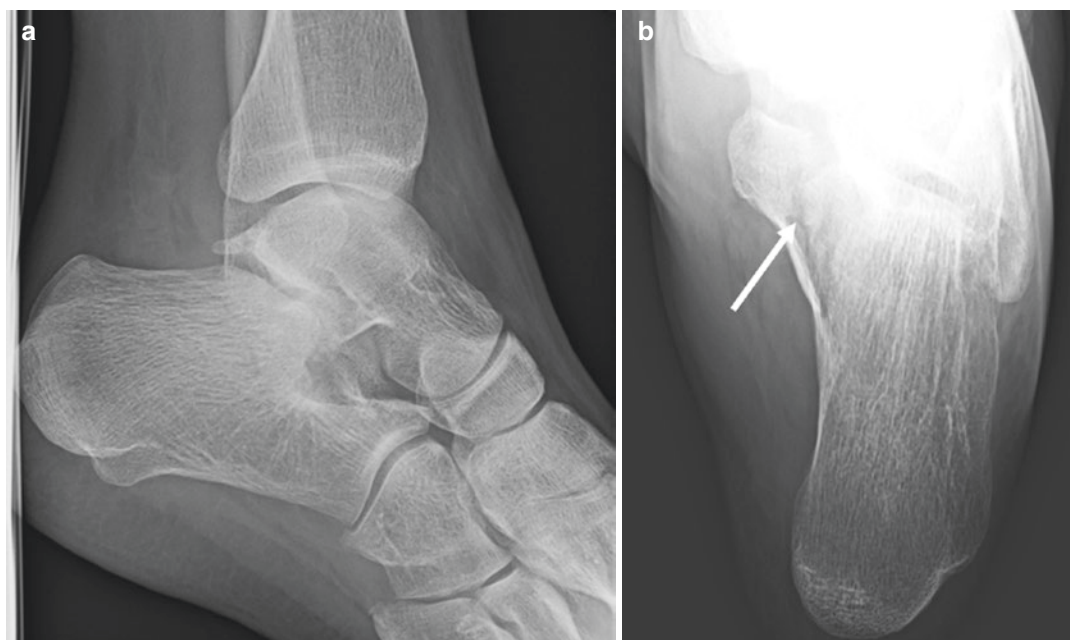
Fig. 9.9 Twenty-two-year-old woman with nondisplaced fracture of the calcaneus involving the sustentaculum tali. Lateral radiograph (**a**) from ankle series shows soft-tissue swelling, but the sagittal fracture of the sustentaculum could only be appreciated on the Harris view (arrow in **b**)

Fig. 9.10 Twenty-seven-year-old man with nondisplaced capsular avulsion fracture of the dorsal talonavicular joint capsule. Lateral radiograph shows linear cortical bone fragments dorsal to the navicular (arrow). This subtle finding can be associated with Chopart joint injuries, but there was evidence (clinical or radiographic) of a Chopart joint injury in this patient

The normal Achilles tendon demonstrates uniform thickness and sharp margins. Radiographic features that are associated with tendon rupture include indistinctness or interruption of the tendon outline and soft-tissue swelling in Kager's fat pad.

9.3 Upper Extremities

9.3.1 Sternum/Clavicle

9.3.1.1 Sternoclavicular Joint Dislocation/Medial Head Clavicle Fracture

The sternoclavicular (SC) joint is a true synovial articulation linking the upper extremity to the axial skeleton. Sternoclavicular joint dislocation is rare, accounting for only 2–3% of all shoulder girdle dislocations. Usually the result of blunt force trauma, SC dislocations are difficult to diagnose clinically, emphasizing the importance of imaging diagnosis [22]. Anterior dislocations are approximately nine times more common than posterior dislocations, and if missed can be associated with chronic degenerative changes including early-onset osteoarthritis or anterior instability [23]. Posterior dislocations, on the other hand, require prompt identification as they can be associated with life-threatening complications secondary to impingement on vital superior mediastinal

structures, including the lungs, esophagus, trachea, and great vessels [23–26].

Radiographic evaluation of the SC joint is usually quite limited on a frontal view or chest radiograph secondary to superimposition of the ribs, mediastinum, and spine, as well as the relative thinness of the sternum and medial clavicular head cortex [25]. The serendipity view of the sternoclavicular joints (Fig. 9.11) is obtained with the X-ray tube angled 40° cephalad, providing improved visualization of both the SC joints and medial third of the clavicles. Evaluation is based on SC joint asymmetry with caudal displacement suggestive of a posterior dislocation and cephalad displacement suggestive of an anterior dislocation [27]. Medial head clavicle fractures may also be recognized, prompting the need for further investigation of mediastinal trauma. However, even if the radiographic evaluation is normal, computed tomography (CT) is the imaging modality of choice, and should be recommended in the clinical setting of suspected SC joint trauma. Ready availability, time-sensitive acquisition, complete anatomical evaluation, and the ability to include angiography underlie the central role for CT evaluation of this potentially life-threatening injury.

9.3.1.2 Acromioclavicular Separation

Acromioclavicular (AC) separation typically results from a fall on an adducted arm. Accounting for 12% of shoulder girdle injuries, AC injuries are classified based upon ligament involvement and clavicular displacement [28, 29]. Differentiating low-grade (I–II) from high-grade (III–VI) injuries is vital in directing management, as low-grade injuries are typically treated conservatively, whereas high-grade injuries usually require surgery [30, 31].

Subtle malalignment of the AC and coracoclavicular (CC) joints may be difficult to assess on the standard three- or four-view shoulder series. The AC stress view taken with bilateral suspended weights provides comparison of both AC joints and CC intervals with and without load-bearing, when evaluating for AC separation. Evaluation is based on asymmetry of the AC and CC spaces, specifically with evidence of widening upon loading (Fig. 9.12). The normal
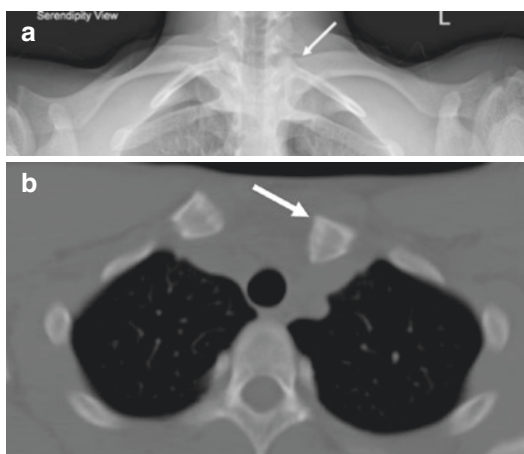

Fig. 9.11 Sixteen-year-old boy with suspected left clavicle injury. AP radiograph (not shown) of the left clavicle is normal. Serendipity view of the sternoclavicular joints (**a**) shows caudal displacement (arrow) of the left clavicular head at the sternoclavicular junction relative to the right clavicle. This finding is concerning for a posterior dislocation. Because of strong clinical suspicion and abnormal radiographs, CT examination was performed. The axial CT image (**b**) shows posterior dislocation of the left clavicle. Posterior dislocation can be associated with mediastinal injury, and close examination of the mediastinum is necessary on the CT to exclude such associated injuries
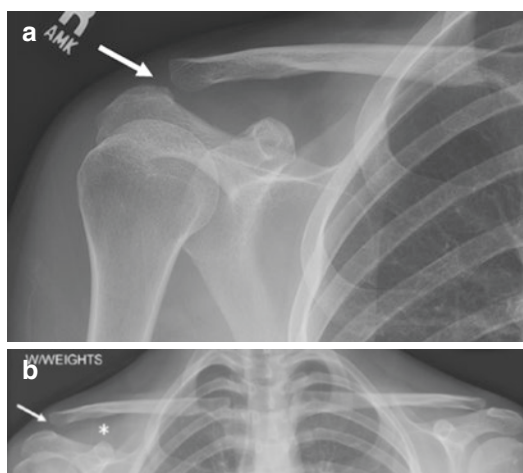

Fig. 9.12 Twenty-four-year-old woman with acromioclavicular separation. AP radiograph (**a**) of the right shoulder demonstrates questionable offset of acromioclavicular alignment (arrow). AP view including both clavicles with weights (**b**) shows asymmetric progressive malalignment of the right acromioclavicular joint (arrow) with widening of the coracoclavicular distance (asterisk), consistent with a type III acromioclavicular separation injury

AC distance measures 1–6 mm in width, with <4 mm of allowable asymmetry. The normal CC distance measures 11–13 mm in width, with <5 mm of allowable asymmetry [31, 32]. Widening of both the AC and CC spaces indicates at least a grade III injury.

9.3.1.3 Glenohumeral Joint

Bipedal evolution has resulted in the glenohumeral joint having the widest range of motion of all the major joints. This adaptation has come at the expense of stability, however, with the glenohumeral joint accounting for ~40% of all joint dislocations, the most common of the major joints.

Imaging evaluation of all shoulder trauma should begin with a four-view radiographic examination including AP internal rotation, AP external rotation, axillary, and trans-scapular Y views. Diagnosis should be evident when a patient presents in the dislocated state, especially in the setting of anterior instability. However, evaluation is more difficult in patients who are post-reduction at the time of initial imaging. Identification of secondary osseous injuries may be the only indication of a recent instability event, and identifying these fractures often influences prognosis and treatment.

9.3.1.4 Anterior Instability

Anterior shoulder dislocations account for the vast majority (~95%) of all shoulder instability events. Excessive force in the setting of abduction/external rotation may result in impaction of the posterolateral humeral head on the antero-inferior glenoid (Hill-Sachs fracture) [33]. Identification of Hill-Sachs fractures is important as larger injuries are associated with recurrent instability and can engage the glenoid resulting in failed reduction or recurrent dislocation [34]. The posterolateral humeral head is best evaluated on the internal rotation view; however, adequate profiling can be difficult, and many Hill-Sachs fractures are unrecognized. The Stryker notch view profiles the posterolateral humeral head, and is a supplemental option if the internal rotation view is indeterminate [35]. Loss of smooth cortical contour or notching of the posterolateral humeral head is highly consistent with a Hill-Sachs lesion (Fig. 9.13).

When anterior instability is suspected, the anteroinferior glenoid must also be closely inspected. While the traditional Bankart lesion refers to a glenoid labral tear, it can be accompanied with a bone fracture fragment (often referred to as a bony Bankart), which is evident on radiographs. The fragment is best identified
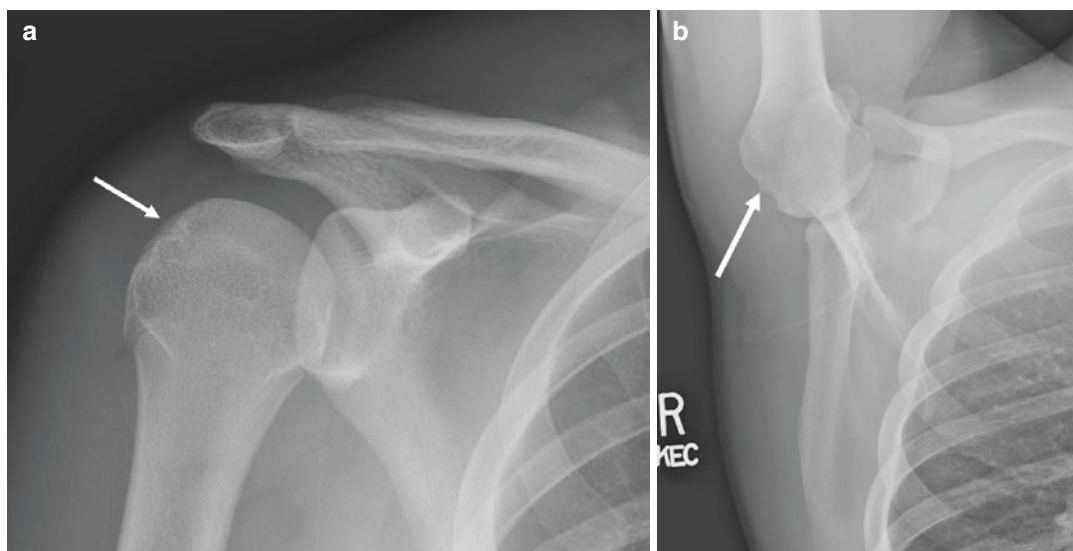

Fig. 9.13 Twenty-year-old man with initially missed anterior instability event. Internal rotation radiograph (**a**) of the right shoulder shows possible flattening of the pos-terior humeral head (arrow). Stryker notch view (**b**) demonstrates a small Hill-Sachs deformity (arrow) confirming a prior anterior instability event

on the AP views with the degree of displacement assessed on the axillary view. Identification of the anteroinferior glenoid rim fragment is important, as it often warrants further evaluation with CT to qualify the size of the defect, potentially altering surgical approach to prevent attrition of glenoid bone stock in the setting of recurrent instability [36].

9.3.1.5 Posterior Instability

Acute posterior glenohumeral dislocations are frequently missed on both clinical and radiographic examinations, often secondary to the subtle findings on the AP views. The humeral head will often have a fixed internal rotation appearance (the "lightbulb sign") on both AP views (Fig. 9.14) [33]. The Grashey view demonstrates abnormal overlap of the humeral head and glenoid. The trans-scapular Y view is often diagnostic; however, this view may be falsely reassuring if the degree of humeral rotation or erroneous technique projects the humeral head over the glenoid. Therefore, an axillary view should always be obtained when suspecting posterior instability [37].

In the setting of relocation, secondary findings of posterior instability include a vertically oriented impaction fracture of the anterior humeral head known as the "trough sign" or reverse Hill-Sachs lesion [38]. Similarly, a posterior glenoid rim fracture, or reverse Bankart lesion, may be present. Both injuries are best evaluated on the axillary view, and again often warrant further evaluation with CT to qualify the extent of the injuries as pre-surgical evaluation [36].

9.3.2 Scapula

Scapular fractures most commonly occur in the setting of high-velocity trauma [39]. Relatively uncommon, accounting for only 3–5% of all shoulder girdle injuries, the diagnosis of scapular fracture is often initially missed and treatment delayed, as clinical focus is commonly on other concurrent potentially acute life-threatening injuries [40, 41] which take precedence. However, a delay in diagnosis of a scapular fracture may lead to instability, chronic pain, weakness, and post-traumatic osteoarthritis [41, 42].

Radiographic evaluation of scapular injuries can be difficult secondary to overlapping complex bony anatomy [43]. Dedicated imaging of suspected scapular injuries typically includes AP, trans-scapular Y, and axillary views. Interrogation of the scapula should also be a part of the radiologist's routine search pattern when evaluating the traumatic shoulder series.
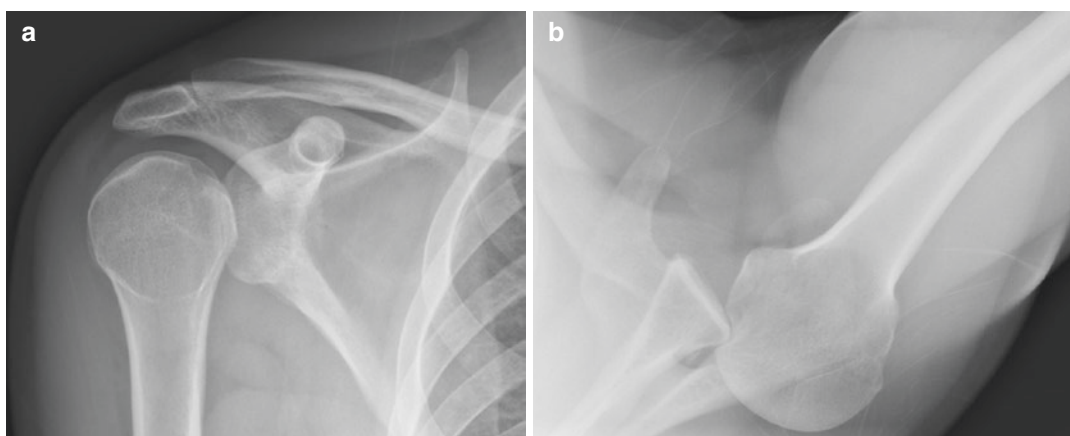
Fig. 9.14 Forty-four-year-old man with posterior shoulder dislocation. (**a**) AP internal (not shown) and external rotation radiographs show persistent internal rotation appearance of the humeral head on both views. Trans-scapular Y view (not shown) demonstrates questionable posterior subluxation of the humeral head in relation to the glenoid. This was interpreted as indeterminate, and an axillary view (**b**) was requested, which confirms acute posterior dislocation of the humeral head

If high clinical suspicion for a scapular fracture persists despite normal radiographs, further evaluation with CT should be recommended. In the authors' experience, given the close association with blunt high-energy trauma, CT of the chest, abdomen, and pelvis is commonly performed regardless in the emergency department setting, providing a more accurate and reliable imaging modality for diagnosis and staging of scapular injuries [41, 44].

9.3.2.1 Intra-articular
Intra-articular fractures of the scapula account for approximately 10% of all scapular injuries [45, 46]. Fractures involving the glenoid are best evaluated on the axillary and Grashey views (Fig. 9.15), secondary to profiling of the glenoid fossa and glenohumeral joint space [41]. Scapular fractures are classified according to the fracture location on the glenoid and articular involvement [46]. Non-displaced fractures are typically treated conservatively, and although criteria for surgical management are controversial, interventional indications traditionally include greater than 20% involvement of the articular surface, or more than 4 mm of depression [41, 47].

9.3.2.2 Extra-articular
Extra-articular fractures may involve any combination of the scapular neck, body, spine, acromion or coracoid process and comprise the largest group of scapular injuries [48]. Conservative management is the treatment of choice, with open reduction and internal fixation reserved for displaced fractures of the acromion, coracoid, and scapular neck, depending on expectant future biomechanical demand of the patient. Fractures of the coracoid and acromion process are best visualized on the axillary view (Fig. 9.16), with classification dependent upon anatomic location, displacement, and functional relationship to the coracoclavicular ligament [49, 50] or association with subacromial impingement, respectively [51, 52]. Displaced acromion fractures may show a double density sign on AP views, with lack of smoothly marginated cortical borders utilized to differentiate fractures from an os acromiale.

9.3.3 Humerus

9.3.3.1 Greater Tuberosity
Isolated fractures of the greater tuberosity are associated with direct impaction injuries and anterior
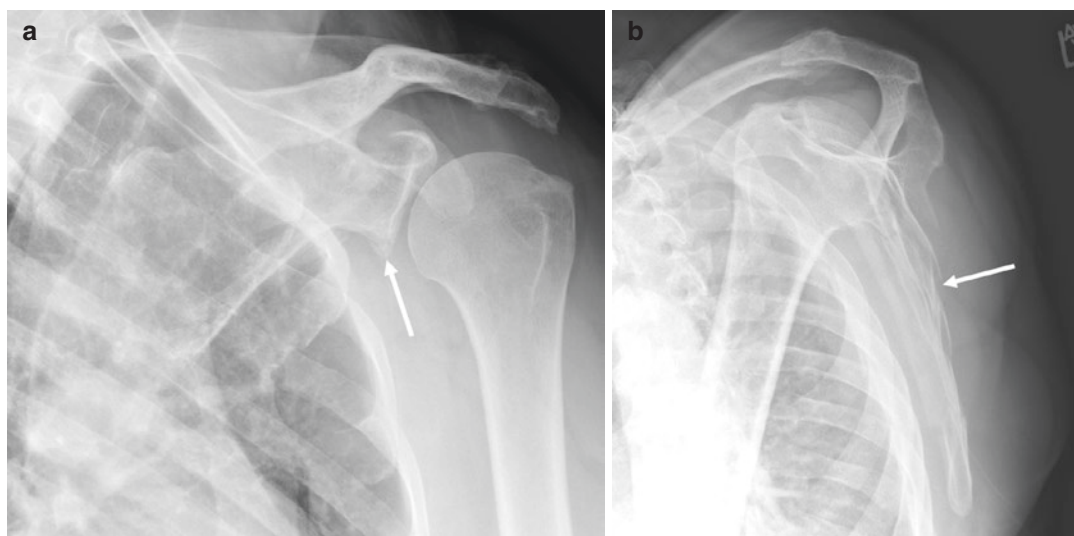

Fig. 9.15 Sixty-two-year-old man with a comminuted intra-articular scapular fracture. AP internal rotation radiograph (not shown) is normal. AP external rotation radiograph (**a**) demonstrates a fracture of the scapular neck with extension into the inferior glenoid (arrow). Trans-scapular Y view (**b**) shows the extent of the comminuted fracture involvement of the body, which was underestimated on the AP views (arrow)
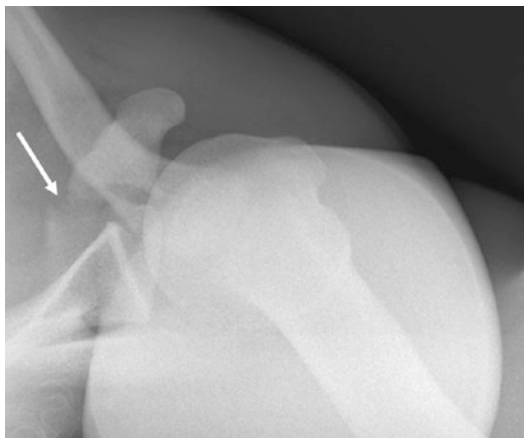
Fig. 9.16 Nineteen-year-old man with initially missed coracoid fracture. AP internal and external rotation radiographs are normal (not shown). Trans-scapular Y view demonstrates a mildly displaced coracoid base fracture (arrow)

Fig. 9.17 Twenty-nine-year-old man with initially missed non-displaced greater tuberosity fracture. AP internal rotation radiograph shows a non-displaced greater tuberosity fracture (arrow). This fracture was occult on the external rotation AP radiograph (not shown)

instability events, accounting for approximately 20% of all proximal humerus fractures. Diagnostic evaluation of these fractures is difficult secondary to bony overlap, with up to two-thirds of greater tuberosity fractures missed on initial radiographic evaluation [53]. On the four-view trauma shoulder series, the greater tuberosity is best evaluated on the external rotation view, where it is seen in profile (Fig. 9.17). The axillary view is useful to determine the degree of anterior or posterior fragment displacement, which is important as fractures displaced <5 mm are typically treated conservatively [54].

9.3.4   Elbow/Forearm

Traumatic injuries to the elbow and forearm are responsible for approximately 15% of all upper extremity-related emergency department visits [55]. Many common injury patterns (Monteggia, Galeazzi, and Essex Lopresti) have been described and are typically not difficult to diagnose with an understanding of elbow biomechanics. However, minimally displaced or non-displaced fractures of the radial head and coronoid process may not be as obvious on the standard three-view radiographic series (AP, oblique, and lateral views), and can result in delayed treatment complications and instability.
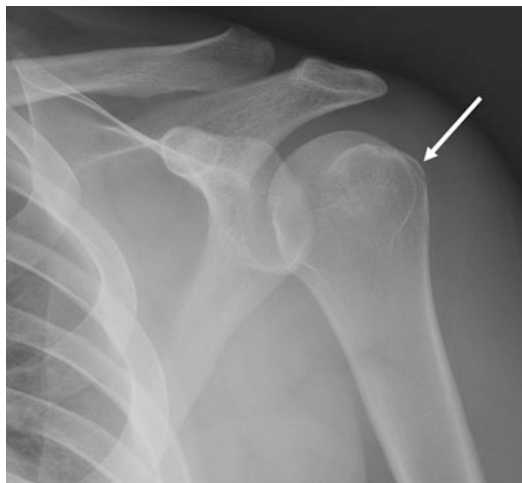
9.3.4.1 Radial Head

In adults presenting with elbow pain post-trauma, the radial head and neck should always be closely inspected for non-displaced fractures. However, an elbow effusion on the lateral view is often the only radiographic indication of intra-articular injury. In this setting, an occult fracture should always be suspected. Fractures of the posterior half of the radial head are particularly difficult to diagnose on the lateral view due to overlap with the ulna. While non-surgical treatment is indicated for minimally or non-displaced fractures, identification is important to ensure adequate follow-up for complications of late displacement or non-union [56]. The radial head-capitellum view is a valuable supplemental view in the evaluation of the traumatic elbow. This view profiles the radiocapitellar joint, depicting articular involvement by separating the ulnotrochlear and radiocapitellar articulations (Fig. 9.18) [57].

9.3.4.2 Coronoid Process

The coronoid process is one of the primary elbow stabilizers, providing restraint against both varus- and valgus-directed forces. Fractures of the coronoid process are typically of the shearing variety secondary to blunt contact, with the trochlea
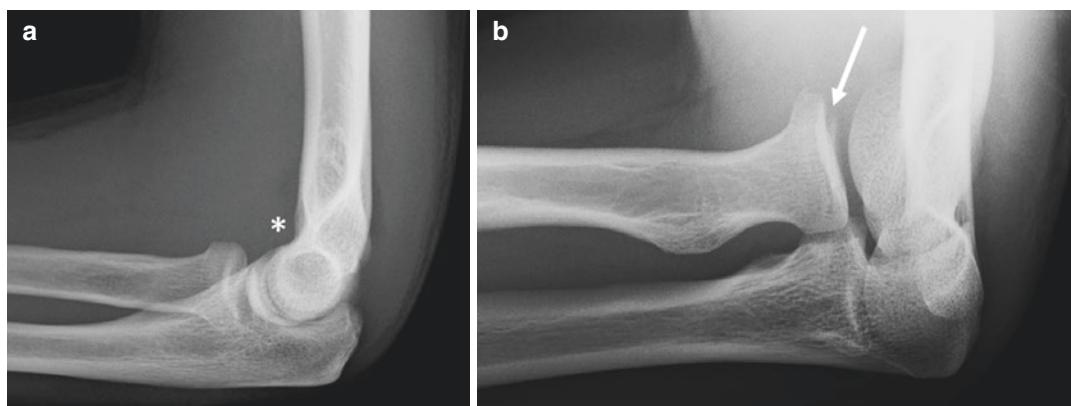
Fig. 9.18 Thirty-three-year-old man with a non-displaced radial head fracture. Lateral radiograph (**a**) demonstrates an elbow effusion (asterisk) without a frac-ture identified. Radial head-capitellum view (**b**) shows a non-displaced radial head fracture (arrow)

Fig. 9.19 Twenty-one-year-old woman with a non-displaced coronoid process fracture. AP and oblique elbow radiographs are normal (not shown). Lateral radiograph shows a non-displaced coronoid process fracture (arrow) overlapped by the radial head and a large elbow effusion (asterisk)

during a posterolateral rotary instability or a posterior dislocation event [58]. The coronoid process is best evaluated on the lateral view. However, fractures can be easily missed secondary to osseous overlap. Similar to the radial head evaluation, the radiocapitellar view provides relief of that overlap, and allows for better investigation of the capitellum (Fig. 9.19). Identification of a coronoid process fracture warrants careful evaluation of the radial head for a concurrent injury, as this combination may have surgical implications [43].

9.3.5   Hand/Wrist

Multiple easily missed fractures and ligamentous injuries affect the wrist. The initial radiographic evaluation of wrist trauma should include a minimum of three views: posteroanterior, lateral, and oblique views. Additional specialized views can be obtained if there is concern for a specific wrist injury not well profiled by the standard views.

9.3.5.1 Scaphoid
The scaphoid is the most commonly fractured carpal bone [59], occurring most frequently in young, physically active patients. The injury results from a combination of hyperextension and axial forces on the wrist. Management of the fracture depends on the location (proximal, central, or distal) and the degree of displacement. The more proximal the fracture, and the greater displacement at the fracture site, the higher the risk for poor healing including nonunion or malunion [59, 60]. The anatomical blood supply to the scaphoid, which enters the distal scaphoid and travels proximally, predisposes to increased risk of osteonecrosis and poor fracture healing with proximal fractures [59, 60].

In addition to the standard three views of the wrist, an ulnar deviation with extension view or scaphoid view of the wrist can be helpful to evaluate the scaphoid (Fig. 9.20) [26]. The oblique and scaphoid views give an elongated view of the scaphoid, improving visualization of the distal
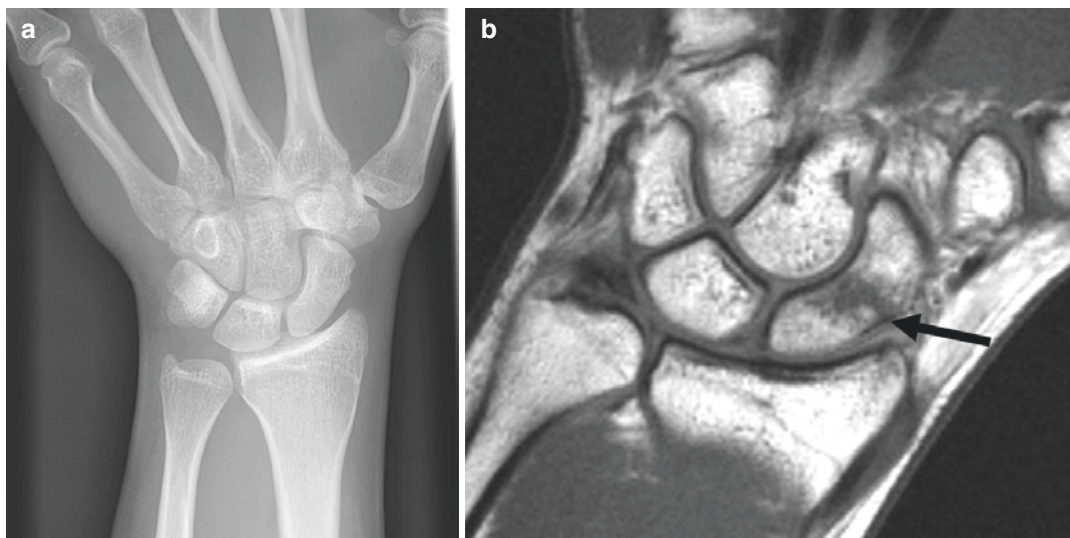
Fig. 9.20 Twenty-two-year-old man with fall on outstretched hand. Scaphoid/ulnar deviation radiograph (**a**) is negative for fracture. Coronal T1-weighted MR image demonstrates a non-displaced fracture of the scaphoid waist (**b**)

and central portions of the bone. Given the potential complications related to delayed diagnosis of scaphoid fracture, if there is persistent clinical concern for non-displaced scaphoid fracture despite negative radiographs, splinting with follow-up radiographs in 7–10 days or MRI should be recommended to exclude fracture.

9.3.5.2 Hamate

The hook of the hamate is a site of attachment for multiple ligaments and tendons along the volar aspect of the wrist. Hook of the hamate fractures typically occur after direct impact or secondary to an avulsion injury at the transcarpal ligament insertion [61, 62]. They result in non-specific pain along the volar-ulnar aspect of the wrist, particularly when making a tight grip. On physical examination, there may be point tenderness at the volar-ulnar wrist at the hook of the hamate.

The hook of the hamate is commonly difficult to visualize on the standard three-view wrist examination, as there are many overlapping carpal structures. The carpal tunnel view [26] may be helpful in diagnosis, as it isolates the hook of the hamate from the remainder of the carpus (Fig. 9.21). In patients with persistent suspicion for fracture of the hook of the hamate, either CT or MRI can help establish the diagnosis.

Fig. 9.21 Twenty-three-year-old man with acute onset left hand pain after swinging a baseball bat. The suspected hamate fracture was occult on the PA radiograph of the wrist (not shown), but is evident (arrow) on the carpal tunnel radiograph of the wrist

9.3.5.3 Perilunate/Lunate Dislocation

Perilunate dislocation is a commonly missed injury in the wrist, with up to 25% undetected on initial evaluation [63]. The lunate is the center of a multitude of ligaments and articulations that stabilize the proximal and distal

carpal rows. A perilunate dislocation is a continuum of carpal instability related to injuries of the ligaments surrounding the lunate, which result in dislocation of adjacent carpal bones, which can progress to lunate dislocation. The injury occurs in the setting of high-energy trauma resulting in hyperextension, intercarpal supination, and ulnar deviation of the wrist [64, 65].

Perilunate dislocations occur in a stepwise manner from the radial side to the ulnar side of the wrist [65]. Stage I injuries result in scapholunate dissociation. Stage II injuries progress to involve the volar radioscaphocapitate ligament, and are associated with dorsal dislocation of the capitate, i.e., perilunate dislocation. Stage III injuries progress to tearing of the long radiolunate ligament and disruption of the lunotriquetral joint. Stage IV injuries lead to disruption of the

dorsal radiotriquetral ligament and rotation, with volar dislocation of the lunate.

The standard radiographic wrist series is typically sufficient to establish the diagnosis of perilunate or lunate dislocation. The appearance of a stage I injury is identical to that of scapholunate dissociation with scapholunate diastasis. The appearance of a stage II injury results in disruption of the "arcs of Gilula" surrounding the lunate margins on the PA view, with dorsal displacement of the capitate on the lateral view. The appearance of stage III injury is complete separation of the lunate from the carpus, with disruption of the "arcs of Gilula" on the PA view, volar tilt, and possible subluxation of the lunate, as well as dorsal subluxation or dislocation of the capitate on the lateral view. The appearance of a stage IV injury on the PA view is arc disruption surrounding the lunate, as well as a "pie-shaped" lunate (Fig. 9.22). On the
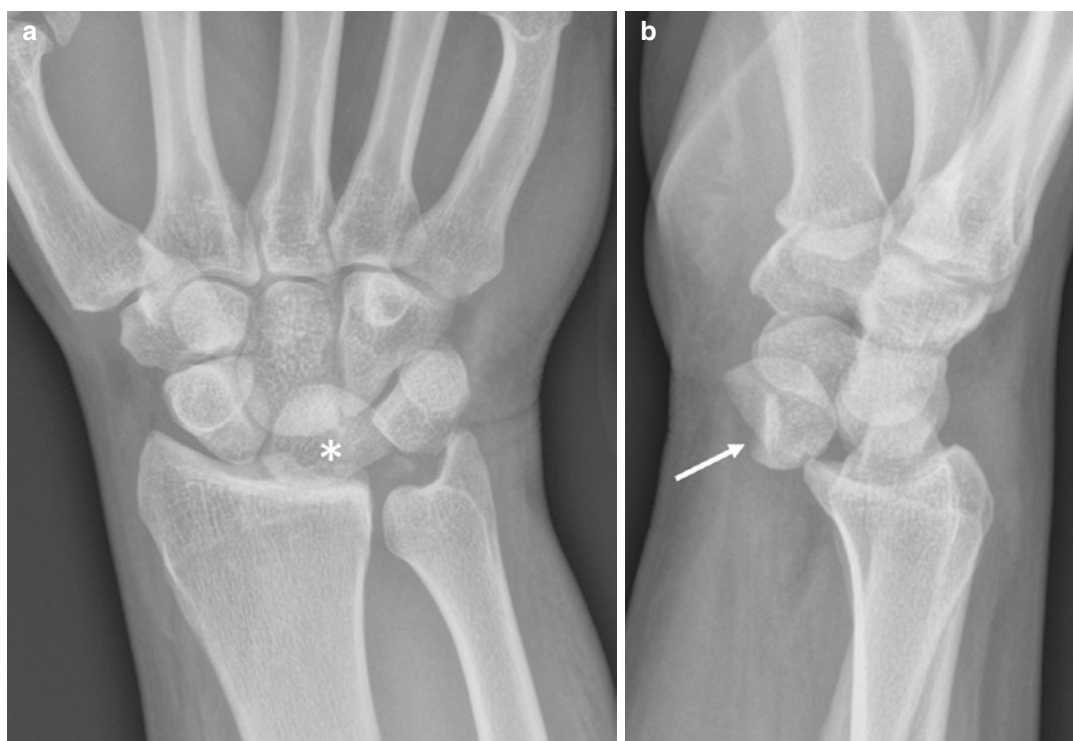

Fig. 9.22 Twenty-eight-year-old man with right hand and wrist pain following motor vehicle collision. PA radiograph of the wrist (**a**) shows a "pie-shaped" appearance of the lunate (asterisk), a small ossific fragment at the ulnar margin of the lunate, and disruption of the "arcs of Gilula." Lateral radiograph (**b**) shows volar dislocation of the lunate (arrow) relative to the wrist. The dislocation was initially missed in the emergency department by the radiologist on call

Fig. 9.23 Forty-three-year-old woman with acute onset right wrist pain. Ulnar deviation radiograph (**a**) of the wrist is normal. Clenched fist view of the wrist (**b**) shows rotatory subluxation with "signet ring" appearance of the scaphoid and widening of the scapholunate interval (white asterisk)

lateral view, the lunate is dislocated volarly, and the capitate is aligned with the distal radius. CT can be helpful to elucidate the various associated fractures.

9.3.5.4 Scapholunate Instability

Scapholunate ligament injuries typically occur in the setting of a fall on an outstretched hand with the force centered on the thenar eminence [66]. The scapholunate ligament has three components; dorsal, volar, and central/membranous. The dorsal component is the strongest and most important for scapholunate joint stability [67]. The volar component provides rotational stability. The central/membranous component contributes very little to stability. Multiple secondary stabilizers around the wrist include the volar and dorsal extrinsic ligaments, which help to maintain normal scapholunate movement.

The standard three-view wrist series is diagnostic of some scapholunate ligament injuries. However, a scaphoid view of the affected wrist and stress views including both wrists, either a clenched fist view or pencil grip view,

can be confirmatory of the scapholunate injury (Fig. 9.23) [26]. Normal static radiographs with abnormal stress views are a common presentation of scapholunate injury. Scapholunate ligament injury associated with extrinsic ligament injury will result in abnormal static radiographs, including diastasis and rotatory subluxation of the scaphoid.

9.3.6 Infectious Typically Radiographically Occult Musculoskeletal Emergencies

Radiologists frequently image patients with musculoskeletal infections in the emergency department setting. The presentation of these infections is highly variable and dependent on multiple patient factors, including immune status, age, and etiology of the infection. The most common route of infection is through broken skin [68]. Radiographs of the body part of concern are typically obtained initially and are usually normal or positive only for non-specific

soft-tissue swelling. Occasionally a more specific diagnosis can be made from the radiographs, including the presence of a foreign body, soft-tissue gas, or erosion of bone with an overlying soft-tissue ulcer. Often cross-sectional imaging or ultrasound will be needed to make a more specific diagnosis and to evaluate for complications of infection. A prompt and accurate diagnosis is important for timely management of the infection and to decrease the risk of potential complications, including limb loss, sepsis, and death.

9.3.6.1 Cellulitis and Abscess
Cellulitis is a superficial bacterial infection of the skin and subcutaneous fat commonly caused by beta hemolytic streptococci or *Staphylococcus aureus*. Clinical diagnosis is made based on the clinical features of skin erythema, warmth, swelling, and pain, often accompanied by fever and leukocytosis. Imaging can be helpful to evaluate for complicating features of cellulitis including abscess, deep soft-tissue infection, or osteomyelitis [69, 70].

Radiographs will demonstrate non-specific soft-tissue swelling and skin thickening. MRI and CT exams show skin thickening, subcutaneous fat edema, and reticulation. With intravenous contrast, there will be enhancement of the affected tissues, distinguishing cellulitis from edema related to congestive heart failure, volume overload, and lymphatic obstruction. If there is an associated abscess, MRI will show a fluid collection with central non-enhancement and irregular rim enhancement (Fig. 9.24). Ultrasound may show hypervascularity on color Doppler images and linear fluid outlining lobules of subcutaneous fat [71].

9.3.6.2 Osteomyelitis
Osteomyelitis is an infection of bone caused by direct extension from an adjacent wound/ulcer, penetrating trauma, or hematogenous spread [72]. Direct extension is more common in adults with a soft-tissue ulcer or cellulitis. Hematogenous spread is more common in children, starting at the metaphysis and spreading from the marrow to involve the adjacent cortical bone and soft tis-

sues. Delay in diagnosis can result in significant morbidity to the patient.

Radiographs are insensitive to acute osteomyelitis and commonly are normal or show only soft-tissue swelling. After several weeks, there typically will be radiographically evident bone destruction with periostitis and sclerosis [73]. Because of this delay in radiographic findings, if there is clinical concern for osteomyelitis despite negative radiographs, MRI should be recommended to evaluate for osteomyelitis and/or adjacent soft-tissue infection. On MRI, marrow edema with T1 signal hypointensity relative to skeletal muscle and water-sensitive sequence hyperintensity adjacent to infected soft tissues are characteristic of osteomyelitis (Fig. 9.25). With contrast administration, viability of soft tissues and bone can be evaluated. Non-enhancement suggests that surgical management in addition to antibiotic therapy will be needed [74–76].

9.3.6.3 Necrotizing Fasciitis
Necrotizing fasciitis is a rapidly progressive infection of the subcutaneous tissue and deep fascia with associated tissue necrosis, systemic toxicity, morbidity, and mortality. Diagnosis is typically made clinically with signs and symptoms including fever, systemic toxicity/sepsis, swelling, erythema, and soft-tissue gas formation leading to crepitus. Group A strep is the most frequently isolated pathogen, although polymicrobial infections are also common [77]. This is a surgical emergency, with early diagnosis leading to improved survival [78].

Imaging should not delay surgical management; however, emergent imaging is commonly performed as part of the evaluation of necrotizing fasciitis. Radiographs can show soft-tissue swelling and soft-tissue gas. CT may be done rapidly and with high sensitivity for detecting the proximal extent and location of gas in the soft tissues, and therefore aids in surgical planning (Fig. 9.26). MRI shows non-specific fascial thickening >3 mm, and edema with enhancement which decreases with progression of necrosis [79, 80]. Soft-tissue gas can be difficult to identify on MRI. In cases where gas is not present, the only imaging findings of
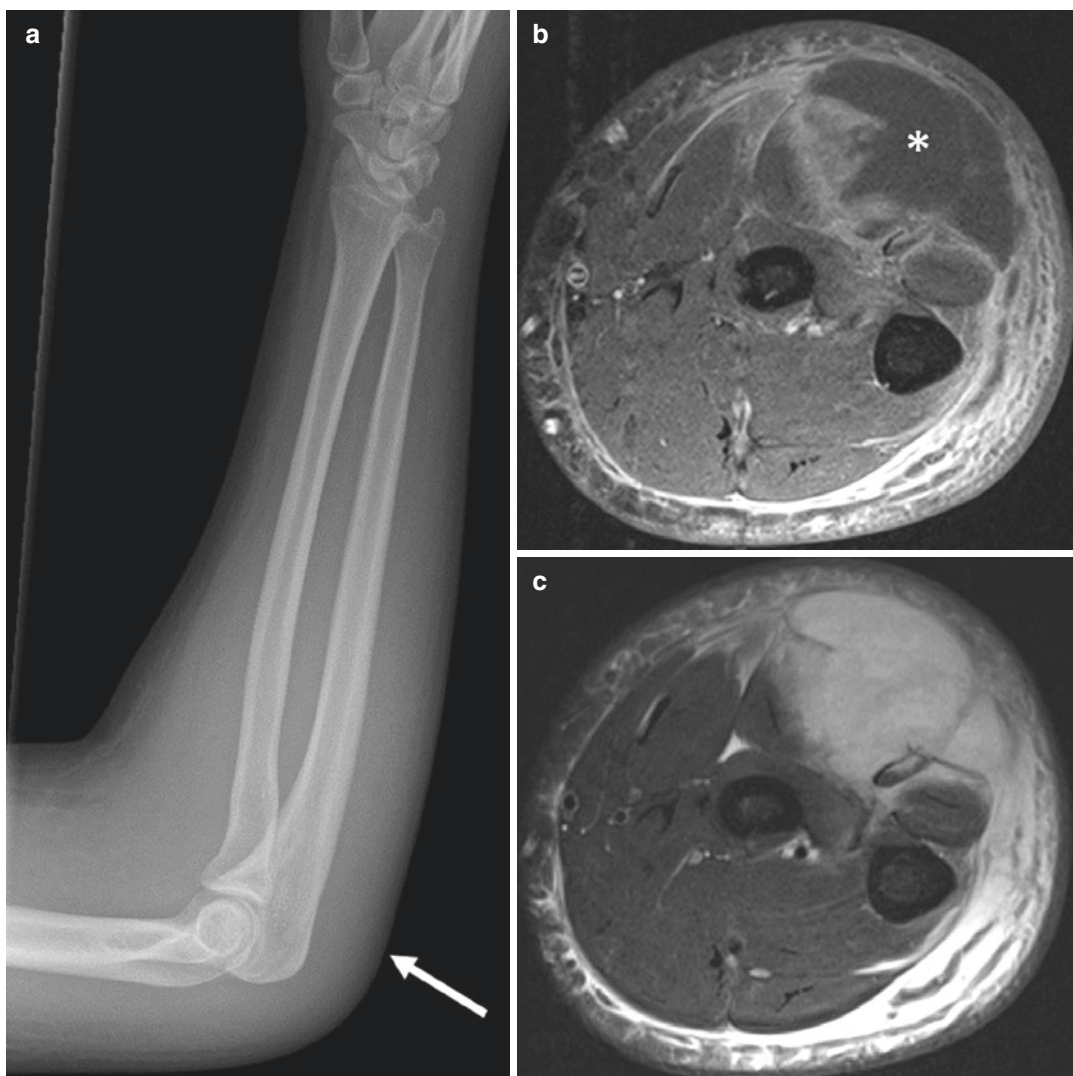
Fig. 9.24 Fifteen-year-old boy with forearm swelling and pain. Lateral radiograph of the forearm (**a**) with non-specific dorsal soft-tissue swelling. Axial T2-weighted fat-suppressed (**b**) and axial T1-weighted fat-suppressed post-contrast (**c**) MR images demonstrate thickened, edematous, and enhancing skin and subcutaneous tissues, consistent with cellulitis, and a non-enhancing collection involving the subcutaneous tissues and the extensor musculature of the forearm consistent with abscess. The patient underwent subsequent incision and drainage; polymicrobial flora grew from the surgical culture

necrotizing fasciitis may be skin thickening, sub-cutaneous edema, and fascial thickening.

9.3.6.4 Septic Arthritis

Septic arthritis is an infection of a joint caused by direct extension or hematologic spread. Predisposing factors include bacteremia, joint injection or surgery, joint prosthesis, direct extension, and an immunocompromised state. With septic arthritis in a native joint, early detection is important to avoid irreversible cartilage damage [81]. Joint pain, fever, elevated inflammatory markers, and elevated serum white blood cell count are commonly found.
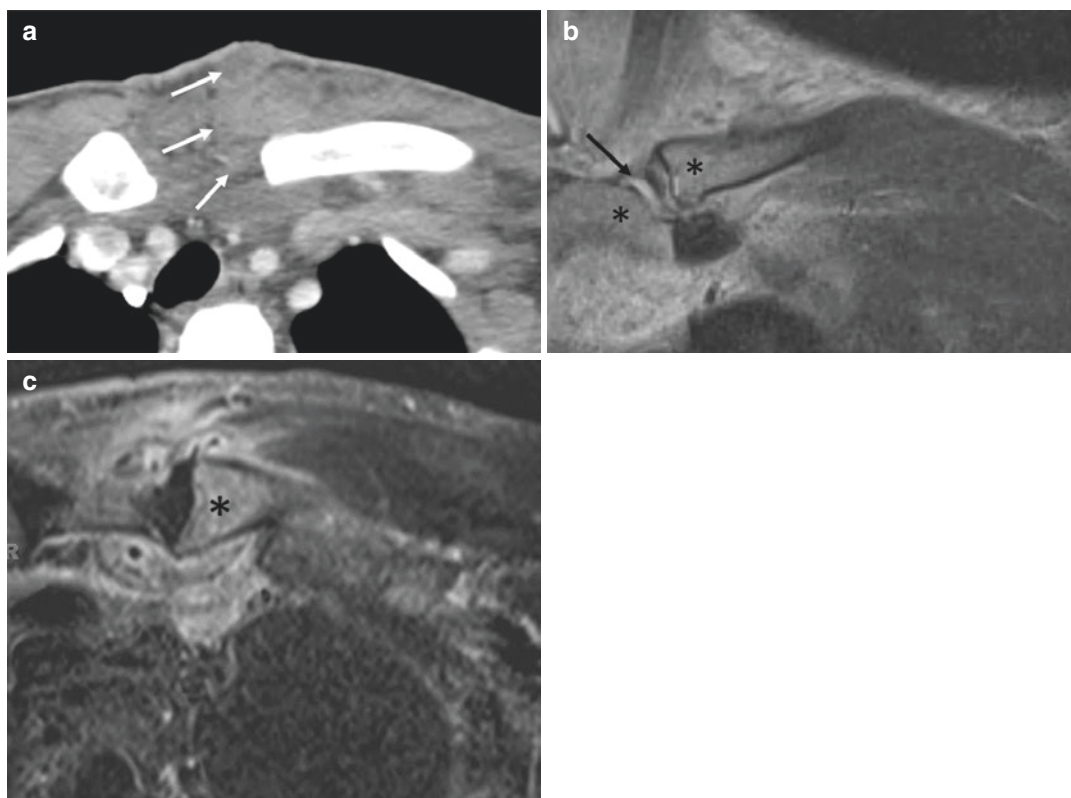
Fig. 9.25 Twenty-seven-year-old man who presented to the emergency department with acute left chest wall pain and swelling. Radiographs of the shoulder and chest were normal (not shown). (**a**) Transverse post-contrast CT image of the chest wall shows skin thickening, small subcutaneous abscess, and inflammation extending to the left sternoclavicular joint (white arrows). Coronal STIR (**b**) and transverse T1-weighted fat-suppressed post-contrast MR (**c**) images of the left chest wall show enhancing marrow edema in the medial clavicle (asterisks) and adjacent sternum, along with sternoclavicular joint fluid and synovitis (black arrow), consistent with septic arthritis and osteomyelitis. Cultures of the site grew methicillin-sensitive *S. aureus*, and the patient was managed with 6 weeks of intravenous antibiotics

If there is a strong clinical suspicion for septic arthritis, arthrocentesis is the diagnostic examination of choice. Initial radiographs may be normal, or there can be effusion and soft-tissue swelling. Later in the disease process, joint space narrowing and/or erosion of bone can be seen. On MRI, there is much overlap between infectious, inflammatory, and crystalline arthropathy. The many non-specific findings include effusion, pericapsular edema, uniform cartilage loss, bone erosions, bone marrow edema, and synovitis (Fig. 9.25) [82].

9.3.7 Non-infectious Typically Radiographically Occult Musculoskeletal Emergencies

9.3.7.1 Compartment Syndrome
Compartment syndrome is increased pressure within a non-distensible space or compartment contained by fascia that exceeds the tissue perfusion pressure [83]. Acute compartment syndrome is a surgical emergency, whereas chronic exertional compartment syndrome is transient and typically related to a specific athletic endeavor. Clinical
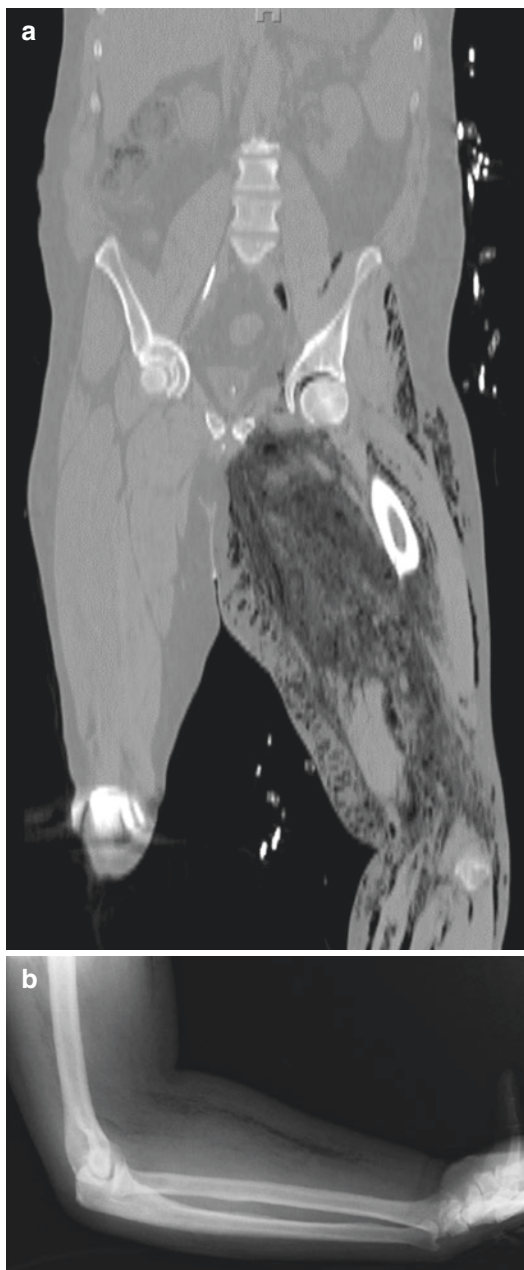
Fig. 9.26 Fifty-one-year-old man who presented with acute mental status changes and was found to have acute leukemia and multifocal *Clostridium septicum* necrotizing fasciitis and myositis. Coronal reformatted CT image of the thighs (**a**) shows extensive deep fascial and intramuscular gas in the left thigh involving all three compartments. Right forearm radiograph (**b**) with soft-tissue gas tracking within the anterior forearm along muscles and fascia. Unfortunately, the patient succumbed to his disease

findings of acute compartment syndrome include severe pain, dysfunction of sensory and motor nerves that pass through the affected compartment, and muscle ischemia/necrosis [83–85]. It most often develops following significant trauma, with fracture accounting for approximately 75% of patients. The most common sites are the leg and forearm. A higher degree of comminution is associated with increased risk of development [86]. Less often, acute compartment syndrome can occur following minor trauma or non-traumatic causes, including hematoma, burns, rhabdomyolysis, muscle hypertrophy, autoimmune vasculitis, and deep venous thrombosis [87].

If there is clinical concern for acute compartment syndrome, direct measures of intracompartmental pressure should be performed emergently, and if positive, fasciotomy should be performed. Rarely, patients who have acute compartment syndrome are imaged by MRI or CT to evaluate for a cause of pain in an extremity. MR imaging features include edema in the muscle and fascia on fluid-sensitive images, with enlargement of the affected muscles, bulging of the surrounding fascia, and decreased enhancement of the muscle (Fig. 9.27) [88, 89].

9.3.7.2 Foreign Body

Retained foreign bodies are commonly encountered in emergency medicine. A retained foreign body may result in soft-tissue infection or incite an inflammatory reaction to the material. Unrecognized retained foreign bodies are a leading cause of emergency medicine litigation [90].

In the emergency setting, radiographs are relatively sensitive, 80–95%, for evaluation of radiodense foreign bodies including metal and glass fragments [91]. However, many foreign bodies, including plastic, wood, and other vegetable material, are radiolucent and are therefore not detectable with radiographs. Ultrasound with a high-frequency probe (7.5 MHz or greater) has become more frequently used to detect superficial foreign bodies. All foreign bodies are initially hyperechoic, with many developing
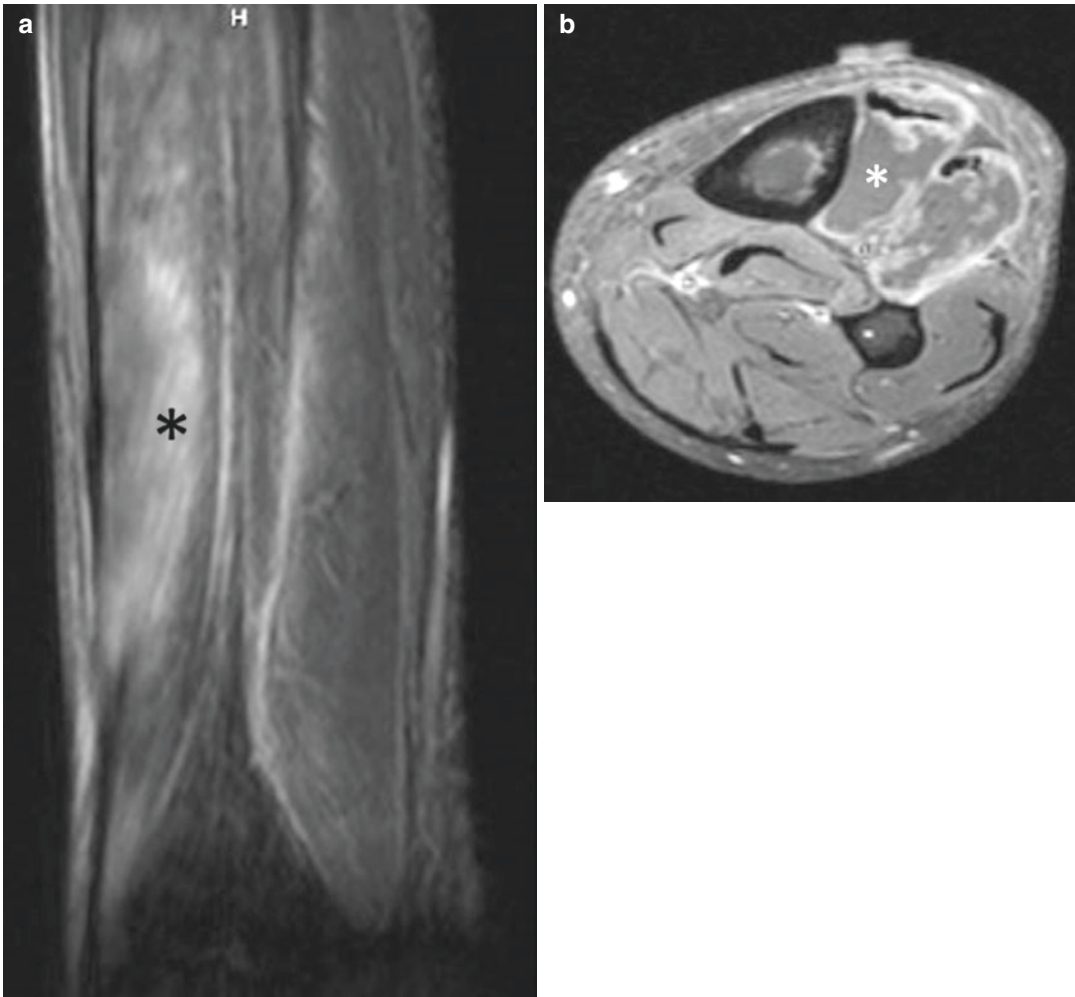
Fig. 9.27 Sixty-four-year-old man with acute onset atraumatic left leg pain with diminished distal pulses 2 days following spinal surgery. Sagittal STIR image of the left leg (**a**) shows edema and swelling in the anterior compartment musculature (asterisk). Transverse T1-weighted fat-suppressed post-contrast MR image (**b**) shows non-enhancement and bulging of the anterior compartment musculature, consistent with compartment syndrome and myonecrosis (asterisk). Elevated anterior compartment intracompartmental pressure was found with compartment pressure measurement, and the patient was managed with a fasciotomy and muscle debridement

a hypoechoic rim over time (Fig. 9.28). Wood products become less hyperechoic over time [92]. Sonographic artifacts related to the surface properties of the foreign body may improve detection and include dirty or clean shadowing and comet tail artifact. Using a standoff pad of gel can be helpful for shallow foreign bodies. Ultrasound can be used to guide removal of the foreign body or to mark the skin overlying the foreign body

for surgical exploration, if needed [93]. MRI and CT are also sometimes used to evaluate for a foreign body and to demonstrate signal intensity or attenuation differences, respectively, between the foreign body and the adjacent soft tissues.

9.3.7.3 Impending Pathologic Fracture

Metastases are the most common malignant tumor of bone. They commonly cause pain and

Fig. 9.28 Fifty-five-year-old woman with puncture wound to the volar right hand. In the emergency department, she had multiple foreign bodies removed and was placed on antibiotics. Three months later, she had a non-healing wound with purulent drainage. PA radiograph of the right hand (**a**) shows no radiopaque foreign body, and an old healed small finger proximal phalanx fracture. Ultrasound image of the volar right hand (**b**) shows a superficial linear hyperechoic foreign body with surrounding hypoechoic phlegmon or abscess. The patient underwent surgical foreign body removal and debridement, with resolution of symptoms

can cause pathologic fracture with associated decreased functional status and independence. The identification of lesions at risk for the development of pathologic fracture can be difficult. The Mirels classification has been used to diagnose impending pathologic fracture by evaluating multiple clinical and radiologic factors and assigning a score of 1–3 for each category. There are four categories: (1) location in the upper limb, lower limb, or peritrochanteric region; (2) cortical bone involvement divided in thirds; (3) bone metastasis described as lytic, blastic, or mixed; and (4) type of pain described as mild, moderate, or functional [94–96]. The highest possible score is 12, and the higher the score, the higher the risk of pathologic fracture.

In the emergency setting, radiographs will commonly demonstrate a non-specific focal abnormality of the bone but can offer information about the location, cortical bone involvement, and type of abnormality. Often cross-sectional imaging is needed to further characterize the degree of involvement of the cortical bone, as well as any associated soft-tissue extension beyond the bone or pathologic fracture (Fig. 9.29).

9.3.7.4 Stress Fractures

Stress fractures can be divided into fatigue fractures and insufficiency fractures. Fatigue fractures are abnormal stress on a normal bone, and insufficiency fractures are normal stress on an abnormal bone [97–99]. A common scenario for the development of a fatigue-type stress fracture would be a young athlete who has recently increased activity and now has foot pain. A common scenario for development of an insufficiency-type stress fracture would be an elderly osteoporotic woman on bisphosphonates chronically, with increasing proximal thigh pain. Early diagnosis is essential, as delayed recognition of bone stress injury may lead to fracture completion and the necessity of surgery rather than rest.

Initial radiographs are commonly normal or may show subtle sclerosis or an incomplete fracture line. MRI will show a T1 and T2 (or its equivalent) weighted sequence hypointense line with surrounding marrow edema (Fig. 9.30) [100].
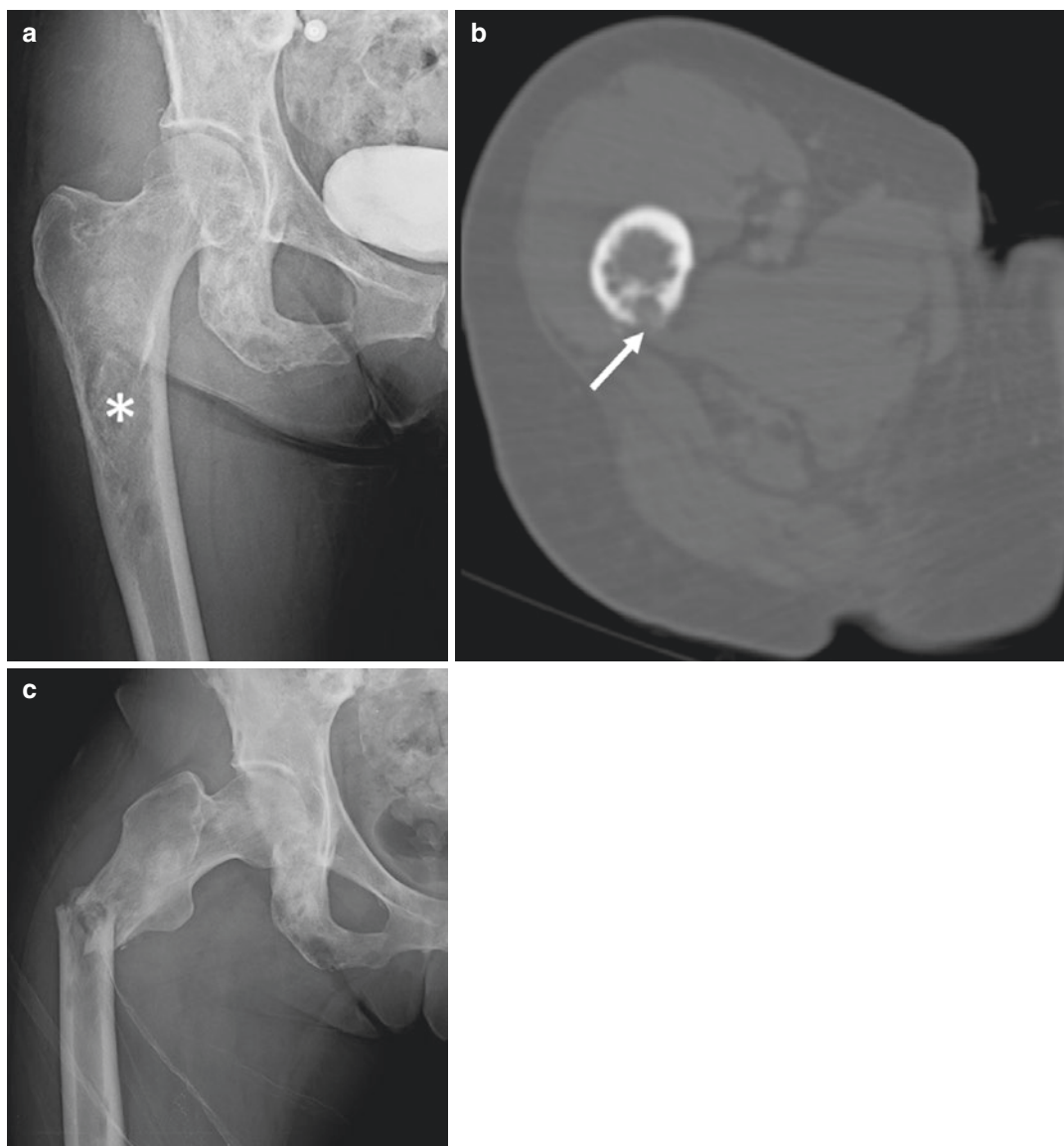
Fig. 9.29 Fifty-seven-year-old woman with metastatic breast cancer and right hip pain. Right hip radiograph (**a**) shows a permeative lytic focus centered in the subtrochanteric right femur and diffuse pelvic metastases (Mirel score >9). CT image (**b**) from a staging CT shows this finding is associated with cortical destruction and is at risk for development of pathologic fracture. (**c**) Right hip radiograph 4 days later with pathologic fracture through the subtrochanteric lytic focus following minimal trauma. Her fracture was managed with intramedullary nail fixation
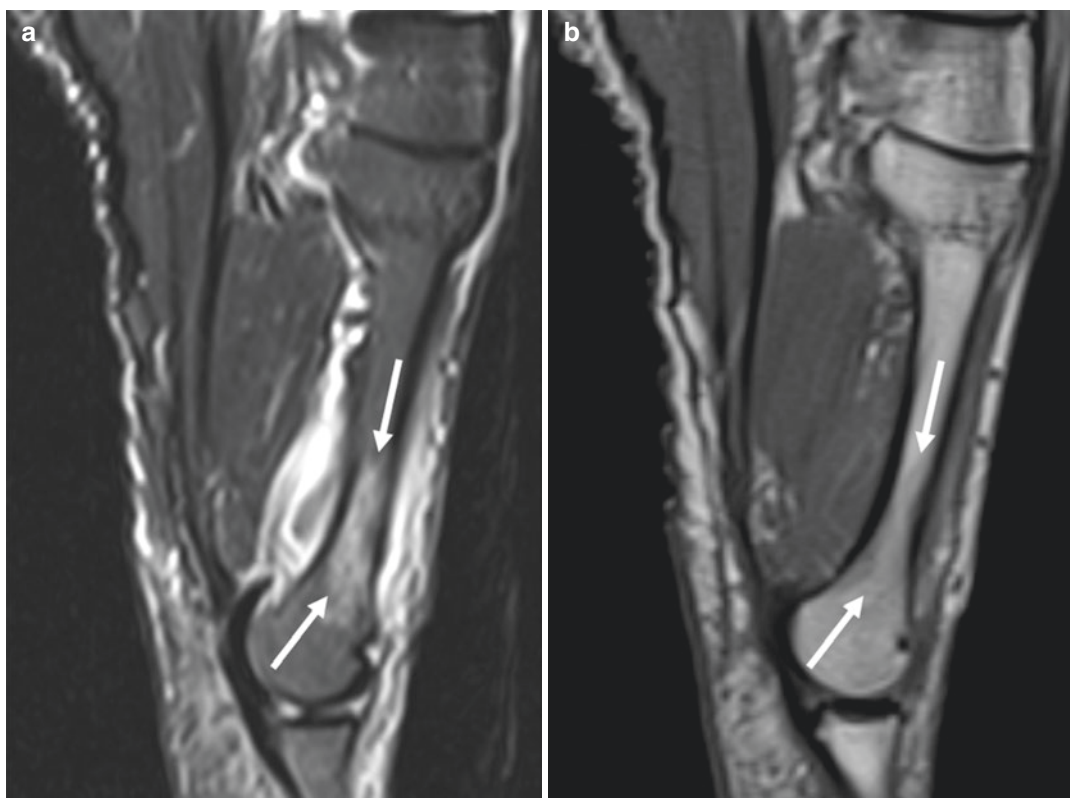
Fig. 9.30 Forty-two-year-old woman runner with increasing right foot pain at the distal second metatarsal. Radiographs are normal. Sagittal STIR (**a**) and T1-weighted (**b**) images of the second metatarsal show marrow edema, periostitis, and mild cortical thickening in the distal metatarsal. Her foot pain resolved with a period of rest

9.4   Conclusion

There are many traumatic and non-traumatic musculoskeletal pathologies encountered in the emergency department. Many of the pathologies are evident to the clinician caring directly for the patient and the emergency department radiologist interpreting the initial radiographic examination. In patients where the diagnosis is not evident, the emergency department radiologist plays an important role in the diagnosis of subtle pathology and as a consultant who recommends the best imaging modality (and the specific use of that modality) for further evaluation of an initially demonstrated or suspected pathology.

References

1. Florschutz AV, Langford JR, Haidukewych GJ, Koval KJ. Femoral neck fractures: current management. J Orthop Trauma. 2015;29:121–9.
2. Sheehan SE, Shyu JY, Weaver MJ, Sodickson AD, Khurana B. Proximal femoral fractures: what the orthopedic surgeon wants to know. Radiographics. 2015;5:1563–84.
3. Parker MJ. Missed hip fractures. Arch Emerg Med. 1992;9:23–7.
4. Ha AS, Porrino JA, Chew FS. Radiographic pitfalls in lower extremity trauma. Am J Roentgenol. 2014;203:492–500.
5. Kirby MW, Spritzer C. Radiographic detection of hip and pelvic fractures in the emergency department. Am J Roentgenol. 2010;194:1054–60.
6. Deutsch AL, Mink JH, Waxman AD. Occult fractures of the proximal femur: MR imaging. Radiology. 1989;170:113–6.

7. Ward RJ, Weissman BN, Kransdorf MJ, et al. ACR appropriateness criteria acute hip pain-suspected fracture. J Am Coll Radiol. 2014;11:114–20.

8. Mlinek EJ, Clark KC, Walker CW. Limited magnetic resonance imaging in the diagnosis of occult hip fractures. Am J Emerg Med. 1998;16:390–2.

9. Khurana B, Okanobo H, Ossiani M, Ledbetter S, Al Dulaimy K, Sodickson A. Abbreviated MRI for patients presenting to the emergency department with hip pain. Am J Roentgenol. 2012;198:W581–8.

10. Hakkarinen DK, Banh KV, Hendey GW. Magnetic resonance imaging identifies occult hip fractures missed by 64-slice computed tomography. J Emerg Med. 2012;43:303–7.

11. Mandell JC, Weaver MJ, Khurana B. Computed tomography for occult fractures of the proximal femur, pelvis, and sacrum in clinical practice: single institution, dual-site experience. Emerg Radiol. 2018;25:265–73.

12. Feldman F, Staron RB. MRI of seemingly isolated greater trochanteric fractures. Am J Roentgenol. 2004;183:323–9.

13. LaLonde B, Fenton P, Campbell A, Wilson P, Yen D. Immediate weight-bearing in suspected isolated greater trochanter fractures as delineated on MRI. Iowa Orthop J. 2010;30:201–4.

14. Matcuk GR, Mahanty SR, Skalski MR, Patel DB, White EA, Gottsegen CJ. Stress fractures: pathophysiology, clinical presentation, imaging features, and treatment options. Emerg Radiol. 2016;23:365–75.

15. Pierce JL, McCrum EC, Rozas AK, Hrelic DM, Anderson MW. Tip-of-the-iceberg fractures: small fractures that mean big trouble. Am J Roentgenol. 2015;205:524–32.

16. Jarraya M, Diaz LE, Arndt WF, Roemer FW, Guermazi A. Imaging of patellar fractures. Insights Imaging. 2017;8:49–57.

17. Ostlere S. The extensor mechanism of the knee. Radiol Clin N Am. 2013;51:391–411.

18. Badillo K, Pacheco JA, Padua SO, Gomez AA, Colon E, Vidal JA. Radiographics. 2011;31:81–92.

19. Friedman MV, Chris S, Baker JC, Hillen TJ. Review of supplemental views and stress radiography in musculoskeletal trauma: lower extremity. Emerg Radiol. 2015;22:589–94.

20. Walter WR, Hirschmann A, Garwood ER, Rosenberg ZS. MRI evaluation of midtarsal (Chopart) sprain in the setting of acute ankle injury. Am J Roentgenol. 2018;210:386–95.

21. Kalia V, Fishman EK, Carrino JA, Fayad LM. Epidemiology, imaging, and treatment of Lisfranc fracture-dislocations revisited. Skelet Radiol. 2012;41:129–36.

22. Garretson RB, Williams GR. Clinical evaluation of injuries to the acromioclavicular and sternoclavicular joints. Clin Sport Med. 2003;22:239–54.

23. Morell DJ, Thyagarajan DS. Sternoclavicular joint dislocation and its management: a review of the literature. World J Orthop. 2016;7:244.

24. Salgado RA, Ghysen D. Post-traumatic posterior sternoclavicular dislocation: case report and review of the literature. Emerg Radiol. 2002;9:323–5.

25. Restrepo CS, Martinez S, Lemos DF, et al. Imaging appearances of the sternum and sternoclavicular joints. Radiographics. 2009;29:839–59.

26. Friedman MV, Smith C, Hillen TJ, Baker JC. Review of supplemental views and stress radiography in musculoskeletal trauma: upper extremity. Emerg Radiol. 2015;22:583–8.

27. Rockwood CA. Dislocations of the sternoclavicular joint. In: Evans E, editor. American academy of orthopaedic surgeons instructional course lectures: volume XXIV. St. Louis, MO: CV Mosby; 1975. p. 144–59.

28. Mazzocca AD, Arciero RA, Bicos J. Evaluation and treatment of acromioclavicular joint injuries. Am J Sports Med. 2007;35:316–29.

29. Rockwood CA, Williams GR, Young DC. Acromioclavicular injuries. In: Rockwood CA, Green DP, Bucholz RW, Heckman JD, editors. Fractures in adults, 4th ed., vol. I. Philadelphia, PA: Lippincott-Raven; 1996. p. 1341–413.

30. Lafferty PM, Min W, Tejwani NC. Stress radiographics in orthopaedic surgery. J Am Acad Orthop Surg. 2009;17:528–39.

31. Kim AC, Matcuk G, Patel D, Itamura J, Forrester D, White E, Gottsegen CJ. Acromioclavicular joint injuries and reconstructions: a review of expected imaging findings and potential complications. Emerg Radiol. 2012;19:399–413.

32. Marinček B, Dondelinger RF. Emergency radiology, imaging and intervention. Berlin: Springer Verlag; 2007. p. 254–6.

33. Sheehan SE, Gaviola G, Gordon R, Sacks A, Shi LL, Smith SE. Traumatic shoulder injuries: a force mechanism analysis–glenohumeral dislocation and instability. Am J Roentgenol. 2013;201:378–93.

34. Kralinger FS, Golser K, Wischatta R, Wambacher M, Sperner G. Predicting recurrence after primary anterior shoulder dislocation. Am J Sports Med. 2002;30:116–20.

35. Rozing PM, De Bakker HM, Obermann WR. Radiographic views in recurrent anterior shoulder dislocation. Comparison of six methods for identification of typical lesions. Acta Orthop Scand. 1986;57:328–30.

36. Sandstrom CK, Kennedy SA, Gross JA. Acute shoulder trauma: what the surgeon wants to know. Radiographics. 2015;35:475–92.

37. Hawkins RJ, Neer CS 2nd, Pianta RM, Mendoza FX. Locked posterior dislocation of the shoulder. J Bone Joint Surg Am. 1987;69(1):9–18.

38. Cisternino SJ, Rogers LF, Stufflebam BC, Kruglik GD. The trough line: a radiographic sign of posterior shoulder dislocation. Am J Roentgenol. 1978;130:951–4.

39. Cole PA, Freeman G, Dubin JR. Scapula fractures. Curr Rev Musculoskelet Med. 2013;6:79–87.

40. Baldwin KD, Ohman-Strickland P, Mehta S, Hume E. Scapula fractures: a marker for concomitant injury? A retrospective review of data in the National Trauma Database. J Trauma. 2008;65:430–5.

41. Ropp AM, Davis DL. Scapular fractures: what radiologists need to know. Am J Roentgenol. 2015;205:491–501.

42. Herrera DA, Anavian J, Tarkin IS, Armitage BA, Schroder LK, Cole PA. Delayed operative management of fractures of the scapula. J Bone Joint Surg Br. 2009;91:619–26.

43. Gyftopoulos S, Chitkara M, Bencardino JT. Misses and errors in upper extremity trauma radiographs. Am J Roentgenol. 2014;203:477–91.

44. Tadros AM, Lunsjo K, Czechowski J, Corr P, Abu-Zidan FM. Usefulness of different imaging modalities in the assessment of scapular fractures caused by blunt trauma. Acta Radiol. 2007;48:71–5.

45. Goss TP, Owens BD. Fractures of the scapula. In: Rockwood Jr CA, Matsen III FA, Wirth MA, Lippitt SB, editors. The shoulder. 4th ed. Philadelphia, PA: Saunders Elsevier; 2009. p. 333–5.

46. Ideberg R, Grevsten S, Larsson S. Epidemiology of scapular fractures: incidence and classification of 338 fractures. Acta Orthop Scand. 1995;66:395–7.

47. Nork SE, Barei DP, Gardner MJ, Schildhauer TA, Mayo KA, Benirschke SK. Surgical exposure and fixation of displaced type IV, V, and VI glenoid fractures. J Orthop Trauma. 2008;22:487–93.

48. Nordqvist A, Petersson C. Fracture of the body, neck, or spine of the scapula: a long-term follow-up study. Clin Orthop Relat Res. 1992;283:139–44.

49. Ogawa K, Matsumura N, Ikegami H. Coracoid fractures: therapeutic strategy and surgical outcomes. J Trauma Acute Care Surg. 2012;72:E20–6.

50. Eyres KS, Brooks A, Stanley D. Fractures of the coracoid process. J Bone Joint Surg Br. 1995;77:425–8.

51. Ogawa K, Naniwa T. Fractures of the acromion and the lateral scapular spine. J Shoulder Elb Surg. 1997;6:544–8.

52. Kuhn JE, Blasier RB, Carpenter JE. Fractures of the acromion process: a proposed classification system. J Orthop Trauma. 1994;8:6–13.

53. Ogawa K, Yoshida A, Ikegami H. Isolated fractures of the greater tuberosity of the humerus: solutions to recognizing a frequently overlooked fracture. J Trauma. 2003;54:713–7.

54. Mattyasovszky SG, Burkhart KJ, Ahlers C, et al. Isolated fractures of the greater tuberosity of the proximal humerus: a long-term retrospective study of 30 patients. Acta Orthop. 2011;82:714–20.

55. Pitts SR, Niska RW, Xu J, Burt CW. National Hospital Ambulatory Medical Care Survey: 2006 emergency department summary. Natl Health Stat Report. 2008;7:1–38.

56. Struijs PA, Smit G, Steller EP. Radial head fractures: effectiveness of conservative treatment versus surgical intervention. A systematic review. Arch Orthop Trauma Surg. 2007;127:125–30.

57. Greenspan A, Norman A, Rosen H. Radial head-capitellum view in elbow trauma: clinical application and radiographic-anatomic correlation. Am J Roentgenol. 1984;143:355–9.

58. Doornberg JN, Ring D. Coronoid fracture patterns. J Hand Surg Am. 2006;31:45–52.

59. Bobyns JH, Linscheid RL. Fractures and dislocations of the wrist. In: Rockwood Jr CA, Green DP, editors. Fractures in adults. 3rd ed. Philadelphia, PA: Lippincott; 1984. p. 411–509.

60. Gelberman RH, Wolock BS, Siegel DB. Fractures and non-unions of the carpal scaphoid. J Bone Joint Surg Am. 1989;71:1560–5.

61. Bryan RS, Dobyns JH. Fractures of the carpal bones other than lunate and navicular. Clin Orthop Relat Res. 1980;149:107–11.

62. Cohen MS. Fractures of the carpal bones. Hand Clin. 1997;13:587–99.

63. Bain GI, McLean JM, Turner PC, Sood A, Pourgiezis N. Translunate fracture with associated perilunate injury: 3 case reports with introduction of the translunate arc concept. J Hand Surg Am. 2008;33:1770–6.

64. Mayfield JK. Mechanism of carpal injuries. Clin Orthop. 1980;149:45–54.

65. Mayfield JK. Patterns of injury to carpal ligaments. Clin Orthop. 1984;187:36–42.

66. Mayfield JK, Johnson RP, Kilcoyne RK. Carpal dislocations: pathomechanics and progressive perilunar instability. J Hand Surg Am. 1980;5:226–41.

67. Kitay A, Wolfe SW. Scapholunate instability: current concepts in diagnosis and management. J Hand Surg Am. 2012;37:2175–96.

68. Turecki MB, Taljanovic MS, Stubbs AY, et al. Imaging of musculoskeletal soft tissue infections. Skelet Radiol. 2010;39:957–71.

69. Rahmouni A, Chosidow O, Mathieu D, et al. MR imaging in acute infectious cellulitis. Radiology. 1994;192:493–6.

70. Schmid MR, Kossmann T, Duewell S. Differentiation of necrotizing fasciitis and cellulitis using MR imaging. Am J Roentgenol. 1998;170:615–20.

71. Loyer EM, DuBrow RA, David CL, et al. Imaging of superficial soft-tissue infections: Sonographic findings in cases of cellulitis and abscess. Am J Roentgenol. 1996;166:149–52.

72. Waldvogel FA, Medoff G, Swartz MN. Osteomyelitis: a review of clinical features, therapeutic considerations and unusual aspects. N Engl J Med. 1970;282:198–206.

73. Wheat J. Diagnostic strategies in osteomyelitis. Am J Med. 1985;78:218–24.

74. Baker JC, Hillen TJ, Demertzis JL. The role of imaging in musculoskeletal emergencies. Semin Roentgenol. 2014;49:169–85.

75. Morrison WB, Schweitzer ME, Bock GW, et al. Diagnosis of osteomyelitis: utility of fat suppressed contrast-enhanced MR imaging. Radiology. 1993;189:251–7.

76. Craig JG, Amin MB, Wu K, et al. Osteomyelitis of the diabetic foot: MR imaging-pathologic correlation. Radiology. 1993;203:849–55.
77. Torralba KD, Quismorio FP. Soft tissue infections. Rheum Dis Clin N Am. 2009;35:45–62.
78. Voros D, Pissiotis C, Georgantas D, et al. Role of early and extensive surgery in the treatment of severe necrotizing soft tissue infections. Br J Surg. 1993;80:1190–1.
79. Kim KT, Kim YJ, Won Lee J, et al. Can necrotizing infectious fasciitis be differentiated from nonnecrotizing infectious fasciitis with MR imaging? Radiology. 2011;259:816–24.
80. Fugitt JB, Puckett ML, Quigley MM, et al. Necrotizing fasciitis. Radiographics. 2004;24:1472–6.
81. Learch TJ, Farooki S. Magnetic resonance imaging of septic arthritis. Clin Imaging. 2000;24:236–42.
82. Karchevsky M, Schweitzer ME, Morrison WB, et al. MRI findings of septic arthritis and associated osteomyelitis in adults. Am J Roentgenol. 2004;182:119–22.
83. Elliott KG, Johnstone AJ. Diagnosing acute compartment syndrome. J Bone Joint Surg Br. 2003;85:625–32.
84. Olson SA, Glasgow RR. Acute compartment syndrome in lower extremity musculoskeletal trauma. J Am Acad Orthop Surg. 2005;13:436–44.
85. Shadgan B, Menon M, O'Brien PJ, Reid WD. Diagnostic techniques in acute compartment syndrome of the leg. J Orthop Trauma. 2008;22:581–7.
86. Patel RV, Haddad FS. Compartment syndromes. Br J Hosp Med (Lond). 2005;66:583–6.
87. Mubarak SJ, Hargens AR. Acute compartment syndromes. Surg Clin North Am. 1983;63:539–65.
88. May DA, Disler DG, Jones EA, et al. Abnormal signal intensity in skeletal muscle at MR imaging: patterns, pearls, and pitfalls. Radiographics. 2000;20:S295–315.
89. Baker JC, Demertzis JD, Rhodes NG, et al. Diabetic musculoskeletal complications their imaging mimics. Radiographics. 2012;32:1959–74.
90. Schlager D. Ultrasound detection of foreign bodies and procedure guidance. Emerg Med Clin North Am. 1997;15:895–912.
91. Blankenship RB, Baker T. Imaging modalities in wounds and superficial skin infections. Emerg Med Clin North Am. 2007;25:223–34.
92. Jacobson JA, Powell A, Craig JG, et al. Wooden foreign bodies in soft tissue: detection at US. Radiology. 1998;206:45–8.
93. Young AS, Shiels WE II, Murakami JW, et al. Self-embedding behavior: radiologic management of self-inserted soft-tissue foreign bodies. Radiology. 2010;257:233–9.
94. Mirels H. Metastatic disease in long bones: a proposed scoring system for diagnosing impending pathologic fractures. Clin Orthop Relat Res. 1989;249:256–64.
95. Jawad MU, Scully SP. In brief: classifications in brief: Mirels' classification: metastatic disease in long bones and impending pathologic fracture. Clin Orthop Relat Res. 2010;468:2825–7.
96. Damron TA, Morgan H, Prakash D, et al. Critical evaluation of Mirels' rating system for impending pathologic fractures. Clin Orthop Relat Res. 2003;415(suppl):S201–7.
97. Kompel A, Murakami A, Guermazi A. Magnetic resonance imaging of nontraumatic musculoskeletal emergencies. Magn Reson Imaging Clin N Am. 2016;24:369–89.
98. Daffner RH. Stress fractures: current concepts. Skelet Radiol. 1978;2:221–9.
99. Porrino JA, Kohl CA, Taljanovic M, et al. Diagnosis of proximal femoral insufficiency fractures in patients receiving bisphosphonate therapy. Am J Roentgenol. 2010;194:1061–4.
100. Umans HR, Kaye JJ. Longitudinal stress fractures of the tibia: diagnosis by magnetic resonance imaging. Skelet Radiol. 1996;25:319–24.

Mistakes in Emergency Imaging of Pregnant Patients

10

Gabriele Masselli and Martina Derme

10.1 Introduction

Radiologists play an important role in the diagnostic assessment of patients in the emergency setting. The imaging literature states that there is a daily risk of radiologic mistakes of approximately 4% [1]. Diagnostic errors are responsible for approximately 10–15% of preventable deaths in trauma center audits, for example [2].

Errors in medical imaging can be classified as follows: (1) observer errors, (2) errors in interpretation, (3) failure to suggest the next appropriate procedure, and (4) failure to communicate in a timely and clinically appropriate manner [3]. Errors of interpretation are the most frequent. Limited clinical information, advanced age, high injury severity, and multiplicity of injury all increase the likelihood of major errors [3].

An acute abdomen in pregnancy represents one of the most challenging diagnostic and therapeutic dilemmas in the emergency setting. The difficulty is due to the anatomical and pathophys-

iological changes related to pregnancy, including the different locations of the abdominal and pelvic structures, displaced by the uterus and adnexae, altered laboratory tests, difficult abdominal and pelvic physical examination, and patient signs and symptoms which are frequently nonspecific. Many factors need to be considered in the management of pregnant women in the emergency setting. First, physicians and other clinicians have to choose the appropriate imaging technique in order to avoid, as much as possible, the use of ionizing radiation to the fetus. Ultrasound (US) is widely considered to be the first imaging examination that should be performed. It is widely and readily available, is inexpensive, and is free of ionizing radiation [1]. However, its accuracy is greater in the first trimester, but decreases in the second and third trimesters, making it necessary to use alternative imaging techniques, including magnetic resonance imaging (MRI) and, if necessary, computed tomography (CT). MRI is preferable to avoid ionizing radiation; no contraindications are reported in the American College of Radiology guidelines on MRI safe practice. The decision to administer IV gadolinium should be based on an individual risk-benefit analysis [1].

The systemization of errors reduces the possibility of recurrence in the future, by providing a valid approach help to learn from these errors.

G. Masselli (✉)
Radiology Dea Department, Umberto I Hospital, Sapienza University of Rome, Rome, Italy
e-mail: gabriele.masselli@uniroma1.it; g.masselli@policlinicoumberto1.it

M. Derme
Department of Gynaecological, Obstetrical and Urological Sciences, Umberto I Hospital, Sapienza University of Rome, Rome, Italy
e-mail: martina.derme@uniroma1.it

10.2 Gynecologic Causes

10.2.1 Ovarian Torsion

Ovarian torsion during pregnancy is a rare event, with a reported incidence of 1–10 per 10,000 spontaneous pregnancies. The highest risk of ovarian torsion is during the first trimester [4].

Torsion of the ovarian tissue on its pedicle leads to reduced venous return, stromal edema, internal hemorrhage, and then infarction. This condition can occur at any age, more frequently (70–80%) during reproductive age. Many cases of ovarian torsion are associated with a preexistent ovarian mass.

Risk factors include a mass size of 5 cm or larger, a benign mass, ovarian hyperstimulation, and pregnancy [5].

The diagnosis must always be suspected when an ovarian mass is found in a woman with severe, localized, or radiating abdominal or pelvic pain, nausea, and/or vomiting. Fever and a minimally increased serum white blood cell count may be present. A timely and correct diagnosis is fundamental.

The first required imaging examination is transvaginal US. US findings include an enlarged ovary with multiple peripherally located follicles, a twisted vascular pedicle (the "whirlpool sign"), and free pelvic fluid. Normal Doppler flow can be observed in 45–61% of all ovarian torsion cases [6]. The absence of both arterial and venous flow in the twisted pedicle is highly suggestive of a definitive diagnosis and can lead to ischemia and necrosis. The fallopian tube can appear as an oblong or fusiform structure close to the ovary with inhomogeneous echogenicity, and absent or decreased color Doppler flow, depending on the number of turns of the torsion.

MRI has a role if US is not diagnostic. Asymmetric enlargement of the ovary and stromal edema are well demonstrated by MRI, especially using T2-weighted sequences. Ovarian hemorrhage can be identified using T1-weighted sequences [5]. Fat-saturated sequences can help in evaluating some conditions, such as hemoperitoneum and a possible underlying ovarian mass on MRI. The use of IV contrast is helpful in the diagnosis of ovarian infarction [1] (Fig. 10.1).

In some patients, it may be necessary to perform a CT in emergency situations, such as when there is large amount of hemoperitoneum in the borderline stable patient.

Early diagnosis and subsequent laparoscopic management are needed to optimize maternal and fetal outcomes.

Many conditions can mimic an ovarian torsion clinically, representing possible pitfalls, and need to be differentiated from it, including hemorrhagic cysts, ovarian hyperstimulation syndrome (OHSS), endometriosis and endometritis, pelvic inflammatory disease, adhesions, and appendicitis. US exam and MRI help to make the correct diagnosis.
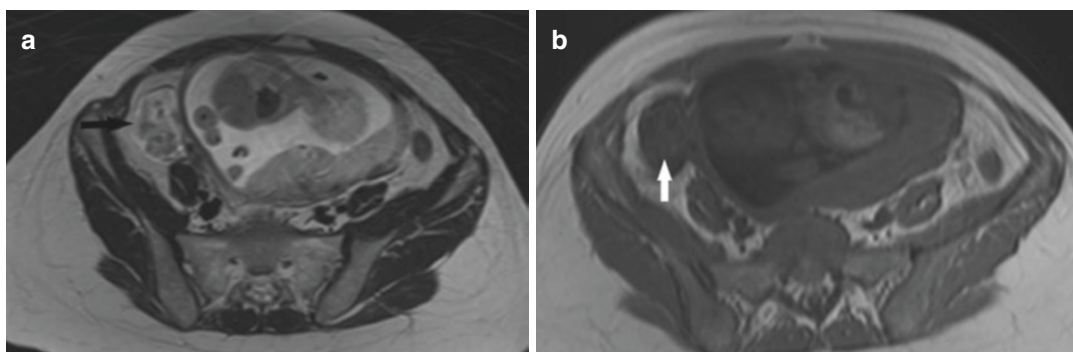

Fig. 10.1 Ovarian torsion in a 30-year-old woman at gestational week 27 with acute pelvic pain. Axial (**a**) T2-weighted HASTE image shows an enlarged, edematous right ovary (black arrow). Axial T1-weighted MR image (**b**) shows areas of increased signal intensity (white arrow) within the right ovary, indicating hemorrhagic infarction

10.2.2 Fibroids (Leiomyomas)

Fibroids (leiomyomas) are the most common pelvic tumors in women. It is estimated that 60% of all reproductive-aged women are affected. Fibroids have a prevalence during pregnancy of up to 20%. They have been associated with a variety of obstetric complications, including spontaneous abortion, fetal malpresentation, intrauterine growth restriction, placenta previa, labor dystocia, retained placenta, preterm labor, premature rupture of membranes, postpartum hemorrhage, and an increased frequency of cesarean section [7].

Fibroids are often asymptomatic. Commonly reported symptoms include heavy menstrual bleeding, dysmenorrhea, noncyclic pain, urinary symptoms, fatigue, and constipation [8].

US is usually used for initial diagnosis. Fibroids appear on US with hypoechoic, isoechoic, hyperechoic, and mixed echo patterns. Uncomplicated fibroids are mostly hypoechoic, but can be isoechoic or hyperechoic compared to normal myometrium [9]. In acute hemorrhagic infarction (red degeneration), US shows heterogeneous or hyperechoic masses and later anechoic components resulting from cystic necrosis. In patients with associated fibroid torsion, Doppler flow is absent.

MR imaging is the most accurate imaging technique for the detection and localization of fibroids, especially when located deep in the pelvis or in the posterior myometrium, and for differential diagnosis from other pelvic masses. Exophytic fibroids can simulate ovarian masses at US, representing the main diagnostic pitfalls. On T2-weighted images, non-degenerated leiomyomas appear as well-circumscribed masses of decreased signal intensity. Leiomyomas with hemorrhagic degeneration often exhibit diffuse or peripheral high signal intensity on T1-weighted imaging and variable signal intensity on T2-weighted imaging [5] (Fig. 10.2).

Conservative therapy is the first option to be considered. Myomectomy may be performed in selected patients, presenting with symptomatic
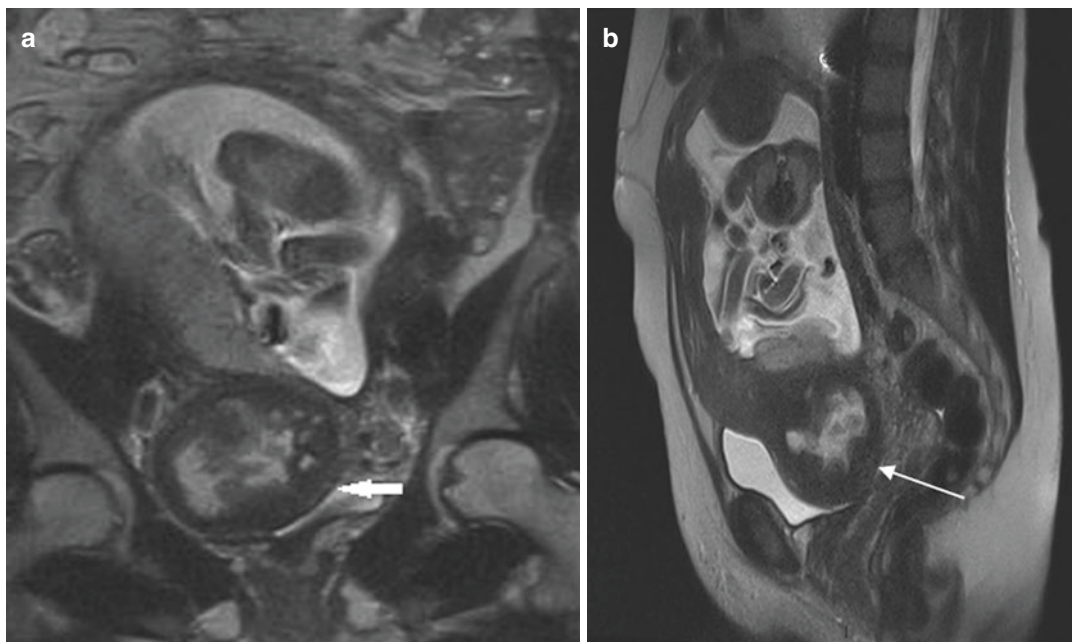
Fig. 10.2 Degenerated leiomyoma in a 28-year-old woman at gestational week 25 with acute pelvic pain. Coronal (**a**) and sagittal (**b**) T2-weighted images show a well-circumscribed uterine mass with variable signal intensity (arrow). The fibroid shows a diameter of 5 cm, with areas of increased internal signal intensity consistent with degeneration

subserosal or pedunculated leiomyomas with signs of degeneration, after the failure of initial conservative treatment, with low perioperative and postoperative morbidity.

10.2.3 Adnexal Masses

The incidence of adnexal masses during pregnancy is approximately 1% [5]. Common adnexal masses include simple cysts, hemorrhagic cysts, and hyperstimulated ovaries in patients who have undergone fertility assistance therapy. Their characterization represents a diagnostic challenge, and it is of great importance in the preoperative setting, in order to plan adequate therapeutic procedures.

Lower abdominal pain is the most common symptom. Ovarian cyst torsion or rupture may require emergency surgery after a correct differential diagnosis from other possible causes of abdominal/pelvic pain.

On imaging the differential diagnosis for the adnexal masses includes ovarian torsion and uterine pedunculated myoma, which represent the main diagnostic pitfalls.

US is the examination of choice for primary evaluation of adnexal masses. Morphological features suggestive of malignancy include thickness (>2–3 mm) and irregularity of walls and septa, the presence of solid areas and papillary projections, as well as other evidence of malignant activity, namely, ascites, peritoneal nodules, and other metastatic foci. Color Doppler is able to demonstrate both the presence and the localization of new tumor blood vessels. A predominantly central blood flow is more often associated with malignancy, while a peripheral one is more typical of a benign mass [10].

MRI is an essential problem-solving tool to determine the site of origin of a pelvic mass, and then to characterize an adnexal mass, especially in patients with indeterminate masses. MRI has been shown to be more specific and accurate than US and Doppler assessment in the diagnosis and characterization of adnexal masses, with an accuracy ranging from 83% to 89%, compared with 63% for sonography [11]. In order to obtain anatomic information and to study morphological and signal intensity characteristics of the mass, both T1- and T2-weighted MR sequences are needed. Fat-saturated T1-weighted images are helpful to detect hemorrhagic areas and fat tissue. The use of intravenous gadolinium improves detection of enhancing septa and solid components within the mass and of peritoneal and omental implants [10] (Figs. 10.3 and 10.4).

Most ovarian masses diagnosed in pregnancy are benign and resolve spontaneously. Surgical management is warranted when masses are suspicious for malignancy, at risk for torsion, or are clinically symptomatic. With increasing numbers of successful laparoscopic procedures reported in pregnancy, laparoscopy seems to be a safe option with trained and experienced providers.

10.3 Obstetric Causes

10.3.1 Uterine Rupture

Uterine rupture is one of the most serious obstetric complications, characterized by a breach in the uterine wall and the overlying serosa. The incidence of spontaneous uterine rupture in a previously intact uterus is approximately 1 in 15,000 [12]. It often occurs during labor or third trimester of pregnancy. The most important predisposing factor is the presence of a uterine scar due to previous surgery for cesarean deliveries, myomectomy, and congenital uterine malformations. The most common symptom is abdominal/pelvic pain.

In case of intrapartum ruptures, US shows the presence of the fetus and placenta in the peritoneal cavity, free intraperitoneal fluid, and a bulky empty uterus with an anterior tear seen as a hypo- or anechogenic scar [1]. US can help in predicting an impending uterine rupture, by demonstrating a uterine segment thinner than
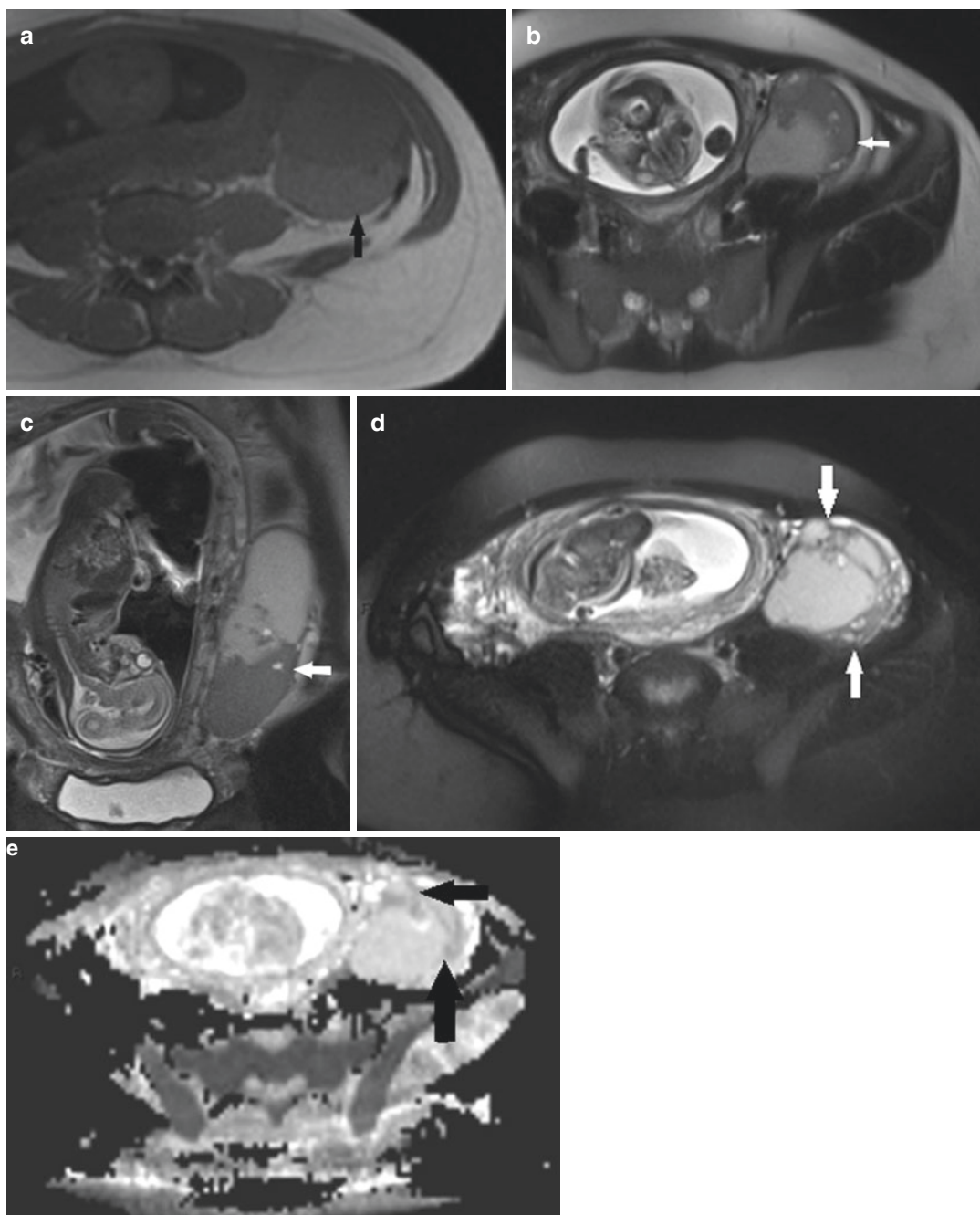
Fig. 10.3 A 31-year-old woman at 29 weeks' gestation with acute left-sided pain. Axial T1 (**a**) and axial (**b**) and coronal (**c**) T2-weighted HASTE MR images show a complex mass, with fluid and solid components in the left ovary (arrow). Axial fat-suppressed T2-weighted MR image (**d**) better demonstrates the solid component, showing restricted diffusion on an axial apparent diffusion coefficients (ADC) map (**e**). Borderline mucinous cystadenoma was confirmed at surgery
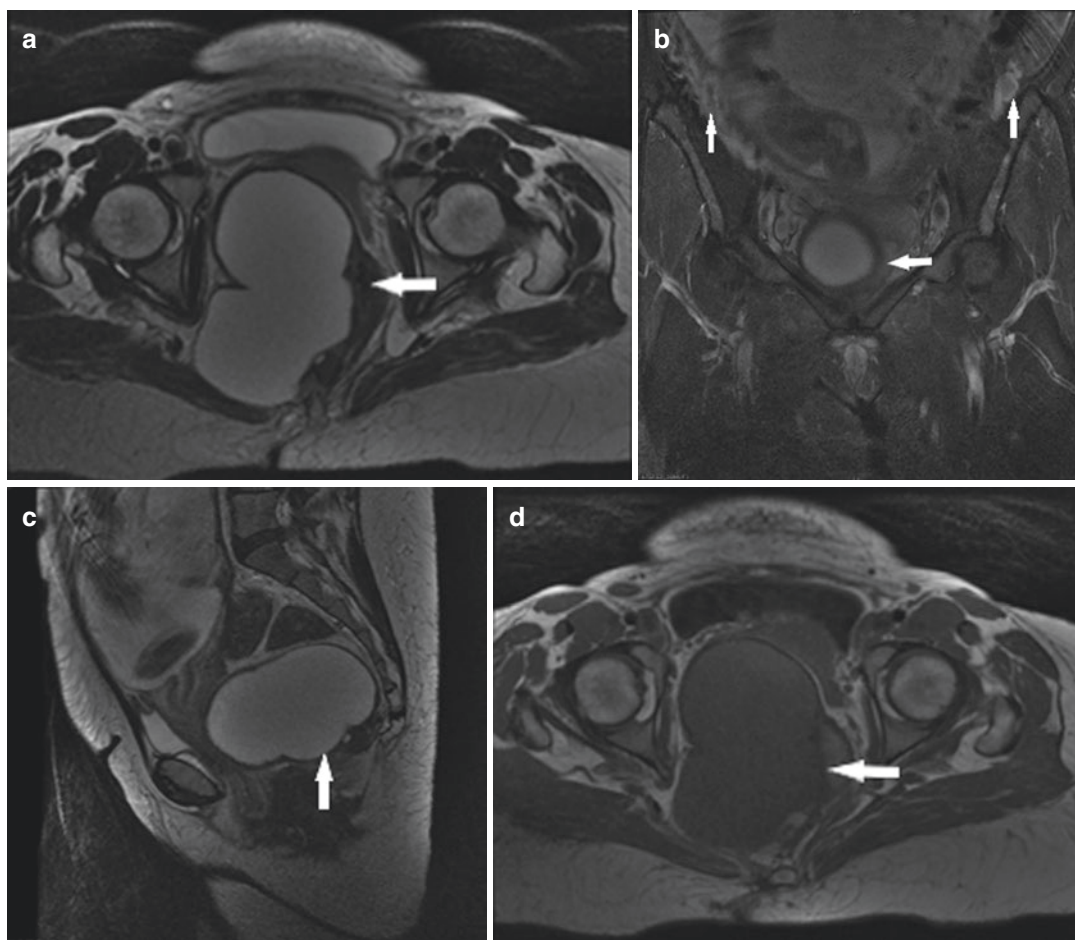
Fig. 10.4 A 30-year-old woman at 28 weeks' gestation with acute pelvic pain. US showed a cyst adjacent to the posterior wall of the uterus. Axial (**a**), sagittal (**b**), and coronal (**c**) HASTE MR images, and axial T1-weighted MR image (**d**), show a large cystic mass displacing the cervix and the rectum, with normal ovaries (arrows in **c**). A tailgut cyst was found at surgery

3.5 mm or a hypoechoic line in the myometrium thinner than 2.0 mm [1].

In comparison with US, MR imaging is less operator dependent and provides a more comprehensive examination with a larger field of view. MR imaging allows a better evaluation of soft tissues than US and CT. Finally, MR imaging allows clear visualization of the uterine wall; therefore, it helps to diagnose antepartum uterine rupture when US is indeterminate, showing the tear itself (Fig. 10.5). Moreover, MR imaging is more accurate than US for the differentiation of

uterine rupture from other uterine wall defects, including uterine sacculation and uterine dehiscence, which usually refers to the process of gradual myometrial rupture without a rupture of membranes. A correct differential diagnosis between complete uterine rupture and uterine dehiscence is important to choose the most appropriate management [5].

When a diagnosis of complete uterine rupture is established, the immediate stabilization of the mother and the surgical delivery of the fetus are imperative.
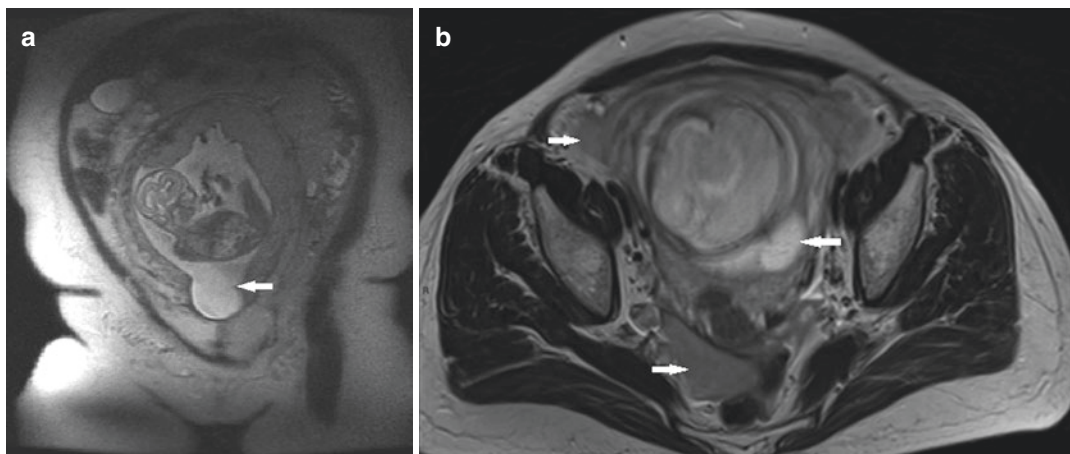
Fig. 10.5 A 34-year-old woman, primipara with a history of three previous myomectomies, was admitted at 25 weeks' gestation, presenting with vomiting, acute abdominal pain, and tenderness in the upper quadrants. Abdominal US revealed only complex intraperitoneal fluid, indicating hemoperitoneum. Coronal (**a**) and axial (**b**) T2-weighted HASTE MR images show posterior extravasation of amniotic fluid into a hernial sac (arrows), which contains a small fluid level. Note the presence of hemoperitoneum (small arrows). The findings are consistent with a sealed uterine rupture

10.3.2 Ectopic Pregnancy

Ectopic pregnancy (EP), or extrauterine pregnancy, is defined as implantation and subsequent development of the zygote outside of the intrauterine cavity. The incidence of EP is 1–2% of all reported pregnancies and remains the main cause of maternal death during the first trimester. Potential risk factors are previous EP, prior pelvic inflammatory disease, previous tubal surgery, abdominal surgery, tubal blockage, advanced maternal age, cigarette smoking, intrauterine device, prior abortions, and a history of subfertility [13]. EP is usually tubal (95%); more rarely, it is ovarian (1–3%), interstitial (2–4%), abdominal (1.4%), or cervical (<1%) [14].

Signs and symptoms are non-specific and include acute abdominal pain, vaginal bleeding, and an adnexal mass. Early diagnosis and treatment of EP are crucial to reduce maternal mortality and to preserve future fertility.

The initial evaluation includes a quantitative measurement of serum human chorionic gonadotropin (hCG) and TV US. If hCG levels increase by less than 50% during a 48-h period, the pregnancy is almost always nonviable [15].

TV US demonstrates a gestational sac (GS) when hCG levels are greater than 2000 mIU/mL, with a sensitivity of 87–99% and a specificity of 94–99.9% [14]. Sometimes US provides a definitive diagnosis showing an extrauterine GS with a yolk sac or embryo; more frequently, it is only suggestive of an EP, showing the presence of an adnexal mass (the most common sonographic finding in EP), and pelvic-free fluid, which is often complex [16–19]. The adnexal mass usually appears as a saclike ring, solid, or complex.

MR imaging is an excellent problem-solving modality to confirm or better define suspected EP, especially when TV US fails to demonstrate focus of EP or to distinguish from incomplete abortion. MR imaging can help to diagnose the rare or complicated form of EP [20]. However, its use may be limited in hemodynamically unstable patients, especially in ruptured EP. Reported MR imaging findings of EP include a GS-like structure with an adnexal or abdominal hematoma, tubal dilatation caused by hemosalpinx, and tubal wall enhancement [20, 21]. MR imaging is also important to make an accurate differential diagnosis between GS and a corpus luteum cyst. On

TV US, a corpus luteum appears as a cystic structure with the "ring of fire" on color Doppler, which resembles the feature of EP. On MR imaging, the distinction may be facilitated by focusing on the signal intensity of the peripheral area, location (intraovarian or extraovarian), and enhancement pattern. MR imaging is also superior to US for demonstrating hemoperitoneum and for differentiating it from simple ascites (Fig. 10.6).

Expectant management is a possible option for clinically stable asymptomatic women with a US diagnosis of EP and a decreasing serum hCG value, initially lower than 1500 mIU/mL. Medical therapy, using methotrexate, should be offered to women with a serum hCG level lower than 5000 mIU/mL and minimal symptoms. Surgery is usually needed when EP causes severe symptoms and bleeding or when high hCG levels are present. Laparoscopic
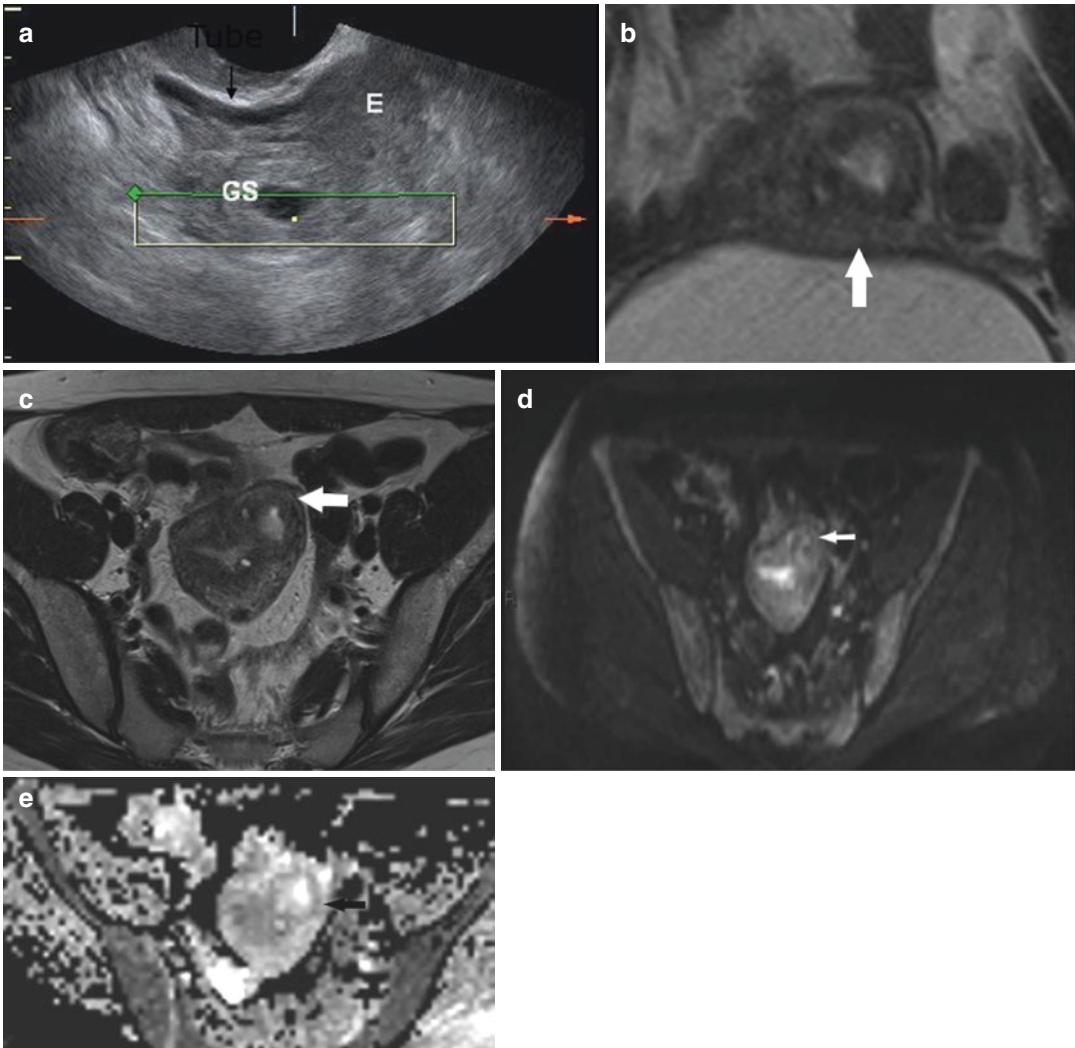
Fig. 10.6 A 32-year-old woman presenting with acute pelvic pain and vaginal bleeding. Transvaginal US (**a**) shows a right complex saclike ring, suggesting an angular ectopic pregnancy (arrow). Coronal (**b**) and axial (**c**) T2-weighted MR images, axial diffusion-weighted imaging (DWI) (**d**), and axial ADC map (**e**) show a left gestational saclike structure measuring 10 mm in diameter, surrounded by a thick wall, indicating an interstitial pregnancy

surgery is typically used. For a ruptured EP, emergency laparotomy is needed.

10.3.3 Placental Abruption

Placental abruption (PA), the premature separation of a normally implanted placenta from the uterine wall before delivery of the fetus, complicates approximately 1% of all pregnancies and is an important cause of maternal and neonatal morbidity and mortality [22].

Hypertensive disorders, advanced maternal age, grand multiparity, thrombopenia, cigarette smoking, illicit drug use, and external abdominal trauma are associated with an increased risk of PA [23].

The main clinical features of PA are vaginal bleeding associated with abdominal pain, uterine contractions or uterine tenderness, and signs of fetal distress.

The most important US criteria for PA (sensitivity, 80%; specificity, 92%) are the detection of preplacental/retroplacental collections, evidence of marginal subchorionic or intra-amniotic hematomas, increased placental thickness (>5 cm), and jelly-like movements of the chorionic plate [24, 25]. However, 25–50% of hematomas, mostly retroplacental in location, remain undetected by US because the echotexture of recent hemorrhage is similar to that of the placenta or because of the small dimensions of the bleed [24–26]. Therefore, the main diagnostic pitfall is the failure to diagnose a real placental abruption using only the US exam.

MR imaging is superior to US for the evaluation of placenta hemorrhage, because it improves soft-tissue contrast and has a wider field of view [27]. Diffusion and T1-weighted sequences (sensitivity, 100% and 94%, respectively; diagnostic accuracy, 100% and 97%, respectively) are more accurate than T2-weighted (sensitivity, 94%; diagnostic accuracy, 87%) and true FISP sequences (sensitivity, 79%; diagnostic, accuracy 90%) for depiction of PA [27, 28].

Additionally, MR imaging can be used to date hemorrhage based on the paramagnetic effects of methemoglobin and to classify intrauterine hematomas as hyperacute (first few hours, intra-cellular oxyhemoglobin), acute (1–3 days, intra-cellular deoxyhemoglobin), early subacute (3–7 days, intracellular methemoglobin), late subacute (14 days, extracellular methemoglobin), and chronic (>4 weeks, intracellular hemosiderin and ferritin) [29] (Fig. 10.7).

Because of the possible rapid and unpredictable worsening of abruption, it is important to avoid any delay in performing MR imaging. Moreover, when taking a pregnant patient with a potentially unstable condition to an MR unit, continuous monitoring and emergency preparedness are mandatory. MR imaging is an extremely accurate investigation that reveals, with an excellent interobserver agreement, the origin of second- and third-trimester uterine bleeding. MR imaging is an extremely accurate modality for the identification of PA, even in patients with negative US findings [27].

10.3.4 Placental Adhesive Disorders

Placental adhesive disorders (PAD) include placenta accreta (placental villi attached to the myometrium), placenta increta (placental villi invading the myometrium), and placenta percreta (placental villi penetrating up to the uterine serosa). The incidence of PAD is approximately 1 in 2000 pregnancies, with a rapid increase in recent years, reflecting the rising number of cesarean sections and other uterine surgery [30].

Placenta percreta can be a cause of acute abdominal pain. US is the first imaging modality used to diagnose PAD. Sonographic features are loss of the normal hypoechoic retroplacental myometrium zone, thinning or disruption of the hyperechoic uterine serosa-bladder interface, a focal exophytic mass, and the presence of lacunae in the placenta, which is the most predictive sonographic sign, with a sensitivity of 79% and a positive predictive value of 92% [31]. Color Doppler can add information and, when three dimensions are available, can help to distinguish placenta accreta from placenta percreta, highlighting areas of increased vascularity with dilated blood vessels which cross the placenta and uterine wall [32].
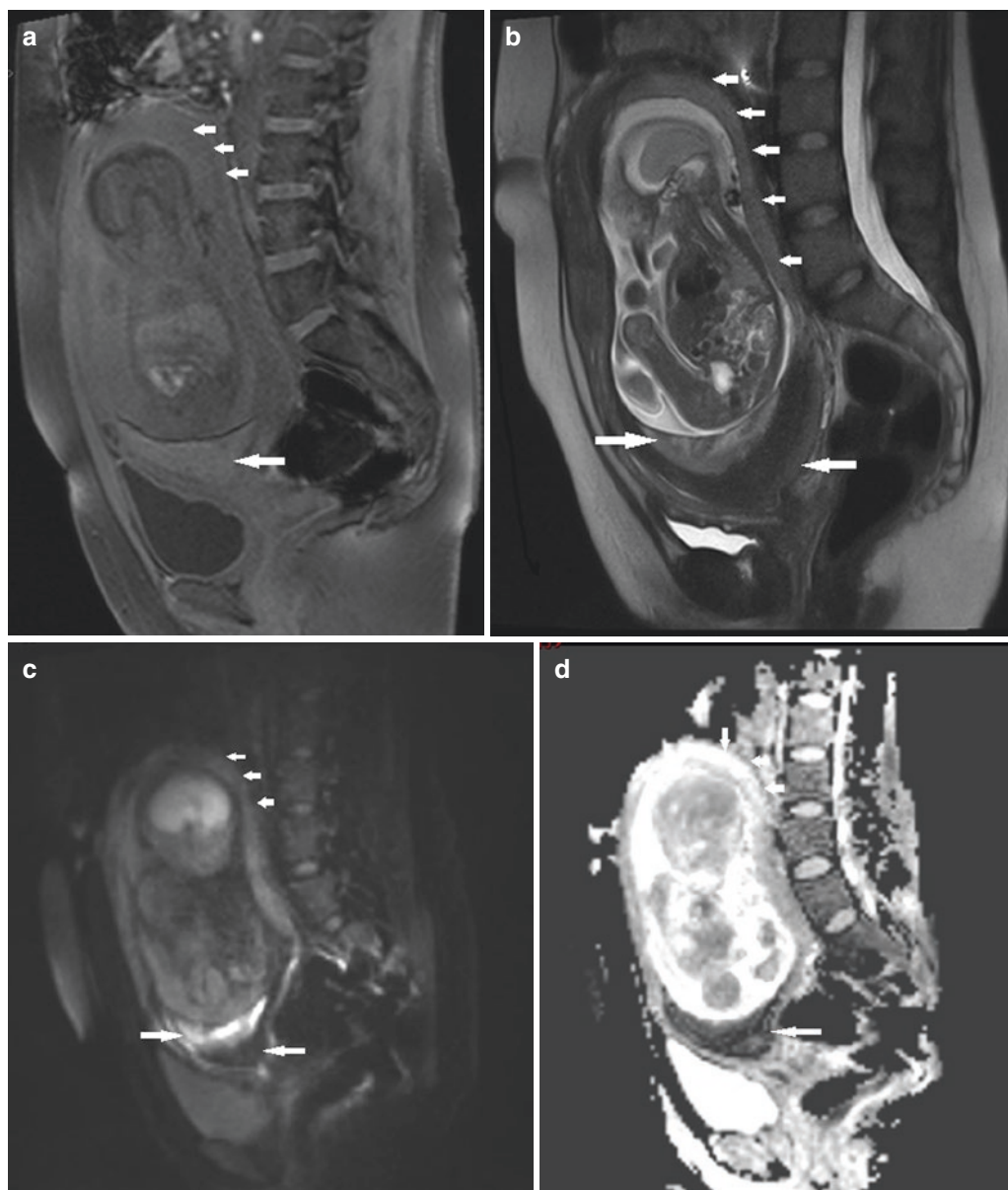
Fig. 10.7 A 25-year-old woman at 28 weeks' gestation with acute pelvic pain and vaginal bleeding. Sagittal T1 (**a**) and sagittal T2-weighted MR images (**b**) show an intrauterine clot with mixed hyperintense and hypointense areas (**c**) along the lower side of the uterine cavity, extend-ing to cover the uterine ostium. Sagittal DWI images (**d**) show mixed signal areas, indicating repeated bleeding. Note the normal placenta located on the posterior aspect (short arrows in a, b and c)

MR imaging is not used as the first imaging modality to diagnose PAD, but can provide additional information in equivocal situations, especially in patients with posterior placenta and previous myomectomy. Lim and colleagues [33] found that the volume of dark pla-

cental bands was the most predictive finding for the identification of PAD. Derman and colleagues [34] confirmed that the most reliable sign is the larger dark band on T2 HASTE images. They added an additional finding: vessels of 6 mm or greater (which presumably

correspond to lacunae). When the placenta is percreta, MR imaging is able to depict infiltration of adjacent organs by evaluating tenting of the bladder, interruption of the myometrial line, and direct infiltration of pelvic organs [32] (Fig. 10.8).

If US findings suggest possible percreta or are inconclusive or negative in an at-risk woman, MR imaging can be useful. Invasion of adjacent organs is better depicted with MR imaging than on US.

Situations in which MR imaging may also contribute additional information include women with placenta previa with a posterior or lateral implantation, a posterior scar from a myomectomy, a history of difficult placental removal in the past with a posterior or lateral placenta in the present pregnancy, or a history of endometrial ablation [32].

The correct and prompt diagnosis of placenta percreta is important, because this condition may cause uterine rupture, requiring an emergency cesarean section.
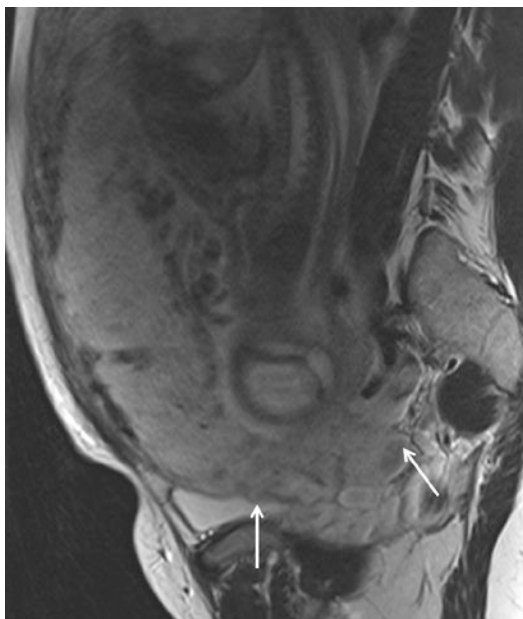
Fig. 10.8 A 28-year-old woman at 30 weeks' gestation with acute pelvic pain. Sagittal T2-weighted MR HASTE image shows multiple irregular areas of the placenta bulging into the myometrium, with invasion of the right parametrium (arrows). These findings indicate placenta percreta. A hysterectomy was performed at delivery, which confirmed the MR findings

10.4 Summary

The cause of acute abdominal/pelvic pain in pregnancy is often difficult to establish because of the presence of multiple confounding factors. Diagnostic imaging with US, the first-line diagnostic test during pregnancy, is limited because of the altered body habitus, the small field of view, and the presence of interfering overlying structures. MR imaging is usually used when US is inconclusive and it helps to avoid a lot of *pitfalls*, providing a systematic evaluation of the entire abdomen and pelvis with a high diagnostic accuracy.

References

1. Casciani E, De Vincentiis C, Mazzei MA, et al. Errors in imaging the pregnant patient with acute abdomen. Abdom Imaging. 2015;40:2112–26.
2. Patlas MN, Dreizin D, Menias CO, et al. Abdominal and pelvic trauma: misses and misinterpretations at multidetector CT: trauma/emergency radiology. Radiographics. 2017;37:703–4.
3. Pinto A, Brunese L. Spectrum of diagnostic errors in radiology. World J Radiol. 2010;2:377–83.
4. Chang SD, Yen CF, Lo LM, et al. Surgical intervention for maternal ovarian torsion in pregnancy. Taiwan J Obstet Gynecol. 2011;50:458–62.
5. Masselli G, Derme M, Laghi F, et al. Evaluating the acute abdomen in the pregnant patient. Radiol Clin N Am. 2015;53:1309–25.
6. Lourenco AP, Swenson D, Tubbs RJ, et al. Ovarian and tubal torsion: imaging findings on US, CT, and MRI. Emerg Radiol. 2014;21:179–87.
7. Rothmund R, Taran FA, Boeer B, et al. Surgical and conservative management of symptomatic leiomyomas during pregnancy: a retrospective pilot study. Geburtshilfe Frauenheilkd. 2013;73:330–4.
8. Sohn GS, Cho S, Kim YM, et al. Working Group of Society of Uterine Leiomyoma. Current medical treatment of uterine fibroids. Obstet Gynecol Sci. 2018;61:192–201.
9. Sarkodie BD, Botwe BO, Ofori EK. Uterine fibroid characteristics and sonographic pattern among Ghanaian females undergoing pelvic ultrasound scan: a study at 3-major centres. BMC Womens Health. 2016;16:10.
10. Foti PV, Attinà G, Spadola S, et al. MR imaging of ovarian masses: classification and differential diagnosis. Insights Imaging. 2016;7:21–41.
11. Anthoulakis C, Nikoloudis N. Pelvic MRI as the "gold standard" in the subsequent evaluation of ultrasound-indeterminate adnexal lesions: a systematic review. Gynecol Oncol. 2014;132:661–8.

12. Mavromatidis G, Karavas G, Margioula-Siarkou C, et al. Spontaneous postpartum rupture of an intact uterus: a case report. J Clin Med Res. 2015;7:56–8.

13. Moini A, Hosseini R, Jahangiri N, et al. Risk factors for ectopic pregnancy: a case-control study. J Res Med Sci. 2014;19:844–9.

14. Petrides A, Dinglas C, Chavez M, et al. Revisiting ectopic pregnancy: a pictorial essay. J Clin Imaging Sci. 2014;4:37.

15. Lipscomb GH, Stovall TG, Ling FW. Nonsurgical treatment of ectopic pregnancy. N Engl J Med. 2000;343:1325–9.

16. RCOG. RCOG guidelines. Diagnosis and management of ectopic pregnancy (green-top guideline no. 21). London: RCOG; 2016.

17. Cacciatore B. Can the status of tubal pregnancy be predicted with transvaginal sonography? A prospective comparison of sonographic, surgical, and serum hCG findings. Radiology. 1990;177:481–4.

18. Brown DL, Doubilet PM. Transvaginal sonography for diagnosing ectopic pregnancy: positivity criteria and performance characteristics. J Ultrasound Med. 1994;13:259–66.

19. Nyberg DA, Mack LA, Jeffrey RB Jr, et al. Endovaginal sonographic evaluation of ectopic pregnancy: a prospective study. Am J Roentgenol. 1987;149:1181–6.

20. Masselli G, Derme M, Piccioni MG, et al. To evaluate the feasibility of magnetic resonance imaging in predicting unusual site ectopic pregnancy: a retrospective cohort study. Eur Radiol. 2018;28:2444–54.

21. Tamai K, Koyama T, Togashi K, et al. MR features of ectopic pregnancy. Eur Radiol. 2007;17:3236–46.

22. Leunen K, Hall DR, Odendaal HJ, et al. The profile and complications of women with placental abruption and intrauterine death. J Trop Pediatr. 2003;49: 231–4.

23. Denis M, Enquobahrie DA, Tadesse MG, et al. Placental genome and maternal-placental genetic interactions: a genome-wide and candidate gene association study of placental abruption. PLoS One. 2014;9:e116346.

24. Jaffe MH, Schoen WC, Silver TM, et al. Sonography of abruptio placentae. AJR Am J Roentgenol. 1981;137:1049–54.

25. Harris RD, Cho C, Wells WA. Sonography of the placenta with emphasis on pathological correlation. Semin Ultrasound CT MR. 1996;17:66–89.

26. Yeo L, Ananth C, Vintzileos A. Placenta abruption. In: Sciarra J, editor. Gynecology and obstetrics. Hagerstown, MD: Lippincott Williams & Wilkins; 2004.

27. Masselli G, Brunelli R, Di Tola M, et al. MR imaging in the evaluation of placental abruption: correlation with sonographic findings. Radiology. 2011;259:222–30.

28. Verswijvel G, Grieten M, Gyselaers W, et al. MRI in the assessment of pregnancy related intrauterine bleeding: a valuable adjunct to ultrasound? JBR-BTR. 2002;85:189–92.

29. Atlas SW, Thulborn KR. Intracranial hemorrhage. In: Atlas SW, editor. Magnetic resonance imaging of the brain and of the spine. 4th ed. Philadelphia, PA: Lippincott Williams & Wilkins; 2009. p. 644–94.

30. Wu S, Kocherginsky M, Hibbard JU. Abnormal placentation: twenty-year analysis. Am J Obstet Gynecol. 2005;192:1458–61.

31. Comstock CH, Love JJ, Bronsteen RA, et al. Sonographic detection of placenta accrete in the second and third trimesters of pregnancy. Am J Obstet Gynecol. 2004;190:1135–40.

32. Comstock CH, Bronsteen RA. The antenatal diagnosis of placenta accreta. BJOG. 2014;121:171–81.

33. Lim PS, Greenberg M, Edelson MI, et al. Utility of ultrasound and MRI in prenatal diagnosis of placenta accreta: a pilot study. Am J Roentgenol. 2011;197:1506–13.

34. Derman AY, Nikac V, Haberman S, et al. MRI of placenta accreta: a new imaging perspective. Am J Roentgenol. 2011;197:1514–21.

Errors and Pitfalls in Emergency Pediatric Imaging

11

Elka Miller, Gali Shapira-Zaltsberg, Rita Putnins, and Kristin Udjus

11.1 Introduction

There are many areas where pediatric radiology differs substantially from adult radiology. This can be related to technical challenges due to lack of patient cooperation or comprehension, a wide spectrum of anatomical and developmental variants which may mimic disease, as well as a difference in pathological processes and diseases affecting children.

It is known that children are at increased risk of the ill effects from ionizing radiation, since the developing tissues in the growing child are more radiosensitive. There is a cumulative radiation risk over a lifetime, and manifestations of the risks are delayed. Children have a longer time in which to express the manifestations of this potential risk [1]. Therefore, careful use of imaging examinations utilizing ionizing radiation is of special importance in pediatric radiology. Routine practice should be according to the ALARA ("as low as reasonably achievable") principle. The risk associated with sedation is yet another consideration which has to be taken into account when choosing an imaging modality. These are additional challenges specific to pediatric radiology.

A review by Taylor et al. in 2011 [2] describes the patterns and potential etiologies of diagnostic errors in pediatric radiology. They found clinically significant diagnostic errors in 265 cases (54% radiographs, 25% CTs, and remaining 20% including MRI, US, and fluoroscopy). The majority of the errors were cognitive, i.e., faulty information processing, faulty data gathering, or insufficient knowledge base. For example, cases of misinterpretation of the position of tubes and lines, and multifactorial, i.e., more than one type of error identified. Other types of errors included perceptual errors, i.e., nonrecognition of an imaging abnormality, for example, a child imaged for a left shoulder mass with multiple unsuspected left posterior medial rib fractures; system-related errors, i.e., technical or organizational flaws, for example, inappropriate scanning parameters or fast MR sequences resulting in images obscuring the salient findings; or unavoidable errors, i.e., abnormal imaging findings were absent or masked or so atypical that arriving at a correct diagnosis would not be expected.

Therefore, since some of the errors occur in a predictable way and frequency, approaches for improvement, including systematic image interpretation, utilization of protocols, awareness of common errors and pitfalls, and sharing and learning from errors related to emergency imaging of the pediatric patient, have potential for improved performance.

E. Miller (✉) · G. Shapira-Zaltsberg · R. Putnins
K. Udjus
Department of Medical Imaging, CHEO, University of Ottawa, Ottawa, ON, Canada
e-mail: emiller@cheo.on.ca;
GShapira-Zaltsberg@cheo.on.ca;
rputnins@cheo.on.ca; udjus@cheo.on.ca

In this chapter we will review some of the common errors which can be encountered in emergency imaging of the pediatric patient using a regional approach.

11.2 Chest and Soft Tissues of the Neck

Radiographs are the pillar of pediatric chest imaging. Adequate technique, correct positioning, and patient cooperation are issues which are not easy to control in the pediatric patient. The "Pigg-O-Stat" is a well-known device used to immobilize the small pediatric patient for upright chest radiographs. It consists of a saddle with a plastic holder that keeps an infant safely secured in an erect position. The use of this device, or something like it, is a must where chest radiographs are performed on small children (Fig. 11.1).

11.2.1 Airway

Croup, or laryngotracheobronchitis, is the most common cause of upper airway obstruction in the pediatric population (usually between 6 months and 3 years) [3]. It is a viral infection, most commonly caused by parainfluenza virus or respiratory syncytial virus. On frontal radiographs it classically presents with symmetrical tapering and loss of shouldering of the subglottic airway, giving it the well-known "steeple sign" (Fig. 11.2a). The lateral radiograph demonstrates narrowing of the subglottic airway and ballooning of the hypopharynx. If the tapering of the subglottic airway is asymmetrical and/or the patient is over 3 years of age, alternative diagnoses should be considered, including a subglottic hemangioma (Fig. 11.2b) and post-tracheostomy fibrosis. However, circumferential hemangiomas or hemangiomas located central to the plane of projection can also cause symmetric narrowing of the trachea [4].

The pediatric neck is a site of frequent infection. This may spread to the retropharyngeal space, producing a retropharyngeal abscess which can cause airway compromise. This is best seen on lateral radiographs as widening of the retropharyngeal soft tissues. These tissues are quite variable and may appear thickened in normal young children, usually less than 2 years. If the image is done with the neck in flexion and taken in expiration, this may appear as a false positive. Repeat radiography with improved technique (extension
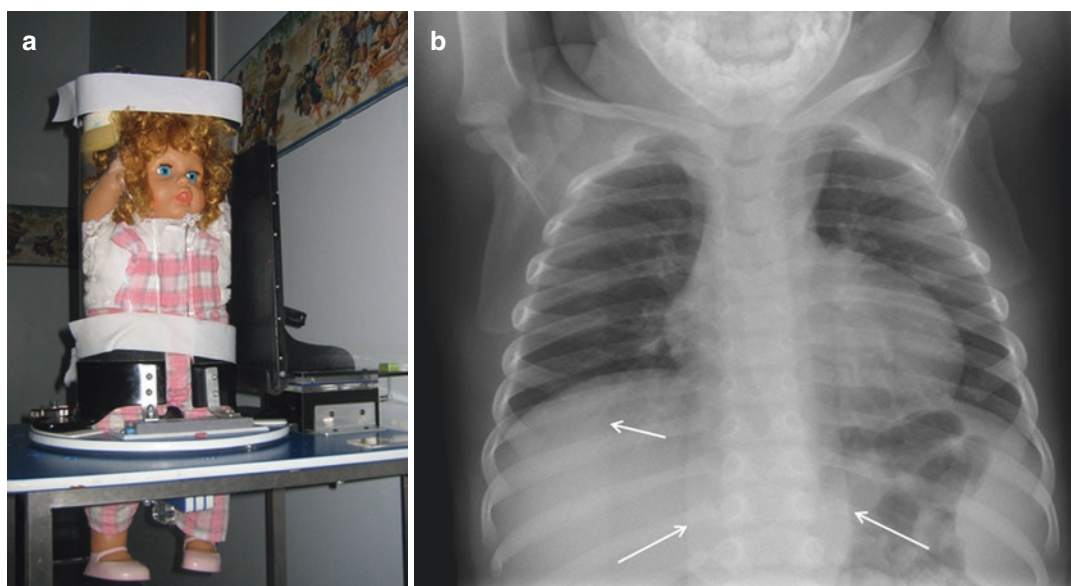
Fig. 11.1 (**a**) "Pigg-O-Stat" device. (**b**) PA chest radiograph of a 2-year-old child obtained using the "Pigg-O-Stat," showing commonly associated linear densities produced by the device (arrows)
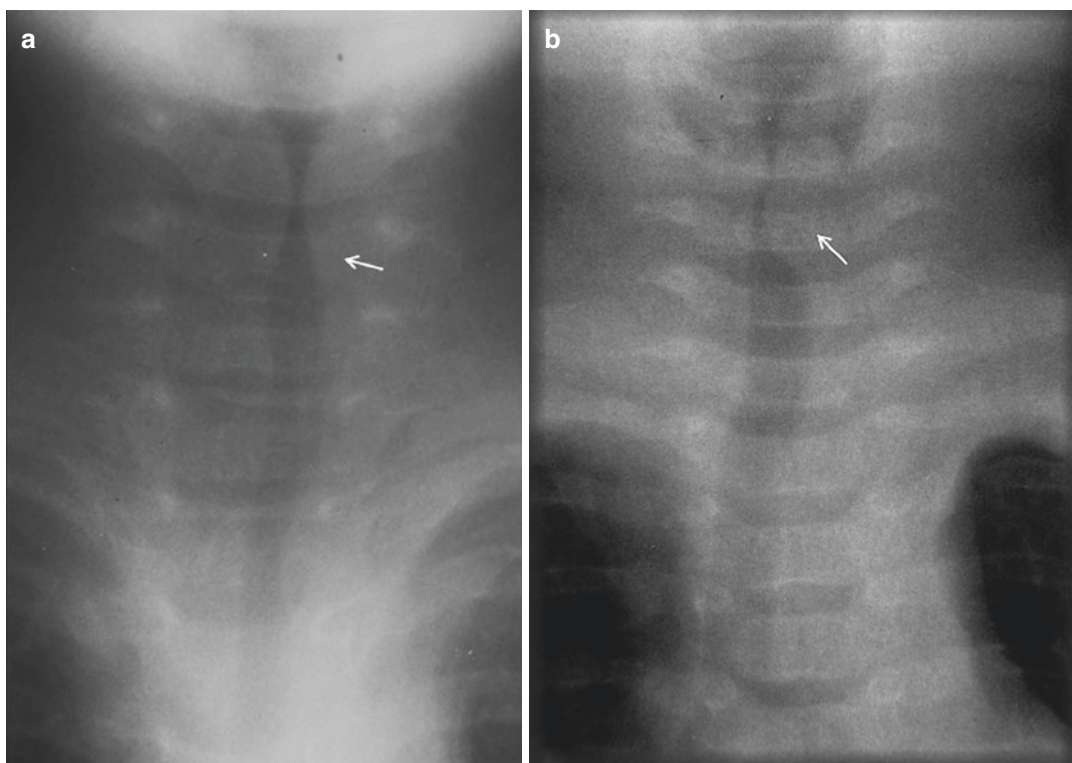
Fig. 11.2 (**a**) Frontal radiograph of the airway of a 2-year-old boy, showing the typical symmetrical "steeple sign" (arrow), which is suggestive of croup. (**b**) There is asymmetric tapering of the subglottic airway in a 3-year-old boy, representing a subglottic hemangioma

and inspiration) is needed for diagnosis. If positive or inconclusive, further evaluation with intravenous contrast CT may be needed (Fig. 11.3).

Teaching Points
- Asymmetric tapering of the subglottic airway and/or the "steeple sign" in a patient older than 3 years of age should not be mistaken for croup and should raise the possibility of another etiology.
- Retropharyngeal soft tissues in young children are often redundant and may mimic an abscess.

11.2.2 Lungs

11.2.2.1 Asymmetrical Lung Lucency
The differential diagnosis for unilateral increased lung lucency includes pneumothorax, foreign body, congenital lobar emphysema, solitary lung cyst, congenital pulmonary airway malformation (CPAM), pulmonary artery hypoplasia, and Poland syndrome. Of these, endobronchial foreign bodies are the most common, especially in children younger than 3 years. Most are not radiopaque (e.g., peanuts, popcorn). They obstruct the bronchus and produce distal hyperinflation due to a ball-valve mechanism [5]. The compliant airway allows air to bypass the foreign body on inspiration but collapses against the foreign body on expiration, thereby trapping the air within the lung. This may not be apparent when the surrounding lung is inflated as on an inspiratory image (Fig. 11.4a). On an expiratory view, it appears as a focal lucency due to the air trapping, with mass effect on surrounding structures. Mediastinal shift to the opposite side and flattening of the diaphragm may be seen (Fig. 11.4b). Other manifestations including atelectasis and consolidation may also be appreciated.
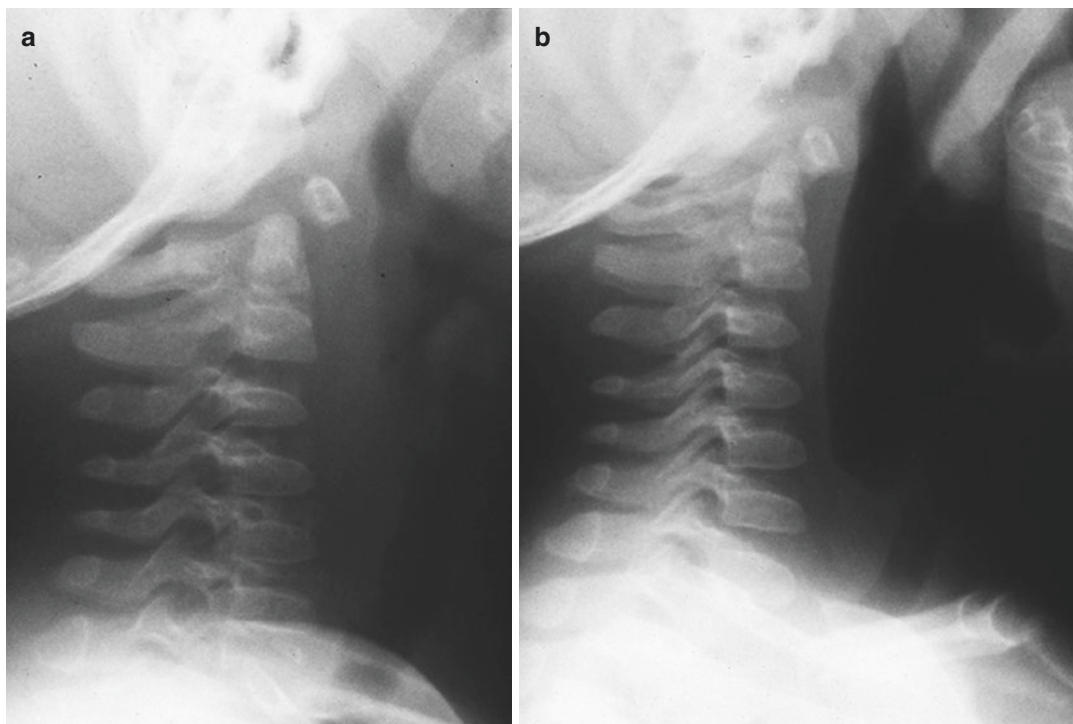
Fig. 11.3 Variable thickness of the retropharyngeal soft tissues of a 3-year-old girl. (**a**) Poor inspiration; (**b**) good inspiration. The apparent widening of the posterior soft tissues on an expiratory radiograph resolves with good inspiration
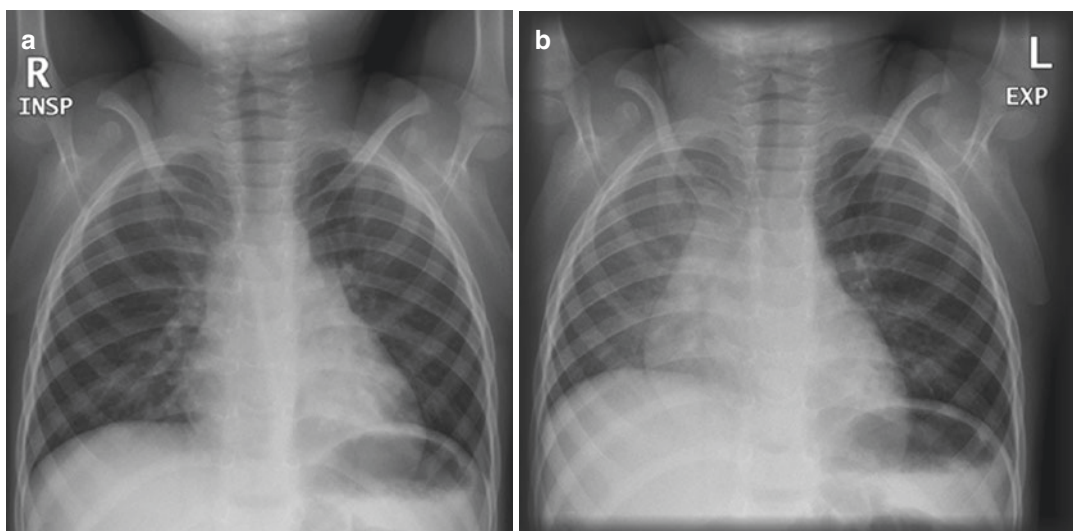

Fig. 11.4 (**a**) Inspiratory and (**b**) expiratory PA chest radiographs in a 4-year-old boy with foreign body aspiration. Air trapping with increased lucency on the left is appreciated only on the expiratory view. The mediastinum shifts to the opposite side

A foreign body can also be lodged in the esophagus and can cause dilatation of the esophagus proximal to the impaction, which sometimes can be seen on chest radiographs. However, if the radiograph is normal and esophageal impaction is suspected, further assessment with an upper GI examination is recommended. Even though transient esophageal air is frequently present in babies as a normal finding, persistent air and dilatation should raise concern for an esophageal obstruction (Fig. 11.5).

In the case of a radiopaque foreign body, it is important to differentiate button batteries from coins. The former needs to be managed more aggressively due to the potential leakage of caustic substances causing damage to the surrounding tissues. Button batteries have a bilaminar structure, making them appear as a double ring when seen "en face" on frontal radiographs. When seen in profile, they have a characteristic beveled edge appearance, distinguishing them from coins [5] (Fig. 11.6).

11.2.2.2 Increased Lung Density

Diagnosis of community-acquired pneumonia is one of the most common reasons for imaging the chest in children. Although pneumonia often responds well to conventional treatment, complications including empyema, lung necrosis, and bronchopleural fistula may occur [6]. A focal lucency within the consolidation with or without an air-fluid level suggests parenchymal necrosis. In children, chest ultrasound has been found useful in assessing necrotizing pneumonias, as well as for evaluating pleural effusions [7] (Fig.11.7).

Round pneumonia is another manifestation of community-acquired pneumonia in children, mainly seen under 8 years of age (Fig. 11.8). Underdeveloped pores of Kohn (openings between adjacent alveoli) and canals of Lambert (bronchoalveolar channels that involve the terminal bronchioles opening into alveolar sacs) predispose young children to round pneumonia. It is important to correlate the radiographs with the clinical presentation, as the differential
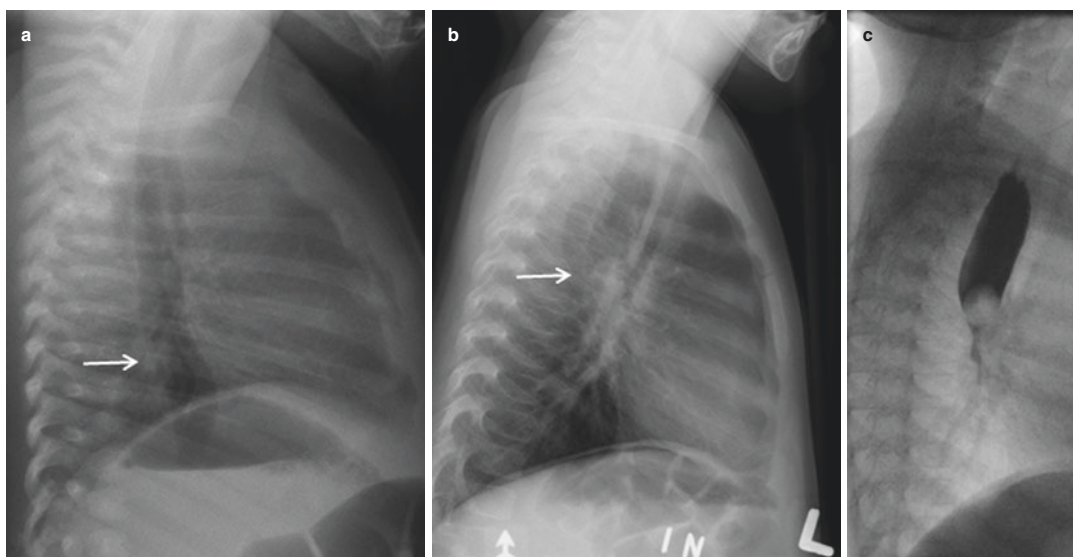
Fig. 11.5 (**a**) Lateral chest radiograph of a 5-week-old girl, showing air throughout the distended esophagus (arrow), which is commonly seen in normal young pediatric patients. (**b**) Lateral view of a 19-month-old girl who presented with a 4-day history of vomiting and fever. The image shows distention of the proximal esophagus to the level of an opacity (arrow). (**c**) An esophagogram showed abrupt cutoff by a well-defined filling defect, representing an impacted food bolus
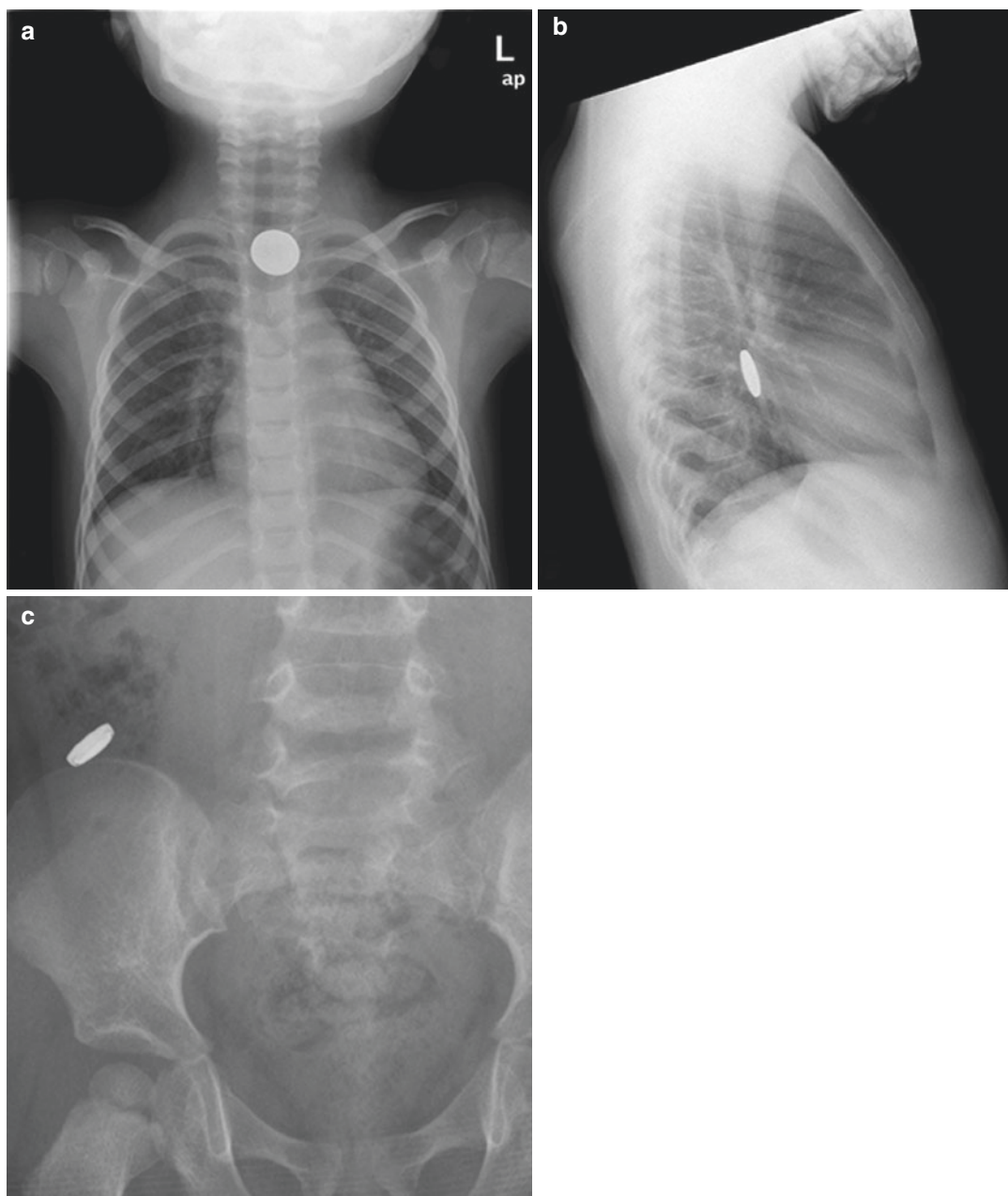
Fig. 11.6 (**a**) Frontal and (**b**) lateral chest radiograph of a child who swallowed a coin and (**c**) frontal abdominal radiograph of a child who swallowed a button battery. Note the bilaminar configuration of the battery, not seen with the coin

diagnosis for a round opacity on chest radiographs includes neoplasm, developmental pulmonary malformation (e.g., congenital pulmonary airway malformation, sequestration, bronchogenic cyst), and atypical infection (e.g., tuberculosis, aspergillosis). Even if the symptoms are consistent with a pneumonic process, follow-up radiography is recommended after completion of treatment in
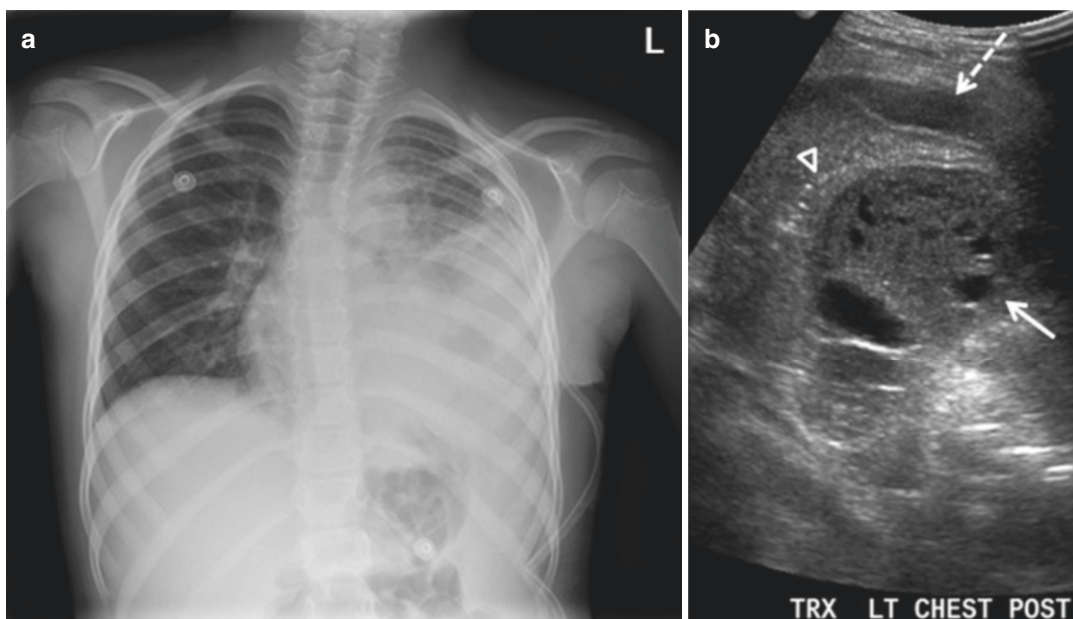
Fig. 11.7 (**a**) Frontal chest radiograph of 6-year-old girl admitted for pneumonia, showing a large left-sided consolidation and pleural effusion with focal lucency within the opacity. (**b**) Ultrasound of the left chest shows hypoechoic lung, with areas of liquefaction representing a focal area of necrotizing pneumonia (solid arrow), adjacent to viable (more echogenic) lung with air broncho-gram (arrowhead), as well as a small pleural effusion (dashed arrow). Doppler images showed no flow in the necrotic lung, with detectable vascularity in the adjacent viable consolidation (not shown)
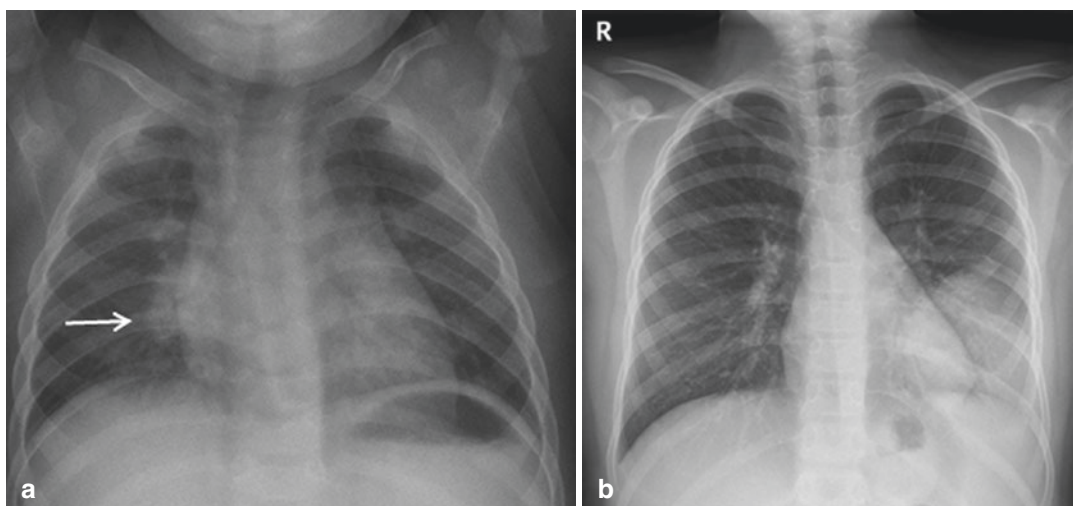
Fig. 11.8 Frontal chest radiograph of (**a**) a 2-year-old boy with an ill-defined right perihilar round pneumonia (arrow), (**b**) a 7-year-old girl showing a well-defined round pneumonia in the left lower lobe (LLL), and (**c**) an 8-year-old girl with recurrent LLL pneumonia and similar imaging findings. This opacity was surgically proven to be a congenital pulmonary airway malformation (CPAM)
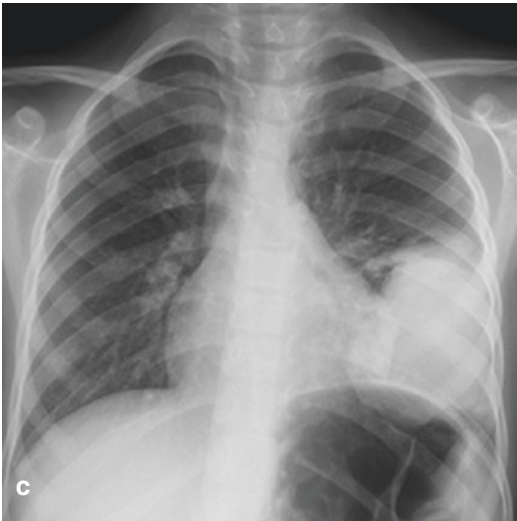
Fig. 11.8 (continued)

order to confirm resolution of the round opacity. CT should be considered in the presence of a round opacity on chest radiographs if the clinical features are not consistent with pneumonia, if the round opacity does not resolve after appropriate antibiotic treatment, or if there are radiographic signs of a non-pulmonary origin on chest radiography [8].

Teaching Points
- Foreign bodies should always be considered when interpreting pediatric chest radiographs.
- Endobronchial foreign bodies can cause air trapping, and this is better appreciated on an expiratory view. The inspiratory view may appear normal.
- Remember to differentiate batteries from other metallic foreign bodies on radiographs.
- Ultrasound is helpful in characterizing lung densities and pleural effusions in pediatric patients.
- Round pneumonias need to be followed up to assure resolution.

11.2.3 Mediastinum

11.2.3.1 Thymus

Assessment of the mediastinum in children can be challenging due to the prominent thymus which is normally present in infancy. The normal mediastinum can have a variable appearance on radiographs, depending on the patient's age. The thymus is a soft gland located in the prevascular space of the mediastinum and is nearly fully developed at birth. It increases in size during early infancy. The gland then gradually involutes and is less apparent after 3 years of age [9].

On a frontal chest radiograph in an infant, the thymus appears as a prominent soft-tissue structure in the superior mediastinum. It appears inseparable from the superior cardiac silhouette. The lateral margins often have smooth undulations related to impressions from the overlying ribs and the costal cartilages on the thymus, giving the so-called "wave" sign (Fig. 11.9a). This is a helpful differentiating feature. The lateral view confirms the location in the anterior mediastinum (Fig. 11.9b), obliterating the retrosternal clear space which is normally seen in older children and adults. The angular corner, usually where the right lobe is flattened at the right minor fissure, gives the classical "sail sign" (Fig. 11.9c). A normal gland may potentially obscure anywhere from one-third to the entire left and/or right upper lung. Due to its embryologic descent along the thymopharyngeal duct, normal ectopic thymic tissue can be found in the neck and submandibular regions [10] (Fig. 11.10). This should not be confused with a neck mass on ultrasound.

Another feature that is helpful in differentiating the normal thymus from a mediastinal mass is the fact that the thymus does not compress adjacent vessels or in other ways exert mass effect on the surrounding structures. Also,
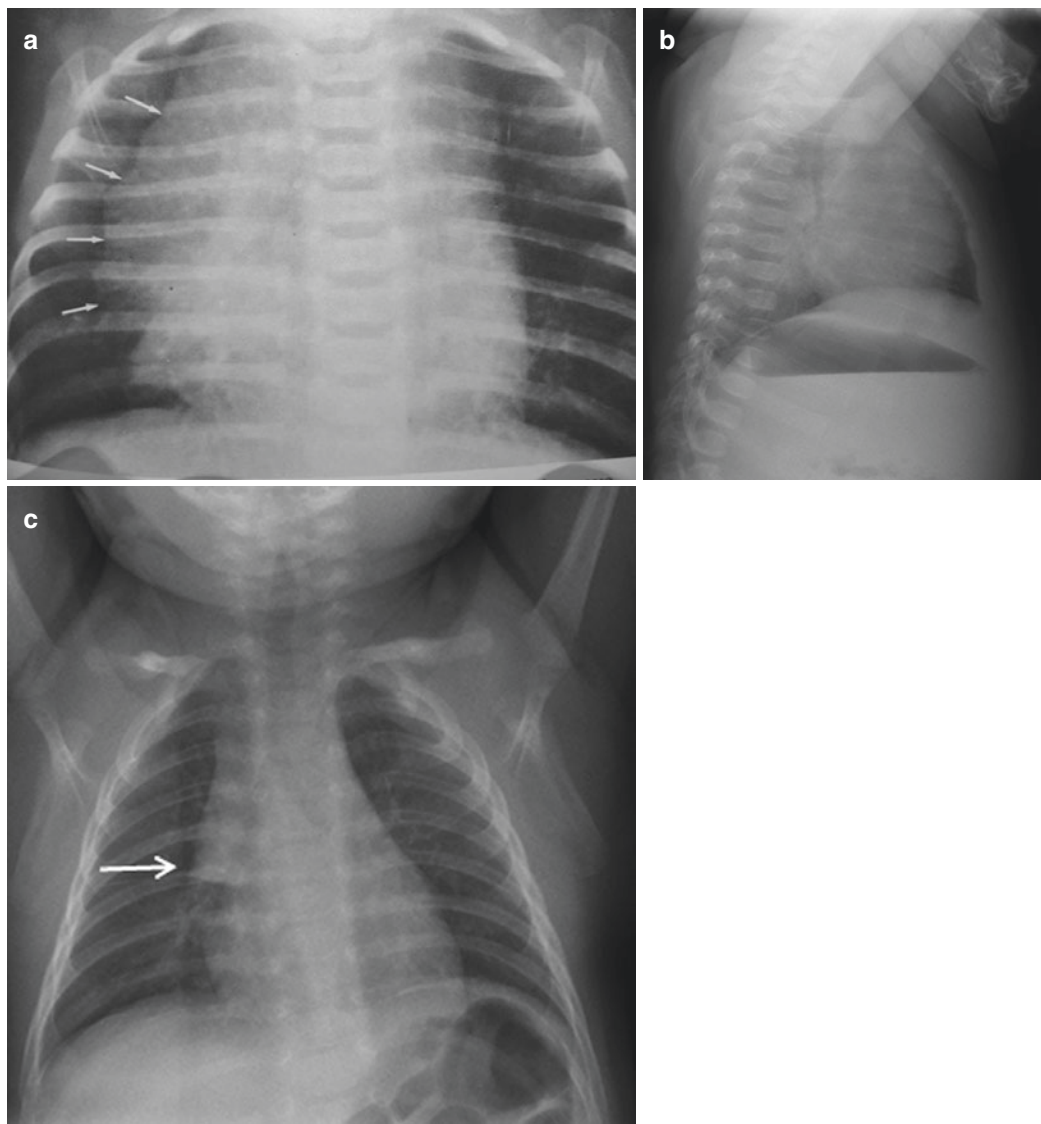
Fig. 11.9 (**a**) Frontal chest radiograph of an infant shows the "wave" sign of the normal thymus (arrows). (**b**) Lateral view in another child shows the thymus in the anterior mediastinum, with absent retrosternal clear space. (**c**) Frontal chest radiograph demonstrates the classic, thymic "sail sign" (arrow)

the gland is relatively lucent, allowing visualization of the underlying pulmonary vasculature. This helps to distinguish the thymus from adjacent dense pulmonary opacities including pneumonia and atelectasis. In the young child, ultrasound can be used to confirm thymic tissue in questionable cases. The gland has a characteristic echo pattern on ultrasound, appearing

predominantly hypoechoic, with uniformly granular parenchyma showing echogenic punctate and linear septa ("dot-dash" pattern) [11] (Fig. 11.11).

Failure to identify the thymus in the young child is also of concern. Absent thymus is associated with severe combined immune deficiency such as in DiGeorge syndrome. It is also important to remember that partial or total thymectomy is routinely performed during cardiac surgery, to allow access to the heart and vessels. Mediastinal widening in patients after heart surgery should therefore not be attributed to thymic shadow or rebound but rather suggests a hematoma or a mass [10, 12, 13].
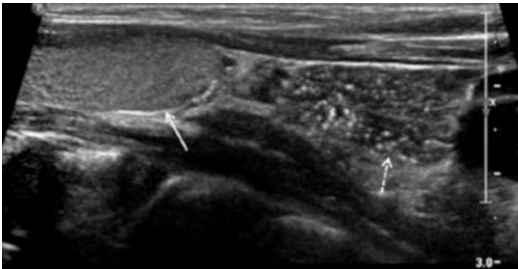
Fig. 11.10 Sagittal ultrasound image of the neck of a 10-year-old boy, showing the left lobe of the thyroid (solid arrow) with adjacent ectopic thymic tissue (dashed arrow), demonstrating typical thymic echotexture ("dot-dash" pattern)

11.2.3.2 Mediastinal Mass

Neuroblastoma is the most common solid extracranial malignancy of childhood. Although the mediastinum is not the most frequent site of origin (19%), a well-circumscribed posterior mediastinal or paraspinal mass associated with calcifications (typically punctate), rib widening, or bone erosion should raise strong suspicion of a mass and prompt further cross-sectional imaging (Fig. 11.12).

11.2.3.3 Vascular Structures

A child in the emergency department often has a chest radiograph as the first imaging examination. Careful evaluation of the caliber and position of the trachea, mediastinal contour, and position of the aortic arch should be performed on every pediatric chest radiograph. In doing this, a vascular ring or other vascular abnormalities may be detected (Fig. 11.13). Of note, tracheal deviation is always to the right in normal children, due to the left aortic arch. Tracheal deviation to the left on a frontal radiograph should raise concern for vascular abnormality or mass.

Teaching Points
- The thymus is a lobulated soft-tissue density in the anterior mediastinum in children under

Fig. 11.11 (**a**) PA chest radiograph of a 3-week-old girl with history of cyanosis with coughing spells. There is a well-defined soft-tissue density in the right upper mediastinum with no associated 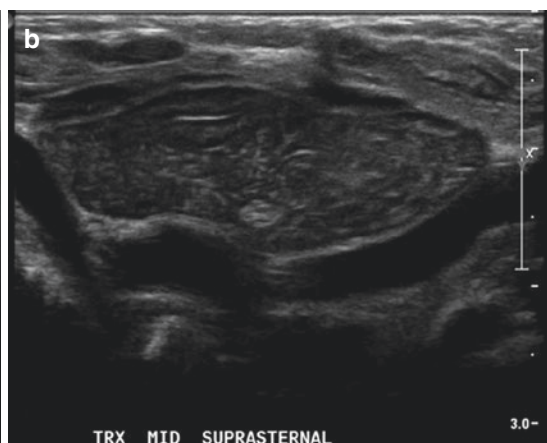mass effect (arrow). (**b**) US image of the upper mediastinum via the suprasternal notch demonstrates normal-appearing thymus, correlating with the density seen on chest radiography
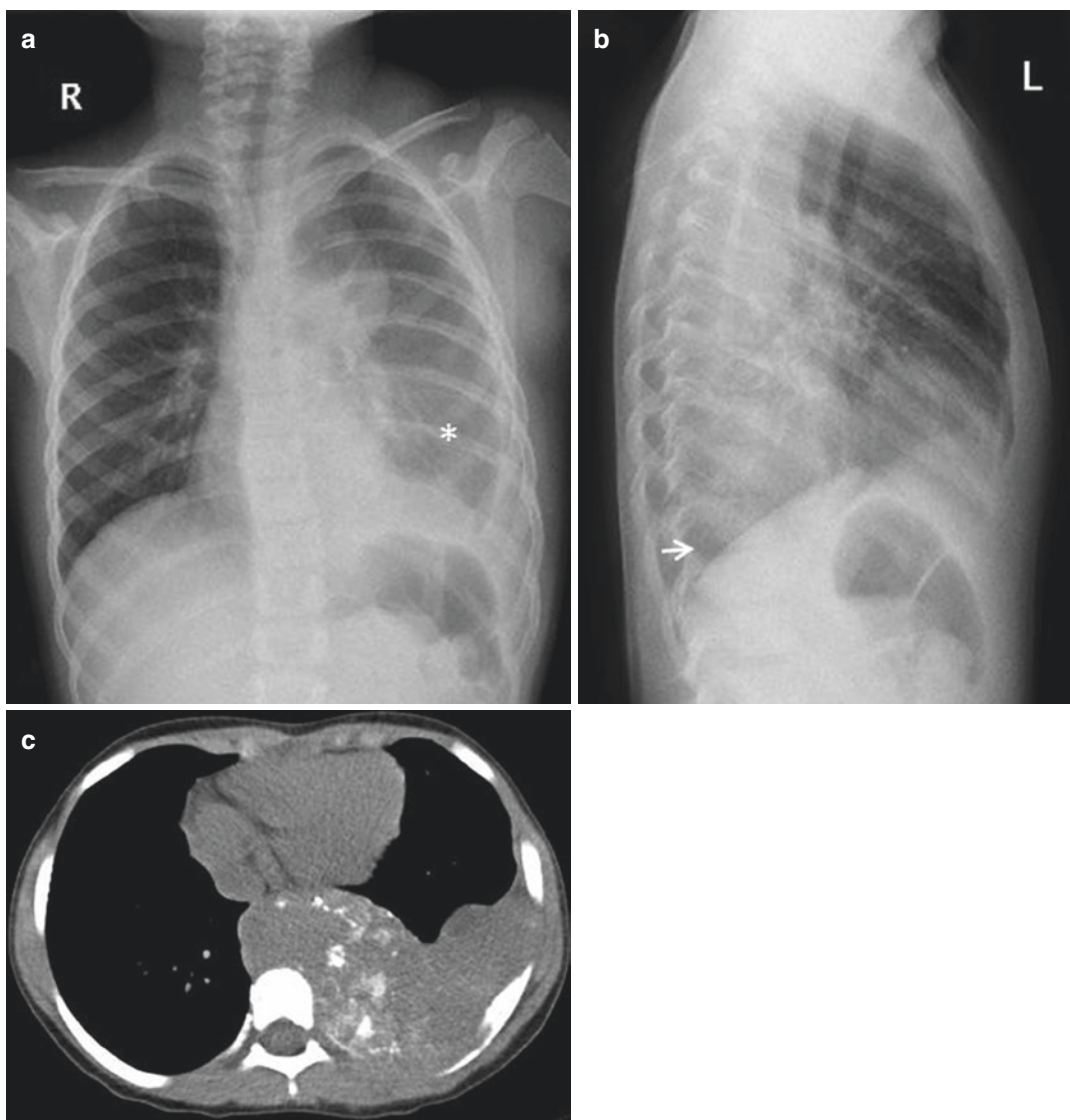
Fig. 11.12 (**a**, **b**) Frontal and lateral chest radiographs of a 2-year-old child with an upper left mediastinal opacity, extending to the left lower hemithorax. The opacity shows internal calcifications. Note the intercostal space widen-ing at multiple levels on the left with rib erosion (asterisk), as well as the enlarged intervertebral foramina (arrow) on the lateral view. CT (**c**) confirms a mediastinal mass with internal calcifications representing a neuroblastoma

3 years. Relative lack of density of the thymus allows visualization of underlying lung vessels and should never compress adjacent structures.

- Failure to identify the thymus in an infant should raise the possibility of a combined immune defi-ciency such as DiGeorge syndrome.
- After cardiac surgery, a widened mediasti-num should not be attributed to a large thy-

mus. It should raise suspicion for hematoma or mass.
- A posterior mediastinal mass in a young child should be considered a neuroblastoma until proven otherwise.
- Deviation of the trachea to the left on frontal chest or airway radiographs should raise con-cern for a vascular abnormality or mass.
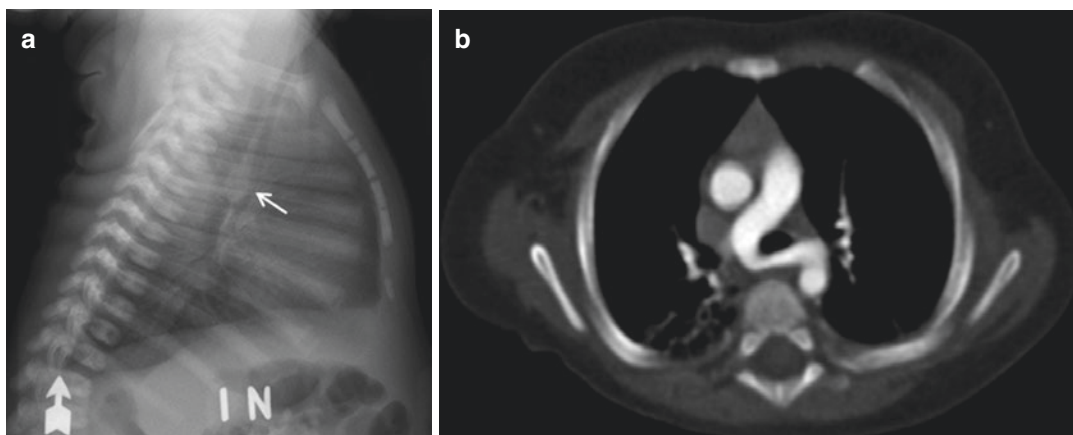
Fig. 11.13 (**a**) Lateral chest radiograph of a 7-month-old girl with a well-defined oval opacity between the trachea and air-filled esophagus (arrow). (**b**) CT confirmed a pulmonary sling

11.2.4 Bones

Careful evaluation of the bones on chest radiography can often yield valuable information. In a small infant, unsuspected rib fractures may be the first indicator of non-accidental injury (NAI). Other findings, including osteopenia, bone destruction, and scoliosis, can be subtle but suggest underlying congenital or metabolic bone disease, infection, or treatment-related changes (Fig. 11.14).

11.3 Abdomen

Abdominal pathology in the pediatric population differs substantially from that in adults. Additionally, both abdominal pathology and normal bowel appearance also change over time as the child grows.

Abdominal pain is a very common complaint among pediatric patients in the emergency department. If appendicitis, gynecologic abnormalities, or intussusception are clinically suspected, ultrasound is the first imaging modality of choice. When a child presents with bilious vomiting, an emergency upper gastrointestinal (GI) series needs to be done to exclude malrotation. CT is used much less frequently, due to concerns about radiation dose and immobilization issues, as well as the great advantage of ultrasound in the young due to the small body habitus.

When the symptoms are non-specific, radiographs of the abdomen are frequently used as the initial imaging of choice, although their diagnostic yield is limited. Rothrock et al. [14] evaluated high-yield criteria for obtaining abdominal radiographs in the emergency assessment of children. They concluded that abdominal radiographs should be restricted to patients with at least one of the following features: prior abdominal surgery, foreign body ingestion, abnormal bowel sounds, abdominal distention, and peritoneal signs.

11.3.1 Bowel Gas Pattern

There is significant variability in the normal bowel gas pattern in children. The findings on abdominal radiographs are often non-specific,
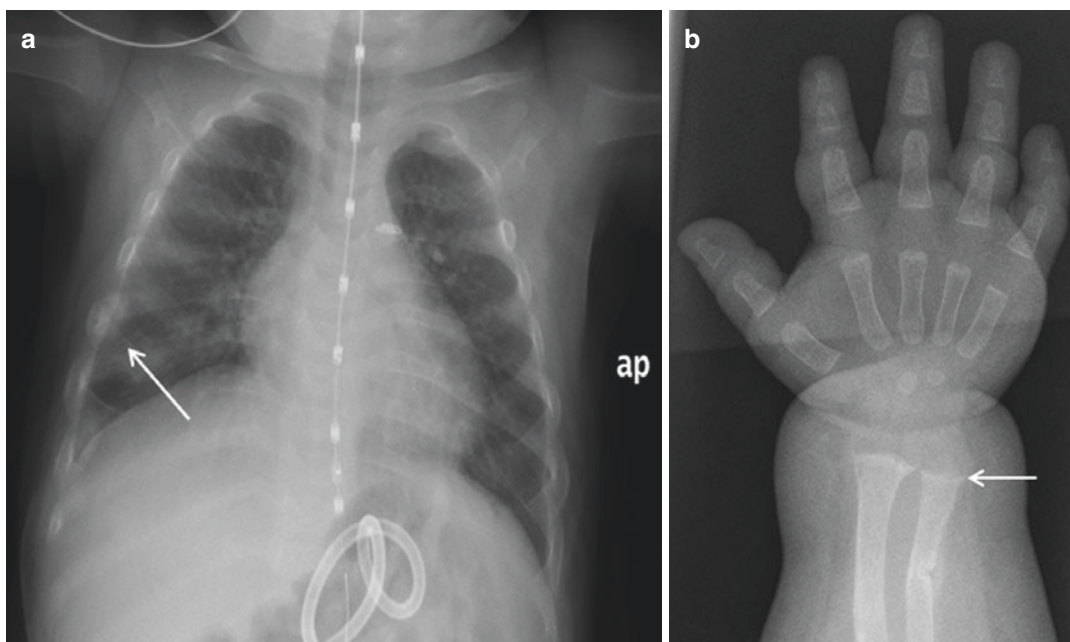
Fig. 11.14 (**a**) The AP chest of a 1-year-old girl admitted for choking episodes. There was subtle callus along the lateral aspect of the right sixth rib (arrow), suggesting a fracture and raising possibility of non-accidental injury. A radiograph of the right wrist (**b**) shows a healing fracture in the distal ulna and metaphyseal cupping and flaring of the distal ulna (arrow) and radial metaphysis. A diagnosis of rickets was confirmed

subtle, or normal. Therefore, one should not rely on the radiographic findings alone to exclude potentially catastrophic diagnoses, including midgut volvulus and intussusception [15]. If clinically suspected, further assessment with other modalities (e.g., upper GI series, US) should be performed (Fig. 11.15). When doing an upper GI series to investigate suspected midgut volvulus, it is important to remember that midgut volvulus often produces partial obstruction, allowing contrast material to advance to distal bowl loops. The hallmark of midgut volvulus is the "corkscrew" appearance of the duodenum (Fig. 11.16). Ultrasound is also useful in diagnosing volvulus and can show a typical "swirl sign" in the upper and mid abdomen.

Other factors to assess are displacement and dilatation of bowel loops on radiographs.

Displacement of bowel loops should raise concern for an abdominal mass (Fig. 11.17). When a mass is identified in the first year of life, it is most commonly benign and of renal origin, particularly hydronephrosis or a multicystic dysplastic kidney. Beyond this age, primary tumor of the kidney (e.g., Wilms tumor) is a more commonly encountered diagnosis [16].

Radiographic evaluation of possible bowel obstruction in children may be challenging. Children typically have more abundant bowel gas than adults. Distension of small and large bowel loops may be seen normally. A normal size of a small bowel loop should be less than the combined height of the L1 and L2 vertebral bodies [17]. Another important feature in diagnosing small bowel obstruction is dilated small bowel loops with absence of identifiable
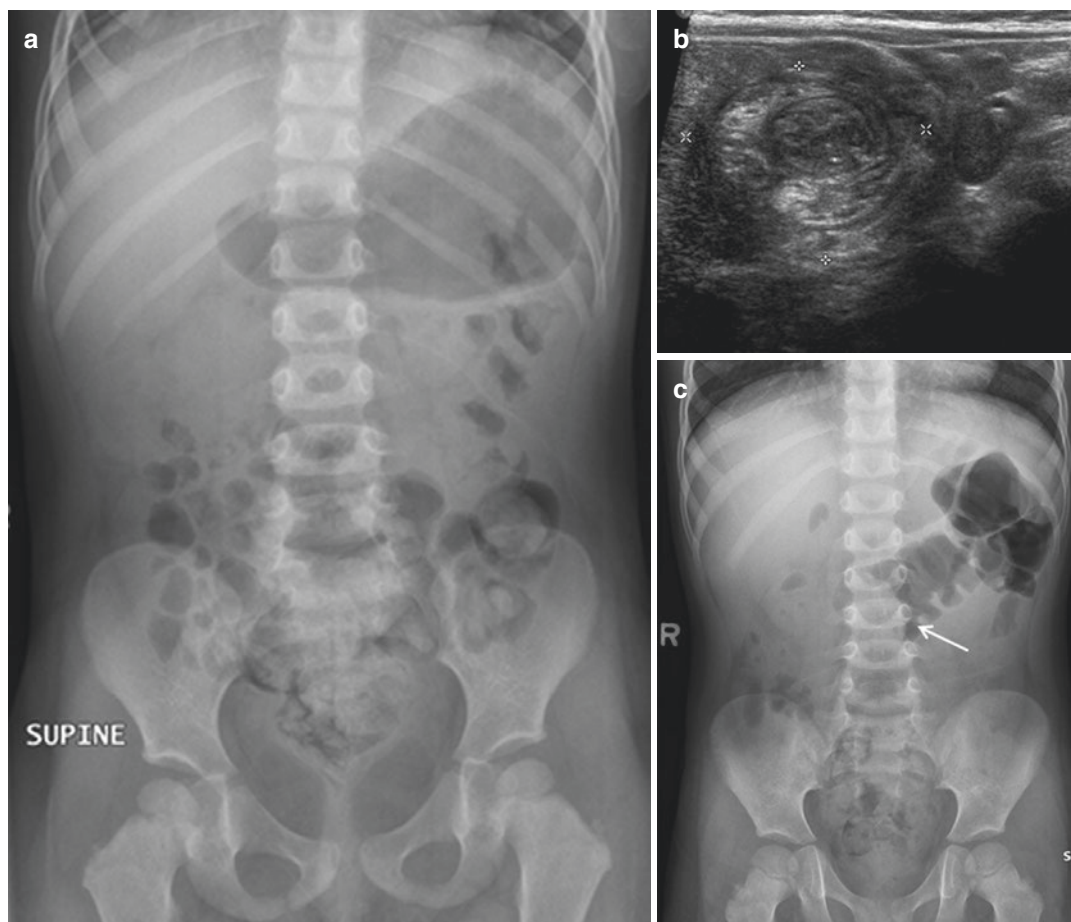
Fig. 11.15 (**a**) Supine abdominal radiograph of a 2-year-old girl with colicky abdominal pain shows no specific bowel abnormality. (**b**) Ultrasound of the same patient demonstrates an ileocolic intussusception. (**c**) Supine abdominal radiograph of another child with suspected intussusception shows the typical soft-tissue density in the mid abdomen, with a crescent of air around the intussus-ceptum in the colon (arrow)

large bowel dilatation. However, in neonates it is often in neonates it is often difficult to differentiate small from large bowel, as the haustral pattern has not yet developed. It is important to use a horizontal beam image (cross-table lateral, left lateral decubitus, or upright view) to assess for air-fluid levels. Also, ultrasound may be helpful in assessing the bowel. With bowel obstruction, the differential diagnosis varies substantially from adults. Congenital causes are much more frequent in children [18].

Teaching Points

- The bowel gas pattern on radiographs is often non-specific and may even appear nor-
mal in the presence of potentially catastrophic diagnoses, including midgut volvulus and intussusception. If clinically suspected, further assessment with other imaging modalities (e.g., upper GI series, US) should be obtained.
- Bowel distension without air-fluid levels can represent a normal bowel gas pattern in infants.

11.3.2 Calcifications

Abdominal calcifications on pediatric radiographs are important. When a renal calculus or

Fig. 11.16 Frontal view of the abdomen from an upper GI examination of a 3-year-old girl shows malrotation with the typical corkscrew appearance (arrow) of the duodenum and proximal jejunum, representing midgut volvulus. Note contrast filling of more distal bowel loops, due to incomplete obstruction

gallstone is seen, the possibility of an underlying metabolic condition should be considered. Tumors including neuroblastoma can show calcifications on at least 30% of radiographs [19] (Fig. 11.18). Although neuroblastoma most typically arises from the adrenal, it can originate anywhere along the sympathetic nervous system [20]. Another cause for adrenal calcifications is remote adrenal hemorrhage, usually from the perinatal period. These tend to be focal triangular-shaped calcifications, and are of no consequence, but require confirmation with other imaging, including ultrasound, to exclude an associated mass. In a neonate the finding of scattered calcifications in the abdomen should raise the possibility of prenatal bowel perforation with meconium peritonitis.

Teaching Point

- When calcification is noted on abdominal radiographs in children, a broad differential diagnosis must be considered. Do not forget the possibility of a mass; further investigation is recommended, starting with ultrasound.
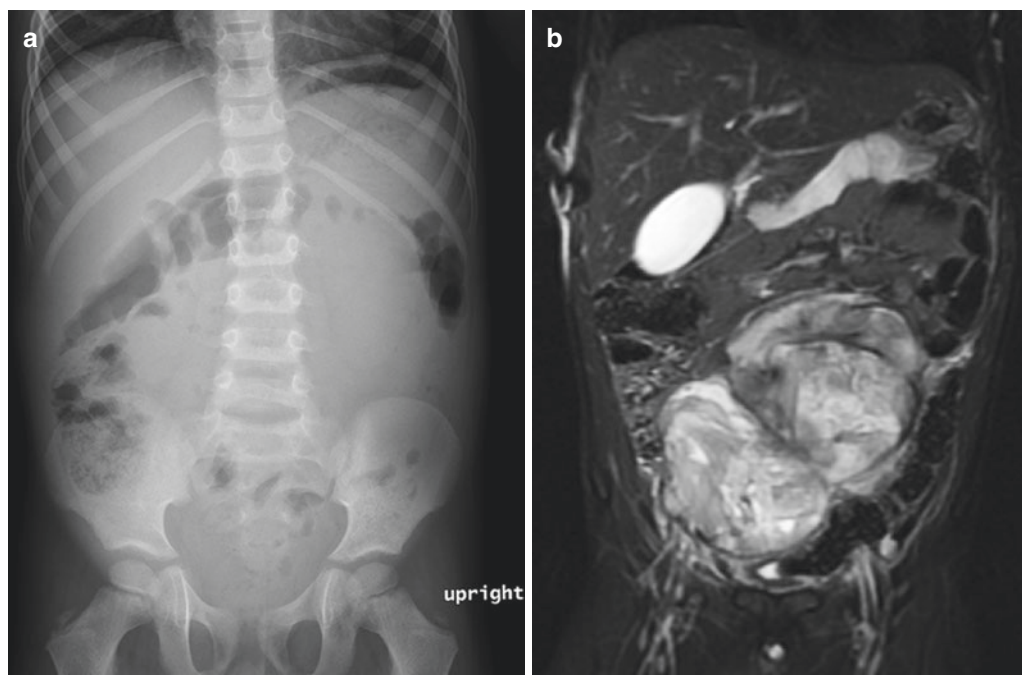

Fig. 11.17 (**a**) Frontal upright view of the abdomen showing soft tissue in the mid abdomen displacing bowel loops. (**b**) A large tumor (rhabdomyosarcoma) was confirmed on MRI
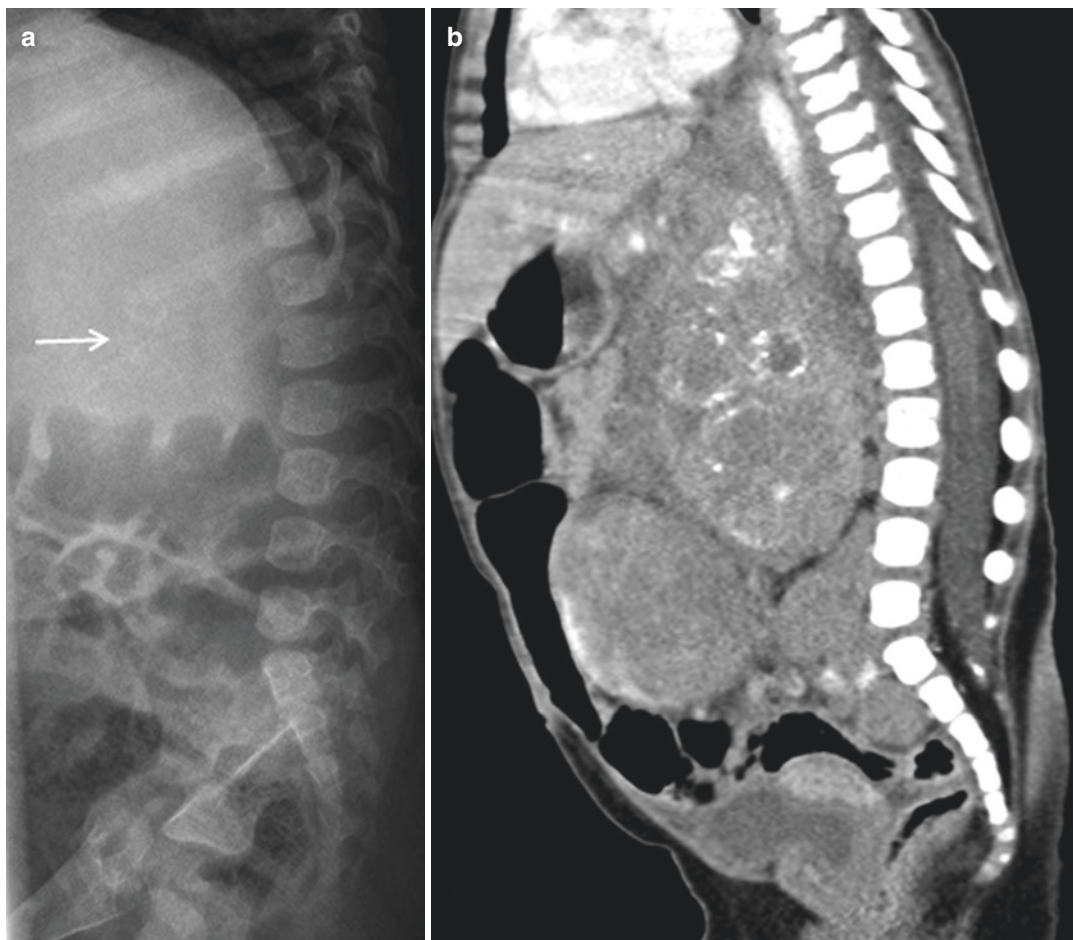
Fig. 11.18 (**a**) Lateral radiograph of the lumbar spine of a 10-month-old girl showing punctate calcifications (arrow) projecting over the liver. (**b**) CT showing a large abdominal mass with internal calcifications, which was subsequently confirmed to be a neuroblastoma

11.3.3 Bones

Evaluation of the osseous structures on plain abdominal radiographs should be done as a routine. As the young patient not always communicates or localizes symptoms, an abdominal radiograph may be the initial imaging examination obtained [16]. Congenital and developmental abnormalities, focal bone abnormality, and infection are occasionally revealed.

Developmental dysplasia of the hip (DDH) can be seen as an incidental finding on an abdominal radiograph (Fig. 11.19). Although DDH is considered highly treatable when detected early,

a missed or late diagnosis is often challenging to manage and can lead to significant disability. Assessment of the hip joints on abdominal radiographs is particularly important in non-ambulatory children in whom hip subluxation may not be evident clinically [16].

Unexpected fractures should also be looked for, to identify unsuspected non-accidental injury. Sacral integrity, Legg-Calvé-Perthes (LCP) disease, and slipped capital femoral epiphysis (SCFE) are additional entities which should be kept in mind when assessing the osseous structures, depending on the age of the patient.

Fig. 11.19 Frontal supine abdominal radiograph of a 14-month-old girl with a G-tube and abdominal distention. In addition to the distended bowel loops, incidental note was made of asymmetry of the femoral heads, superior dislocation of the left hip, and a very shallow left acetabulum, representing left- sided developmental dysplasia of the hip. Note the small pseudo-acetabulum at the superior acetabular corner

Teaching Point
- It is essential to evaluate the osseous structures on abdominal radiographs as well as to be aware of the disorders specific for the pediatric age group.

11.3.4 Foreign Bodies

Ingested foreign bodies are common, as young children will put anything into their mouths and will often inadvertently swallow them. Special attention should be paid if the ingested foreign body is metallic, as it may represent a magnet. Differentiating magnets from other metallic objects is a challenge. However, if two or more metallic foreign bodies are seen adjacent to each other, magnet ingestion should be suspected [5]. Multiple small magnets are
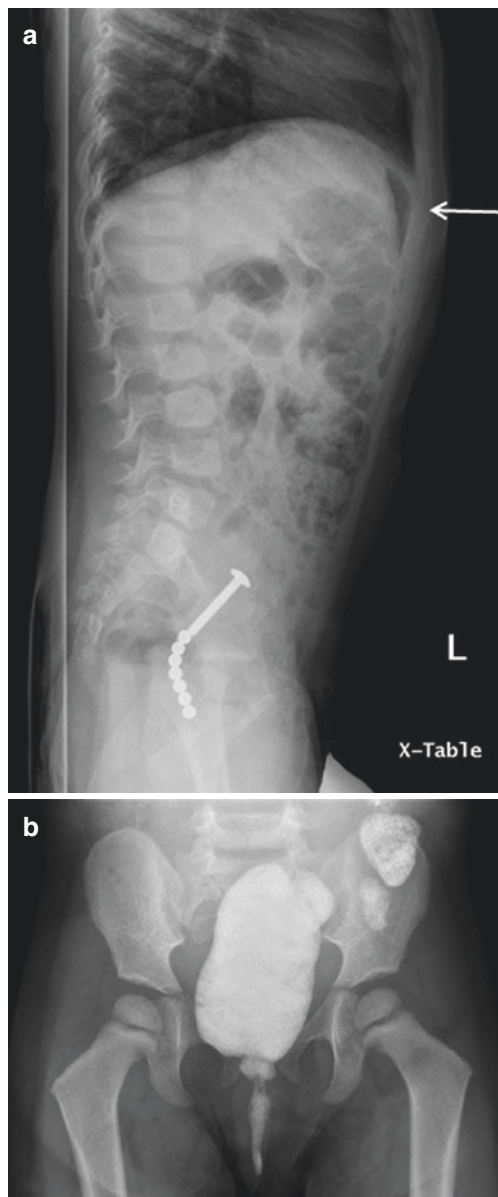

Fig. 11.20 (**a**) Lateral cross-table radiograph of the abdomen of a 3-year-old boy who swallowed a screw and multiple round magnets. Note the small amount of free air anteriorly (arrow). (**b**) Frontal radiograph of the pelvis of a 2-year-old with an incidental finding of radiopaque material filling the rectosigmoid and correlating with the clinical history of large amount of sand ingestion

of particular concern as they can cause bowel complications, including perforation and volvulus (Fig. 11.20a). Other foreign bodies such as sand can be radiopaque on radiographs and

may have the appearance of contrast material in the bowel (Fig. 11.20b).

Teaching Point

• There can be serious consequences if multiple magnets are ingested. It is therefore important to image the neck, chest, and abdomen, if foreign body ingestion, in particular magnets, is suspected.

11.4 Musculoskeletal

Interpretive errors by pediatric radiologists reviewing musculoskeletal (MSK) radiographs are relatively rare. An assessment of radiologists' errors was performed by Bisset et al. in 2014 [21]. They reviewed 3865 radiographs of the elbow, wrist, knee, and ankle of children and young adults with pain and/or trauma and found a 1.6% miss rate and a 1.1% overcall rate by radiologists. Misses and overcalls were most common in the ankle. Interpretive performance by emergency physicians, on the other hand, was assessed by Smith et al. [22] and found 19.4% of misses on evaluating 1000 cases. The bones most associated with missed fractures were the pelvic, carpal bones, vertebrae, and patellae.

Many of the pitfalls in pediatric musculoskeletal imaging are related to misleading history (e.g., minor trauma that is not the cause of the detected finding or trauma which has been forgotten or unwitnessed) and/or poor localization of pain by the young child. This is especially common in the setting of a limping child, in which the abnormalities may be subtle and easily missed. It sometimes requires imaging of the lower extremities and pelvis for diagnosis [23]. Delayed images to detect evidence of healing are also frequently helpful.

The increased elasticity of the skeletal structures in children allows for specific fracture types which may be subtle and difficult to detect. A typical and common example is that of toddler's fracture of the tibia. These may not be apparent until evidence of healing, including subperiosteal new bone formation, is present on follow-up imaging. This is not to be confused with the

physiologic periosteal reaction seen in small infants along the shafts of long bones before the age of 6 months. This is always symmetrical in distribution (Fig. 11.21).

The torus fracture is also commonly seen in children. It can be easily missed, as it consists of only a contour abnormality without a visualized cortical break. This typically affects the metaphysis of a bone, and its detection requires familiarity with the normal contours of the bones.

The presence of unfused growth plates in skeletally immature children has given rise to the Salter-Harris classification of pediatric fractures. Undiagnosed growth plate injuries can lead to long-term deformities, and therefore they are important to recognize. If in doubt, a view of the contralateral extremity may be performed to assess for symmetry [24].

The variable appearance of the ossifications and physeal plates is another common source of error in pediatric MSK imaging, especially in the setting of trauma. Ossification is not a homogenous process, and although generally the ossification is predictable timewise, there is substantial variability.

11.4.1 Elbow

The multiple ossification centers of the elbow joint are a source of imaging pitfalls. The ossification centers appear radiographically in a predictable fashion following the mnemonic CRITOE: capitellum, radial head, internal (medial) epicondyle, trochlea, olecranon, and external (lateral) epicondyle. The age of appearance of these ossification centers is approximately 1, 3, 5, 7, 9, and 11 years of age, respectively. These ages may vary between individuals, and girls frequently ossify 1–2 years earlier than boys when nearing puberty. This predictable order is key in evaluating the elbow in children [24]. The absence of an expected ossification center may indicate a fracture, such as a displaced medial epicondyle (Fig. 11.22).

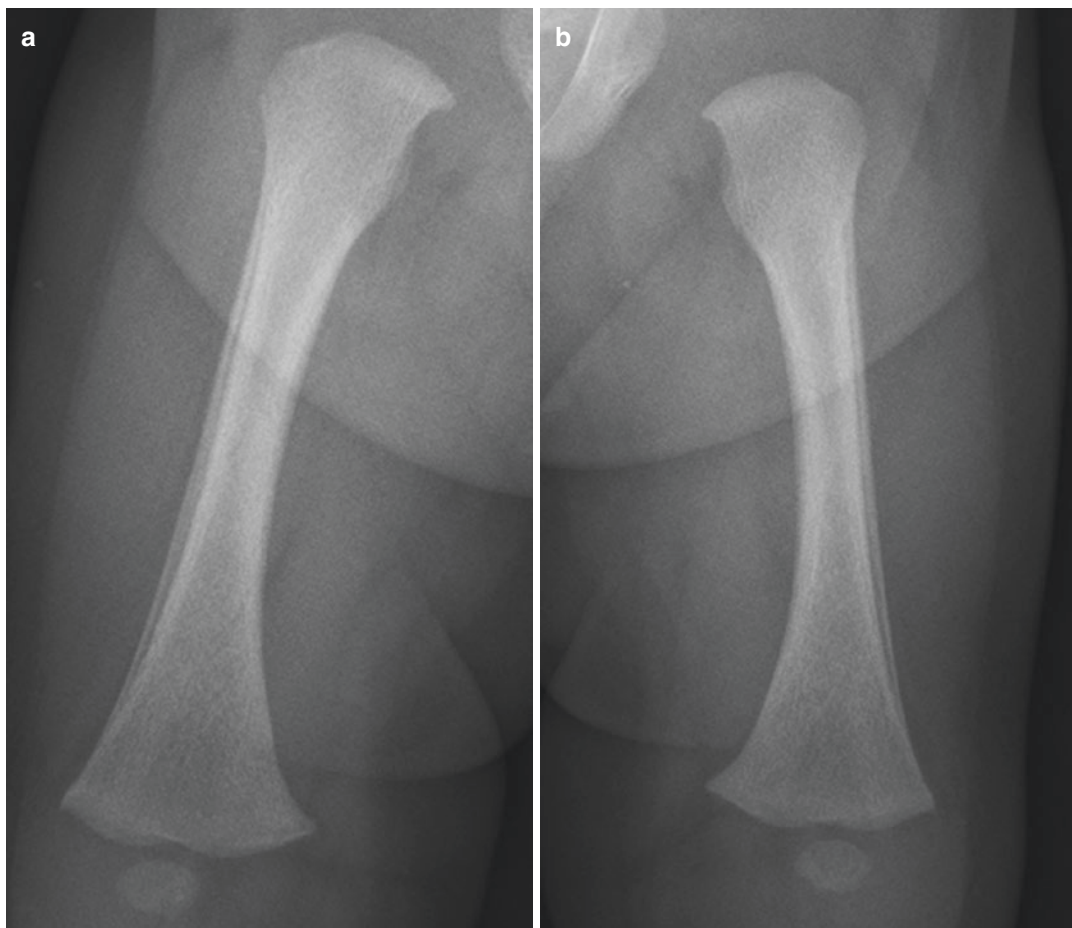When assessing the elbow, it is also very important to look for a joint effusion, seen as

Fig. 11.21 A 3-month-old boy with physiological, symmetrical, periosteal bone reaction along the shafts of the right (**a**) and left (**b**) femora

elevated anterior and posterior fat pads on the lateral view (Fig. 11.23). With a joint effusion, a fracture is presumed to be present, even when not seen on radiographs [25]. A prospective study demonstrated that the posterior fat pad sign was predictive of an occult fracture of the elbow following trauma in 76% of 45 children who had no other evidence of fracture on anteroposterior, lateral, and oblique radiographs after the injury [26]. Children with elbow joint effusion without identifiable bony abnormality after trauma are usually treated with posterior splinting for a presumptive non-displaced fracture. The anterior humeral line may be helpful in assessing for subtle supracondylar fracture of the humerus.

The radiocapitellar line is important to evaluate for radial head dislocation (Fig. 11.24). This can be easily missed, as alignment is usually maintained on the frontal view, and the malalignment must be specifically evaluated on a true lateral projection.

Teaching Points
- The ossification centers of the elbow should follow the CRITOE mnemonic. If they do not, consider a fracture.
- Elbow joint effusion should always be mentioned as it usually implies an occult fracture in children. Follow-up imaging is recommended.
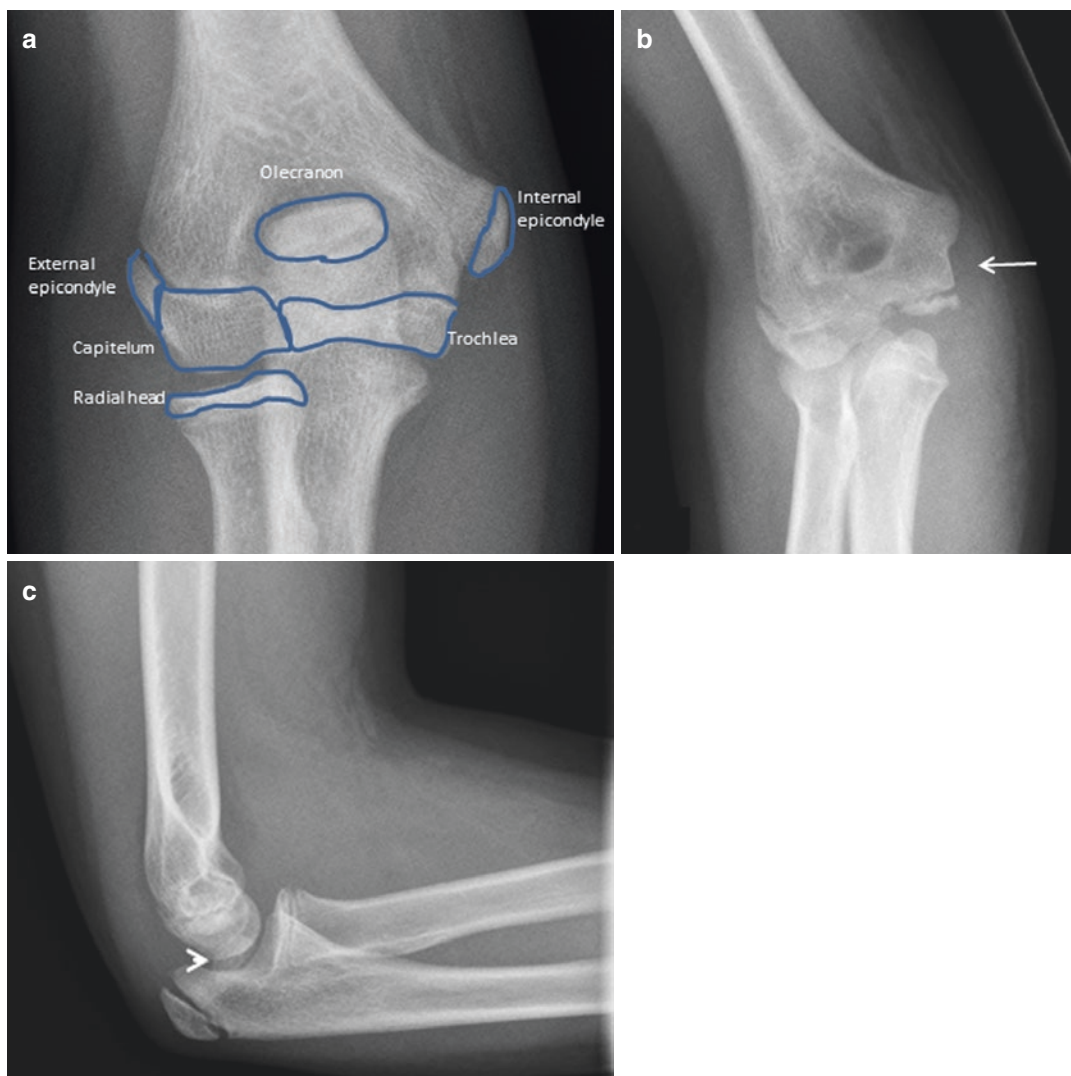
Fig. 11.22 (**a**) Frontal radiograph of the elbow of a 12-year-old boy, showing the normal appearance of the ossification centers (CRITOE). (**b**) Frontal view of an 11-year-old boy with absence of the normal position of the medial epicondyle (arrow), in the presence of a well-ossified trochlea. (**c**) The avulsed, displaced medial epicondyle is faintly visualized on the lateral view (arrowhead). Also note a joint effusion

11.4.2 Shoulder

The skeletal maturation of the shoulder also follows a normal sequential pattern. In the glenoid, the subcoracoid secondary ossification center is the first scapular secondary ossification center to ossify and forms the upper one-third of the glenoid articular surface. It typically appears at 8–10 years of age and fuses completely by 16–17 years of age. The lower accessory ossification centers normally appear at 14–15 years of age. These should not be confused with fractures.

The acromioclavicular joint is cartilaginous at birth. The adjacent bones are not fully ossified until 14–16 years. It is important not to misinterpret the non-ossified area as acromioclavicular joint widening and acromioclavicular separation [27].

Fig. 11.23 Lateral radiograph of the elbow of a 9-year-old boy who fell from a trampoline. There is elevation of the posterior and anterior fat pads, indicating that there is a joint effusion. There is a fracture of the radial neck. A subtle olecranon fracture is also present which was not appreciated initially (arrow)

Fig. 11.24 Lateral radiograph of the elbow of a 6-year-old girl with a history of fall off a trampoline, with pain in the left elbow, and decreased mobility. The radial head is not aligned with the capitelum, indicating an anterior radial head dislocation

Failure of fusion of the ossification center for the acromion by 18–25 years results in an os acromiale, which may cause shoulder impingement, rotator cuff tear, or degenerative acromioclavicular joint disease. The unfused acromion ossification center in children should not be confused with a fracture.

Fig. 11.25 AP radiograph of the left shoulder of a 14-year-old girl shows the normal undulating growth plate as two separate lines traversing the proximal humerus (arrows), which should not be mistaken for a fracture

The proximal humeral physis frequently manifests as two separate lines traversing the proximal humerus on the AP projection due to an undulating configuration. This can be misinterpreted as a fracture. Familiarity with this appearance, the absence of cortical discontinuity, and the absence of adjacent soft-tissue swelling, help to distinguish the normal growth plate from a proximal humeral fracture [23, 27] (Fig. 11.25).

Teaching Point
- Be aware of mimickers: ossification centers of the glenoid, acromioclavicular distance, os acromiale, and proximal humeral physis.

11.4.3 Pelvis and Hip

The ischiopubic synchondrosis usually closes between the age of 4 and 12 years, often asymmetrically. It can manifest as unilateral swelling with irregular mineralization on radiographs. This normal ossification pattern of the synchondrosis should not be mistaken for an aggressive bone process. Although it is usually an incidental finding, it can be associated with pain. In these symptomatic patients, further assessment with MRI is recommended to assess for possible associated pathology, including stress reaction or infection [23] (Fig. 11.26).

Apophyseal avulsion fractures of the pelvis and hip typically occur in the adolescent involved

Fig. 11.26 (**a**) Frontal pelvis radiograph of a 6-year-old boy with acute right hip pain, showing bony expansion and irregularity in the expected location of the right ischiopubic synchondrosis. This was thought to represent a normal variant. Due to ongoing pain in this area, an MRI was performed. (**b**) Axial T2-weighted fat-suppressed image shows marked bone marrow edema around the right ischiopubic synchondrosis, indicating a stress reaction, which is also known as ischiopubic synchondrosis syndrome, or Van Neck-Odelberg disease

in active sports. It is due to sudden forceful muscle contraction which causes the apophysis attached to the tendon to avulse. This most commonly occurs at the ischial tuberosity (hamstrings) and anterior superior iliac spine (sartorius) but also at the anterior inferior iliac spine (rectus femoris) and lesser trochanter (iliopsoas) [28]. Assessment of symmetry with the asymptomatic side is very helpful in accurate diagnosis (Fig. 11.27).

Legg-Calvé-Perthes (LCP) disease and slipped capital femoral epiphysis (SCFE) are pathologies which should be kept in mind when assessing the pediatric pelvis. In LCP disease, early radiographs may show very subtle flattening of the femoral head and subchondral lucency (i.e., a "crescent sign") (Fig. 11.28). In SCFE, the epiphysis slips posteriorly, and it is therefore better appreciated on the lateral view. It is also important to remember that SCFE may occur bilaterally in up to one-third of patients; therefore slippage of the contralateral side should be looked for acutely, as well as on follow-up images (Fig. 11.29).

Irregular density of pelvic bones related to overlying bowel contents may be seen over the medial two-thirds of the iliac wings. If the irregularity is seen involving the lateral one-third, it is unlikely to be related to bowel, and an osseous abnormality including infection or tumor should be considered (Fig. 11.30).
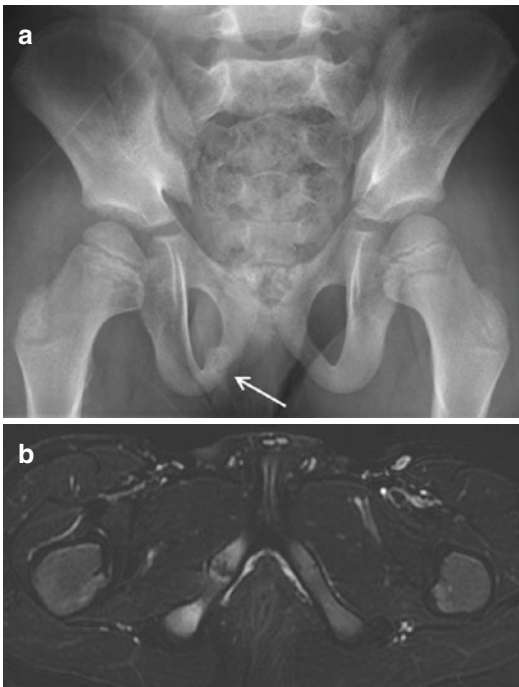
Teaching Points
- Do not mistake an asymmetric ischiopubic synchondrosis for an aggressive process.
- In adolescents with acute pelvic trauma, remember the many sites of possible pelvic apophyseal injury.
- Bowel contents should not superimpose over the lateral outer third of the iliac wings.

11.4.4 Knee

In children aged 2–12 years, more so in boys than in girls, the normal ossification of the posterior non-weight-bearing portion of the distal femoral
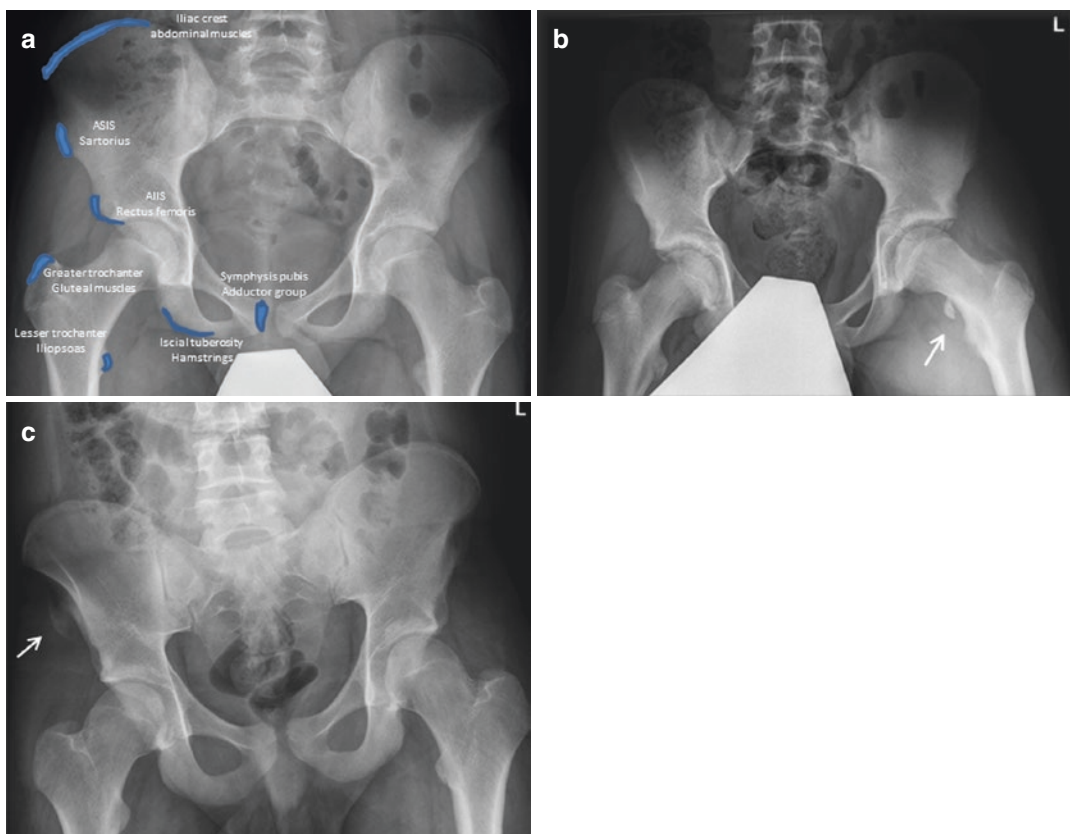
Fig. 11.27 AP views of the pelvis (**a**) showing the possible locations of pelvic avulsion fractures. (**b**) A 17-year-old boy with an avulsion fracture of the left lesser trochanter (arrow). (**c**) A 14-year-old boy with an avulsion fracture of the right anterior superior iliac spine (arrow)

Fig. 11.28 Frontal radiograph of the pelvis, showing mild flattening and subchondral lucency ("crescent sign") of the left femoral head (arrow), indicating Legg-Calvé-Perthes disease

epiphysis can appear irregular, fragmented, and spiculated, resembling abnormal processes including osteochondritis dissecans on radiographs [24, 29, 30] (Fig. 11.31).

Focal cortical irregularity along the postero-medial aspect of the distal femoral metaphysis in children and adolescents (typically 10–15 years of age) should not be mistaken for an aggressive process. It is thought to be related to reactive change at the medial supracondylar ridge due to repetitive stress at the attachment of the medial head of the gastrocnemius or adductor magnus (Fig. 11.32).

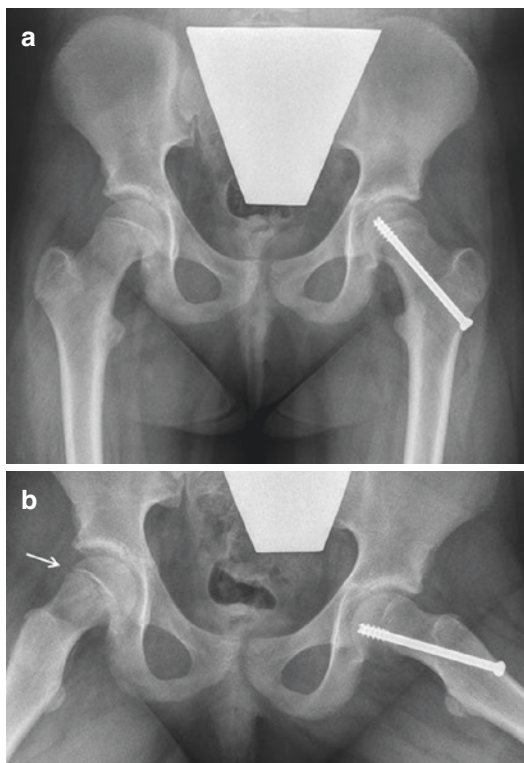Abnormal conditions unique to children are seen at the extensor mechanism of the knee [31].

Fig. 11.29 AP (**a**) and lateral (**b**) views of the hips of an 11-year-old girl, following pinning for left slipped capital femoral epiphysis, who presented 1 year later with right hip pain. The slippage of the right femoral epiphysis is better appreciated on the lateral view (arrow)

Fig. 11.30 (**a**) AP view of the pelvis of an 11-year-old boy, showing apparent bowel contents superimposed on the lateral third of the right iliac bone, which is suspicious for a tumor. There is also a soft-tissue component along the superior aspect of the iliac crest (arrows). (**b**) On MRI, axial T1-weighted fat-suppressed post-contrast image shows an abnormal right iliac bone with a surrounding large soft-tissue mass, representing a Ewing sarcoma

Osgood-Schlatter disease is generally seen in the 10- to 15-year-olds, in boys more than in girls, with a history of jumping or kicking. It is due to chronic microtrauma at the patellar tendon insertion onto the tibial tubercle. Radiographically, soft-tissue swelling, increased density of the most inferior part of Hoffa's fat pad, thickening of the patellar tendon, and fragmentation of the tibial tubercle should suggest the diagnosis in the presence of clinical abnormality. Remember that in isolation, the normal tibial tubercle can have a very irregular appearance (Fig. 11.33). Sinding-Larsen-Johanssen disease is a similar entity affecting the lower pole of the patella. Both conditions require clinical correlation for accurate diagnosis.

Tibial tubercle fractures are most common in teenage boys, usually associated with jumping sports. Sometimes the normal physis of the tibial tubercle can be confused with a fracture, as there
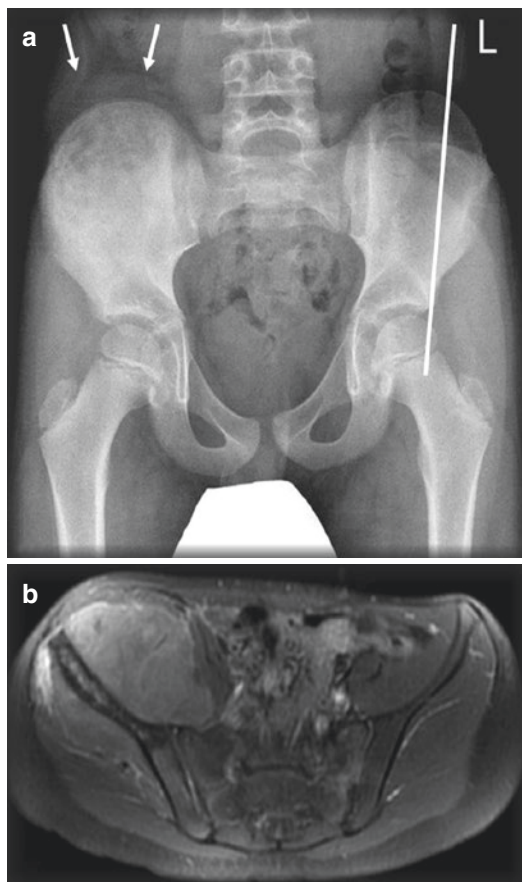
can be a prominent lucency on the frontal projection (Fig. 11.34).

In the context of acute trauma, it is important to exclude inferior patellar sleeve fracture. In this fracture, the cartilage of the inferior patella is avulsed, often with a small bony fragment. Radiographs can show patella alta and a small bone fragment of the inferior patella, with or without an associated knee joint effusion. In isolation, a normal secondary ossification center of the inferior pole of the patella should not be confused with an avulsion fracture (Fig. 11.35).

Fig. 11.31 Lateral radiograph of the knee of a 10-year-old boy, showing irregularity along the posterior non-weight-bearing portion of the femoral epiphysis (arrow), which is normal for his age

Fig. 11.32 Lateral view of the knee of a 12-year-old boy showing focal cortical irregularity along the posterior aspect of the distal femoral metaphysis, a normal variant which should not be mistaken for an aggressive process

Teaching Points
- The normal ossification of the posterior non-weight-bearing margin of the femoral condyles often appears irregular, fragmented, and spiculated.

- Focal cortical irregularity in the posteromedial aspect of the distal femoral metaphysis in children and adolescents can mimic an aggressive process.
- In the region of the knee, osteochondritis dissecans, Osgood-Schlatter disease, Sinding-Larsen-Johanssen disease, and patellar sleeve avulsion should be considered. However, consider that irregularity of the lower pole of the patella and tibial tubercle in isolation can be seen normally on radiographs in children.

11.4.5 Foot and Ankle

The apophysis of the proximal fifth metatarsal bone is the source of a common pitfall in the setting of foot trauma. The apophysis typically appears at around 10 years of age in girls and 12 years of age in boys. It fuses after approximately 2 years. Fractures in this location typically are oriented transversely, whereas the apophysis growth plate is oriented along the long axis of the bone [24] (Fig. 11.36).

In the ankle, a joint effusion does not necessarly imply an occult fracture, as it does in the elbow. Salter-Harris type 3 fracture of the distal tibia may be quite subtle on radiographs but is always accompanied by fluid in the joint. When it occurs in adolescence during incomplete growth plate closure, the characteristic pattern of a Tillaux fracture is commonly seen. This affects the lateral part of the distal tibial epiphysis and may be obscured by the overlapping distal fibula. A tibial triplane fracture (Salter-Harris type 4) is also seen during adolescence and should be considered when ankle trauma is encountered in this age group (Fig. 11.37).

Teaching Points
- Orientation of the apophysis at the base of the fifth metatarsal helps differentiate it from a fracture.
- Tillaux and triplane fractures of the distal tibia are typical fractures seen during adolescence.
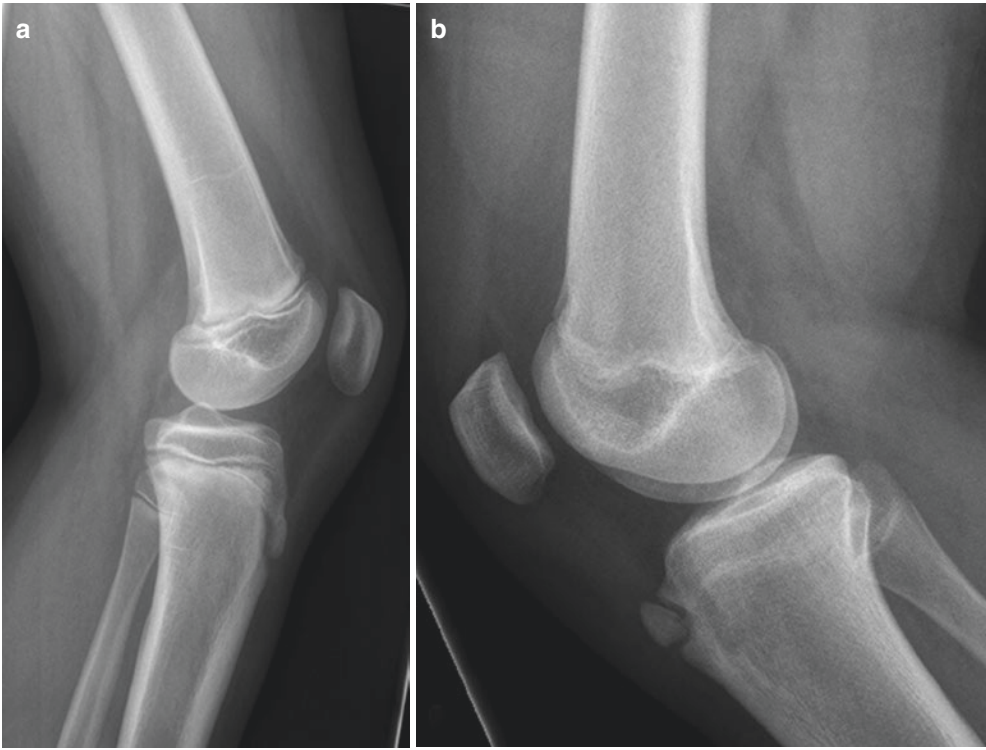
Fig. 11.33 Lateral radiographs of the knee. (**a**) A 9-year-old boy, showing a normal appearance of the tibial tuberosity and patellar tendon. (**b**) A 12-year-old girl, showing fragmentation of the tibial tuberosity and thickening of the patellar tendon, which is suggestive of Osgood-Schlatter disease
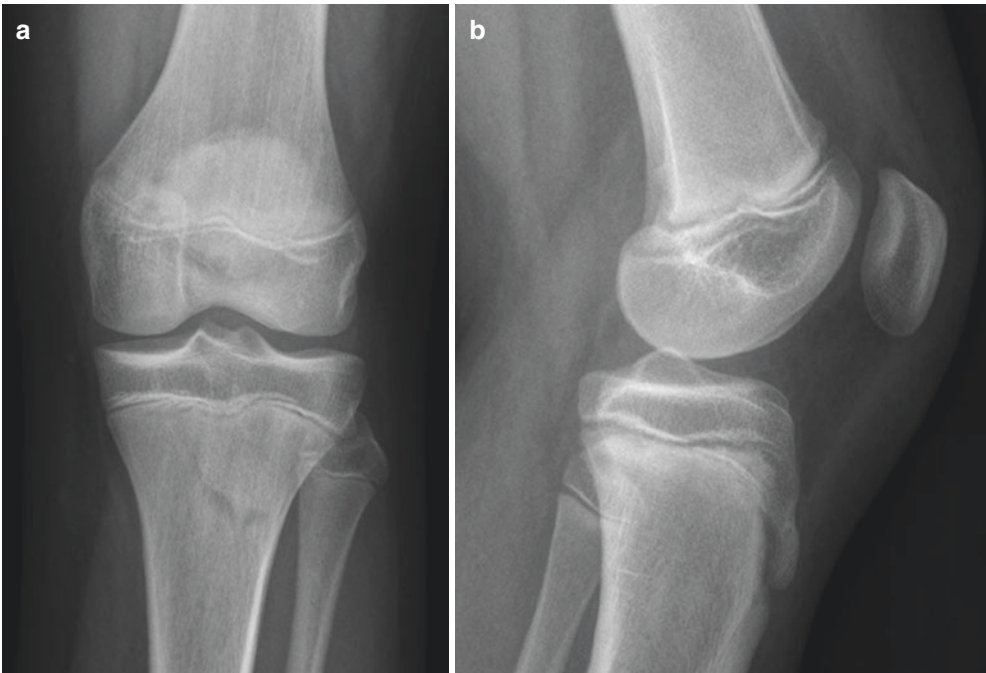

Fig. 11.34 (**a**) Frontal radiograph of the knee, showing an apparent fracture line in the tibial metaphysis. (**b**) Lateral view confirming that this represents the physis of a normal tibial tubercle
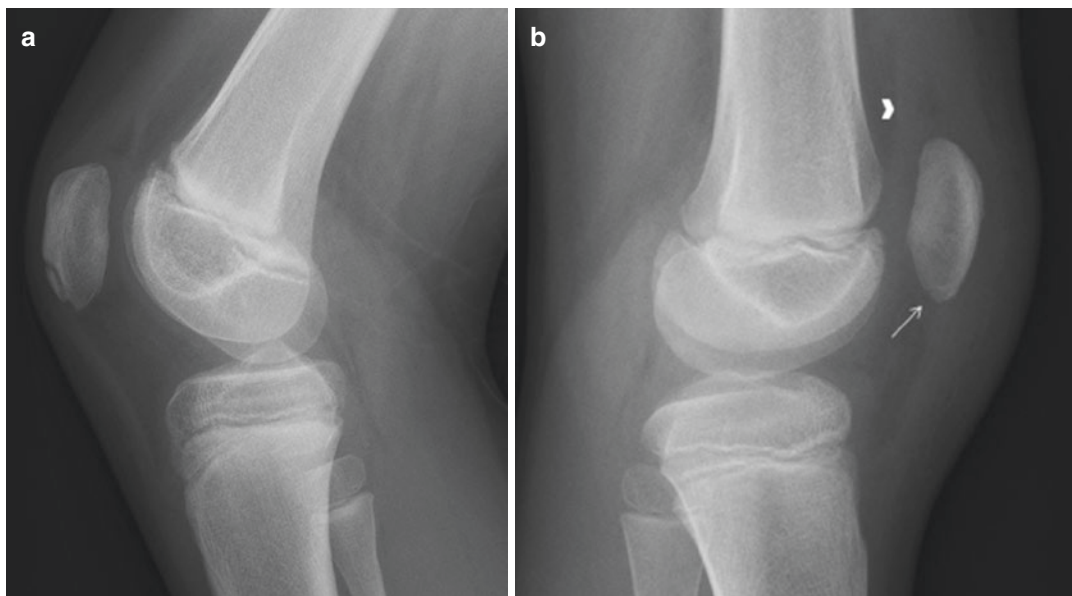
Fig. 11.35 Lateral radiographs of the knee. (**a**) Bony fragment at the anterior inferior pole of the patella, which is well defined with sclerotic margins. This represents a normal secondary ossification center, which is often seen in this location. (**b**) Avulsion fracture of the inferior patella with a subtle fracture line (arrow) and associated soft-tissue swelling and a joint effusion (arrowhead)

11.5   Neuroimaging

The most common indications for neuroimaging of the pediatric patient presenting to the emergency department include trauma (accidental or non-accidental), suspected shunt malfunction, first-time afebrile seizure, suspected vascular abnormality (arterial ischemic event, venous event, vasculitis, and dissection), and infection (meningitis/encephalitis).

11.5.1   Brain Parenchyma

Head trauma is one of the most common reasons for an emergency department (ED) visit in pediatrics. Children are more susceptible to traumatic brain injury because of a larger head-to-body size ratio, a thinner cranial vault, and less myelinated neural tissue, which makes them more vulnerable to damage [32]. All patients with abnormal examination findings, altered mental status, or major mechanisms of injury should undergo a CT. Debate exists as to which patients with minor head injury require CT [33]. However, a multicenter Canadian study of 3886 children with minor head injury (defined as history of loss of consciousness, amnesia, or disorientation in a patient who is conscious and responsive in the ED with a Glasgow Coma Scale score of 13–15) suggested that if any of the following exist, head CT is recommended: Glasgow Coma Scale score less than 15 at 2 h, suspected open or depressed skull fracture, worsening headache, persistent irritability, sign of a basal skull fracture, a large boggy scalp hematoma, and a dangerous mechanism of injury [34].

One confounder in pediatric brain imaging, specifically in the setting of trauma, is benign enlargement of the subarachnoid spaces (BESS) mimicking a subdural collection. BESS typically presents as rapid head growth and/or macrocephaly between 3 months and 3 years of age in normally developing infants. It is characterized on imaging by enlarged subarachnoid spaces, particularly involving the bi-frontal spaces. Mild ventriculomegaly may be associated with BESS. A simple way to distinguish between

Fig. 11.36 Oblique radiographs of the foot. (**a**) Normal unfused apophysis at the base of the fifth metatarsal bone, oriented along the long axis of the bone. (**b**) Additional lucent line oriented transversely in the same region, representing a fracture

BESS and a subdural fluid collection is by identifying the position of the subarachnoid vessels. These are displaced toward the pial surface by a subdural collection but traverse freely through the prominent subarachnoid spaces in BESS [24, 35] (Fig. 11.38). In equivocal patients, this can easily be appreciated using color Doppler prior to closure of the anterior fontanelle or on IV contrast-enhanced CT or MRI. On cross-sectional imaging, changing the window and

Fig. 11.37 Oblique radiograph of the ankle of a 13-year-old girl with right ankle trauma showing a vertical fracture line through the distal tibial epiphysis (arrow), with widening of the lateral physis (arrowhead), indicating a Tillaux fracture

level of the images may also help to differentiate between these conditions.

The hematocrit level at birth is normally high. It decreases more or less linearly in the first 28 days of life [36]. An elevated hematocrit results in increased attenuation of cerebral vessels and venous sinuses on non-enhanced CT, simulating cerebral sinus venous thrombosis (CSVT) or intracranial hemorrhage. CT is not commonly performed in the neonate. However, when performed, correlation with the hematocrit level is important to differentiate between hemoconcentration and CSVT (Fig. 11.39).

When interpreting a head CT, it is essential to carefully evaluate for the presence of hypoattenuation in the brain parenchyma to exclude the possibility of ischemia. This is especially true in the pediatric patient, as the clinical level of suspicion is usually low for a cerebral vascular accident. In addition, an atypical presentation can lead to a delay in diagnosis. Subtle loss of gray-white matter differentiation and/or hypo-/hyperattenuation can also point to the presence of encephalitis or tumor (Fig. 11.40).

Although MR imaging in the pediatric population can be difficult to obtain at times, often requiring sedation or general anesthesia, its use has expanded over time. There are now a growing number of emergency indications, including stroke, cerebral sinus thrombosis, meningitis/encephalitis, discitis/osteomyelitis, transverse myelitis, and trauma. This shift is a reflection of the many advantages of MR in depicting soft-tissue processes and bone marrow edema, as well as the heightened awareness of the radiation exposure associated with pediatric CT. Additionally, rapid MR imaging protocols have reduced the length of MR imaging examinations while still providing clinically valuable information. This has been especially useful in the clinical setting of shunt evaluation in children treated for hydrocephalus [37, 38].

Sutures, accessory sutures, and Wormian bones can mimic calvarial fractures. Sutures typically have a zigzag course and sclerotic borders and are found in expected locations. Nonetheless, suture diastasis is the most common type of pediatric skull fracture. The use of symmetry is helpful in identifying suture diastasis. When CT is performed, additional 3D reformatted images are helpful in assessing the skull and the sutures [39] (Fig. 11.41).

Teaching Points
- Look at the distribution of subarachnoid vessels in extra-axial fluid collections on ultrasound, CT, or MRI, to differentiate between the subarachnoid and the subdural spaces.
- Sutures have a typical zigzag course and sclerotic borders, which can help differentiate them from fractures.
- Be meticulous in the evaluation of the gray-white matter differentiation in children on CT, as this can give clues to underlying pathology.
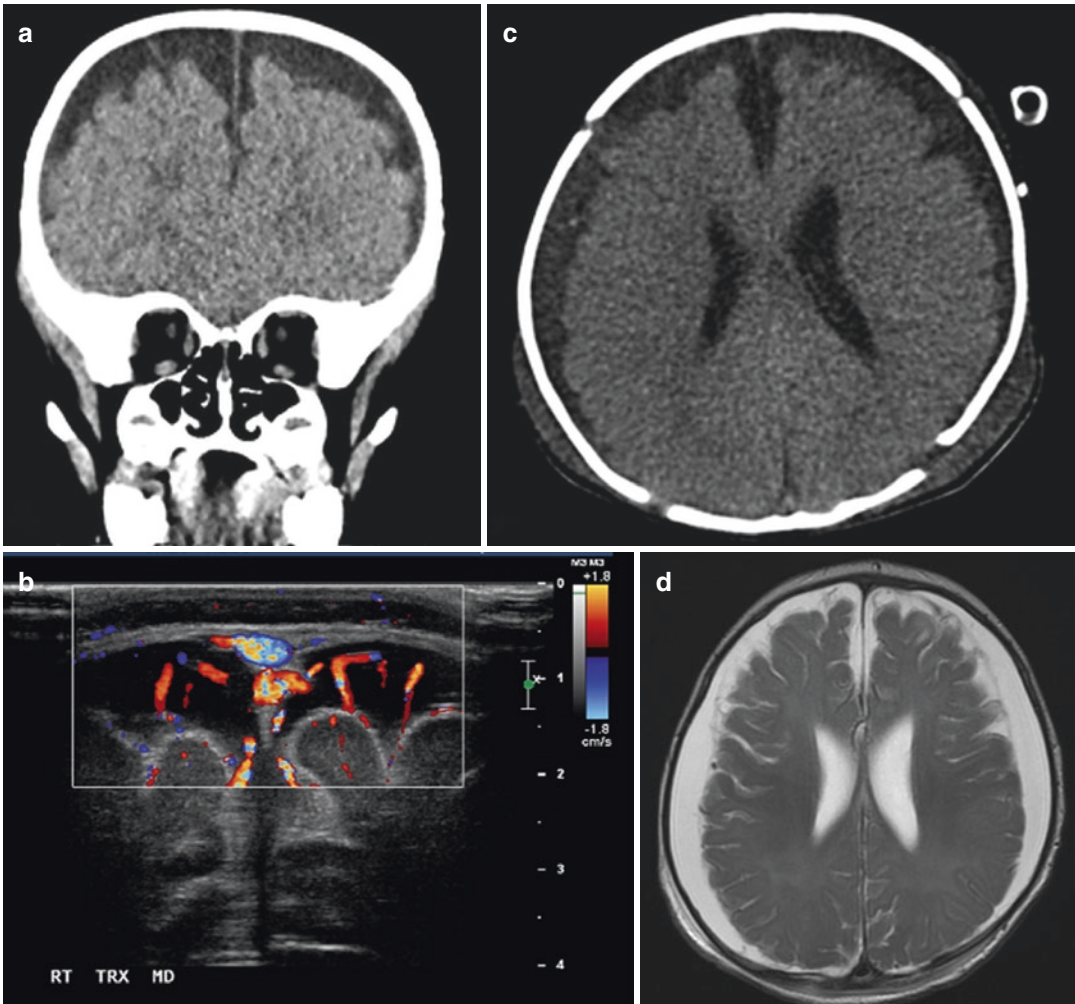
Fig. 11.38 (**a**) Coronal image of a non-contrast CT of the brain of a 9-month-old baby demonstrating prominence of the extra-axial CSF spaces over the frontal lobes. (**b**) Color Doppler ultrasound image showing subarachnoid vessels traversing this space, confirming that this is subarachnoid fluid. This is suggestive of "benign enlargement of subarachnoid spaces" (BESS) in the presence of normal development. (**c**) Axial image of a non-contrast CT of the brain of an age-matched baby post-trauma showing prominence of the extra-axial fluid spaces over both frontal lobes. (**d**) MRI confirms that this is subdural, the extra-axial T2 bright fluid being devoid of crossing vessels

11.5.2 Paranasal Sinuses

The paranasal sinuses do not reach adult size until the second decade of life; therefore, interpretation errors occur if one is unfamiliar with their development [40]. At birth, the sphenoid bone contains red (erythropoietic) marrow which converts to yellow (fatty) marrow at around 7 months to 2 years. These fatty changes that normally occur before pneumatization should not be misinterpreted for hemorrhage, proteinaceous fluid, or a dermoid cyst on MRI [41].

When evaluating a child with sinusitis and/or mastoiditis, especially if there is poor response to treatment, it is important to assess for complications. This requires cross-sectional imaging. Subtle changes around an affected sinus must be looked for. Complications can be divided into superficial (osteomyelitis, subgaleal abscess or "Pott puffy tumor," and septic thrombophlebitis), orbital (preseptal

cellulitis/abscess, subperiosteal postseptal abscess, extraocular myositis, optic neuritis, and septic thrombophlebitis), and intracranial (meningitis, epidural abscess, subdural emphy-sema, cerebritis, brain abscess, and cavernous sinus thrombosis) (Fig. 11.42).

Teaching Point

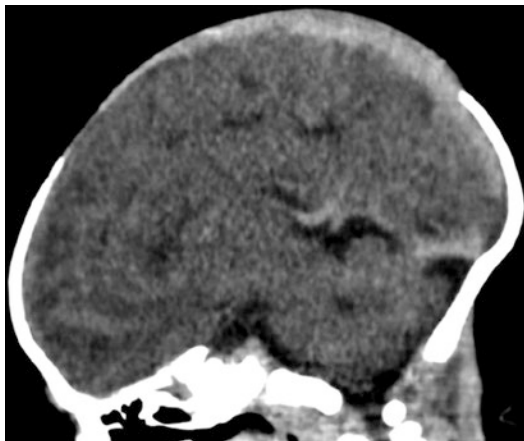- Cross-sectional imaging is required if complications of sinusitis are suspected.

11.5.3 Cervical Spine

Emergency radiologic evaluation of the pediatric cervical spine can be challenging because of the presence of synchondroses, normal anatomic variants, and injuries which are unique to children. Upper cervical spine injuries most commonly occur in children younger than 8 years of age [40]. It is important to remember that the anatomy of the developing cervical spine predisposes children to injury of the upper cervical spine and that these injuries are associated with a high risk of neurologic damage, with a 25–50% prevalence of associated head injuries [42]. Thoracic and lumbar spine injuries
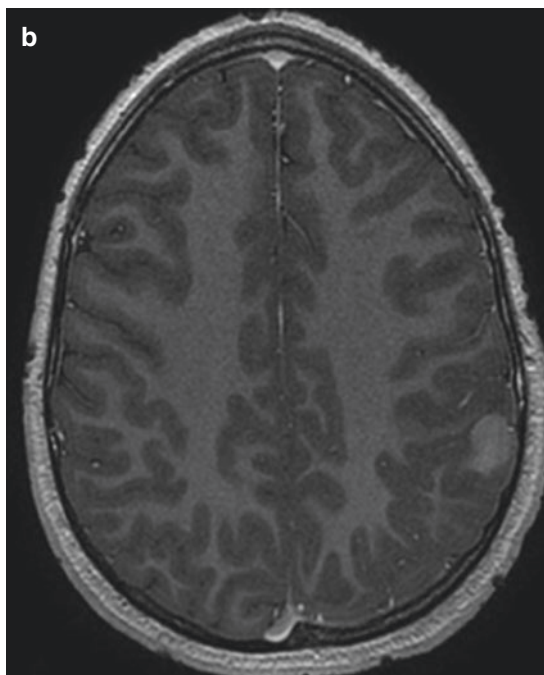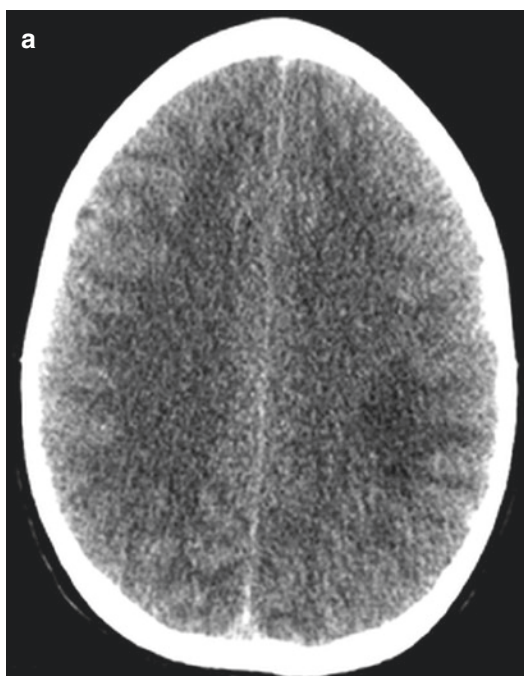

Fig. 11.39 Sagittal reconstruction of a head CT of a newborn. No contrast was given. There is hyperdensity of the dural sinuses, simulating *cerebral* sinovenous thrombosis, which is related to the normal high hematocrit in this age group

Fig. 11.40 (**a**) Non-contrast CT of an 11-year-old boy presenting with first-time focal seizures, showing ill-defined hypodensity in the left parietal lobe. (**b**) MRI demonstrates a left parietal cortical mass. (**c**) Non-contrast CT of another child after minor head injury. There is sub-tle hyperdensity in the posterior fossa, causing mass effect on the fourth ventricle (arrow), which was overlooked. (**d**) MRI done 3 years later demonstrates a large posterior fossa tumor
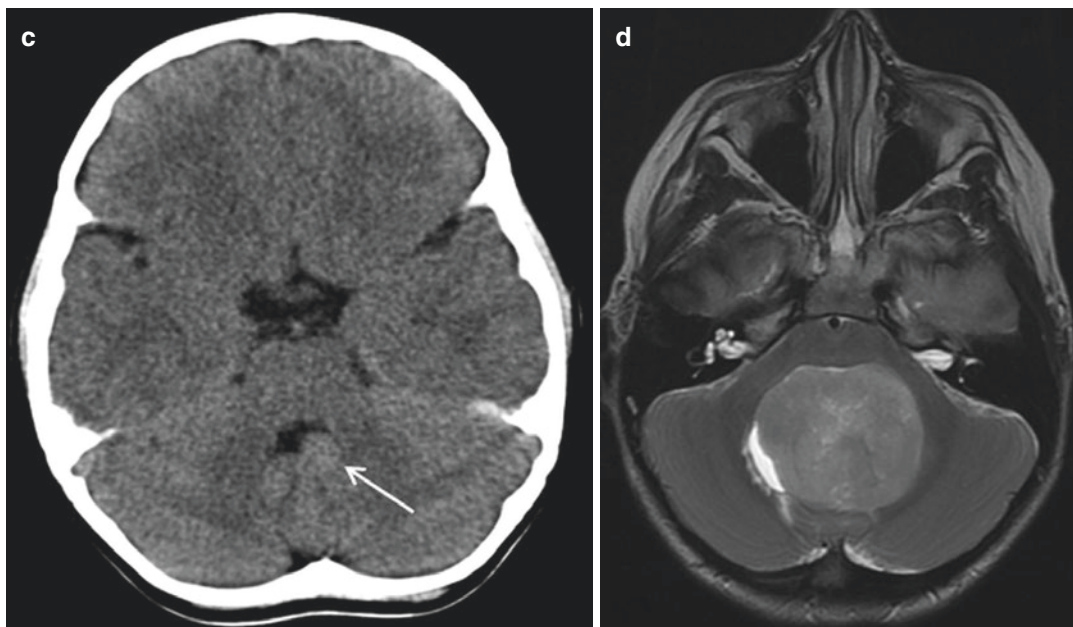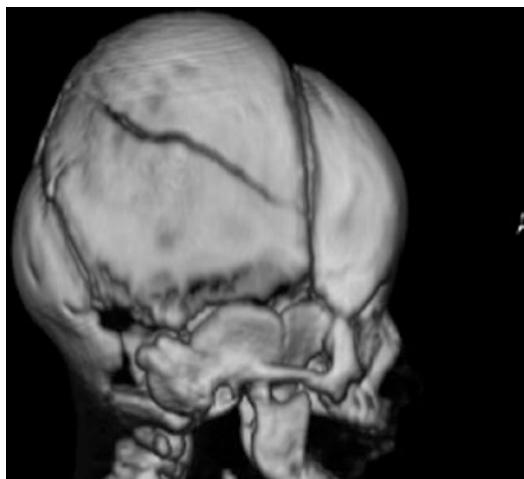
Fig. 11.40 (continued)

Fig. 11.41 Sagittal 3D reformatted image of the skull of a 26-day-old infant who fell from 3 feet onto a hard floor. Note linear parietal skull fracture

are more frequent in teenagers and show similar patterns to adult fractures.

The body of C2 usually fuses with the odontoid process by 3–6 years of age. The subdental synchondrosis at the base of the odontoid process can be seen until age 11 years, however. It is seen as a lucent line, not to be mistaken for a transverse fracture of the dens (type 2 fracture).

There is also a secondary ossification center, the os terminale, at the tip of the odontoid process, which appears between 3 and 6 years of age. It fuses by 12 years of age. Normal synchondrosis and physeal plates should be recognized as smooth, regular structures with subchondral sclerotic lines, unlike acute fractures, which are irregular and are not sclerotic [42] (Fig. 11.43).

The C1 vertebral body ossifies at a faster pace compared to C2. As a result, the C1 lateral masses may appear laterally offset with respect to C2 on the open-mouth odontoid view, simulating a C1 ring fracture (i.e., "pseudo-Jefferson" fracture) (Fig. 11.44). Up to 6 mm lateral offset of the lateral masses may be normally seen up to 4–7 years of age [24, 42]. The atlanto-axial interval, defined as the distance between the anterior aspect of the dens and the posterior aspect of the anterior ring of the atlas, can be up to 5 mm normally in children, compared to up to 3 mm in adults [42].

Approximately 50% of children less than 8 years old have pseudosubluxation of C2 on C3 and, to a lesser degree, C3 on C4. This is caused by ligamentous laxity in children, which permits normal mobility at these levels. In physiologic pseudosubluxation, the posterior spinolaminar line (drawn along the anterior margin
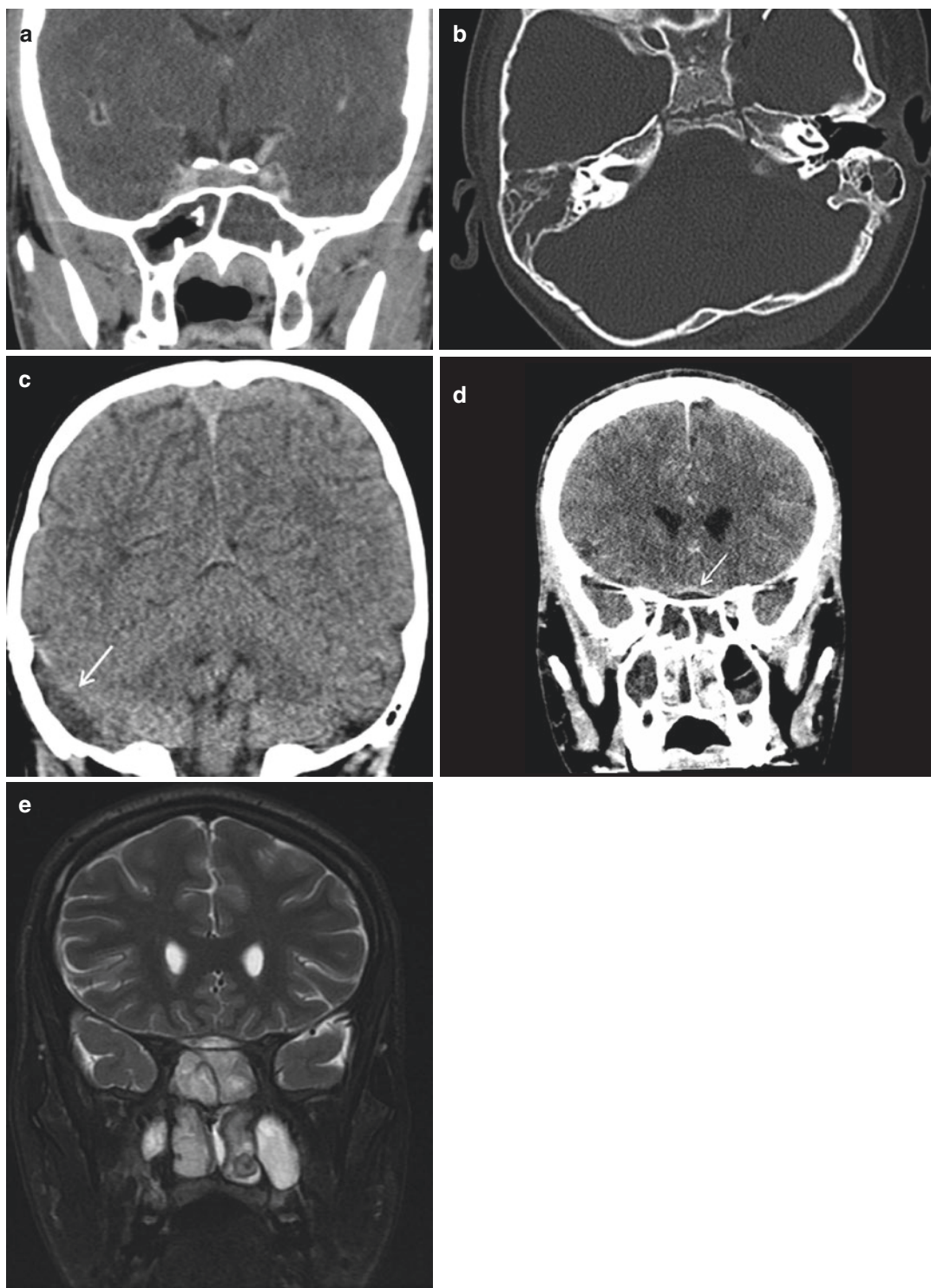
Fig. 11.42 (**a**) IV contrast-enhanced coronal CT of the brain of a 12-year-old boy with sinusitis showing left cavernous sinus thrombosis. (**b**, **c**) Axial and coronal images of a non-contrast CT of a 2-year-old girl with right mastoiditis and epidural abscess (arrow). (**d**) IV contrast-enhanced coronal CT of the brain of a 15-year-old boy with sinusitis, showing an epidural abscess along the planum sphenoidale (arrow). (**e**) T2-weighted coronal MR images demonstrate this better
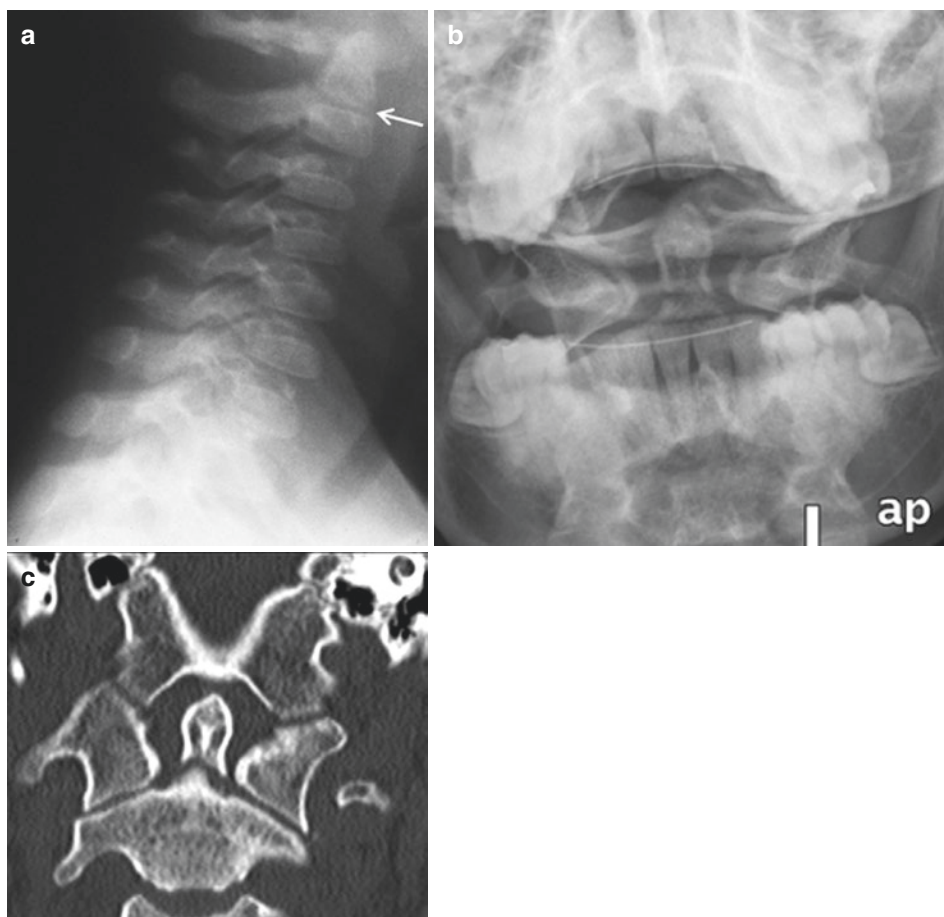
Fig. 11.43 (**a**) Lateral radiograph of the cervical spine in a 3-year-old boy shows a normal subdental synchondrosis with subchondral sclerotic lines (arrow). (**b**) Open-mouth view of the cervical spine in an 8-year-old trauma patient, showing an acute fracture of the dens. (**c**) This was confirmed on CT
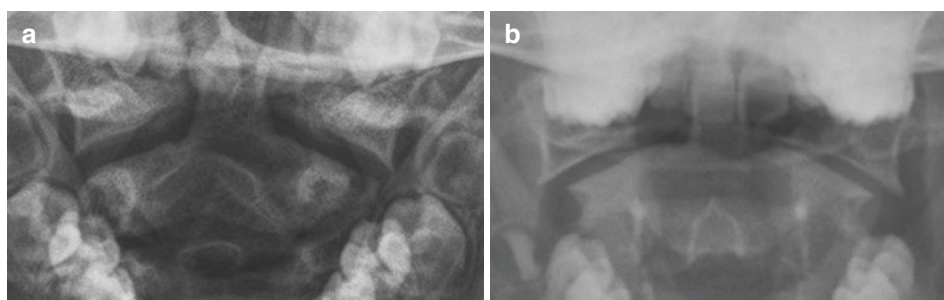

Fig. 11.44 Open-mouth views of the cervical spine in a 7-year-old boy. (**a**) There is a "pseudo-Jefferson" appearance with mild spread of the atlas on the axis. (**b**) There is a Jefferson fracture in this second patient, showing more pronounced lateral displacement of the lateral masses of C1

of the spinous processes of C1 and C3) touches or is 1 mm anterior to the corresponding C2 spinolaminar line. If the distance is greater than 2 mm, it indicates the presence of an injury, and CT should be done [24, 35, 42] (Fig. 11.45).

Straightening of the cervical lordosis can be seen normally in children up to 16 years of age when the neck is in a neutral position [35, 42].

Cervical vertebral bodies have an oval shape in early infancy and become rectangular with
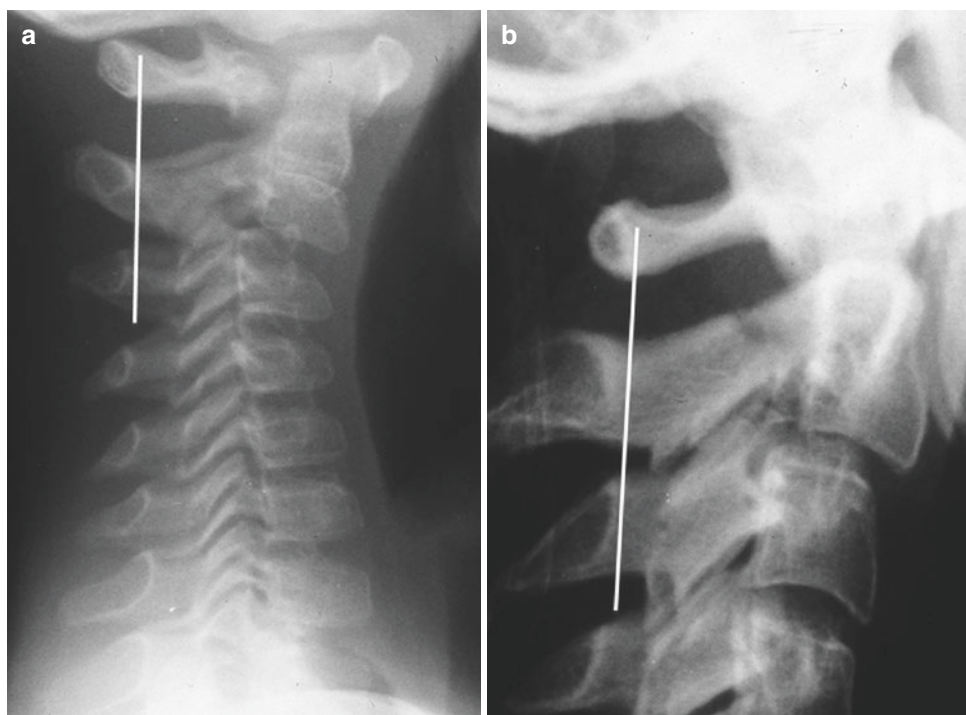
Fig. 11.45 Lateral cervical spine views. (**a**) Pseudosubluxation, the C2 vertebral body is mildly anteriorly displaced on C3. However, the spinolaminar line from C1 to C3 touches or is within 1 mm of the corresponding C2 spinous process. Also note the anterior wedging of the vertebral body of C3, a normal appearance for age, which should not be confused with a compression fracture. (**b**) True subluxation, the distance between the spinolaminar line and the C2 spinous process is greater than 2 mm. A fracture of the pars interarticularis at C2 is also shown

age. This is most conspicuous at the C3 level. Anterior wedging of up to 3 mm of the vertebral bodies should not be interpreted as a compression fracture [35, 42] (Fig. 11.45a).

SCIWORA, defined as "spinal cord injury without radiographic abnormality" depicted on conventional radiographs or CT, is more common in children due to anatomic features which predispose them to hypermobility of the spinal column in the absence of bony injury. MR imaging should therefore be performed to evaluate for spinal cord injury when neurological abnormality (transient or persistent) is present, despite the absence of radiographic abnormalities [42, 43].

Calcifications of the intervertebral discs are quite common in adults, are mainly degenerative in nature, and occur most commonly at the level of mid thoracic and upper lumbar spine. Disc calcification in children, however, is a rare condition of uncertain etiology which occurs predominantly in the cervical spine and, when it occurs, presents with neck pain. Leukocytosis

and elevated erythrocyte sedimentation rate may be present. In the acute period, disc protrusion may occur and lead to neurological signs. On radiographs, there may also be alteration of the adjacent vertebral bodies, including loss of body height of the anterior half, anterior "pseudo-osteophytes," and endplate irregularity. The vertebral body above the calcification is usually more affected. Awareness of the condition is important, to obviate unnecessary surgical intervention, as calcifying discopathy in children typically resolves spontaneously within a few months [44, 45] (Fig. 11.46).

Teaching Points
- The cervical spine assumes an adult configuration by 8–9 years; until this age, children tend to be more susceptible to upper cervical spine injury.
- Thoracic and lumbar spine injuries are more frequent in teenagers and are similar to adult fractures.

Fig. 11.46 Lateral radiograph of the cervical spine of a child showing calcification in the intervertebral disc space, indicating calcifying discopathy with changes in the adjacent vertebrae

- A lateral radiograph is usually adequate for the initial assessment of suspected cervical spine injury. On this radiograph, it is important to differentiate pseudosubluxation from true subluxation and to recognize the normal anatomy of the pediatric craniocervical junction.

11.5.4 Thoracic and Lumbar Spine

In later childhood and during puberty, secondary ossification centers encircle the margins of the superior and inferior endplates, known as ring apophyses. The bony apophysis is separated from the vertebral body by a thin layer of cartilage, until fusion occurs at about 18 years. The normal non-fused ring apophysis may mimic a fracture on radiographs, as it is separated from the vertebral body by a small radiolucent line [46, 47]. Apophyseal ring fractures may be difficult to appreciate on radiographs (Fig. 11.47). However, on CT/MR, a bone or cartilage fragment, or disc herniation, can be better shown.
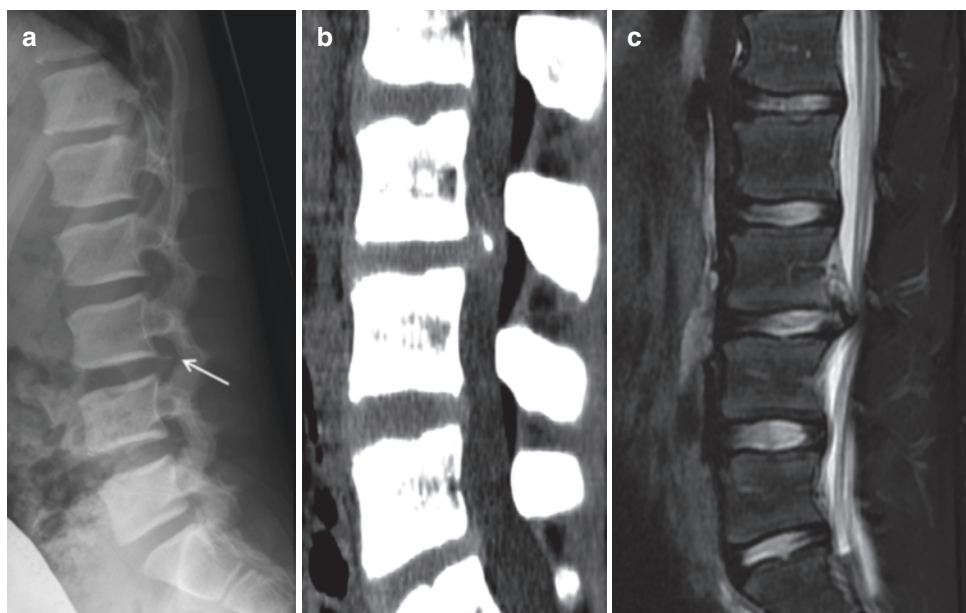

Fig. 11.47 (**a**) Lateral radiograph of the lumbar spine of a 14-year-old boy with worsening lower back pain. There is a subtle bone density posterior to the inferior endplate of L3 (arrow). Note the normal non-fused ring apophysis in the anterior aspect of the vertebral bodies. (**b**) CT and (**c**) MRI show an apophyseal ring fracture with disc herniation
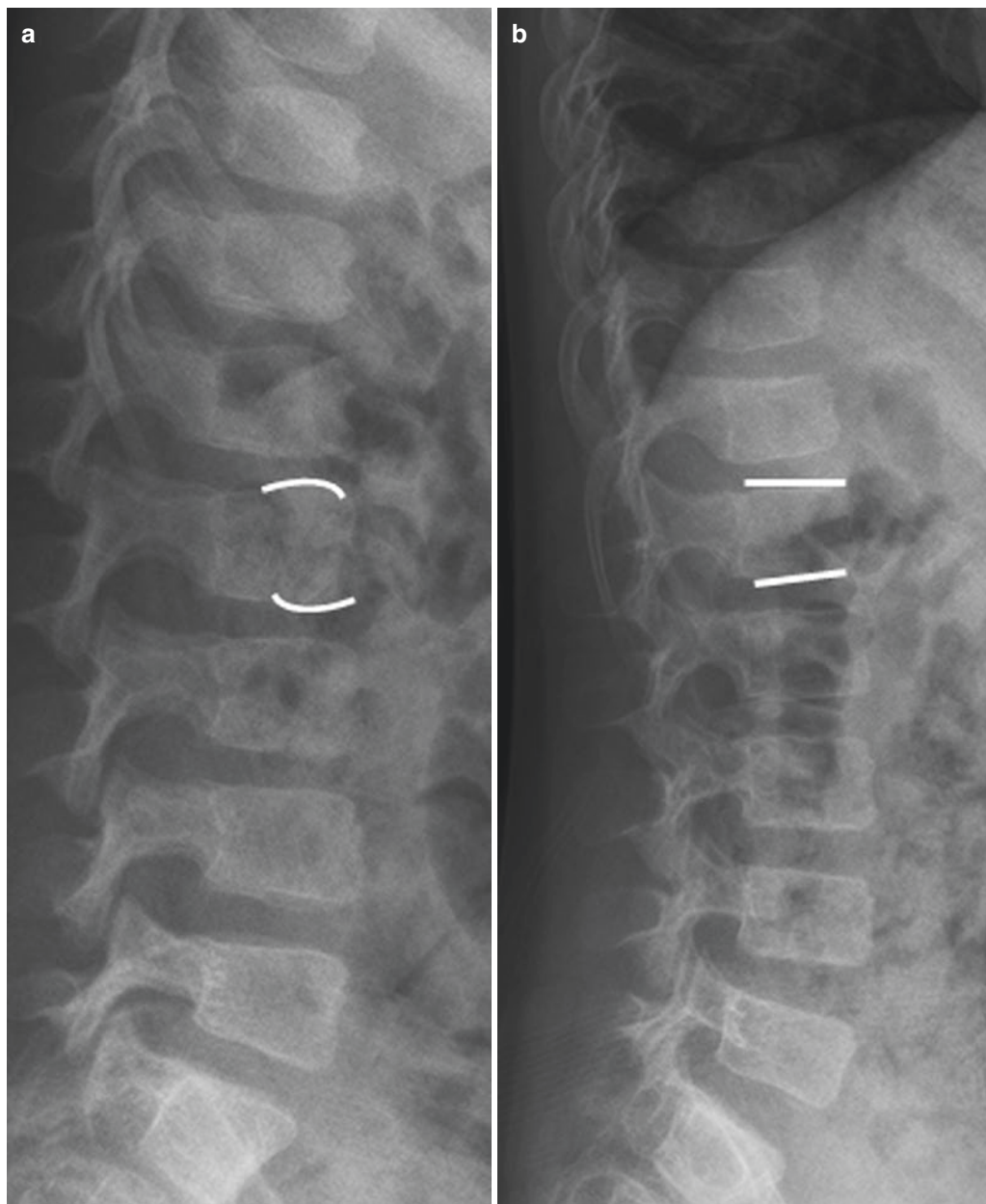
Fig. 11.48 Lateral lumbar spine images of (**a**) a 5-year-old girl with normal appearance of the endplates, retaining their normal childhood biconvexity, (**b**) age-matched girl with osteogenesis imperfecta, showing a minimal anterior wedge shape of several lower thoracic vertebrae and flattening of the lumbar endplates, with loss of the normal convexity

Loss of endplate parallelism is a key sign of vertebral fracture in adults. However, endplates in children are not usually parallel to each other. Vertebral bodies in normal young children typically appear convex outward with a gradual transition to a more square adult shape in later childhood. Loss of this normal outward convexity of the endplates suggests a compression fracture [46] (Fig. 11.48).

Teaching Points

- The normal ring apophysis may mimic a fracture.
- In young adults with disc herniation, remember to look for fragments and to exclude ring apophyseal fracture.
- Loss of the normal outward convexity of the vertebral endplates in young children suggests a compression fracture.

References

1. Arthurs OJ, Bjorkum AA. Safety in pediatric imaging: an update. Acta Radiol. 2013;54:983–90.
2. Taylor GA, Voss SD, Melvin PR, Graham DA. Diagnostic errors in pediatric radiology. Pediatr Radiol. 2011;41:327–34.
3. Darras KE, Roston AT, Yewchuk LK. Imaging acute airway obstruction in infants and children. Radiographics. 2015;35:2064–79.
4. Koplewitz BZ, Springer C, Slasky BS, Avital A, Uwyyed K, Piccard E, Bar-Ziv J. CT of hemangiomas of the upper airways in children. AJR Am J Roentgenol. 2005;184:663–70.
5. Pugmire BS, Lim R, Avery LL. Review of ingested and aspirated foreign bodies in children and their clinical significance for radiologists. Radiographics. 2015;35:1528–38.
6. Al-Saleh S, Grasemann H, Cox P. Necrotizing pneumonia complicated by early and late pneumatoceles. Can Respir J. 2008;15:129–32.
7. Lai SH, Wong KS, Liao SL. Value of lung ultrasonography in the diagnosis and outcome prediction of pediatric community-acquired pneumonia with necrotizing change. PLoS One. 2015;10:e0130082.
8. Restrepo R, Palani R, Matapathi UM, Wu YY. Imaging of round pneumonia and mimics in children. Pediatr Radiol. 2010;40:1931–40.
9. Enriquez G, Garcia-Pena P, Lucaya J. Pitfalls in chest imaging. Pediatr Radiol. 2009;39(Suppl 3):356–68.
10. Nasseri F, Eftekhari F. Clinical and radiologic review of the normal and abnormal thymus: pearls and pitfalls. Radiographics. 2010;30:413–28.
11. Khan NT, Dimakatso C, Suleman F, Van De Werke I. Pitfalls and mimics: the many facets of normal paediatric thymus. S Afr J Radiol. 2015;19:1–5.
12. Eysteinsdottir JH, Freysdottir J, Haraldsson A, Stefansdottir J, Skaftadottir I, Helgason H, Ogmundsdottir HM. The influence of partial or total thymectomy during open heart surgery in infants on the immune function later in life. Clin Exp Immunol. 2004;136:349–55.
13. Afifi A, Raja SG, Pennington DJ, Tsang VT. For neonates undergoing cardiac surgery does thymectomy as opposed to thymic preservation have any adverse immunological consequences? Interact Cardiovasc Thorac Surg. 2010;11:287–91.
14. Rothrock SG, Green SM, Hummel CB. Plain abdominal radiography in the detection of major disease in children: a prospective analysis. Ann Emerg Med. 1992;21:1423–9.
15. Daneman A, Navarro OM. Common pitfalls in paediatric abdominal imaging. Pediatr Radiol. 2009;39(Suppl 3):369–71.
16. Menashe SJ, Iyer RS, Parisi MT, Otto RK, Weinberger E, Stanescu AL. Pediatric abdominal radiographs: common and less common errors. AJR Am J Roentgenol. 2017;209:417–29.
17. Edwards DK. Size of gas-filled bowel loops in infants. AJR Am J Roentgenol. 1980;135:331–4.
18. Hryhorczuk AL, Lee EY. Imaging evaluation of bowel obstruction in children: updates in imaging techniques and review of imaging findings. Semin Roentgenol. 2012;47:159–70.
19. Lonergan GJ, Schwab CM, Suarez ES, Carlson CL. Neuroblastoma, ganglioneuroblastoma, and ganglioneuroma: radiologic-pathologic correlation. Radiographics. 2002;22:911–34.
20. David R, Lamki N, Fan S, Singleton EB, Eftekhari F, Shirkhoda A, Kumar R, Madewell JE. The many faces of neuroblastoma. Radiographics. 1989;9:859–82.
21. Bisset GS III, Crowe J. Diagnostic errors in interpretation of pediatric musculoskeletal radiographs at common injury sites. Pediatr Radiol. 2014;44:552–7.
22. Smith J, Tse S, Barrowman N, Bilal A. P123: missed fractures on radiographs in a pediatric emergency department. CJEM. 2016;18:S119.
23. Kellenberger CJ. Pitfalls in paediatric musculoskeletal imaging. Pediatr Radiol. 2009;39(Suppl 3):372–81.
24. Baheti AD, Iyer RS, Parisi MT, Ferguson MR, Weinberger E, Stanescu AL. "Children are not small adults": avoiding common pitfalls of normal developmental variants in pediatric imaging. Clin Imaging. 2016;40:1182–90.
25. Major NM, Crawford ST. Elbow effusions in trauma in adults and children: is there an occult fracture? AJR Am J Roentgenol. 2002;178:413–8.
26. Skaggs DL, Mirzayan R. The posterior fat pad sign in association with occult fracture of the elbow in children. J Bone Joint Surg Am. 1999;81:1429–33.
27. Zember JS, Rosenberg ZS, Kwong S, Kothary SP, Bedoya MA. Normal skeletal maturation and imaging pitfalls in the pediatric shoulder. Radiographics. 2015;35:1108–22.
28. Stevens MA, El-Khoury GY, Kathol MH, Brandser EA, Chow S. Imaging features of avulsion injuries. Radiographics. 1999;19:655–72.
29. Jans LB, Jaremko JL, Ditchfield M, Verstraete KL. Evolution of femoral condylar ossification at MR imaging: frequency and patient age distribution. Radiology. 2011;258:880–8.
30. Jaimes C, Chauvin NA, Delgado J, Jaramillo D. MR imaging of normal epiphyseal development

and common epiphyseal disorders. Radiographics. 2014;34:449–71.

31. Dupuis CS, Westra SJ, Makris J, Wallace EC. Injuries and conditions of the extensor mechanism of the pediatric knee. Radiographics. 2009;29:877–86.

32. Sookplung P, Vavilala MS. What is new in pediatric traumatic brain injury? Curr Opin Anaesthesiol. 2009;22:572–8.

33. Thiessen ML, Woolridge DP. Pediatric minor closed head injury. Pediatr Clin N Am. 2006;53:1–26.

34. Osmond MH, Klassen TP, Wells GA, et al. CATCH: a clinical decision rule for the use of computed tomography in children with minor head injury. Can Med Assoc J. 2010;182:341–8.

35. Kocaoglu M, Bulakbasi N. Common pitfalls in paediatric imaging: head and spine. Pediatr Radiol. 2009;39(Suppl 3):347–55.

36. Jopling J, Henry E, Wiedmeier SE, Christensen RD. Reference ranges for hematocrit and blood hemoglobin concentration during the neonatal period: data from a multihospital health care system. Pediatrics. 2009;123:e333–7.

37. Chang PT, Yang E, Swenson DW, Lee EY. Pediatric emergency magnetic resonance imaging: current indications, techniques, and clinical applications. Magn Reson Imaging Clin N Am. 2016;24:449–80.

38. Rozovsky K, Ventureyra EC, Miller E. Fast-brain MRI in children is quick, without sedation, and radiation-free, but beware of limitations. J Clin Neurosci. 2013;20:400–5.

39. Idriz S, Patel JH, Ameli Renani S, Allan R, Vlahos I. CT of normal developmental and variant anatomy of the pediatric skull: distinguishing trauma from normality. Radiographics. 2015;35:1585–601.

40. Miller EDJ, Rotaru C, Koujak K. Pediatric skeletal trauma. In: Donavon A, Schweitzer ME, editors. Imaging musculoskeletal trauma interpertation and reporting. Hoboken, NJ: Wiley-Blackwell; 2012. p. 31–50.

41. Scuderi AJ, Harnsberger HR, Boyer RS. Pneumatization of the paranasal sinuses: normal features of importance to the accurate interpretation of CT scans and MR images. AJR Am J Roentgenol. 1993;160:1101–4.

42. Lustrin ES, Karakas SP, Ortiz AO, Cinnamon J, Castillo M, Vaheesan K, Brown JH, Diamond AS, Black K, Singh S. Pediatric cervical spine: normal anatomy, variants, and trauma. Radiographics. 2003;23:539–60.

43. Brown RL, Brunn MA, Garcia VF. Cervical spine injuries in children: a review of 103 patients treated consecutively at a level 1 pediatric trauma center. J Pediatr Surg. 2001;36:1107–14.

44. Donmez H, Mavili E, Ikizceli T, Koc RK. Pediatric intervertebral disc calcification. Diagn Interv Radiol. 2008;14:225–7.

45. Urso S, Colajacomo M, Migliorini A, Fassari FM. Calcifying discopathy in infancy in the cervical spine: evaluation of vertebral alterations over a period of time. Pediatr Radiol. 1987;17:387–91.

46. Jaremko JL, Siminoski K, Firth GB, et al. Common normal variants of pediatric vertebral development that mimic fractures: a pictorial review from a national longitudinal bone health study. Pediatr Radiol. 2015;45:593–605.

47. Afshani E, Kuhn JP. Common causes of low back pain in children. Radiographics. 1991;11:269–91.